

Year

2008-2010

Role of Computational Fluid Dynamics in the Analysis of Haemodynamic and Morphological Characteristics of Intracranial Aneurysms

Pankaj Singh

MBBS, MS, MRCS

Departments of Cardiovascular Sciences,
Medical Physics & Neurosurgery
Royal Hallamshire Hospital,
University of Sheffield
Sheffield UK,
S10 2JF



Submitted for the degree of MD

Contents

	List of Abbreviations	3
	List of Figures & Illustrations	4
	List of Tables	7
	Acknowledgements	9
	Ethical Approvals	11
	Abstract	12
	Awards	14
	Publications/ Abstracts/ Presentations	15
Chapter-1	Summary	21
Chapter-2	Review of Literature	29
	<i>Introduction</i>	29
	<i>Materials and Methods</i>	30
	<i>Understanding the Natural History and Aetiopathogenesis of Intracranial Aneurysms</i>	30
	<i>Importance of Haemodynamic Factors</i>	43
	<i>Management of Intracranial Aneurysms: the History of a Paradigm Shift</i>	48
	<i>Computational fluid dynamics: the concept and need</i>	59
	<i>How Long We Have Come So Far: A Focused Review of Literature of the Studies Published on the Application of Computational Fluid Dynamics in the Field of Intracranial Aneurysms</i>	62
	<i>Conclusions</i>	78
Chapter-3	Materials & Methods	79
	<i>Introduction</i>	79
	<i>Project @neurIST</i>	69
	<i>Ethical Approvals</i>	81
	<i>Recruitment of Patients</i>	81
	<i>Data Collection and Organization</i>	85
	<i>Software @neuFuse</i>	87
	<i>Boundary Conditions used in different studies: Measured and 1D model</i>	96
	<i>Statistical analysis</i>	98
	<i>Designing and Performing Different CFD Studies</i>	98
Chapter-4	Validation of the Common Concepts used in Computational Fluid Dynamics	99
	<i>Introduction</i>	99
	<i>Effects of Different Velocity Profiles on the Haemodynamics of Intracranial Aneurysms</i>	100
	<i>Effects of Measured vs. Modelled Boundary Conditions on the Haemodynamics of Intracranial Aneurysms</i>	120
	<i>Overall conclusions form this section</i>	139
Chapter-5	Evaluations and Controlled Exposures of @neuFuse Tool-chain	140
	<i>Introduction</i>	140
	<i>The role of computational fluid dynamics in the management of unruptured intracranial aneurysms: a clinicians' view</i>	142
	<i>Background and Objectives</i>	142
	<i>Material and methods</i>	143
	<i>Results</i>	148
	<i>Discussion</i>	155
	<i>Conclusions</i>	161
	<i>Appendix-1</i>	162
Chapter-6	Computational Fluid Dynamics as a Tool to Explore the Aetiopathogenesis of Intracranial Aneurysms	165
	<i>Introduction</i>	165
	<i>Effects of changing blood viscosity on computed wall shear stress and oscillatory shear index at the site of intracranial aneurysm formation</i>	167
	<i>Analysis of Different Haemodynamic Factors During Initiation and Rupture of an Intracranial Aneurysm and Possible Influence of Low Molecular Weight Heparin Mediated Change in the Blood Viscosity on Computed Values of These Haemodynamic Factors</i>	180
	<i>The Effects of Aortic Coarctation on Cerebral Haemodynamics and its Possible Role in the Aetiopathogenesis of Intracranial Aneurysms</i>	192
Chapter-7	Conclusions & Future Work	213
Chapter-8	References	216

LIST OF ABBREVIATIONS

SAH	Subarachnoid hemorrhage	POD	Para-operational Device
IA	Intracranial Aneurysms	TCVC	Therapeutic transcatheter vessel-occlusion
UIAs	Unruptured IAs	GDC®	Guglielmi detachable coils
CFD	Computational Fluid Dynamics	DMSO	Dimethyl sulfoxide
WSS	Wall Shear Stress	CAP	Cellulose acetate polymer
BCs	Boundary Conditions	TIA s	Transient Ischemic Attacks
BV	Blood Viscosity	ROI	Region of Interest
CoA	Coarctation of Aorta	VMTK	Vascular Modeling Toolkit
OSI	Oscillatory Shear Index	GAMBIT	Geometry and Mesh Building Intelligent Toolkit
MRI	Magnetic Resonance Imaging	TCD	Transcranial Doppler
MRA	Magnetic Resonance Angiogram	LDV	Laser Doppler Velocimetry
MRFD	Magnetic Resonance Fluid Dynamics	NA	Not Available
pc-MR	phase contrast MR	CoW	Circle of Willis
NMR	Nuclear Magnetic Resonance	TOF	Time-Of-Flight
3DRA	3 Dimensional Rotational Angiography	MIP	Maximum intensity projections
DSA	Digital Subtraction Angiogram	CRIM	Clinically Relevant Information Model
CTA	CT Angiogram	ANSYS®-ICEM™	Ansys CFD Software
ROI	Region of Interest	ANSYS®-CFX™	Ansys CFD Software
AVM	Arteriovenous Malformations	GB	Gigabyte
APKD	Adult Polycystic Kidney Disease	MB	Megabyte
EDRF	Endothelial Derived Relaxation Factors	RAM	Random Access Memory
ATP	Adenosine triphosphate	CAM-application	Computer-aided medicine-application
ICA	Internal Carotid Artery	IT system	Information Technology system
MCA	Middle Cerebral Artery	iNOS	Inducible N2O synthase
ACA	Anterior Cerebral Artery	eNOS	Endothelial N2O synthase
ACoM	Anterior Communicating Artery	MABP	Mean Arterial BP
PCoM	Posterior Communicating Artery	JAG	Juxta apical groove
BA	Basilar Artery	MMP-13	Matrixmetalloproteinases-13
PCA	Posterior Cerebral Artery	NO	Nitric oxide
PICA	Posterior Inferior Cerebellar Artery	t-pa	Tissue plasminogen activator
SCA	Superior Cerebellar Artery	ISUIA	International Study of Unruptured Intracranial Aneurysms
CCA	Common Carotid Artery	ISAT	International Subarachnoid Aneurysm Trial
AbCoA	Abdominal Aortic Coarctation	CT	Computed Tomographic

LIST OF FIGURES & ILLUSTRATIONS

	PAGE
Chapter-1	
None	
Chapter-2	
Figure-2.1: The common anatomical locations for IAs in cerebral vasculature. (Source: http://www.usmle-forums.com)	32
Figure-2.2: Graphs showing the average size of aneurysms at the time of rupture during follow-up (left) and the average aneurysm size as function of patient age (right). For high mean growth rates almost all aneurysms rupture in the first 40 years of follow-up but small rupture rates indicate towards the nonlinear pattern of the growth. Source: Koffijberg et al J Neurosurg 2008	39
Figure-2.3: Showing the intra-aneurysmal flow pattern inside an aneurysm before and after the growth. (Source: Tateshima et al)	40
Figure-2.4: Showing the endothelial cells losing their normal alignment when exposed to abnormally low WSS. (Source: Malek et al JAMA)	43
Figure-2.5: Thomas Willis (Source: http://www.accu-check.com)	49
Figure-2.6: John Hunter (Source: http://citizenscientistsleague.com)	50
Figure-2.7: Sir Victor Horsley (Source: Medscape)	50
Figure-2.8: Walter Dandy (Source: Medscape)	50
Figure-2.9: Temporal Evolution of different surgical modalities Neurosurg Focus, 2006, © AANS	51
Figure-2.10: GDC® Detachable coils. Source: http://synapse.koreamed.org	57
Figure-2.11: Claude Navier -Source: Medscape	59
Figure-2.12: Equations for Poiseuille's parabolic velocity profile Source: universe-review.ca	60
Figure-2.13: Discretization and generation of polygonal mesh in a pipe flow fluid region	61
Chapter -3	
Figure-3.1: Project @neurIST	79
Figure-3.2: @neuQuest GUI (Graphical User Interface)	85
Figure-3.3: @neuQuest GUI –Data Collection	85
Figure-3.4: @neuBrowser- showing graphical representation of data	86
Figure-3.5: @neuFuse Software architecture	87
Figure-3.6: @neuFuse CFD processing toolchain. Form top right clockwise: DICOM images ate loaded and the vessel geometry segmented. Then a topologically correct geometric model is processed to extract vessel Centre line (axis). This information is then used to map 3D vessels with a 1D circulatory model. This mapping allows deriving flow boundary conditions for haemodynamic model.	89
Figure-3.7: Operation workflow from medical image to haemodynamic results. A) Orthoslice visualization of the 3DRA medical image in @neuFuse. B) Visualisation of the extracted vessel surface. C) Visualisation of reduced region of interest with location of inlet and outlet openings. D) 1D circulation model. E) Visualisation of predicted streamlines. F) Visualisation of predicted wall shear stress.	90
Figure-3.8: A snapshot of 3D volume generation, segmentation and clipping of the ROI	91
Figure-3.9: A typical example of geometric healing where an artifact (a) and (b)“kissing vessels” can cause distortion of real geometry due to lack of the image resolution. Two close vessels are glued together by the reconstruction algorithm, but in reality they are separate	92

Figure-3.10: Process of defining the centre line and Skeletonization	93
Figure-3.11: Application of BCs at the inlets and outlets using 1D Model dictionary	94
Figure-3.12: Visualization of haemodynamic simulation in @neuFuse. On top right, flow particle tracing erythrocytes are animated according to the velocity field. On top left picture, streamlines represented with pressure-coded colouring. In the bottom left picture, WSS drawn on the vessel wall. On bottom right, complex visualization showing streamlines crossing an arbitrary plane coloured according a colour-code where red regions represent inward flow whilst represent outward flow regions.	95
Chapter -4	
Figure-4.1: Representation in one of @neurIST application suites of a typical cerebral arterial tree, with locations of geom.1, geom.1b, geom.2, and geom.3 indicated by white spheres and black arrows.	101
Figure-4.2: Reconstructed geometries: geom.1, basilar artery aneurysm, geom.1b, basilar artery aneurysm including vertebral arteries, geom.2, internal carotid artery aneurysm, geom3, middle cerebral artery aneurysm. Black arrows show secondary smaller aneurysms, excluded from the study. Labels indicate the openings where boundary conditions were applied.	103
Figure-4.3: Flow-rate (top) and pressure waveforms (bottom) applied in geom.1	106
Figure-4.4: Flow-rate (top) and pressure waveforms (bottom) applied in geom.1	107
Figure-4.5: Flow-rate (top) and pressure waveforms (bottom) applied in geom.1	108
Figure-4.6: Flow-rate (top) and pressure waveforms (bottom) applied in geom.1	109
Figure-4.7: Velocity contours across the aneurysmal sac for a) Womersley BC at lowest Re during diastole, b) plug-flow BC at lowest Re during diastole, c) Womersley BC at highest Re during systole, d) plug-flow BC at highest Re during systole. From top to bottom: geom.1, geom.2, and geom.3. Grey arrows indicate areas of discrepancies.	111
Figure-4.8: WSS contours for a) Womersley BC at lowest Re during diastole, b) plug-flow BC at lowest Re during diastole, c) Womersley BC at highest Re during systole, d) plug-flow BC at highest Re during systole. From top to bottom: geom.1, geom.2, and geom.3	113
Figure-4.9: Time-averaged WSS contours for a) Womersley boundary conditions, b) plug-flow BC. From top to bottom: geom.1, geom.2, and geom.3.	114
Figure-4.10: OSI contours for a) Womersley BC, b) plug-flow BC. From top to bottom: geom.1, geom.2, and geom.3.	115
Figure-4.11: Velocity vectors on cross-sections along the afferent vessel at peak systole for geom.1 (a,b) and geom.1b (c). The distance between the cross-sections is 1.5D, where D is the diameter of the inlet boundary in geom.1.	116
Figure-4.12: Locations of aneurysms 1-5 in a typical cerebral vasculature (illustration generated using the @neurIST software)	122
Figure-4.13: Mesh particulars and BC types used. QMRI is the velocity-based boundary condition from MRI patient-specific measurements, Q1D is the velocity-based boundary condition from 1D model, Q1D-S is the WSS-scaled velocity-based boundary condition	124
Figure-4.14: Contour plots of $tavWSS$ for method I (pc-MR), method II (1D-model), and method III (WSS-scaled).	128
Figure-4.15: Contour plots of normalized values of $tavWSS$ ($ntavWSS$) for method I (pc-MR), method II (1D-model), and method III (WSS-scaled).	129
Figure-4.16: Contour plots of OSI for method I (pc-MR), method II (1D-model), and method III (WSS-scaled).	130
Figure-4.17: Boxplots showing the distribution percentage differences between methods I and II (top) and method I and III (bottom). Asterisks denote outliers above or below 1.5 times the inter quartile range.	132

Figure-4.18: VFR waveforms for a typical healthy individual and aneurysm patients included in this study, measured using pc-MR at internal carotid level. Typical waveform was taken from Radaelli et al 2008.	135
Chapter-5	
Figure-5.1: Snapshot of a Questionnaire used to gather Feedback	141
Figure-5.2: Participants' demographic constitution	143
Figure-5.3: Clinical Vignette: typical challenging case scenario	144
Figure-5.4: Operation workflow from medical image to haemodynamic results. A) Orthoslice visualization of the 3DRA medical image in @neuFuse. B) Visualization of the extracted vessel surface. C) Visualization of reduced region of interest with location of inlet and outlet openings. D) 1D circulation model. E) Visualization of predicted streamlines. F) Visualization of predicted wall shear stress.	146
Chapter-6	
Figure-6.1: Reconstructed geometry of the IA and surrounding vasculature for patient-1 (A). Contours of WSS (B,C) and OSI (D,E) for μ typical (B,D) and μ atypical (C,E) are displayed. Arrows indicate the site of IA along the parent vessel before removal.	171
Figure-6.2: Reconstructed geometry of the IA and surrounding vasculature for patient-2 (A). Contours of WSS (B,C) and OSI (D,E) for μ typical (B,D) and μ atypical (C,E) are displayed. Arrows indicate the site of IA along the parent vessel before removal.	172
Figure-6.3: Reconstructed geometries showing the IAs and connecting vessels reconstructed with software @neuFUSE. Labels indicate the openings where boundary conditions were applied.	178
Figure-6.4: The qualitative differences in the patterns of t-av-WSS and OSI in pre (a,b) and post heparinized (c,d) blood. Top two rows are contour plots for t-av-WSS. Bottom two rows are contour plots for OSI. a&b; front views, c&d; back views. Row 1&3; Aneu-1, row 2&4; Aneu-2.	186
Figure-6.5: 24 hours ambulatory Non-invasive BP (NIBP) monitoring showing satisfactory BP control for both systolic and diastolic values.	195
Figure-6.6: Intracranial aneurysm included in the study shown in (a) circle of Willis (yellow sphere) and (b) in subclinoid part of ICA (arrow)	196
Figure-6.7: A comparison of VFR waveforms from CoA patient (marked-red) measured in proximal ICA and average VFR waveforms from healthy volunteers (marked-blue) in the same location. The flow-rates in presence of CoA are 1.5 times higher (5.44 ml/sec) as compared to the normal healthy individuals (3.62 ml/sec). Solid horizontal lines represent average values of VFR for CoA (red) and typical (blue).	199
Figure-6.8: Time-averaged WSS (top) and OSI (Oscillatory shear index) (bottom) contour plots in the left subclinoid intracranial aneurysm of CoA patient. Whereas, the areas affected by high WSS are increased in CoA patient (top, right) as compared to healthy volunteers (top, left) the OSI values are minimally changed	200
Figure-6.9: Transthoracic Doppler echocardiogram showing aortic coarctation with a diastolic tail. A coarctation gradient of 30-40 mmHg was seen (arrowhead) while the average aortic pressure was 16 mmHg. The peak velocity in aorta was 276 cm/sec.	202

LIST OF TABLES

	Page
Chapter-1	
None	
Chapter-2	
Table-2.1: The frequency of Intracranial Aneurysms as per different arterial locations (%)	31
Table-2.2: Classifications for Intracranial Arterial Aneurysms	33
Table-2.3: Aetiologies of Intracranial Arterial Aneurysms	35
Table-2.4: The factors involved in the initiation	35
Table-2.5: Activities or Events preceding Aneurysmal SAH	41
Table-2.6: The ratio of normal growth mediators is reversed in endothelial cells exposed to abnormally low WSS in right column. Source: Malek et al JAMA, 1999	44
Table-2.7: The literature-based evidence on the importance of haemodynamics in the aetiopathogenesis of IAs	47
Table-2.8: Showing the Journals publishing 2 and more papers in CFD in PubMed search	63
Table-2.9: CFD Analysis of Intracranial Aneurysms & Arteries: Some Main Studies, their Methodology and Results	69
Chapter -3	
Table-3.1. Demographic details for all recruited cases in project @neurIST	83
Table-3.2. Main known risk factors for IA development and SAH in the recruited population	84
Table-3.3: Radiological characteristics of IAs included in the study along with the location, type and method of BC application	97
Chapter -4	
Table-4.1: Geometrical properties of geom.1-3.	104
Table-4.2: Grid properties for geom.1-3	105
Table-4.3: Haemodynamic indices extracted for geom.1-3 and percentage error between Womersley and plug-flow results. 1) Elevation defined as 50% of peak pressure minus average pressure in the aneurysm at systole. 2) Elevation defined as 50% of maximum time- _{averag}	117
Table-4.4: Patient demographics and aneurysm radiological features	123
Table-4.5: Boundary conditions location, type and method	125
Table-4.6: Time-average volumetric flow-rates and inlet radii for the 6 aneurysms in study	135
Table-4.7: A comprehensive review of the methods adapted by different authors while applying BCs	138
Chapter-5	
Table-5.1: Aneurysm Radiological Characteristics	145
Table-5.2: Questionnaire sections and objectives	148
Table-5.3: General feedback	149
Table-5.4: Course design and conduct	150
Table-5.5: Experience with the software	151
Table-5.6: Haemodynamics understanding	152
Table-5.7: Impact of CFD in neurosurgery	153
Table-5.8: Bringing this software into routine use	154
Table-5.9: Attendees' performance	155
Table-5.10: The literature-based evidence on the importance of haemodynamics in the aetiopathogenesis of IAs	159

Chapter-6	
Table-6.1: Patients' demography, clinical presentations of IAs included in the study, their management, and the known risk factors	168
Table-6.2: Quantitative comparison of areas and values of WSS the effects for μ_{atypical} and μ_{typical}	170
Table-6.3: The literature-based evidence on the importance of WSS and OSI in the aetiopathogenesis of IAs	173
Table-6.4: WSS-induced vascular remodeling: an overview of some important mechanisms proposed	175
Table-6.5: Radiological characteristics of IAs	183
Table-6.6: Inter-aneurysmal comparison of haemodynamic indices in Aneu-1 and Aneu-2 for typical BV ($\mu_{\text{untreated}}$)	184
Table-6.7: The Quantitative comparison of effects of heparin on haemodynamic indices	185
Table-6.8: The literature-based evidence on the importance of haemodynamics in the aetiopathogenesis of IAs	188
Table-6.9: Radiological characteristics of the IA included in the study, the pc-MR measurements in CoA patient and healthy volunteers along with the locations, types and methods of BC application	198
Table-6.10: Absolute values of WSS, OSI, velocity and pressure for IA, obtained using BCs derived from healthy volunteers and measurements taken in CoA patient by pc-MR	201
Table-6.11: A comprehensive review of different mechanisms proposed for the increased incidence of IAs in CoA patients	208

ACKNOWLEDGEMENTS

First of all, I would like to thank the European Commission, VI Framework Program, Priority 2, Information Society Technologies, and Project @neurIST for allowing these studies as well as all their financial and logistic support.

Words are not enough to express my gratitude to my friend and colleague Dr. Alberto Marzo. The studies included in this manuscript would have not been possible without his generous help and support. Alberto and me shared an excellent chemistry throughout my stay in the project, travelled the world together to present our work, came close to each other's families, and in fact, started a lifelong friendship.

Special thanks go to my supervisors Prof. Rod Hose and Mr. Umang Patel for their constant guidance and invaluable supervision. Rod has been much more than a mentor to me who showed great trust in my abilities, and has always been ready to go beyond his limits to help me out. In spite of holding such a high academic and research position, he is an amazingly approachable and humble person. He will be a role model to me for rest of my life for hard work, perseverance, and generosity. Being a neurosurgeon is busy enough. I am grateful to Umang who always took time from his extremely busy schedule to discuss a number of scientific hypotheses with me. He was always available for 'brainstorming' on any topic when I needed his invaluable input. I am also grateful to him for allowing me to approach patients from his Neurovascular Clinics, which played an instrumental role in our patient recruitment from Sheffield Center.

Prof. Patricia Lawford and Dr. Stuart Coley deserve special mention for their support and time-to-time help they provided. Dr. Richard Lycett deserves special thanks for his support in conducting the CFD analyses on a number of cases.

I would also like to extend my regards to Prof. Alex Frangi, Dr. Daniel Rufenacht, and Dr. Philippe Bijlenga for believing in my capabilities and giving me numerous opportunities to work in many key roles. I am also grateful to all members of @neurIST for their dedicated efforts in developing the software @neuFuse and other tools especially Dr. Mari-Cruz Villa-Uriol, Dr. Alessandro Chiarini, Dr. Inacho Larrabide, Dr. Juan Macho, and rest of the team. I duly acknowledge that the 1D circulation model used in a number of analyses here was a result of the work done by

Dr. Philippe Reymond and Dr. Nikos Stergiopoulos from Laboratory of Haemodynamics and Cardiovascular Technology, Ecole Polytechnique, Fédérale de Lausanne EPFL, Switzerland.

Whereas, Dr. Andy Narracott helped me in understanding in the basic principles of Computational Fluid Dynamics initially, Dr. Alan Waterworth and Dr. Steven Wood always made sure that anonymized patient images are available in time for my analyses. I gratefully acknowledge the help of Dr. Matt Gwilliam, Dr. Iain Wilkinson, and other members of MRI Department in Royal Hallamshire Hospital who helped me in performing Q-Flow pcMRI measurements that formed important basis for a number of studies included in this thesis.

I must thank Dr. Guntram Berti and other members from NEC Laboratories Europe, for all their help and support. Acknowledgements will not be complete without thanking Dr. Keith McCormack who always made sure things went smoothly on a number of occasions especially during exposures and multicentric synchronization of @neuFuse.

I am also grateful to my beloved wife Juhi Tomar for her help, motivation and support in preparing this draft as well as bearing with my absences during my regular visits to other countries to present my work and conduct @neuFuse workshops.

Last but not least, I highly appreciate the help of a number of visiting fellows and BMedSci students including Ms. Alice Pitt, Mr. Kiyanouche Jash, Mr. Hannan Tahir, Mr. Tissa Weeratunge, Ms. Gwen Mulder and Ms. Sneha Varkey. I am also grateful to Mr. Steve Parkin for the technical support in the department.

In retrospect, working in Project @neurIST was one of the best things I ever did in my life. It was like working in a big family of all incredibly supportive and kind people who will go beyond their limits to make you happy.

Pankaj Singh

Pankaj Singh

39, Aldrich Drive

Milton Keynes

MK15 9HP

ETHICAL APPROVALS

The project has appropriate ethical approvals for the required research. All partners involved in the project took separate ethical approvals from their local ethical committees after satisfying their requirements. The ethical matters for UK managed by Project Ethical Committee, Oxford, UK (Oxfordshire Research Ethics Committee-A Study Number: 07/Q1604/53). The research was supported by a research grant from Project Aneurist (www.aneurist.org) - Research Grant Account N° RU 110017. Registration N° for MD is 070237465 while the RTP N° is MED6950.

ABSTRACT

Aneurysmal subarachnoid hemorrhage (SAH) carries a high morbidity and mortality. The current protocols used to treat the unruptured Intracranial Aneurysms (IAs) are inadequate underscoring the need of finding new descriptors.

As demonstrated by the studies performed in this manuscript, haemodynamics plays an important role in the aetiopathogenesis of IAs. An evaluation of haemodynamic indices can provide a useful alternative to predict the behavior of an unruptured IA at an early stage. Studies performed by me demonstrate that Computational Fluid Dynamics (CFD) can be used successfully to predict haemodynamic indices where detailed in vivo measurement of haemodynamic flow variables is not possible owing to technical limitations.

European Commission funded Project @neurIST was the first project of its kind that brought together a number of multidisciplinary professionals from 32 European institutions and made possible development of state-of-the-art tools for personalised risk assessment and treatment IAs using CFD. These tools have been constantly improved and amended in the light of feedback gathered from their controlled exposures conducted world over, as described in the manuscript. However, need of a well-designed Randomized Controlled Trial in this context cannot be overemphasized, before these tools can be accepted by clinicians and patients.

In my study on the validation of different concepts used in CFD, I demonstrated that there is no added advantage of complex Womersley-flow-profile over the much simpler plug-flow profile.

One of my studies on initiation and rupture of IAs showed that the haemodynamic patterns of IAs during these two phases are significantly different with values of supra-physiological Wall Shear Stress (WSS) being higher in initiation while lower in rupture phase. I also investigated the effects of pharmacological agents on the aetiopathogenesis of IAs and found that heparin induces significant derangements in the haemodynamics of both, pre-aneurysmal as well as ruptured IA. I propose that heparin (and its derivatives) can, on the one hand may facilitate the rupture of existing IAs, on the other hand they may suppress the formation of new IAs.

I have also found significant differences in the results using patient-specific vs. Modeled Boundary Conditions and showed that the 1D

circulation model adopted by @neurIST performs better than other approaches found in the literature.

I also proposed a novel mechanism of increase in Blood Viscosity leading to high WSS as one of the important underlying mechanisms responsible for the increased incidence of IA formation in smokers and hypertensive patients.

In my study on patients with pre-existing Coarctation of Aorta (CoA) and Intracranial Aneurysms, I demonstrated that the cerebral flow-rates in CoA patients were significantly higher when compared to average flow-rates in healthy population. It was also seen that the values and the area affected by supraphysiological WSS ($>15\text{Pa}$) were exponentially higher in patients with CoA indicating the possible role of increased haemodynamic WSS secondary to the increased flow-rates playing an important role in the pathogenesis and rupture of IAs in CoA patients.

AWARDS

- **Codman Educational Fellowship and Grant:** to present my work at 9th International Conference on Cerebrovascular Surgery, Nagoya, Japan in November 2009.
- **Young Neurosurgeon Award-2009:** by American Association of Neurological Surgeons-World Federation of Neurosurgical Societies (AANS-WFNS), XVI World Congress of Neurological Surgery, for the study *-Analysis of different haemodynamic factors during initiation and rupture of intracranial aneurysms and influence of various drugs on their natural history*, presented at Boston, MA, in September 2009.

PUBLICATIONS/ ABSTRACTS/ PRESENTATIONS

PUBLICATIONS

As a first or second author

1. **Singh PK**, Marzo A, Kumar K, Tahir H, Weeratunge TF, Lycett R, Boutarbouch M, Lawford P, Frangi A, Hose DR, Coley SC, Patel UJ. Effects of heparin on the haemodynamics of intracranial aneurysms. Published in **J Neuroradiol** (*J Neuroradiol*. 2010 Dec;37(5):300-1. Epub 2010 Apr 5.)
2. **Singh PK**, Marzo A, Lawford P, Frangi A, Patel UJ, Hose, DR, Coley SC. Effects of smoking and hypertension on the wall shear stress and oscillatory shear index at the site of intracranial aneurysm formation. **Clin Neurol Neurosurg**. 2010 May;112(4):306-13. Epub 2010 Jan 21.
3. **Singh PK**, Marzo A, Staicu C, Gwilliam MN, Lawford P, Wilkinson I, Frangi A, Patel UJ, Hose, DR, Coley SC. The effects of aortic coarctation on cerebral haemodynamic and its importance in the aetiopathogenesis of intracranial aneurysms. **J Vascular and Interventional Neurology** 2009;2(3):1-14
4. **Singh PK**, Marzo A, Coley SC, Berti G, Bijlenga P, Lawford PV, et al: The role of computational fluid dynamics in the management of unruptured intracranial aneurysms: a clinicians' view. **Comput Intell Neurosci**:760364, 2009
5. **Singh PK**, Erlalil G, Nicolae L, Prakash S, Marzo A, Iyer V, Patel J, Hose R. Management of Intracranial Aneurysms: History of a Paradigm Shift. Accepted for publication by **J Cerebrovascular & Endovascular Neurosurgery**: Nov 2013
6. **Singh PK**, Kumar K, Tarik, J, Marzo, A, Hose R, Coley S, Patel J. Superficial Temporal Artery Aneurysm Associated With Paintball Injury Successfully Treated by Endovascular Glue: A Technical Case Report and Review of Literature. Accepted for publication by **J Cerebrovascular & Endovascular Neurosurgery**: Aug 2013
7. Marzo A, **Singh P**, Reymond P, Stergiopulos N, Patel U, Hose R: Influence of inlet boundary conditions on the local haemodynamics of intracranial aneurysms. **Comput Methods Biomech Biomed Engin** 12:431-444, 2009
8. Marzo A, **Singh PK**, Radaelli A, Hose, DR, Reymond P, Lawford P, Stergiopulos N, Gwilliam M, Wilkinson I, Frangi A, Patel UJ, Coley SC. Numerical Predictions of Haemodynamics in Intracranial Aneurysms: the Effects of Modeled versus Patient-Specific Boundary Conditions. **Annals of Biomedical Engineering**. (Ann Biomed Eng. 2011 Feb;39(2):884-96. Epub 2010 Oct 23.)

Other publications from collaborations

1. **Risk of rupture of small anterior communicating artery aneurysms is similar to posterior circulation aneurysms**. Bijlenga P, Ebeling C, Jaegersberg M, Summers P, Rogers A, Waterworth A, Iavindrasana J, Macho J, Pereira VM,

- Bukovics P, Vivas E, Sturkenboom MC, Wright J, Friedrich CM, Frangi A, Byrne J, Schaller K, Rufenacht D, Narata AP, Clarke A, Yarnold J, Kover F, Schatlo B, Hudak S, Teta P, Blasco J, Gonzalez AM, Lovblad KO, Coley S, Doczi T, Risselada R, Sola T, Lawford P, Patel U, **Singh P**, Wickins J, Elger B, Beyleveld D, Wood S, Hasselmeyer P, Arbona A, Meyer R, Hose R, Lonsdale G, Hofmann-Apitius M. **Stroke**. 2013 Nov;44(11):3018-26. doi: 10.1161/STROKEAHA.113.001667. Epub 2013 Jul 30.
2. **@neurIST Complex Information Processing toolchain for the integrated management of cerebral aneurysms.** Villa-Uriol MC, Berti G, Hose DR, Marzo, Chiarini A, Penrose J, Pozo J, Schmidt JG, **Singh P**, Lycett R, Larrabide I, Frangi AF. **Interface Focus (official Journal of The Royal Society)** April 6, 2011, doi: 10.1098/rsfs.2010.0033.
 3. **Genome-wide association study of intracranial aneurysms identifies 5 risk loci.** Katsuhito Yasuno, Kaya Bilguvar, Philip Bijlenga, Amanda Low Siew Kee, Boris Krichek, Georg Auburger, Matthias Simon, Dietmar Krex, Zulfikar Arlier, Nikhil Nayak, Ynte M Ruigrok, Mika Niemela, Atsushi Tajima, Mikael von und zu Fraunberg, Doczi Tamas, Florentina Wirjatijasa, Akira Hata, Blasco Jordi, Agi Oszvald, Hidetoshi Kasuya, Zilani Gulam, Beate Schoch, **Singh Pankaj**, Carsten Stürer, Risselada Roelof, Jürgen Beck, Teresa Sola, Filomena Ricciardi, Arpo Aromaa, Thomas Illig, Stefan Schreiber, Cornelia M van Duijn, Leonard H van den Berg, Perret Claire, Proust Carole, Constantin Roder, Ali K. Ozturk, Emilia Gaal, Wickins Jeremy, Daniela Berg, Christof Geisen, Friedrich Christoph, Summers Paul, Frangi Alex, Matthew W State, H Erich Wichmann, Monique M B Breteler, Cisca Wijmenga, Shrikant Mane, Leena Peltonen, Elio Vivas, Sturkenboom Miriam, Lawford Patricia, Byrne James, Macho Juan, I. Erol Sandalcioğlu, Bernhard Meyer, Andreas Raabe, Rufenacht Daniel, Juha E Jääskeläinen, Juha Hernesniemi, Gabriel J E Rinkel, Hitoshi Zembutsu, Ituro Inoue, Aarno Palotie, Francois Cambien, Yusuke Nakamura, Richard P Lifton, Murat Gunel. Published in **Nature Genetics (Nat Genet. 2010 May;42(5):420-5. Epub 2010 Apr 4.)**
 4. **MR derived volumetric flow rate waveforms at locations within the common carotid, internal carotid, and basilar arteries.** Gwilliam MN, Hoggard N, Capener D, **Singh P**, Marzo A, Verma PK, Wilkinson ID. **J Cereb Blood Flow Metab (Nature Publishing Group)**. 2009 Dec;29(12):1975-82.

ABSTRACTS/ CONFERENCE PROCEEDINGS

1. **Singh PK**, Marzo A, Coley SC, Lawford P, Frangi A, Hose DR, Patel UJ. The @neurist Project: Development of a Computational Model to Improve Management of Intracranial Aneurysms. Published in the **Proceedings of XIV-AANS-WFNS (American Association of Neurological Surgeons-World Federation of Neurosurgical Societies)**, World Congress, Boston, MA, USA, 30th Aug – 4th Sep 2009, 1512-1520.
2. **Singh PK**, Marzo A, Coley SC, Lawford P, Frangi A, Hose DR, Patel UJ. Computational Simulation of Haemodynamic Characteristics in Intracranial

Aneurysms with @neufuse. Published in the **Proceedings of XIV-AANS-WFNS (American Association of Neurological Surgeons-World Federation of Neurosurgical Societies)**, World Congress, Boston, MA, USA, 30th Aug – 4th Sep 2009, 2505.

3. **Singh PK**, Marzo A, Lawford P, Frangi A, Patel UJ, Hose, DR, Coley SC. Effects of smoking and hypertension on the wall shear stress and oscillatory shear index at the site of intracranial aneurysm formation. Published as an abstract in the **Proceedings of 9th International Conference on Cerebrovascular Surgery**, Nagoya, Japan, 08;2, 2009.
4. **Singh PK**, Marzo A, Tahir H, Weeratunge TF, Hose DR, Lawford P, Patel UJ, Coley SC. Computational study of the effects of drugs on growth and rupture of intracranial aneurysms: Published in the **Proceedings of VI International Conference on Computational Bioengineering**, Bertinoro, Italy, 2009, p 67.
5. **Singh PK**, Marzo A, Tahir H, Weeratunge TF, Hose DR, Lawford P, Patel UJ, Coley SC: **A novel approach for computational haemodynamic characterisation of cerebral aneurysms. Proceedings of the VI International Conference on Computational Bioengineering**, Bertinoro, Italy, 2009, p 67.
6. **Singh PK**, Pitt A, Chiarini A, Marzo A, Lawford P, Coley SC, Rufenacht DA, Frangi A, Patel UJ, Hose, DR. Cerebral Aneurysms: from Carotid Ligations to Computational Fluid Dynamics: Published in **2nd Proceedings of ESMINT Society**.
7. Marzo A, **Singh PK**, Lawford P, Patel UJ, Coley SC Hose DR. A novel approach for computational haemodynamic characterisation of cerebral aneurysms. Published in the **Proceedings of VI International Conference on Computational Bioengineering**, Bertinoro, Italy, 2009, p 65.
8. Marzo A and **Singh PK**. Computational haemodynamics characterization of intracranial aneurysms with @neuFuse. **1st Proceedings of the ESMINT (European Society of Minimally invasive Neurological Therapy) Conference**, September 2008, Lisbon, Portugal.
9. Pitt A, Marzo A, **Singh P**, Larrabide I, Aguilar M, Lawford P, Coley SC, Frangi A, Patel UJ, Hose, DR. Haemodynamics in intracranial aneurysms of the anterior and posterior circulation and its association with rupture. Abstract Published in **Br J Neurosurg (Mar 2010)**.
10. Hose DR, Howard B, Marzo A, **Singh PK**, Lawford P. Haemodynamic Characterization of Aneurysms by Computational Fluid Dynamics. Published in **2nd Proceedings of ESMINT Society**.

PRESENTATIONS

1. **Effects of smoking and hypertension on the wall shear stress at the site of intracranial aneurysm formation:** (Presenting Author) presented in 9th International Conference on Cerebrovascular Surgery, Nagoya, Japan 11th- 13th Nov 2009
2. **Recent Advances and the Role of CFD in the Management of Unruptured Intracranial Aneurysms:** (Presenting Author) presented in Cardiovascular Surgery Meeting, Royal Hallamshire Hospital, Sheffield on 2nd Oct 2009
3. **Recent Advances in the Management of Unruptured Intracranial Aneurysms:** (Presenting Author) presented during Sheffield Clinical Neurosurgery Meeting (B. Braun), 25, 26th Sept 2009
4. **Computational study of the effects of drugs on growth and rupture of intracranial aneurysms:** (Presenting Author) presented in VI International Conference on Computational Bioengineering, Bertinoro, Italy, 16-18th Sept 2009
5. **Computational Predictions to Improve Management of Intracranial Aneurysms:** (Presenting Author) Presented in American Association of Neurological Surgeons-World Federation of Neurosurgical Societies (AANS-WFNS), XVI World Congress of Neurological Surgery, Boston, MA, Sept 2009.
6. **The effects of heparin on the natural history of intracranial aneurysms:** (Presenting Author) Presented in Young Neurosurgeons' Forum as an Award winning paper during American Association of Neurological Surgeons-World Federation of Neurosurgical Societies (AANS-WFNS), XVI World Congress of Neurological Surgery, Boston, MA, Sept 2009.
7. **The @neurist Project: Development of a Computational Model to Improve Management of Intracranial Aneurysms:** (Presenting Author) Presented in American Association of Neurological Surgeons-World Federation of Neurosurgical Societies (AANS-WFNS), XVI World Congress of Neurological Surgery, Boston, MA, Sept 2009.
8. **A Computational Fluid Dynamics (CFD) Based Analysis of Different Haemodynamic Factors in Six Patient-Specific, Typical, Saccular Intracranial Aneurysms at Common Locations in Circle of Willis:** (Presenting Author) presented in Annual Research Day, University of Sheffield, UK, Aug 2009.

RELEVANT PERMISSIONS

Publication used in thesis	Journal/ Publisher	Permission from Journal/ Publisher
Effects of heparin on the haemodynamic characteristics of intracranial aneurysms	J Neuroradiol/ Elsevier	Yes. Attached is the generalized permission that covers all articles published by Elsevier (parent publisher for J Neuroradiol)
Effects of smoking and hypertension on the wall shear stress and oscillatory shear index at the site of intracranial aneurysm formation	Clin Neurol Neurosurg/ Elsevier	Yes. Attached is the generalized permission that covers all articles published by Elsevier
The effects of aortic coarctation on cerebral haemodynamics and its importance in the aetiopathogenesis of intracranial aneurysms.	J Vascular and Interventional Neurology/ JVIN	Yes. Permissions granted by the Editor in Chief of JVIN. Proof attached
The role of computational fluid dynamics in the management of unruptured intracranial aneurysms: a clinicians' view.	Comput Intell Neurosci/ Hindawi	Yes. The paper was published as an Open Access Publication by Comput Intell Neurosci (Hindawi publishers)- As per Journal's Policy- these articles are distributed under the terms of the Creative Commons Attribution License, which permits unrestricted use, distribution and reproduction in any medium , provided that the original work is properly cited. The Policy Statement form Journal's website is enclosed.
Management of Intracranial Aneurysms: History of a Paradigm Shift.	J Cerebrovascular & Endovascular Neurosurgery/ Korea Med	Yes. Authors retain Copyright to use their own work for any non-commercial purposes. Policy statement form Korea Med attached.
Influence of inlet boundary conditions on the local haemodynamics of intracranial aneurysms.	Comput Methods Biomech Biomed Engin/ Taylor & Francis	Yes. Attached is the generalized permission that covers all articles published by Taylor & Francis (parent company for CMBBE)
Numerical Predictions of Haemodynamics in Intracranial Aneurysms: the Effects of Modeled versus Patient-Specific Boundary Conditions.	Annals of Biomedical Engineering/ Springer	Yes. Permission obtained from Springer (parent publisher for Annals of Biomedical Engineering) to reuse the full text of the article for the purpose of thesis, is attached

Co-author	Permission acquired
Alberto Marzo	Yes. Received on 23/03/2014
Rod Hose	Yes. Received mail on 21/03/2014
Patricia Lawford	Yes. Verbally
Umang Patel	Yes, verbally
Alex Frangi	Yes. Got the mail on 23/03/2014
Stuart Coley	Yes, received mail
Philippe Bijlenga	Yes. Got the mail on 23/03/2014
Daniel Rufenacht	Yes. Got the mail on 23/03/2014
Keith McCormack	Mailed on 23/03/2014
Hannan Tahir	Yes. Got the mail on 23/03/2014
Richard Lycett	Yes, received email
Matt Gwilliam	Yes. Got the mail on 23/03/2014
Tissa Weeratunge	Mail bounced back. Unable to contact!
Ian Wilkinson	Yes. Got the mail on 23/03/2014
Christina Staicu	Mail bounced back. Unable to contact!
Mari-Cruz Villa-Uriol	Mailed on 23/03/2014
Alessandro Chiarini	Yes, received email
Guntram Berti	Mail bounced back. Unable to contact!
Alessandro Radaelli	Mailed on 23/03/2014
Philippe Reymond	Mailed on 23/03/2014
Nikos Stergiopoulos	Mailed on 23/03/2014
Kuldeep Kumar	Yes, verbally
Mahjouba Boutarbouch	Yes. Got the mail on 23/03/2014
George Erlalil	Yes, verbally
Liviu Nicolae	Yes, verbally
Savithru Prakash	Yes, verbally
Ven Iyer	Yes, verbally

CHAPTER 1.0: SUMMARY

Overview

- 1.1 Background
- 1.2 Dilemmas with current management plans
- 1.3 Importance of Haemodynamic Factors
- 1.4 Limitations of current technology in measuring haemodynamic indices and role of CFD in this context
- 1.5 CFD and its various applications in medicine
- 1.6 Application of CFD in the field of Intracranial Aneurysms
- 1.7 Validation of common concepts used in CFD
- 1.8 CFD as a tool to explore the aetiopathogenesis of Intracranial Aneurysms

1.1 Background

An aneurysm is an abnormal dilatation or ballooning of a part of a blood vessel due to weakness in its walls. Whereas, we can find aneurysms virtually anywhere in the body, one of the most fatal locations to have one is inside the cerebral vasculature, known as intracranial aneurysms (IAs). The work presented in this thesis is focussed on addressing different aspects of aetiopathogenesis and management of this particular variety using Computational Fluid Dynamics (CFD).

The term aneurysm, derived from Greek word *aneúrýsma* (*ana*; throughout + *eurus*; wide), meaning ‘to dilate’, was introduced by Claudius Aelius Galen, a philosopher of Greek origin in 200 AD. The earliest description of the intracranial or subarachnoid haemorrhage (SAH) as a cause of death in human beings, dates back to the ancient Biblical times. The first anecdotal evidence of an intracranial aneurysm as well as the earliest attempt to treat it come from Egypt. It is recorded in *Ebers Papyrus*, one of the oldest preserved medical documents that in 2725 BC, Imhotep, who was an Egyptian architect cum physician, tried to treat an aneurysm by using a fire glazed instrument [Lippi 1990].

History as a whole plays a paramount role in motivating scientists as well as providing us a foundation for future work. The history of management of Intracranial Aneurysms, history of Computational Fluid Dynamics (CFD) and the current status of CFD in the field of Intracranial

Aneurysms, is therefore analyzed in detail by conducting a focused review of relevant literature in the section Review of Literature.

1.2 Dilemmas with current management plans

In spite of recent advancements in the management, aneurysmal subarachnoid hemorrhage (SAH) remains a major cause of morbidity and mortality in neurosurgical patients [Hop et al. 1997]. Whereas, the treatment protocols for a ruptured intracranial aneurysm (IA) have become clearer with time, the management of unruptured IAs remains one of the most controversial topics in neurosurgery. These uncertainties are multi-factorial, owing mainly to incomplete and conflicting data about natural history of these lesions and the risks associated with the active management [ISUIA 1998, Raaymakers 1998, Rinkel 1998]. In order to offer the best possible treatment to the patient with the least side effects, formulation of a clear management protocols, directed by the natural history of unruptured IAs and, the risks associated with the active management, is required. Whereas, there are no strict guidelines, most of the studies [Juvela 2000, Komotar et al. 2008, Mayberg et al. 1994] including ISUIA trials [ISUIA 1998, Wiebers et al. 2003], almost unanimously recommend certain factors as indications of surgery or endovascular coiling in unruptured IAs: large aneurysmal size, symptomatic lesions, evidence of growth, multiple lesions, posterior circulation location, past history of SAH, history of smoking and hypertension, etc. All these criteria are found to have good correlation with increased risk of rupture and hence, active intervention is advocated in these situations to avoid the poor outcome. However, it is interesting to note that all of these factors also remain the underlying descriptors for poor surgical or endovascular outcome [Khanna et al. 1996, Solomon et al. 1994, Wirth et al 1983]. In other words, by the time we take a decision to treat an IA based on the current guidelines, the patient has already become predestined for a poor outcome.

1.3 Importance of Haemodynamic Factors

Whereas, current evidence convincingly supports a multifactorial aetiology for IA formation, there is a growing body of literature underlining the importance of haemodynamic [Burleson et al. 1996, Byrne et al. 1998, Gao et al. 2008, Morimoto et al. 2002, Cebal et al. 2013, Sadasivan et al. 2013, Omodaka et al. 2012, Meng et al. 2013] and morphological [Lall et al. 2009, Sadatomo et al. 2008, Xu et al. 2013, Kashiwazaki et al. 2013] factors in this context. The haemodynamic variables often considered in these studies are wall shear stress (WSS), oscillatory shear index (OSI), blood pressure and other quantities used to

characterize blood flow, while important morphological indices are shape, aspect ratio, Zernike Moments, etc. An evaluation of these variables can provide a useful alternative to predict the behavior of an unruptured IA at an early stage before it changes in size, shape or becomes symptomatic. These factors therefore can guide us in selecting the IAs with greatest risk of rupture and thus warranting the active interventions before they join a cohort of IAs who are destined for a poor outcome if we take this decision based on current guidelines. At the same time, these factors can indicate the IAs with relatively low risk of rupture that can be safely monitored, thus avoiding the unnecessary interventions.

I envision that, this prediction of risk of rupture in an *Aneurysm-specific way* will eventually revolutionize the treatment of Intracranial Aneurysms taking it to the next level.

1.4 Limitations of current technology in measuring haemodynamic indices and role of CFD in this context

Whereas, haemodynamic and morphological indices show great potential in guiding the correct management of IAs, limitations in current technology greatly restrict our ability to measure these factors in patients. In spite of some recent studies [Boussel et al. 2008, Isoda et al. 2009, Rayz et al. 2009] showing possibility of measuring some of the haemodynamic quantities *in-vivo* using magnetic resonance fluid dynamics (MRFD), inherent limitations in the technology impede its use in large cohort studies and aneurysms of <5 mm diameter. It is therefore fair to say that, the detailed *in-vivo* measurements of these relevant flow variables in the regions affected by the disease are currently very difficult and impractical [Shojima et al. 2004, Steinman et al. 2003].

Computer modeling and simulation techniques are playing an increasingly important role in the way medicine is being practiced and has been successfully applied in a number of medical disciplines.

1.5 CFD and its various applications in medicine

Computational fluid dynamics (CFD) is one of the most important tools used for computer modeling and simulation that can represent a valuable alternative to extract additional non-observable information from patient-specific data for IAs.

CFD is the science of predicting fluid flow, heat and mass transfer, chemical reactions, and related phenomena by solving numerically the set of mathematical equations that govern a particular physical system

(conservation of mass, momentum, energy, species etc.). Since its early development in the 1960s and 1970s in the field of aerospace, where it was used mainly to improve the design and efficiency of aircrafts [Agarwal et al. 1999] CFD has been successfully used in many other clinical applications.

One of the most important clinical areas where CFD is widely used is Circulatory System. It has been applied for assessing the blood flow through stenoses [Feng et al. 2011, Bark et al. 2010, Siouffi et al. 1998], analysis of physiology of blood flow through heart valves [Chan et al. 2013] as well as the turbulence through prosthetic heart valves [Kaufmann et al. 2011], flow and patency of aortic grafts [Vardoulis et al. 2011, Prasad et al. 2011] and mechanics of arterial diseases [Tang et al. 2013]. It has also been used for assessing the flow through Arterio Venous Fistulas [Ene-Iordache et al. 2011, Kharboutly et al. 2010] and modelling of thrombosis of blood [Corbett et al. 2010]. CFD has also been applied to the Respiratory System for the simulation of airflow and evaluation of respiratory functions [Malvè et al. 2011] as well as characterization of respiratory aerosol drug delivery [Lou et al. 2004, Tian et al. 2011]. Investigators have also applied numerical modelling to the fluid dynamics inside the human Gastrointestinal System [Ferrua et al. 2010], the urinary flow-rates through the Genitourinary System [Frawley et al. 2009] and the flow dynamics of Cerebrospinal Fluid (CSF) and its correlation with the development of hydrocephalus [Linge et al. 2011, Penn et al 2011].

1.6 Application of CFD in the field of Intracranial Aneurysms

Success of CFD in other medical disciplines played an important role in inspiring biomedical scientists and paved a path for its further application in the field of cerebral vasculature and intracranial aneurysms [Boussel et al. 2008, Castro et al. 2006, Cebal et al. 2005, Shojima et al. 2004, Singh et al. 2009, Steinman et al. 2003, Morales et al. 2011, Lu et al. 2011, Wong et al. 2011, Hassan et al. 2011, Marzo et al. 2011, Doenitz et al. 2010, Zeng et al. 2010, Sun et al. 2010, Sforza et al. 2010, Ford et al. 2005, Ford et al. 2008, Sun et al. 2012, Alfano et al. 2013, Weichert et al. 2013]. Apart from that; two other important factors behind the successful application of CFD in this field were; growing evidence emphasizing the important role played by haemodynamic indices in the aetiopathogenesis of Intracranial Aneurysms and difficulty of conducting detailed *in-vivo* measurement of these variables.

The application of CFD in this relatively new field, however, was not without challenges. There were a number of prerequisites to be met and

hurdles to overcome, before the potential of CFD as a tool could be tapped, in predicting the risk of rupture in Intracranial Aneurysms. These challenges were met one by one in the project @neurIST.

The initial step in computing these haemodynamic and morphological variables is building three-dimensional (3D) computer models of the Region of Interest (ROI) from patient specific medical images (e.g. 3D Rotational Angiograms, CT Angiograms, or MR Angiograms). This is achieved with the help of a software tool-chain (called herein tool-chain). First and foremost, prerequisite therefore was building a user-friendly robust tool-chain that is not observer dependent and can be used by a common user, consistently and repeatedly [Villa-Uriol et al. 2011]. This major breakthrough achieved by teams of dedicated biomedical scientists and computer engineers across a number of centers as a part of project @neurIST. This goal was accomplished in three main steps: a) development of software @aneuFuse or the tool-chain, b) continuing evaluation of the tool-chain by conducting its controlled exposures to the relevant audiences and users to collect useful feedback and, c) modifying the tool-chain by integrating this feedback as well as conducting a Multi-centric Synchronization. The tool-chain is described in detail under materials and methods section along with an overview of its development process as undertaken by different teams.

1.7 Validation of common concepts used in CFD

After building a robust tool-chain, the next step was to establish the reliability of the common basic concepts applied while using CFD as a tool in the analysis of haemodynamic and morphological indices in the Cerebral Vasculature and Intracranial Aneurysms.

Specification of Boundary Conditions is an important prerequisite for solving the governing equations in the extraction of these non-observable indices. As direct measurements of these flow-rate waveforms at the inlets and outlets of the domain are usually impracticable [Marzo et al. 2009], the Boundary Conditions are mostly derived using the available 1D Circulation models [Westerhof et al. 1969, Stergiopoulos et al. 1992, Vignon-Clementel et al. 2006, Balossino et al. 2009, Bove et al. 2008]. A number of assumptions are made while applying these Boundary Conditions that can strongly perturb the numerical calculations. One such assumption is application of Womersley flow profile at inlet Boundary of the domain [Marzo et al. 2009]. The first study therefore was conducted to investigate the effects of different inlet velocity profiles on the

haemodynamics of IAs and compared them with the more important determinants of the haemodynamics like geometry of the domain.

The study on the effects of Boundary Conditions on the haemodynamics of IAs further extended by taking phase contrast MR (pc-MR) measurements for flow-rates in 19 IAs from nine patients recruited in the study [Marzo et al. 2011]. The effects of the Boundary Conditions derived using these patient-specific pc-MR flow-rates and the traditional 1D-model, on the haemodynamic characterization of IAs, were then compared and analyzed in order to quantify the agreements and differences in the values of derived haemodynamic indices.

1.8 CFD as a tool to explore the aetiopathogenesis of Intracranial Aneurysms

The final sections of this manuscript are devoted towards exploring the different factors that can influence the aetiopathogenesis of Intracranial Aneurysms by altering their haemodynamic environments. A number of studies were designed in this context and CFD was used to prove or refute the hypotheses.

The first study in this section was conducted on the two well-known risk factors for Intracranial Aneurysm formation: smoking and hypertension. Whereas, smoking and hypertension are well-established risk factors in IA formation [Bonita 1986, de la Monte et al. 1985, Inci et al. 2000, Juvela 2000, Kondo et al. 1997] their roles in the mechanisms that regulate aneurysm formation are poorly understood and are essentially limited to their statistical associations. In this study, I hypothesized that smoking and hypertension lead to intracranial aneurysm formation by changing the haemodynamic environment of the cerebral vasculature secondary to their effect on Blood Viscosity. There is good evidence in the literature that smoking and hypertension increase the Blood Viscosity in individuals [de Simone et al. 2005, Letcher et al. 1983]. CFD was used to compute the effects of these risk factors on wall shear stress (WSS) and oscillatory shear index (OSI) at the site of IA initiation, two most important factors for the development of Intracranial Aneurysms [Burlison et al. 1996, Byrne et al. 1998, Gao et al. 2008, Morimoto et al. 2002].

In the next study, I analyze the differences in the haemodynamic environments of intracranial aneurysms during the stages of their initiation versus rupture. 3D Rotational Angiograms were used to build the three-dimensional computer models of aneurysms included in the study followed by their qualitative and quantitative comparisons. The study

further extended by investigating the effects of heparin (and enoxaparin) on the haemodynamic characteristics of aneurysms. Heparin (and its derivative enoxaparin) is a widely used injectable anticoagulant for preventing venous thrombosis and pulmonary embolism. It inhibits the factors involved in blood clotting (factor Xa), causing instantaneous inactivation of thrombin, thereby reducing Blood Viscosity [Hitosugi et al. 2001) and, in turn altering the haemodynamics of the blood circulation. Values of WSS and OSI were computed with the help of CFD in a ruptured Intracranial Aneurysm and compared with a tiny aneurysm in the stage of initiation. Possible link between the low Blood Viscosity, and alterations in values of WSS/ OSI, leading to the rupture of Intracranial Aneurysm was explored. Potential effects of other pharmacological agents on the aetiopathogenesis of intracranial aneurysms are also discussed.

Another interesting study was conducted to analyze the haemodynamic changes in the cerebral circulation of patients with Coarctation of Aorta and its possible effects on the increased incidence and rupture of Intracranial Aneurysms in these patients. After a thorough search (PubMed®, Embase® and Google-Scholar™ searched from the year 1900 up to 2009) I could retrieve only two relevant studies. Whereas, Hafkenschiel et al [Hafkenschiel et al. 1949) demonstrated a significant increase in cerebral arterial flow-rates in patients with Coarctation of Aorta in 1949, Rowe and colleagues [Rowe et al. 1964] found no significant differences in the flow-rates before and after the repair of Coarctation of Aorta in their study performed in 1964. I therefore performed pc-MR measurements in the cerebral arteries of a Coarctation of Aorta patient with coexisting IA and five healthy volunteers to establish the flow-rates at different locations in the cerebral vasculature.

Amongst other aetiologies proposed, Coarctation of Aorta has been highlighted as a major risk factor in the aetiopathogenesis of IAs [Abbott 1928, Ahmetoğlu et al. 2003, Connolly et al. 2003, DuBoulay 1965, Eppinger 1871). Incidence of Intracranial Aneurysms among patients with CoA is approximately 5 times higher than that of the general population [Connolly et al. 2003]. The incidence of IA rupture in CoA patients (4.8%) [70,83 Mercado et al. 2002, Reifenstein et al. 1947] is also higher than the estimated rate of rupture in the general population, which is less than 1% [Weir et al. 1996]. In spite of CoA being a well-established risk factor for IA formation, [Abbott 1928, Ahmetoğlu et al. 2003, Connolly et al. 2003, DuBoulay 1965, Eppinger 1871] the exact underlying mechanisms for this association remain poorly understood. After measuring the flow-rates in the cerebral vasculature in patients with Coarctation of Aorta, an analysis of the different haemodynamic factors

inside Intracranial Aneurysms was performed. The possible role of haemodynamics is discussed in this context in a background of relevant literature.

A better understanding of the aetiopathogenesis of the IA formation and rupture may help clinicians in preventing and treating the disease effectively.

No study is perfect. It is therefore imperative to analyze the strengths and weaknesses of any work objectively. Towards the end of each section, limitations of the each study are discussed. This will provide readers and future workers a comprehensive insight in the methodology as well as enable them to reduplicate the studies, if required.

Overall inferences and conclusions drawn from the work as a whole are given at the end of the manuscript along with scope for future work.

CHAPTER 2.0: REVIEW OF LITERATURE

OVERVIEW

2.1: Introduction

2.2: Materials and Methods

2.3: Understanding the Natural History and Aetiopathogenesis of Intracranial Aneurysms

2.4: Importance of Haemodynamic Factors

2.5: Management of Intracranial Aneurysms: the History of a Paradigm Shift

2.6: Computational fluid dynamics: the concept and need

2.7: How Long We Have Come So Far: A Focused Review of Literature of the Studies Published on the Application of Computational Fluid Dynamics in the Field of Intracranial Aneurysms

2.8: Conclusions

My contribution: I performed all literature reviews included in this chapter, independently.

2.1 Introduction

In the first section of this chapter I have reviewed the pertinent literature exploring the natural history of Intracranial Aneurysms (IAs) including incidence, anatomical locations, and different classifications. The phenomenon of ‘initiation’, ‘growth’ and ‘rupture’ are addressed separately with their possible mechanisms and different theories behind them with a focus on the possible role played by different haemodynamic factors in each stage.

History as a whole plays a paramount role in motivating scientists as well as providing us a foundation for future work. The history of management of Intracranial Aneurysms, the history of Computational Fluid Dynamics (CFD) and the current status of CFD in the field of Intracranial Aneurysms, is therefore analysed in detail by conducting a focused review of relevant literature in the later sections of this chapter.

2.2 Materials and Methods for Conducting Review of Literature

A thorough search of different medical and non-medical databases was conducted. The databases searched were Pubmed[®], Cochrane[®], Medline[®], Embase[®], Experta Medica[®], Cinahl[®], Citation Index[®], National Library for

Health[®]. General-purpose search engines such as Google[™], Google-scholar[™], and AltaVista[™] were also used to generate search leads, which were further followed, by searching specific medical databases. I searched the different databases from the years 1910 to 2014. Strings from the bibliographies and references used by different authors of the published papers were also followed to retrieve the articles. The full text articles sourced through Sheffield Health Sciences Library, Northern General Hospital Library, The British Library, British Medical Association Library and British Museum. The full-text of the required articles was also obtained from the concerned journals. The authors of some papers were contacted directly if I was unsuccessful in retrieving the paper from any other source. Help of professional translators was taken to translate the articles obtained in languages other than English. Some unpublished work is also included in the data analysis after obtaining the relevant permissions from the concerned authors.

The different key words used for searching were: "intracranial/ cerebral + aneurysm + management", "intracranial/ cerebral + aneurysm + treatment", " intracranial/ cerebral + aneurysm + surgery", " intracranial/ cerebral + aneurysm + coiling", " intracranial/ cerebral + aneurysm + history", "intracranial/ cerebral + aneurysm + management + unruptured", "intracranial/ cerebral + aneurysm + aetiology", "intracranial/ cerebral + aneurysm + aetiopathogenesis" "intracranial/ cerebral + aneurysm + initiation" "intracranial/ cerebral + aneurysm + growth", "intracranial/ cerebral + aneurysm + rupture", "intracranial/ cerebral + aneurysm + natural + history", "computational + fluid + dynamics", "CFD", "numeric simulations", "CFD + validations", "CFD + applications + medicine", etc.

2.3: Understanding the Natural History and aetiopathogenesis of Intracranial Aneurysms

2.3.1: Incidence

Depending upon the population sample, observers' competence and the method used, the incidence of intracranial aneurysms varies in different autopsy series from 0.9% to 11% [Chason et al 1958, Cohen 1955, Jakubowski et al 1978]. The average annual prevalence of unruptured aneurysms in a population can be considered around 5% [ISUIA 1998, Kondo et al 1997]. The incidence is expectedly increasing with the advent of non-invasive techniques such as CTA, MRI and MRA. Intracranial aneurysms are rare in children, especially in first decade, with the incidence being highest during 4th, 5th and 6th decades [Kondo et al 1997]. The sex ratio changes with location. They are more common in women in

the internal carotid location (2:1) while the ratio is reversed in the middle cerebral artery (2:3). Multiple aneurysms can occur in 15 to 31% of the population [Kondo et al 1997]. The regional variations are reported with publications claiming higher incidence from Japan [Suzuki et al 1971].

2.3.2: Anatomic Location

Most intracranial aneurysms arise in and around the circle of Willis, with peripheral aneurysms remaining a rarity. The frequency of IAs at different locations is given in Table-2.1. An aneurysm is usually formed at an arterial bifurcation or at the convexity of an arterial bend, the direction the axial blood stream would have taken if the curve were not there (Figure-2.1) [Rhoton 1980].

Table 2.1: The frequency of Intracranial Aneurysms as per different arterial locations (%)

Author/ Year	Type of Study	No. Of Cases	MCA	ACA	ICA	VA
Kassell et al 1990	Cooperative	3521	22	39	30	4
Sah et al 1969	Cooperative	2630	20	34	41	4
Stebhns 1972	Case Series	5267	20	31	38	5
Stebhns 1972	Autopsy	8000	33	30	24	12

NB: MCA; middle cerebral, ACA; anterior cerebral, ICA; internal carotid, VA; vertebro-basilar

2.3.3: Classification of Intracranial Arterial Aneurysms

Intracranial aneurysms are typically classified on the basis of their location (on the artery, anterior or posterior circulation), morphology (saccular, fusiform, dissecting), aetiology (traumatic, inflammatory, neoplastic), size etc., as given in Table-2.2 and Table-2.3. In addition, the microaneurysms of Charcot and Bouchard can be found on the small perforating arteries in hypertensive individuals.

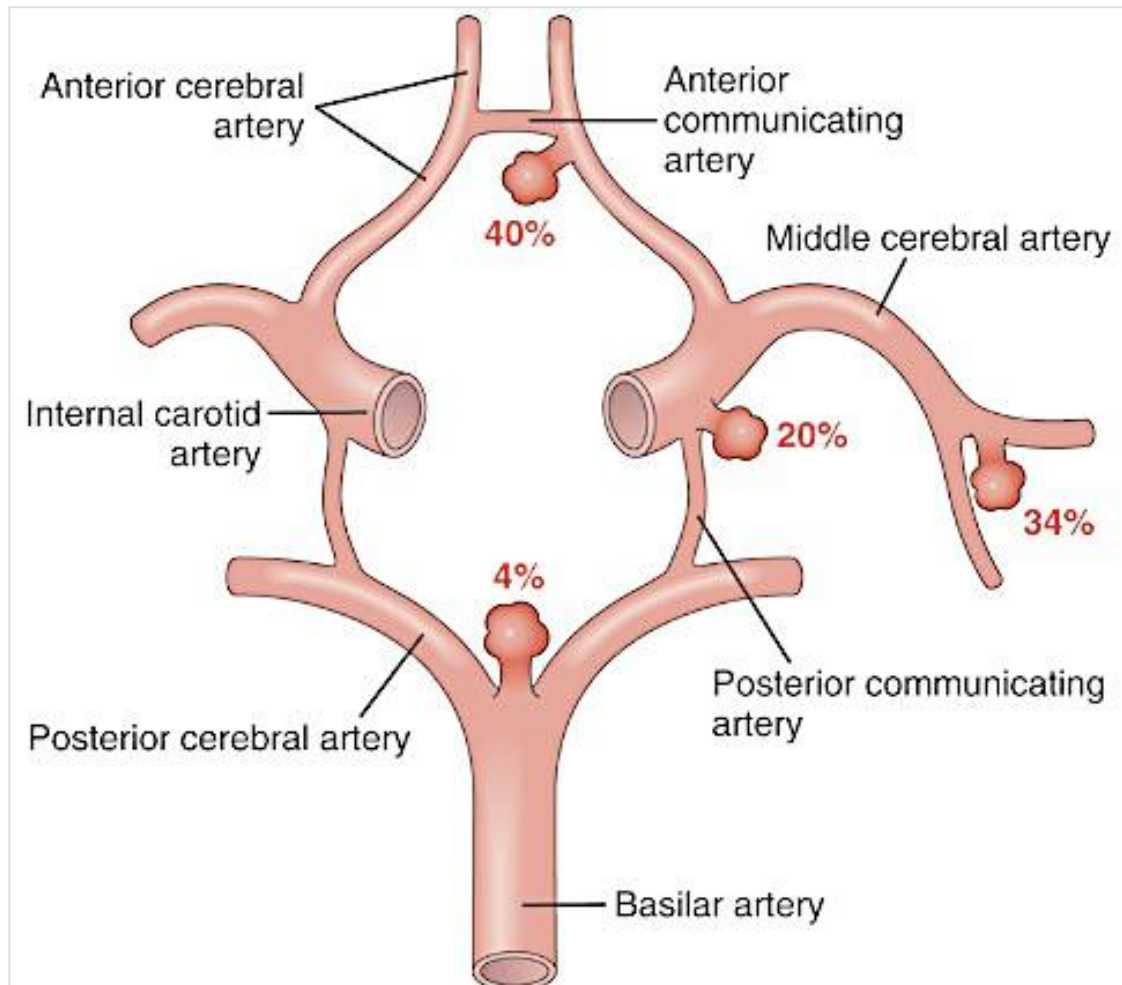


Figure 2.1: The common anatomical locations for IAs in cerebral vasculature. (Source: <http://www.usmle-forums.com>)

2.3.4: Histopathological Considerations

An understanding of the histological structure of a cerebral arterial wall is essential before the exact aetiopathogenesis of intracranial aneurysms can be discussed. A typical cerebral artery contains three layers: an outer adventitia, a prominent muscular media and, the inner most intima lined by a layer of endothelial cells. The intima is separated from media by means of an internal elastic lamina. However, contrary to the systemic arteries the external elastic lamina is absent in cerebral arteries. Intimal fat pads are localised thickening of intima seen around bifurcations mostly at lateral angles, face, dorsum and apex.

‘Medial defects of Forbus’, encountered occasionally, are the places where the muscularis media is deficient leaving the remaining two layers with elastic lamina. The important histopathological differences between the walls of an artery and an aneurysm are summarized in Table-2.3. The wall of an aneurysm is usually deficient in media, which ceases abruptly at the

Table 2.2: Classifications for Intracranial Arterial Aneurysms

Morphology	Size	Location	Aetiology
Saccular	<3mm	Anterior Circulation	Idiopathic
Fusiform		Internal Carotid	
Dissecting	3-6mm		Inflammatory
	7-10mm	a.Carotid canal b. Intracavernous c.Paraclinoid (Ophthalmic)	a.Main Trunk b.PICA Posterior Inferior Cerebeller Region Neoplastic
	1-25mm	d.Posterior Communicating Region e.Carotid Bifurcation	Basilar Traumatic
	>25mm	Anterior Cerebral a.A1 (Main Branch) b.Anterior Communicating Region c.A2 (Distal Region)	a.Bifurcation b.Superior Cerebeller Region c.AICA (Anterior Inferior Cerebeller Region) d.Basilar Trunk e.Vertebrobasilar Junction Region
		Middle Cerebral	Posterior Cerebral
		a.M1 (Main Branch) b.Bifurcation c.Peripheral	a.P1 (Proximal PCA) b.P2 (Distal PCA)

Source: Wilkins RH, Rengachary SS. Neurosurgery. pp. 2198, 2nd ed, 1996, McGraw Hill, USA.

neck. The aetiopathogenesis of an intracranial aneurysm can be divided in to three phases: initiation, growth and evolution and rupture.

2.3.5: The Initiation-Growth-Rupture Continuum

The natural history of an intracranial aneurysm can be divided into three phases: initiation, growth and rupture. It is quite intuitive to speculate that the factors, which are responsible for the formation of an intracranial aneurysm, will promote its growth as well, eventually leading to its rupture. Current evidence suggests, that some continue to work on all three phases, there are other factors superimposed on these background forces that act exclusively on each phase. The different aetiological factors playing roles in the pathogenesis of an intracranial aneurysm are shown in Table-2.3. The important theories for each phase are discussed in detail in the following sections. Whereas trauma, infection, tumours, radiation and other factors can play a role in 1-2% intracranial aneurysms, most develop spontaneously.

Table 2.3: Aetiologies of Intracranial Arterial Aneurysms

Saccular Aneurysms			
A. Hemodynamic	B. Structural	C. Genetic	D. Traumatic
a) Uneven pulsatile pressure head distribution e.g. at bifurcations/ branching/ convex surface of curves, leading to change in different hemodynamic factors b) Increased Blood Flow i. AVM ii. Aplasia/Hypoplasia/Agensis/ Contralateral vessel ligation iii. Persistent Foetal Circulation- a) Carotid Basilar- Trigeminal/Otic/ Hypoglossal/ Proatlantal b) Basilar Middle Meningeal iv. Increased Blood Pressure (+/-Vessel Wall Defects) *Essential Hypertension *Coarctation of aorta *APKD *Fibromuscular Dysplasias *Renal Artery Stenosis	a) Combined Media/ Elastica defects b) Preaneurysmal lesions – Infundibula – Thin Areas – Microaneurysms	a) Familial intracranial aneurysms b) Syndromes Associated with Aneurysms *Ehlers-Danlos syndrome *Marfans’s syndrome *Pseudoxanthoma elasticum *Rendu-Osler-Weber syndrome *Klippel-Trenaunay-Weber syndrome *Type III collagen deficiency	a) Skull fracture b) Penetrating Injuries c) Iatrogenic- in Surgery
E. Infectious	F. Neoplastic	G. Disorders affecting blood Vessels	G. Radiation
i. Bacterial ii. Fungal	i. Metastatic *Choriocarcinoma *Atrial Myxoma *Undifferentiated Ca ii. Primary iii. Aneurysms associated with tumours – Pituitary adenomas	i. Giant Cell Angiitis ii. SLE iv. Moyamoya disease v. Sickle cell anaemia	Radian induced saccular aneurysms
Fusiform Aneurysms			
A. Atherosclerosis	B. Structural	C. Genetic	D. Infectious
Most common cause of Fusiform Aneurysm	i. Loss of normal Elastica/ Media ii. Fibromuscular Dysplasias	*Marfans’s syndrome *Pseudoxanthoma elasticum	Syphilis
E. Other disorders of Vs	F. Hemodynamic	G. Radiation	
Giant cell arteritis	Coarctation of aorta	Radian induced saccular aneurysms	

Source: Wilkins RH, Rengachary SS. Neurosurgery. pp. 2198, 2nd ed, 1996, McGraw Hill, USA.

2.3.5.1: The Initiation

Different workers over a period of time have tried to explain the formation of intracranial aneurysms based on various factors. These factors can broadly be divided into congenital and acquired, as detailed in Table-2.4. The important theories, their positive points and limitations are discussed below.

Table 2.4: The factors involved in the initiation

Congenital Factors	Acquired Factors
Medial defects	Elastic degeneration
Elastica defects	Stehbens defects
Origin of small vessels	Inflammation
Failure of branch involution	Atherosclerosis
	Hypertension
	Haemodynamic stresses

Medial defect theory: The theory is also known as congenital theory. Eppinger [Eppinger 1887] in 1887 was the first person to draw attention that the congenital defects in the elastic properties of an arterial wall can lead to aneurysm formation. Forbus [Forbus 1930] published his observations in 1930 describing the medial defects in detail. In his study involving 33 subjects (14 children, 19 adults), he found that the medial defects were present in two third of each group. He stated that the aneurysms are the acquired lesions arising at the sites these congenital medial defects due to continuous overstretching of the elastic membrane caused by the haemodynamic stresses and facilitated by the degenerative process of the elastic lamina itself.

Elastic Lamellar Theory: In a case control study Glynn [Glynn 1940] compared the arterial walls from the healthy persons and the patients diagnosed with aneurysms and noted that the medial defects were present in about 80% of the arteries in both groups. As the medial defects were far more common than the incidence of aneurysms, he raised strong suspicion about the validity of medial defect theory. In order to assess the strength of the different arterial layers he created artificial defects in the arterial walls and noted that defects were able to withstand an intraluminal pressure of up to 600 mmHg exerted by an external pump without bulging. He consequently proposed degeneration of internal elastic lamina rather than the medial defects as a cause of aneurysms.

Degenerative Theory: In an autopsy study, Stehbens [Stehbens 1959] found that apical and lateral angle defects were more common after the age of 6 years, suggesting a possible acquired nature, at least for some of them. He also observed that these medial defects were more common at the lateral angles of a bifurcation, whereas the most common location for an intracranial aneurysm is carina. Moreover, these defects are present in all extra and intracranial arteries of humans and animals in equal proportions but the aneurysms occur preferably in intracranial arteries of humans and remain rare in extracranial arteries and animals. He turned

down Forbus theory on the basis of these observations. In an extensive histopathological study conducted on 454 cerebral arteries [Stehbens 1963] he described three types of ‘preaneurysmal’ lesions: *funnel shaped dilatations*, *areas of thinning* and *microscopic evaginations*. These funnel shaped dilatations described by him correspond to the infundibula seen in angiography mostly found at the origin of posterior communicating artery. Unlike Forbus’ medial defects, the media was not ending abruptly in these lesions and the adventitia was not thickened. Later, by various angiographic studies it has been demonstrated that these infundibula can lead to the formation of aneurysm over time [Stuntz 1970, Waga 1979]. The areas of thinning were present at the apex of arterial bifurcations. These areas had relatively thin walls, with attenuated adventitia and, absent media and internal elastic lamina. He considered these areas as pre-aneurysmal lesions because of their occurrence in the areas where the aneurysms are most commonly formed. He also noticed that these lesions bulging when subjected to a pressure of 30-mmHg pressures contrary to the medial defects. Small evaginations, the third pre-aneurysmal lesions described by him were the herniation of intima through medial defects, visible microscopically.

Congenital vestigial vessels theory: Some authors like Bremer proposed that when primitive capillary plexus fail to obliterate the aneurysms can be formed. However, as no vessels are seen originating from the apex of an aneurysm, this theory was not well accepted. Drennan thought that origin of small vestigial vessels from the apex of arterial bifurcations could provide a weak spot for the aneurysms to form. No such vestigial vessels originating from the arterial forks were found in the studies done by various pathologists [Carmichael 1950].

Anomalies and variations in the circle of Willis: Variations and anomalies of the circle of Willis have been long associated with increased risk of aneurysm formation. Among all variations, a definitive correlation between the increased aneurysm incidence and an anomaly has only been found in cases of anterior communicating-anterior cerebral artery complex variations [Stehbens 1963, Stehbens 1963b]. In spite of claims of having a congenital basis, the possible underlying factors in the genesis of an aneurysm in these cases may be the haemodynamic stresses originating from an imbalance in the circulation secondary to the anomalous vasculature [Kayembe 1984].

Inflammatory theory: The theory was postulated by Handler and Blumenthal who reported nine patients developing aneurysms after post-arteritis destruction of internal elastic lamina [Handler 1954]. The

hypothesis however, could not get a widespread reorganization due to lack of confirmation of similar findings by other authors.

Atherosclerotic theory: Atheromatous degeneration of the arterial wall in the genesis of an intracranial aneurysm was proposed by Kerpola and was supported by Walker and Allegre [Walker and Allegre 1954]. In spite of these reports, a definitive cause and effect relationship could not be established.

Hypertensive theory: Hypertension has long been speculated as an underlying cause of cerebral aneurysms, working on the background of congenital medial defects. The Co-operative study of Intracranial Aneurysms showed that the incidence of hypertension was higher in the group with larger aneurysmal size. This however may reflect the high incidence of hypertension in elderly population where aneurysms are more common as well. Quite the contrary, the study demonstrated a negative correlation between the age at which ruptured aneurysms reached a critical size and hypertension, although the duration of hypertension in this group of patients was not known [Walker and Allegre 1954]. Similar findings were reproduced by McCormick and Schmlasteig [McCormick and Schmlasteig 1977] when they found no difference in the incidence of hypertension in a group of patients harbouring cerebral aneurysms at autopsy.

In their study on 212 age-matched patients, Andrews and colleagues [Andrews and Spiegel 1979] found that the incidence of hypertension was significantly higher in the population with aneurysms. Both men and women with hypertension were twice as likely to develop aneurysm as compared to their non-hypertensive counterparts. They concluded that increasing age; high systolic and, diastolic pressure had good correlation with increased incidence of cerebral aneurysms in women, but not in men. Kwak and co-workers reported similar findings from Japan [Kwak et al 1979]. The increased incidence of intracranial aneurysms in animal models with experimentally induced hypertension also testifies to the role of hypertension in the genesis of cerebral aneurysms. Therefore, on the basis of the available clinical and experimental data it can be concluded that the hypertension plays a crucial role in the initiation of the cerebral aneurysms. However, its role in growth and rupture remained controversial.

2.3.5.1.1 Association of intracranial aneurysms with other diseases:

Arteriovenous malformations (AVMs): The co-existence of intracranial arteriovenous malformations and related saccular aneurysms was initially described in 1925, and later further documented in 1930 and 1931. The incidence of a coexisting aneurysm in patients harbouring an AVM ranges from 2.7% to 16% (in the majority of studies diagnosed by means of cerebral angiography). Aneurysms associated with an AVM have also been reported in 5-7% of intracranial haemorrhage [Kim et al 2004]. Following the recent significant advancements in neuroradiology it has now been recognised the two lesions may co-exist more often than estimated before. Such association is mostly thought to be secondary to haemodynamic imbalance and is discussed in detail in haemodynamic section.

Association with other diseases and genetic aspects: Genetic factors have also been implicated in the pathogenesis of intracranial aneurysms. Several epidemiological studies have demonstrated increased occurrence of these lesions in the first-degree relatives of the patients with cerebral aneurysms [Ronkainen et al 1998, Schievink et. al. 1995]. As it is evident from Table-2.3, the higher prevalence of cerebral aneurysms have been noted in various hereditary conditions like adult polycystic kidney disease (APKD), Ehlers-Danlos syndrome, Marfans's syndrome, Pseudoxanthoma elasticum, Rendu-Osler-Weber syndrome, Klipple-Trenaunay-Weber syndrome, and Type III collagen deficiency. A number of studies have been done in order to establish the genetic link by analysing the encoding for protein synthesis in the genes [Kuivaniemi et al 1993, Peters et al 1999]. Apart from the associations with some genetic mutations, a clear evidence for the genetic basis for the aetiopathogenesis an intracranial aneurysm is missing. Associations of cerebral aneurysms have also been suggested with pituitary tumours [Jakubowski and Kendall 1978] and moyamoya [Adams et al 1979] disease. Stebehns [Stehbens 1962] conducted an autopsy study to compare the incidence of congenital anomalies in the patients having intracranial aneurysms with the normal population. He found no difference in the occurrence of these anomalies in both the groups. However, the sample size taken was not statistically significant. After reviewing the relevant literature he later concluded that only coarctation of aorta and adult polycystic kidney disease (APKD) had a significant association with cerebral aneurysms. The increased incidence of hypertension in these two conditions can be a contributory factor.

2.3.5.2: The Growth

Most of the aneurysms don't grow in size is a general observation of Neurosurgeons and Neuroradiologists. However, sometimes it is difficult to imagine that an aneurysm will remain static in size forever. Recent evidence indicates that these are dynamic lesions with de-novo formation in the later life and growth in size of those already formed. In their recent publication (Aug 2008) in Journal of Neurosurgery Koffijberg and co-

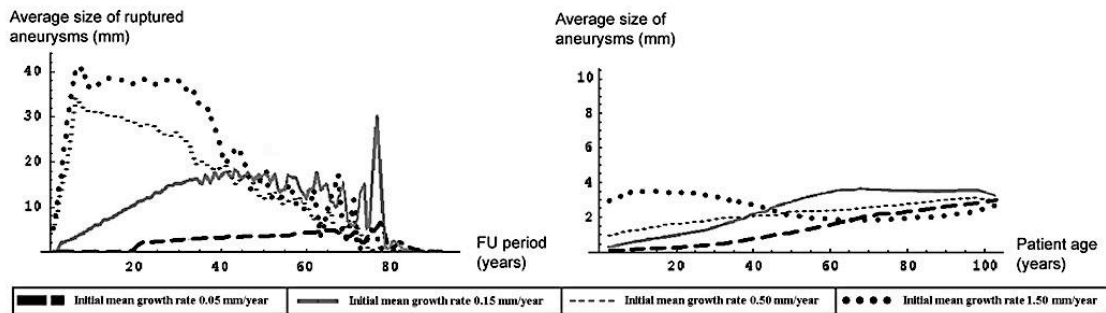


Figure 2.2: Graphs showing the average size of aneurysms at the time of rupture during follow-up (left) and the average aneurysm size as function of patient age (right). For high mean growth rates almost all aneurysms rupture in the first 40 years of follow-up but small rupture rates indicate towards the nonlinear pattern of the growth. Source: Koffijberg et al J Neurosurg 2008

authors [Koffijberg et al 2008] conclude that the intracranial aneurysms don't follow a linear pattern of growth (Figure-2.2). They grow in spurts with periods of no growth in between and don't follow a strict growth pattern. Most of the aneurysms they grow initially to attain a particular size, stabilize there and then some rupture suddenly without changing their size. In a follow-up study Wermer et al [2005] over a period of 10 years 13 out of 53 (24.5%; 95% CI-0.31-0.71%) aneurysms enlarged in size. Eleven aneurysms increased in size by 1-3 mm, one enlarged 3-5mm while one grew >5mm. The mean enlargement rate calculated by them was between 0.12 and 1.3 per year. The main risk factors for aneurysmal analysis were current smoking (HR 3.5, 95% CI-1.4-8.7), history of hypertension (HR 1.9, 95% CI 0.9-4.4) and multiple aneurysms. Other risk factors were positive family history and female sex. Smoking and female sex have also previously been shown as risk factors for aneurysmal growth by Juvela et al [Juvela et al 2001]. The growth of an intracranial aneurysm is mostly explained on the basis of pathological alterations in the mechanobiological properties of aneurysmal wall (e.g. stretching of collagen fibres and re-deposition of more collagen leading to fibrosis and thickening of aneurysmal wall), haemodynamic factors (WSS, OSI, Jet of blood stream, etc.) and as a passive yield to blood pressure. Tateshima et al in 2007 [Tateshima et al 2007] showed differences in the enlargement in their study as assessed by univariate Cox regression haemodynamic patterns of Intracranial Aneurysms that grew over a period of time (Figure-2.3). In an effort to analyse the mechanisms responsible for the

growth of an aneurysm Crompton [Crompton 1966] suggested that the cellular and fibrin proliferation of the wall of an unruptured aneurysm might result in it's weakening. The weak point subsequently may give way leading to aneurysmal rupture or it may organise perhaps forming a 'bleb'

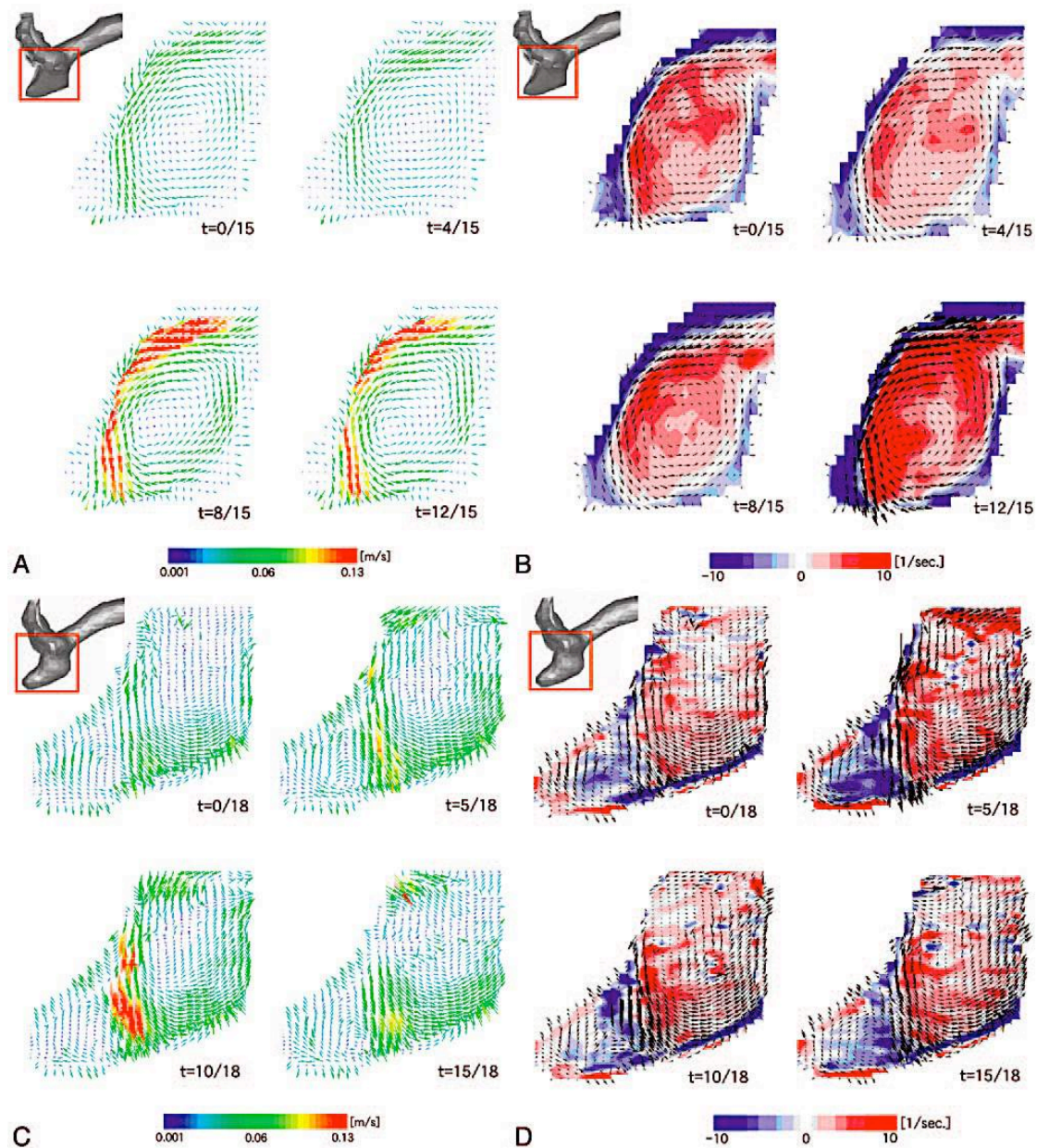


Figure 2.3: Showing the intra-aneurysmal flow pattern inside an aneurysm before and after the growth. (Source: Tateshima et al)

(a small nipple shaped outpouching of the wall) with resultant growth in the size. Due to repeated organization and fibrosis the wall of a larger aneurysm may actually get thicker, however more friable with less tensile strength.

2.3.5.3: The Rupture

Rupture of an intracranial aneurysm unfortunately remains the least well-understood phenomenon. Rupture occurs typically when the stresses in the aneurysm wall exceed its strength. Different authors have suggested various risk factors for rupture. Hypertension has been found to be associated with rupture in up to 60% of the cases, as shown in both clinical [Inagawa 2005] as well as the necropsy series [Crompton 1964].

Table 2.5: Activities or Events preceding Aneurysmal SAH

Activity/Event	Patients	
	No.	Percent %
Chatting/Watching television/ Staying home	71	13.8
Defecation/micturition	65	12.7
Working at workplace	63	12.3
Taking a bath/Shower	44	8.6
Sleeping/resting	41	8.0
Housework/Housekeeping	39	7.6
Shopping/outing	31	6.0
Brushing teeth/ washing face	25	4.9
Eating/drinking	24	4.7
Sport/exercise	14	2.7
Driving/riding a bike	12	2.3
Others	27	5.3
Unknown	57	11.1
Total	513	100.0

Source: Matsuda et al 2007

Most of the clinical series testify to this fact [Broderick et al 2003, Knekt et al 1991, Leppala et al 1999, Mhurchu et al 2001] whilst some contradict it [Juvela et al 1993, Longstreth et al 1992]. In his case control study on 247 patients and equal number of healthy volunteers, Inagawa [Inagawa 2005] found hypertension, cigarette smoking and hypercholesterolemia significantly more common in the patients with SAH.

Diurnal and seasonal variations in the incidence of SAH have been reported in previous studies [Inagawa et al 2002, Inagawa 2000]. SAH exhibits two peaks during the day; between 6 am to 10 am and, between 4pm to 8pm. Again, high incidence of SAH in winters has been noted as compared to summers [Inagawa et al 2002, Inagawa 2000]. The instantaneous peaks in the blood pressure have been suggested as possible factor responsible for these variations and likely to play an important role in affecting the rupture [Inagawa et al 2002, Inagawa 2000]. The relationship between cigarette smoking and increased SAH has widely been studied [Broderick et al 2003, Mhurchu et al 2001, Juvela et al 1993,

Longstreth et al 1992]. It has been suggested that smoking can increase the risk of rupture by accelerating the rate of formation of de-novo aneurysms as well as growth. Alpha -1 antitrypsin deficiency [Gaetani et al 1996] and degradation of internal elastic lamina in vessel walls [Qureshi et al 1998] have been asserted as a basic mechanism affected by smoking. Cigarette smoking causes acute rise in systolic blood pressure [Cellina et al 1975], these instantaneous spikes, in turn can be trigger the rupture [Longstreth et al 1992]. Increasing size and the presence of multi-loculations has also been implicated in the aneurysmal rupture. In Crompton's [Crompton 1966] series the majority of the ruptured aneurysms were more than 5mm in their maximum diameter. A size of 2 - 5mm was the critical size suggested by Crompton at which an aneurysm becomes suddenly unstable. Many studies including the recent ISUIA studies [Wiebers 2003, ISUIA 1998] have reiterated the importance of the larger size making aneurysm more prone for rupture. The critical size however, suggested by more recent studies is 7mm. It is seldom possible in vivo to determine the exact site of rupture. However, in 271 of 289 cases where the site of rupture could be localised by Crompton [Crompton 1966], the ruptured had occurred from the apex in 227 cases. 57% of the ruptured aneurysms in the same series had multiple loculations or blebs or daughter nuclei as against 16% of the unruptured aneurysms. Various activities have been proposed as risk factors for the aneurysmal rupture. Like Inagawa and colleagues [Inagawa et al 2002, Inagawa 2000], Matsude et al [Matsude et al 2007] also found a bimodal peak pattern for the aneurysmal SAH during a day. Peaks occurred during early morning (6-9 am) and late evening (6-9 pm), the period corresponding to the daily routine activities such as defecation, micturition, brushing teeth, washing face, dressing, drinking, and taking bath. 8% of all SAHs, however occurred during sleep or rest. Whereas they explained the morning peaks in the SAH on the basis of circadian spike of the blood pressure, no explanation could be found for the evening peaks. Some of the daily routine activities, like defecation and micturition, associated with a significant risk of bleed, have a predominant physiologic response essentially similar to Valsalva manoeuvre [Matsuda et al 2007]. The sudden changes in the arterial pressure during these activities can precipitate the aneurysmal rupture [Matsuda et al 2007]. Apart from the intramural factors, the peri-aneurysmal environment has also been proposed to influence the risk of rupture. In a retrospective analysis, Ruiz et al found that the existence of contact constraints between an intracranial saccular aneurysm and the surrounding structures had a significant influence on its shape and risk of rupture [San Millan Ruiz et al 2006]. The main activities at the time of rupture are given in the Table-2.5.

2.4: Importance of Haemodynamic Factors

Haemodynamic factors are believed to play an important role in the initiation, growth and, rupture of an intracranial aneurysm. The initiation is usually attributed to the impingement of the axial blood stream on the carina of the arterial bifurcation and the arterial bends, explaining the common occurrence of aneurysms on these locations. Different type of haemodynamic forces working on the arterial wall or inside the aneurysm can influence the aetiopathogenesis of a cerebral aneurysm. The forces can broadly be divided into hydrostatic forces and dynamic forces. Whereas the hydrostatic forces work constantly in the background e.g. blood pressure; the dynamic forces exert their effect by momentary variations with time like impinging jet of blood. The different haemodynamic factors, their role in the aneurysmal aetiopathogenesis and the possible scientific explanations are provided below.

Wall shear stress or shear stress is a tangential frictional force exerted by the flowing blood on the endothelial cells. WSS is typically expressed as a product of shear rate and viscosity

$$\tau = \frac{\mu \times \partial u}{\partial x}$$

Where τ = WSS, μ = viscosity, du/dx = shear rate

Human blood, which is considered non-Newtonian fluid under normal circumstances, can behave as a Newtonian fluid at high shear stresses [Oka 1981]. u is constant in above equation for Newtonian fluid whereas is variable and, in fact is a function of shear rate in non-Newtonian fluids.

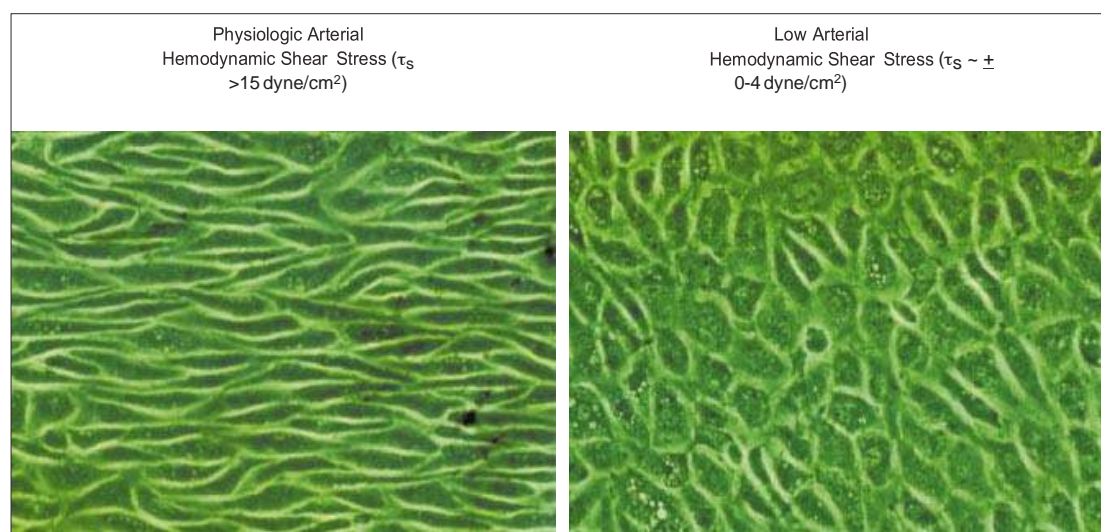


Figure 2.4: Showing the endothelial cells losing their normal alignment when exposed to abnormally low WSS. (Source: Malek et al JAMA)

The normal physiological range of WSS is crucial for endothelial cells to maintain their normal function and integrity. One of the important properties of WSS is to influence the behaviour of endothelial cells. In their study on the haemodynamics of the intracranial aneurysms Malek et al [Malek et. al. 1999] demonstrated a good correlation between the low WSS and aneurysmal growth. They found that the endothelial cells subjected to low WSS in a bovine artery lost their normal alignment (Figure-2.4). It was seen that whereas the normal endothelial cells produced high growth inhibitors and low growth promoters, the ratio was reversed in endothelial cells subjected to low WSS (Table-2.6).

Table. Endothelial Response to Hemodynamic Shear Stress*

	Hemodynamic Shear Stress	
	Physiologic Arterial Magnitude ($\tau_s > 15$ dyne/cm ²)	Low Arterial Magnitude ($\tau_s \sim \pm 0-4$ dyne/cm ²)
Endothelial cell morphology	Fusiform aligned	Polygonal unaligned
Endothelial cell function		
Vasoactive agents		
Vasoconstrictors		
ET-1 ¹⁰² /ECE ⁸⁶	Low	High
ACE ⁸⁰	Low	High
Vasodilators		
NO/NO syntase ^{67-69,81-83}	High	Low
PGI ₂ /PGI ₂ synthase ⁶⁶⁻⁸⁴	High	Low
CNP ⁸⁵	High	Low
Adrenomedullin ⁸⁷	High	Low
Antioxidant enzymes		
COX-1, 2 ⁸⁵	High	Low
Mn SOD ⁸⁵	High	Low
Cu/Zn SOD ⁸⁹	High	Low
Growth regulators		
Growth factor		
PDGF-B ^{78,97}	Low	High
PDGF-A ⁸⁹	Low	High
Growth inhibitor		
TGF- β ⁸⁸	High	Low
Inflammatory mediators		
MCP-1 ¹⁰¹	Low	High
Adhesion molecules		
VCAM-1 ^{100,101,103}	Low	High
Thrombosis/fibrinolysis		
tPA ^{89,90}	High	Low
TM ⁸⁹	Low	High
Endothelial proliferation ⁷⁸	Low	High
Endothelial apoptosis ⁷⁹	Low	High

*ET-1 indicates endothelin 1; ECE, endothelin-converting enzyme; ACE, angiotensin-converting enzyme; NO, nitric oxide; PGI₂, prostacyclin; CNP, C-type natriuretic peptide; COX, cyclooxygenase; Mn SOD, manganese-containing superoxide dismutase; Cu/Zn SOD, copper/zinc-containing superoxide dismutase; PDGF-A, B, platelet-derived growth factor A-chain, B-chain; TGF- β , transforming growth factor beta; MCP-1, monocyte chemotactic peptide 1; VCAM-1, vascular cell adhesion molecule 1; tPA, tissue-type plasminogen activator; and TM, thrombomodulin.

Table 2.6: The ratio of normal growth mediators is reversed in endothelial cells exposed to abnormally low WSS in right column. *Source: Malek et al JAMA, 1999*

WSS is directly proportional to the velocity and viscosity of blood flow inside the vessel or sac and will be highest in an end-on aneurysm while will be lowest in a side-on aneurysm, with bend-on aneurysm lying in between. Tateshima et al [Tateshima et al 2003] noted high WSS at the neck of the parent aneurysm and at the margin of the daughter bleb. The pre and post growth peak WSS were 5.61 n/m^2 and 7.38 n/m^2 respectively they attributed this high WSS to the flow separation and flow impingement at the margin of the bleb. Luscher et al 1993 [Luscher et al 1993], found that the release of the endothelial derived growth and relaxation factors are WSS dependant, which in turn regulate the vascular remodelling endothelial cells and have a capacity to remodel the blood vessel in response to change in WSS. Increased WSS stimulates the endothelial cells to produce the matrixmetalloproteases, which are responsible for the degradation of the internal elastic lamina [Sho et al 2002]. Tromp et al in 2004 [Tromp et al 2004], showed elevated expression of metalloproteases-13 in abdominal aortic aneurysm and thought them to be responsible for destructive remodelling present in extracellular matrix of AAA. Focal high WSS is the predisposing factor in formation of aneurysm in healthy cerebral artery. Drexler in 1999 [Drexler and Hornig 1999] demonstrated that low WSS leads to endothelial dysfunction in coronary arteries. Pohl et al 1991 [Pohl et al 1991] proved that increased flow leading to increased WSS accelerates the release of endothelial derived relaxation factors (EDRF) from endothelium resulting in dilatation of an artery and demonstrated marked flow dependant dilatations in small arterioles in vivo and in vitro. The same authors also showed increased dilatation responses with an increasing viscosity indicating that the shear stress is the stimulus for the flow dependant dilatation. These flow-induced dilatations were abolished by inhibition of EDRF. Flow shear stress increases the production of N_2O leading to increased EDRF release. It has been suggested by experimental studies that the shear stress may be directly or indirectly linked to the activation of Ca^{++} dependant endothelial N_2O synthase [Busse et al 1990]. Elevated shear stress augments the release of ATP and substance-p from endothelium [Milner et al 1990], which in a paracrine manner may enhance EDRF production more directly [Pohl et al 1991]. Increased shear stress leads to the hyperpolarisation of the endothelial cells by mobilising the Ca^{++} from intracellular stores in the cultured endothelial cells [Ando et al 1988] probably via activation of phospholipase C [Bhagyalakshmi and Frangos 1989] and activation of K^+ channels [Olesen et al 1988]. How shear stress transduces the signals to endothelial cells to release EDRF production is not clear. It has been hypothesised that stress acts on the structures anchored in the endothelial membrane and mechanically enhances their interaction between regulatory proteins and their targets.

Neuraminidase inhibits the flow dependant dilatation by clearing the sialic acids, which are present in high concentration at the endothelial surface [Born and Palinski 1988] as an integral component of glycoproteins and lipoproteins, may act as mechanoreceptors. Fukuda et al [Fukuda et al 2000] examined the role of N_2O in the degenerative changes associated with and, preceding to the formation of a cerebral aneurysm in experimental models they found high localisation iNOS (Inducible N_2O synthase) at the site of aneurysm formation in both rat and human arteries, as demonstrated by increased immunoreactivity. In contrast to its counterpart eNOS, iNOS is not commonly present in arterial walls it is usually synthesised or used within the endothelial cells and the smooth muscle cells by a number of different stimuli including high WSS. They showed that an NOS inhibitor, amino guanidine attenuated the early degenerative changes associated with new aneurysm formation. They also showed that a blood-thinning agent Batroxobin (a defibrinogenic agent) also prevented early iNOS induction and thus early aneurysm formation by lowering the WSS. This phenomenon was explained by virtue of primarily decreasing the blood viscosity. Blood viscosity is determined by the haematocrit, which in turn is dependent upon its fibrinogen concentration [Oka 1981]. Bx can reduce the blood viscosity by lowering its fibrinogen concentration [Ohba and Aoyama 1985], which in turn decreases the wall shear stress. Bx doesn't have any effect on cerebral blood flow and MABP. They concluded that N_2O especially one derived from iNOS is a prerequisite for a development for a new aneurysm in cerebral blood vessel. In their earlier studies they experimentally induced cerebral aneurysms in rat and monkeys. They found that the degenerative changes associated with aneurysm formation was almost exclusively localised at arterial bifurcation especially the intimal fat pad and neighbouring distal portion known juxta apical groove (JAG).

The role of N_2O in the vessel wall damaged was proven by Beckman et al [Beckman et al 1990] and Geng et al [Geng et al 1992] in 2 independent studies. Mattson et al [Mattson et al 1998] linked iNOS with high blood pressure. Burleson [Burleson and Turitto 1996] and Steiger [Steiger et al 1988] were the other investigators who agreed with the association of site of high WSS and aneurysm formation. In their study on high WSS induced damage to endothelium and smooth muscle cells at JAG, Fukuda and colleagues [Fukuda et al 2000] classified the histopathological changes into 5 grades. Grade-1 changes are where no damage can be demonstrated, grade-2 is mild endothelial cell damage e.g. a wavy rippling of plasma membrane without smooth muscle cell damage, grade-3 corresponds to moderate endothelial cell damage and grade-4 is severe

endothelial cell damage. The changes are called grade-5 when damage involved smooth muscle cell in addition to severe endothelial cell damage.

Table 2.7: The literature-based evidence on the importance of haemodynamics in the aetiopathogenesis of IAs

Haemodynamic factors	Intracranial Aneurysm			Proposed mechanism(s)	References
	Initiation	Growth	Rupture		
Dynamic					
Wall Shear Stress (WSS)	High	Low	Low	Increased WSS increases the production of MMP-13 which in turn leads to vessel wall damage Decreased WSS increases iNOS synthesis- NO induced damage to vessel wall Low WSS increases endothelial proliferation and apoptosis	Boussel et al 2008, Fukuda et al 2000, Gao et al 2008, Jou et al 2008, Malek et al 1999, Meng et al 2007, Shojima et al 2004, Ujie et al 1999
Oscillatory Shear Index (OSI)	High/Low	High	High	Degenerative changes in endothelium	Glor et al 2004, Goubergrits et al 2008, Mantha et al 2006
Jet of Blood Stream	Impingement	Impingement	Impingement	Localized endothelial cell injury	Foutrakis et al 1999, Cebral et al 2005, Cebral et al 2009
Flow Pattern	-	-	Complex	Statistical association	Cebral et al 2005, Cebral et al 2009
Hydrostatic					
Pressure	High	High	High	Passive yield/ water hammer effect	Inci and Spetzler 2000, Morimoto et al 2002, Steiger et al 1989

NB: WSS; wall shear stress, MMP-13; matrixmetalloproteinases-13, iNOS; inducible-nitric oxide synthase, NO; nitric oxide, OSI; oscillatory shear index

In 1993 Resnick and co-workers [Resnick et al 1993a, Resnick et al 1993b] identified a shear stress responsive element for iNOS on endothelial genes inducing the t-pa (tissue plasminogen activator), intracellular adhesions molecule- 1 and TGF- beta. Cooke et al in 1990 [Cooke et al 1990] demonstrated the association between high NOS and atherosclerosis. Both magnitude of WSS and duration of exposure of endothelial cells to that high WSS, played an important role in the induction of iNOS in their experimental study. Wagner et al [Wagner et al 1997] found that no iNOS was induced when the smooth muscle cells were exposed to the lower shear stresses in the order of 1.1 to 2.5 dynes per cm² for a smaller period of time i.e. less than 24 hours. Table-2.7 below summarizes literature-based evidence on the role of haemodynamic factors in the aetiopathogenesis of Intracranial Aneurysms.

Analysis of the haemodynamic factors thus, may act as a crystal ball where we can see the future of an intracranial aneurysm and can take necessary interventions to modify it, as and when required.

2.5 Management of Intracranial Aneurysms: The History of a Paradigm Shift

2.5.1: Background and Objectives

With the advent of technology, management of intracranial aneurysms (IAs) have undergone a tremendous evolution. In order to appreciate the modern achievements, it is imperative to analyse the past.

Apart from the masterly inactivity the initial treatment for IA was confined to the ligation of ipsilateral carotid artery mostly resulting in high morbidity and mortality. In 1927 Egas Moniz introduced cerebral angiography following which Dandy clipped the first aneurysm in 1937. This led to the surge in neurological surgeries to clip all ruptured aneurysms. Owing to the disastrous consequences originating from indiscriminate surgeries and poor surgical and neuroanaesthetic techniques, the euphoria however didn't last long.

Inherent limitations associated with surgical management inspired physicians to search for new and safer alternatives. Whilst the roots of some of these endovascular techniques can be traced back to the early nineteenth century, it's only through the incredible progress in the technology over last couple of decades that made their safe and widespread clinical application possible. Since then, it has rapidly become a primary therapeutic option in most of centres worldwide.

Present article summarises these diagnostic and therapeutic developments, in chronological order with an eye on the potential scope for research and future progress.

2.5.2: Introduction

With the advancements in modern microsurgical and endovascular techniques coupled with improved neuroanaesthetic approaches, the morbidity and mortality figures associated with aneurysmal subarachnoid haemorrhage (SAH), have improved significantly. Whereas most of the recent advancements in the neurological therapy of IAs are achieved in past 200 years, the journey of success began over 4000 years ago. The following sections discuss the temporal evolution of different diagnostic and treatment modalities along with an analysis of the important milestones achieved and their long-term implications.

With all this recent technological progress, the protocols to treat the *ruptured* IAs became quite clear over time however, the management of *unruptured* IAs (UIAs) still remains controversial. These uncertainties are

mainly due to an incomplete understanding of natural history of IAs and risks associated with active management [ISUIA-1998] The difficulties are further enhanced by the fact that the poor surgical outcome is dictated by the same factors [Komotar et al 2008] that currently form the basis of surgical decision making [Khanna et al 1996].

2.5.3: The Early Developments

The earliest description of intracranial or subarachnoid haemorrhage (SAH) as a cause of death in human beings dates back to the ancient



Figure 2.5: Thomas Willis
(Source:<http://www.accu-chek.com>)

Biblical times. The first anecdotal evidence of an IA as well as the earliest attempt to treat it comes from Egypt. It is recorded in Ebers Papyrus, one of the oldest preserved medical documents that in 2725 BC Imhotep, who was an Egyptian architect cum physician, tried to treat an aneurysm by using a fire glazed instrument [Lippi 1990]. The term aneurysm, derived from Greek word *aneúrysma* (*ana*; throughout + *eurus*; wide), meaning ‘to dilate’, was introduced by Claudius Aelius Galen, a philosopher of Greek origin in 200 AD.

In 1664, Thomas Willis [Willis 1664], (Figure-2.5) an Oxford-based physician provided the first scientific account of the cerebral vasculature later being honoured by the eponym ‘circle of Willis’. Almost a century later in 1761 [Morgagni 1761] an Italian anatomist from the city of Padua, published the first anatomical write-up describing the entity of an intracranial aneurysm. It however, took another four decades to recognize the definitive clinical importance of IAs until Blane in 1800 published the clinical and autopsy findings of a patient with bilateral carotid cavernous aneurysms, described by John Hunter in 1792. The credit of first clinical diagnosis of an intracranial aneurysm goes to Hutchinson [Hutchinson 1875] in 1861. Based on the neurological signs he successfully diagnosed an intracranial aneurysm in a patient 11 years before his death. However, in spite of the handful of clinical diagnoses, the exact preoperative localization of an IA remained a challenge to clinicians until late.

2.5.4: The Surgical Era

Understanding the deadly nature of these lesions, the earliest efforts of modern times to treat them by surgery were started in the form of carotid ligation. The concept presumably stems from an important observation made by Jean-Louis Petit in 1760s that there were no significant adverse effects on the human brain even after the complete occlusion of one carotid artery by thrombosis. The carotid



Figure 2.6: John Hunter
(Source: <http://citizenscientistsleague.com>)

ligation was initially popularised by John Hunter (Figure-2.6) in 1800s, and was known as ‘Hunterian ligation’ after him [Hutchinson 1875]. The first ever attempt to treat an aneurysm by ‘Hunterian ligation’ was endeavoured by Cooper in 1808 [Cooper 1852]. Carotid ligation remained popular and appeared a reasonably successful treatment except for the fact that in most of the cases it carried a significant risk of cerebral infarction and hemiplegia. Given the high mortality and morbidity produced by the acute occlusion of the carotids, the concept of gradual occlusion was introduced [Crutchfield 1959]. Numerous metallic clamps were designed



Figure 2.7: Sir Victor Horsley
(Source: Medscape)

that could be tightened over a period of several days. The clamp could be reopened should the patient become symptomatic. Because of unacceptably high complication rates, the ICA ligation was gradually replaced by common carotid artery ligation.

Due to the lack of preoperative localization, most of the initial ‘direct surgical encounters’ of IAs were unplanned and were limited to their accidental surgical exposures. Sir Victor Horsley (Figure-2.7) [Drake 1985] was one of the first surgeons to witness an IA during a craniotomy in 1885, when he was operating on a patient with a preoperative diagnosis of a middle fossa tumour, which turned out to be an IA. He treated the patient by ipsilateral carotid ligation.

Two other important discoveries that altogether changed the ways of diagnosis and management of IAs can be considered as contributing to the dawn of modern neurovascular surgery. Quincke introduced the technique of lumbar puncture in 1891 [Quincke 1891] while Egas Moniz discovered the cerebral angiography in 1927 [Moniz 1927]. The first direct planned surgical intervention to treat an intracranial aneurysm however, was endeavoured by Norman Dott on April 22 1931, when he stopped bleeding from an intraoperatively



Figure 2.8: Walter Dandy
(Source: Medscape)

ruptured carotid aneurysm by wrapping a muscle around it [Dott 1933]. The preoperative diagnosis of a carotid bifurcation IA was localised clinically and the procedure was tolerated well.

The efforts were further matured by Walter Dandy (Figure-2.8) who gets the credit for the first successful *clipping* of a preoperatively diagnosed IA

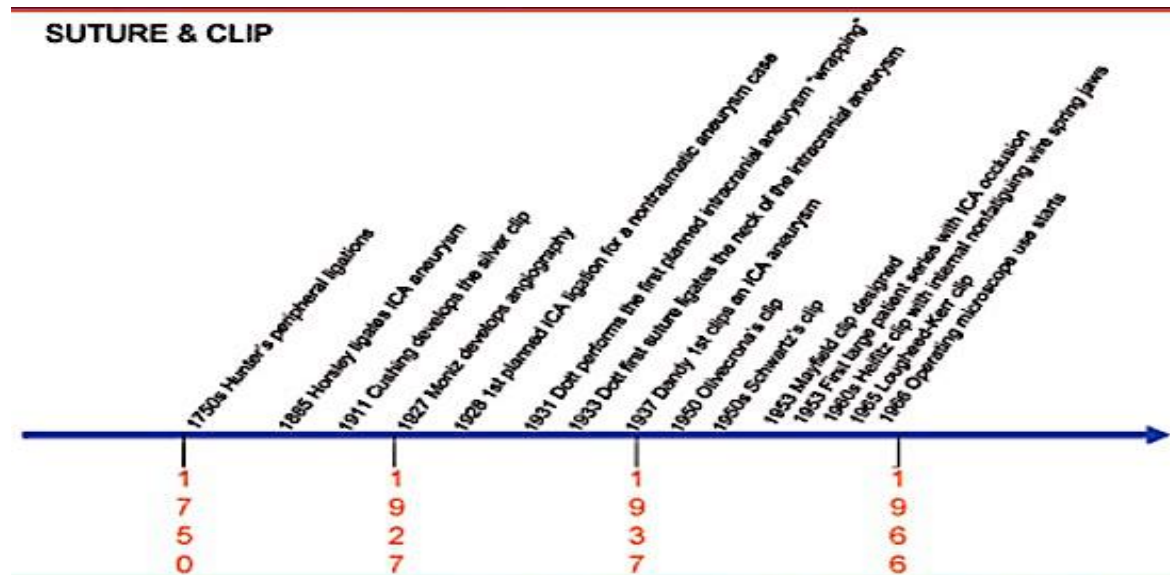


Figure 2.9: Temporal Evolution of different surgical modalities Source: Neurosurg Focus, 2006, © AANS

[Dandy 1938]. In March 1937 he treated a man of 43 by applying an ordinary flat silver clip to a pea sized IA of distal ICA. The operation was performed around six-years after Egas Moniz demonstrated the first IA by cerebral angiography in 1931. The diagnosis however, was localised solely on the basis of clinical signs. Dandy himself admits that such a precise clinical localization of an IA warranting a surgical attack is but a rare phenomenon [Dandy 1938]. Clipping became established as a new procedure to secure the ruptured IA, soon after Dandy published his monograph in 1938.

Justification of Surgery: In absence of clear scientific evidence it was often difficult for earlier neurosurgeons to justify their surgical decisions against medical or conservative management. Strong doubts were raised about the effectiveness of surgery as most of the studies failed to show any advantage of surgery as compared with medical management (Figure-10).

Continuing refinement in surgical techniques and instruments, coupled with the advancements in the neurocritical care, made the surgery progressively safer. Greenwood [Greenwood 1942] brought in the bipolar cautery in 1940, while the hypothermia was introduced by Loughheed, White and Sweet [Loughheed et al 1955] in 1953 for cerebral protection

during cerebrovascular procedures. Almost a decade later Uihlein et al [Uihlein et al 1962] performed the first intracranial aneurysm clipping using induced hypothermia and total circulatory arrest. The entity of vasospasm was demonstrated by Ecker and Riemenscheidner in 1951 [Ecker and Riemenscheidner 1951]. The first operating microscope was introduced by Carl Zeiss Inc. in 1953 [Krampe 1984] a company established by the visionary German optician Carl Zeiss in 1846. Theodore Kurze from Los Angeles was the first neurosurgeon to use an operating microscope in neurosurgery in 1957 [Kurze 1964]. The twin benefits of illumination and magnification offered by the operating microscope, laid the pavement for microneurosurgery, led by Yaşargil and others.

One of the earliest publications to attract the attention towards ineffectiveness of medical management of SAH came from Tappura in 1962 [Tappura 1962]. He showed that rebleeding rates were as high as 55% without any active intervention with 75% mortality. In the same year Norlén [Norlén 1963] published the results from his series of 134 patients of IAs managed surgically. He reported an astonishing success with a mortality of less than 2.5%. Over a period of time, the growing scientific evidence unequivocally established the superiority of intracranial surgery as compared to both, carotid ligation and bed rest. By the late 1970s direct clipping was accepted unanimously as a 'gold-standard' for the treatment of ruptured IAs.

2.5.5: Neuroradiological Developments & Invent of Cerebral Angiography

The radiological localization of an intracranial pathology remained a challenge to neurosurgeons until late. In this context the discovery of cerebral angiography by Egas Moniz in 1927 [Moniz 1927] a multitalented physician from Portugal, and the demonstration of an IA by this technique in 1931 was a breakthrough research.

A group of researchers, including Sir Godfrey Hounsfield [Hounsfield 1973] developed the first computed tomographic (CT) head scanner which became operational by 1971. The CT scan proved to be a crucial aid to the diagnosis of SAH due to its ability to pick subarachnoid and intraventricular blood. The early report about the first NMR image of a live human body was published by Damadian and colleagues [Damadian et al 1977] in 1977 and MRI came into clinical practice in 1982 after Sir Peter Mansfield [Mansfield et al 1979] and Paul Lauterbur [Lauterbur 1989] developed mathematical techniques that allowed rapid acquisition of MR Images possible making it a practical tool. It surpassed every

available imaging modality in providing exquisite soft tissue differentiation.

2.5.6: Endovascular Interventions

The history of the evolution of endovascular treatment of the aneurysms is a fascinating story of ground-breaking work done by the early geniuses. Whereas roots for some of these endovascular techniques can be traced to the early nineteenth century it's only through incredible progress in the technology over last couple of decades that made their safe and widespread clinical application possible.

2.5.6.1: Extracranial Endovascular Interventions

Medical measures: Apart from masterly inactivity, workers started trying various medical compounds to induce thrombosis in aneurysmal sacs. The most commonly used pharmacological compound was potassium iodide [Keen 1916] administered systemically. Various other medical measures tried were; vinegar, iron perchloride solutions, alcohol, gelatin, ergot salts, and even hypothermia by local ice packing [Keen 1916]. These procedures however, soon had to be discontinued due to inconsistent and unpredictable results.

Insertion of foreign bodies/ wiring techniques: After abandonment of medical measures various investigators started attempting to treat aneurysms by inserting foreign bodies. The earliest description of such an endovascular procedure to treat an aneurysm is given by Ransohoff [Ransohoff 1886] reciting Sir E Herne who by the turn of eighteenth century induced thrombosis in an iliac artery aneurysm by inserting heated needles into it. The same concept was later applied to treat aortic aneurysms by many authors who replaced needles with metallic wires. In spite of initial enthusiasm among its advocates the overall results from these 'wiring' procedures remained poor. These procedures were ultimately abandoned during the first half of the twentieth century.

Emergence of the concept of electrothrombosis: The limited success of these 'wiring' techniques stimulated investigators to search for more efficient alternatives. It was realised that one of the important reasons for failure was the lack of sufficient thrombus formation attributed mostly to inadequate aneurysmal packing. The idea of using galvanic current as an adjunct to enhance the thrombogenicity of these metallic coils presumably has taken its inspiration from the early experimental works done by Scudamore [Duncan and Fraser 1867] in 1824. It was however Phillips in

1832 [Phillips 1832] who gave birth to the concept of electrocoagulation in aneurysms. CH Moore introduced wiring for the treatment of aortic aneurysms in 1864. Another dimension to it was added when Corradi in 1879 [Matas 1914] who passed the electric current through the wire. The technique was later called Moore-Corradi method after both the workers. The method remained in use for next 40 years and was adopted by many investigators.

2.5.6.2: Transcranial Approaches

Due to understandable limitations in the precise localization and difficulties in accessing an IA, the early endovascular interventions were limited to the large and extracranial arteries. The initial attempts to treat an IA by iatrogenically induced thrombosis were therefore carried under direct vision during a craniotomy. In 1936 WJ Gardner [Gardner 1936] packed an accidentally opened giant IA with cotton sponges. The credit of the first successful ‘thermocoagulation’ of an IA however, goes to Werner [Werner et al 1941]. Working with Blakemore and King, in 1941 he treated a giant paraclinoid IA in a young girl. The aneurysm, resistant to multiple Hunterian ligations, was approached transorbitally. A ten-foot long silver wire was inserted through its fundus and heated for 40 sec, reportedly curing the aneurysm.

Transition from transcranial to intravascular approach: The idea of using blood vessels as natural access to treat the cerebrovascular lesions may probably have taken motivation from the pioneering work done by Brooks [Brooks 1930]. He is credited with the first endovascular intervention to treat a cerebrovascular pathology. After exposing the ICA surgically, he embolised a traumatic carotid cavernous fistula in 1930 by placing a strip of muscle intravascularly. Switching from the transcranial to intravascular approach was nevertheless, not straightforward. Tortuosity, delicacy and narrowness of intracranial vasculature as well as the presence of the carotid siphon were the main obstacles for intracranial catheter navigation. This important shift could only be made possible through the development of sophisticated micro-catheter systems and intravascular delivery devices.

Luessenhop and Spence [Luessenhop and Spence 1960] remained pioneers in cerebral endovascular navigation; they successfully cannulated an ICA to embolise an arteriovenous malformation (AVM) using flow-directed silastic spheres in 1960. They also set another important milestone in endovascular navigation in 1964; what is believed to be the first successful catheterization of intracranial vessels in a human being, finally shifting the focus from a transcranial to intravascular approach. With the help of a

glass chamber, surgically connected to the external carotid artery, they delivered a length of silastic tubing into intracranial arteries. The balloon at the tip of this flow-directed catheter was inflated temporarily to occlude the neck of a posterior communicating artery aneurysm.

Superselective catheterization and magnetic navigation: Frei and colleagues [Frei 1966] from Rehvoth, Israel, added another dimension to endovascular navigation by introducing their novel microcatheter system in 1966. This high-tech system, also called POD (para-operational device) by its inventors, made superselective catheterization of intracranial vessels possible. The tip of the catheter was made of specialised soft silicone rubber to minimise vessel trauma. A micromagnet of 1 millimetre diameter, strategically placed inside the tip of the microcatheter was used to manipulate it with the help of external magnetic fields. In 1974 Hilal et al [Hilal et al 1974] published their experience with safe intracranial catheterization in 120 patients. Using a slightly modified version of magnetically directed POD catheter they catheterized many difficult to reach intracranial vessels and more importantly performed electrocoagulation of one basilar tip aneurysm, giving birth to the concept of neuroendovascular electrothrombosis.

Following their initial success the magnetically directed catheters remained in use until the late 70s, however the lack of precise operator control and distortion of the fluoroscopic images by strong magnetic fields drove researchers to look for alternative methods of intracranial catheter navigation.

Balloons: Convinced with the idea first given by Luessenhop and Rothenberg as early as in 1960s, [Luessenhop and Spence 1960] most of the investigators started realising with time that the best force to propel the endovascular catheter was the antegrade flow of blood itself. TJ Fogarty [Fogarty 1963] and co-workers introduced a novel balloon-tipped catheter system in 1963 to extract the arterial emboli. Fogarty catheter system proved as a milestone in the advancement of catheter technology and opened doors for the development of a range of endovascular catheters including the modern balloon-tipped catheters. The most important discovery in microcatheter technology however, was the invention of Tracker[®] microcatheter system in mid 1980s by Engelson [Engelson 1986]. By virtue of its unique externally steerable tip it revolutionised the way intracranial arteries were negotiated.

Montgomery et al from Massachusetts Institute of Technology (MIT), USA, designed the first detachable balloon catheter in 1970 using a modified POD catheter by mounting a balloon on its tip. However, it was

Fedor A. Serbinenko [Serbinenko 1974] from Burdenko Neurosurgery Institute, Moscow, who not only established endovascular interventions as a treatment modality for IAs but also gets the credit for founding Endovascular Neurosurgery as a new medical discipline. Inspired by a simple observation of helium-filled balloons at May Day celebrations in Moscow's Red Square in 1959, he spent relentless hours in the laboratory to create prototype silicone and latex balloon catheters. Using these flow-directed balloon-tipped catheters he mastered the art of balloon embolization of IAs and AVMs and performed 304 balloon endovascular procedures between 1969 and 1972 with just two mortalities [Kwan et al 1991] laying the foundation stone for modern endovascular neurosurgery. The seminal works done by him changed the management of IAs forever and he is therefore rightfully called father of endovascular neurosurgery.

From balloons to endovascular coiling: Due to wide spread application and growing experience, a number of shortcomings of the balloon embolization started to become apparent. Owing to the fixed and rigid shape (round or oval) of the balloons, it was difficult to achieve 100% occlusion of the IAs, frequently leaving an insecure aneurysm at the end of the procedure. Furthermore, this potential space and the balloon-aneurysm complex together, when subjected to the continuous pulsations arising from the pulsating arterial blood column, were thought to produce a 'water-hammer' effect. This 'water-hammer' effect was reported to facilitate the IA recanalization, enlargement or delayed rupture [Kwan et al 1991]. Additionally, the balloons have also been reported to undergo slow-deflation, slowly loosening the packing further. All these drawbacks together formed the basis for the shift from balloons to coils for the endovascular treatment of the IAs.

Transcatheter electrocoagulation: Therapeutic transcatheter vessel-occlusion (TCVC), which was introduced in 1930s for the treatment of carotid-cavernous fistulae, [Greenfield 1980] slowly became a well-established technique by the 70s. Thompson and colleagues provided a thorough and methodical description of the technique and uncovered its various merits and shortcomings. They also demonstrated that the clot size and the extent of thrombosis were directly related to the product of amount and duration of the current applied. Due to difficulties in precise placement of the anode in IA, TCEC was mostly used to occlude the vessels only.

From 'pushable' coils to 'detachable' coils (GDC®): In the quest of selective and safe embolization of IAs Gianturco and colleagues invented a novel mechanical device in 1975, called 'wool coils' [Gianturco et al

1975]. It was one of the earliest ‘pushable’ coils where the ‘wool’ could be ‘pushed’ into target using a guide wire. In 1989 Hilal et al reported another use of short ‘pushable’ coils for the treatment of IAs. Although being relatively stiff, it was almost impossible to achieve a dense packing of IAs with these coils. Moreover, these coils were inherently non-retrievable and hence difficult to control. These ‘pushable’ coils later formed the basis of more advanced ‘detachable’ coils.

The credit of inventing the modern detachable coils (commonly known as GDC®) can safely be attributed to Guido Guglielmi [Guglielmi 2009] Guido Guglielmi (Figure-2.10) was born in Rome, Italy and initially studied engineering for a while before opting for medicine as a career. Due to his great interest in engineering he studied the concept of electrothrombosis of IAs in detail and conducted a series of animal experiments in the 1980s. Guglielmi later moved to Los Angeles where he

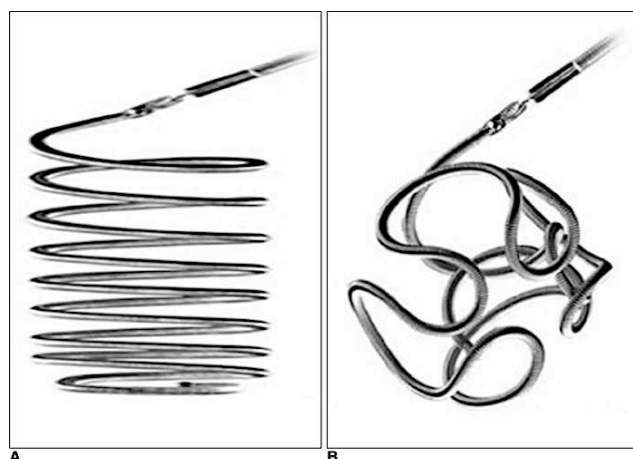


Figure 2.10: GDC® Detachable coils
Source: <http://synapse.koreamed.org>

came in contact with Ivan Sepetka, a research and development engineer at Target® Therapeutics. The genesis of this state-of-the-art coiling system has changed the way Neurovascular surgery is practiced and is a unique example of a creative interdisciplinary collaboration between these two masterminds.

Working together they mounted soft platinum coils of

different sizes to a stainless steel guide-wire. The thrombosis was achieved by passing an electric current to the coil once it is placed inside the IA. The coil would ‘detach’ from the delivery wire during the process of electrothrombosis due to the low melting point of the metal used to attach it to the guide wire. Another very important feature of these coils was their retrievability and softness, which at gave the operator added control over the procedure. The first GDC® was used in a human by Dr Viñuela on 6th March 1989 by treating a cavernous sinus fistula. The first IA was treated by GDC® in January 1991 at UCLA, Los Angeles. The techniques of endovascular interventions for the treatment of IAs have exploded in the past few decades. From a second line treatment in the early 1990s it has rapidly become a primary therapeutic option in most of the centres worldwide.

A large, multicentric, prospective, randomised, controlled, clinical trial, the International Subarachnoid Aneurysm Trial (ISAT), was conducted

under the leadership of Neurovascular Research Unit, Oxford, UK. It has indicated that the outcome in terms of survival free of disability at 1 year is significantly better with endovascular coiling as compared to surgical clipping. It however, showed that the risk of re-bleed is slightly higher with coiling.

2.5.7: Recent Advancement and Future of Neurovascular Surgery

The easy availability and widespread use of non-invasive neurodiagnostic modalities, has brought to clinical attention a large and ever increasing group of patients harbouring unruptured and asymptomatic IAs. These UIAs are also diagnosed coincidentally at the time of catheter angiography done for a ruptured IA in a patient with multiple lesions. The increasing awareness of the relatively bleak prognosis related to aneurysmal rupture amongst the general public and clinicians, forces neurosurgeons to come up with a definitive answer for these asymptomatic lesions.

Turjman et al [Turjman et al 1994] introduce a GDC into the sac of aneurysm with the help of micro catheter passing through the mesh of a stent. This technique provides tight packing without danger of the coil being herniating through arterial wall. Kinugasa et al [Kinugasa et al 1992] used a polymerising plastic material, bismuth trioxide dissolved in dimethyl sulfoxide (DMSO) and cellulose acetate polymer (CAP), for endovascular packing of UIAs. However distal embolism and toxicity to DMSO are still cause of concern. Recently a few researchers used micro catheter to deposit viable migration capable fibroblasts as a promising endovascular technique to treat UIAs [Abruzzo et al 2007].

Though therapeutic management of IAs has evolved in past few decades but the issues, which still remain unresolved, is to identify patients at risk of developing IAs and take preventive measures. The flow of blood inside the intracranial vasculature, the shape of the IA and its structural properties, has long been thought to play a role in their aetiopathogenesis. Computational Fluid Dynamics (CFD) is providing a useful alternative to predict blood flows where detailed *in vivo* measurement of haemodynamic flow variables is not possible. Important haemodynamic factors to be considered are Wall Shear Stress (WSS) and Oscillatory shear index (OSI). In future these factors can be used as new descriptors to predict the risk of rupture for these lesions.

2.6: Computational fluid dynamics: the concept and need

2.6.1: A Brief History

Flow of fluid has always caught the attention of man since the beginning of civilisation, whether it is the water in river or ocean, air in the atmosphere or blood in human body. The first idea on this topic was introduced by Heraclitus (536-460), though it was in a philosophical sense rather than a scientific one. Archimedes (287-212 BC) gave a scientific meaning to the concept and worked on hydrostatics and static mechanics. During European Renaissance (15th century) Leonardo Da Vinci started depicting the natural world of fluid through his drawings. His findings on fluid mechanics are presented in a nine-part treatise (Del moto e misura



Figure 2.11: Claude Navier
Source: Medscape

dell'acqua- in Latin 'Mensura motus et aqua', in English- 'Motion and measure water'). The pictorial representation of Leonardo was followed by quantification and prediction of the fluid flow phenomena by Newton in the late 17th century. Again, in the 17th century the foundations for experimental fluid dynamics were laid in England and France. In the 18th and 19th century, theoretical fluid dynamics gradually developed, again primarily in Europe. As a result, throughout most of the 20th century the study and practice of fluid dynamics involved the use of pure theory on the one hand and pure experiment on the other hand. In 18th and 19th century Daniel Bernoulli (1700-1782) and Leonhard Euler (1707-1783) tried to mathematically describe the flow of fluid using for the first time the concept of infinitesimal calculus.

Further, Claude Louis Marie Henry Navier (1785-1836) (Figure-2.11) and, George Gabriel Stokes (1819-1903) modified the Euler equation and gave birth to the now famous Navier-Stokes equation, which forms the basis of modern CFD.

2.6.2: Navier-Stokes Equations

The Navier-Stokes equations are set of nonlinear partial differential equations that describe the flow of fluids in terms of fluid velocity and pressure. The Navier-Stokes equations are:

$$\frac{\partial \rho}{\partial t} + \nabla \cdot (\rho \mathbf{u}) = 0 \quad \dots\dots\dots \text{Continuity equation (1)}$$

$$\frac{\partial}{\partial t} (\rho \mathbf{u}) + \nabla \cdot (\rho \mathbf{u} \otimes \mathbf{u} + \rho \mathbf{I}) = \nabla \cdot \boldsymbol{\tau} + \rho \mathbf{g} \dots\dots\dots \text{Momentum equation (2)}$$

Where ρ is density of the fluid, u its velocity, p its pressure, μ its viscosity and F represents body forces (e.g. gravitational forces).

The Navier-Stokes equations are time-dependent and consist of a continuity equation for conservation of mass and conservation of momentum equations which is equivalent to Newton's second law of motion (Force=Mass x Acceleration) but applied to a fluid. These equations can be used to describe and predict the fluid flow in any applications.

When the fluid flow is simple these equations can be simplified and a solution can be computed. A typical example is the steady viscous flow of a fluid through a straight circular pipe, in which case the simplified version of the Navier-Stokes, leads to the well-known Poiseuille's solution-

$$u = -\frac{1}{4\mu} (R^2 - r^2) \frac{\partial p}{\partial x}$$

Which represent the famous Poiseuille's parabolic velocity profile (see Figure-13), expressed in terms of viscosity μ , radius r , and pressure drop dp/dx .

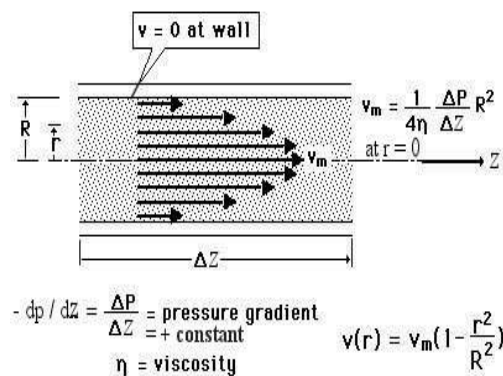


Figure 2.12: Equations for Poiseuille's parabolic velocity profile
 Source: universe-review.ca

Current knowledge in mathematics limits the analytical solution of the Navier-Stokes equations only to a restricted group of relatively simple applications (e.g. straight circular pipes and the likes). In most applications however, where fluid flows around or through more complex geometries, a solution of these equations is not readily available and it is necessary to recur to computational

fluid dynamics, whose underlying concepts are further treated in the following chapters.

2.6.3: Why Computational Fluid Dynamics? The Concept And The Need

Computational fluid dynamics constitutes a relatively new approach in the study and the development of the whole discipline of fluid dynamics. Around 1960, with the advent of high-speed digital computers and the development of accurate numerical algorithms a new third revolutionary approach developed that strongly affected the way we study and practice fluid dynamics today, the approach of computational fluid dynamics. This approach nicely and synergistically complements the other two approaches of pure theory and pure experiment, but it will never replace either of these. The interpretation and understanding of any fluid dynamics problem should rest upon a proper balance of all three approaches.

Computational fluid dynamics is the science of predicting fluid-flow, heat & mass transfer, chemical reactions, and related phenomena by solving numerically the set of mathematical equations (conservation of mass, momentum, energy, species etc.) that govern a particular physical system. In the past decades it has been successfully used mainly in the engineering field for conceptual studies of new designs, troubleshooting redesign, or improving the physical understanding of a novel fluid mechanical phenomenon. Successful examples are found in the automotive sector, where it has helped to improve the aerodynamics of vehicles, civil engineering, where it has been used to design more efficient cooling systems, and nautical architecture, where it has been used in the design of more efficient keels. Accompanied to an in depth knowledge of the physical problem (theory) and supported by experimental data, CFD can be used as a powerful tool to reduce the total effort required in the experiment, design, and data acquisition.

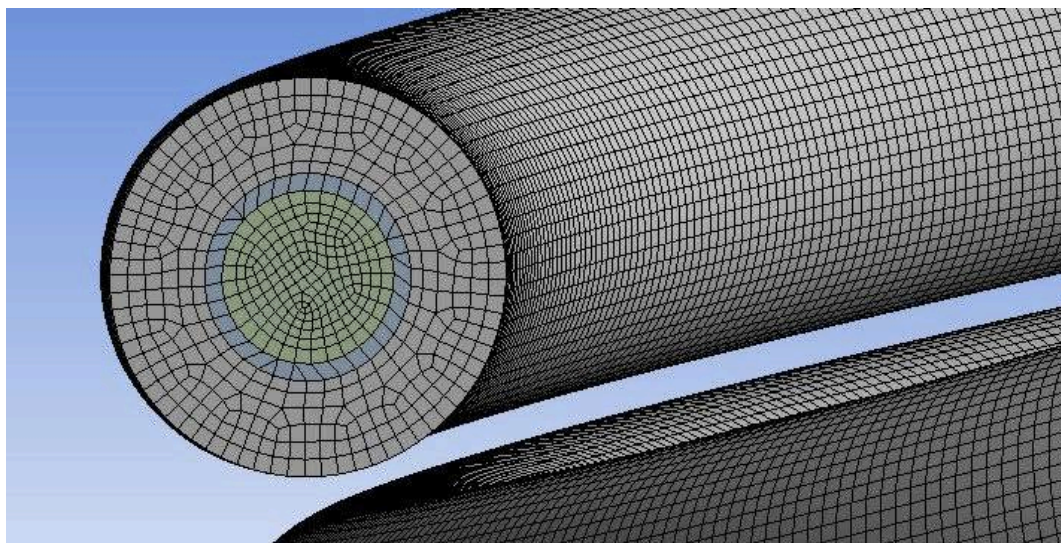


Figure 2.13: Discretization and generation of polyhedral mesh in a pipe flow fluid region

The behaviour of a particular physical problem is often represented by a set of partial differential equations (governing equations, i.e. conservation of continuity, momentum, energy, etc.) whose exact solution is sometimes tedious, if not impossible. In the case of fluid flows these equations are the Navier-Stokes equations. In complex physical problems the solution is often not available. In these contexts CFD offers the possibility to solve the governing equations by approximation. CFD solvers are based on the discretization of the fluid flow domain (i.e. the region traversed by flow). The domain is subdivided into a set of sub-volumes or cells called mesh or grid. The figure 2.13 shows the discretization and generation of polygonal mesh in a pipe flow fluid region. By using this discretization the governing differential equations of Navier-Stokes can be approximated and solved, but only at certain points (i.e. cell corners) of the domain, thus providing the solution in terms of pressure or velocity of the fluid at these points.

While screening of patients (with high risk of cerebral aneurysm) through invasive techniques continues to play a paramount role in deciding the course of treatment, it has some disadvantages that explain the increasing emphasis many neurosurgeons are placing on computer simulation.

2.7: How Long We Have Come So Far: A Focused Review of Literature of The Studies Published on the Application of Computational Fluid Dynamics in the Field of Intracranial Aneurysms

2.7.1: Background and introduction

A focused review of literature was conducted to assess the progression of Computational Fluid Dynamics research in the field of Intracranial Aneurysms. Twenty-six (26) full text publications were reviewed for past seventeen years (17 years) from 1998 to 2014. Table -2.8 shows the major journals publishing papers in the field. Efforts were made to cover the most important landmark studies of each year and at least one study was included in the review from each year except year 2000, as I could not find any relevant study conducted that year. A brief account of important studies reviewed is given below in Table-2.9.

2.7.2: Initial work, current research groups involved and publication trends

Initial studies: The initial studies were conducted using idealised rather than patient-specific models [Low et al 1993, Burleson et al 1995, Aenis et al 1997]. With the progression of time it was realised that the patient-

specific models will be more appropriate to give a better approximation of the haemodynamic parameters in a given patient, and hence the researchers started using the patient specific models. The first simulations studies using the patient specific models were conducted in 2003 by Steinman and colleagues and Jou et al [Steinman et al 2003, Jou et al 2003]. Apart from having other flaws, the earlier studies also had inconsistent methodology and less explicit in describing their materials and methods e.g. no clear description of software used for mesh generation and CFD analysis, imaging modality used, boundary conditions applied, type of analysis, assumptions made, etc. [Foutrakis et al 1999, Cebal et al 2001, Butty et al 2002]. Whereas, most of these shortcomings can definitely be attributed to the rudimentary technology available that time, there also seem to be a lack of appreciation among few author groups [Cebal et al 2001, Foutrakis et al 1999], on the importance of stating the material and methods clearly in their publications.

Table 2.8: Showing the Journals publishing 2 and more papers in CFD in PubMed search

No	Journal	Number of publications	% of Total
1	AJNR	37	20%
2	J Biomech	19	10%
3	Neurosurgery	11	5.6%
4	Ann Biomed Eng	10	5%
5	J Biomech Eng	9	4.6%
6	Stroke	8	4%
7	Int J Numer Method Biomed Eng	8	4%
8	IEEE Trans Med Imaging	5	2.5%
9	Acta Neurochir (Wein)	5	2.5%
10	Med Phys	5	2.5%
11	J Neurosurg	4	2%
12	Med Biol Eng Comput	4	2%
13	Conf Proc IEEE Eng Med Biol Soc	4	2%
14	Neurol Res.	3	1.5%
15	Neuroradiology	3	1.5%
16	Academic Radiology	3	1.5%
17	J Neurointerv Surg	3	1.5%
18	Proc Soc Photo Opt Instrum Eng	2	1%
19	Biorheology	2	1%
20	Surg Neurol	2	1%
21	Comput Math Methods Med	2	1%
22	Med Eng Phys	2	1%
23	NMR Biomed	2	1%
24	Phys Med Biol	2	1%
25	Physiol Meas	2	1%
26	PLoS One	2	1%

2.7.3: Salient Features of the Studies Reviewed

Demography of the population in the publications reviewed: CFD analyses can be conducted either in human beings (patients or healthy subjects), animal models (e.g. experimental studies), *in vitro* models or virtual models (*in silico*). All of these methods have their own positives and negatives. Whereas, studies in human beings provide best chance to simulate the disease process of IAs *in vivo* and help in improving their ultimate management, they may be difficult to conduct and may limit

researchers' ability to try new therapeutic options due to ethical and technical issues. In the publications reviewed here, most of the studies were conducted in human beings (19 out of 26, 73%), either in patient specific 3D geometries or healthy volunteers. Second method is *in vitro* experiments where 3D models are created (e.g. with the help of 3D printers) and experiments are conducted by simulating human tissues and blood by setting a rig. These *in vitro* studies are mainly used to simulate the human vasculature and IAs. These models serve excellent platform for validation of CFD results as used by many authors in my review (3, 11%) [Bordas et al. 2013, Acevedo-Bolton et al. 2006]. Animal models provide closest approximation to the human pathophysiology and give flexibility of experimentation to researchers, however, may lack specificity of the human disease process. *In silico* or computer generated virtual 3D models of idealized vessel/ IA geometries are popular among biomedical scientists who use them frequently to test mesh reliability and finite element solution methods (2, 8%).

Cohort size: Most of the studies (>80%) were conducted on small number of subjects (cohorts of 10 or less). Less than 20% studies had a cohort size of more than 10 with biggest being analysing 114 IAs in 31 patients [Alfano et al, 2013] followed by 61 IAs in 57 patients [Cebral et al, 2005], 29 IAs in 26 patients [Shojima et al, 2005] and 20 IAs in 19 patients [Shojima et al, 2004]. **Location:** Location-wise the studies can be divided into two categories; a) Analyses of haemodynamics of IA and b) Analyses of haemodynamics of cerebral arteries. Out of the 32 locations for IAs analysed 20 (60%) were in anterior circulation (ICA=7, MCA=7, ICA-PCoM Junction=2, ACA=2, ACoM=2) while 10 (31%) were in Posterior circulation (BA=5, PCoM=4, VA-BA=1). Locations for 2 (6%) IAs were not available (NA=2). These figures differ from the Juvela et al [Juvela et al 2000] who found in their study that 97% of IAs were located in anterior circulation while only 3% were in Posterior circulation.

Type of IAs: Consistent with findings of other authors [Juvela et al 2000, Keedy 2006], the most common type of IAs in papers I reviewed was Saccular (81%) followed by Fusiform (2%) while for 11% type was either not available or not applicable (NA).

Imaging modalities used in different studies for CFD analyses; Comparison of 3DRA/ CTA and MRA: Most common imaging modality used in most of the studies is 3DRA (3 Dimensional Rotational Angiography, also known as DSA= Digital Subtraction Angiogram) for creating 3D models and performing CFD analyses. Other imaging modalities used were CTA (CT Angiogram) and MRA (MR Angiogram).

In 3DRA the contrast is injected directly into the cerebral arteries leading to a high concentration of contrast material inside the arteries and Intracranial Aneurysm. This produces a very high-resolution image of the arterial ROI (Region of Interest) and the Intracranial Aneurysm making it the 'Gold Standard' modality for creating 3D Models and performing CFD Analyses. In rest two modalities (CTA and MRA) the contrast is injected systemically into a vein at a remote location (usually antecubital vein in the forearm of patient). The 'bolus of the contrast' material injected peripherally has to travel a long distance (via heart) before it reaches the cerebral arteries as well as is 'diluted significantly' by the time it reaches the cerebral arteries. Due to these two factors, the concentration of the contrast material inside the arterial (and aneurysmal) lumen remains significantly low in these two modalities resulting in lower resolution images compared to 3DRA.

In spite of its ability to produce high quality better resolution images, 3DRA remains a fairly invasive procedure carrying higher risks to patients when compared to CTA and MRA. The main risks of 3DRA [Dion et al. 1987, Fifi et al. 2009] include Cerebral Ischemic Events (Stroke; including TIAs and Permanent Neurologic Deficits), intracranial bleed secondary to perforation of a vessel or the aneurysm itself, allergy to contrast media, acute kidney failure (Acute Tubular Necrosis), bleeding and hematoma formation at the puncture site, dissection of blood vessels, femoral abscess, femoral occlusion leading to distal ischemia, etc. CTA and MRA are relatively straightforward procedures carrying significantly lower risks that can be performed on outpatient basis and therefore used widely for monitoring unruptured aneurysms as well as post-procedural follow-ups. The risk of radiation exposure is common to both 3DRA as well as CTA while all three carry risk of developing allergy to contrast media. The MRA is least invasive of all three and supposed to be safest as well. However, as the effects of radiofrequency fields and the loud acoustic environment on a foetus remain unknown, further research is needed to establish the long-term safety of MRA on pregnant patients [Bulas 2013]. Furthermore, with advance in technology and introduction of sophisticated neuro-endovascular catheters, the risk profile of 3DRA is falling rapidly. Recent studies [Thiex et al. 2010] quote figures as low as approaching to zero in well-equipped centres, carefully selected cases and experienced operator.

Software used for 3D Modelling and CFD Analyses: The process of analysing the haemodynamic variables and deducing other non-observable data can be divided into following steps: a) Importing the medical images into a suitable software interface and generation of 3D Models, b) Surface

extraction and mesh generation c) Application of appropriate boundary conditions on inlet and outlets of the geometry d) Simulation of blood-flow into the geometrical models of arteries and IAs created in previous steps, d) Post-processing of the results obtained to display the haemodynamic variables. Different researchers used a number of software at each step.

a) Generation of 3D Models: The medical data is ‘raw’ and need to be ‘processed’ to create 3D Models that can be used for further processing. This is done by importing the medical images (e.g. 3DRA/ CTA/ MRA) into a suitable software-interface that generates Anatomical 3D Models of the ROI (Region of Interest), i.e. the IAs and surrounding vasculature. A number of software are available for generation of 3D models from medical images. The most common software used in my review of 26 publications was In House Developed Software (7, 27%). Other software used were Rapidform™ (INUS Technology, Seoul, South Korea) (3, 12%), VMTK (Vascular Modelling Toolkit, an open source software containing C++ based algorithms, developed by VMTK Community, Bergamo, Italy; www.vmtk.org) (2, 8%), Alatoview™ (Toshiba, Japan), Altair HyperMesh™ (Altair Engineering, Inc., MI, USA), (X)-MedCon™ V0.5.10 (Open Source Software), AVS/Express Visual Development Tool V5.1 (Advanced Visual System Inc.), e.soft@LEONARDO™ (Siemens Medical Solutions USA, Inc.), VTK/ Paraview™ (Kitware Inc., NY, USA), Amira™ V 3.0 (Mercury Computer Systems, Berlin, Germany), ICEM™-CFD software (Ansys, Berkeley, CA), Matlab™ R2006b (The Mathworks, Natick, MA, USA), and CAD software RHINOCEROS™ V 4.0 (McNeel & Associates, Indianapolis, IN, USA). For generating the 3D Models of Intracranial Aneurysms and surrounding vasculature in Project @neurIST, I used in house developed software @neuFuse.

b) Mesh generation and Fluid flow simulation: Mesh or volume generation after surface extraction is the second step in the processing followed by application of Boundary Conditions and simulation of Fluid Flow by solving the equations iteratively, either as a steady-state or transient (also called as pulsatile) fluid flow.

Two biggest giants building software in the field of CFD Simulation are Ansys® and Fluent® (bearing in mind that after acquisition in 2006, Fluent® has become a part of Ansys®). In my review of 26 publications, these two companies shared equal proportion of software used for mesh generation and blood flow simulation. Software provided by both Ansys® and Fluent® were used in 12 studies (46% each) totalling to 92% together. Main Ansys® software used for mesh generation is Ansys® ICEM™ used

in 7 studies (27%). Its counterpart from Fluent® is GAMBIT (Geometry and Mesh Building Intelligent Toolkit), which also used extensively in mesh generation and was used by equal number of authors (7, 27%) as ICEM™ from Ansys® in my review. Other popular software from Ansys are CFX™, CFD-Flo™, Ansys Fluent™, Ansys CFD Professional™. Ansys® has also integrated its all fluid dynamics solution products into the Ansys® Workbench™. Other software used for meshing and blood flow simulations by different authors are; FIDAP –CFD Software (Fluent Europe, Sheffield, UK), CFD-ACE+ package (CFD Research Corporation, Huntsville, AL, USA), STARCD, (CD Adapco, Melville, NY, USA), SC/Tetra V-5 (Software Cradle Co Ltd, Osaka, Japan), FeatFlow V1.3 release candidate 3 (University of Dortmund, Germany), Gridgen V15.12 (Pointwise Inc., TX), Nektar Spectral/ HP Element Framework (Division of Applied Mathematics, Brown University, USA, Department of Aeronautics, Imperial College London, UK, and Scientific Computing and Imaging Institute, University of Utah, USA), etc. In the studies included in this thesis, whereas Ansys® ICEM™ software was used for mesh generation, Ansys® CFX™ was used for blood flow simulations in the ROI (Region of Interest), as a part of Project @neurIST.

Boundary conditions applied: Boundary conditions (BCs) are required as due to limitation in current technology it is currently impossible to simulate the whole body vasculature at the same time. The region of interest (ROI) despite the fact being simulated in isolation is naturally affected by the region outside it. In order to perform a realistic simulation this information is passed to the solver by applying the Boundary Conditions. These boundary conditions can be either measured directly on the patient by using different techniques e.g. Transcranial Doppler (TCD) or MR Q Flow measurements or if not available has to be taken from the other sources. In my review total 35 Boundary Conditions were considered (including inlet and outlet Boundary Conditions in the same study). Out of these 35 BCs, 17 (approx. 49%) were measured in the patients. The most common method for measuring the BCs was Transcranial Doppler (TCD) Ultrasound (5, 30%), followed by Phase Contrast MRI (pcMRI) in 4 (24%), MR Velocimetry (2, 12%), Laser Doppler Velocimetry (LDV) (2, 12%). All of these methods, in spite of their advantages, have some inherent shortcomings. The most recent advancement in the field of measuring the BCs is taking the measurements of pressure and velocity by Intravascular Probe Sensors directly in the Intracranial Vessels and IAs as demonstrated by Levitt and colleagues in a ground breaking study done this year [Levitt et al. 2014]. However, it will

take some time before these methods can become a practical adjunct in routine clinical settings.

Whenever this information is not available for a particular patient, we use the values observed in age sex matched other patients or the healthy volunteers or values from literature, also known as 'modelled' or 'phantom-boundary conditions'. In author's review of 26 studies; 16 (46%) were modelled BCs, out of which while 12 (34%) were literature based, rest 4 (11%) were measured in healthy age and sex matched volunteers. The variables often used as phantom-boundary conditions are heart rate, blood flow velocity, pressure, velocity profile, and usually applied at outlets in most of the studies, sometimes also called 'Universal Boundary Conditions' by some authors. Methods of obtaining BCs were not available in 2 studies.

Table 2.9: CFD Analysis of Intracranial Aneurysms & Arteries: Some Main Studies, their Methodology and Results

No	Author/ Year	Journal/ Year	Human/ Animal/ <i>in-vitro</i>	Patients/ Animals/ Aneurysms	Location	Aneurysm type	Imaging Modality	Software used	Haemodynamic Variables analyzed	Results	Boundary Condition Applied	Type of Analysis	Assumptions Made	Salient features of study
1	Ortega	<i>J Med Eng Technol</i> 1998	Animal	3/3	CCA	Saccular	3DRA	*Surface Extraction and 3D Modeling: -In house developed software *CFD: - FIDAP –CFD Software, Fluent Europe, Sheffield, UK	Flow patterns Jet stream impingement	Flow patterns inside the IAs change with time during a cardiac cycle- this may lead to increased WSS in the IAs	Measured with Doppler	Transient	Newtonian Fluid, Rigid Vessel Wall, Non Slip BC	One of the early study to show potential application of CFD in the prediction of haemodynamics of IAs
2	Foutrakis et al	<i>AJNR</i> 1999	<i>In vitro</i>	2/0	Cerebral artery Curves Bifurcations +/- Aneurysm -models	Saccular	NA	*Surface Extraction and 3D Modeling: NA *CFD: NA	Pressure Velocity Flow Pattern Impingement WSS	High Pressure High Velocity, High WSS, Impingement – Initiation	Measured	NA	Newtonian Fluid, Rigid Vessel Wall, Non Slip BC	One of the early study, used 2D Finite Element Models
3	Cebral et al	<i>JBiomech</i> 2001	Human	1/0	ICA and ECA of a healthy volunteer	NA	MRA	*Surface Extraction and 3D Modeling: NA *CFD: NA	NA	Study describes a new method for mesh generation	NA	NA	NA	A new method for Mesh Generation described
4	Butty et al	<i>Biorheology</i> 2002	Human	1/2	ICA	Saccular	CTA	*Surface Extraction and 3D Modeling: - Altair HyperMesh, Altair Engineering, Inc., MI, USA *CFD: - CFD-ACE+ package, by CFD Research Corporation, Huntsville, AL, USA	Flow patterns Residence time Basins of attraction	Complex flow patterns and mixing of blood seen inside the IAs	NA	NA	Newtonian Fluid, Rigid Vessel Wall, Non Slip BC	Early study, methodology not very clear esp. re: Boundary Conditions
5	Steinman et al	<i>AJNR</i> 2003	Human	1/1	ICA- PcomA	Saccular	3DRA	*Surface Extraction and 3D Modeling: -NA *CFD: - In house developed finite element CFD Solver	WSS Flow Pattern OSI	Neck - High flow Aneurysmal sac – persistent & transient vortices Distal neck – high OCI & WSS	Measured in Age/Sex matched volunteers	Transient	Newtonian Fluid, Rigid Vessel Wall, Non Slip BC	Validations done by comparing the CFD findings with the cine angiography showed good agreement

No	Author/ Year	Journal/ Year	Human/ Animal/ <i>in-vitro</i>	Patients/ Animals/ Aneurysms	Location	Aneurysm type	Imaging Modality	Software used	Haemodynamic Variables analyzed	Results	Boundary Condition Applied	Type of Analysis	Assumptions Made	Salient features of study
6	Shojima et al	<i>Stroke</i> 2004	Humans	19/20	MCA	Saccular	3 D CTA	*Surface Extraction and 3D Modeling: Alatoview, Toshiba, Japan *CFD: ICEM CFD, Ansys	WSS	High WSS – Initiation Low WSS – Growth & rupture	Inlet: measured in One Pt. by TCD Outlet: Modeled	Stationary	Newtonian Fluid, Rigid Vessel Wall, Non Slip BC	
7	Hoi et al	<i>J Neurosurg</i> 2004	<i>In vitro</i>	10	ICA Models	Saccular	3D DSA	*Surface Extraction and 3D Modeling: In House Software *CFD: -Gambit, Fluent, Lebanon, NH -STARCD, CD Adapco, Melville, NY	Effects of arterial geometry and Neck Size WSS Velocity	WSS increases with Curvature and Neck Size	Measured	Transient	Newtonian Fluid, Rigid Vessel Wall, Non Slip BC	Effects of arterial geometry and Neck Size on WSS were investigated
8	Hassan et al	<i>AJNR</i> 2004	Human	1/1	Vertebro- Basilar	Saccular	3DRA	*Surface Extraction and 3D Modeling: -(X) MedCon, V0.5.10, Open Source Software -AVS/Express visual development tool (V5.1, Advanced Visual System Inc.) *CFD: -ICEM CFD, Ansys -Gambit, Fluent, Lebanon, NH *Post Processing: Enight, version 7.3.0 (Computational Engineering International, Inc., Berkley, CA)	Pressure, after therapeutic occlusion of VA- one by one	Balloon occlusion of Rt VA better than the Lt VA	Measured, TCD, Pt. Specific	Transient	Newtonian Fluid, Rigid Vessel Wall, Non Slip BC	CFD of a Giant IA showing growth

No	Author/ Year	Journal/ Year	Human/ Animal/ <i>in-vitro</i>	Patients/ Animals/ Aneurysms	Location	Aneurysm type	Imaging Modality	Software used	Haemodynamic Variables analyzed	Results	Boundary Condition Applied	Type of Analysis	Assumptions Made	Salient features of study
9	Jou et al	<i>AJNR</i> 2005	Humans	2/2	Basilar Artery	Fusiform	MRA	*Surface Extraction and 3D Modeling: Rapidform (INUS Technology, Seoul, South Korea) *CFD: -Gambit (Fluent, Lebanon, NH) -Fluent (Fluent Inc., Lebanon, NH)	WSS Flow Pattern Pressure Impingement	Low WSS correlates with IA growth	Pt. Specific- Inlet: pcMRA Outlet: MR Velicimetry	Transient	Newtonian Fluid, Rigid Vessel Wall, Non Slip BC	CFD on growing IAs
10	Shojima et al	<i>Stroke</i> 2005	Humans	26/29	ICA MCA ACA	Saccular	3D DSA	*Surface Extraction and 3D Modeling: ImageDesign (Quint Corporation) *CFD: SC/Tetra V-5 , Software Cradle Co Ltd, Osaka, Japan	Pressure Velocity Flow Pattern Impingement WSS	High Pressure- No correlation with Rupture, High Pressure- correlated with High WSS	Inlet: Measured in one pt., used in all Outlet: modeled	Transient	Newtonian Fluid, Rigid Vessel Wall, Non Slip BC	Contrary to the common belief study shows Blood Stream Jet Impaction and Local Pressure Elevation less important factors in IA rupture
11	Cebral el al	<i>AJNR</i> 2005	Humans	57/62	ICA MCA PComA ACA NA	Saccular	3DRA	*Surface Extraction and 3D Modeling: In House Software *CFD: Ansys	Peak Pressure OSI WSS	Ruptured IAs: Complex, unstable flow, Small Impingement Area Small Jet Size	Modeled Literature based Based on MRA	Transient	Newtonian Fluid, Rigid Vessel Wall, Non Slip BC	Cebral el al found correlations with Complex, Unstable flow, and ruptured IAs
12	Karmonik et al	<i>IEEE Proceedings</i> 2006	Human	3/3	Basilar Artery	Saccular	3DRA	*Surface Extraction and 3D Modeling: - e.soft@LEONARDO, Siemens Medical Solutions USA, Inc. -VTK/ Paraview- Kitware Inc. *CFD: Meshing: Gambit CFD: Fluent, CFD Solver, Fluent, Lebanon, NH	WSS- time dependent	WSS varies with time	Modeled, from literature	Transient	Newtonian Fluid, Rigid Vessel Wall, Non Slip BC	One of the early studies on CFD of IAs

No	Author/ Year	Journal/ Year	Human/ Animal/ <i>in-vitro</i>	Patients/ Animals/ Aneurysms	Location	Aneurysm type	Imaging Modality	Software used	Haemodynamic Variables analyzed	Results	Boundary Condition Applied	Type of Analysis	Assumptions Made	Salient features of study
13	Acevedo- Bolton et al	<i>Neurosurgery</i> 2006	Human/ <i>in vitro</i>	1/1	Basilar Artery	Fusiform	MRI/ MRA	Surface Extraction and 3D Modeling: Amira (version 3.0; Mercury Computer Systems, Berlin, Germany) and Rapidform 2004 (INUS Technology, Seoul, South Korea) CFD: GAMBIT, Fluent	Inflow Jet WSS	*Low WSS- corresponds to Aneurysm growth *CFD can be used to model interventions	Measured pcMRI	Transient	Newtonian Fluid, Rigid Vessel Wall, Non Slip BC	* <i>in vitro</i> and <i>in vivo</i> validations done *Increasing the WSS proposed as treatment
14	Castro et al	<i>AJNR</i> 2006	Humans	4/4	PComA Rt MCA Lt MCA AComA	Saccular	3DRA	*Surface Extraction and 3D Modeling: NA *CFD: NA	WSS Flow Velocity Flow Pattern	Significant effect of upstream parent vasculature on aneurysmal haemodynamics	Modeled, based on the MR measurements in Normal Subjects	Transient	Newtonian Fluid, Rigid Vessel Wall, Non Slip BC	Effects of Geometry of the upstream parent artery on IA haemodynamics demonstrated
15	Mantha et al	<i>AJNR</i> 2006	Humans	3/3	ICA	Saccular	3D DSA	*Surface Extraction and 3D Modeling: In House Software *CFD: Gambit (Fluent, Lebanon, NH)	WSS OSI Velocity	Low WSS/ Stagnant flow correlates IA Initiation	Modeled Literature based	Transient	Newtonian Fluid, Rigid Vessel Wall, Non Slip BC	First one to use technique of removing the IA and computing WSS after reconstructing the parent wall
16	Alnaes et al.	<i>Stroke</i> 2007	Human	10/0	Complete Circle of Willis	-	CTA MRA 3DRA	*Surface Extraction and 3D Modeling: In House Software *CFD: FeatFlow (version 1.3, release candidate 3; Uni of Dortmund, Germany) *Post Processing: ParaView software (version 2.4; Kitware Inc., Los Alamos National Laboratory, Los Alamos, NM)	WSS	*WSS changes with Vessel radii and Branch Angles. *High WSS at the sites where Aneurysms are common	*Modeled *Literature Based	Stationary	Newtonian Fluid, Rigid Vessel Wall, Non Slip BC Blood Density: 1g/cm ³ Viscosity: 0.0035 Pa.s	Study provides CFD model of circle of Willis and values of WSS in it

No	Author/ Year	Journal/ Year	Human/ Animal/ <i>in-vitro</i>	Patients/ Animals/ Aneurysms	Location	Aneurysm type	Imaging Modality	Software used	Haemodynamic Variables analyzed	Results	Boundary Condition Applied	Type of Analysis	Assumptions Made	Salient features of study
17	Meng et al	<i>Stroke</i> 2007	Animals	6	CCA- surgically created vessel branch	Saccular/ Nascent aneurysm formation	3DRA	*Surface Extraction and 3D Modeling: ICEM-CFD software (Ansys, Berkeley, CA). *CFD: Star-CD (CD- Adapco, Melville, NY)	Impingement zones WSS WSS Gradients	High WSS, Impingement- Initiation	Measured	Transient/ Stationary	Newtonian Fluid, Rigid Vessel Wall, Non Slip BC	Experimental study in animals showing histological changes in vessel walls of IA initiation
18	Boussel et al	<i>Stroke</i> 2008	Human	7/7	Basilar ICA MCA	Saccular	MRA	*Surface Extraction and 3D Modeling: Rapidform (INUS Technology, Seoul, South Korea) *CFD: Fluent (Fluent Inc., Lebanon, NH)	WSS _{TA} (Time Averaged WSS)	Low WSS correlates with Growth of IA	Measured by pcMRI	Transient	Newtonian Fluid, Rigid Vessel Wall, Non Slip BC,	Correlation of Low WSS to Aneurysm Growth
19	Cebral et al	<i>AJNR</i> 2009	Human	1/1	Basilar Tip	Saccular	3DRA	*Surface Extraction and 3D Modeling: In House Software *CFD: Ansys	WSS Velocity Flow Pattern	Haemodynamic Characteristics of Ruptured IAs: *Concentrated inflow jet *Unstable Flow *Small Impaction zone *Low WSS	Modeled Based on MRA Of Volunteers	Transient	Newtonian Fluid, Rigid Vessel Wall, Non Slip BC, Haemodynamic and Morphology of IA remains same before and after rupture	CFD analysis done just 2 hours before the IA rupture

20	Baek et al	<i>Interface Focus</i> 2010	Human	3/3	ICA PComA	Saccular	3DRA CTA	*Surface Extraction and 3D Modeling: Matlab R2006b (The Mathworks, Natick, MA, USA) *CFD: Mesh: Gridgen V15.12 (Pointwise Inc., TX) CFD: Nektar, Spectral/ HP Element Framework	WSS OSI VFR	Flow instability occurs in certain IAs - esp. wide necked IAs that may be responsible for their growth or rupture	Inlet: literature Based Outlet: Universal BC	Transient	Newtonian Fluid, Rigid Vessel Wall, Non Slip BC,	
No	Author/ Year	Journal	Human/ Animal/ in- vitro	Patients/ Aneurysms	Location	Aneurysm type	Imaging Modality	Software used	Haemodynamic Variables analyzed	Results	Boundary Condition Applied	Type of Analysis	Assumptions Made	Salient features of study
21	Bernardini et al	<i>Interface Focus</i> 2011	Virtual	0/1	NA	Saccular	Idealized vessel and IA geometry	*Surface Extraction and 3D Modeling: CAD software RHINOCEROS v. 4.0 (McNeel & Associates, Indianapolis, IN, USA) *CFD: Meshing: Ansys ICEM CFD: Ansys CFX, (ANSYS, Canonsburg, Pennsylvania)	Position and deployment of stent WSS Impact zone	Position of stent influences the WSS and impact zone in the IAs	Inlet: literature Based Outlet: Universal BC	Transient	Newtonian Fluid, Rigid Vessel Wall, Non Slip BC,	Position of stent influences the WSS and impact zone in the IAs
22	Kono et al	<i>Neurosurgery</i> 2012	Human	1/1	ACA	Saccular	3DRA CTA	*Surface Extraction and 3D Modeling: NA *CFD: Meshing: Ansys ICEM CFD: Ansys CFX, (ANSYS, Canonsburg, Pennsylvania)	WSS OSI Velocity Static pressure	Site of rupture corresponds with Low End-Diastolic WSS and High Peak-Systolic Pressure	Inlet: Measured by Doppler Outlet: Universal BC	Transient	Newtonian Fluid, Rigid Vessel Wall, Non Slip BC,	Rare study that computed Haemodynamic variables during IA rupture

23	Li et al	<i>JNeurosurg</i> 2012	Human	17/17	ICA AComA PComA	Saccular	3DRA	*Surface Extraction and 3D Modeling: In house software *CFD: Meshing: Ansys ICEM CFD: Ansys CFX, (ANSYS, Canonsburg, Pennsylvania)	Max WSS Spatially Ave WSS	Values of Max WSS and Spatially Ave WSS at peak systole were significantly higher at the neck in recanalized IAs after coiling	Inlet: Measured by Doppler in healthy volunteers Outlet: Universal BC	Transient	Newtonian Fluid, Rigid Vessel Wall, Non Slip BC,	Study addresses a common problem of recanalization in IAs
24	Alfano et al	<i>Neurosurgery</i> 2013	Human	31/114-10 common locations	Vessel bifurcations	-	3DRA CTA	*Surface Extraction and 3D Modeling: Vascular Modeling Toolkit *CFD: ICEM Ansys	WSS WSS Gradient Av WSS Max WSS Impact zones	High WSS correlates with the site of IA formation	Literature based	Stationary	Newtonian Fluid, Rigid Vessel Wall, Non Slip BC,	-

No	Author/Year	Journal	Human/Animal/ <i>in-vitro</i>	Patients/Aneurysms	Location	Aneurysm type	Imaging Modality	Software used	Haemodynamic Variables analyzed	Results	Boundary Condition Applied	Type of Analysis	Assumptions Made	Salient features of study
25	Bordas et al	<i>Interventional Med Applied Sci</i> 2013	<i>In vitro</i>	1	PComA MCA AComA	Saccular	MRA	*Surface Extraction and 3D Modeling: NA *CFD: Meshing: Ansys ICEM CFD: Fluent, (ANSYS, Canonsburg, Pennsylvania)	WSS Velocity	Good agreement was found between experimental and CFD results	MRA LDV =Laser Doppler Velocimetry	Transient	Newtonian Fluid, Rigid Vessel Wall, Non Slip BC,	Validates CFD for analysis of Haemodynamic indices in IAs

26	Levitt et al	<i>AJNR</i> 2014	Human	4/4	ICA	Saccular	3DRA	<p>*Surface Extraction and 3D Modeling: Vascular Modeling Toolkit (Bergamo, Italy; www.vmtk.org)</p> <p>*CFD: Meshing: Gambit CFD: Fluent, (ANSYS, Canonsburg, Pennsylvania)</p>	Blood Flow Pressure WSS	Flow diverter stents lead to significant intra-IA reduction in WSS and WSS Gradient and a trend in reduced blood flow- that may induce thrombosis in IA	Pressure and velocity was measured by Intravascular Probe Sensors directly in the Intracranial Vessels and IA	Transient	Newtonian Fluid, Rigid Vessel Wall, Non Slip BC,	CFD simulations of Flow Diverter Stents, Use of Intravascular Probe Sensors to measure the Pressure and Velocity directly in the Intracranial Vessels and IA
----	--------------	---------------------	-------	-----	-----	----------	------	--	-------------------------	---	---	-----------	--	--

Transient vs. stationary analyses: Whereas, the blood-flow entering into the domain is pulsatile (varying according to the stage of cardiac cycle), for the sake of simplicity, sometimes authors perform analyses considering blood-flow as stationary or steady state. Most of the analyses in my review (19, 73%) however, were performed using pulsatile blood-flow shown, as transient analyses in the Table-9. 12% (3) analyses were stationary while the information was not available in another 12% (3) studies. One analysis was performed using both methods, transient as well as stationary.

Assumptions made: As stated above, it is often difficult and impractical to measure all Boundary Conditions in a given patient, most of the authors tend to make some assumptions while performing CFD Analyses of Intracranial Aneurysms. In this review author found that 24 (92%) studies made assumptions that blood is a Newtonian fluid, vessel walls are rigid, and boundaries of domain are non-slip. In addition to these assumptions, one study also made assumption that shape and size of the intracranial aneurysm does not change before and after rupture. Information was not available in one study.

Haemodynamic variables analysed: Wall shear stress (WSS) is the most important haemodynamic variable receiving attention of maximum number if researchers worldwide. In this review I found the same pattern with 22 (85%) studies computing WSS. Different types of WSS computed were; WSS gradient, time-dependent WSS, time-averaged WSS, max and min WSS, spatially-averaged WSS, etc. Next two haemodynamic variables analysed were Flow Patterns and Jet Stream Impingement (8, 31% each) followed by Pressure and Velocity (7, 27% each), Flow-rates, Residence Time, Basins of Attraction, Effects of Geometry of Parent Vessel and Neck Size on the haemodynamics, Position of deployment of Stent, etc.

Results and Salient Features: This short review draws attention towards a number of important factors. Most common unanimous conclusion from the studies reviewed was that High WSS favours Initiation of Aneurysm as well as Low WSS promoting the Aneurysmal Growth and Rupture (12, 46% studies). Good correlations were also demonstrated between Rupture of IAs and Complex Blood Flow, Unstable Blood Flow, Mixing of Blood, and Small Impingement Zone by 9 (35%) authors. Other parameters analysed were; High Pressure and High Velocity correlates with Initiation, Flow patterns inside IAs change with cardiac cycle, High flow seen at neck, WSS increases with curvature of vessel and Neck size of IAs, CFD can be used to model interventions, Significant effects of Upstream Parent Vessel on the IA Haemodynamics, WSS changes with Time and Radii of Vessels, Position of Stent Affects WSS and Impact Zones, High WSS

associated with Re-canalization of coiled IAs, Experimental Validations of CFD show Good Correlation, etc.

2.8: Conclusions

Intracranial Aneurysms share a multifactorial aetiology with haemodynamics playing an important role. Though therapeutic management of IAs has evolved in past few decades but the issues that still remain unresolved are to identify patients at risk of developing IAs and take preventive measures. The flow of blood inside the intracranial vasculature, the shape of the IA and its structural properties, has long been thought to play a role in their aetiopathogenesis. Computational Fluid Dynamics (CFD) is providing a useful alternative to predict blood flows where detailed in vivo measurement of haemodynamic flow variables is not possible. Important haemodynamic factors to be considered by a number of authors are Wall Shear Stress (WSS), Oscillatory Shear Index (OSI), Pressure, Jet Impingement, Flow Patterns and Stability over time and space, Complexity of Flow, etc. In future these factors can be used as new descriptors to predict the risk of rupture for these lesions.

CHAPTER 3.0: MATERIALS AND METHODS

OVERVIEW

- 3.1. Introduction
- 3.2. Project @neurIST
- 3.3: Ethical Approvals
- 3.4: Recruitment of patients
- 3.5: Data collection and organization
- 3.6. Software @neuFuse: Development and
- 3.7. Boundary conditions used in different studies: Measured and 1D model
- 3.8. Statistical analysis
- 3.9. Designing and Performing Different CFD Studies

**My contribution: The tool-chain (e.g. @neuFuse) were primarily developed by computer scientists (including Dr Alberto Marzo, Dr Mari-Cruz Villa-Uriol, etc., as detailed in acknowledgement section) working in project @neurIST, however, I played major role in the clinical evaluation to gather users' feedback that was used in the improvement of these tools. I was also responsible for recruitment of the patients/ volunteer form Sheffield Centre including consenting and facilitating Scans, etc.*

3.1. Introduction

One of the most important parameters that can be used to assess the quality of a good study is the ease with which it can be replicated and, ability to reproduce similar results by other researchers independently. Results of any study can only be replicated consistently and reliably if materials and methods are constant across the researchers who are trying to replicate the research. A clear and detailed description of materials and methods used in any research is thus of paramount importance. The materials and methods used in different studies while conducting the work presented in this thesis are described here in detail.

3.2. Project @neurIST

Overview

@neurIST [@neurIST Project 2007, Project Identifier: IST-2004-027703, www.aneurist.org], was a major multidisciplinary European initiative funded by the European Commission with a budget €17 million. The main co-ordination of the project



Figure 3.1- Project @neurIST

is done from Center for Computational Imaging & Simulation Technologies in Biomedicine, Universitat Pompeu Fabra, Barcelona, Spain.

The total duration of the project @neurIST was 4 years- from January 2006 to December 2009. The period was extended further for another three months until March 2010. The studies included in this thesis were conducted as a part of project from March 2008 to March 2010. Studies were mainly done jointly in the Departments of Neurosurgery and Neuroradiology, Royal Hallamshire Hospital, and the Academic Unit of Medical Physics, Department of Cardiovascular Science, University of Sheffield, Sheffield, UK, with collaborations and support from other project partners.

The project brings together neurosurgeons, neuroradiologists, epidemiologists, engineers, biologists and computer scientists from 32 European institutions, both public and private, in 12 countries (Figure-3.1) to develop a usable interface for personalised risk assessment and treatment of patients with IAs and SAH. The University of Sheffield and the Sheffield Teaching Hospitals NHS Trust played a major role in the development of image-processing and computational tools to provide new, non-observational measures for the characterisation of the disease. Activities in the project are executed through different suites, as outlined below briefly:

1. **@neuLink:** The suite is aimed at exploring the genetic aspects of IAs and linking them to their initiation, growth and rupture. It also facilitates successful application of data-mining, text-mining or micro array analysis leading to the development a model of the molecular mechanisms involved in the disease forming a platform for the future genetic epidemiological studies thus facilitating the process of molecular genetics.
2. **@neuFuse:** @neuFuse is the state of art software developed in the project that fuses diagnostic, modelling and simulation data into a coherent representation of the patient's condition. 3 dimensional models of the intracranial vasculature and intracranial aneurysms can be created starting from the patient medical image @neuFuse can solve these models to provide a prediction of haemodynamic, morphological and structural indices inside an IA. More details of @neuFuse are given below in the relevant section.
3. **@neuRisk:** @neuRisk provides clinicians a tool to facilitate the personalised risk assessment and guidelines establishment to treat patients by integrating the various sources of information (molecular to

clinical level). The management of unruptured intracranial aneurysms will be improved by optimizing the decision-making process. The goal of @neuRisk is to reduce the number of unnecessary treatments by 50%, leading to reduction of risks to the patient and economic savings.

4. **@neuEndo:** @neuEndo is developing computational tools to optimise and customise the design of endovascular devices. These tools simulate the structural, haemodynamic and biological responses of the body to the deployment of stents and coils before the procedure. This will serve not only the manufacturers in the design of these implants, but also the medical end-user in the planning of an intervention. Additionally, with the help of advanced numerical-simulation tools it can predict the occurrence of device-induced thrombosis and drug elution processes.
5. **@neuInfo:** @neuInfo enables accessing clinical and epidemiological data distributed in different databases. Different data sources can be searched using a query user interface linked to the actual physical data sources. It allows direct navigation through different specific knowledge domains.
6. **@neuCompute:** @neuCompute provides distributed (remote) computing capabilities to @neurIST ensuring secure data transport. This integration of computing resources supports computationally demanding tasks such as complex modelling and simulation demanded by the integrative suites @neuRisk, @neuLink, @neuEndo and @neuFuse. A focus is placed on interoperability and integration, leveraging on existing technologies.
7. **@neuQuest:** This data entry software was used to enter the clinical, social, radiological etc. data about the recruited patients across the project.
8. **@neuBrowser:** The data entered through @neuQuest at different locations is integrated through this suite. With the help of this unique software categorization and basic analysis of the data can be done along with its graphical representation.

3.3. Ethical Approvals

The project has appropriate ethical approvals for the required research. All partners involved in the project took separate ethical approvals from their local ethical committees after satisfying their requirements. The ethical matters for UK are managed by Project Ethical Committee, Oxford, UK (Oxfordshire Research Ethics Committee-A Study Number: 07/Q1604/53).

3.4. Recruitment of patients

The patients involved in different studies were recruited through seven clinical centres across Europe after taking informed consents. The clinical

centres responsible for the patient recruitment and data collection are: Royal Hallamshire Hospital and Sheffield Teaching Hospitals NHS Trust, Sheffield, UK; John Radcliffe Hospital, Oxford, UK; Université de Genève, Geneva, Switzerland; Medical University of Pecs, Hungary; Erasmus Medical Centre, Rotterdam, The Netherlands; Hospital General de Catalunya, Barcelona, Spain; and Hospital Clinical i Provincial de Barcelona. More recently, Dr. A. Asenjo Institute of Neurosurgery & Neuroradiology, Santiago, Chile, and Beaumont Hospital, Dublin, Ireland have also started the process of joining the project. Total number of cases was 1591, recruited through all clinical centres.

3.4.1: Demography of Recruited Cases

A total number of 1591 cases were recruited to @neurIST through all 7 clinical centres. A brief overview of different demographic characteristics of the recruited population is given in Tables-3.1 and Table-3.2.

The patients were recruited randomly either in a retrospective or prospective manner through Neurosurgical Clinics and Wards. However, due to low risk of rupture majority of the population was recruited retrospectively. Depending upon the type of consent patients gave, blood samples were also collected and analysed for exploring the genetic aspects of the disease. In order to compare the characteristics of the case cohort, population matched controls were also recruited through the same sources.

Table: 3.1. Demographic details for all recruited cases in project @neurIST

Location	No.	Aneurysmal aspect	No.	Side of the IA	
Total recruited	1591	Total recruited	1591	Total recruited	1591
Info about IA location available	1264	Info about IA aspect available	1036	Info about IA side available	893
No-info about IA location available	327	No info about IA aspect available	555	No info about IA side available	698
Intracavernous internal carotid	61	Smooth	812	Left	347
Ophthalmic segment carotid	111	Rough	224	Midline	183
Medial wall carotid	31	Presence of blebs on IA		Right	363
Posterior Communicating	200	Total recruited	1591	Endovascular treatment	
Ant Choroidal segment carotid	25	Info about IA blebs available	1102	Total recruited	1591
Anterior and superior wall carotid	6	No info about IA blebs available	489	Info about IA endovascular treatment available	750
Carotid bifurcation	56	No bleb present	841	No info about IA endovascular treatment available	841
A1 segment ant	26	One bleb present	190	Parent vessel occlusion	6
Ant communicating artery	231	Two blebs present	44	Coil - Balloon remodelling	23
A2 segment ant	10	Multiple blebs present	27	Coil - 3D Bare	142
Pericallosal cerebral artery	24	Presence of lobules in IA		Coil - 3D Coated	98
Distal ant cerebral artery	4	Total recruited	1591	Coil – Random Shape -Bare	428
M1 segment middle cerebral artery	130	Info about IA lobules available	1117	Coil – Random Shape –Coated	53
Sylvian bifurcation	175	No info about IA lobules available	474	Stent - Covered stent - self expanding	5
Distal to sylvian bifurcation	10	No lobule present	835	Stent - Leo - self expanding	4
V4 segment vertebral artery	5	One lobule present	160	Stent - Neuroform - balloon expandable	10
PICA	32	Two lobule present	107	Stent - open entry - balloon expandable	9
AICA	7	Multiple lobule present	15	Other endovascular procedures	15
Superior cerebellar artery	24	Total recruited	1591	Stimulant abuse	
Basilar trunk	10	Ruptured vs. Unruptured IAs		Total recruited	1591
Basilar Tip	74	Total recruited	1591	Info about stimulant abuse available	822
P1 Posterior cerebral artery	4	Info about IA rupture available	1260	No info about IA stimulant abuse available	709
P1-P2 junction posterior cerebral artery	5	No info about IA rupture available	331	Cocaine	12
P2 posterior cerebral artery	1	Unruptured	693	Amphetamine	2
Distal posterior cerebral artery	0	Ruptured	567	Diet pills	2
Ophthalmic artery	2	Total recruited	1591	Nasal spray	28
Type	No.	Genetic tissue samples collected		Oral decongestants	7
Total recruited	1591	Total recruited	1591	None	771
Info about IA Type available	1263	Total samples collected	2658		
No info about IA Type available	328	Blood	928		
Saccular side wall	377	Tissue from IA dome	14		
Saccular bifurcation	869	Leucocytes	271		
Fusiform dissecting	12	Plasma	315		
Fusiform non-dissecting	3	DNA	299		
Fusiform segmental ectasia	1	PAXgene	792		
Fusiform transitional	1	No info about sample available	39		

Table: 3.2. Main known risk factors for IA development and SAH in the recruited population

Risk factor	No.	Moyamoya	
Total recruited	1591	Info about moyamoya available	1132
Sex		No-info about APKD available	459
Info about sex available	1327	Moyamoya absent	1129
No info about sex available	264	Moyamoya present	3
Males	455	Associated AVM	
Females	872	Info about AVM available	1133
Ethnicity		No-info about AVM available	458
Info about ethnicity available	1075	Associated AVM absent	1125
No-info about ethnicity available	516	Associated AVM present	8
Arab	5	ED syndrome	
Japanese	1	Info about EDS available	1132
Eurasian, Albanian	2	No-info about EDS available	459
Eurasian, Anglo-Celt	298	EDS absent	1131
Eurasian, Baltic	1	EDS present	1
Eurasian, Basque	4	Aortic coarctation (CoA)	
Eurasian, Caucasian	42	Info about CoA available	1130
Eurasian, French	77	No-info about CoA available	461
Eurasian, German	10	CoA absent	1125
Eurasian, Hungarian	161	CoA present	5
Eurasian, Italian	21	Family history (FH) of SAH	
Eurasian, Other	152	Info about FH available	1141
Eurasian, Portuguese	10	No-info about FH available	450
Eurasian, Romanian	2	FH of SAH absent	965
Eurasian, Slav	6	FH of SAH present	176
Eurasian, Spanish	175	Smoking	
Iranian-Median, Kurd	1	Info about smoking available	1090
Latin-Caribbean Americans	14	No-info about smoking available	501
Malay, Filipino, Java	2	Never smoked	482
North American	1	Active smokers	341
South Asian, Indian, Nepali	2	Ex-smokers	267
Undefined	87	Hypertension (HTN)	
Coagulopathy		Info about HTN available	1198
Info about coagulopathy available	775	No-info about HTN available	393
No-info about coagulopathy available	816	No HTN	794
No coagulopathy	766	HTN – not treated	73
Coagulopathy present	9	HTN - treated and controlled	301
Abdominal aneurysm (AAA)		HTN - treated and poorly controlled	30
Info about AAA available	1130	Multiple IAs	
No-info about AAA available	461	Info about multiplicity available	1119
AAA absent	1125	No-info about multiplicity available	472
AAA present	5	Solitary lesions	200
APKD		Multiple IAs	919
Info about APKD available	1129	Past SAH	
No-info about APKD available	462	Info about past SAH available	1151
APKD absent	1118	No-info about past SAH available	440
APKD present	11	No past SAH	1105
Alpha-1 antitrypsin deficiency (A-IAD)		Past SAH present	46
Info about A-IAD available	1132	Marfan's syndrome	
No-info about A-IAD available	459	Info about Marfan's Synd. available	1133
A-IAD absent	1131	No-info about Marfan's Synd. available	458
A-IAD present	1	No Marfan's Synd.	1131
Oral contraceptives (OCP) use		Marfan's Synd. Present	2
Info about OCP use available	1142	Heart disease	
No-info about OCP use available	449	Info about heart disease available	1131
No OCP	1090	No-info about heart disease available	460
OCP users	52	No heart disease	1120
		Heart disease Present	11

3.5. Data collection and organization

3.5.1: @neuQuest & CRIM (Clinically Relevant Information Model)

The relevant clinical, demographic, social and radiological information of the participants was collected using the data entry software @neuQuest (Figures 3.2 and 3.3) @neuQuest is a GUI (Graphical User Interface) based software developed in Sheffield initially to collect local data but finally used by most of the clinical centres in @neurIST.

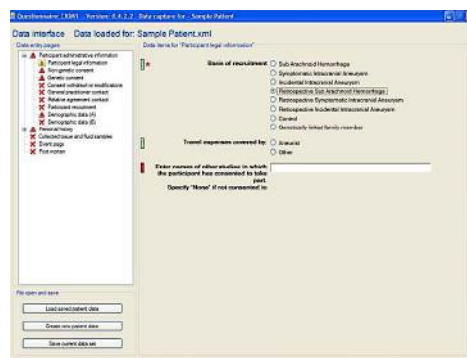


Figure 3.2: @neuQuest GUI (Graphical User Interface)

3.5.2: Data collection using @neuQuest: An editable definition file lists

the data fields to be collected both in terms of data type (date, text, number, etc.) and description of the item. All data entered into @neuQuest is recorded with audit information. Whereas, as much as possible information was collected, a minimum number of dataset also defined to prioritize the entry of information at the fastest possible pace without

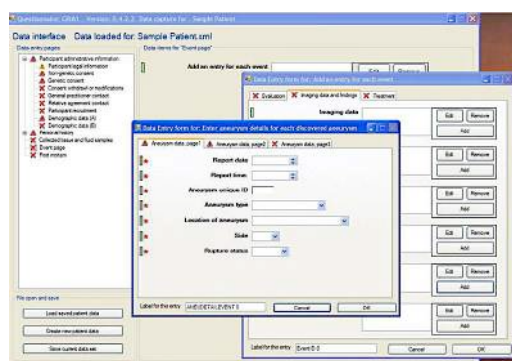


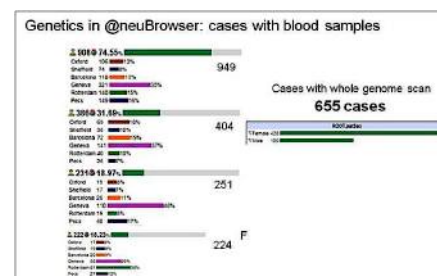
Figure 3.3: @neuQuest GUI –Data Collection

missing the most vital bits through CRIM (clinically relevant information model). Collected data is made available outside the clinical environment after a rigorous anonymization process. The medical DICOM images selected in @neuQuest are also anonymized prior to export. Files anonymized for export are uploaded to an @neurIST DataNode where the data is imported into a database ready for users to query. @neuQuest also includes the functionality to scan patient DICOM imaging studies and automatically completes data sets.

3.5.3: Testing of the software and processing events: The @neuQuest suite and the routines for collecting data, anonymizing data and distributing data have constantly been tested by the clinical sites. Feedback has allowed new functionality to be added and issues to be fixed. The ultimate goal is @neuQuest to be adapted by many centres world over once the @neurIST and its products are taken over by ESMINT (European Society for Minimally Invasive Neurological Therapy).

3.5.4: @neuBrowser

The anonymized data in @neuQuest software from all clinical centres were finally uploaded to a common server. This data was then passed to a central server called @neuBrowser (Figure-3.4) @neuBrowser is another state of the art



tool developed with project @neurIST. Apart from organizing and categorizing the data it can also present the information in nice and easy to understand graphs.

Figure-3.4 @neuBrowser- showing graphical representation of data

3.5.5: Image Acquisition and Processing

The medical images used in different studies were obtained using rotational acquisition in a Philips® Integris™ Allura™ machine (Philips® Medical Systems, Best, The Netherlands), producing 100 images in 6 seconds, with 5 milliseconds exposure per image. Voxel size (Voxel is a 'blend word' derived from 'volume' and 'pixel' whereas 'pixel' itself is a combination of 'picture' and 'element'. A Voxel therefore represents the smallest distinguishable boxed shaped part of a 3D image) in the reconstructed 3D images was either 121 microns or 234 microns (depending on the study, as specified in the beginning of each study) with reconstruction matrix of either 512x512x512 or 256x256x256 (depending on the study, as specified in the beginning of each study). All images were anonymized, respecting the @neurIST ethical approval for use of patient data.

The current version of the @neuFuse software (prototype 4), based on the Multimod Application Framework [Viceconti et al 2004] and developed within the @neurIST project, was used to reconstruct the vessel surfaces, create the model and set up the haemodynamic analysis. The solvers used within @neuFuse to solve the fundamental equations describing the blood flow behavior within the region of interest were ANSYS®-ICEM™ and ANSYS®-CFX™ (Ansys®, Inc., Canonsburg, PA, USA).

All analyses performed were pulsatile except for the workshops conducted for the evaluation of @neuFuse software, where simple stationary analyses (non-pulsatile but constant flow rate and pressure at the openings of the region of interest) were performed by the participants using Intel® core duo 2.4 GHz machines, with 2 GB RAM and 512 MB of dedicated graphic memory.

3.6. Software @neuFuse

By definition, @neuFuse is a computer-aided medicine-application (CAM-application) software that integrates the visualization, modelling and simulation of multimodal biomedical data with specific respect to Intracranial Aneurysms. In the broad context of an integrated IT system for IA management, the *role* of such a suite is to gather clinical structured information from electronic medical records, and the unstructured functional imaging, to provide a state-of-the-art environment for medical imaging processing and modeling aimed at producing a structure of three distinguished complex derived indicators: morphological, haemodynamic, and structural. The derived data is then used by epidemiologists to find the definitive correlations to assess the risk of rupture. Innovative key elements are the capability of combining medical imaging data, simulation results and morphological indicators into a coherent set of patient-specific data, properly fused and interactively accessible from within an easy-to-use application and the development of a *fat client* that exploits the client hardware capabilities in advanced visualization while being fully integrated with the backend Grid infrastructure [Rajasekaran 2008].

3.6.1 Development of @neuFuse: Contributions and Process

@neuFuse is a result of joint collaboration received from several project partners that contributed at different layers by providing specific algorithmic *plug-ins*, or by providing application's modules for a specific task, or by providing software libraries to connect to a specific service. In brief, **Universitat Pompeu Fabra (UPF)**, Barcelona (Spain) provided the advanced medical imaging functionalities such as the segmentation and the skeletonization *plug-ins*. **NEC Europe Ltd** (Germany) contributed to

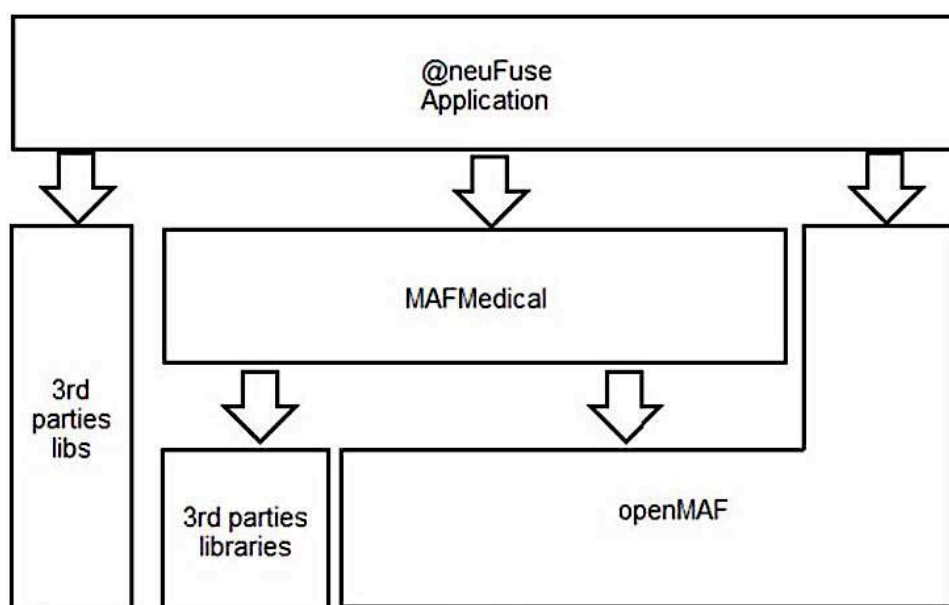


Figure-3.5: @neuFuse Software architecture

the data model design and provided routines for preprocessing the geometric models of vessel in an appropriate format for CFD solvers. **Erasmus Medical Centre** (The Netherlands) contributed in enhanced imaging filtering *plug-in*. **The University of Sheffield** (UK) and **Ecole Polytechnique Federale de Lausanne** (Switzerland) provided and integrated the 1D circulatory model. **GridSystems S.A.** (Spain), **NEC Europe Ltd** (Germany) and **University of Vienna, Institute of Scientific Computing** (Austria), provided the Grid-connectors libraries. **University of Bedfordshire (former University of Luton)** (UK) contributed to develop advanced graphics interface to visualize and manipulate vessel geometries. **Super Computing Solution (s.r.l. B3C)**, Bologna, (Italy) was responsible for most of the development of the software, the integration and the maintenance. Major versions of @neuFuse applications have been released routinely every six months and it is being used by six clinical pilot centers (UPF, UNIGE, USFD, EMC, OXF, PEC).

All these software components were integrated on an existing backbone, provided by the Multimod Application Framework. MAF is an open source freely available framework (MAF, <http://www.openmaf.org>) for the rapid development of applications based on the Visualisation Toolkit (www.vtk.org) and other specialized libraries. It provides high-level components that can be easily combined to develop a vertical application in different areas of scientific visualization (Figure-3.5). *OpenMAF* is further extended by an additional software layer, called *MafMedical* that contains all MAF components specific to the biomedical application domain. A generic *MafMedical* application, such as @neuFuse, is defined by choosing from the framework the necessary components, and eventually specialising them. It is also possible to develop *ad hoc* components that are necessary only to the application itself, and plug additional third party libraries.

There are four types of components that form any MAF application: *Virtual Medical Entities (VME)*; that are the data objects, *Views*; that provide interactive visualisation of the VMEs, *Operations*; that create new VMEs or modify existing ones, and interface elements; generic *graphic user interface (GUI)* components that define the user interface of the application.

3.6.2 @neuFuse: Work Flow at a Glance

Haemodynamic modeling of cerebral aneurysms involves several steps (Figure-3.6). It starts with the retrieval of medical images in DICOM or

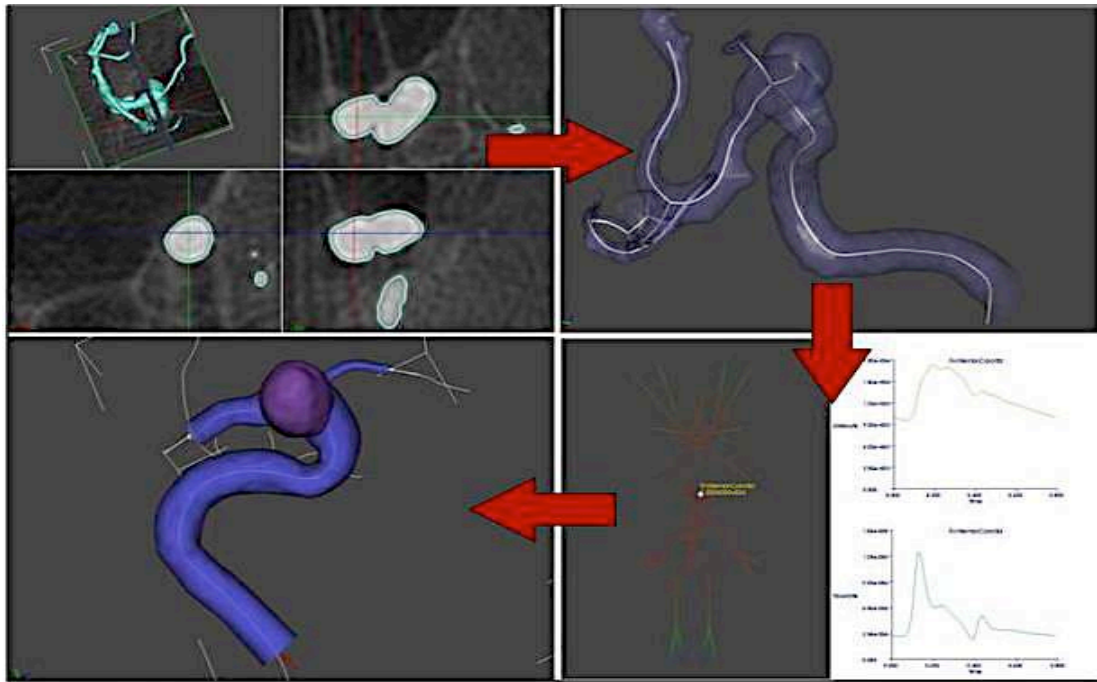


Figure-3.6: @neuFuse CFD processing toolchain. Form top right clockwise: DICOM images ate loaded and the vessel geometry segmented. Then a topologically correct geometric model is processed to extract vessel Centre line (axis). This information is then used to map 3D vessels with a 1D circulatory model. This mapping allows deriving flow boundary conditions for haemodynamic model.

V3D format; creation of a geometric model of the vasculature; topological reconstruction of the vasculature, assignment of boundary conditions to the domain from the 1D flow model and, solution of the flow equations that are actually demanded for a specific off-the-shelf software. The main steps involved in the process are given below.

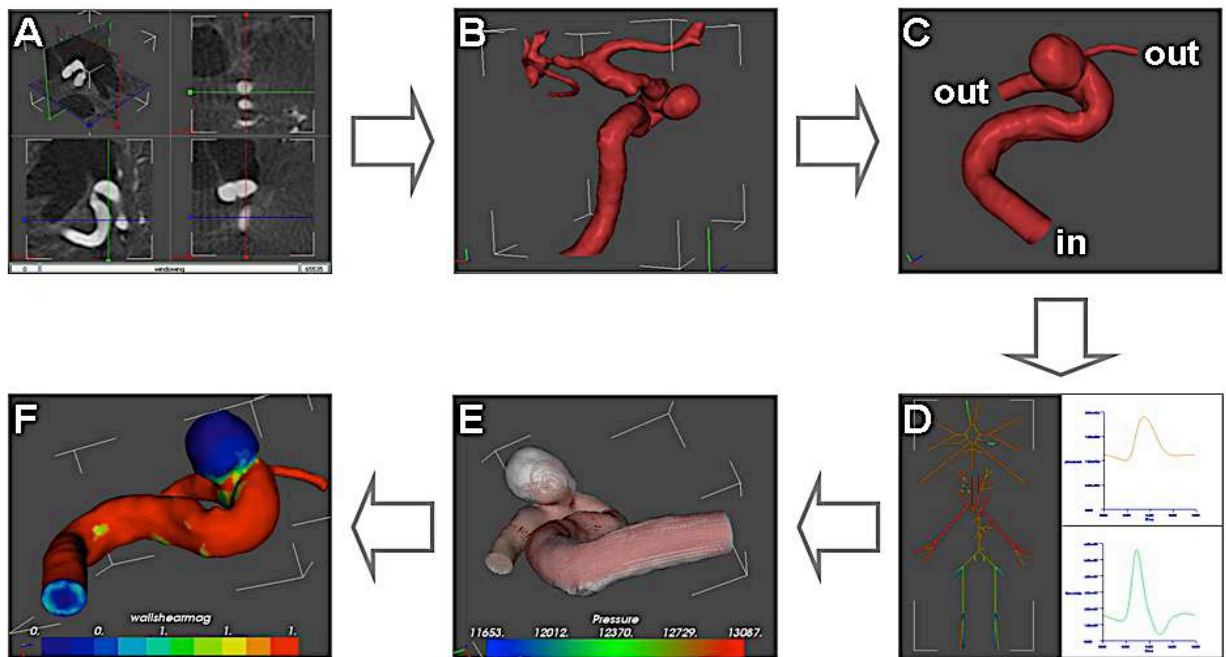


Figure 3.7: Operation workflow from medical image to haemodynamic results. A) Orthoslice visualization of the 3DRA medical image in @neuFuse. B) Visualisation of the extracted vessel surface. C) Visualisation of reduced region of interest with location of inlet and outlet openings. D) 1D circulation model. E) Visualisation of predicted streamlines. F) Visualisation of predicted wall shear stress.

Segmentation: The very first step to build CFD models of an IA is extraction of geometrical representation of the cerebral arteries from a medical image. Segmentation is a process where every pixel (or voxel in case of a medical images stack) of the image is labeled in order to form a small set of pixel clusters known as segments, to obtain a representation that is easier to analyze. The first product obtained here as a result of segmentation is the set of voxels that have been labeled as interior surface of the vasculature corresponding. In the literature, many different approaches are documented, but whereas some of these methods give acceptable results with a particular imaging modality; other methods are too operator-dependent. To combat the issue an automatic, multi-modal algorithm [Hernandez and Frangi 2007] has been developed and integrated in @neuFuse. Automatic segmentation could compute an accurate model of the arteries in few minutes.

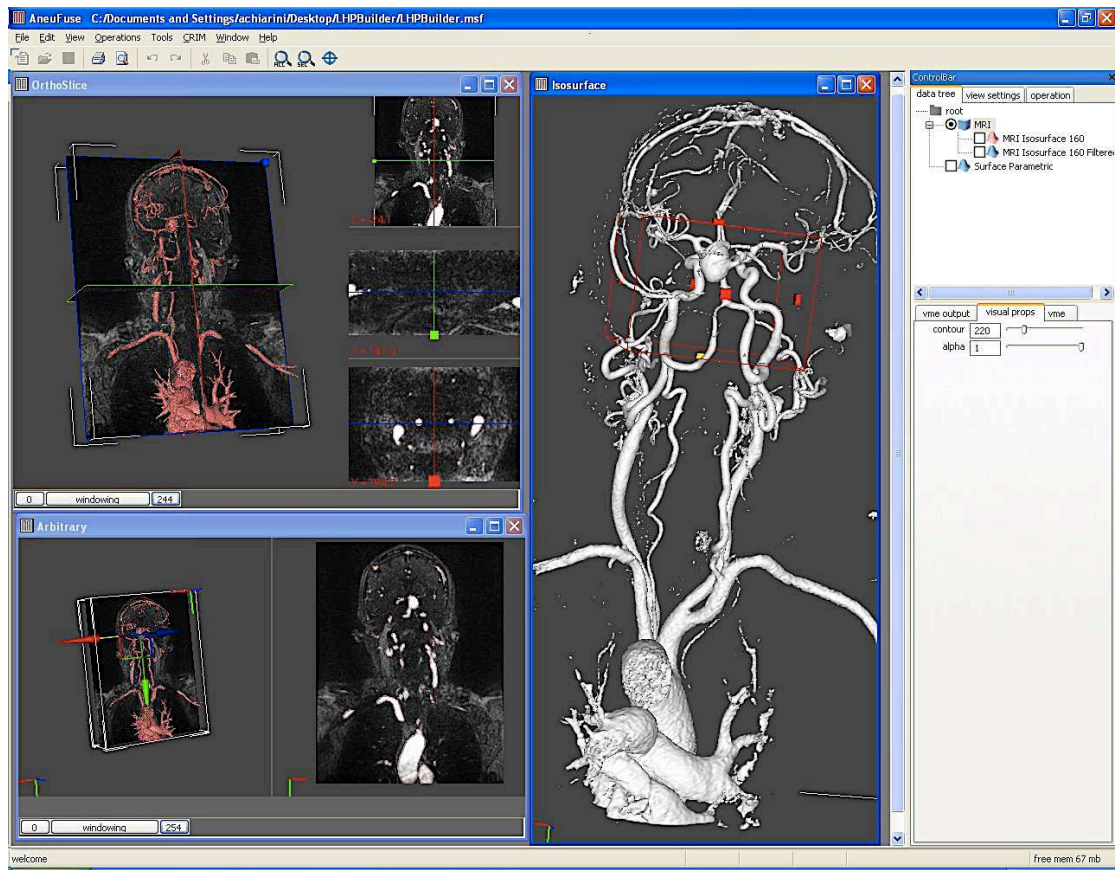


Figure-3.8: A snapshot of 3D volume generation, segmentation and clipping of the ROI

Geometric Healing: Lack of resolution or other contrast medium artifacts could generate errors in the automatic segmentation process that should be resolved by the operator. A typical example is the “kissing vessels” problem due to a lack of the image resolution. Two close vessels are glued together by the reconstruction algorithm, but in reality they are separate. If this problem is not solved before modeling, it may result in a gross error. To address this kind of problem, the @neuFuse operator should check that the resulting geometry is a topologically correct representation of the cerebral arteries and eventually fixes with a set of general-purpose tools, in a way which is similar to photo editing software.

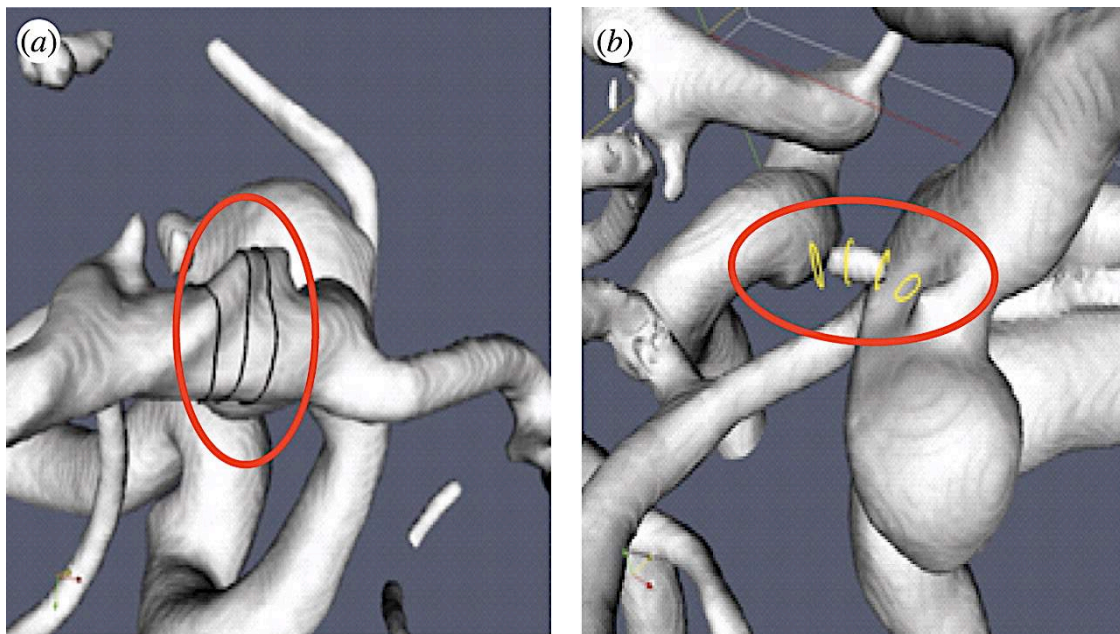


Figure-3.9: A typical example of geometric healing where an artifact (a) and (b) “kissing vessels” can cause distortion of real geometry due to lack of the image resolution. Two close vessels are glued together by the reconstruction algorithm, but in reality they are separate

Vasculature Topology- Skeletonization: Once the geometric model is topologically correct, the next step is to extract the vasculature network. This process is called skeletonization because the result is a kind of graph that represents the vessels [Mellado et al 2007]. This representation is fundamental for many purposes; with this information it is possible to navigate the vessels, to check vessel diameters along a specific artery and, to plan an endovascular treatment choosing the position for deploying a stent.

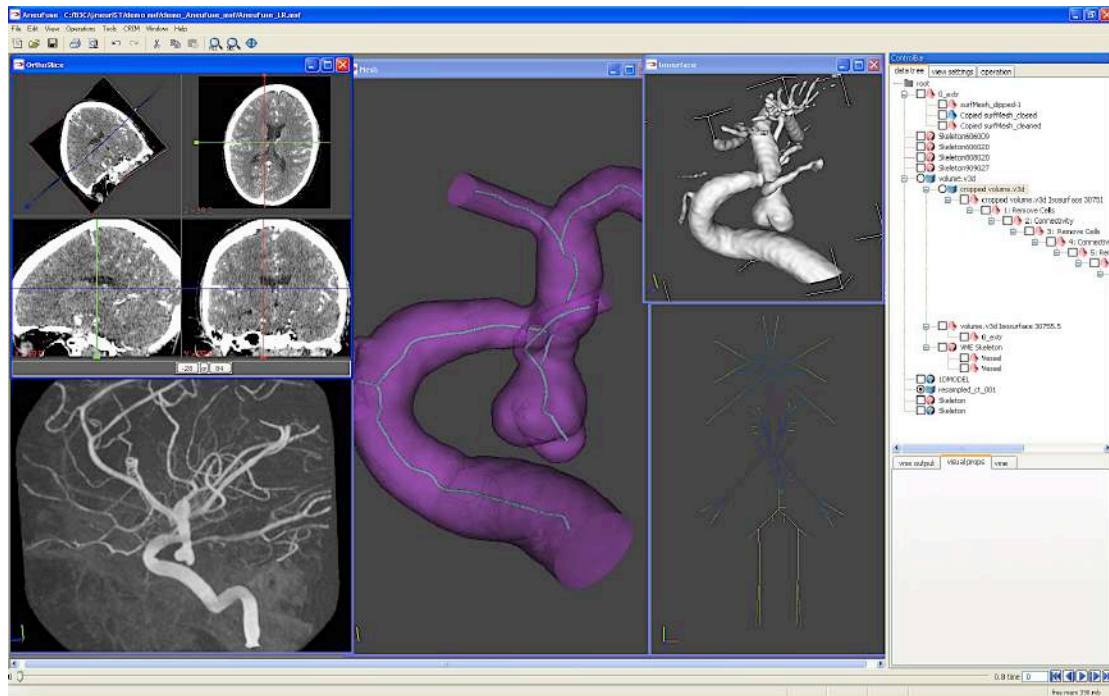


Figure-3.10: Process of defining the centre line and Skeletonization

Boundary Conditions assignment: In this step the operator defines the domain of the flow simulation by localizing the inlets and outlets in relation to the vessel skeleton. Followed by this each vessel in the patient specific geometry is literally matched with the corresponding vessel in the 1D circulatory system model. The Boundary Conditions were derived from two main sources as described below in section 3.6.

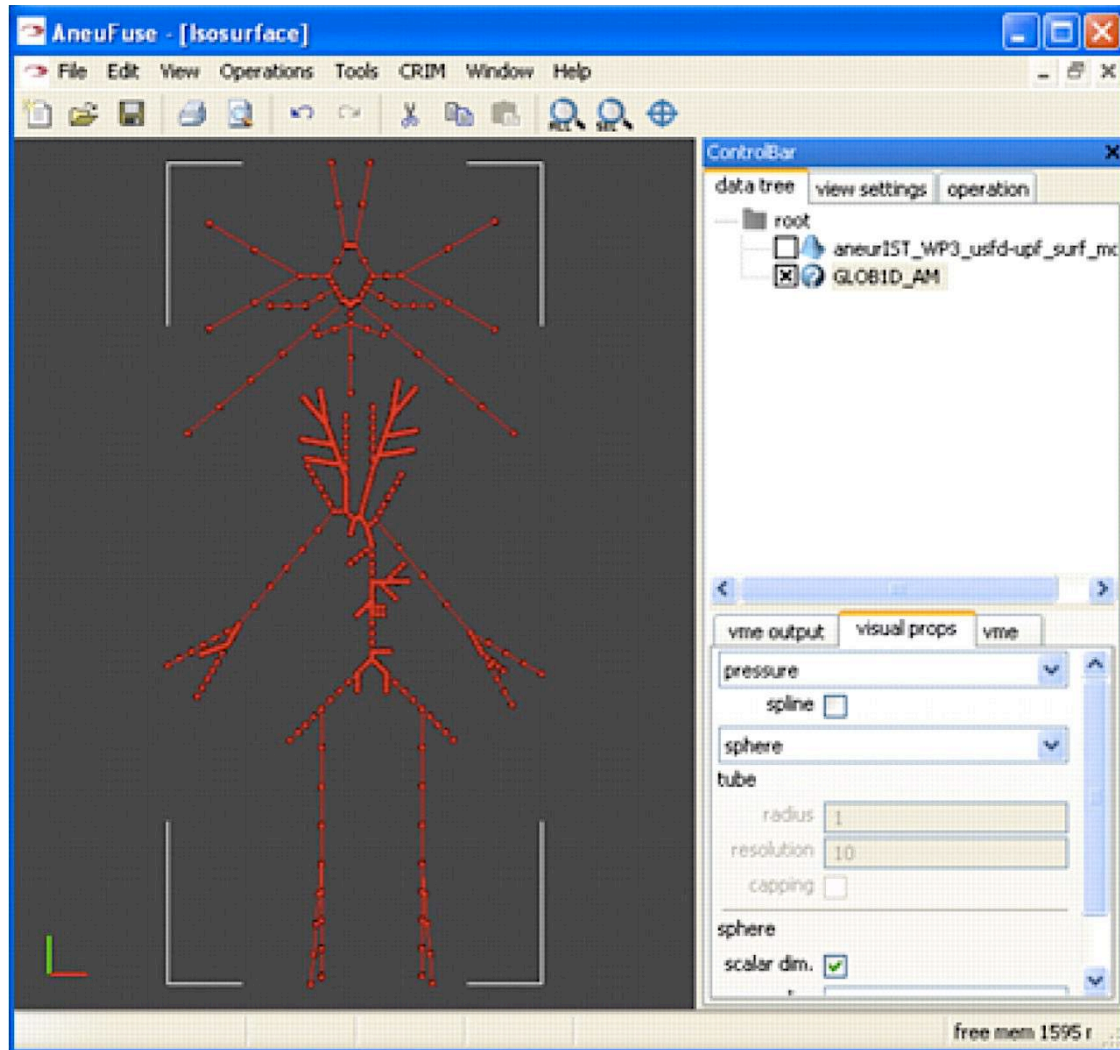


Figure-3.11- Application of BCs at the inlets and outlets using 1D Model dictionary

Solving flow equations: Once the model is completely defined, flow equations are solved. @neuFuse could launch the simulation software locally, or it can connect to the Grid infrastructure and request a remote simulation. To do so, data should be stored in a neutral format, as the simulation software could have several implementations. Then, data are processed and stored in the particular file format depending upon the solver used. The solver used in @neuFuse is ANSYS® ICEM-CFX™, which is then launched and finally results are loaded in @neuFuse.

Presenting results: The CFD solution is a very complex collection of data and it is a challenge to present them in an environment, which is coherent with the medical images and the clinical context (Figure-7). Results are composed by multi-scalar and multi-vector time-variant fields sampled on a tridimensional unstructured mesh, where each element represents an infinitesimal solid cell (typically tetrahedral).

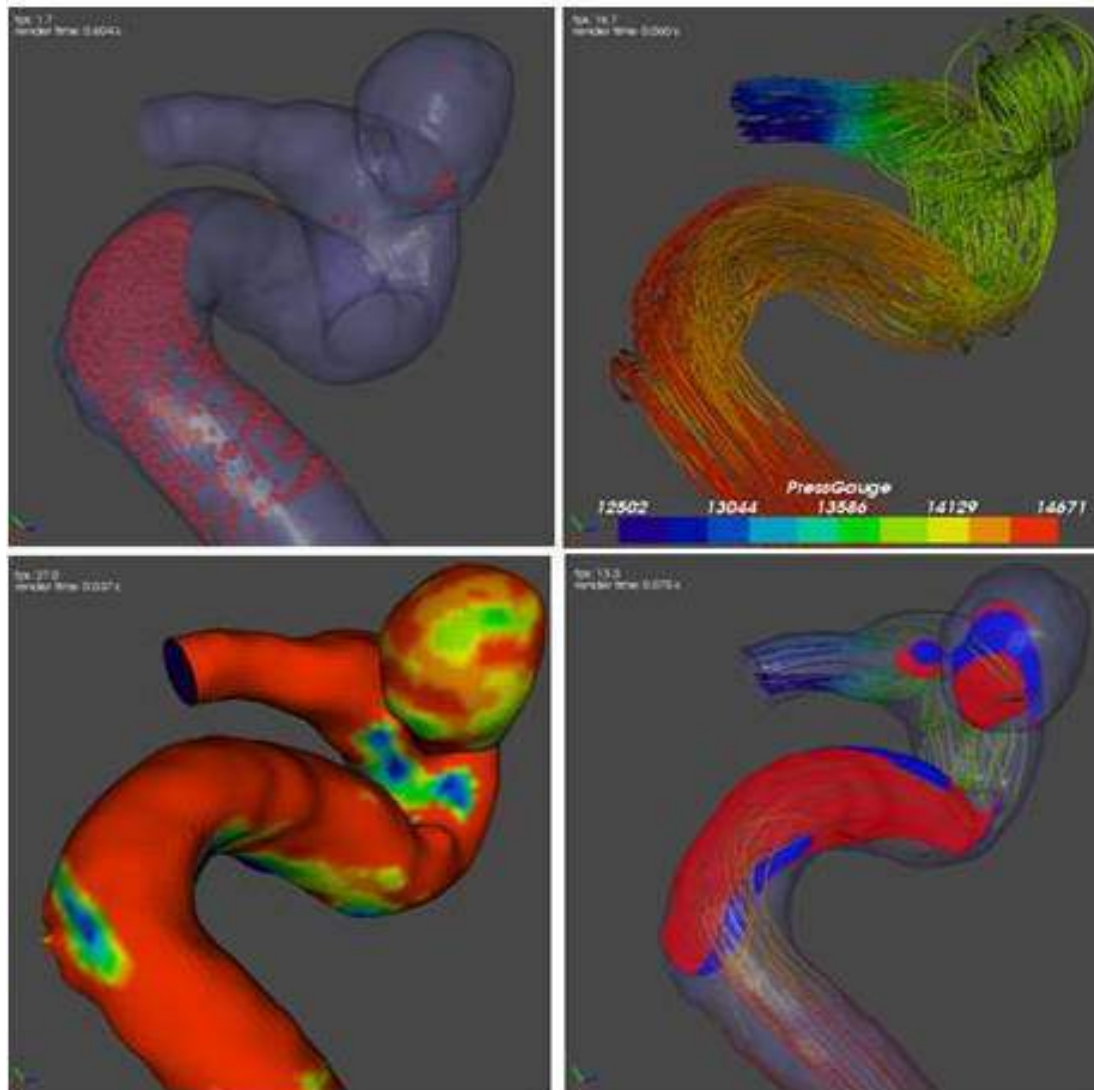


Figure-3.12: Visualization of haemodynamic simulation in @neuFuse. On top right, flow particle tracing erythrocytes are animated according to the velocity field. On top left picture, streamlines represented with pressure-coded colouring. In the bottom left picture, WSS drawn on the vessel wall. On bottom right, complex visualization showing streamlines crossing an arbitrary plane coloured according a colour-code where red regions represent inward flow whilst represent outward flow regions.

Typical representations for flow (velocity) fields are streamlines that represent the tangent of the velocity fields. Streamlines then are usually colored according the pressure gradients. To give an idea of the flow pattern, I introduced a particle tracer. It enables the visualization of flow particles' position and to follow their trajectories in the boundaries for

each time-stamp of the simulation, by integrating the velocity field. The operator can also visualize 3D representation of the scalar fields. Vessel walls can be colored according to WSS values. Furthermore, it is also possible to superimpose scalar values on 2D original medical images. More complex, representations can also be obtained by combining those already presented.

3.7. Boundary conditions used in different studies: Measured and 1D model

Application of appropriate Boundary Conditions at the inlets and outlets of the ROI (Region of Interest or domain) remains an essential prerequisite for any accurate CFD analysis. Accuracy of our predictions obviously depends upon the accuracy of the Boundary Conditions applied. The Boundary Conditions applied here in the studies done are derived from following sources:

1) Phase Contrast MRI (pc-MR) Scan: pcMR was used to measure the flow-rates in arteries at different locations to get the boundary conditions. All MR imaging and measurements were performed at high field strength (Achieva™ 3.0T, Philips® Medical Systems, Best, The Netherlands) using a standard 8-channel, radiofrequency receive-only head coil. The same radiographer imaged all patients to maximize the reproducibility of the overall acquisition technique. A pre-designed protocol guided the radiographer through the desired measurement locations for subsequent application of CFD BCs. As afferent vasculature has an important influence on intra-aneurysmal haemodynamics [Cebal et al 2005, Castro et al 2006, Moyle et al 2006, Oshima et al 2005], proximal measurements were taken at a distance of approximately 12 parent vessel diameters from the aneurysm. Measurements in distal arteries were taken four diameters away from the IAs. To minimize patient discomfort, table-occupancy time was no greater than 1 hour. Within this period, it was difficult to ensure that all measurements were obtained for all patients. The tortuous nature of the vasculature also made slice selection perpendicular to the artery difficult to achieve. To maintain integrity in the final measurement dataset, data was rejected if there was doubt about the placement of the measurement plane. Locations of pc-MR measurements are reported in Table-3.3. The manufacturer's proprietary postdata-acquisition software (Q-Flow™, Philips® Medical Systems, Best, The Netherlands) was used to estimate volumetric flow rate (VFR) waveforms at each location.

Table-3.3: Radiological characteristics of IAs included in the study along with the location, type and method of BC application

Pt.	IA No	IA Location	Size* (mm)	Neck (mm)	BC location	BC type [†]	BC Method
A	1	Lt ICA Cavernous	5.0/3.5	4.3	1.Lt ICA Proximal 2.Lt ICA Distal 3.Lt OphthA	Inlet/ velocity Outlet/ velocity Outlet/ pressure	pc-MR pc-MR 1-D
B	2	Lt MCA	11.1/7.3	4.3	1.Lt MCA Proximal 2.Lt MCA Supr-Div M-2 3. Lt MCA Infr-Div M-2	Inlet/ velocity Outlet/ pressure Outlet/ pressure	pc-MR 1-D 1-D
C	3	Lt ICA Cavernous	3.4/3.3	3.1	1.Lt ICA Proximal 2.Lt ICA Distal 3.Lt OphthA	Inlet/ velocity Outlet/ pressure Outlet/ pressure	pc-MR 1-D 1-D
D	4	Rt MCA Bifurcation	4.4/7.3	3.0	1.Rt MCA Proximal 2.Antr Temp branch of Rt MCA 3.Rt MCA Supr Div M-2 4.Rt MCA Infr Div M-2	Inlet/ velocity Outlet/ pressure Outlet/ pressure Outlet/ pressure	pc-MR 1-D 1-D 1-D
E	5	Lt ICA Subclinoid	2.9/2.5	3.1	1.Lt ICA Proximal 2.Lt ICA Distal 3.Lt OphthA	Inlet/ velocity Outlet/ velocity Outlet/ pressure	pc-MR pc-MR 1-D
	6	Lt MCA Bifurcation	2.5/2.0	2.2	1.Lt MCA Proximal 2.Lt MCA Supr-Div M-2 3.Lt MCA Infr-Div M-2	Inlet/ velocity Outlet/ pressure Outlet/ pressure	pc-MR 1-D 1-D

NB: Lt; left, Rt; right, ICA; internal carotid artery, MCA; middle cerebral artery, OphthA; ophthalmic artery, Supr; superior, Infr; inferior, Div; division, Antr; anterior, Temp; temporal. *size is reported as max diameter/max length. †BC method refers to the analyses based on patient-specific BC.

2) 1D Model: In studies where patient-specific boundaries were not available (this is specified in the beginning of each study in their respective Materials and Methods sections), the Boundary Conditions were derived from the flow-rate and pressure waveforms computed by using the 1D circulation model developed by Reymond et al [Reymond et al 2009]. Development of this 1D Model was also a part of the @neurIST Project. This is a distributed model of the systemic arterial tree, including a detailed description of the cerebral arteries, and coupled to a heart model. Authors, Reymond and colleagues, have extensively validated the 1D Model given by them by measuring the flow and pressure in a number of arterial locations in healthy volunteers and found good agreement between these measurements with the corresponding values computed using the 1D Model [Reymond et al 2009]. The distal vessels and vascular beds of the model are terminated with three-elements Windkessel models to account for proximal and distal resistance and compliance of the peripheral vasculature. Flow-rate waveforms were used for all primary inlets and pressure waveforms for all primary outlets.

3.8. Statistical analysis:

Robust and appropriate statistical tools were applied to analyze the results from different studies. Significance was calculated using Student's t-test wherever required. Quantitative comparisons of the data obtained from different methodologies were made using boxplot diagrams. SPSS™ and Excel software were used to perform advanced statistical analyses as and where required.

3.9. Designing and Performing Different CFD Studies

A number of studies were designed and performed as a part of this thesis. Next three sections of this manuscript are devoted to cover these studies as summarized below:

First section: Validations of few common concepts used often in Computational Fluid Dynamics are covered in this section. Studies were designed by applying these concepts to CFD and their validity tested. Main concepts tested are; assessing effects of two common velocity profiles and effects of measured vs. modeled Boundary Conditions are also assessed on haemodynamics of Intracranial Aneurysms.

Second section: This section covers Development and Controlled Exposures of Tool-chain.

Third section: In this section, Computational Fluid Dynamics is used as a Tool to Explore the Aetiopathogenesis of Intracranial Aneurysms. The main studies conducted were: Analysis of different haemodynamic factors during initiation and rupture of intracranial aneurysms, assessing the influence of various drugs, smoking, and hypertension on the haemodynamic characteristics of intracranial aneurysms, and effects of Aortic Coarctation on cerebral haemodynamics and aetiopathogenesis of intracranial Aneurysms.

CHAPTER 4.0: VALIDATIONS OF THE COMMON CONCEPTS USED IN COMPUTATIONAL FLUID DYNAMICS

Overview

4.1: Introduction

4.2: Effects of Different Velocity Profiles on the Haemodynamics of Intracranial Aneurysms

4.3: Effects of Measured vs. Modeled Boundary Conditions on the Haemodynamics of Intracranial Aneurysms

4.4: Discussion and conclusions

**My contribution: In both studies described in this chapter, I played major role in concept, study design, conducting review of literature, performing analyses, performing statistical calculations, writing and submission of manuscripts to journals for publications. Dr Alberto Marzo (and other biomedical scientists, as detailed in acknowledgement section) gave important support and contribution in retrieval of medical images, performing CFD analyses, and post-processing of the results.*

4.1. Introduction

Once a robust tool-chain is build by the software engineers and biomedical scientists as described earlier, the next step was to establish the reliability of the common basic concepts applied while using CFD as a tool in the analysis of haemodynamic and morphological indices in the cerebral vasculature and IAs.

Specification of boundary conditions is an important prerequisite for solving the governing equations in the extraction of these non-observable indices. As direct measurements of these flow-rate waveforms at the inlets and outlets of the domain are usually impracticable [Marzo et al. 2009], the boundary conditions are mostly derived using the available 1D Circulation models [Westerhof et al. 1969, Stergiopoulos et al. 1992, Vignon-Clementel et al. 2006, Balossino et al. 2009, Bove et al. 2008]. A number of assumptions are made while applying these boundary conditions that can strongly perturb the numerical calculations. One such assumption is application of Womersley flow profile at inlet boundary of the domain [Marzo et al. 2009]. The first study therefore was conducted to investigate the

effects of different inlet velocity profiles on the haemodynamics of IAs and compared them with the more important determinants of the haemodynamics like geometry of the domain.

The study on the effects of boundary conditions on the haemodynamics of IAs further extended by taking phase contrast MR (pc-MR) measurements for flow-rates in 19 IAs from nine patients recruited in the study [Marzo et al. 2011]. The effects of the boundary conditions derived using these patient-specific pc-MR flow-rates and the traditional 1D-model, on the haemodynamic characterization of IAs, were then compared and analyzed in order to quantify the agreements and differences in the values of derived haemodynamic indices.

4.2. Effects of Different Velocity Profiles on the Haemodynamics of Intracranial Aneurysms

4.2.1 Background and Objectives

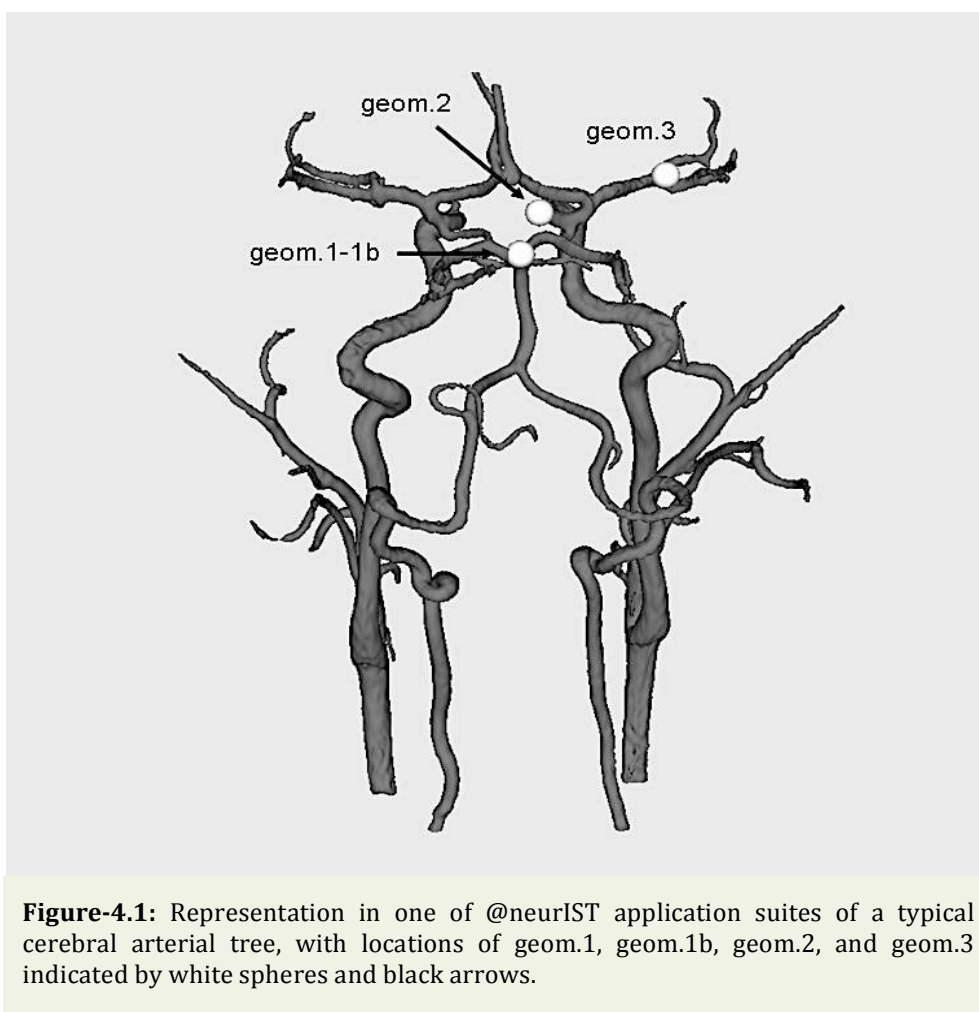
Pressure or flow rate waveforms are often available, from say magnetic resonance or 1D circulation models, as 1D values averaged over the cross sectional area of the vessel, and at specific instants along the cardiac cycle. The solution of the 3D Navier-Stokes equations, on the other hand, requires these quantities to be specified as point wise values at each node of the 3D boundary mesh. Assumptions made while completing such deficient data at boundaries is not trivial and can strongly perturb the numerical results.

Many authors rely on the theory of Womersley (Womersley 1955) for the specification of the velocity profile of flow rate-based boundary conditions, assuming that flow is fully and axially developed and behave similarly to flow in a circular pipe. This is certainly the most realistic guess but it is known that geometry remains the most important factor (Cebal et al. 2005, Moyle et al. 2006, Oshima et al. 2005) that ultimately determines the flow development in cardiovascular vessels. The over-complication of applying a Womersley velocity profiles might be unnecessary and in some circumstances unrealistic in the determination of the haemodynamics within the aneurismal sac.

Studies done so far (Myers et al. 2001) to assess the effect of these assumptions on systemic vessel haemodynamics have shown that geometry takes over within a relatively short distance from the location of the inlet boundaries, thus nullifying the effects of these assumptions.

However, the effects have only marginally been studied in the context of saccular cerebral aneurysms [Oshima et al. 2005], which often presents more complex haemodynamic patterns [Cebal et al. 2005a)] when compared to the simpler geometries of the studies reported so far [Myers et al. 2001; Moyle et al. 2006].

The current study investigates the effects of using different velocity profiles on the haemodynamics of intracranial aneurysms, and their secondary role when compared to anatomical geometry and extension of afferent vasculature, in three typical anatomical locations.



4.2.2 Materials and Methods

Three typical intracranial aneurysms found in the circle of Willis were considered in this study: an aneurysm at the tip of the basilar artery (herein called geom.1), an aneurysm of the right ophthalmic segment of the internal carotid artery (geom.2), and an aneurysm of the terminal bifurcation of the right middle cerebral artery (geom.3). Locations are shown in Figure-4.1. In order to study the flow development at the confluence of the vertebral arteries an additional geometry for the basilar artery aneurysm was reconstructed (geom.1b), which contains the junction of the two vertebral arteries. Essentially speaking geom.1 and geom.1b are same except for the presence of some extra proximal segment of vertebral arteries in geom.1b.

Some images, in addition to the aneurysm of interest, contain additional minor aneurysms. These are highlighted by black arrows in Figure-2, and were excluded from the study. The aneurysm in each of geom.1 and geom.3 was saccular bilobular. The aneurysm in geom.2 was saccular with a single lobe. These geometries present a progressively higher level of tortuosity of the aneurysmal afferent loop from geom.1, where the basilar artery is only slightly curved, to geom.3, where the feeding vasculature presents several bends, changes in the lumen diameter and bifurcations, before reaching the aneurysm of interest. Properties of these geometries are given in Table-4.1.

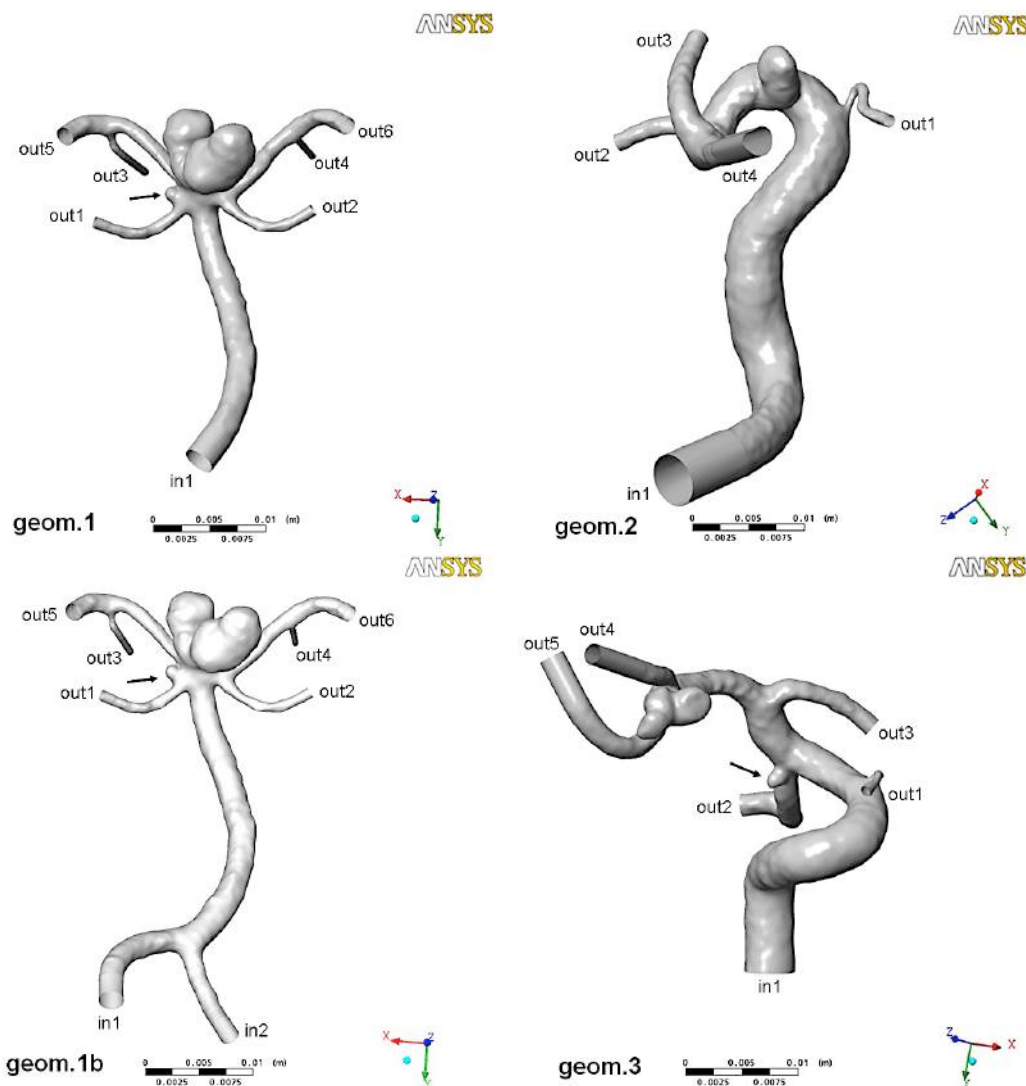


Figure-4.2. Reconstructed geometries: geom.1, basilar artery aneurysm, geom.1b, basilar artery aneurysm including vertebral arteries, geom.2, internal carotid artery aneurysm, geom.3, middle cerebral artery aneurysm. Black arrows show secondary smaller aneurysms, excluded from the study. Labels indicate the openings where boundary conditions were applied.

Rotational acquisitions were obtained using a Philips® Integris™ BV 5000 machine (Philips® Medical Systems, Best, The Nederland), producing 100 images in 4 seconds, with 5ms exposure per image. A built-in x-ray image intensifier was used, with a close-circuit-digital camera and software to correct for geometrical deformation. Voxel size in the reconstructed 3D images was 303 microns with reconstruction matrix 512x512x512. Images were anonymized, respecting the ethical approval for @neurIST's for use of patient data.

Table-4.1: Geometrical properties of geom.1-3.

Aneurysm size [mm]					
	<i>Depth</i>	<i>Max diameter</i>	<i>Neck (max width)</i>	<i>Length of afferent vessel (normalized with inlet diameter)</i>	<i>Complexity of afferent loop</i>
<i>geom.1</i>	5.5-6.5*	4.6-5.8*	5.5	10D	low
<i>geom.1b</i>	5.5-6.5*	4.6-5.8*	5.5	12D**	low
<i>geom.2</i>	5.5	4.6	4.3	8.2D	medium
<i>geom.3</i>	4.4-3.8*	3.3-2.3*	3.1	12D	high

*Values for the two lobes, **values for both inlet afferent vessels, i.e. vertebral arteries, D= inlet diameter.

The @neurIST computational tool chain was used to segment, extract and repair the vessel surfaces. In particular, vessel triangular surfaces were created using a threshold isosurface extraction tool, based on the marching cubes algorithm developed by Lorensen et al. (1987). Artifacts and unnecessary vasculature were removed and surface repaired using tools based on the Visualization Toolkit (VTK) (www.vtk.org), further developed within the Multimod Application Framework (Viceconti et al. 2004) in @neurIST. All inlet openings were extruded and morphed into circular edges for the appropriate application of Womersley-based boundary conditions. Extrusion of some outlets was necessary to ensure that spatially constant pressure represented an appropriate boundary condition at the termination of the 3D domain. The results of the geometry reconstruction process are shown in Figure-4.2.

During vessel reconstruction the neck of the aneurysms was manually identified and marked to define the aneurysmal sac that was used for the haemodynamic characterization of each aneurysm.

Volumetric meshes were generated using ANSYS® ICEM CFD 11.0™ and based on the octree approach. Grids were made finer at the walls and progressively coarser towards the vessel axis. Tetrahedral elements were used for the discretization of the domain core, with three layers of prismatic elements adjacent to the wall, thus ensuring accurate computation of wall shear stresses (WSS) and oscillatory shear indices (OSI). Element size and number were set accordingly to the outcome of a mesh dependency study performed on similar aneurysmal geometries (Radaelli et al. 2008, private communications). In this study, results were found to be grid independent for meshes greater than 1700 el/mm³. In order to maintain consistency across the meshes used for all geometries, similar element density and the same wall element size and maximum core element size were used in the discretization of the domains. Mesh details are reported in Table-4.2 below.

Table-4.2: Grid properties for geom.1-3

	volume [mm ³]	elements	nodes	average density [el./mm ³]	max el. size [mm]	max wall el. size [mm]
geom.1	433.9	1321449	411331	3046	0.4	0.12
geom.1b	540.4	1678606	527615	3106	0.4	0.12
geom.2	1375.5	3173174	912842	2307	0.4	0.12
geom.3	848.2	2292777	694172	2703	0.4	0.12

The 3D unsteady Navier-Stokes equations were solved by using the finite-control-volume software, ANSYS®-CFX™. The default second order high-resolution advection-differencing scheme was used. The solution algorithm is an implicit coupled solution scheme, based on an algebraic multigrid method for the coupled linear equations. Blood was assumed to be incompressible, with density $\rho=1050$ kg/m³, and Newtonian, with viscosity $\mu=0.0035$ Pa s. All analyses were run in parallel, using the communication mode MPICH on two Itanium2 900MHz 64-bit processors of a Tiger-2 Linux cluster node with 4GB of registered DDR-SDRAM PC1600.

4.2.3 Boundary conditions

Patient-specific flow measurements at boundaries were not available for the data sets under consideration, thus boundary conditions were derived from the flow-rate and pressure waveforms computed by using the 1D circulation model developed by Reymond et al. (2008), which is part of the @neurIST computational tool chain. This is a distributed model of the entire systemic arterial tree, coupled to a heart model and including a detailed description of the cerebral arteries. The 1D form of the fluid equations are applied over each arterial segment and intimal wall shear stress is modeled using the Womersley theory. A non-linear viscoelastic constitutive law for the arterial wall is considered. The systemic arterial tree dimensions and properties were taken from literature and extended to include a description of the cerebral arterial tree obtained from real patient scans.

Flow-rate waveforms were used for all primary inlets and pressure waveforms for all primary outlets. All pressure and flow rate waveforms used for the analyses are reported in Figure-3 to Figure-6. Flow-rate waveforms were used to specify, in turn, plug-flow (i.e. flat velocity profile) and Womersley velocity profiles at the inlet boundaries.

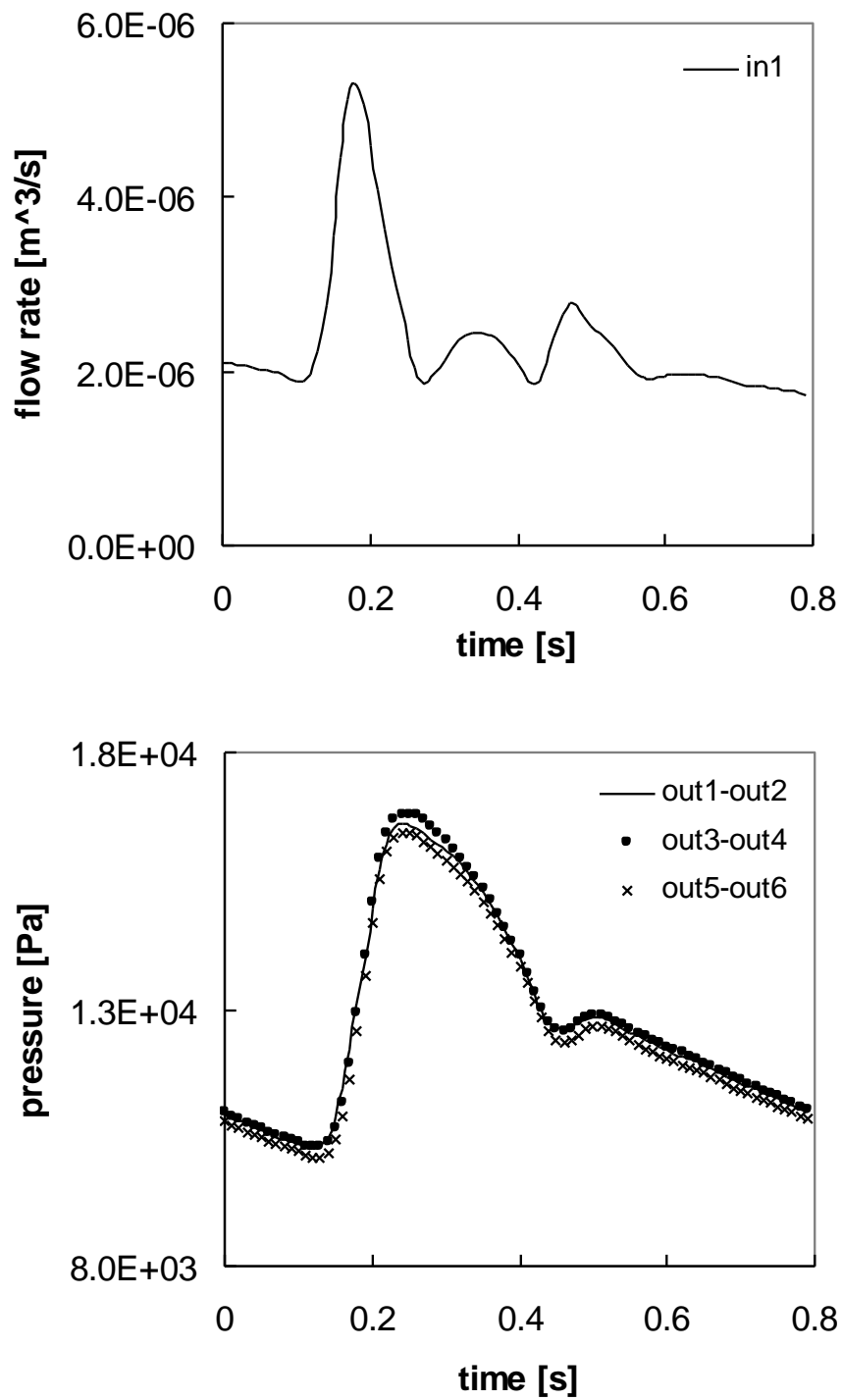


Figure 4.3 Flow-rate (top) and pressure waveforms (bottom) applied in geom.1

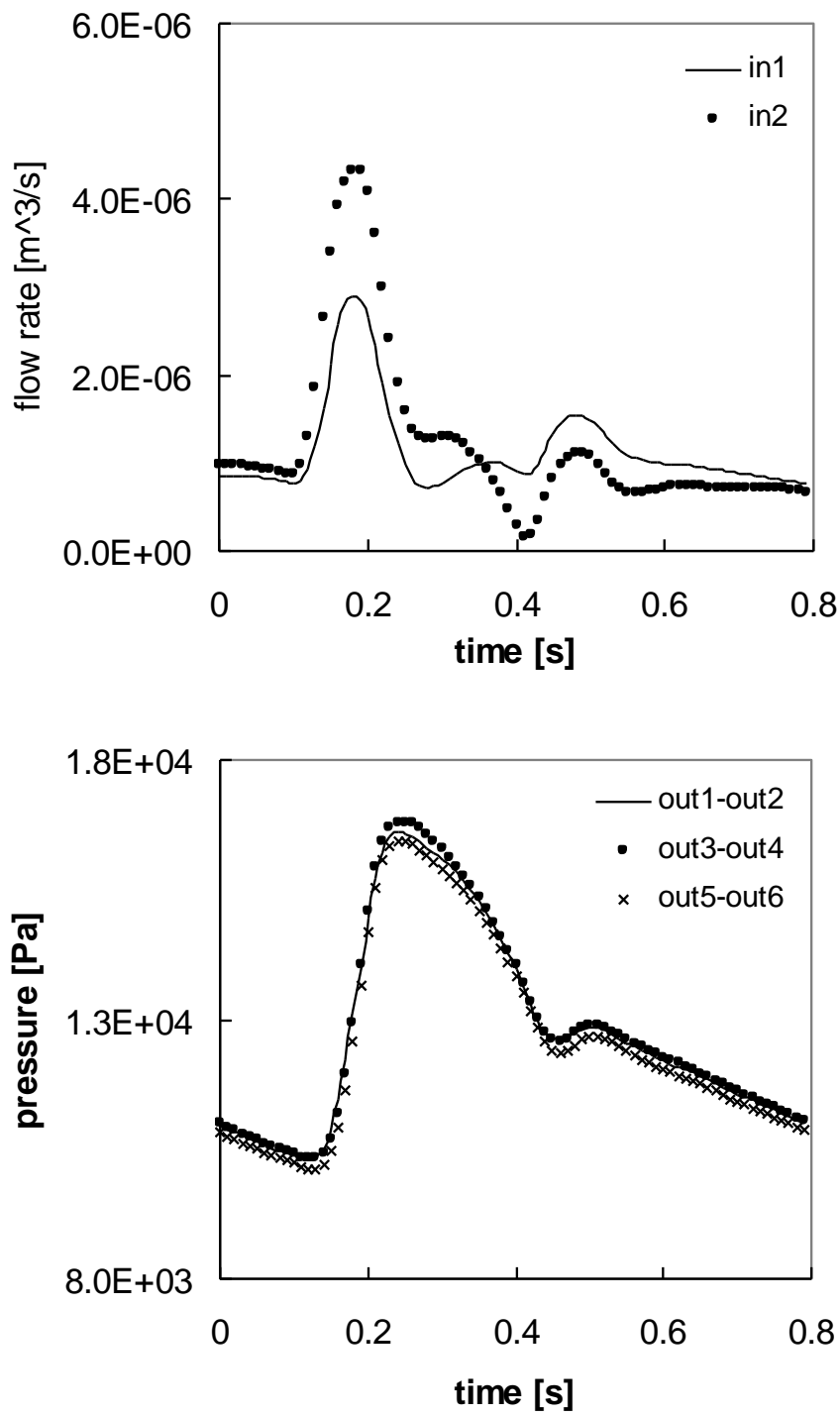


Figure 4.4 Flow-rate (top) and pressure waveforms (bottom) applied in geom.1b

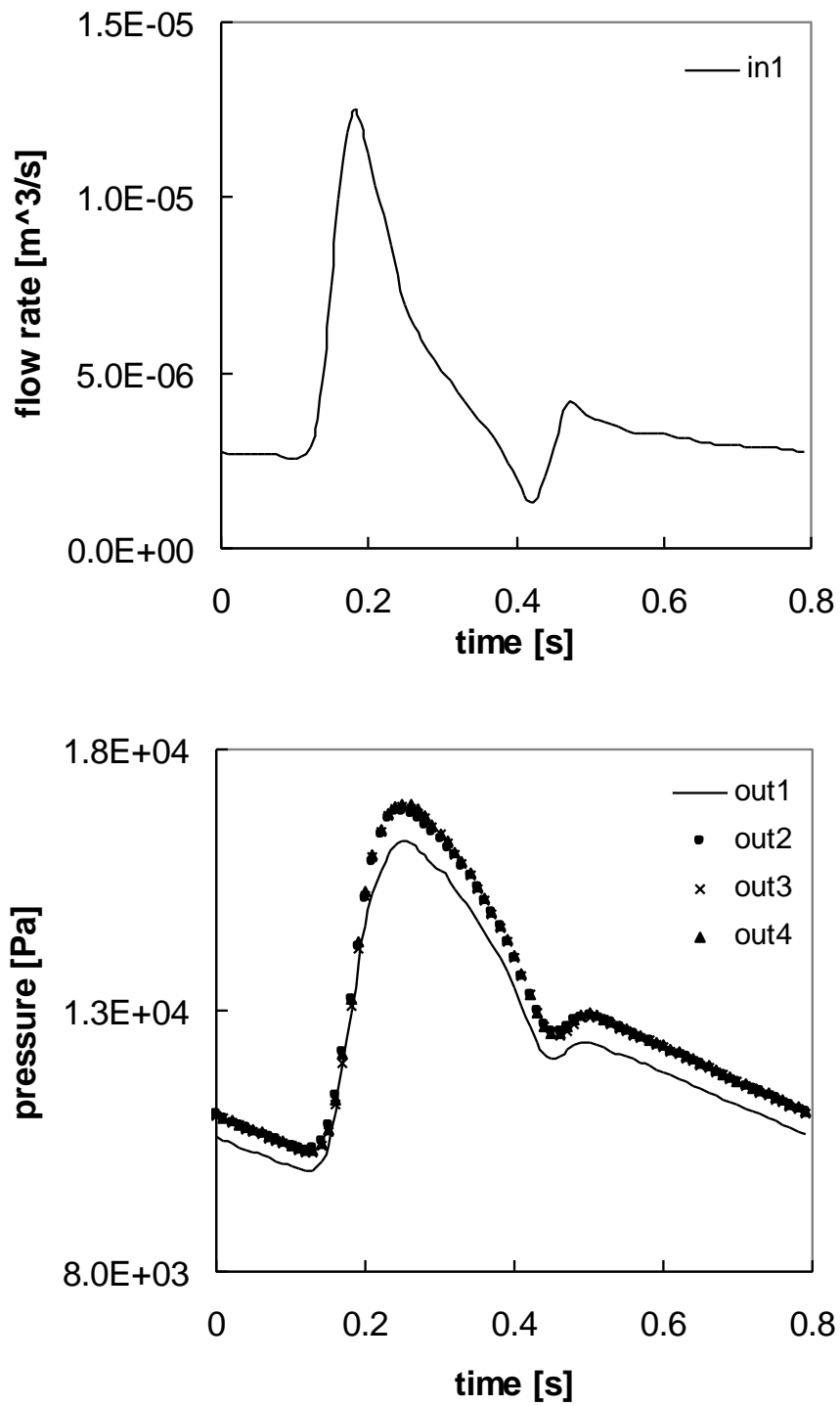


Figure 4.5 Flow-rate (top) and pressure waveforms (bottom) applied in geom.2

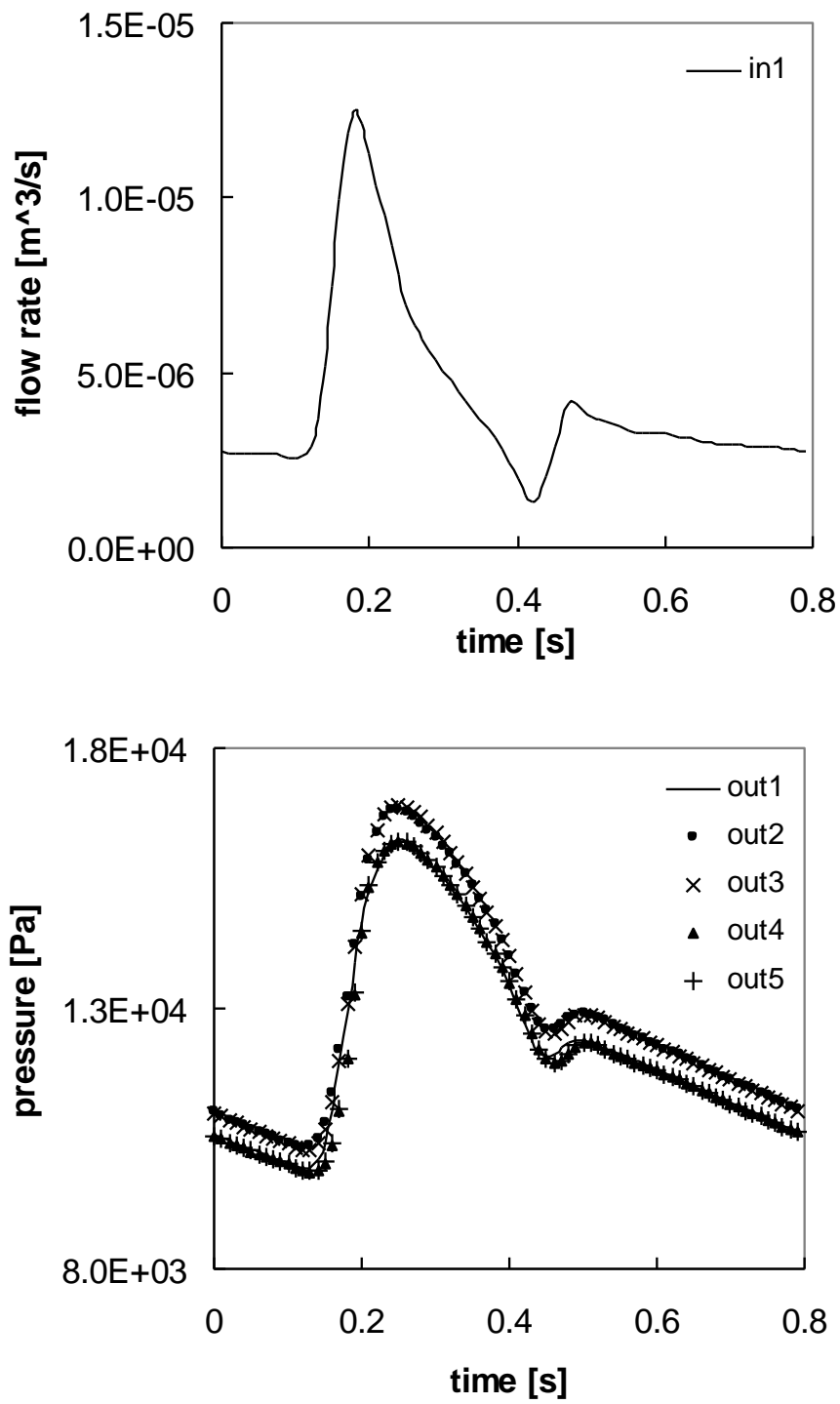


Figure 4.6 Flow-rate (top) and pressure waveforms (bottom) applied in geom.3

The waveforms were decomposed into Fourier series as indicated in equation (1)

$$Q(t) = \sum_{n=0}^N Q_n e^{in\omega t} \dots\dots\dots(1)$$

where N is the number of harmonics, and ω is the angular frequency derived from the period of the cardiac cycle $T=0.8$ s. The Womersley velocity profile was expressed in terms of the Fourier representation of the flow rate waveforms as indicated in equation (2)

$$v(r,t) = \frac{2Q_0}{\pi R^2} \left[1 - \left(\frac{r}{R} \right)^2 \right] + \sum_{n=1}^N \frac{Q_n}{\pi R^2} \left[\frac{1 - \frac{J_0\left(\beta_n \cdot \frac{r}{R}\right)}{J_0(\beta_n)}}{1 - \frac{2J_1(\beta_n)}{\beta_n \cdot J_0(\beta_n)}} \right] \cdot e^{in\omega t} \dots\dots\dots(2)$$

where R is the radius of the inlet boundary, Q_0 is the first harmonic coefficient responsible for the parabolic profile of a steady flow (i.e. Poiseuille's flow), J_0 and J_1 are Bessel functions of order zero and one, respectively, and

$$\beta_n = i^{\frac{3}{2}} \cdot \alpha_n \dots\dots\dots(3)$$

$$\alpha_n = R \cdot \sqrt{\frac{n \cdot \omega \cdot \rho}{\mu}} \dots\dots\dots(4)$$

where α_n is the Womersley number of the n-th harmonic. A Fortran subroutine was created and interfaced to the ANSYS®-CFX™ solver for the computation of the velocity inlet profiles within each time loop.

Analyses were run for four cardiac cycles to nullify the transient artifacts generated by the initial conditions, and only data from the 4-th cycle were used in the post-processing phase.

4.2.4 Results

Relevant haemodynamic variables were compared qualitatively and quantitatively for the two velocity profile assumptions both at two time-points along the cardiac cycle (corresponding to the lowest and highest Reynolds numbers achieved during diastole and systole, respectively), and as time-averaged quantities across the cardiac cycle. The haemodynamic variables chosen for these comparisons have been associated to

aneurysmal initiation, growth, and rupture in the literature (Shojima et al. 2004, Cebal et al. 2005)

4.2.4.1: Qualitative comparison using instantaneous velocity contours

Figure-4.7 shows the comparison between Womersley and plug-flow boundary conditions during diastole and systole, using velocity contours at specific cross sections. The cross-sections were selected as those, which subjectively, best illustrated the complexity of the flow within the three domains. Results for geom.1 show that for both flow regimes; the Womersley and plug-flow flow patterns are essentially the same with some minor discrepancy in the magnitude of the velocity field, as shown by the arrows in Figure-4.7.

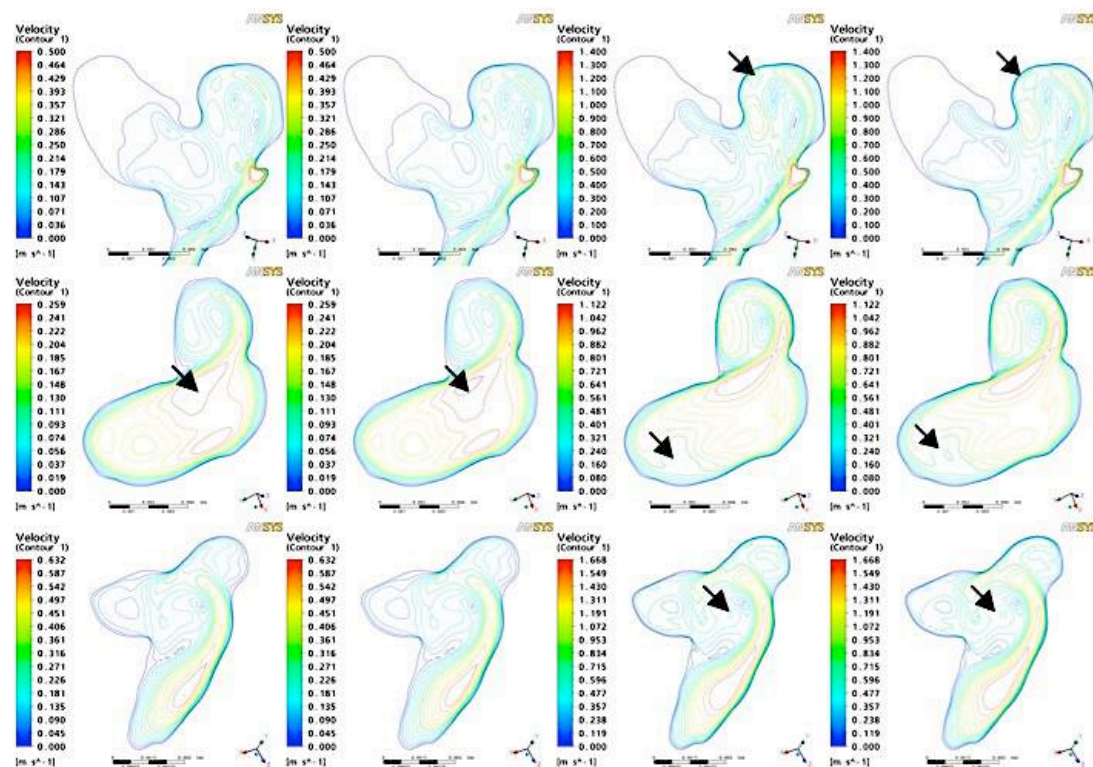


Figure-4.7: Velocity contours across the aneurysmal sac for a) Womersley BC at lowest Re during diastole, b) plug-flow BC at lowest Re during diastole, c) Womersley BC at highest Re during systole, d) plug-flow BC at highest Re during systole. From top to bottom: geom.1, geom.2, and geom.3. Grey arrows indicate areas of discrepancies.

Results for geom.2 are consistent with geom.1 except that discrepancies in velocity magnitudes are more pronounced in the lower part of the cross section, representing the velocity patterns within the parent vessel. Finally, results for geom.3 show good agreement in the patterns as well as the magnitude of the velocity field. Contours in geom.2 and geom.3 show the presence of a jet of fluid entering the aneurysm and impinging onto the distal side of the aneurysmal wall. Moreover, results for all geometries show that flow is rather stable (according to the definition of Cebal et al. 2005), exhibiting the same characteristics during diastole and systole.

4.2.4.2: Qualitative comparison using instantaneous WSS contours

Figure-4.8 shows the comparison between Womersley and plug-flow boundary conditions during diastole and systole, using contours of WSS on the wall of the aneurysmal sac. Results for geom.1 show that Womersley and plug-flow boundary conditions at inlet develop essentially the same WSS distribution in the aneurysm in both flow regimes. It was noticed that the bigger lobule of geom.1 is one, which is subjected to comparatively low WSS at both reported time-points in the cardiac cycle, whereas in the smaller lobule WSS values reach their highest values. Results for geom.2 and geom.3 show essentially the same WSS patterns for both inflow assumptions and for both flow regimes, with some minor variations for geom.2 during diastole near the aneurysmal neck, and for geom.3 during systole as shown by the arrows in Figure 4.8.

As for velocity distributions, WSS present similar patterns during diastole and systole, showing stability of the flow.

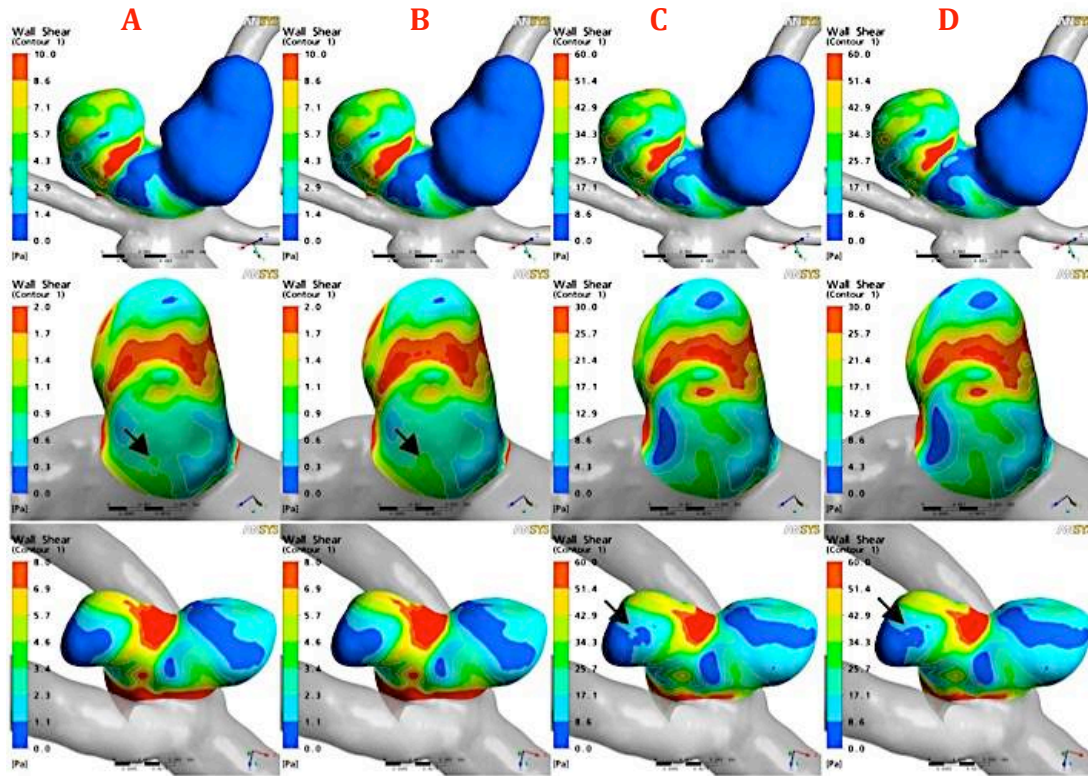


Figure-4.8: WSS contours for a) Womersley BC at lowest Re during diastole, b) plug-flow BC at lowest Re during diastole, c) Womersley BC at highest Re during systole, d) plug-flow BC at highest Re during systole. From top to bottom: geom.1, geom.2, and geom.3

4.2.4.3: Qualitative comparison using time-averaged WSS and OSI contours

Time-averaged haemodynamic quantities can be used to assess the agreement between results over the whole cardiac cycle, and not solely at specific snap-shots in time. Time-averaged WSS are reported, together with Oscillatory Shear Index (OSI) for further comparison. OSI is defined in equations 5, 6 and 7, and was used to quantify the oscillatory shears experienced by the cells of the inner part of the arterial vessel and aneurysm (endothelial layer).

$$OSI = \frac{1}{2} \left(1 - \frac{\tau_{mean}}{\tau_{abs}} \right) \dots\dots\dots(5)$$

$$\tau_{mean} = \left| \frac{1}{T} \int_0^T t_s \cdot dt \right| \dots\dots\dots(6)$$

where t_s represents the surface traction vector. Figure 4.9 and Figure 4.10 show the time-averaged WSS and OSI contours, respectively, on the aneurysmal wall of all three geometries and for both inlet boundary conditions.

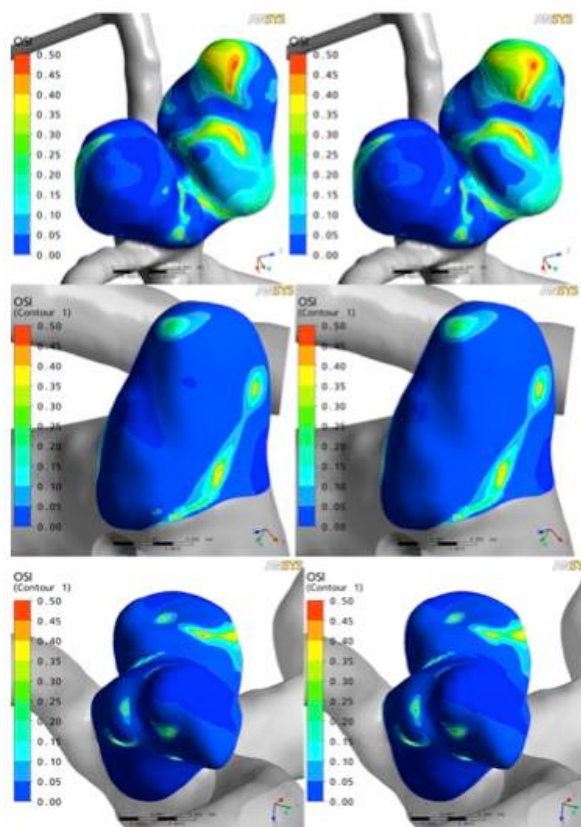


Figure-4.9: Time-averaged WSS contours for a) Womersley boundary conditions, b) plug-flow BC. From top to bottom: geom.1, geom.2, and geom.3.

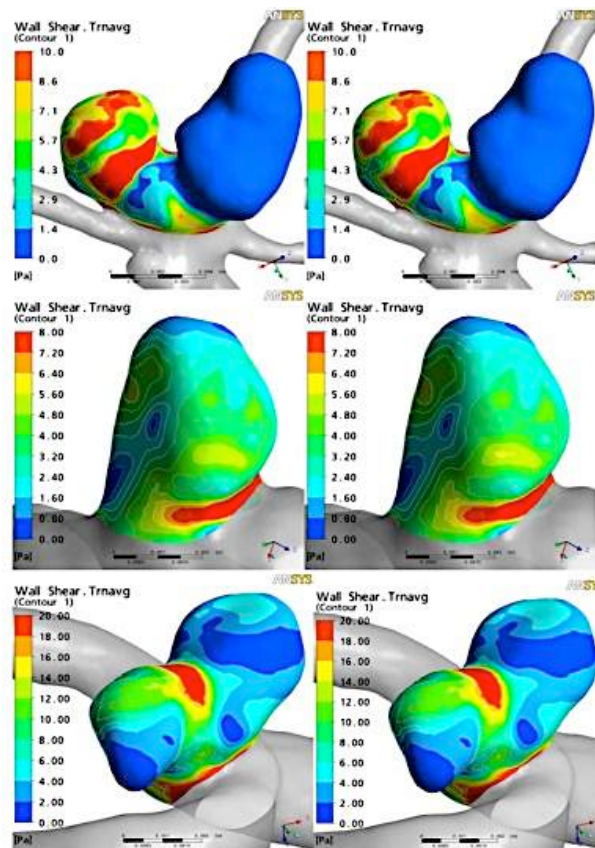


Figure-4.10: OSI contours for a) Womersley BC, b) plug-flow BC. From top to bottom: geom.1, geom.2, and geom.3.

The results are consistent with those of the instantaneous measures, i.e. very little differences are observed between WSS and OSI patterns, and only minor differences in magnitudes, from Womersley and plug-flow boundary conditions. For these aneurysms, exhibiting stable flow patterns over the cardiac cycle, it is noted that the time-averaged WSS stress pattern is qualitatively very similar to that of its instantaneous counterparts.

4.2.4.4: Qualitative comparison on flow development

Figure 4.11a and Figure 4.11b show the development of the flow for Womersley and plug-flow boundary conditions for geom.1. Although the two flows start from different assumptions at the inlet opening, both develop into a very similar velocity pattern before reaching the aneurysmal sac. Figure 4.11c, illustrating the results for the extended domain of geom.1b, shows that the two converging vessels produce a ring-like velocity profile that is significantly different from both the Womersley and flat profiles, but in fact closer to the latter.

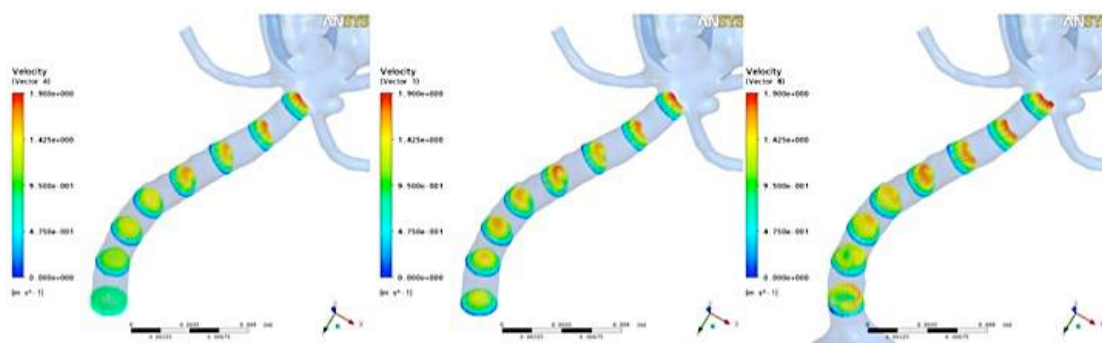


Figure-4.11: Velocity vectors on cross-sections along the afferent vessel at peak systole for geom.1 (a,b) and geom.1b (c). The distance between the cross-sections is $1.5D$, where D is the diameter of the inlet boundary in geom.1.

This indicates clearly that there are geometries (of course those that are least like a straight tube) for which the Womersley profile is actually a worse choice than the flat profile. Nevertheless, once again the flow close to the aneurysm is relatively similar for all boundary conditions considered.

4.2.4.5: Quantitative comparison

For a more accurate and direct evaluation of the effects that different boundary conditions may have on local haemodynamics, several haemodynamic indices were extracted from the flow field of the three aneurysmal sacs, for both inflow boundary conditions. These are reported in Table-3 with the percentage discrepancy between Womersley and plug-flow results. In geom.1, the maximum discrepancy was observed in the spatial-average speed in the aneurysmal sac (4.3%) and in the area of elevated pressure in the aneurysmal wall (also 4.3%). Relatively high discrepancies were also observed in the values predicted for the maximum speed within the aneurysm at systole (2.3%) and the location of maximum OSI (2.8%). In geom.2, the maximum discrepancy was observed in the

predictions of area of elevated pressure (4.1%) and for geom.3 in the values of max OSI (3.7%) and its location (4.1%).

Table 4.3. Haemodynamic indices extracted for geom.1-3 and percentage error between Womersley and plug-flow results. 1) Elevation defined as 50% of peak pressure minus average pressure in the aneurysm at systole. 2) Elevation defined as 50% of maximum time-averag

	Geom.1			Geom.2			Geom.3		
	Wom	Plug	Err%	Wom	Plug	Err%	Wom	Plug	Err%
Max speed within aneurysm at systole [m/s]	1.774	1.733	-2.3	1.154	1.155	0.1	1.555	1.544	-0.7
Spatial mean speed in aneurysm at systole [m/s]	0.331	0.317	-4.3	0.557	0.557	0.0	0.619	0.619	0.0
Peak static wall pressure at systole [Pa]	16131	15950	-1.1	15770	15750	-0.1	14560	14550	-0.1
Location X of max pressure [m]	3.51E-02	3.51E-02	0.0	4.20E-02	4.20E-02	0.0	1.73E-02	1.73E-02	0.0
Location Y of max pressure [m]	1.64E-02	1.64E-02	0.0	2.33E-02	2.33E-02	0.0	3.11E-02	3.11E-02	0.0
Location Z of max pressure [m]	-3.67E-02	-3.67E-02	0.0	-3.48E-02	-3.48E-02	0.0	-3.65E-02	-3.65E-02	0.0
Spatial mean static pressure in aneurysm at systole [Pa]	15260	15130	-0.9	15140	15120	-0.1	13770	13770	0.0
Area of elevated pressure ¹ [m ²]	0.123E-06	0.118E-05	-4.3	4.18E-06	4.01E-06	-4.1	7.06E-06	7.13E-06	1.1
Max time-averaged WSS [Pa]	25.79	25.52	-1.1	16.44	16.87	2.6	49.07	50.52	2.95
Location X of max time-averaged WSS [m]	3.604E-2	3.604E-2	0.0	4.18E-02	4.18E-02	0.0	1.79E-02	1.79E-02	0.0
Location Y of max time-averaged WSS [m]	0.196E-03	0.196E-03	0.0	0.232E-03	0.232E-03	0.0	0.291E-03	0.291E-03	0.0
Location Z of max time-averaged WSS [m]	-3.48E-02	-3.48E-02	0.0	-3.49E-02	-3.49E-02	0.0	-3.36E-02	-3.36E-02	0.0
Area of elevated time-averaged WSS ² [m ²]	1.83E-06	1.82E-06	-0.9	6.39E-07	6.39E-07	0.0	2.60E-07	2.56E-07	-1.4
Max OSI in aneurysmal wall []	0.491	0.487	-0.8	0.471	0.472	0.2	0.494	0.475	-3.7
Location X of max OSI [m]	3.21E-02	3.12E-02	-2.8	4.13E-02	4.13E-02	0.0	1.95E-02	1.97E-02	1.2
Location Y of max OSI [m]	1.80E-02	1.79E-02	-0.9	2.34E-02	2.34E-02	0.0	3.12E-02	2.99E-02	-4.1
Location Z of max OSI [m]	-3.20E-02	-3.12E-02	-2.7	-3.75E-02	-3.75E-02	0.0	-3.67E-02	-3.68E-02	0.3
Area of elevated OSI [m ²]	6.44E-05	6.37E-05	-1.0	3.39E-07	3.35E-07	-1.2	7.30E-07	7.70E-07	5.4
RMS error %			1.9			1.2			1.98

The root mean square of the errors of the different indices was also computed and is reported in the last row of Table-4.3.

Overall, the maximum discrepancy between Womersley and plug-flow results was observed in geom.3, where the RMS is 2%. Lower RMS values were calculated for geom.1, RMS = 1.9%, and geom.2, RMS = 1.2%

4.2.5 Discussion

The purpose of this section is to compare the results from two common methods of application of proximal velocity boundary conditions for haemodynamic analysis of cerebral aneurysms. The context is that of

specification of a robust protocol for routine haemodynamic analysis as part of a clinical workflow.

The isolation of the vessel of interest from the rest of the cardiovascular tree and its surroundings (e.g. tissues, bones) implies that wall and flow conditions will have to be specified at the boundaries of the vessel. Patient-specific assessment of the properties of the vessel walls and its surroundings are difficult. There is some evidence that pulsatility of the vessel wall might have negligible effect on haemodynamics even when the wall motion is of the order of the radius of a vessel (Jeays et al. 2007) and even less so in the context of cerebral aneurysms in the confined compartment of the skull (Dempere-Marco et al. 2006). For the purposes of the current study, (and probably for a routine clinical analysis protocol) the walls of the vessel are considered fixed.

Patient-specific flow measurements are in principle attainable from MRI or Doppler ultrasound but the intricacy of the cerebral vasculature, the small size of its vessels, and the fact that these are not part of the clinical procedure make them rarely available. Even when they are, it is unusual to rely on the spatial distribution of velocity (due to resolution of MRI and difficulties of location of Doppler ultrasound measures). To overcome these difficulties several authors use lumped-parameters or 1D models for the description of the remaining vascular systems (Formaggia et al. 1999, Quarteroni et al. 2001). Flow boundary conditions, whether from patient-specific ultrasound MRI measures or computed using simple models of the cardiovascular system, are available as cross-sectional average values of velocity or pressure along the cardiac cycle. Thus assumptions on their 3D development across the same boundaries are to be made to match the level of details required by 3D modeling. While imposing inflow boundary conditions from the flow-rate waveforms computed by a 1D distributed model, for instance, one assumption often imposed at the inlet boundary is that of axisymmetric flow with a velocity distribution determined by the Womersley theory.

The results of the comparative analyses with Womersley and flat velocity profiles indicate that there is no change in qualitative flow patterns, and detailed examination of the flow fields yields maximum differences of less than 5%, and RMS differences between 1 and 2%. It is suggested that these differences are unimportant in the context of interpretability against known thresholds, and particularly in the context of other uncertainties in the analysis (patient blood pressure, beat-to-beat variations, alternative physiological states including exercise, patient haematocrit and viscosity models). Certainly, the errors are small compared with those that might

arise from inaccurate segmentation of the patient specific geometry, when variability up to 48% has been reported (Moyle et al. 2006). Whilst the true significance and relevance of discrepancies between Womersley and plug-flow results can only be assessed once associations are found between haemodynamic indices and aneurysmal evolution, it is probably safe to assume that the uncertainties of any thresholds and the safety factors that will be built into any clinical interpretation and recommendations will always remain greater than that associated with analysis errors from the inlet velocity profile provided the inlet development domain is of adequate length.

The computational savings associated with a recommendation of the simplest inlet-velocity-boundary-condition that of a flat profile, are not significant. More important is that the simpler the analysis protocol adopted, the more likely it is that other centers will contribute to the growth of an established database of haemodynamic characterizations, ultimately reflecting on its power to provide meaningful, peer-reviewed and clinically implementable associations of the characteristic haemodynamic measures with observed clinical outcome. Until such associations are established, the impact of CFD on the management of cerebral aneurysms will be minimal.

A limitation of the current study is that results are reported for only three aneurysms, with one further variation. Nevertheless, these aneurysms have been selected as typical of those that arise most commonly in the cerebral vasculature and, given the consistency of the results and their resonance with expectations based on the physics of the problem, it is suggested that it provides strong evidence that haemodynamic characterizations are indeed likely to be insensitive to details of the inlet velocity distribution.

Although specific analysis and comment on the haemodynamic results for any one aneurysm is not the focus of the current study, the analysis of geom.1 revealed some interesting haemodynamic characteristics that are worthy of mention. Primary haemodynamic activity is clearly confined to one of the lobules, whilst the other is subject to very low wall shear stresses. In fact it is the smaller lobule that exhibits strong haemodynamic activity and the larger that is relatively stagnant. It is noted that the larger lobe has a more irregular shape. No follow-up data is available and so it is impossible to determine which, if either, lobe is growing or which might rupture. Nevertheless, it is noteworthy that the haemodynamic environment in the smaller lobes is more similar to that in the parent vasculature rather than that in the larger lobe, and that the mean shear stress in the larger lobe is below that threshold that has been associated

with negative outcome and the onset of disease in other vascular applications [Malek et al. 1999].

4.2.6. Conclusions

The following conclusions can be drawn from this study:

1. The haemodynamic characterization of a cerebral aneurysm, under given proximal flow conditions is relatively insensitive to the details of the velocity profile on inlet boundaries that are sufficiently far from the aneurysm.
2. Wider adoption of a given analysis protocol is more likely if it is simple to implement, and the specification of a flat velocity profile at the inlet to a 3D domain provides an adequate and justifiable description for the purposes of haemodynamic characterization.

4.3. Computational Haemodynamics in Intracranial Aneurysms: the Effects of Modeled versus Patient-Specific Boundary Conditions

4.3.1 Background and Objectives

There is growing consensus that haemodynamics plays an important role in the growth, rupture and initiation of IAs [Cebal et al 2005, Sekhar and Heros 1981, Shojima 2004]. Two haemodynamic indices, WSS (wall shear index) and OSI (oscillatory shear index), have received particular attention due to their influence on endothelial cell behavior [Cebal et al 2005, Shojima 2004].

Although the studies from Rayz et al [Rayz et al 2008], Boussel et al [Boussel et al 2008], and Isoda et al [Isoda et al 2010], showed that in-vivo measurements of these quantities are possible using magnetic resonance fluid dynamics (MRFD), inherent limitations in the technology impede its use in large cohort studies where detailed haemodynamics is needed also for smaller aneurysms (max diameter < 5 mm).

In this context, numerical modeling can provide detailed predictions for WSS and OSI using input parameters derived from medical imaging, blood sampling, and other patient information. In fact, CFD has been used by many authors in the context of IAs to find correlations between haemodynamics and risk of rupture or growth. For convenience, in these works the extension of the computational domain is often limited to a restricted area around the aneurysm. The specification of boundary conditions at the interfaces with the rest of the cardiovascular network

thus remains a pre-requisite for the solution of the governing equations. Different authors approach this particular aspect differently.

Some studies use patient-specific Boundary Conditions (BCs) based on measurements obtained using phase contrast – magnetic resonance (pc-MR) or transcranial Doppler (TCD) ultrasound, to record blood velocity; and applanation tonometry, to infer pressure. However, because of the inherent difficulty in obtaining these measures in the small and intricate vessels of the cerebral vasculature, and the fact that these measurements are to date rarely justifiable as part of the clinical routine, such studies are often based on small cohort sizes and lack statistical significance [Jou et al 2008, Hassan et al 2004, Jou et al 2005, Boussel et al 2008, Rayz et al 2008, Rayz et al 2008b]. Furthermore when patient-specific-BC data is available, these are often limited to the inflows of the fluid domains [Hassan et al 2004, Jou et al 2005, Boussel et al 2008, Rayz et al 2008, Rayz et al 2008b] where vessels are larger and easily accessible by the available measurement techniques.

Larger cohort studies, in contrast, rely on inflow BCs based on measurements taken from typical healthy individuals, in some cases [Jou et al 2008, Radaelli et al 2008, Venugopal et al 2007, Cebal et al 2009, Mantha et al 2006] scaled to achieve a supposedly more realistic mean WSS of 1.5 Pa, and outflow BCs that assume the same peripheral resistance at all openings (traction free or zero pressure BCs). The assumptions associated with this type of BCs may also lead to unrealistic results.

As detailed comparison with in-vivo measurements is currently difficult, the validity of CFD tools in the context of IAs rupture risk assessment and management relies upon the extent to which the correlations between haemodynamic predictions and rupture are statistically matched for a large cohort study. One of the important aims of @neurIST (www.aneurist.org), a multidisciplinary EU project of which this study forms a part, is to establish these correlations by processing a large number of cases. The lack of patient-specific data for use at computational boundaries remains an important limiting factor in the project. This issue has been addressed by deriving a complete set of BCs for 3D CFD analysis from a 1D-model of the circulatory system, including the cerebral vasculature [Reymond et al 2009].

This study explores and analyzes the effects that BCs derived using in turn the 1D-model, patient-specific pc-MR measurements, and other

approaches found in the literature, have on the haemodynamics within typical intracranial aneurysms.

4.3.2 Materials and Methods

Study design, demographics and clinical details: The study was conducted in cooperation between the Departments of Neurosurgery and Neuroradiology, Royal Hallamshire Hospital, and the Academic Units of Medical Physics and Radiology, University of Sheffield, Sheffield, UK. A total of 5 patients diagnosed with IAs between Dec 2006 and Jan 2009, were identified retrospectively and followed prospectively according to the data collection protocol of the @neurIST project upon appropriate ethical approval and patient consent. Table-4.4 gives the demographic constitution of the population along with the relevant aneurysm details. All IAs were sidewall saccular aneurysms and their location is shown in Figure-4.12.

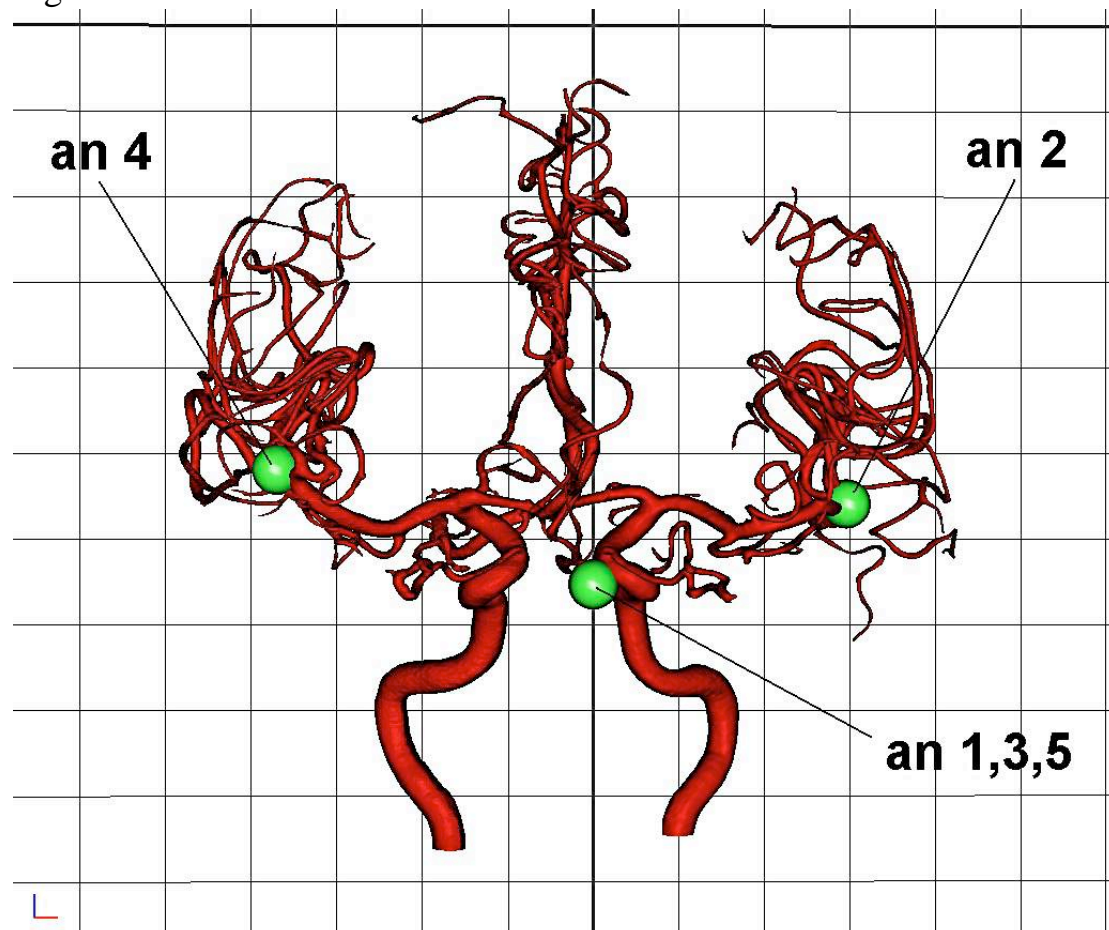


Figure: 4.12. Locations of aneurysms 1-5 in a typical cerebral vasculature (illustration generated using the @neurIST software)

Table 4.4 Patient demographics and aneurysm radiological features

Patient			Aneurysm				
#	Sex	Age	#	Side	Location	Rupture	Size(diam/neck)[mm]
1	M	44	1	Left	ICA	No	5/4.3
2	M	52	2	Left	MCA	No	11.1/4.3
3	F	50	3	Left	ICA	No	3.4/3.1
4	F	41	4	Right	MCA	Yes	4.4/3
5	F	51	5	Left	ICA	No	2.9/3.1

ICA = Internal Carotid Artery; MCA = Middle Cerebral Artery bifurcation

Image acquisition: The medical images used for surface reconstruction were obtained using 3D rotational acquisition (3DRA) in a Philips® Integris™ Allura machine (Philips® Medical Systems, Best, The Netherlands), producing 100 images in 6 seconds, with 5ms exposure per image. Voxel size in the reconstructed 3D images was 121 microns with reconstruction matrix of 512x512x512.

pc-MR protocol: All MR imaging was performed at high field strength (Achieva™ 3.0T, Philips® Medical Systems, Best, The Netherlands) using a standard 8-channel, radiofrequency receiver-only head coil. The same radiographer imaged all patients to maximize reproducibility of overall acquisition technique. Macroscopic vascular flow and IA location were visualized using a qualitative Time-Of-Flight (TOF) MR angiography sequence. Maximum intensity projections (MIP) from this 3D dataset were used to define the placement of each quantitative phase contrast measurement plane perpendicular to the vessel under investigation. A 2D acquisition sequence (TR=7.7ms, TE=3.7ms, flip angle=10°; field of view=270x179mm, acquisition matrix=1.7x1.60mm, slice thickness=5mm) was used to acquire 40 velocity-encoded ‘time-point’ over the cardiac cycle at each vascular location. Vector Electro Cardiography (ECG) triggering was used to standardize each quantitative acquisition. Appropriate maximum velocity-encoding (VENC) values

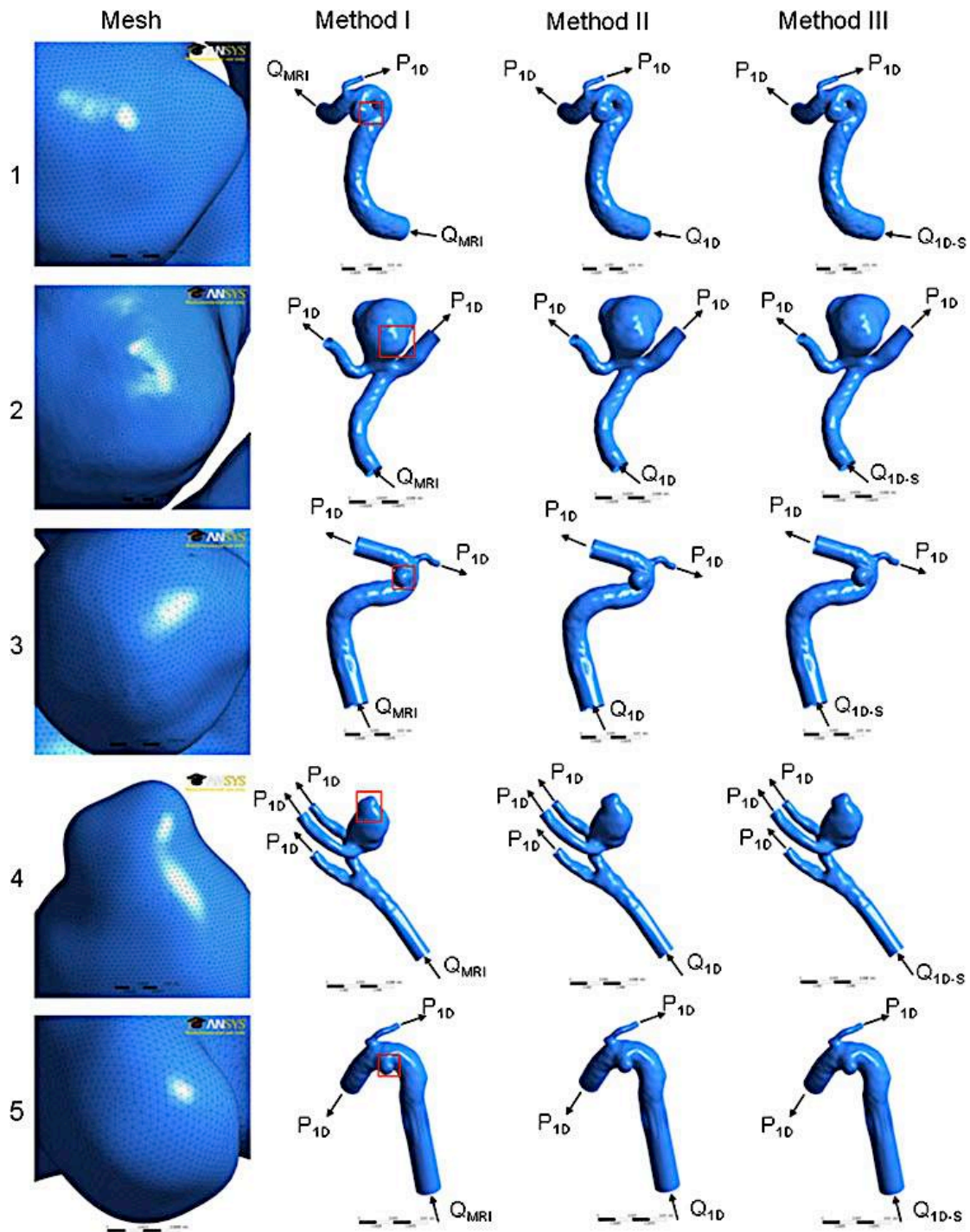


Figure-4.13: Mesh particulars and BC types used. QMRI is the velocity-based boundary condition from MRI patient-specific measurements, Q1D is the velocity-based boundary condition from 1D model, Q1D-S is the WSS-scaled velocity-based boundary condition

condition from 1D model, and P1D is the pressure boundary condition from 1D Model was chosen (150 cm/sec for ICA and 120 cm/sec for MCA regions) to ensure that appropriate dynamic ranges were sampled in all cases. A pre-designed protocol guided the radiographer through the desired measurement locations for subsequent application of CFD BCs. As afferent vasculature has an important influence on intra-aneurysmal

haemodynamics [Cebal et al 2005, Castro et al 2006, Marzo et al 2009, Moyle et al 2006, Oshima et al 2005] proximal measurements were taken at a distance of approximately 10 parent vessel diameters from the aneurysm. Measurements in distal arteries were taken 3 diameters apart from the IAs. Patient table-occupancy time was no greater than 1 hour. Within this period it was difficult to ensure that all measurements were obtained for all volunteers. The tortuous nature of the vasculature also made slice selection perpendicular to the artery difficult to achieve. To maintain integrity in the final measurement dataset, data was rejected if there was doubt about the placement of the measurement plane.

Table-4.5: Boundary conditions location, type and method

Aneurysm	BC Location	type	Method I	Method II	Method III
1	ICA proximal	inlet	pc-MR/velocity	1D/velocity	1D/velocity scaled
	ICA distal	outlet	pc-MR/velocity	1D/pressure	1D/pressure
	OphthA	outlet	1D/pressure	1D/pressure	1D/pressure
2	MCA M1	inlet	pc-MR/velocity	1D/velocity	1D/velocity scaled
	MCA M2 supr	outlet	1D/pressure	1D/pressure	1D/pressure
	MCA M2 infr	outlet	1D/pressure	1D/pressure	1D/pressure
3	ICA proximal	inlet	pc-MR/velocity	1D/velocity	1D/velocity scaled
	ICA distal	outlet	1D/pressure	1D/pressure	1D/pressure
	OphthA	outlet	1D/pressure	1D/pressure	1D/pressure
4	MCA M1	inlet	pc-MR/velocity	1D/velocity	1D/velocity scaled
	TempA	outlet	1D/pressure	1D/pressure	1D/pressure
	MCA M2 supr	outlet	1D/pressure	1D/pressure	1D/pressure
5	MCA M2 infr	outlet	1D/pressure	1D/pressure	1D/pressure
	ICA proximal	inlet	pc-MR/velocity	1D/velocity	1D/velocity scaled
	ICA distal	outlet	pc-MR/velocity	1D/pressure	1D/pressure
	OphthA	outlet	1D/pressure	1D/pressure	1D/pressure

ICA=internal carotid artery, OphthA=ophthalmic artery, MCA M1=middle cerebral artery, MCA M2 supr/infr=superior/inferior division of the middle cerebral artery, TempA=temporal artery

Locations of pc-MR measurements are reported in Table-4.5 (column “BC Location”). The manufacturer’s proprietary post-data-acquisition software (Q-Flow™, Philips® Medical Systems, Best, The Netherlands) was used to estimate volumetric flow rate (VFR) waveforms at each spatial location.

1D circulation model: The finite-difference model developed by Reymond et al [Reymond et al 2009], was used to compute pressure and VFR waveforms at the desired boundaries of the 3D domain. The model solves the 1D form of the Navier-Stokes equation in a distributed model of the main human systemic arteries including the main arteries of the circle of Willis. It accounts for ventricular-vascular interaction and wall viscoelasticity, and it was recently validated through a comparison with in-vivo measurements taken using applanation tonometry, B-mode, and colour-coded duplex flow imaging, and pc-MRI. Although the model could be personalized tuning input parameters such as heart rate (HR), cardiac contractility, age (vessel elasticity), height (vessel geometry), and blood properties, in this study the model was used with the properties of a

typical young individual as patient-specific data was not available for all patients. A typical analysis is solved in approximately 8 min.

CFD models: The @neurIST computational tool-chain was used to reconstruct vessel and aneurysmal geometries, following the workflow described in Marzo et al [Marzo et al 2009]. The 3D transient Navier–Stokes equations were solved by using the finite-control-volume software, ANSYS®-CFX™. Blood was assumed to be incompressible, with density $\rho=1060$ kg/m³, and Newtonian, with viscosity $\mu=0.0035$ Pa·s. Boundary conditions were applied following three different approaches, as reported in Table-4.5. Method I used pc-MR VFR measurements at the openings for which these could be measured, and 1D model pressure waveforms at every remaining interface. For aneurysm-1 and 5 measurements were available at all vessel openings but one. Method II used VFR and pressure waveforms from the 1D circulation model. Method III used the typical waveforms derived using the 1D model, where VFR curves were scaled to obtain a mean WSS of 1.5 Pa at inlets. For all velocity-based BCs a flat velocity profile was applied, in line with the recent findings of Marzo et al [Marzo et al 2009]. Arterial walls were assumed to be rigid. The validity of this assumption has been extensively tested in the context of intracranial aneurysms by other authors [Dempere-Marco et al 2006]. Tetrahedral elements were used to discretize the core of the computational domain, with 3 layers of prismatic elements at the wall to ensure accurate computation of the velocity gradients. Grid sizes with an average density of 2000 el/mm³ were used as a result of a mesh dependency study in which WSS, pressure and velocity values, were monitored at several points within aneurysm and parent vessel. Figure-4.13 shows the meshes and BC types used in the analyses. Three cardiac cycles were computed for each analysis and haemodynamic data were extracted from the last cardiac cycle, herein assumed to be independent from the initial numerical conditions. Analyses were run in parallel using 30 cluster nodes Xeon® 2.8 GHz 2GB RAM. The average time required to solve a complete 3-cycle analysis was approximately 5 hrs.

Statistical analysis: Quantitative agreement between data obtained with the different BC methodologies was analyzed using boxplot diagrams.

4.3.3 Results

Relevant haemodynamic variables were compared qualitatively and quantitatively for the BC methods analyzed. For the qualitative comparison I considered values of WSS time-averaged along the cardiac cycle (tavWSS) and OSI. The qualitative analysis of the results also included a comparison of the normalized values of tavWSS (ntavWSS), where normalization was done by dividing the absolute values of tavWSS to the spatial average of tavWSS at the aneurismal wall.

4.3.3.1 Qualitative comparison

Figure-4.14 shows contour distributions of tavWSS at the wall of the IAs considered.

For all methods, areas of relatively high WSS concentrate around the aneurysmal neck and apex, for aneurysms 1, 2, whilst for aneurysms 5 an area of relatively higher WSS is also present at the body. In aneurysms 3 and 4 only the neck is affected by high WSS, leaving the remaining part of the aneurysmal wall exposed to lower values of WSS. For all aneurysms, areas of relatively low WSS concentrated around their bodies.

From a visual comparison of the contour plots, the most pronounced differences between method I (pc-MR) and method II (1D-model) are in the distribution of tavWSS for aneurysms 1, 3, and 5 whereas aneurysms 2 and 4 showed closer agreement. As an effect of the quantitative differences between patient-specific and 1D model waveforms, for all IAs except 2, tavWSS values were underestimated when 1D-model BCs were applied.

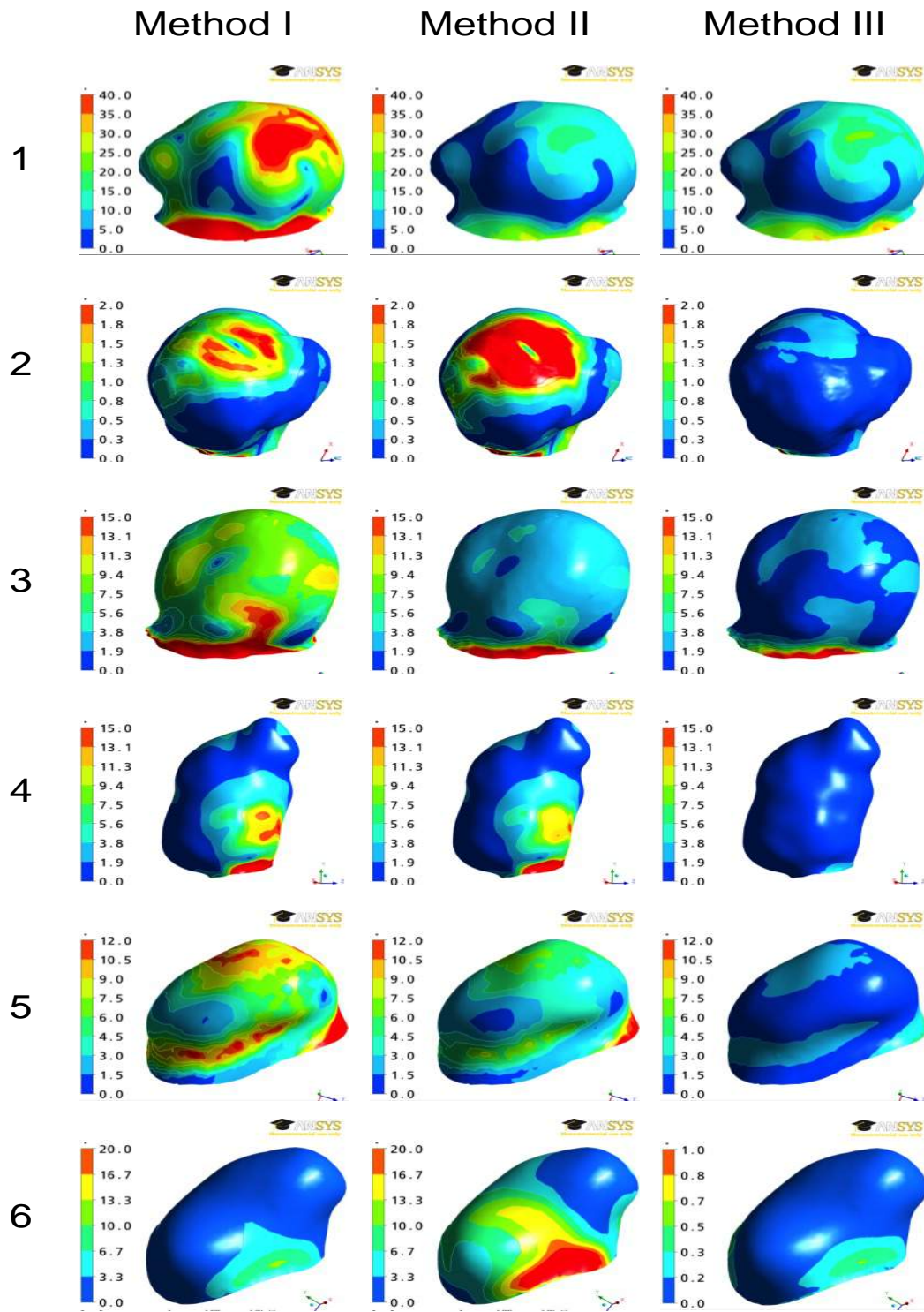


Figure- 4.14: Contour plots of tavWSS for method I (pc-MR), method II (1D-model), and method III (WSS-scaled).

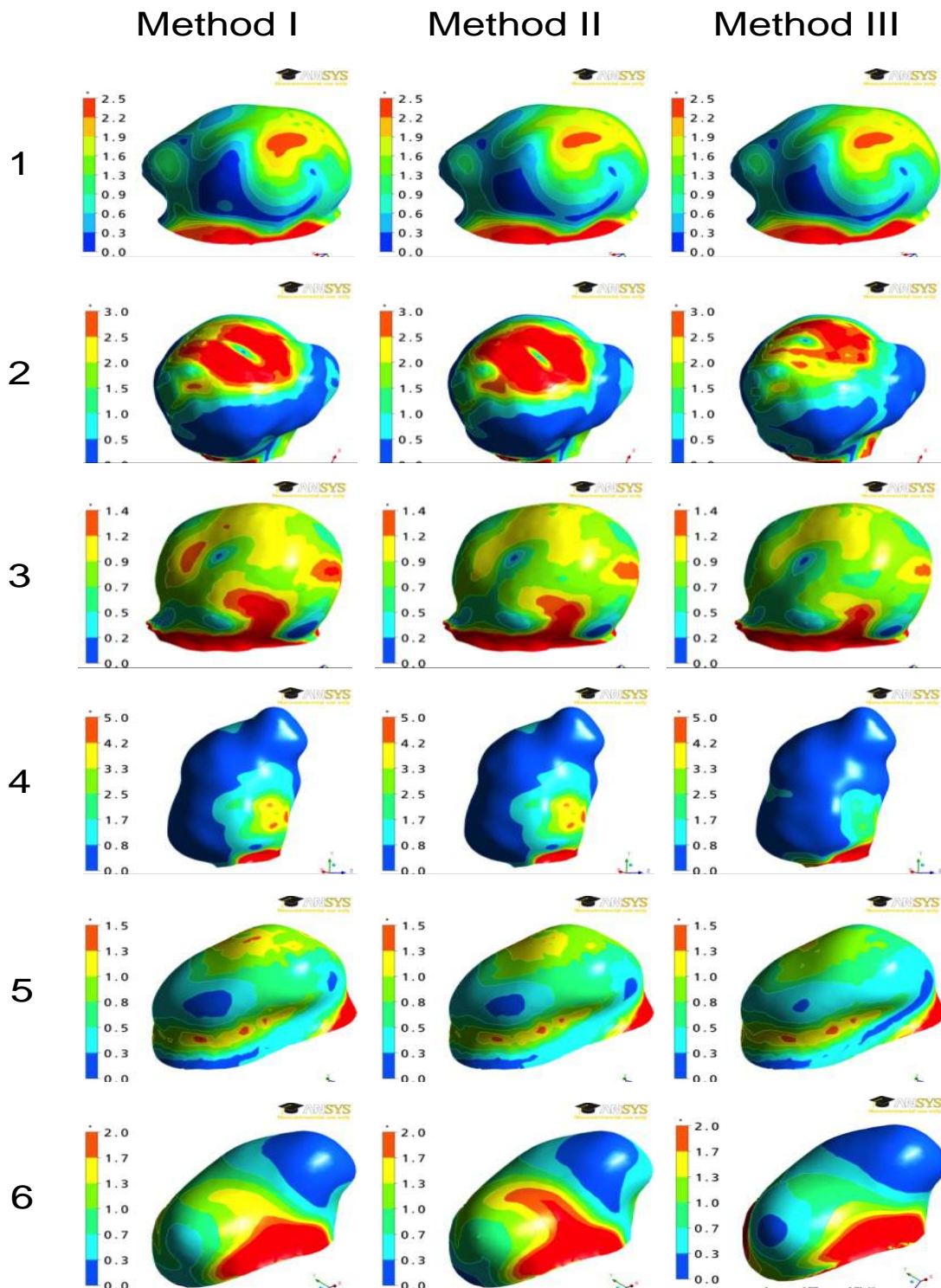


Figure-4.15: Contour plots of normalized values of tavWSS (ntavWSS) for method I (pc-MR), method II (1D-model), and method III (WSS-scaled).

The qualitative comparison between method I (pc-MR) and method III (WSS-scaled) showed larger discrepancies than those observed when comparing method I and II, except from aneurysm 1 where contour values of tavWSS are closer to the method I predictions. Values of tavWSS

obtained with method III are for all IAs smaller than those observed in method I. Figure-4.15 shows contours of normalized values of $\tau_{av}WSS$ ($ntavWSS$). Interestingly, the overall distribution of areas of proportionally higher, or lower, WSS is quantitatively similar for all methods.

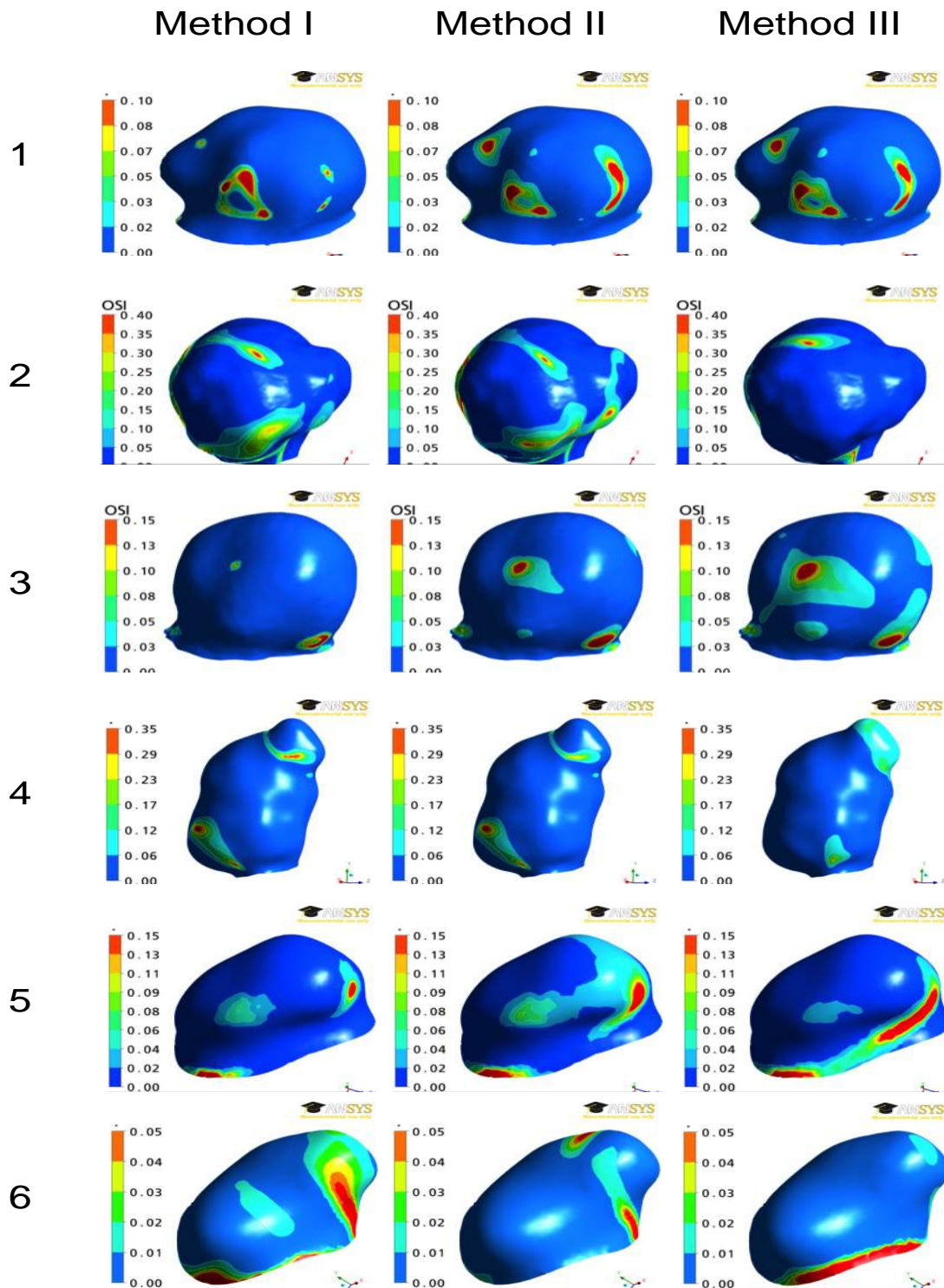


Figure-4.16: Contour plots of OSI for method I (pc-MR), method II (1D-model), and method III (WSS-scaled).

Figure-4.16 shows contour distributions of OSI on the surface of the aneurysms. Although some small differences can be observed, the OSI patterns are very similar, with areas of higher values occupying the same locations for all methods employed. As expected, areas of elevated OSI tend to concentrate where tavWSS is low. OSI values obtained with method II look closer to the pc-MR-based values, than those obtained using method III.

4.3.3.2 Quantitative comparison

For some selected indices computed within the aneurismal sac, namely maximum OSI (mOSI), normalized maximum value of time-average WSS (nmtavWSS), maximum time-average WSS (mtavWSS), maximum time-average velocity (mtavU) and spatial and time-average velocity (stavU), Figure-4.17 reports the boxplots diagrams of the percentage differences between method I and method II (top boxplot) and method I and method III (bottom boxplot). Percentage error was calculated as equal to

$$(\text{index_valuemethodI} - \text{index_valuemethodX}) / \text{index_valuemethodI} \times 100$$

As previously observed in the qualitative comparison, both quantitative comparisons show that the smallest discrepancies are observed in the values of mOSI and nmtavWSS (median value 17.5-23.5% for mOSI and 11-20.5% for nmtavWSS). On the other hand, the haemodynamic index showing highest discrepancies is mtavWSS with median values of 46% for method I vs. II and 69% for method I vs. III.

When considering the cross-comparison of the methods II (1D-model) and III (WSS-scaled) with method I (pc-MR), herein assumed as gold standard, the larger discrepancies are observed for the comparison between methods III and I. If I consider only the median values of each index we observe that all indexes in method I perform better than their counterpart in method III.

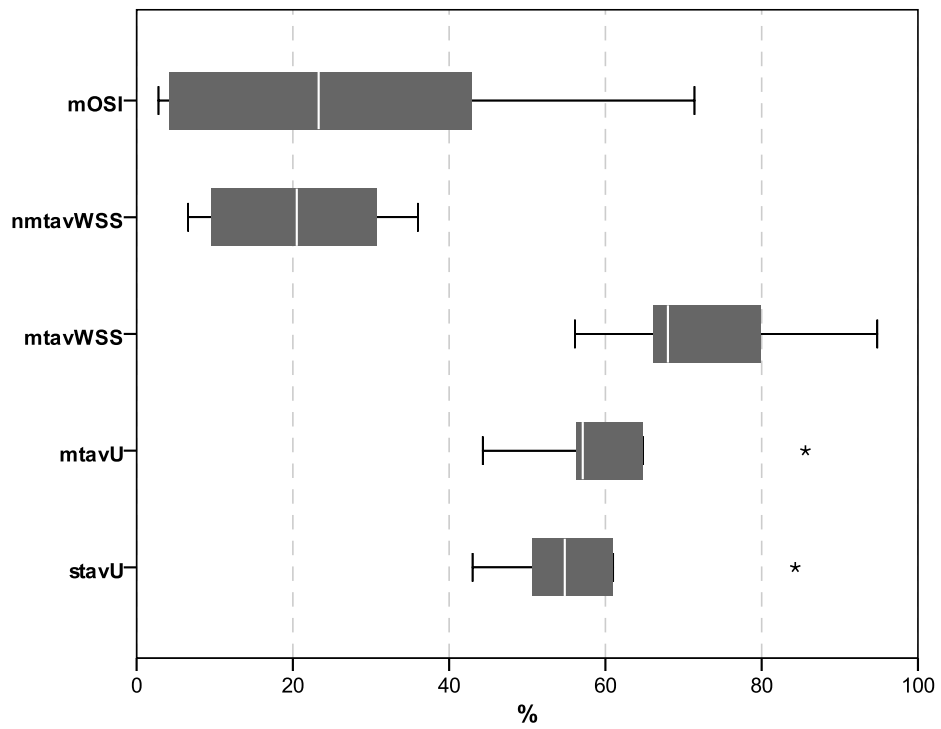
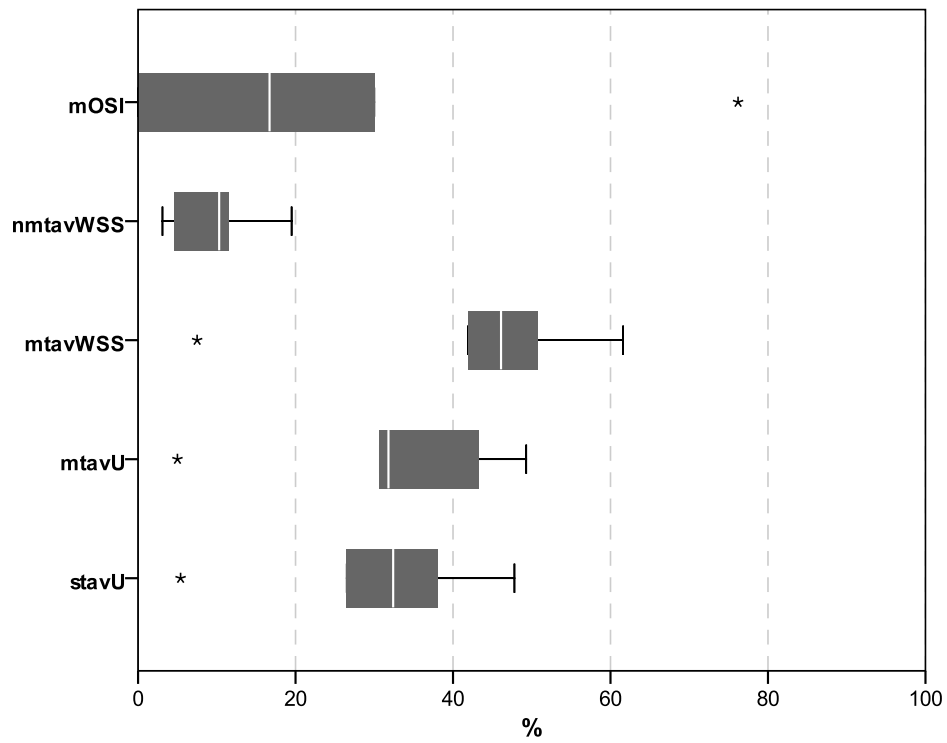


Figure-4.17: Boxplots showing the distribution percentage differences between methods I and II (top) and method I and III (bottom). Asterisks denote outliers above or below 1.5 times the inter quartile range.

4.3.4 Discussion

The creation of a computational model for the prediction of haemodynamics in IAs requires assumptions that can adversely affect the numerical results. One of the most important areas where assumptions are frequently required is the application of BCs. Several authors have demonstrated the major influence of BCs on computed haemodynamic indices [Hassan et al 2004, Chatziprodromou et al 2003, Rayz et al 2008, Venugopal et al 200].

Depending on their method of derivation, BCs can be broadly divided into two categories: patient-specific and non-patient-specific BCs.

4.3.4.1 Patient-specific BC:

Patient-specific-BCs are deservedly considered as ‘gold-standard’ [Hassan et al 2004, Chatziprodromou et al 2003, Venugopal et al 2007]. Unfortunately, these are rarely available. Of the 24 articles on CFD in IAs reviewed for this study (Table-4.7), only six (25%) used patient-specific BCs [Jou et al 2003, Hassan et al 2004, Jou et al 2005, Boussel et al 2008, Rayz et al 2008, Rayz et al 2008b]. In these studies, pc-MR remained the most common modality (5 out of 6) for obtaining patient-specific measurements, while TCD was used by one author [Hassan 2004]. Most authors (5 out of 6) applied these measurements only at inlets. Jou and colleagues [Jou et al 2005] was the only group to use patient-specific pc-MR measurements both at inlets and outlet for analyzing a basilar artery fusiform aneurysm. Thus, even when patient-specific measurements can be justified in a busy clinical setting, technical difficulties may compromise their application at all openings, further limiting their use in establishing statistical correlations with rupture. In fact, a major constraint when adopting patient-specific BCs is that due to current restrictions in obtaining these measurements, they have not been applied in large cohort studies, thus compromising the possibility of using CFD to find significant statistical correlations between haemodynamics and aneurysmal evolution (initiation, growth and rupture). In the current review, the mean cohort size in the patient-specific group was significantly smaller, i.e. 3 (range 1-7) [Boussel et al 2008, Castro et al 2006, Castro et al 2006b, Castro et al 2006c, Cebal et al 2005, Cebal et al 2009, Chatziprodromou et al 2003, Dempere-Marco et al. 2006, Hassan et al 2004, Jou et al 2003, Jou et al 2003, Karmonik et al, Mantha et al 2006, Marzo et al 2009, Mitsos et al 2008, Radaelii et al 2008, Rayz et al 2008, Rayz et al 2008b, Shimogonya et al 2009, Steinman et al 2003, Venugopal et al 2007] as compared to 9.5 (range 1-62) where non-patient-specific BCs were used [Shojima et al

2004, Cebral et al 2005, Shojima et al 2005, Jou et al 2008]. There is another important aspect one has to consider. There may be significant diurnal variations in a person's day-to-day life associated with stress or anxiety [Ford et al 2008, Kulikov et al 2005] physical exertion [Gonzalez-Alonso 2004, Ide and Secher 2000] and other day-to-day activities [Hajjar et al 2007]. It can be argued that patient-specific BCs, invariably measured with a patient lying quietly in a scanner surrounded by an artificial environment or stressed by the overall clinical experience (e.g. white-coat hypertension), might not represent the normal day-to-day physiology for that individual, and therefore might not represent exactly the type of BCs I need for our statistical associations. Gonzalez-Alonso et al [Gonzalez-Alonso 2004] recorded population-average flow rate variation as high as 1 ml/s at middle cerebral artery level between a rest and exercise status.

Table-4.6: Time-average volumetric flow-rates and inlet radii for the 6 aneurysms in study

	$Q_{av-MR}(ml/s)$	$Q_{av-ID}(ml/s)$	$Q_{av-wss}(ml/s)$	$r_{pt}(mm)$	$r_{ID}(mm)^*$
Aneu-1	7.53	3.95	4.31	2.3	2.1-2.6
Aneu-2	1.46	1.90	0.74	1.3	1.4-1.5
Aneu-3	6.36	3.94	3.11	2.1	2.1-2.6
Aneu-4	2.00	1.91	0.42	1.1	1.4-1.5
Aneu-5	5.44	3.95	2.21	1.9	2.1-2.6

NB: Aneu; aneurysm, Pt.; patient, Q_{av-MR} ; average flow measured using pc-MR, Q_{av-ID} ; average flow predicted by 1D-model, Q_{av-wss} ; average flow predicted by 1D-model scaled to obtain WSS=1.5 Pa at boundary, r_{pt} ; radius of the vessel as measured in the patient, r_{ID} ; average radius of the vessel used in 1D-model, * min and max radii in 1D model vessel where BCs was originated

4.3.4.2 Non patient-specific BC:

In absence of patient-specific-BCs many investigators use typical or modeled BCs. Out of 24 authors in the current review 18 (75%) [Steinman et al 2003, Bousset et al 2008, Castro et al 2006b, Castro et al 2006c,

Lt ICA before ophthalmic

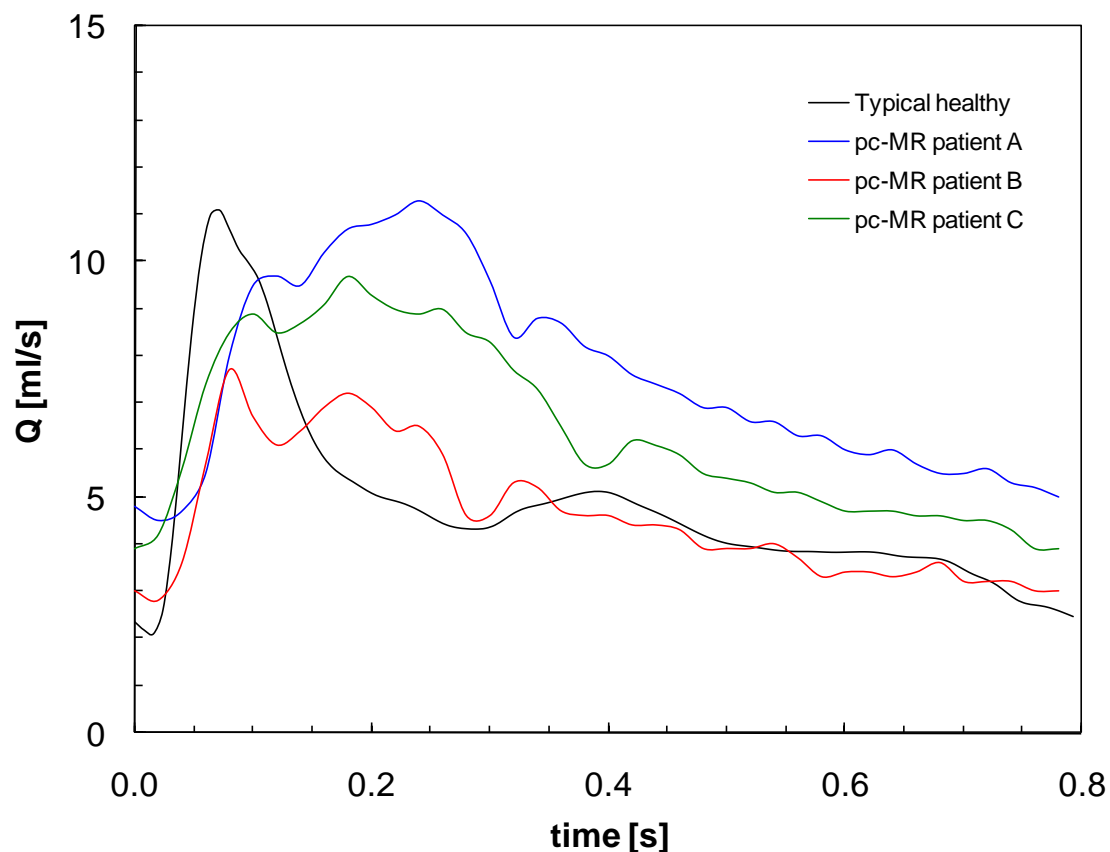


Figure-4.18: VFR waveforms for a typical healthy individual and aneurysm patients included in this study, measured using pc-MR at internal carotid level. Typical waveform was taken from Radaelli et al 2008.

Castro et al 2006d, Cebal 2005a, Cebal 2009, Chatziprodromou et al 2003, Hassan et al 2004, Jou et al 2003, Jou et al 2005, Karmonik et al 2006, Mantha et al 2006, Marzo et al 2009, Mitsos et al 2008, Radaelli et al 2008, Rayz et al 2008, Rayz et al 2008b, Shimogonya 2009, Venugopal et al 2007] used this approach, reflecting their common usage. Non-patient-specific waveforms are usually obtained from population-averaged

measurements taken on healthy volunteers [Ford et al 2008, Chatziprodmou et al 2003]. While the use of such waveforms remains the most popular method of BC application (17 out of 18 non-patient-specific BCs in my review) [Shojima et al. 2004, Cebal et al 2005, Steinman et al 2003, Shojima et al. 2003, Jou et al 2008, Radaelli et al 2008, Chatziprodmou et al 2003, Cebal et al 2005, Karmonik et al 2006, Castro et al 2006, Castro et al 2006b, Castro et al 2006c, Cebal et al 2009, Mantha et al 2006, Mitsos et al 2008, Shimogonya 2009] they carry important limitations. First, as these measurements are taken in a healthy population, they may well differ from patient waveforms. This difference is apparent in Figure-4.18, where waveforms from a healthy volunteer show differences both in shape and values, when compared with those for patients 1,3, and 5.

Second, these waveforms represent average values of pressure and velocity across the population, and lack adaptability in terms of location and vessel geometrical properties. In an attempt to address these issues and make these typical waveforms more patient-specific, Cebal and colleagues in 2008 [Cebal et al 2008] suggested ‘scaling’ the inflow rates to the inflow boundary area to keep the WSS within a ‘physiological’ range (around 1.5 Pa). The same approach has been adopted by other scientists [Jou et al 2008, Radaelli et al 2008, Mitsos et al 2008]. Although Cebal and co-workers [Cebal et al 2008] found an important flow-area correlation based on experimental evidence at some specific vessel locations, their approach is very sensitive to the boundary location along the vessel, due to diameter variations along the vessel, and to segmentation error and image modality. More importantly, Cebal’s work is based on an important assumption derived from Murray’s law, which states that WSS should be constant across the branches of the vascular tree in order to minimize the energy used to drive blood flow. This hypothesis may be true for a typical healthy individual but, as reported by many authors in the field, it is mostly atypical variations in haemodynamics (e.g. WSS) that are believed to influence the aetiopathogenesis of IAs [Sekhar and Heros 1981, Shojima et al. 2004, Cebal et al 2005, Cheng et al 2007] challenged this hypothesis in their recent review, which showed large variations of average WSS (variation range: 0.2-1.6 Pa). Atypical values of WSS have been associated with other conditions such as maladaptive growth, congenital malformations, patent ductus arteriosus, and atherosclerosis [Cheng et al 2007].

Quarteroni and collaborators [Quarteroni et al 2004] pioneered the concept of using lumped and 1D-circulation-models in a quest to provide realistic BCs to 3D circulation models [Formaggia et al 2001, Lagana et al 2002].

More recently in 2009, Marzo and colleagues [Marzo et al 2009] introduced the use of a 1D-circulation-model to derive BCs while studying haemodynamics within IAs. This is the same model used in the current study. The parameters of the 1D model used in the current study are relative to a healthy typical individual, an approach exposed to the limitations mentioned above for typical “healthy” waveforms. Indeed, this might explain in part the discrepancies observed in the quantitative comparisons.

The use of a 1D model, however, as opposed to other methods allows flexibility in the locations of the model boundaries and, more importantly, has the potential of being adaptable to the patient specific parameters, when available, to obtain more representative values at the boundaries. The comparison in Figure-4.17 (top) shows important differences between 1D-model and pc-MR data ranging from a minimum median value of 11% (OSI) to a maximum of 46% (mtavWSS).

These discrepancies, however, are determined by differences in flow rates between the 1D model and patient specific waveforms, which are of the same order of magnitude of the physiological variations reported by Gonzalez-Alonso et al [Gonzalez-Alonso et al 2004], see Table-4.6.

As reported in the results session, differences among the different methods analyzed are only quantitative, while the distribution of WSS remains the same as shown by the comparison on the normalized data. This confirms once again the major role played by geometry in determining the haemodynamic development within the aneurysm [Cebal et al 2005, Marzo et al 2009].

For all methods scrutinized, the comparisons performed on the OSI values showed good agreement. This is in line with the fact the OSI in its definition uses the normalization of local WSS.

Table-4.7: A comprehensive review of the methods adapted by different authors while applying BCs

No	Author/ Year	Cohort size (IAs)	IA location (s)	BC type/ location	BC source (method)
1	Steinman et al 2003	1	Terminal ICA	Inlet/ ICA Outlets/ MCA, ACA	Healthy Subjects (pc-MR) Traction-free
2	Chatziprodromou et al, 2003	2	Supraclinoid ICA	Inlets/ ICA Outlets/ ICA	Healthy Subjects Traction-free
3	Jou et al, 2003	1	BA – Fusiform	Inlets/ VA Outlet/ BA	Patient-Specific (pc-MR) Patient-Specific (pc-MR)
4	Hassan et al, 2004	1	Vertebro-Basilar	Inlet/ VA Outlet/ BA	Patient-Specific (TCD) Traction-free
5	Shojima et al, 2004	20	MCA	Inlets/ MCA-M1 Outlets/ MCA-M2	Healthy Subjects (TCD) Traction-free
6	Cebral et al, 2005	62	ICA(22), MCA(14), Pcom(13), ACA(1), Post(9), (3 NA)	Inlets/ ICA, MCA, ACA, BA Outlets/ NA	Healthy Subjects (pc-MR) NA
7	Jou et al, 2005	2	BA (fusiform)	Inlets/ VA Outlets/ PCA	Patient-Specific (pc-MR) NA
8	Shojima et al, 2005	29	ICA (14), MCA (14), MCA (1)	Inlets/ ICA Outlets/ ICA, MCA	Healthy Subjects (TCD) Traction-free
9	Cebral et al, 2005	4	ICA (1), SCA (1), ICA (1), Pcom (1)	Inlets/ NA Outlets/ NA	Healthy Subjects (pc-MR) Traction-free
10	Karmonik et al, 2006	3	BA top	Inlets/ BA, VA Outlet	Healthy Subjects, (pc-MR/ TCD) NA
11	Castro et al, 2006	4	Pcom (1), Acom (1), MCA (2)	Inlets Outlets/ NA	Healthy Subjects (pc-MR) Traction-free
12	Castro et al, 2006	7	Acom (1), BA (1), ICA (2), MCA (1), SCA (1), PCA (1)	Inlets/ NA Outlets/ NA	Healthy Subjects (pc-MR) Traction-free
13	Castro et al, 2006	2	Acom	Inlets/ ICA Outlets/ NA	Healthy Subjects (pc-MR) Traction-free
14	Mantha et al, 2006	3	ICA	Inlets/ NA Outlets/ NA	Healthy Subjects (Scaled) NA
15	Venugopal et al, 2007	1	Acom	Inlet/ A1 Outlet/ A2	Healthy Subjects (Scaled) Traction-free
16	Boussel et al, 2008	7	BA(3), ICA(3), MCA(3)	Inlets/ NA Outlets/ NA	Patient-Specific (pc-MR) NA
17	Mitosos et al, 2008	1	Acom	Inlet/ NA Outlet/ NA	Healthy Subjects (LDV) Traction-free
18	Rayz et al, 2008	4	BA	Inlets/ VA Outlets/ PCA	Patient Specific (pc-MR) Traction-free
19	Radaelli et al, 2008	1	ICA	Inlet/ ICA-proximal Outlet/ ICA-distal	Healthy Subjects (Scaled) Traction-free
20	Rayz et al, 2008	3	BA	Inlet/ VA Outlet/ PCA	Patient-Specific (pc-MR) Likely traction free
21	Shimogonya et al, 2008	1	ICA	Inlet/ ICA-proximal Outlet/ ICA-distal	Healthy Subjects waveforms Traction-free
22	Jou et al, 2008	26	ICA-clinoidal	Inlets/ ICA Outlet/ NA	Healthy Subjects (Scaled) NA
23	Marzo et al, 2009	3	BA, ICA	Inlet/ BA, ICA-proximal Outlet/ BA, ICA-distal	Computed (1-D Model) Traction free
24	Cebral et al, 2009	1	BA top	Inlet/ Mid BA Outlets/ PCA	Healthy Subjects (Scaled) Traction-free

NB: BCs; boundary conditions, PC-MR; phase contrast magnetic resonance angiography, TCD; trans-cranial Doppler's ultrasound, LDV; laser Doppler Velocimetry, ICA; internal carotid artery, ACA; anterior cerebral artery, Acom; anterior communicating artery, MCA; middle cerebral artery, Pcom; posterior communicating artery, SCA; superior cerebellar artery, BA; basilar artery; VA; vertebral artery, Post; posterior circulation

The current study will benefit from a larger cohort size (5 aneurysm only in current study), although this is bound to the difficulties experienced while performing pc-MR measurements in a clinical environment, and from a wider range of aneurysm locations, for example aneurysm of the anterior communicating artery (AComA) or basilar artery, which were not available for this study.

4.3.5 Conclusions

Significant differences were found between results obtained with patient-specific and modeled BCs. These are largely attributable to the underlying differences in the waveforms (similar peak but higher mean flow was observed in the measured values). It is most likely that in future patient-specific BCs will be provided as a part of the routine clinical procedure. Before that, CFD has to affirm itself in finding statistical correlations using non-patient-specific-BCs. The results of this study show that the 1D circulation model adopted by @neurIST performs better than other approaches found in the literature and offers a viable means to find correlation with rupture in large cohort size studies.

4.4: Overall Conclusions form this Section

In the study on the validation of different concepts used in CFD, I demonstrated that there is no added advantage of complex Womersley-flow-profile over the much simpler plug-flow profile.

The second study in this section on Modeled vs. Patient-Specific Boundary Conditions it I found that there are significant differences in the results obtained with these two methods. These are largely attributable to the underlying differences in the waveforms (similar peak but higher mean flow was observed in the measured values). It is most likely that in future patient-specific BCs will be provided as a part of the routine clinical procedure. The results of this study show that the 1D circulation model adopted by @neurIST performs better than other approaches found in the literature and offers a viable means to find correlation with rupture in large cohort size studies.

CHAPTER 5.0: EVALUATIONS AND CONTROLLED EXPOSURES OF @NEUFUSE TOOL-CHAIN

OVERVIEW

5.1. Introduction

5.2 The role of computational fluid dynamics in the management of unruptured intracranial aneurysms: a clinicians' view

5.2.1 Background and Objectives

5.2.2 Materials and Methods

5.2.3 Results

5.2.4 Discussion

5.2.5 Conclusions

5.3 Appendix-1

****My contribution:** In the study described in this chapter, I played a major role in concept, study design, conducting review of literature, conducting workshops for exposure of the tools, collecting feedback, performing analyses, performing statistical calculations, writing and submission of manuscripts to journals for publications. Dr Alberto Marzo, Dr Alessandro Chiarini and Dr Keith McCormack gave important support and contribution in conducting workshops at different venues.*

****Declarations:** Whereas, as mentioned below, a total of six evaluations of the software @neuFuse were performed at different international locations by conducting the workshops, due to unavailability of the data only the first workshop conducted during the meeting of ESMINT (European Society of Minimally invasive Neurological Therapy), in Lisbon, Portugal, is included in this chapter.*

5.1. Introduction

The tool-chain @neuFuse was developed under Project @neurIST by teams of computer and biomedical scientists working across a number of centers as described in Chapter 3 - Materials and Methods. The development of the tool-chain was a process of trial and error where the perfect final product could only be achieved due to continuous improvements made hand in hand while it was still under development.



 	
Edifício "Egas Moniz", Hospital de Santa Maria Faculdade de Medicina da Universidade de Av. Professor Egas Moniz 1649-028 Lisboa, Portugal http://www.fm.ul.pt	
Workshop Evaluation - @neufuse	
Personal Details	
Title: _____	First Name: _____ Surname: _____ Age: _____
Degree: _____	
Job Title: _____	
Institution/Department: _____	
Background: _____	Clinical Engineering Scientific Other: _____
Address: _____	
Email: _____	
Telephone: _____	
Section 1: General Feedback	
Q1. Why did you decide to participate to this workshop?	Working in the field Suggestion by colleague Interested in computational haemodynamics Improve management of aneurysms Other: please specify
Q2. How useful did you find this workshop?	Not 1 2 3 4 5 Very
Q3. Would you recommend a friend to attend?	No Yes
Q4. Would you recommend the software to a friend	No Yes
Q5. Any specific shortcomings, surprises?	1. 2. 3.
Q6. Any suggestions for course improvements?	No Yes, I've described them below

Figure-5.1: Snapshot of a Questionnaire used to gather Feedback

Due to the importance of haemodynamics in the aetiopathogenesis of intracranial aneurysms (IAs), mathematicians and engineers are increasingly using computational fluid dynamics (CFD) for haemodynamic predictions. However, whilst engineers and computer scientists devote their efforts towards the development and validation of these computational tools, it is imperative to collect the opinion of the clinical and other scientific community and evaluate their experience with the software.

5.1.1 Methods in general: The evaluation of these tools was done by conducting six hands-on workshops on CFD analysis. The workshops are designed by keeping in mind a wide range of audience including clinicians (Neurosurgeons/ Neuroradiologists/ Neurologists/ Nursing etc.), Biomedical Engineers, Computer Scientists, Software Programmers, Epidemiologists, CFD scientists and Residents still in training. The workshops were typically of 75 minutes consisting of an initial overview of the IAs and their current management followed by explanation of basic concept of CFD and role of haemodynamic and morphological indices in the aetiopathogenesis of these lesions. The participants were then presented with a clinical vignette treated using the current management protocols. They were then asked to perform the CFD analysis on the IA of the same patient using a printed 'Ready Reckoner' and see the results at

the end. The case was reappraised again in the light of available CFD results at the end of CFD analysis. The management was then discussed with participants in the form of an open question that if they had offered a different treatment to the patient if they would have these results beforehand? A Preformed Questionnaire (Figure-5.1, also given as an Appendix at the end of this chapter) was used to gather feedback on all these issues as well as about the different aspects of software @neuFuse. The data was analysed later and which was used to improve the on-going development of the software.

A total of six evaluations of this type were performed at different international locations. The first planned exposure of this series, conducted during the meeting of ESMINT (European Society of Minimally invasive Neurological Therapy), in Lisbon, Portugal, is described below in detail in this chapter. The findings of this exposure have been published in the form of a peer-reviewed paper the journal *Computational Intelligence and Neuroscience*: [Singh et al 2009]

5.2 The role of computational fluid dynamics in the management of unruptured intracranial aneurysms: a clinicians' view

5.2.1 Background and Objectives

The management of unruptured cerebral aneurysms remains one of the most controversial topics in neurosurgery. These uncertainties are multifactorial owing mainly to incomplete natural history of these lesions and risks associated with active management [Juvela et al 2004, Raaymakers et al 1998, ISUIA 1998, Wiebers et al 2003]. Recent evidence, however, suggests a good correlation between different haemodynamic factors and aetiopathogenesis of intracranial aneurysms [Burlison et al 1996, Gao et al 2008, Morimoto et al 2002, Byrne et al 1998]. This, together with the fact that current technologies do not allow detailed in-vivo measurements of blood flow [Shojima et al 2004, Steinman et al 2003] in cerebral arteries have given computational fluid dynamics (CFD) new strength and a chance to affirm itself as a technology that can help in the management of unruptured intracranial aneurysms. Many studies have been published where patient-specific medical images and CFD are used to predict relevant haemodynamic variables that correlate well with initiation, growth, and rupture of an IA [Boussel et al 2008, Cebal et al 2005, Cebal et al 2005, Castro et al 2006, Steinman et al 2003, Shojima et al 2004, Mantha et al 2006]. Until recently, engineers, physicists or mathematicians performed these works in collaboration with select clinicians. However, in order to make an impact on clinical practice and to enhance trust among clinicians, a controlled and extensive exposure of the software and its

concepts to the broader clinical community is crucial along with its continuing validations.

The current study is the first effort of its kind where the concept and application of CFD software was exposed to the clinical community, followed by analysis of their views, understanding and performance.

5.2.2 Materials and Methods

The first gathering of the ESMINT (European Society of Minimally Invasive Neurological Therapy) Teaching Course on intracranial aneurysms was chosen as an ideal opportunity to expose the computational tools being developed within the European project @neurIST (@neurIST), to the attention of its audience. The workshop was held near the birthplace of angiography at the “Edificio Egas Moniz” of the Hospital Santa Maria in Lisbon, Portugal between 6th and 12th September 2008.

5.2.2.1 Participants’ Demography and Overview

The workshop was attended mainly by neurosurgeons and neuroradiologists. Out of all participants 86% had a clinical, 8% and engineering, and 6% a scientific background. Participants broadly fell into four age groups: 20-30 yrs. old (3 participants, 8%), 31-40 (22, 61%), 41-50 (9, 25%), 50+ (2, 6%). Participants were prevalently male with a ratio M: F = 8:1. These data are summarized in Figure-5.2.

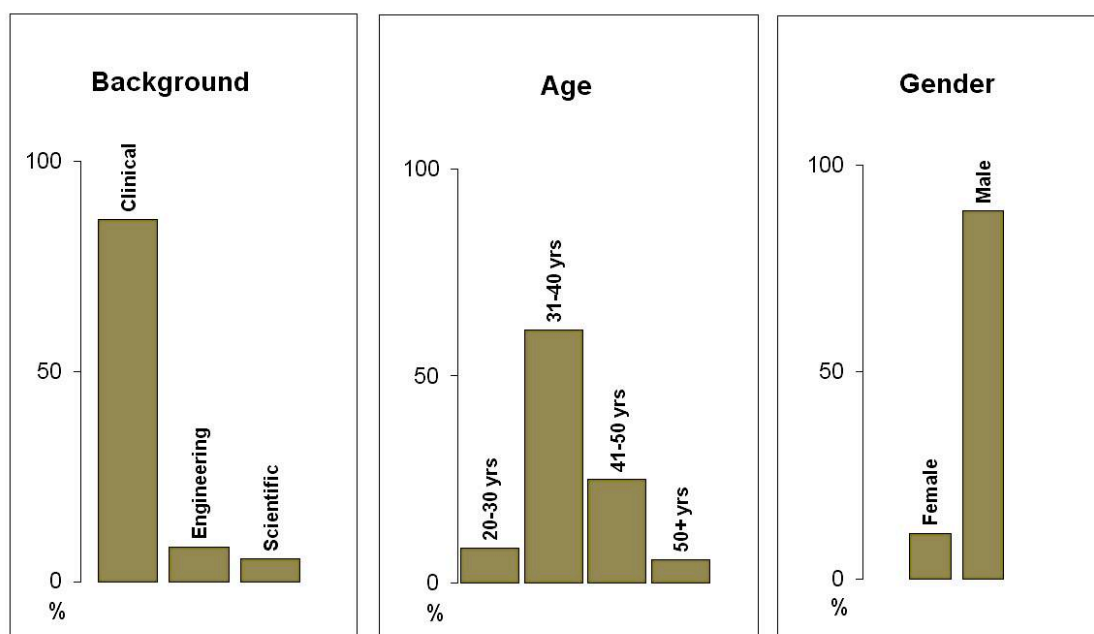


Figure -5.2: Participants’ demographic constitution

Participants were subdivided into groups of about 8 individuals per session to maximize teacher-to-attendee ratio. Two tutors were available during each session, one with a clinical background, (neurosurgeon= Pankaj Singh, the author) and one with an engineering background (biomedical engineer= Alberto Marzo). Teaching was delivered via a lecture of 75 minutes, which included a discussion of the clinical background and relevance of haemodynamic factors in aetiopathogenesis of IAs, a brief introduction on the use of CFD in haemodynamic predictions, and explanation of key fluid dynamics concepts in this context e.g. wall shear stress (WSS), boundary conditions etc. This was followed by a supervised hands-on experience with the software.

Clinical Vignette:

A 23-year lady attends neurovascular clinic with her partner. Her mom died one month back due to subarachnoid hemorrhage from a cerebral aneurysm. She smokes around 10 cigarettes a day but is otherwise fit and asymptomatic. After a long discussion it was decided to screen her for the possibility of an intracranial aneurysm. The MRA revealed the presence of an aneurysm of 5 millimetre maximum diameter in the region of left terminal ICA. She expresses great concerns about the diagnosis and is keen on exploring the active treatment options rather than being observed by routine follow-up.

Figure 5.3: Clinical Vignette: typical challenging case scenario

The exercise was presented to the audience via a clinical vignette of a typical difficult scenario encountered in the clinic, represented in Figure-5.3.

The vignette illustrates a typical case of an incidentally discovered IA in an anxious young patient. Due to its size (5 mm maximum diameter) and absence of any other major known risk factors, the aneurysm should be managed conservatively as per ISUIA (International Studies for Unruptured Intracranial Aneurysms) guidelines [ISUIA-1998, Wiebers et al 2003]. However due to patient's concerns and insistence for active intervention the management plan becomes controversial.

The participants were then asked to use the software @neuFuse to extract additional and non-observable haemodynamic data from the 3 dimensional rotational angiographic (3DRA) image of this case. Attendees performed the tasks independently with the help of a ready-reckoner containing the complete guided procedure with illustrations to facilitate the exercise. One-to-one support and supervision was provided during each session, as required.

5.2.2.2 Image Acquisition and Processing

The medical image used in the workshop was obtained using rotational acquisition in a Philips® Integris™ Allura™ machine (Philips® Medical Systems, Best, The Netherlands), producing 100 images in 6 seconds, with 5ms exposure per image. Voxel size in the reconstructed 3D images was 234 microns with reconstruction matrix 256x256x256. Images were anonymized, respecting the @neurIST ethical approval for use of patient data. The characteristics of the aneurysm considered in this study are reported in Table-5.1.

Table-5.1: Aneurysm Radiological Characteristics

Localisation:	Carotid artery/ ophthalmic segment/ medial wall
Side:	Left
Dome status:	Unruptured
Depth:	4.2 mm
Max diameter:	5 mm
Max neck width:	3.7 mm
Type:	Side-wall, saccular
Aspect:	Smooth

The current version of the @neuFuse software (prototype 4), based on the Multimod Application Framework [Viceconti et al. 2004] and developed within the @neurIST project, was used to reconstruct the vessel surfaces, create the model and set up the haemodynamic analysis. The solvers used within @neuFuse to solve the fundamental equations describing the blood flow behavior within the region of interest were ANSYS®-ICEM™ and ANSYS®-CFX™ (Ansys®, Inc., Canonsburg, PA, USA).

For the purpose of the workshop a simple stationary analysis (non-pulsatile but constant flow rate and pressure at the openings of the region of interest) was performed by the participants using Intel® core duo 2.4 GHz machines, with 2 GB RAM and 512 MB of dedicated graphic memory.

5.2.2.3 CFD Analysis

Figure 5.4 shows the overall workflow of the operations performed from uploading the raw medical image to the software through the visualization of relevant haemodynamic data in @neuFuse.

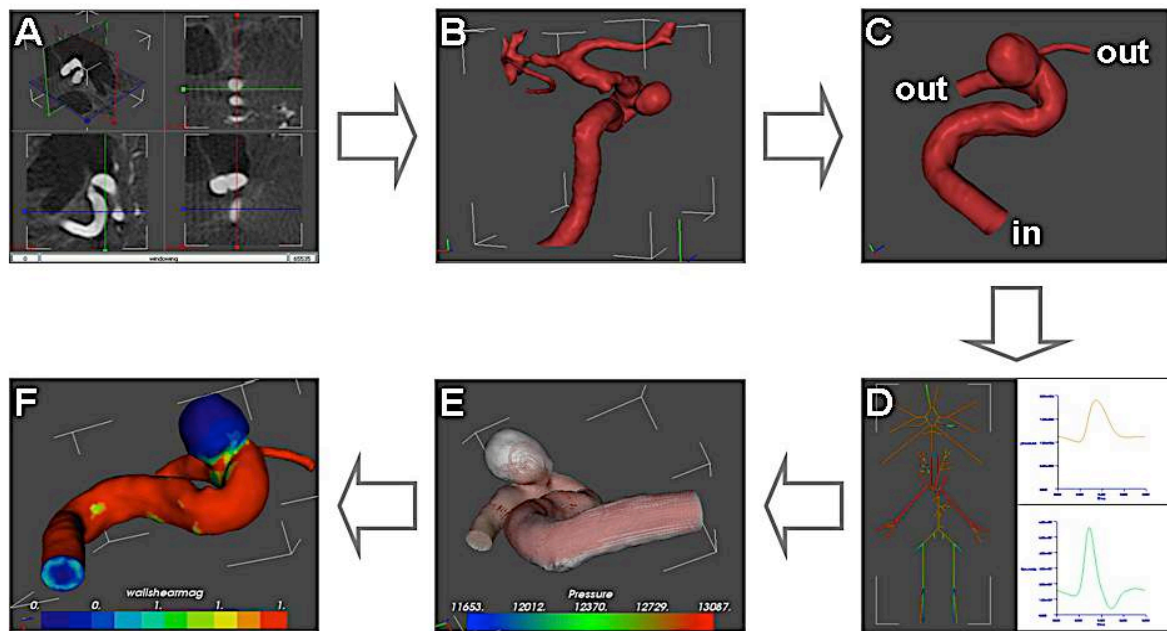


Figure 5.4: Operation workflow from medical image to haemodynamic results. A) Orthoslice visualization of the 3DRA medical image in @neuFuse. B) Visualization of the extracted vessel surface. C) Visualization of reduced region of interest with location of inlet and outlet openings. D) 1D circulation model. E) Visualization of predicted streamlines. F) Visualization of predicted wall shear stress.

Any CFD analysis requires knowledge of the volumetric region traversed by the fluid (i.e. aneurysm including connected surrounding vasculature) plus information about velocity and pressure of the fluid at the boundaries of the chosen region of interest (boundary conditions). Participants were asked to reconstruct the region of interest starting from the medical image, and specify the boundary conditions using the software @neuFuse. The first step was to launch @neuFuse and import the medical image (Figure 5.4A). The geometry of the vessel, including the IA, was then extracted from the imported image (Figure-5.4B). As only a sub-region of the extracted vasculature around the aneurysm has influence on the haemodynamic computation, all vessels entering or leaving the IA were identified and cropped at desired locations to define the region of interest (ROI). The ascending carotid artery, which was an inlet (blood enters the domain through it), was cropped at ten vessel diameters proximal to the IA as shown in Figure-5.4C. The distal carotid artery in the region of cavernous sinus and the ophthalmic artery were identified as the two outlets of ROI (blood exits the domain through these two vessels). These are shown in Figure-5.4C. For the sake of simplicity and time constrains the mesh used in the analysis was coarse and was constructed using simple tetrahedral elements. As is often the case in real-life clinical situations,

information on pressure or velocity of the blood at these locations for the patient under examination was not available. Boundary conditions were therefore provided by using a 1D mathematical model of the systemic tree, which has been developed within @neurIST [Reymond et al 2008]. A representation of the @neurIST 1D circulation model is depicted in Figure 3D. This model provides values of pressure and flow of blood at several locations along the systemic arterial tree, including locations in the circle of Willis for a typical individual. Plug-flow BCs were applied at inlet and pressure BC at outlet, using average values from the waveforms provided by the 1D circulation model. Typical values of blood viscosity ($\mu=0.004$ Pa.s) and density ($\rho=1066$ kg/m³) were applied to define the blood properties. Although the blood is a non-Newtonian fluid for the sake of simplicity and time-constraints, and also in view of recent findings from Cebal et al [Cebal et al 2005], I decided to assume constant blood viscosity.

Whilst arterial walls move under the effect of the propagating pressure waves, it has been shown that the effects of this movement on haemodynamic predictions are negligible [Jeays et al 2007]. Fixed walls were thus considered in this analysis. The computation was automatically performed by the software and participants were asked to display different predicted haemodynamic variables like flow streamlines (Figure-5.4E), pressure distribution within the aneurysm or arterial wall, and WSS (Figure-5.4F). Participants were then asked to compare the WSS values computed within the aneurysm with the critical values found in the experimental studies of Malek et al [Malek et al 1996] below which the endothelium is affected by cell loss, desquamation and deranged activity of wall-growth regulators.

5.2.2.4 Evaluation

Finally, the feedback was collected via a questionnaire consisting of 48 questions. These were broadly divided into 6 categories (Table-5.2); general feedback, course design and conduct, experience with the software, haemodynamics understanding, impact of CFD in neurosurgery, and bringing this software into routine use. Each section of the questionnaire was carefully designed to collect information on different aspects of the participant experience as described in Table-5.2. The questionnaire with the complete list of questions is reported in Appendix-1 at the end of this chapter.

Performance of participants was measured by analyzing the file containing an audit trail of the operations performed during the analysis. The performance criteria were based on the analysis settings that have major

influence on the outcome of the numerical predictions: The quality of the reconstructed geometry, its extension, the locations in the 1D circulation model from which boundary conditions were extracted, and the correctness of the applied boundary condition type (i.e. whether it was correctly set to inlet or outlet). Each correct operation was assigned one point, leading to a maximum score of four. Expert performance was considered as gold standard (4 out of 4) and participants' performance rate was compared against this,

5.2.3 Results

For each section of the questionnaire only data gathered for the most representative questions were reported in this manuscript. Results were represented using tables with percentage distribution for a ready appreciation of feedback across the participants. These are reported section by section below.

Table-5.2: Questionnaire sections and objectives

Section	Category	Objectives
1	General feedback	To gather impressions on the overall experience
2	Course design and conduct	To gather suggestions on possible improvements and identify any shortcomings in the design of the workshop
3	Experience with the software	To identify weak points as perceived by clinicians in the graphical user interface of the current version of the software
4	Haemodynamics understanding	To assess their current knowledge and understanding in the role of haemodynamics in the aetiopathogenesis of intracranial aneurysms
5	Impact of CFD in neurosurgery	To assess their faith in the principles of CFD and its use in the clinical environment, along with the need of validation through a multicentre trial
6	Bringing this software into routine use	To explore the participants view on cost related issues and gather information on future marketing potentials of this kind of software

Section 1: General feedback: As shown in Table-5.3, the overall feedback about the workshop was positive. The 86 % of participants would recommend the software to a colleague, 75 % found the workshop useful and 78% rated their overall experience between good and very good. Negative feedback was confined averagely within less than 5%. Most participants recognized the need to improve management of IAs and for 47% this was the main reason for attending the workshop.

Table-5.3: General feedback

<i>Question/Answer options</i>	<i>No of participants (%)</i>	
<i>Would you recommend the software to a colleague?</i>		
Yes	31	(86)
No	3	(8)
n.a.	2	(6)
<i>Why did you decide to participate to this workshop?</i>		
Working in the field	16	(45)
Interested in CFD	2	(6)
Improve management of aneurysms	17	(47)
Other	1	(2)
<i>How useful did you find this workshop?</i>		
Not useful	1	(3)
Not sure	8	(22)
Useful	16	(45)
Very useful	11	(30)
<i>Rate your overall experience</i>		
Poor	1	(3)
Average	7	(19)
Good	15	(42)
Very good	13	(36)

Section 2: Course design and conduct: 80% of candidates found the workshop to be of the right duration, 14% found it to be too short while for 6% it was too long (Table 5.4). Participants-to-instructor ratio was right for 91% while 6% thought that there were too many participants. Most of the participants did not have any difficulty in understanding the instructions. On a scale of 1 to 5, where 1 is not clear and 5 is very clear, 86% rated it 4-5, while 14% were not sure. 94% of the participants thought that the course content was scientifically appropriate.

Table-5.4: Course design and conduct

Question/Answers	No of participants (%)	
<i>Was the duration of the workshop ...</i>		
Right	29	(80)
Short	5	(14)
Long	2	(6)
<i>Was the participant-to-instructor ratio...</i>		
Right	33	(91)
Too-many	2	(6)
n.a.	1	(3)
<i>Were the instructions given in a clear way?</i>		
Not sure	5	(14)
Clear	18	(50)
Very clear	13	(36)
<i>Was the content of the course scientifically appropriate?</i>		
Yes	34	(94)
No	2	(6)

Section 3: Experience with the Software: 34% of the candidates found the current version of the software user friendly, 11% think it needs some improvement, while 6% found it was not user-friendly (Table-5.5). The remaining 46% were unsure. 48% of the participants think that clinicians with limited IT skills will find using the software challenging, 11% disagree with this assumption and 33% were not sure. 86% of all attendees were able to complete all the steps of the haemodynamic analysis within the time allocated (approx. 50 minutes). 11% missed one or more steps. Application of boundary conditions and clipping the region of interest were amongst the most difficult steps reported by majority of participants. These were equally distributed among participants with scientific and clinical background.

Table-5.5: Experience with the software

<i>Question/Answers</i>	<i>No of participants (%)</i>	
<i>Do you find the software user friendly?</i>		
No	2	(6)
Needs improvement	4	(11)
Not sure	17	(46)
User friendly	11	(31)
Very user friendly	1	(3)
n.a.	1	(3)
<i>Will clinicians without tech/IT experience have trouble?</i>		
Yes	17	(48)
Not sure	12	(33)
No	4	(11)
n.a.	3	(8)
<i>Were you able to complete all the steps of the haemodynamic analysis?</i>		
Yes	30	(86)
No	4	(11)
n.a.	1	(3)

Section 4: Haemodynamics understanding: Whereas for 78% of the participants it was easy to understand the technical concepts used throughout the course (Table-5.6), 19% faced some difficulties in understanding the terminology, mostly related to concepts such as boundary conditions and WSS.

36% of the participants showed trust in the results predicted by the software and think they are realistic. However, 58% were unsure. 48% believe that there is good scientific evidence to justify the role of haemodynamics in the aetiopathogenesis of IAs, 3% did not agree with this. 43% of the candidates were not sure. Whereas 50% of the participants were aware of the use of CFD as a tool in the prediction of rupture in IAs, 42% were hearing the concept for the first time.

Interestingly, 84% of all participants were willing to read further peer-reviewed articles published on CFD and role of haemodynamics in IAs.

Table-5.6: Haemodynamics understanding

Question/Answers	No of participants (%)	
<i>Did you have difficulty with the technical concepts (boundary conditions, wall shear stress, etc.)?</i>		
Yes	7	(19)
No	28	(78)
n.a.	1	(3)
<i>Are the results from this software realistic?</i>		
Yes	13	(36)
Not sure	21	(58)
No	0	(0)
n.a.	2	(6)
<i>Is current evidence sufficient to justify a role for haemodynamics in the pathogenesis of aneurysms?</i>		
No	1	(3)
Not sure	15	(43)
Yes	17	(48)
n.a.	2	6
<i>Were you previously aware of the use of CFD to predict the risk of rupture in intracranial aneurysms?</i>		
No	15	(42)
Yes	18	(50)
n.a.	3	(8)
<i>If you see a publication on computational predictions for IA in a peer-reviewed journal, will you read it?</i>		
No	3	(8)
Yes	30	(84)
n.a.	3	(8)

Section 5: Impact of CFD in neurosurgery: Responding to the question “Who should perform the CFD analysis for your patient”, 19% answered a consultant, 6% thought it should be done by a registrar or a junior member of the team (Table 5.7). 25% believed that analysis should be performed by a dedicated clinical scientist/engineer, while another 25% think that it can be done by anyone provided that they have adequate training.

84% of the participants were of the view that the software can be used as a diagnostic tool on outpatient basis, 8% did not agree with them. 84% of the participants were aware of similar software, whereas for 8% of them it was the first exposure to this kind of software. When asked about automated versus user-controlled software, interestingly 35% expressed a wish to retain user control. 26% preferred a fully automated tool, while another 26% were unsure.

Although the majority of participants (88%) were convinced that there is a future for CFD as a risk prediction tool, and that there is a significant, or emerging clinical need for these kinds of innovative tools (84%), most of them (75%) thought that the current version of the software was not yet ready and would require refinement before it could be introduced into clinical practice.

Table-5.7: Impact of CFD in neurosurgery

Question/Answers	No of participants (%)	
<i>Ideally, who should perform this type of computational analysis for patients?</i>		
Consultant	7	(19)
Dedicated clinical scientist	9	(25)
Registrar	2	(6)
Anyone with training	14	(38)
Office member	1	(3)
All	1	(3)
n.a.	2	(6)
<i>When ready could this software be used diagnostically in an outpatient clinic?</i>		
Yes	30	(84)
No	3	(8)
n.a.	3	(8)
<i>Are you aware of any similar software?</i>		
Yes	30	(84)
No	3	(8)
n.a.	3	(8)
<i>Should this type of analysis be fully automated, or is it better that the user has control?</i>		
Automated	10	(26)
User control	14	(35)
Not sure	10	(26)
n.a.	5	(13)
<i>Is there a future for computational tools for risk prediction of intracranial aneurysm rupture?</i>		
Yes	29	(80)
No	2	(6)
Not sure	2	(6)
n.a.	3	(8)
<i>How great a clinical need is there for this software?</i>		
Significant	17	(48)
Emerging	13	(36)
Low	3	(8)
n.a.	3	(8)
<i>Do you think that this type of analytical software is ready for introduction into the clinical environment?</i>		
Ready	4	(11)
Needs work	26	(75)
n.a.	5	(14)
<i>In which cases might this software influence your decision-making about patient management?</i>		
All	7	(19)
Small unruptured asymptomatic	14	(39)
Other	2	(6)
Not sure	1	(3)
None	3	(8)
n.a.	9	(25)
<i>Would you be interested in participating in a multi-centre trial on the evaluation of this software?</i>		
Yes	25	(69)
No	5	(14)
n.a.	6	(17)

64% of the candidates believed that an early prediction of the risk of rupture computed with the help of this software could influence their decision making in the management of an IA. Out of the 64% over half (39%) think that small asymptomatic unruptured cases specially falling in the border-line category based on current evidence, are the best cases where such software can provide definitive help. Interestingly, 19% thought that it could be useful in all cases. 69% of the participants were convinced of the need for a multi-centric trial for the evaluation of the software and expressed their willingness to participate in it.

Section 6: *Bringing this software into routine use:* Once the software is in routine use, 30% of the participants believed that it should be an integral part of the scanner (Table-5.8). 27% thought that it should be supplied as a standalone product, while 32% say it could be provided in either way.

Cost will be an important deciding factor for 72% and another 81% prefer it to be a freeware or shareware. However, cost is a low priority for 17% and another 11% won't mind paying for it.

Table-5.8: Bringing this software into routine use

Question/Answers	No of participants (%)	
<i>Would you expect this software to be provided as part of a scanner. or as a stand-alone product?</i>		
Scanner	11	(30)
Standalone	10	(27)
Both	12	(32)
n.a.	4	(11)
<i>Would the price of this software be an important factor in your deciding to obtain/use it?</i>		
Important	26	(72)
Low priority	6	(17)
n.a.	4	(11)
<i>Would you expect to pay for this software, or would you prefer a freeware/shareware arrangement?</i>		
Pay	4	(11)
Shareware	14	(37)
Freeware	17	(44)
n.a.	3	(8)

Performance: Attendees totalized an average score of 63% of experts' performance (Table-5.9). When age is taken into consideration youngest delegates in the group 20-30 yrs. scored highest (65%) with score figures reducing progressively with age. Age group 50+ obtained the lowest scores (56%). Performance was slightly higher in scientific community (2.7), as compared to the clinicians (2.5)

Table-5.9: Attendees' performance

	Score	%
<i>Average</i>	2.52	(63)
<i>Performance with</i>		
20-30 yrs	2.58	(65)
31-40 yrs	2.50	(63)
41-50 yrs	2.36	(59)
50+ yrs	2.22	(56)
<i>Performance with background</i>		
Clinicians	2.5	(63)
Scientists	2.7	(68)

5.2.4 Discussion

5.2.4.1 The current challenges posed by unruptured IAs

The easy availability and widespread use of relatively non-invasive and sophisticated neurodiagnostic modalities such as high resolution CT, MRI and MRA, have brought to clinical attention a large and ever increasing group of patients harboring unruptured and asymptomatic cerebral aneurysms. These unruptured lesions are also diagnosed coincidentally at the time of catheter angiography done for a ruptured aneurysm in patients having multiple aneurysms. The increasing awareness of relatively bleak prognosis related to aneurysmal rupture in general public and clinicians, forces neurosurgeons to come up with a definitive answer for these unruptured lesions.

With the advancements in the microsurgical techniques and improved neuroanaesthetic and interventional neuroradiological approaches, the morbidity and mortality figures associated with the active management of the ruptured aneurysms has improved significantly when compared to their conservative management. In other words, the indications for the active interventions in ruptured intracranial aneurysms are now well established. The situation unfortunately is not as straightforward in cases of unruptured aneurysms and, the management of these lesions remains one of the most controversial topics in Neurosurgery [Juvela et al 2004, Raaymakers et al 1998, ISUIA 1998, Wiebers et al 2003]. Most of the large series including ISUIA studies agree on the low risk of rupture for unruptured intracranial aneurysms. The cumulative rupture rates in ISUIA studies were between 0.05 to <1 percent per annum [ISUIA-1998, Wiebers

et al 2003]. The fact that the prevalence of unruptured aneurysms in general population outnumbers the incidence of subarachnoid hemorrhage shows that not all unruptured intracranial aneurysms share a common natural history. The annual prevalence of unruptured aneurysms in a population is around 5% [ISUIA-1998] while the incidence of subarachnoid hemorrhage in the corresponding population is observed up to a maximum of 10 cases per 100,000 persons per year [ISUIA-1998]. It is clear from the above-mentioned figures that 80 to 85% of all intracranial aneurysms will never rupture.

The current uncertainties in the management of unruptured intracranial aneurysms are well accepted by the clinical community, and were amongst the most important motivating factors for majority of the participants (47%) to attend this workshop.

In order to offer the best possible treatment to the patient with least side effects, the formulation of a clear management protocol, directed by the natural history of the unruptured intracranial aneurysms and the risks associated with the active management, is required. Whereas the endovascular coiling is increasingly being accepted as a preferred treatment modality for ruptured intracranial aneurysms, surgery has been advocated as a first line treatment for unruptured lesions [Juvela et al 2004, Wiebers et al 2003]. Although there are no strict guidelines, most of the studies [Juvela et al 2000, Komotar et al 2008, Mayberg et al 1994] including ISUIA trials (ISUIA-1998, Wiebers et al 2003), almost unanimously recommend certain factors as indications of surgery in unruptured aneurysms: large aneurysmal size, symptomatic lesions, evidence of growth, multiple lesions, posterior circulation location, and past history of SAH. All these criteria have been established to have good correlation with increased risk of rupture and hence, surgery is advocated in these situations to avoid the poor outcome. It is interesting to note that whereas on the one hand the above-mentioned criteria are used to decide the need and suitability for surgery in an unruptured intracranial aneurysm, all of these factors also remain the underlying descriptors for poor surgical outcome [Solomon et al 1994, Khanna et al 1996, Wirth et al 1983].

In the light of current evidence it is clear that the group which will stand best chances of an excellent outcome after surgery will be one with solitary, very small (<5 mm), truly asymptomatic aneurysms located in the anterior circulation, without any evidence of growth. Quite the contrary, current protocols dictate clinicians not to operate upon this group [ISUIA-1998, Wiebers et al 2003, Komotar et al 2008]; and in fact contraindicate

any active management option in such patients [ISUIA-1998, Wiebers et al 2003, Komotar et al 2008). Moreover, the small aneurysms of <5 mm size which are traditionally thought to be 'safe', are not 'rupture-proof'. In a study Yasui et al [Yasui et al 1996] found that in a group of 25-ruptured aneurysms, 16 (64%) were <5 mm in size. Similarly, Juvela and colleagues [Juvela et al 1993] who followed 142 patients with 181 aneurysms for a mean period of 13.9 years with an aneurysmal size of <4 mm, demonstrated a 19% rupture rate i.e. 27 out of 142 patients had a rupture.

In order to improve the surgical outcome if we choose to operate on these smaller and 'safe' lesions, we have to operate on every single patient. The ideal situation, however, would be if we could identify the aneurysms at greater risk of rupture while they are still small in size and operate upon them, leaving others to be monitored expectantly.

5.2.4.2 The emerging need for new alternatives

It is evident that due to limitations associated with conventional risk factors used to assess the risk of growth and rupture, it is currently impossible to identify those patients who are at an increased risk in this subset having a real need of an early surgery from those who can be monitored safely without any active intervention. The situation consequently leaves us with no options other than searching some new descriptors that can predict the risk of rupture independently in small cerebral aneurysms before they join the cohort destined for a poor surgical outcome. This is in part reflected by the large number of participants (84%, Table-5.7) who believe that there is a significant or emerging need of new alternatives.

There is a rapidly growing body of literature affirming the importance of haemodynamics in the aetiopathogenesis of cerebral aneurysms [Burleson et al 1996, Gao et al 2008, Morimoto et al 2002, Byrne et al 1998]. The haemodynamic variables often considered in these studies are wall shear stress (WSS), oscillatory shear index (OSI), blood pressure and other quantities used to characterize blood flow. Proportional to blood viscosity and its velocity, WSS is the tangential frictional force exerted by the flowing blood on the walls of each vessel. High supraphysiological and low infraphysiological values of WSS have been associated with initiation, growth and rupture of aneurysms [Gao et al 2008, Fukuda et al 2000, Meng et al 2007, Shojima et al 2004, Jou et al 2008, Malek et al 1996, Ujje et al 1999, Boussel et al 2008]. A measure of the oscillatory nature of these viscous forces is given by the oscillatory shear index (OSI), often associated with endothelial cells degeneration [Mantha et al, 2006, Glor et

al 2004, Goubergrits et al 2008]. Table 10 below gives a comprehensive list of haemodynamic variables from the literature and their association with intracranial aneurysm evolution.

An evaluation of these variables can provide a useful alternative to predict the behavior of an unruptured IA at an early stage before it changes in size, shape or becomes symptomatic. Unfortunately, the detailed in-vivo measurements of all relevant flow variables in the regions affected by the disease are currently impossible [Shojima et al 2004, Steinman et al 2003].

5.2.4.3 Computational Fluid Dynamics: a brief overview

Motivated by the important role played by haemodynamics and the difficulty of conducting detailed in-vivo observations of relevant haemodynamic variables, engineers and computer scientists have started using Computational Fluid Dynamics (CFD) to predict blood flows in intracranial aneurysms [Boussel et al 2008, Cebal et al 2005, Cebal et al 2005, Castro et al 2006, Steinman et al 2003, Shojima et al 2004, Mantha et al 2006].

Computational fluid dynamics is the science of predicting fluid flow, heat and mass transfer, chemical reactions, and related phenomena by solving numerically the set of mathematical equations that govern a particular physical system (conservation of mass, momentum, energy, species etc.) Since its early development in the 1960s and 1970s in the aerospace field, where it was mainly used to improve the design and efficiency of aircrafts [Anderson 1995], CFD has been successfully used in many other applications. In the past decades, engineers used CFD in the automotive, nautical, and civil engineering industries for conceptual studies of new designs, troubleshooting redesign, or improving the physical understanding of a novel fluid mechanical phenomenon. Supported by experimental studies and a profound theoretical knowledge of the application at hand, CFD can be applied anywhere the flow of a fluid is important. Validation, through comparisons with experimental data, has always been a key aspect in successful applications of CFD. In the context of its use in intracranial aneurysms, although some early validation work has shown promising results [Ford et al 2008, Ford et al 2005, Radaelli et al 2008, Karmonik et al 2008], a more systematic validation remains a prerequisite before CFD can be adopted as a routine tool in clinical practice. Whereas the majority of participants (78%) did not find any difficulty in understanding the technical concepts used in CFD, only 36% of them believed that the results produced by its application were realistic. The mistrust in the results indicates the need for validation. This is further

supported by the fact that most of the participants (84%) readily wanted to participate in a multi-centric clinical trial.

Although participants showed a manifest interest in computational predictions (Table 5.6), there is a clear lack of awareness concerning the role of haemodynamics in the aetiopathogenesis of IAs and the use of CFD in this context (42%, Table 5.6). More efforts therefore are required by the scientific community to enhance understanding of the role of haemodynamics and awareness of the use of CFD in this field.

Table 5.10: The literature-based evidence on the importance of haemodynamics in the aetiopathogenesis of IAs

Haemodynamic factors	Intracranial Aneurysm			Proposed mechanism(s)	References
	Initiation	Growth	Rupture		
<i>Dynamic</i>					
Wall Shear Stress (WSS)	High	Low	Low	Increased WSS increases the production of MMP-13 which in turn leads to vessel wall damage Decreased WSS increases iNOS synthesis- NO induced damage to vessel wall Low WSS increases endothelial proliferation and apoptosis	Boussel et al 2008, Fukuda et al 2000, Gao et al 2008, Jou et al 2008, Malek et al 1999, Meng et al 2007, Shojima et al 2004, Ujie et al 1999
Oscillatory Shear Index (OSI)	High/Low	High	High	Degenerative changes in endothelium	Glor et al 2004, Goubergrits et al 2008, Mantha et al 2006
Jet of Blood Stream	Impingement	Impingement	Impingement	Localized endothelial cell injury	Foutrakis et al 1999, Cebal et al 2005, Cebal et al 2009
Flow Pattern	-	-	Complex	Statistical association	Cebal et al 2005, Cebal et al 2009
<i>Hydrostatic</i>					
Pressure	High	High	High	Passive yield/ water hammer effect	Inci and Spetzler 2000, Morimoto et al 2002, Steiger et al 1989

NB: WSS; wall shear stress, MMP-13; matrixmetalloproteneseases-13, iNOS; inducible-nitric oxide synthase, NO; nitric oxide, OSI; oscillatory shear index

5.2.4.4 The concept of controlled exposure

The use of CFD in this context represents a significant change in the clinical workflow and a successful transfer of knowledge will only happen via carefully planned, controlled exposure. Clinical sites must be supported locally, underpinning the training for clinicians with the involvement of clinical scientists. The effectiveness of interdisciplinary transfer of knowledge is largely dependent on the course design and the methodology used. As reflected by the results (Table-5.9), a hands-on workshop using multimedia PowerPoint presentation, one-to-one supervision, and low participants-to-instructor ratio with a carefully designed course based on sound scientific principles, can lead to good

results. The correct duration of such a course is also an important factor (Table 5.4). A close collaboration between engineers and the clinical community is also a pre-requisite for successful transfer of knowledge. Supervision during this workshop was hence, jointly provided by a biomedical engineer and a clinician. Given a short training period of only 75 minute, the first ever exposure of the software and its concepts to most of the participants (Table 5.6), together with the fact that the software is still in its prototype stage, the overall response and average performance of 63% was remarkable. It is anticipated that performance can be enhanced to the level of the expert-user by means of a user-friendlier version of the software and more intensive training. The results also show a decline in performance with age. It may be associated with the IT skills necessary to use this type of software efficiently. This fact should be kept in mind when interpreting the results and formulating future training and translational requirements.

5.2.4.5 Software design improvement

Many valuable suggestions were collected from participants on the possible improvements in the software design and its functionalities. Among the important suggestions included automating the steps for which user intervention is not strictly necessary, improving user friendliness through a more intuitive graphical user interface (GUI) where the user is guided through the number of operations required, or use of the icons in place of the more cumbersome operation from the menu bar and, finally graphical representation of the 1D circulation model for easier application of boundary conditions. After discussing the feasibility with developers, most of these suggestions were implemented in the latest version of the software @neuFuse.

5.2.4.6 The expected place of CFD in Neurosurgery

It is interesting to note that the majority of the participants (63%, Table 5.7) want these analyses to be performed either by an expert clinical scientist/engineer or a person with the same level of expertise, rather than a clinician. The fact may reflect clinicians' reluctance to conduct the analyses themselves due to their understandable concern over time-constraints and may indicate the requirement of a dedicated team with sufficient infrastructure for the purpose. In spite of this, most of the clinicians (84%, Table 5.7) see the software as a handy tool, which can be used on an outpatient basis (e.g. ophthalmoscope, otoscope, etc.) rather than a specialist department-based facility (e.g. 3DRA, MRA etc.). On comparing the software in terms of the different properties of a diagnostic modality, which makes it an ideal outpatient tool versus those requiring a dedicated set-up, I found that this software has some important features of

an ideal outpatient tool. It is non-invasive and is not directly performed on the patient (patients do not have to come prepared, e.g. empty stomach). As it is totally non-invasive, there is no risk of cross-infection or contamination. Due to no associated side effects, no admission or post-operative care is necessary. Although only time will decide, in my view only a dedicated department with sufficient IT facilities and dedicated biomedical engineers can take the burden of the extensive computational time required by more realistic transient analyses and, effort to visualize and extract the haemodynamic characteristics required for clinical decision making.

Whereas the current study indicates a positive response among the clinical community for CFD and its use in IAs, it will be necessary to expose the software to a larger number of clinicians before definitive conclusions can be drawn.

5.2.5 Conclusions

Although participants showed a manifest interest in computational predictions, there is a clear lack of awareness concerning the role of haemodynamics in the aetiopathogenesis of IAs and the use of CFD in this context. More efforts therefore are required by the scientific community to enhance awareness and understanding of the clinicians in the subject. There is a clear willingness to use such software as an outpatient tool. The mistrust in the results indicates the need for validations, and most of the participants supported with the need of a multi-centric trial, when software is ready. Keeping in mind the very first exposure to CFD for most of the participants and the inherent difficulties associated with a developing-software, the average performance of 2.5 (63% of an expert) was remarkable. Adequate training, controlled exposure, and further development of these tools is necessary before these can be efficiently used by a common clinician.

5.3 Appendix-1: Questionnaire used for feedback



ESMINT 2008
European Society of Minimally Invasive Neurological Therapy



aneurist
Integrated biomedical informatics for the management of cerebral aneurysms

Edifício "Egas Moniz", Hospital de Santa Maria Faculdade de Medicina da Universidade de Av. Professor Egas Moniz 1649-028 Lisboa, Portugal
<http://www.fm.ul.pt/>

Workshop Evaluation - @neuFuse

Personal Details

Title:	First Name:	Surname:	Age:
Degree:			
Job Title:			
Institution/Department:			
Background:	Clinical	Engineering	Scientific Other:
Address:			
Email:			
Telephone:			

Section 1: General Feedback

Q1. Why did you decide to participate to this workshop?	Working in the field Suggestion by colleague Interested in computational haemodynamics Improve management of aneurysms Other: please specify
Q2. How useful did you find this workshop?	Not 1 2 3 4 5 Very
Q3. Would you recommend a friend to attend?	No Yes
Q4. Would you recommend the software to a friend	No Yes
Q5. Any specific shortcomings, surprises?	1. 2. 3.
Q6. Any suggestions for course improvements?	No Yes, I've described them below
Q7. Rate your overall experience...	Bad 1 2 3 4 5 Good

Section 2: Course Design and Conduct

Q8. Was the participant-to-instructor ratio...	OK Too many students
Q9. Were the instructions given in a clear way?	No 1 2 3 4 5 Very
Q10. Was the content of the course scientifically appropriate?	No Yes
Q11. Do you think the instructors were helpful?	No 1 2 3 4 5 Very
Q12. How useful was the presentation and notes?	Not 1 2 3 4 5 Very
Q13. Did you have any difficulty with terminology?	No Yes, I've described it below

Q14. Were the IT facilities satisfactory?	No 1 2 3 4 5 Very
Q15. Was the duration of the workshop...	Too short Just right Too long

Section 3: Experience with the Software

Q16. Do you find the software user-friendly?	No 1 2 3 4 5 Very
Q17. Will clinicians without tech/IT experience have trouble?	No Not Sure Yes
Q18. Were you able to complete all the steps of the haemodynamic analysis?	No, I missed those below Yes
Q19. Is there any obvious limitation which may prevent the use of this software in future?	No Yes, I've described it below
Q20. Please, identify the easiest and most difficult steps in the use of @neuFuse	Easiest: Most Difficult:
Q21. What would you change/improve in the software?	1. 2. 3.
Q22. In particular, do you think that the Graphical User Interface (GUI) can be improved in any way?	No Yes, I've described it below
Q23. Do you now feel confident in the use of this software?	No 1 2 3 4 5 Very
Q24. Would you like to be kept informed about developments of this software?	No Yes

Section 4: Haemodynamic Understanding

Q25. Did you have difficulty with the technical concepts (boundary conditions, wall shear stress, etc.)?	No Yes, I've named them below
Q26. Are the results from this software realistic?	No Yes Not sure
Q27. Is current evidence sufficient to justify a role for haemodynamics in the pathogenesis of aneurysms?	No Yes Not sure
Q28. Were you previously aware of the use of CFD to predict the risk of rupture in intracranial aneurysms?	No Yes
Q29. If you see a publication on computational predictions for IA in a peer-reviewed journal, will you read it?	No Yes
Q30. Would you be interested in receiving high-quality peer-reviewed publications on haemodynamics in IA?	No Yes

Section 5: Impact of CFD in Neurosurgery

Q31. Ideally, who should perform this type of computational analysis for patients?	Consultant A dedicated clinical scientist/ engineer Registrar/ junior member of team Anyone provided with adequate training It should be simplified so it's an office job Other, please specify:
Q32. Could this software be used diagnostically in an outpatient clinic?	No Yes
Q33. Are you aware of any similar software?	No Yes, I've named it below
Q34. Should this type of analysis be fully automated, or is it better that the user has control?	Automate Not Sure User control
Q35. Is there a future for computational tools for risk prediction of intracranial aneurysm rupture?	No Yes Not sure
Q36. How great a clinical need is there for this software?	Significant Low Emerging

Q37. Do you think that this type of analytical software is ready for introduction into the clinical environment?	Ready Not required Needs work
Q38. In which cases might this software influence your decision-making about patient management?	None All Those below...
Q39. Would you be interested in participating in a multi-center trial on the evaluation of this software?	No Yes
Q40. Can you see any legal or ethical implications in the use of this software?	No Yes, I've described them below
Q41. The principles employed in @neurIST are applicable to other diseases; is this important?	Important Only care about IA
Q42. More complex and informative analyses take longer to calculate; are quick results better?	Quick Complex Let me choose
Q43. @neurIST IA rupture risk assessment can use more than haemodynamic data; is this important?	Important Only need haemodynamics
Q44. @neurIST offers tools for researchers as well as clinicians; are these important?	Important Only need clinical

Section 6: Bringing this Software into Routine Use

Q45. Would you expect this software to be provided as part of a scanner, or as a stand-alone product?	Scanner Standalone Both
Q46. Would you expect such software to be provided by a scanner company or an independent specialist?	Scanner Co Independent
Q47. Would you expect to pay for this software, or would you prefer a freeware/shareware arrangement?	Pay Freeware Shareware
Q48. Would the price of this software be an important factor in your decision to obtain/use it?	Important Cost is a lower priority

Any other comments?

OFFICE USE ONLY

Instructor's evaluation of individual's performance

CHAPTER 6.0: COMPUTATIONAL FLUID DYNAMICS AS A TOOL TO EXPLORE THE AETIOPATHOGENESIS OF INTRACRANIAL ANEURYSMS

OVERVIEW

6.1: Introduction

6.2: Effects of Smoking and Hypertension on the Formation of IAs

6.3: Analysis of Different Haemodynamic Factors During Initiation and Rupture of an Intracranial Aneurysm and Possible Influence of Low Molecular Weight Heparin Mediated Change in the Blood Viscosity on Computed Values of These Haemodynamic Factors

6.4: The Effects of Aortic Coarctation on Cerebral Haemodynamics and its Possible Role in the Aetiopathogenesis of Intracranial Aneurysms

6.5: Conclusions

**My contribution: In the studies described in this chapter, I played a major role in concept, study design, recruitment of patients, consenting them, conducting review of literature, performing analyses, performing statistical calculations, writing and submission of manuscripts to journals for publications. Dr Alberto Marzo (and other biomedical scientists, as detailed in acknowledgement section) gave important support and contribution in retrieval of medical images, performing CFD analyses, and post-processing of the results.*

****Declaration:** In my study on The Effects of The Effects of Aortic Coarctation on Cerebral Haemodynamics and its Possible Role in the Aetiopathogenesis of Intracranial Aneurysms, apart from CoA patient, the measurements were also taken in five healthy volunteers to establish the flow-rates at different locations in the cerebral vasculature. The data from these volunteers however, could not be included in the study as unfortunately this data is not currently available.

6.1. Introduction

CFD is used as a tool for exploring the different factors that can influence the aetiopathogenesis of Intracranial Aneurysms by altering their haemodynamic environments. A number of studies are conducted in this context and CFD was used to prove or refute the hypotheses.

The first study in this section was conducted on the two well-known risk factors for Intracranial Aneurysm formation: smoking and hypertension. Whereas, smoking and hypertension are well-established risk factors in IA formation [Bonita 1986, de la Monte et al. 1985, Inci et al. 2000, Juvela 2000, Kondo et al. 1997] their roles in the mechanisms that regulate aneurysm formation are poorly understood and are essentially limited to their statistical associations. In this study, I hypothesized that smoking and hypertension lead to intracranial aneurysm formation by changing the haemodynamic environment of the cerebral vasculature secondary to their effect on Blood Viscosity. There is good evidence in the literature that smoking and hypertension increase the Blood Viscosity in individuals [de Simone et al. 2005, Letcher et al. 1983]. CFD was used to compute the effects of these risk factors on wall shear stress (WSS) and oscillatory shear index (OSI) at the site of IA initiation, two most important factors for the development of Intracranial Aneurysms [Burleson et al. 1996, Byrne et al. 1998, Gao et al. 2008, Morimoto et al. 2002].

In the next study, I analyze the differences in the haemodynamic environments of intracranial aneurysms during the stages of their initiation versus rupture. 3D Rotational Angiograms were used to build the three-dimensional computer models of aneurysms included in the study followed by their qualitative and quantitative comparisons. The study further extended by investigating the effects of heparin (and enoxaparin) on the haemodynamic characteristics of aneurysms. Heparin (and its derivative enoxaparin) is a widely used injectable anticoagulant for preventing venous thrombosis and pulmonary embolism. It inhibits the factors involved in blood clotting (factor Xa), causing instantaneous inactivation of thrombin, thereby reducing Blood Viscosity [Hitosugi et al. 2001) and, in turn altering the haemodynamics of the blood circulation. Values of WSS and OSI were computed with the help of CFD in a ruptured Intracranial Aneurysm and compared with a tiny aneurysm in the stage of initiation. Possible link, between the low blood viscosity, and alterations in values of WSS/ OSI, leading to the rupture of IAs was explored. Potential effects of other pharmacological agents on the aetiopathogenesis of intracranial aneurysms are also discussed.

Another interesting study was conducted to analyze the haemodynamic changes in the cerebral circulation of patients with Coarctation of Aorta and its possible effects on the increased incidence and rupture of Intracranial Aneurysms in these patients. After a thorough search (PubMed®, Embase® and Google-Scholar™ searched from the year 1900 up to 2009) I could retrieve only two relevant studies. Whereas, Hafkenschiel et al [Hafkenschiel et al. 1949) demonstrated a significant

increase in cerebral arterial flow-rates in patients with Coarctation of Aorta in 1949, Rowe and colleagues [Rowe et al. 1964] found no significant differences in the flow-rates before and after the repair of Coarctation of Aorta in their study performed in 1964. We therefore performed pc-MR measurements in the cerebral arteries of a Coarctation of Aorta patient with coexisting IA and five healthy volunteers to establish the flow-rates at different locations in the cerebral vasculature.

Amongst other aetiologies proposed, Coarctation of Aorta has been highlighted as a major risk factor in the aetiopathogenesis of IAs [Abbott 1928, Ahmetoğlu et al. 2003, Connolly et al. 2003, DuBoulay 1965, Eppinger 1871). Incidence of Intracranial Aneurysms among patients with CoA is approximately 5 times higher than that of the general population [Connolly et al. 2003]. The incidence of IA rupture in CoA patients (4.8%) [Shimogonya et al 2009, Mercado et al. 2002, Reifenstein et al. 1947] is also higher than the estimated rate of rupture in the general population, which is less than 1% [Weir et al. 1996]. In spite of CoA being a well-established risk factor for IA formation, [Abbott 1928, Ahmetoğlu et al. 2003, Connolly et al. 2003, DuBoulay 1965, Eppinger 1871] the exact underlying mechanisms for this association remain poorly understood. After measuring the flow-rates in the cerebral vasculature in patients with CoA, an analysis of the different haemodynamic factors inside Intracranial Aneurysms was performed. The possible role of haemodynamics is discussed in this context in a background of relevant literature.

A better understanding of the aetiopathogenesis of the IA formation and rupture may help clinicians in preventing and treating the disease effectively.

6.2. Effects of changing blood viscosity on computed wall shear stress and oscillatory shear index at the site of intracranial aneurysm formation

6.2.1 Introduction

Aneurysmal subarachnoid hemorrhage (SAH) remains a major cause of morbidity and mortality in neurosurgical patients [Inagawa et al 2001, Numminen et al 1996]. Smoking and hypertension are well-established risk factors in IA formation [Bonita 1986, de la Monte 1985 et al, Inci and Spetzler 2000, Juvola 2000, Kondo et al 1997]. However, their roles in the mechanisms that regulate aneurysm formation are poorly understood and are essentially limited to their statistical associations.

Recent evidence indicates WSS and OSI as important underlying haemodynamic factors in IA formation [Burleson and Turitto 1996, Gao et al 2008, Morimoto et al 2002]. One of the important parameters influencing WSS is blood viscosity, which in turn is influenced by smoking and hypertension [de Simone et al 1990, Letcher et al 1983]. The current study employs CFD to predict the effect of smoking and hypertension on the WSS patterns at the site of IA initiation with aim to explore the possible underlying mechanisms leading to their formation.

6.2.2 Materials and Methods

6.2.2.1 Study design and patient recruitment: The study was conducted jointly in the Departments of Neurosurgery and Neuroradiology, Royal Hallamshire Hospital, and the Department of Cardiovascular Science, University of Sheffield, Sheffield, UK. A total of two (n=2) patients diagnosed with IAs between Jan 2004 and March 2009, were identified retrospectively and recruited with appropriate consent and ethical approval. In order to avoid age and sex bias both patients were selected from the same age group (45 years) with one male and one female. Their relevant demographic and clinical data are reported in Table-6.1.

Table-6.1: Patients' demography, clinical presentations of IAs included in the study, their management, and the known risk factors

Pt .	Age /Sex	Clinical presentation	Ruptured/ Unruptured	Management	Location of IA	Smoking	Hypertension	Other risk factors
1	45/ M	Asymptomatic	Unruptured	Observed	Lt terminal ICA	>60 cigarettes/ day/ 25 years	Poorly controlled	None
2	45/ F	Asymptomatic	Unruptured	GDC embolization	Rt terminal ICA	>40 cigarettes/ day/ 22 years	Controlled on medication	None

NB: Pt.; patient, GDC; Guglielmi detachable coils, Lt; left, Rt; right, ICA; internal carotid artery

3DRA acquisitions: Medical images were obtained using rotational acquisition in a Philips® Integris™ Allura machine (Philips® Medical Systems, Best, The Netherlands), producing 100 images in 6 seconds, with 5ms exposure per image. Voxel size in the reconstructed 3D images was 121 microns with reconstruction matrix 512x512x512.

6.2.2.1 Numerical 3D model: @neuFuse, the computational tool-chain developed within the EU project @neurIST was used to reconstruct vessel and aneurysmal geometries. Vessel triangular surfaces were reconstructed using a threshold isosurface extraction tool, based on the marching cubes algorithm developed by Lorensen and Cline [Lorensen and Cline 1987]. The removal of IAs was performed with the help of software @neuFuse. In order to mark the location of the IA in the parent artery after its removal, the image with IA in situ was superimposed over the image where the IA was removed. This step was done during the post-processing

of data with the help of software ANSYS®-CFX Postprocess™. A virtual marker (a sphere) was placed at the location of IA in the parent vessel from where the IA was removed. Now the first image (image with IA intact) was taken out and the location of IA (as localized by the virtual marker) was displayed by the arrows. Understanding the importance of the issue I have used exactly the same views for comparing the haemodynamic indices with and without intracranial aneurysms, so that the readers can make out the location of IAs easily in the view where there no IAs are present.

Volumetric meshes were generated using ANSYS® ICEM™ CFD 11.0 (Ansys®, Inc., Canonsburg, PA, USA) based on the octree approach. The mesh was refined at the wall (using prismatic elements) for more accurate computation of WSS and OSI. For computational efficiency a progressively coarser mesh was used towards the vessel axis. Tetrahedral elements were used for the discretization of the domain core, with three layers of prismatic elements adjacent to the wall, thus ensuring accurate computation of WSS and OSI. Element size and number were set according to the outcome of a mesh dependency study performed on similar aneurysmal geometries [Radaelli et al 2008]. In this study results were found to be grid independent for meshes greater than 1700 el/mm³. In order to maintain consistency across the meshes used for all geometries, similar element density and the same wall element size and maximum core element size were used in the discretization of the domains.

The 3D transient Navier-Stokes equations were solved using the finite-control-volume software, ANSYS®-CFX™. In view of the recent findings of [Marzo et al 2009] I used the ‘plug-flow’ or ‘flat’ velocity profile at inlet instead of Womersley flow profile. The default second-order high-resolution advection-differencing scheme was used. Blood was assumed to be incompressible, with density $\rho=1060$ kg/m³ and Newtonian, with viscosity $\mu_{\text{typical}}=3.5$ mPa·s. The effects of hypertension and smoking were modeled by increasing BV values by 8.1% ($\mu_{\text{typical}}=3.78$ mPa·s) according to the findings of De Simone et al [de Simone et al 1990] and Price et al [Price et al 1999]. Boundary conditions (BCs) for the 3D models were provided in form of typical volumetric flow rate waveforms at inlet and pressure waveforms at outlet. These were computed using the 1-D circulation model developed by Reymond et al [Reymond et al 2009]. The authors validated their model and found that the predictions of this 1-D model have good agreement with the measurements performed in the real patient/ healthy volunteers.

6.2.3 Results

Values of WSS and OSI were time-averaged for one cardiac cycle and a qualitative and quantitative comparison made for the two BVs. WSS contours reported in Figures-6.1 and 6.2, and the data reported in Table-6.2, show that, in the case of

Table-6.2: Quantitative comparison of areas and values of WSS the effects for $\mu_{typical}$ and $\mu_{atypical}$

	Patient 1			Patient 2		
	$\mu_{typical}$	$\mu_{atypical}$	%	$\mu_{typical}$	$\mu_{atypical}$	%
Area of WSS > 15 Pa at aneurysm location [mm ²]	1.24	1.42	+14.5	0.67	0.68	+1.5
Area of WSS > 15 Pa in parent vessel [mm ²]	7.01	8.24	+17.5	148.8	160.0	+7.5
Maximum WSS at aneurysm location [Pa]	21.3	22.2	+4.2	56.54	58.73	+3.9
Average WSS in parent vessel [Pa]	4.5 Pa	4.7 Pa	+4.4	12.12	12.68	+4.6

NB: $\mu_{typical}$: typical blood viscosity, $\mu_{atypical}$: blood viscosity in smokers and hypertensive patients

both patients, the aneurysm formed at a location where WSS was higher than the mean value in the parent vessel. At physiological BV, the maximum WSS at the site of IA initiation for patient-1 (21.3Pa) was approximately 5 times higher than the mean value in the parent vessel (4.5Pa).

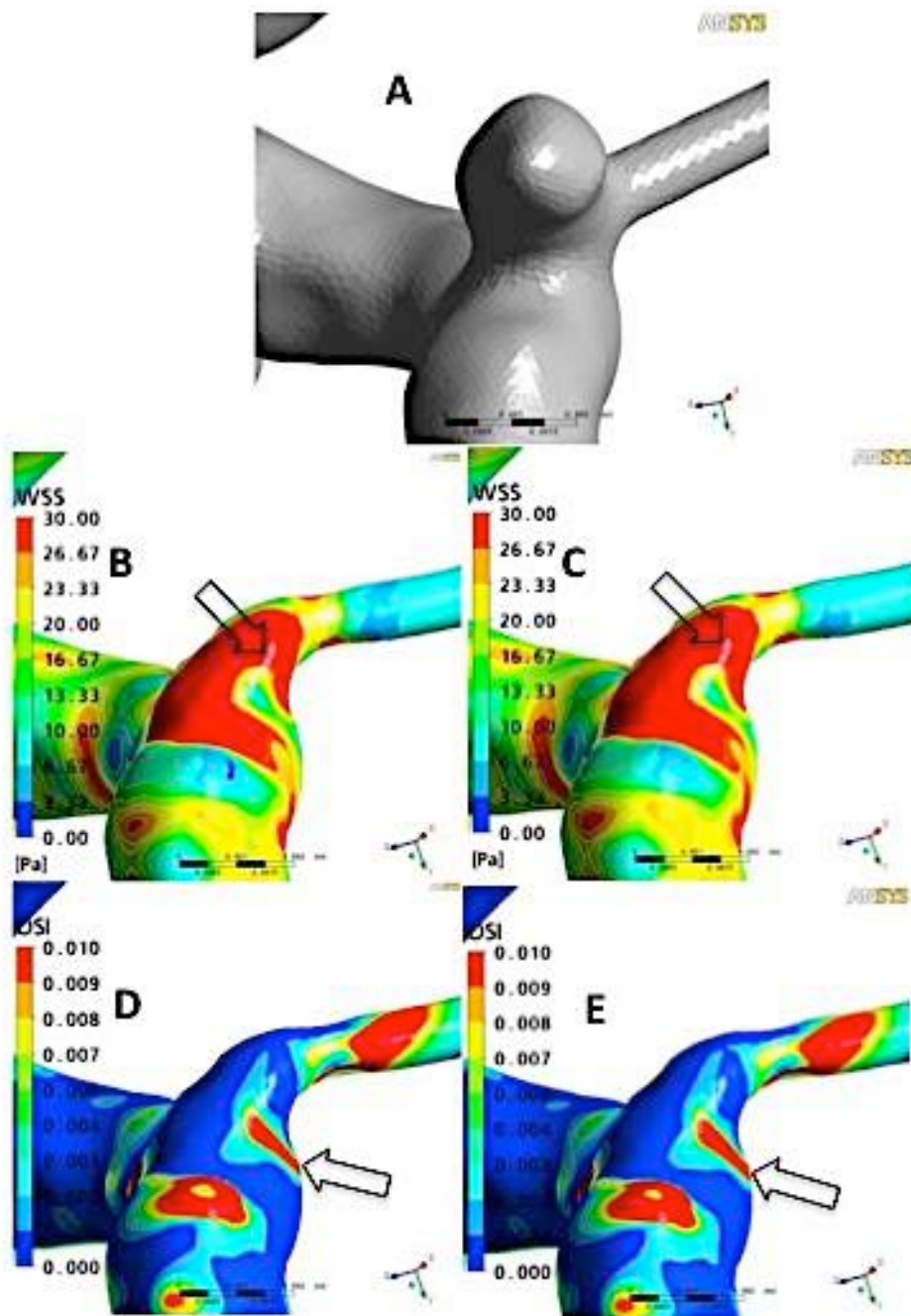


Figure-6.1: Reconstructed geometry of the IA and surrounding vasculature for patient-1 (A). Contours of WSS (B,C) and OSI (D,E) for μ_{typical} (B,D) and μ_{atypical} (C,E) are displayed. Arrows indicate the site of IA along the parent vessel before removal.

Similarly, for patient-2, the maximum WSS at the initiation site (56.5Pa) was approximately 5 times higher than in the parent vessel (12.1Pa). OSI also followed the same trend with relatively higher values at the sites of aneurysmal development for both patients, compared to that in the respective parent vessel (Figures 6.1 and 6.2, Table-6.2). However, it must

be noted that areas of relatively high WSS and OSI were not exclusively limited to the sites of IA formation.

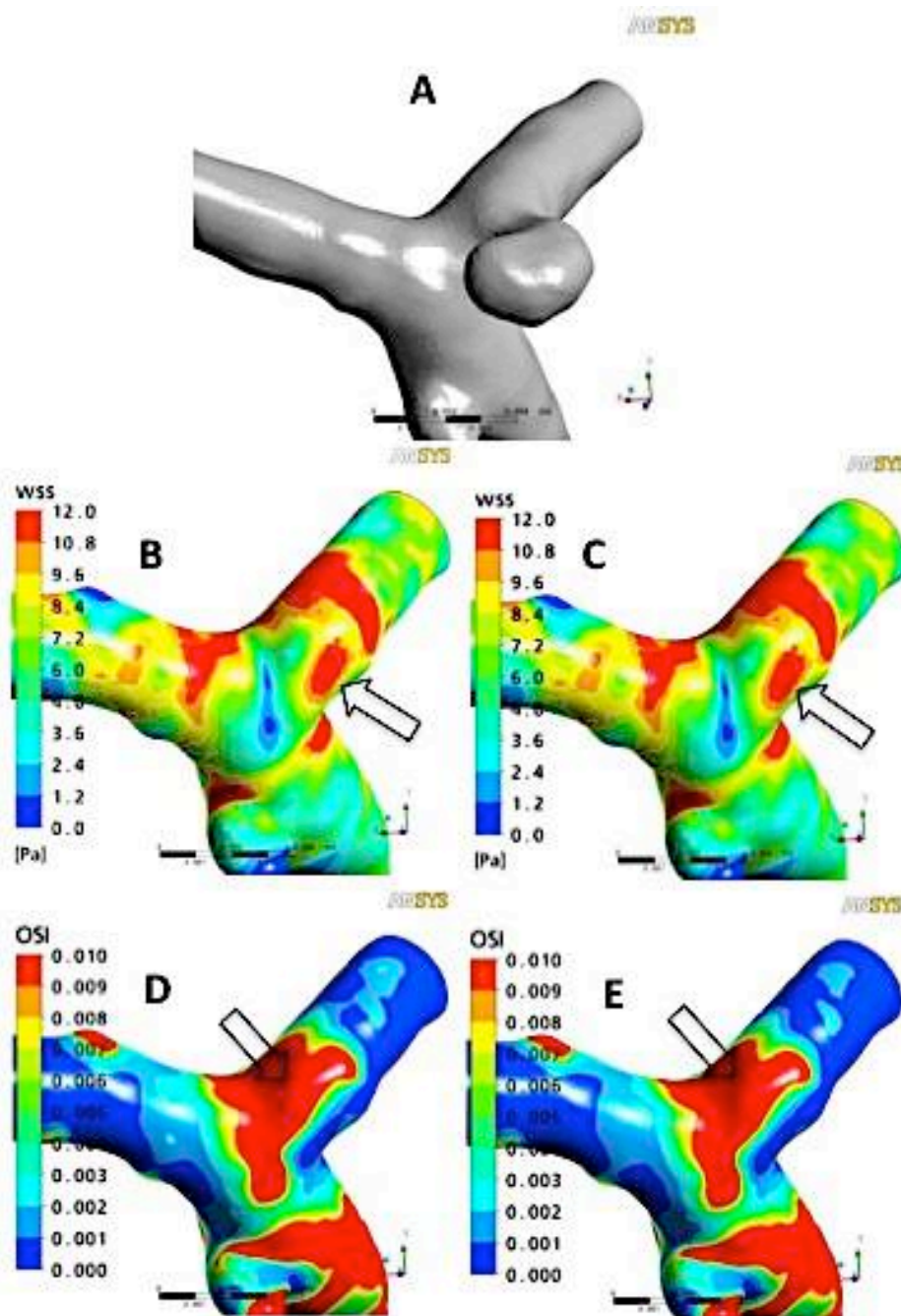


Figure-6.2: Reconstructed geometry of the IA and surrounding vasculature for patient-2 (A). Contours of WSS (B,C) and OSI (D,E) for μ_{typical} (B,D) and μ_{atypical} (C,E) are displayed. Arrows indicate the site of IA along the parent vessel before removal.

The threshold value of 15Pa for WSS used in the study was chosen as an arbitrary limit to highlight the areas of relatively higher WSS where the IAs were initiated and to appreciate/ quantify the effects of changes in BV in smokers and hypertensives on WSS. Whereas it was possible to identify

a threshold for infra-physiological WSS (<0.4Pa) [Malek et al 1996], no such values could be found in the literature for supra-physiological WSS. An increase in BV, to represent the effects of smoking and hypertension, is reflected in the values of WSS and OSI, reported in Table-6.2. For patient-1 the area of high WSS (>15Pa) increased by 17.5%, whereas for patient-2 the increment was 7.5%. The maximum values of WSS at initiation sites followed a similar trend, but the increment was around 4% for both patients. Interestingly, the increase in the value of WSS does not correlate linearly with the increment in BV. Furthermore, from the data in Table-2, it can be seen that changes in BV do not have a significant or consistent effect on the value of OSI at the site of aneurysmal development.

Table 6.3: The literature-based evidence on the importance of WSS and OSI in the aetiopathogenesis of IAs

Haemodynamic factors	Intracranial Aneurysm			Proposed mechanism(s)	References
	Initiation	Growth	Rupture		
<i>Dynamic</i>					
Wall Shear Stress (WSS)	High	Low	Low	Increased WSS increases the production of MMP-13 which in turn leads to vessel wall damage Decreased WSS increases iNOS synthesis- NO induced damage to vessel wall Low WSS increases endothelial proliferation and apoptosis	Boussel et al 2008, Fukuda et al 2000, Gao et al 2008, Jou et al 2008, Malek et al 1999, Meng et al 2007, Shojima et al 2004, Ujje et al 1999
Oscillatory Shear Index (OSI)	High/Low	High	High	Degenerative changes in endothelium	Glor et al 2004, Goubergrits et al 2008, Mantha et al 2006

NB: WSS; wall shear stress, MMP-13; matrixmetalloproteinases-13, iNOS; inducible-nitric oxide synthase, NO; nitric oxide, OSI; oscillatory shear index

6.2.4 Discussion

The exact aetiopathogenesis of IA formation is poorly understood [Sekhar and Heros 1981]. Whilst there is some indication of a congenital link [Forbus 1930], IAs are believed primarily to be acquired lesions [Crawford 1959, Stehbens 1975]. Recent evidence suggests a strong correlation between different haemodynamic factors and the aetiopathogenesis of IAs [Burlison and Turitto 1996, Byrne 1998, Gao et al 2008, Morimoto et al 2002]. In particular, a number of studies suggest a link between aneurysmal initiation, growth and rupture and the magnitude and distribution of WSS and OSI (Table-6.3).

6.2.4.1 Wall Shear Stress (WSS)

WSS is a tangential frictional force exerted by flowing blood on the arterial endothelium, and is proportional to the blood viscosity and the velocity gradients. Mean arterial WSS has been suggested by Malek et al to lie within the range of 1.5-2.0Pa [Malek et al 1996]. There is an increasing body of literature suggesting that high WSS plays a role in the initiation of IAs [Burlison and Turitto 1996, Byrne 1998, Gao et al 2008, Gonzalez et al 1992, Morimoto et al 2002, Sacco et al 1984]. This is

further supported by the observation that IAs most frequently occur at bifurcations and arterial bends. These are regions, which are exposed to constantly high WSS [Foutrakis et al 1997, Rossitti 1998].

A number of different mechanisms have been proposed to explain how WSS influences the natural history of an IA. It has been established that the normal behavior of arterial endothelial cells (ECs) is regulated by haemodynamic shear stress. Sho et al [Sho et al. 2002] observed that increased WSS stimulates ECs to produce matrix metalloproteinase (MMP-13), which, in turn, leads to degeneration of the internal elastic lamina. In 1993 Luscher and Tanner [Luscher and Tanner 1993] found that the release of EC-derived growth and relaxation factor (EDRF – later recognized as nitric oxide) is shear stress dependent and is responsible for vascular remodeling. It has been demonstrated by a number of workers [Cooke et al 1990, Fukuda et al 2000, Pohl et al 1991] that WSS increases the production of NO by the ECs by inducing an enzyme responsible for its synthesis (iNOS; inducible nitric oxide synthase). Fukuda et al [Fukuda et al 2000] found a high localization of iNOS at the site of IA formation, in both rat and human arteries. They also demonstrated that iNOS inhibitors such as Aminoguanidine and Batroxobin (DF-521) attenuate the early degenerative changes associated with IA formation. The preventive effects of these drugs are thought to be mediated by lowering BV and hence WSS [Fukuda et al 2000]. They concluded that iNOS is a prerequisite for de novo development of IAs in cerebral vessels. In 1995, Wang et al [Wang et al 1995] showed that smooth muscle cells (SMCs) in arterial wall can also respond to WSS in intact arteries by virtue of interstitial flow generated by transmural flow gradients, further accentuating the vessel wall damage.

A number of authors have attempted to explain the mechanisms linking WSS with EDRF/NO production. Experimental studies conducted by Busse et al [Busse et al 1990] revealed that WSS activates calcium ion-dependent endothelial iNOS leading to its increased production. Furthermore, WSS augments the release of adenosine tri-phosphate (ATP) and substance-P from EC [Milner et al 1990]. Increased concentrations of these two mediators are believed to enhance NO production in a paracrine manner [Pohl et al 1991]. More directly, increased WSS leads to hyperpolarization of the ECs by mobilizing the calcium ions from intracellular stores in cultured ECs [Ando 1988] probably via activation of phospholipase-C [Bhagyalakshmi and Frangos 1989] and/ or K⁺ channels [Olesen et al 1988]. Several authors have attempted to explain the mechanism of WSS transduction by the endothelium [Born and Palinski 1985, Pohl et al 1991, Radaelli et al 2008]. Born and Palinski [Born and

Palinski 1985] identified 3D mechanoreceptors anchored to the endothelial membrane. They hypothesized that WSS acts on these mechanoreceptors, mechanically enhancing the interaction between regulatory proteins and their targets [Born and Palinski 1985]. Resnick and colleagues [Resnick et al 1993] located a WSS-responsive element for iNOS on endothelial genes in 1993.

Table-6.4 gives an overview of the important mechanisms proposed on the role of WSS in vascular remodeling.

Table-6.4: WSS-induced vascular remodeling: an overview of some important mechanisms proposed

Author/ Journal/ Year	Proposed mechanism(s)/ Observations	Implications
Rossitti et al (<i>Acta Radiol</i> , 1998); Foutrakis et al (<i>Neurol Res</i> , 1997)	IAs mostly occur at arterial bends and bifurcations exposed constantly to high WSS	High WSS can be a possible culprit in the development of IAs
Sho et al (<i>Exp Mol Pathol</i> , 2002)	Increased WSS stimulates endothelial cells to produce matrix metallo-proteinases (MMP-13)	Degeneration of the arterial internal elastic lamina by MMP-13
Luscher et al (<i>Am J Hypertens</i> , 1993)	Release of endothelium derived EDRF is shear stress dependent	Vascular remodeling by WSS
Cooke et al (<i>Am J Physiol</i> , 1990), Pohl et al (<i>Am J Physiol</i> , 1991) Fukuda et al (<i>Circulation</i> , 2000)	WSS induces iNOS, an enzyme responsible for NO synthesis	Increased production of NO in the endothelium, EC injury
Fukuda et al (<i>Circulation</i> , 2000)	Found high concentrations of iNOS at the site of IA formation, both in rat and human arteries	Levels of iNOS correlate with IA initiation
Fukuda et al (<i>Circulation</i> , 2000)	iNOS inhibitors; Aminoguanidine and Batroxobin (DF-521) attenuate the early degenerative changes associated with IA formation	Aminoguanidine and Batroxobin (DF-521) have preventive effects on IA formation by lowering WSS
Wang et al (<i>J Biomech Eng</i> , 1995)	SMCs in arterial walls also respond to shear stress	WSS induced vessel wall damage can extend to SMCs
Busse et al (<i>FEBS Lett</i> , 1990)	WSS activate the calcium ion dependent endothelial iNOS	WSS increases the synthesis of iNOS
Milner et al (<i>Proc Biol Sci</i> , 1990), Pohl et al (<i>Am J Physiol</i> , 1991)	WSS also augments the release of adenosine triphosphate (ATP) and substance-P from ECs	These two mediators increase EDRF production in a paracrine manner
Ando et al (<i>In Vitro Cell Dev Biol</i> , 1988)	High WSS leads to the hyperpolarization of the ECs by mobilizing the calcium ions from intracellular stores	EC damage
Bhagyalakshmi et al (<i>Biochem Biophys Res Commun</i> , 1989)	Hyperpolarization of ECs and mobilization of intracellular calcium is via activation of phospholipase-C	EC damage
Olesen et al (<i>Nature</i> , 1988)	Hyperpolarization of the ECs and mobilization of intracellular calcium is via activation of K ⁺ channels	EC damage
Born et al (<i>Br J Exp Pathol</i> , 1985)	Identified presence of 3D mechanoreceptors anchored to the EC membrane, WSS acts on these mechanoreceptors, mechanically enhancing the interaction between regulatory proteins and their targets	Link is established on how WSS transduces signals to ECs
Resnick (<i>Proc Natl Acad Sci USA</i> , 1993)	Located a WSS responsive element for iNOS on EC genes	Role of WSS in EC damage
Fukuda et al (<i>Circulation</i> , 2000)	Both, the magnitude of WSS as well as the duration of exposure for the endothelium remain important determinants for the induction of iNOS	Duration and magnitude of WSS play important role in IA formation
Wagner et al (<i>J Clin Invest</i> , 1997)	Demonstrated that no iNOS was induced when the SMCs were exposed lower WSS (1.1-2.5 Pa) for shorter durations (<24 Hrs.)	Chronic and significant exposure of WSS are required for the initiation of IAs

NB: MMP-13; matrixmetalloproteinases-13, NO; nitric oxide, iNOS; inducible-NO synthase, EC; endothelial cells

The findings of the current study support the correlation between high WSS and initiation of IA. Maximum values of WSS at the site of aneurysm formation were approximately 5 times higher than the mean values observed in the parent vessels, in both patients (Table-6.2).

6.2.4.2 Oscillatory shear index (OSI)

The OSI is a measure of the oscillatory nature of shear forces [Glor et al 2004, Glor et al 2003, Goubergrits et al 2008, Marzo et al 2009]. This index, which has a range of between 0 and 0.5, represents the fraction of the cardiac cycle over which the instantaneous shear force vector forms an angle greater than 90 degrees to the time-average direction of the same force. Consistently high values of OSI have been associated with EC dysfunction [He et al 1996] and changes in cell structure secondary to cyclic mechanical stress have been demonstrated by Wang et al. [Wang et al 1995] reporting disruption of the actin cytoskeleton of ECs.

Glor and colleagues propose that an OSI of 0.2 represents a threshold value above which endothelial damage is initiated [Glor et al 2004, Glor et al 2003]. Damage to ECs produced by high OSI may contribute to IA formation. Areas of relatively high OSI predicted at the site of aneurysm formation for patient-2 in my CFD simulations support such theories; the maximum values observed approached the threshold value of OSI (0.2) identified in the literature. In contrast, for patient-1, the OSI at the site of IA initiation fell well below the threshold. This may indicate a less significant role for OSI in IA formation, at least in the case of this particular patient.

Whilst, for both patients, areas of high WSS and OSI were located primarily at the bifurcations where the two IAs were observed, areas of high value for these indices were also predicted at other sites in the parent vessels. This raises a further question; why are these other critical areas unaffected? One explanation is that, in addition to the key haemodynamic triggers, IA initiation is governed by many other factors including amongst others; smoking, hypertension, genetics, polycystic kidney disease, Ehlers-Danlos syndrome, Marfan's syndrome, etc. In addition, the possibility of de novo IA formation in these patients in other locations in the future cannot be excluded without a long-term follow-up.

6.2.4.3 Role of smoking and hypertension in the IA formation

Smoking and hypertension are two well-established risk factors for IA formation. A number of clinical studies have highlighted the strong association between smoking [Anderson et al 2004, Bonita 1986, Qureshi et al 1998, Sacco et al 1984, Sauerbeck et al 2008] and hypertension [Inci

and Spetzler 2000, Sakaki et al 1993, Solenski et al 1995, Taylor et al 1995, Teunissen et al 1996] and de novo IA formation. Indeed, both risk factors also correlate with the presence of multiple IAs [Erbengi et al 1997, Juvela 2000, Ostergaard et al 1985, Qureshi et al 1998, Rinne et al 1994]. Experimental studies, where IA has been induced by hypertension, confirm these findings [Handa et al 1993, Hashimoto et al 1987, Kim et al 1992, Kondo et al 1997, Nagata et al 1980, Strother et al 1992]. Furthermore, autopsy studies conducted to assess the relationship between the IA formation and hypertension demonstrate even stronger correlations [Chason and Hindman 1958, Crompton 1964, de la Monte et al 1985, Sarner et al 1965, Toftdahl et al 1995].

Whilst being well-established risk factors for IA formation, the exact mechanisms by which smoking and hypertension lead to increased IA formation remain controversial [Inci and Spetzler 2000]. A number of explanations have been offered including; endothelial cell injury, occlusion of vasa vasorum and disturbances in the synthesis of elastin and collagen [Inci and Spetzler 2000]. It has been proposed that protease/protease-inhibitor factor imbalance is a factor in smokers and a quantitative deficiency of alpha-1-antitrypsin has been reported both in patients with SAH and in smokers [Gaetani et al 1996, Schievink et al 1995, St Jean et al 1996]. Alpha-1-antitrypsin is an inhibitor of elastase, a proteolytic enzyme that enhances collagen catabolism. This link is not supported universally; Sakai et al [Sakai et al 1999] attribute the increased plasma protease levels found in patients with IAs to leukocytosis after SAH thus disputing the significance of plasma protease/protease-inhibitor imbalance as a marker for IA formation. Another hypothesis suggests that IA formation is a part of a vascular degenerative process similar to atherosclerosis and that smoking leads to IA initiation by facilitating this process [Adamson et al 1994, Greenhalgh et al 1980].

One widely recognized effect of smoking and hypertension is an increase in BV [de Simone et al 1990, Price et al 1999]. I propose that the missing link between these risk factors and increased IA formation is via high WSS secondary to an increase in BV. This hypothesis is supported by my findings, which show an increase in the area of vessel wall subject to high WSS and elevated maximum values of WSS coincident with the IA initiation site for the two patients studied. For patient-1 both qualitative (Figure-6.3) and quantitative (Table-6.2) comparisons show that increased BV results in a substantial increase in the maximum WSS of 4.2%. The area of wall affected by very high WSS (>15Pa), up by 14.5% and 17.5% for the site of the IA and parent vessel respectively. Similar trends were

observed for patient-2 but the relative differences were lower (Figure-6.4, Table-6.2).

There is strong evidence to indicate that induction of iNOS in ECs is dependent on both the magnitude and duration of exposure to WSS [Fukuda et al 2000]. In an experimental study, Wagner et al [Wagner et al], found that iNOS was not induced when the vessel walls were exposed to low WSS (1.1-2.5 Pa) for short durations (<24 Hrs.). The study suggests that the chances of IA development are increased if an artery is exposed to high WSS on chronic basis. Both patients included in my study were exposed to these two risk factors chronically for an extended period (20-25 years). Long-term exposure to high WSS, and the increase in the area of vessel wall affected, may have led to EC damage in these patients and contributed to an increased risk of IA development.

Changes in OSI at the sites of IAs were less marked than changes in WSS, and had no consistent trend. Whilst OSI is not directly dependent on BV, changes in haemodynamics resulting from altered rheology may be reflected in the OSI. However, the results indicate its less significant dependency from the haemodynamic changes secondary to altered BV.

It is important to note that my findings differ in some respects from those reported for previous studies, based on similar methodology [Marzo et al 2009, Shimogonya et al 2009]. These sought to develop novel indices in an attempt to link initiation with a haemodynamic trigger whilst indicating that WSS was relatively low at the site of IA initiation. Shimogonya et al [Shimogonya et al 2009] reported a significant correlation between IA formation and a self-proposed haemodynamic index which they termed the 'gradient oscillatory number' (GON) and Mantha et al [Mantha et al 2006] showed a correlation between IA initiation and their newly-proposed haemodynamic index; aneurysm formation indicator (AFI). In considering these results in the light of the current work, it is important to note that Shimogonya et al used a simplified geometry that may have influenced their results. Furthermore, as there are bodies of literature associating low [Boussel et al 2008, Byrne 1998, Jou et al 2005, Malek et al 1996] and high [Burlison and Turitto 1996, Byrne 1998, Fukuda et al 2000, Gao et al 2008, Gonzalez et al 1992, Morimoto et al 2002, Rossitti 1998] WSS with endothelial dysfunction and the aetiopathogenesis of IA, it could be argued that both supra-physiological and infra-physiological WSS lead to perturbation of normal EC behavior. My findings agree with the majority of studies [Burlison and Turitto 1996, Byrne 1998, Fukuda et al 2000, Gao et al 2008, Gonzalez et al 1992, Morimoto et al 2002, Rossitti 1998] that support the role of high WSS in IA formation.

It is evident that the IA formation is likely to have a multi-factorial aetiology with haemodynamic factors acting as an important cog in this process. Many factors are likely to act in parallel rendering the vessel wall more susceptible to the effects of increased pressure and WSS.

6.2.5 Limitations of the study

Before drawing any conclusions it is important to emphasize that my study, in common with other CFD analyses, carries inherent limitations associated with the assumptions necessary to create the models. First, whilst very high quality images (3DRA) were used to reconstruct the vessel geometries, these represent the volume of the vessel occupied by contrast agent. If vessel filling with contrast is incomplete, this may generate errors in surface prediction. Unfortunately, due to the limitations of current technology this remains an unresolved problem. Second, the BCs used in the analyses were obtained from a generic 1D circulation model and were not patient-specific [Reymond et al 2009]. Here it is important to note that recent validation of this model against flow waveforms measured for young volunteers justify its use [Reymond et al 2009]. Third, despite being non-Newtonian, blood was considered as a Newtonian fluid for the purposes of these analyses. This assumption was based on the observations that, blood behaves as a Newtonian fluid at the high shear-rates which apply at most sites in the cerebral circulation ($>100\text{s}^{-1}$) [Bonert et al 2002], in particular in areas coinciding with sites of IA formation. Fourth, the arterial wall was considered rigid, neglecting wall motion, as this has been shown to have a negligible effect on CFD predictions [Ford et al 2008, Jeays 2007]. Finally, the study was performed on a small cohort of two IAs. The work must be considered as a preliminary study; analyses will be required for a significantly larger number of IAs before firm conclusions can be drawn.

6.2.6 Conclusions

The current study suggests that if the smoking and hypertension affect the blood viscosity as per the values given in the literature, the high values of blood viscosity can change the haemodynamic environment of the IAs. Furthermore, when I substituted these high blood viscosity values in CFD simulation I found that the values of computed WSS and OSI for patient were significantly higher.

6.3 Analysis of Different Haemodynamic Factors During Initiation and Rupture of an Intracranial Aneurysm and Possible Influence of Low Molecular Weight Heparin Mediated Change in the Blood Viscosity on Computed Values of These Haemodynamic Factors

6.3.1 Introduction

Aneurysmal subarachnoid haemorrhage (SAH), despite improvement in surgical and medical management, remains a major cause of morbidity and mortality [Inagawa 1998]. Whereas the exact aetiopathogenesis of IA formation and rupture is poorly understood, recent evidence indicates haemodynamics as an important underlying factor [Baskurt 2003, Danesh et al 2000, Sekhar and Heros 1981, Shojima et al 2004]. Most of the IAs are formed at arterial bends and bifurcations corresponding to the areas exposed to highest WSS. [Danesh et al 2000] Contrary to the initiation, aneurysmal growth has been demonstrated to coincide with regions where endothelial cell lining is exposed to abnormally low WSS. [Baskurt 2003] The rupture typically occurs when the stresses and strains in the aneurysmal wall exceed its strength and have been correlated to the complex intra-aneurysmal flow patterns, jet impingement, and areas of low WSS [Cebal et al 2005, Cebal et al 2008].

As confirmed by many authors [Baskurt 2003, Danesh et al 2000] haemodynamics of intracranial vasculature is dependent upon the rheological properties of blood, including BV. It is intuitive to speculate that the factors, which affect BV, may influence the haemodynamic environment of an IA, affecting in turn its initiation, growth, and rupture. Various workers have demonstrated the influence of commonly used drugs on BV including heparin, [Hosoda and Iri 1966] amlodipine, [Linde et al 1996], metoprolol [Hosoda and Iri 1966], pentoxiphilline [Schmetterer 1996], nitrates [Brugger et al 1985], oral contraceptives [Coata et al 1995], statins [Rosenson and Tangney 1998], various chemotherapeutic agents [Mark et al 2001], etc.

As correctly feared by Sekhar and Heros [Sekhar and Heros 1981] in their classical review; with ever increasing use of more and more pharmacological agents there is a pragmatic possibility that a certain medical or surgical treatment modality may alter the delicate balance, leading to increased aneurysm formation or rupture. In the current study I analyzed and compared the important haemodynamic factors in two IAs, one in the stage of initiation (a preaneurysmal lesion, Aneu-1) and other a ruptured aneurysm (Aneu-2). Followed by this, the study investigates the effects of heparin on the haemodynamics of these IAs, and discusses its possible long-term implications on their natural history.

6.3.2 Material And Methods

The study was conducted jointly in the departments of Neurosurgery and Neuroradiology, Royal Hallamshire Hospital, and the Academic Unit of Medical Physics, School of Medicine and Biomedical Sciences, University of Sheffield, Sheffield, UK. After obtaining appropriate consent and ethical approval the patient was recruited to the project @neurIST (www.aneurist.org).

6.3.2.1 Clinical Details

The patient included in the study was a 58-years-old woman presented in March 2008 with a history of sudden onset of severe headache, nausea vomiting, photophobia and loss of consciousness. She had a past medical history of deep vein thrombosis (DVT) and was on long-term warfarin for that. The Glasgow Coma Score (GCS) at the time of admission was 13/15 (E3V4M6) with bilateral normally reacting pupils and no signs of meningism. An urgent CT scan of the head revealed presence of subarachnoid blood with normal ventricles.

6.3.2.2 Endovascular Intervention and Postoperative Period

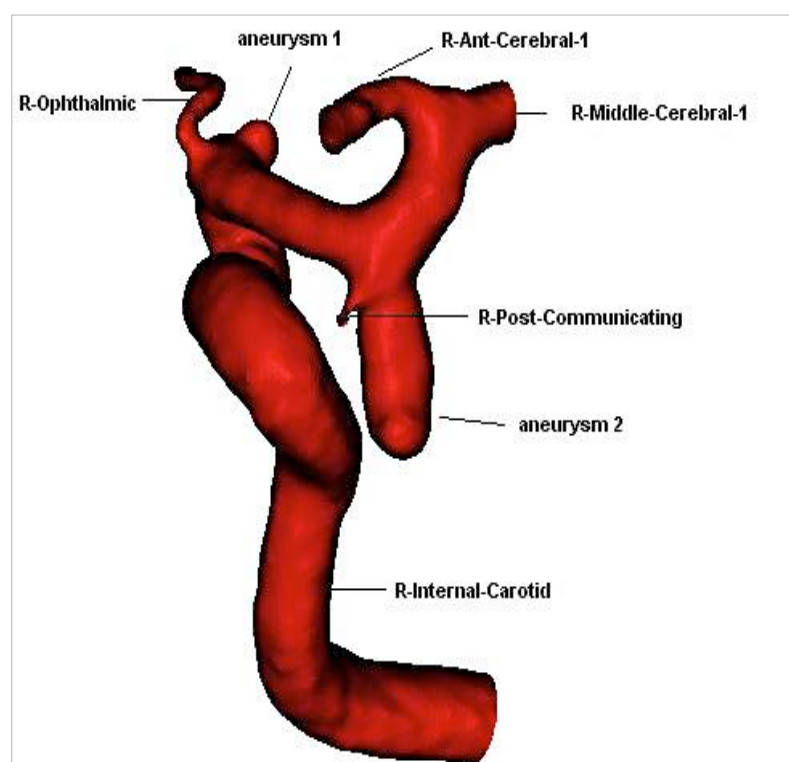


Figure-6.3: Reconstructed geometries showing the IAs and connecting vessels reconstructed with software @neuFUSE. Labels indicate the openings where boundary conditions were applied.

A CT angiogram performed later demonstrated the presence of two IAs, further confirmed by a four-vessel 3DRA (Figure-6.3). First aneurysm (Aneu-1) was a tiny ‘bleb’ type IA in the ophthalmic segment of right internal carotid artery (ICA) and is considered as preaneurysmal lesion here. The second IA (Aneu-2) considered as source of bleed here was present in right

ICA at the level of right posterior communicating artery (PComA). The radiological characteristics of the IAs are given in Table-6.5. It was decided to coil the tubular right ICA-PComA aneurysm in the same sitting using GDC® (Guglielmi Detachable Coils) embolization. A 6-French guide-wire catheter was positioned distally within the right extracranial ICA. The aneurysm was catheterized with an Excelsior® microcatheter using a Transend® 14 guide wire (Boston Scientific®, USA). The IA was packed satisfactorily using four Micrus® endovascular bare platinum coils. Patient's hospital stay was unfortunately complicated by bouts of chest infections necessitating prolonged hospitalization. Throughout the hospital stay, she received low molecular weight (LMW) heparin (enoxaparin, Clexane®) for her DVT prophylaxis. The tiny 'bleb' IA was found unsuitable for coiling and therefore decided to be followed by MRAs.

Table-6.5: Radiological characteristics of IAs

	Aneu-1	Aneu-2
<i>Location</i>	Rt. ICA –Ophthalmic segment	Rt. ICA at the origin of PComA
<i>Size</i>	1.4x2mm	9x3 mm
<i>Neck size</i>	2.3mm	3.6mm
<i>Dome status</i>	Unruptured	Ruptured
<i>Type</i>	Bleb/ preaneurysmal/ side wall	Saccular/ side wall
<i>Aspect</i>	Smooth	Smooth
Connected vessels		
<i>Inlets</i>	Rt. ICA, Rt. PComA	Rt. ICA, Rt. PComA
<i>Outlets</i>	Rt. Ophthalmic, Rt. MCA, Rt. ACA	Rt. Ophthalmic, Rt. MCA, Rt. ACA

NB: Rt; Right, PComA; posterior communicating artery, ICA; internal carotid artery, MCA; middle cerebral artery, ACA; anterior cerebral artery. Connected vessels are used as outlets or inlets in the flow simulation, as indicated.

6.3.2.3 Image acquisition protocol

The medical images used in the study to reconstruct the aneurysm geometries were obtained using rotational acquisition in a Philips® Integris™ Allura™ machine (Philips® Medical Systems, Best, The Netherlands), producing 100 images in 6 seconds, with 5ms exposure per image. Voxel size in the reconstructed 3D images was 121 microns with a reconstruction matrix of 512x512x512.

6.3.2.4 Numerical 3D model

The @neurIST computational tool-chain was used to reconstruct the vessel surfaces as described by Singh and colleagues (Figure-3). Volumetric meshes were generated using ANSYS®-ICEM™ CFD-11.0, based on the octree approach. Grids were made finer at the walls and progressively coarser towards the vessel axis. Tetrahedral elements were used for the discretization of the domain core, with three layers of prismatic elements adjacent to the wall thus ensuring accurate computation of haemodynamic indices. In order to maintain consistency across the meshes used for all geometries, similar element density, same wall element size and maximum core element size were used in the discretization of the domains.

6.3.2.5 CFD Analysis

The 3D transient Navier–Stokes equations were solved by using the finite-control-volume software, ANSYS®-CFX™. The default second-order high-resolution advection-differencing scheme was used. Blood was assumed to be incompressible, with density $\rho=1060$ kg/m³ and Newtonian, with viscosity $\mu_{\text{untreated}}=0.0045$ Pa.s; for untreated blood, and $\mu_{\text{heparin}}=0.0025$ Pa.s; 22 for heparinized blood. This simulates the effect of heparin at an average therapeutic concentration of 0.0075 mg/ml. All analyses were run in parallel on two Itanium2 900MHz 64-bit processors of a Tiger-2 Linux cluster. The average time required to solve one cardiac

cycle was approximately 8.6 Hrs. The relevant haemodynamic variables were computed for both the viscosity values. Qualitative and quantitative comparisons of all the computed haemodynamic variables were performed.

6.3.3 Results

6.3.3.1 Comparison of the haemodynamics in initiation (Aneu-1) and rupture (Aneu-2) phase

Table-6.6 gives the details of all haemodynamic indices computed using typical BV ($\mu_{\text{untreated}}=0.0045$ Pa.s) and their quantitative comparison between Aneu-1 and Aneu-2. The WSS, OSI and blood velocity values used in the present study are time-averaged along the cardiac cycle while the area of elevated pressure was considered at peak systole. Whereas, the flow was stable throughout the cardiac cycle in both the IAs and was momentum driven, it was more vortical in the ruptured lesion (Aneu-2) with higher flow velocities.

Table-6.6: Inter-aneurysmal comparison of haemodynamic indices in Aneu-1 and Aneu-2 for typical BV ($\mu_{\text{untreated}}$)

Haemodynamic variable	Aneu-1	Aneu-2	Difference (%)
Max-t-av-velocity in IA (m/s)	0.049	1.024	+95.2
Space t-av-velocity in IA (m/s)	0.085	0.085	0
t-av-WSS _{min} (Pa)	1.066	0.055	-1838.18
t-av-WSS _{max} (Pa)	35.9	67.75	+47
Area of infra-physiological WSS (<0.4 Pa)	00%	0.8%	+100
Area of supra-physiological WSS (>1.5 Pa)	99.9%	91.2%	-9.6
OSI max	0.21	0.43	+51
Area of elevated OSI (>0.2)	0.1%	2.6%	+96
Area of elevated pressure (%)	2.1%	3.5%	+40
No. Of Vortices	1	2-3	

NB: Aneu-1; preaneurysmal lesion, Aneu-2; ruptured aneurysm, $\mu_{\text{untreated}}$; untreated viscosity values used = 0.0045 Pa.s, WSS; wall shear stress, OSI; oscillatory shear index, Max-t-av-velocity; maximum time-averaged velocity over the cardiac cycle; Space t-av-velocity; space and time-averaged velocity, t-av-WSS_{min}; minimum time-averaged WSS, t-av-WSS_{max}; maximum time-averaged WSS. The values of WSS between 0.4 and 1.5 Pa are considered as physiological range after Malek et al. (1996) and the values of OSI above 0.2 were considered as a threshold value above which endothelial damage is initiated after Glor and colleagues. [Glor et al 2003 and 2004, Goubergrits 2008].

The most striking differences however were observed in the values of WSS, OSI and pressure. Whereas the values for minimum time-averaged WSS (t-av-WSS_{min}) were substantially lower (by 1838.18%) in the ruptured lesion the values for maximum time-averaged WSS (t-av-WSS_{max}) showed an opposite trend. The area affected by infra-physiological WSS (<0.4Pa) was larger in the ruptured lesion (0.8%) as compared to the preaneurysmal stage (0%). Quite the contrary, the area affected by supra-physiological WSS (>1.5 Pa) was larger in preaneurysmal stage. Both, the maximum values of OSI (OSI_{max}) as well as the areas affected by the elevated OSI (>0.2) were higher in the ruptured lesion. Ruptured aneurysm also exhibited approximately 40% rise in the pressure on it wall as compared to its preaneurysmal counterpart.

6.3.3.2 Comparison of the effects of heparin on aneurysmal haemodynamics

6.3.3.2.1 Qualitative comparison

The comparisons of qualitative contour plots of WSS and OSI with and without effects of heparin show (Figure-6.4) that whereas the distributions of both the indices follow similar patterns for both values of BV, the areas affected by their high or low values have changed significantly. It is evident from Figure-6.4 that heparin as a rule increasing the areas affected by relatively low WSS while decreasing the areas affected by relatively high WSS. This pattern of change in the distribution is observed consistently across both the geometries. Whilst for both BV values, areas of low WSS remain confined within the dome and body of the aneurysms, zones of comparatively higher WSS were concentrated around the distal part of the neck and in areas within the aneurysmal body, where the jet generated at the base of the aneurysm impinges against its wall. Figure-6.4 shows the increasing ‘low-WSS’ (black arrows) and decreasing ‘high-WSS’ patterns for Aneu-1 and Aneu-2 (red arrows).

Contrary to the t-av-WSS, it is observed that heparin treatment has peculiar effect on OSI. Whereas in some of the areas the areas of low OSI (black arrows) are increasing with heparin treatment, in other areas it is increasing the areas affected high OSI (red arrows).

6.3.3.2.2 Quantitative comparison

Table-6.7 shows a quantitative comparison between minimum and maximum values of WSS and OSI,

Table-6.7: The Quantitative comparison of effects of heparin on haemodynamic indices

	Aneu-1			Aneu-2		
	$\mu_{\text{untreated}}$	μ_{heparin}	Change %	$\mu_{\text{untreated}}$	μ_{heparin}	Change %
$t\text{-av-WSS}_{\min}$ (Pa)	1.066	1.086	+1.8	0.055	0.048	-12.7
$t\text{-av-WSS}_{\max}$ (Pa)	35.9	28.08	-21.8	67.75	45.11	-33.4
Area of infra-physiological WSS (<0.4 Pa)	0.009%	0.07%	+677.8	0.8%	1.2%	+50.0
Area of supra-physiological WSS (>1.5 Pa)	99.9%	99.6%	-0.3	91.2%	88.7%	-2.7
OSI_{\max}	0.21	0.17	-19.0	0.43	0.46	+7.0
Area of elevated OSI (>0.2)	0.1%	00%	-100.0	2.6%	4.1%	+57.7
Area of elevated pressure (%)	2.1%	2.5%	-19.0	3.5%	4.0%	+14.3

NB: Aneu-1; preaneurysmal lesion, Aneu-2; ruptured aneurysm, $\mu_{\text{untreated}}$; untreated viscosity values used = 0.0045 Pa.s, WSS; wall shear stress, OSI; oscillatory shear index, Max-t-av-velocity; maximum time-averaged velocity over the cardiac cycle; Space t-av-velocity; space and time-averaged velocity, $t\text{-av-WSS}_{\min}$; minimum time-averaged WSS, $t\text{-av-WSS}_{\max}$; maximum time-averaged WSS. The values of WSS between 0.4 and 1.5 Pa are considered as physiological range after Malek et al. (1996) and the values of OSI above 0.2 were considered as a threshold value above which endothelial damage is initiated after Glor and colleagues. [Glor et al 2003, 2004, Goubergrits 2008]

areas where values for these indices are outside their normal physiological range, [Glor et al 2003, 2004, Goubergrits 2008] and areas of elevated pressure for both the geometries. The change in values of these indices

before and after heparin treatment is represented in percentage, in the last columns.

Qualitative and quantitative comparisons for only three most relevant haemodynamic indices i.e. WSS, OSI and pressure were performed.

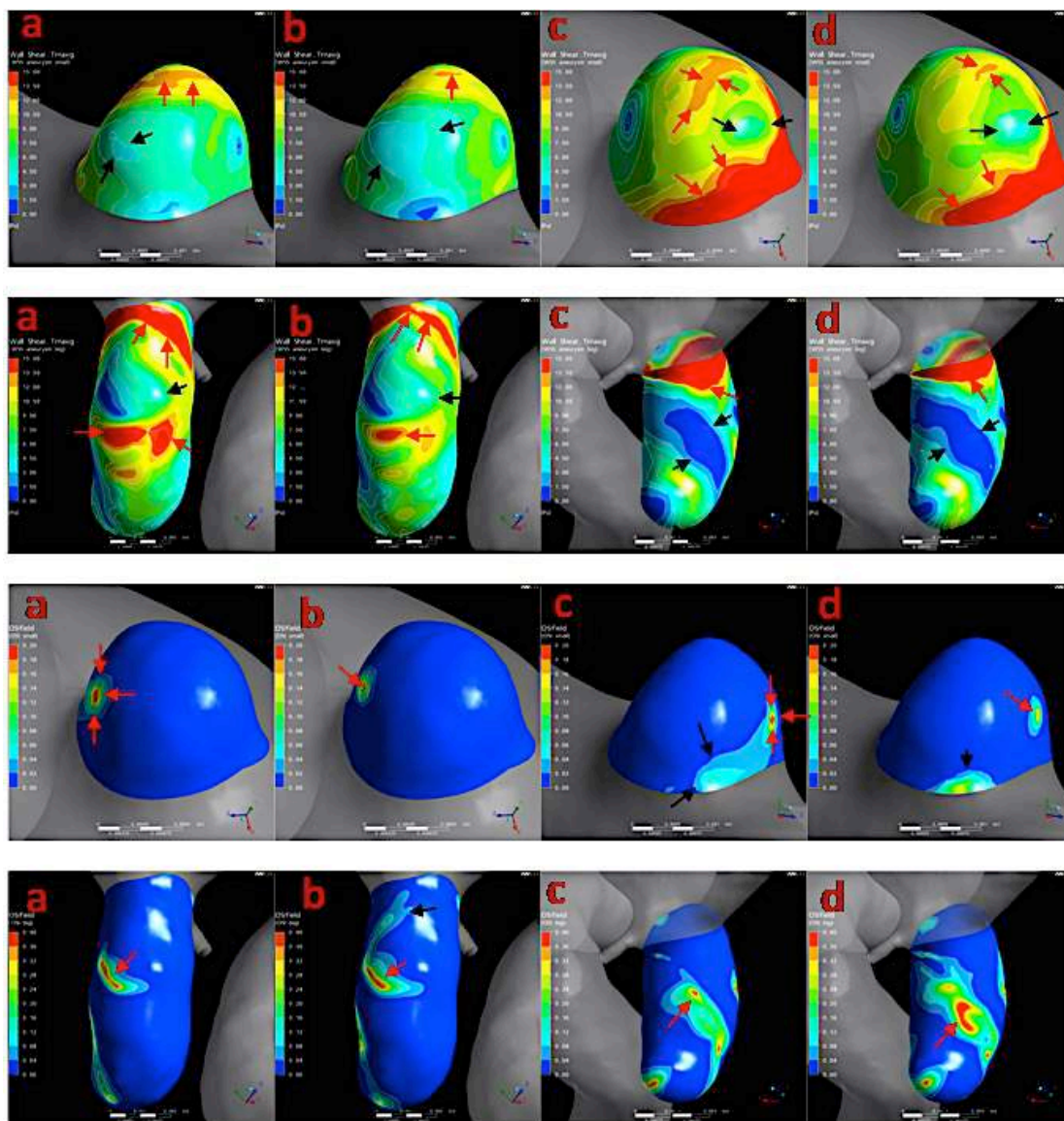


Figure-6.4: The qualitative differences in the patterns of t-av-WSS and OSI in pre (a,b) and post heparinized (c,d) blood. Top two rows are contour plots for t-av-WSS. Bottom two rows are contour plots for OSI. a&b; front views, c&d; back views. Row 1&3; Aneu-1, row 2&4; Aneu-2.

Whereas t-av-WSSmin was decreased in Aneu-2 after heparin administration by 12.7%, the values were minimally (1.8%) increased in Aneu-1. t-av-WSSmax was decreased in both IAs. An increase in the areas affected by infra-physiological WSS ($<0.4\text{Pa}$) was observed in both the lesions. The increments however were substantially higher (+677.8%) in the preaneurysmal lesion (Aneu-1) as compared to the ruptured IA (50%). The areas affected by supra-physiological WSS ($>1.5\text{ Pa}$) were decreased

in both the lesions when BV values specific to heparin were used. Whereas, the values for OSI_{max} and the areas of elevated OSI (>0.2) were decreased in Aneu-1, the corresponding values were increased in Aneu-2 after treatment with heparin. The distribution of elevated pressure areas followed the similar trend to that of OSI.

6.3.4 Discussion

There is a rapidly growing body of literature affirming the importance of haemodynamics in the aetiopathogenesis of IAs [Baskurt 2003, Burleson et al 1996, Castro et al 2006, Cebal et al 2005, Cebal et al 2008, Danesh et al 2000, Fukuda et al 2000, Gao et al 2008, Glor et al 2003, 2004, Goubergrits 2008, Inci and Spetzler 2000, Malek et al 1999, Mantha et al 2006, Morimoto et al 2002, Shojima et al 2004, Steinman et al 2003]. The haemodynamic variables often considered in these studies are WSS, oscillatory shear index (OSI), blood pressure, and other quantities used to characterize blood flow. Proportional to blood viscosity and its velocity, WSS is the tangential frictional force exerted by the flowing blood on the walls of each vessel. High supra-physiological and low infra-physiological values of WSS have been associated with initiation, growth and rupture of aneurysms [Baskurt 2003, Fukuda et al 2000, Gao et al 2008, Glor et al 2003, Shojima et al 2004]. A measure of the oscillatory nature of these viscous forces is given by the OSI, often associated with endothelial cells degeneration. [Glor et al 2003, 2004, Goubergrits 2008] Table-8 below gives a comprehensive list of haemodynamic variables from the literature and their association with IA evolution.

An evaluation of these variables can provide a useful alternative to predict the behavior of an unruptured IA at an early stage before it changes in size, shape or becomes symptomatic. Unfortunately, the detailed in-vivo measurements of these relevant flow variables in the regions affected by the disease are currently impossible [Shojima et al 2004, Steinman et al 2003]. Motivated by the important role played by haemodynamics and the difficulty of conducting detailed in-vivo observations of relevant haemodynamic variables, engineers and computer scientists have started using CFD to predict blood flows in IAs [Baskurt 2003, Castro et al 2006, Cebal et al 2005, Cebal et al 2008].

In this study, I observed that both aneurysms, representing the two extreme stages in the natural history of an IA, were peculiar in their haemodynamic characteristics (Table-6.6). Max-t-av-velocity was approximately 95% higher in Aneu-2 than the preaneurysmal lesion IA (Aneu-1). This might represent a correlation of high max-t-av-velocity and aneurysmal rupture. On the other hand the space and t-av velocity was

identical in both IAs making it difficult to draw any conclusions on its effect IA pathogenesis.

Table 6.8: The literature-based evidence on the importance of haemodynamics in the aetiopathogenesis of IAs

Haemodynamic factors	Intracranial Aneurysm			Proposed mechanism(s)	References
	Initiation	Growth	Rupture		
<i>Dynamic</i>					
Wall Shear Stress (WSS)	High	Low	Low	Increased WSS increases the production of MMP-13 which in turn leads to vessel wall damage Decreased WSS increases iNOS synthesis- NO induced damage to vessel wall Low WSS increases endothelial proliferation and apoptosis	Boussel et al 2008, Fukuda et al 2000, Gao et al 2008, Jou et al 2008, Malek et al 1999, Meng et al 2007, Shojima et al 2004, Ujje et al 1999
Oscillatory Shear Index (OSI)	High/Low	High	High	Degenerative changes in endothelium	Glor et al 2004, Goubergrits et al 2008, Mantha et al 2006
Jet of Blood Stream	Impingement	Impingement	Impingement	Localized endothelial cell injury	Foutrakis et al 1999, Cebral et al 2005, Cebral et al 2009
Flow Pattern	-	-	Complex	Statistical association	Cebral et al 2005, Cebral et al 2009
<i>Hydrostatic</i>					
Pressure	High	High	High	Passive yield/ water hammer effect	Inci and Spetzler 2000, Morimoto et al 2002, Steiger et al 1989

NB: WSS; wall shear stress, MMP-13; matrixmetalloproteneseases-13, iNOS; inducible-nitric oxide synthase, NO; nitric oxide, OSI; oscillatory shear index

WSS is one of the most extensively studied haemodynamic indices. Whereas high supra-physiological values have been associated with initiation, the low values are thought to be responsible for growth and rupture. Cebral et al 2005, Cebral et al 2008 Values of t-av-WSSmin in the preaneurysmal lesion (Aneu-1) were significantly (1838.18%) higher as compared to the ruptured IA where it was significantly lower. t-av-WSSmax also showed the similar patterns being higher in the Aneu-1 as compared to Aneu-2. As suggested by Malek et al [Malek et al 1999] the values of WSS between 0.4 Pa and 1.5 Pa were considered physiological range in the study. Whereas, the area affected by infra-physiological WSS (<0.4Pa) was larger in ruptured IA, the area affected by supra-physiological WSS (>1.5 Pa) was bigger in initiation stage. It has been suggested that supra-physiological WSS increases the production of MMP-13, which in turn leads to vessel wall damage [Boussel et al 2008] leading to IA formation, especially at arterial bends and bifurcations. Infra-physiological WSS on the other hand increases iNOS (inducible Nitric Oxide) synthesis. [Fukuda et al 2000] NO induced damage to vessel wall increases endothelial proliferation and apoptosis.

The increased values of OSI (>0.2) are found to be associated with aneurysmal pathogenesis by producing degenerative changes in endothelium. [Glor et al 2003, 2004, Goubergrits 2008]. In my study, both

OSI_{max} and the area of elevated OSI (>0.2) were higher in ruptured IA as compared to one in the stage of initiation (Aneu-1). This observation may indicate that possibly the high values of OSI play more important role during the rupture of an IA than its initiation.

High pressure has long been implicated in aneurysmal rupture [Inci and Spetzler 2000]. The rupture is thought to be an effect of passive yield to pressure leading to tissue failure and the water hammer effect [Inci and Spetzler 2000]. Keeping in consistent with the previous authors' findings, the area affected by high pressure in the current study was greater in the ruptured IA (Aneu-2). The number of vortices inside an IA represents complexity of its flow, which in turn correlates with aneurysmal rupture [Cebal et al 2005, Cebal et al 2008]. Whereas, only one vortex was observed in Aneu-1 (preaneurysmal lesion) the flow was relatively complex in Aneu-2 (ruptured) with 2-3 vortices.

Various pharmacological agents including Beta aminopropionitrile fumarate (BAPN), a lathyrogen, have been successfully used in the induction of IAs in experimental animal models [Hosoda et al 1966, Inci and Spetzler 2000, Kim et al 1989]. BAPN irreversibly inhibits lysyl oxidase enzyme preventing the cross-linkage between elastin and collagen fibers, critical for the maintenance of normal structure and strength of vessel wall. The net effect is disruption or loss of internal elastic lamina, possibly facilitating the IA formation. Apart from the experimental animal models, there are reports describing the bilateral IA formation in human beings after the anticoagulation therapy [Turowski et al 2007]. The dissecting aneurysms regressed when aspirin replaced warfarin. It has been suggested that a combination of increased pressure (hypertension) and anticoagulation can play a role in the development of IAs in these situations thus contraindicating the use of anticoagulants in these patients [Pezzini et al 2006]. In their novel experimental studies Aoki and colleagues [Aoki et al 2007, Aoki et al 2007, Aoki et al 2008, Aoki et al 2008, Aoki et al 2009] showed various inflammatory mediators playing a crucial role in the initiation and progression of IAs. More recently, the same group also demonstrated preventive effects of different drugs on the formation or progression of IAs including simvastatin [Aoki et al 2008], pitavastatin [Aoki et al 2009], and nifedipine [Aoki et al 2008]. It has been suggested that protective effects of these drugs are mediated through their property of inhibiting the inflammatory reactions in the IA wall.

The effects of various pharmacological agents on the rheological properties of blood have extensively been studied by many authors. It has been shown that drugs like heparin [Hosoda and Iri 1966]

antihypertensives [Hosoda and Iri 1966], pentoxiphiline [Schmetterer 1996] nitrates [Brugger et al 1985] oral contraceptives [Coata et al 1995] statins [Rosenson et al 1998], various chemotherapeutic agents [Mark et al 2001], etc., can influence the BV. Heparin, a highly sulfated glycosaminoglycan, is a widely used injectable anticoagulant. Heparin and its newer derivatives like enoxaparin are very effective in preventing deep vein thrombosis and pulmonary embolism in the patients at risk. By binding with plasma-protease inhibitor antithrombin III, heparin accelerates its action, which in turn inhibits factors involved in blood clotting most notably factor Xa. Heparin increases the rate of this inactivation complex formation 1000-fold, thus causes instantaneous inactivation of thrombin, lowering the BV [Hosoda and Iri 1966]. This reduction in the BV then alters the haemodynamics of blood circulation [Baskurt 2003, Danesh et al 2000, Hitosugi and co-workers [Hitosugi et al 2001] demonstrated that there was a decrease in the BV by 55.6% by heparin at a therapeutic concentration of 0.75 IU/lit. These values are used in the current study to simulate the BV in the patient when she was receiving this drug for DVT prophylaxis.

As noted above the high values of $t\text{-av-WSS}_{\text{min}}$ favor initiation and low values favor the rupture. Whereas the values of $t\text{-av-WSS}_{\text{min}}$ in Aneu-2 were decreased by heparin by 12.7%, the same values were affected minimally in Aneu-1, an observation that may promote rupture of an IA without much affecting the initiation. Quite the contrary, the heparin administration decreased $t\text{-av-WSS}_{\text{max}}$ in both Aneu-1 and Aneu-2 by 21.8% and 33.4%, respectively. Whereas, the situation favors rupture of the existing IAs, it may actually provide protection against formation of new ones. A dramatic increase of 677.8% was seen in the area affected by infra-physiological WSS ($<0.4\text{Pa}$) in preaneurysmal lesion (Aneu-1) after heparin administration. The same values were also increased by 50% in ruptured IA. Again, the deranged values are expected to facilitate the rupture of the existing IAs; but can be protective against formation of new lesions. The area affected by supra-physiological WSS was minimally affected by heparin. The values of OSI_{max} are associated with both initiation as well as rupture of IAs. [Glor et al 2003 and 2004, Goubergrits 2008]. Whereas, heparin decreased both OSI_{max} as well as area of elevated OSI in preaneurysmal lesion (Aneu-1) the effect was opposite in the ruptured IA (Aneu-2) where both the values were increased. The findings further indicate that whereas heparin administration may accelerate the rate of rupture in the existing aneurysms it may suppress the formation of new IAs.

6.3.5 Conclusions

Haemodynamics plays important role in the aetiopathogenesis of IAs. CFD can offer valuable alternative to extract this non-observable data from IAs that can be used to improve the prognosis and management of disease. The current study demonstrates that the haemodynamic patterns of IAs during initiation and rupture are significantly different. Whereas, values of $t\text{-av-WSS}_{\min}$ and areas affected by supra-physiological WSS were higher in preaneurysmal lesion the corresponding values were lower in ruptured IA. The area affected by infra-physiological WSS ($<0.4\text{Pa}$) was significantly higher in ruptured lesion as compared to preaneurysmal IA. Furthermore, by changing the blood viscosity, heparin can induce significant derangements in the haemodynamics of both, preaneurysmal as well as ruptured IA. In the light of evidence from this study, it is expected that whereas on the one hand such alterations in haemodynamics may facilitate the rupture of existing IAs, on the other hand they may suppress the formation of new IAs. Similar effects may be associated with other pharmacological agents, warranting further investigations.

6.3.6 Limitations of the Study

Before drawing any conclusions it is important to emphasize that my study, in common with other CFD analyses, carries inherent limitations associated with the assumptions necessary to create the models. First, whilst very high quality images (3DRA) were used to reconstruct the vessel geometries, these represent the volume of the vessel occupied by contrast agent. If vessel filling with contrast is incomplete, this may generate errors in surface prediction. Unfortunately, due to the limitations of current technology this remains an unresolved problem. Second, the BCs used in the analyses were obtained from a generic 1D circulation model and were not patient-specific. Here it is important to note that recent validation of this model against flow waveforms measured for young volunteers justify its use [Reymond et al 2009]. Third, despite being non-Newtonian, blood was considered as a Newtonian fluid for the purposes of these analyses. This assumption was based on the observations that, blood behaves as a Newtonian fluid at the high shear-rates which apply at most sites in the cerebral circulation ($>100\text{s}^{-1}$), 7 in particular in areas coinciding with sites of IA formation. Fourth, the arterial wall was considered rigid, neglecting wall motion, as this has been shown to have a negligible effect on CFD predictions [Ford et al 2008, Jeays et al 2007]. Finally, the study was performed on a small cohort of two IAs. The work must be considered as a preliminary study; analyses will be required for a significantly larger number of IAs before firm conclusions can be drawn.

6.4 The Effects of Aortic Coarctation on Cerebral Haemodynamics and its Possible Role in the Aetiopathogenesis of Intracranial Aneurysms

6.4.1 Introduction

Estimated annual incidence of IAs in most western countries is 1 to 2% [Atkinson et al 1989, Inagawa et al 1990]. Aneurysmal subarachnoid haemorrhage (SAH) is feared with unacceptably high overall mortality rates of 45% (32-67%) [Hop et al 1997]. About 30% of survivors have moderate to severe disabilities and 66% of those who have 'successful' clipping, never return to same quality of life as before SAH [Hop et al 1997, Drake et al 1981]. The current evidence convincingly supports a multi-factorial basis for the initiation and rupture of IAs [Sekhar and Heros 1981, Yong-Zhong et al 1990, Stehbens 1989].

Amongst other aetiologies proposed, Coarctation of Aorta (CoA) has been highlighted as a major risk factor in the aetiopathogenesis of IAs [Eppinger et al 1871, Abbott et al 1928, Walton et al 1956, Laitinen et al 1960, DuBoulay 1965, Patel 1971, Orsi 1993, Schievink 1996, Ishii 2001, Mercado 2002, Ahmetoğlu 2003, Connolly 2003, Cowan 2004, Hudaoglu 2006, Kan 2007]. A wide range for the incidence of IAs in patients with CoA has been reported starting from 2.5% [Abbott 1928] to as high as 50% [Shearer 1970]. All quoted figures nevertheless are above the estimated incidence of 1-2% of IAs in general population. It is however found by Connolly and colleagues in their recent study that the frequency of IAs among patients with CoA is approximately 5 times higher than that of the general population [Connolly 2003]. Apart from that the incidence of IA rupture in CoA patients (4.8%) [Reifenstein 1947] also outnumbers the estimated rate of rupture in the general population, which is less than 1% [Weir 1996]. In spite of CoA being a well-established risk factor for IA formation [Eppinger 1871, Abbott 1928, Walton 1956, Laitinen 1960, DuBoulay 1965, Patel 1971, Orsi 1993, Schievink 1996, Ishii 2001, Mercado 2002, Ahmetoğlu 2003, Connolly 2003, Cowan 2004, Hudaoglu 2006, Kan 2007], the exact underlying mechanisms for this association remain poorly understood. Hypertension [Orsi 1993, Walton 1956, Stehbens 1962, Stehbens 1989, DuBoulay 1965, Patel 1971, Banna 1973, Orsi 1993, Ishii 2001, Ahmetoğlu 2003] and developmental errors of neural crest resulting in abnormal vessel wall collagen [Laitinen 1960, Schievink 1996, Mercado 2002, Connolly 2003, Cowan 2004, Hudaoglu 2006, Kan 2007] are two main factors thought to facilitate the formation of IAs in presence of CoA. It is surprising to note that in spite of well-established role of WSS in the genesis of IAs [Burlison 1996, Gao 2008, Morimoto 2002, Handa 1983, Hashimoto 1987,

Hashimoto1980, Mantha2006, Meng2007, Wang2009], none of the workers explored this important link in this context.

Owing to their direct origin from the pre-coarctation segment of aorta cerebrocephalic arteries are most likely to be affected by the haemodynamic changes occurring in this part of aorta. Secondary to the increased resistance to outflow increased aorto-cranial pressure gradients have been demonstrated by a number of authors correlating to the severity of stenosis [Gupta1951, Abbott1928, Hom2008, Varaprasathan2002, Mohiaddin1993]. Dilatation of cervicocephalic arteries in CoA secondary to this increased pressure gradient is has also been reported [Rowe et al 1964, Abbot1928].

An increase in the radius (r) of cerebral arteries and increased arorto-cranial pressure gradient (ΔP) in CoA are expected to result in an exponential rise in flow-rates (Q) as per the Hagen-Poiseuille's law (Equation-1), given the viscosity (μ) and length (L) remain constant.

$$Q = \frac{\Delta P}{8\mu L} \pi r^4 \dots\dots\dots (\text{Eq-1})$$

Furthermore, bradycardia coupled with increased stroke volume and cardiac output is a known feature of CoA [Gupta1951]. These increments will further increase the cerebral blood-flow (CBF).

An increased flow-rate (Q) on the other hand remains one of the major factors responsible for increased wall shear stress (WSS) in the intracranial arteries (Equation-2).

$$\tau = 4\eta \frac{Q}{\pi r^3} \dots\dots\dots (\text{Eq-2})$$

Where τ is WSS and η is average blood viscosity.

Literature seems to be particularly deficient and controversial on the effects of CoA on cerebral flow-rates. After a thorough search (Pubmed[®], Embase[®] and Google-Scholar[™] searched from the year 1800 up to 2009) I could retrieve only two studies done in this field. Whereas, in 1949 Hafkenschiel et al [Hafkenschiel1949] demonstrated a significant increase in cerebral flow-rates in patients with CoA, Rowe and colleagues [Rowe 1964] found no significant differences in the flow-rates before and after the repair of CoA in their study done in 1964. No apparent efforts were done since then to measure the cerebral flow-rates in patients with CoA.

Paucity of information about the flow patterns inside the cerebral circulation in presence of CoA provided us a rationale to measure the cerebral flow-rates in the present patient. Furthermore, given the widely accepted importance of haemodynamics in the aetiopathogenesis of IAs [Burleson1996, Gao2008, Morimoto2002, Handa1983, Hashimoto1987, Hashimoto1980, Mantha2006, Meng2007, Wang2009] it is logical to analyse the haemodynamic factors in the coexisting IA of our patient. A better understanding of the aetiopathogenesis of the IA formation and rupture may help clinicians in preventing and treating the disease effectively.

In the current study I performed pc-MR (phase contrast magnetic resonance) measurements in the cerebral arteries of an IA patient with coexisting CoA and five healthy volunteers followed by an analysis of the different haemodynamic factors inside IA. The possible role of haemodynamics is discussed in this context in a background of relevant literature.

6.4.2 Materials and Methods

The study was conducted jointly in the departments of Neurosurgery and Neuroradiology, Royal Hallamshire Hospital, and the Academic Units of Medical Physics, and Radiology, School of Medicine and Biomedical Sciences, University of Sheffield, Sheffield, UK. After obtaining appropriate consent and ethical approval the patient was recruited to the @neurIST project (www.aneurist.org).

6.4.2.1 Clinical details: This 51-years old lady, presented for the first time to cardiovascular surgeons in 1989 at the age of 31 years through obstetric unit. She had hypertension in both her pregnancies but was otherwise asymptomatic. She was a smoker, smoking 10-15 cigarettes per day. On clinical examination, she was generally fit and well with a BP of 160/90. No femoral pulses were palpable and there was an ejection systolic murmur in the aortic area coupled with a continuous machinery murmur at left scapula. She was taking oral antihypertensives (Atenolol and Nifedipine) to control her hypertension. Subsequent investigations including DVI (digital vascular scan) done that time revealed a severe (>80% reduction in diameter) post-ductal aortic coarctation distal to origin of left subclavian artery. X-ray chest showed typical inferior notching of 3rd and 8th ribs, bilaterally. No other congenital anomalies were detected apart from a pseudo-bicuspid aortic valve, without any evidence of regurgitation or stenosis. One year later, the patient was treated with

Dacron onlay patch graft (DOPG) repair for her coarctation with an uneventful postoperative recovery.

A follow-up MRI of the heart and great vessels done in July 2004 after 15 years of primary procedure demonstrated evidence of re-coarctation with significant (60-70%) loss of luminal diameter. The stenosis occurred just distal to the origin of left subclavian artery coinciding with the site of

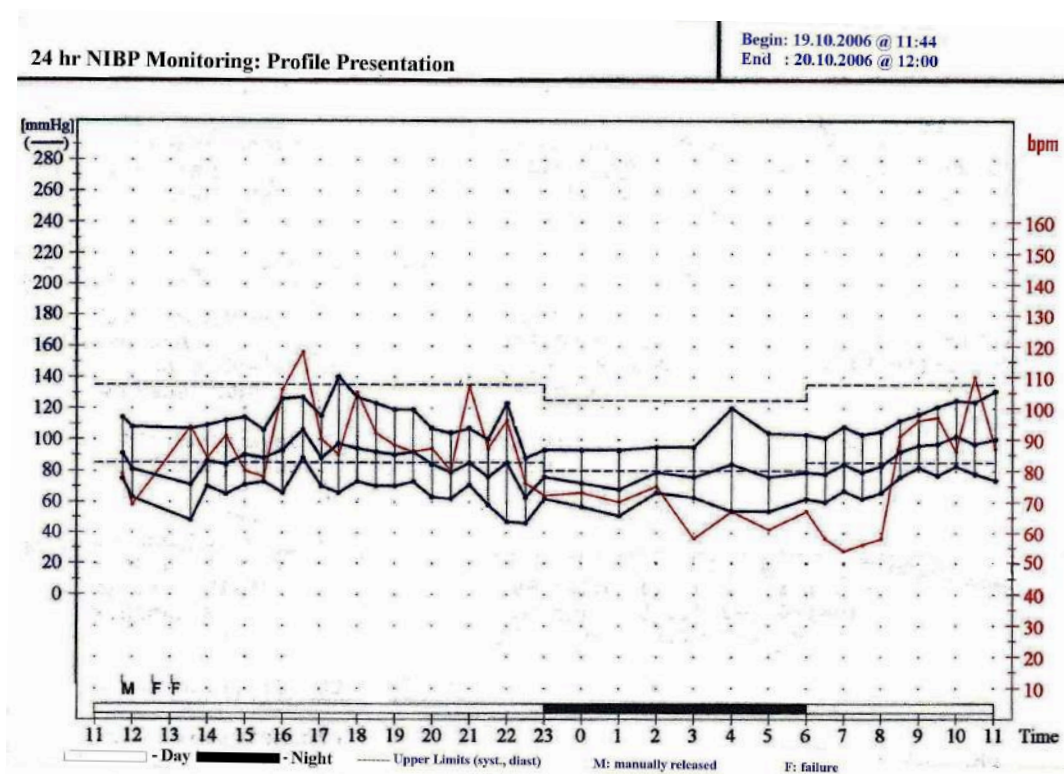


Figure-6.5: 24 hours ambulatory Non-invasive BP (NIBP) monitoring showing satisfactory BP control for both systolic and diastolic values.

repair. Presence of significant collaterals was also noted along with marginal concentric hypertrophy of left ventricle but satisfactory ejection fraction. A BRUCE treadmill stress test done to evaluate cardiac fitness demonstrated an appropriate exercise tolerance without any chest pain or ECG changes. 24-hour BP monitoring further confirmed a satisfactory BP control (Figure-6.5). Being completely asymptomatic and no signs of cardiac failure whatsoever it was decided to manage her conservatively.

The patient was referred to the neurosurgeons in May 2007 with complaints of tingling and numbness affecting right side of her face. On further interrogation she gave history of a similar episode three years back resulting in spontaneous resolution, but no other neurological symptoms. On clinical examination she had an unremarkable neurology. An MRI done to investigate it further demonstrated presence of two incidental IAs. First aneurysm was located in the pericallosal artery and was 4.2 mm in maximum diameter. A second small broad necked 1 mm aneurysm was also present at the origin of left anterior temporal artery arising from the proximal left middle cerebral artery (MCA). The findings were further confirmed by a 3D rotational angiogram (3DRA), which apart from two previous IAs, also revealed an approximately 1.8 mm aneurysm in the subclinoid segment of left internal carotid artery (ICA), pointing medially (Figure-6.6). The case was discussed in a multidisciplinary meeting with neuroradiologists and it was found that due to its small neck the pericallosal IA was suitable for coil embolization.

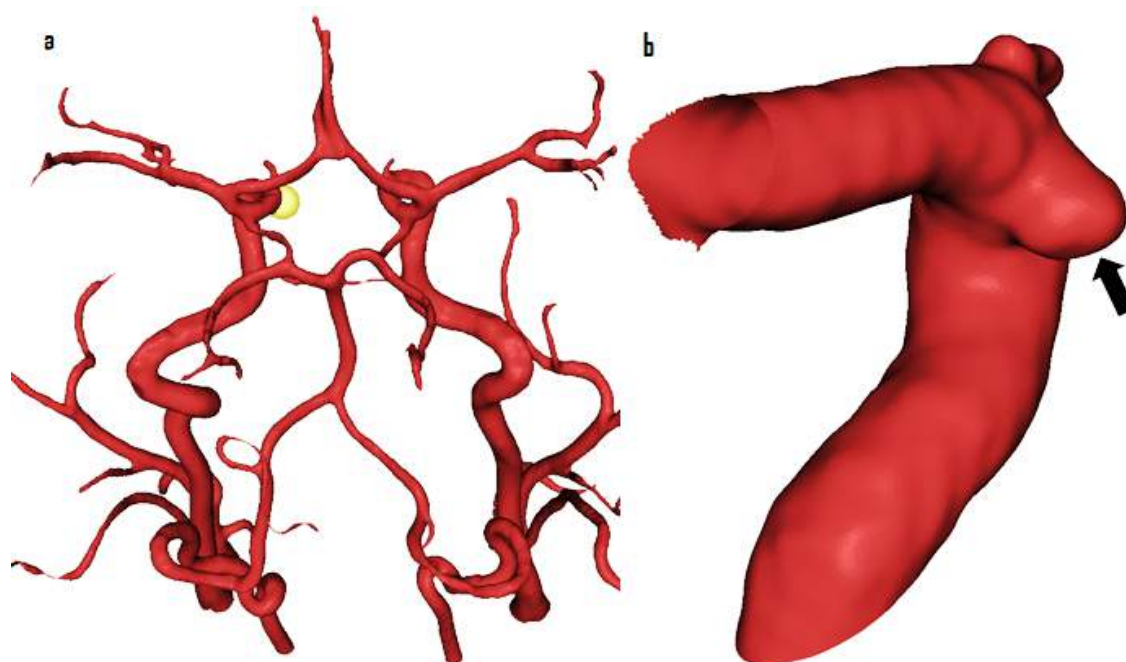


Figure-6.6: Intracranial aneurysm included in the study shown in (a) circle of Willis (yellow sphere) and (b) in subclinoid part of ICA (arrow)

6.4.2.2 3DRA acquisition: All medical images were obtained using rotational acquisition in a Philips® Integris™ Allura machine (Philips® Medical Systems, Best, The Netherlands), producing 100 images in 6 seconds, with 5 ms exposure per image. Voxel size in the reconstructed 3D images was 121 microns with reconstruction matrix of 512x512x512.

6.4.2.3 Endovascular Interventions: The pericallosal artery aneurysm was coiled under general anaesthetic in May 2008 with GDC[®] (Guglielmi Detachable Coils) embolization. A 6-French guided catheter was gently placed within the distal right ICA. The aneurysm was catheterized with an Excelsior[®] SL-10 microcatheter using a Transend[®] 14 guide-wire (Boston Scientific, USA). The IA was packed satisfactorily using four Micrus[®] Cerecyte[®] endovascular bare platinum coils. She made an uneventful recovery from the procedure. Owing to their small size and unsuitability for endovascular coiling (broad neck) remaining two aneurysms were decided to be observed by follow-up MRAs.

6.4.2.4 Flow Measurements & pc-MR protocol: MR imaging was performed at high field strength (Achieva[™] 3.0T, Philips[®] Medical Systems, Best, The Netherlands) using a standard 8-channel, radiofrequency receive-only head coil. The same radiographer imaged the patient and all volunteers to maximize reproducibility of overall acquisition technique. Macroscopic vascular flow and IA location were visualized using a qualitative Time-Of-Flight (TOF) MR angiography sequence (TR=25ms; TE=3.5ms; $\alpha=20^\circ$; visualization voxel size=0.39x0.39x1.00mm³). Maximum intensity projections from this 3D dataset were used to define the placement of each quantitative phase-contrast measurement plane perpendicular to the vessel under investigation. A 2D acquisition sequence (TR=8ms; TE=4.4ms; $\alpha=10^\circ$; field of view=220x179mm²; in-plane acquisition matrix=128x112; slice thickness=5mm) was used to acquire 40 velocity-encoded ‘time points’ over the cardiac cycle at each vascular location. Vector ECG triggering was used to standardize each quantitative acquisition.

The measurements were performed at three locations, both in healthy volunteers and in patient: left proximal ICA, left distal ICA, and left ACA A-1 segment. An appropriate maximum velocity-encoding (VENC) value was chosen (100 cm/sec) for ICA to ensure that appropriate dynamic ranges were sampled in all cases and no phase-aliasing occurred. As proximal vessels geometry has an important influence on intra-aneurysmal haemodynamics [Castro 2006], measurements were taken at a distance of approximately 10 vessel diameters from the aneurysm location. Measurement location in distal vessels was approximately 3 diameters from the IA.

Measurements are reported in Table-6.9, and are consistent with boundary conditions (BCs) in the 3D models. The manufacturer’s proprietary post-data-acquisition processing software (Q-Flow[™], Philips[®] Medical Systems,

Best, The Netherlands) was used to estimate VFR waveforms at each spatial location.

Table-6.9: Radiological characteristics of the IA included in the study, the pc-MR measurements in CoA patient and healthy volunteers along with the locations, types and methods of BC application

IA Location, Size* and Neck Size*	Q-flow measurements using pc-MR and BC application						
	Location of Q-Flow measurements	Q-av-Typical Healthy Volunteers (ml/s)	Q-av-CoA patient (ml/s)	Change (%)	BC location	BC type	BC Method [†]
Lt ICA Subclinoid, 1.8mm, 3.1mm	1. Lt ICA Proximal	3.95	5.44	+27.4	1. Lt ICA Proximal	Inlet/ velocity	pc-MR
	2. Lt ICA Distal	3.7	5.07	+27.1	2. Lt ICA Distal	Outlet/ velocity	pc-MR
	4. Lt ACA	1.2	2.66	+54.9	3. Lt OphthA	Outlet/ pressure	Typical/ population average

NB: Q-av; average blood flow, BC; boundary condition, Lt; left, Rt; right, ICA; internal carotid artery, MCA; middle cerebral artery, OphthA; ophthalmic artery, *size is reported as max diameter. [†]BC method refers to the analyses based on patient-specific BC from CoA patient.

6.4.2.5 Transthoracic Doppler echocardiography: Flow and pressure measurements were performed using transthoracic Doppler echocardiography (Philips[®] Sonos[™] 5500). The results are reported in Figure-6.9.

6.4.2.6 Numerical 3D models and computational fluid dynamics (CFD) analysis: The @neurIST computational tool-chain was used to reconstruct vessel and aneurysmal geometries, as described by Marzo et al [Marzo 2009]. The 3D transient Navier–Stokes equations were solved by using the finite-control-volume software ANSYS[®]-CFX[™]. Blood was assumed to be incompressible, with density $\rho=1060 \text{ kg/m}^3$ and Newtonian, with viscosity $\mu=0.0035 \text{ Pa}\cdot\text{s}$. The relevant haemodynamic indices were computed (Table-6.10) in the IA located in subclinoid part of left ICA (Figure-6.6) of the patient using the VFR values measured in the patient as BCs. A second analysis was performed with BCs derived from the average VFR values measured in healthy volunteers. Location, type and method of BC applied in the study are indicated in Table-6.9. All analyses were run on two Itanium2[®] 900MHz 64-bit processors. The average time required to solve one cardiac cycle was approximately 8.6 Hr.

6.4.3 Results

On comparing the patient-specific waveforms (Figure-6.7) from CoA patient (red) with that of typical normal individual (blue) it becomes apparent that the VFR waveform in the proximal ICA of CoA patient is higher than the one for the healthy volunteers. This is also reflected by the average values reported in Table-6.9 where the flow-rates for the CoA patient are 1.5 times higher (5.44 ml/sec) as compared to the normal healthy individuals (3.62 ml/sec).

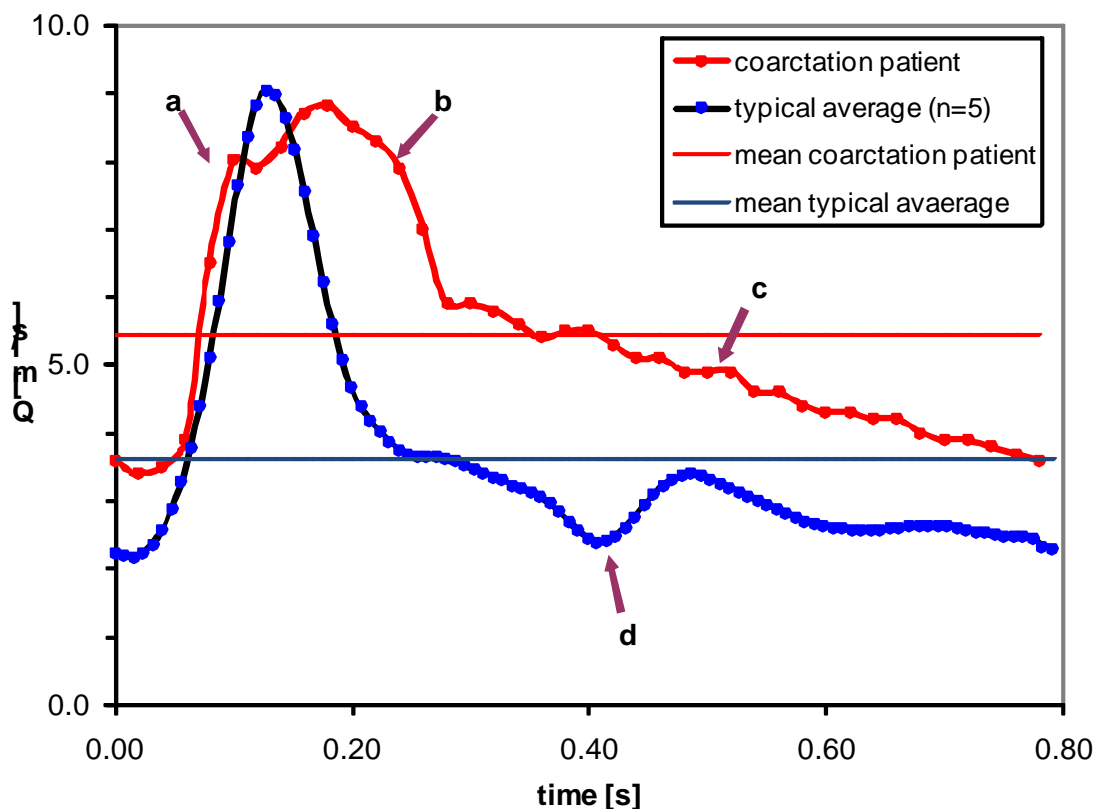


Figure-6.7: A comparison of VFR waveforms from CoA patient (marked-red) measured in proximal ICA and average VFR waveforms from healthy volunteers (marked-blue) in the same location. The flow-rates in presence of CoA are 1.5 times higher (5.44 ml/sec) as compared to the normal healthy individuals (3.62 ml/sec). Solid horizontal lines represent average values of VFR for CoA (red) and typical (blue).

The flow waveforms further illustrate that the cerebral flow in CoA rises and falls slowly than that of a typical individual but the overall volume over one cardiac cycle is increased from 3.48 ml to 4.54 ml. A new broad hump (arrow-a) is seen just after the original peak (arrow-b). The systolic upstroke is delayed and slow; the peak is broader (between arrows a & b), slightly lower and rounded. The flow during diastole is almost a smooth decline curve (arrow-c) and the notch indicating the beginning of diastole is absent (arrow-d).

The contour plots for haemodynamic indices and their absolute values

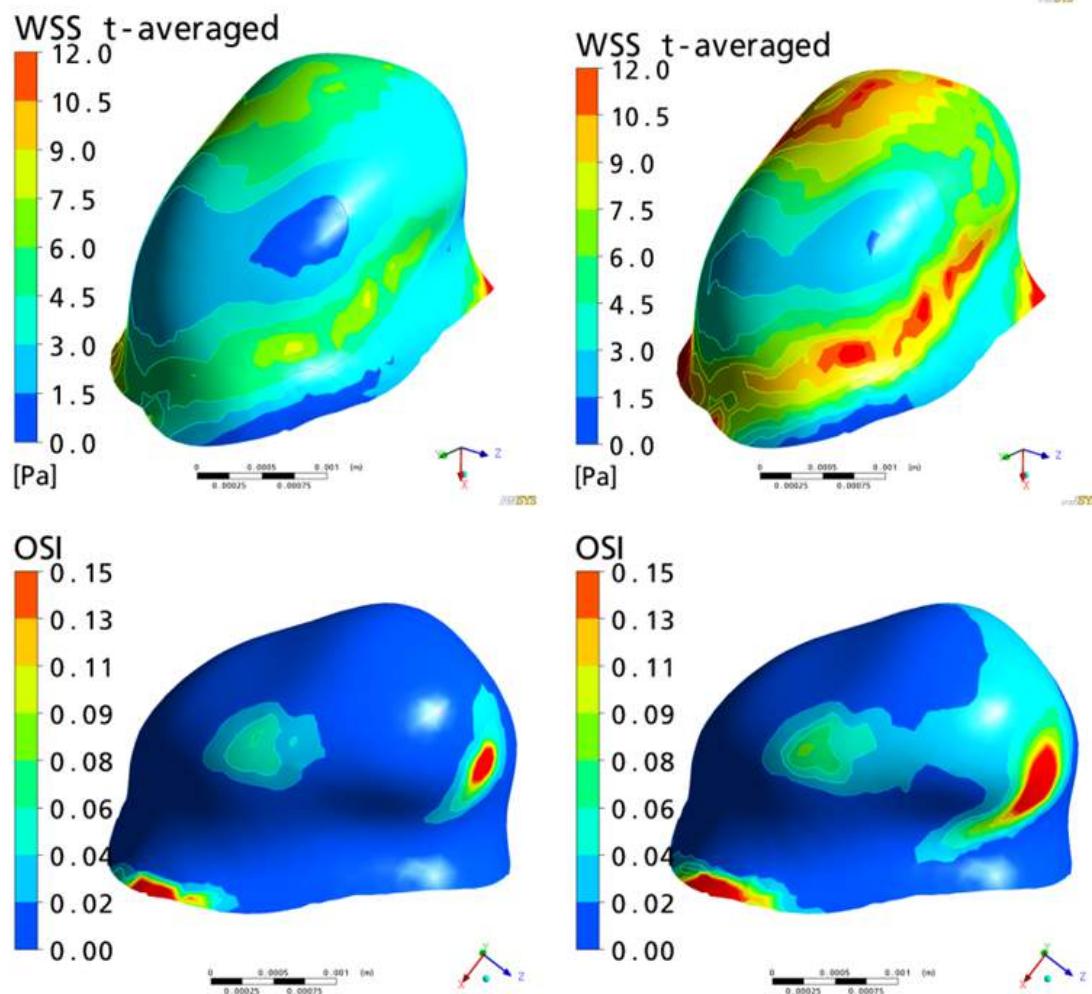


Figure-6.8: Time-averaged WSS (top) and OSI (Oscillatory shear index) (bottom) contour plots in the left subclinoid intracranial aneurysm of CoA patient. Whereas, the areas affected by high WSS are increased in CoA patient (top, right) as compared to healthy volunteers (top, left) the OSI values are minimally changed

Table-6.10 below shows the absolute values of WSS, OSI, velocity and pressure for IA, obtained using BCs derived from healthy volunteers and measurements taken in CoA patient by pc-MR.

Table-6.10: Absolute values of WSS, OSI, velocity and pressure for IA, obtained using BCs derived from healthy volunteers and measurements taken in CoA patient by pc-MR

Haemodynamic Indices	BCs derived from healthy volunteers (without CoA)	BCs derived from patient (with CoA)	% difference
Max t-ave velocity (m/s)	0.5	0.72	+44
Space and t-ave velocity (m/s)	0.072	0.097	+35
Max OSI	0.3	0.3	0
Area of WSS below 0.4 Pa (mm ²)	0.05 (0.3%)	0.03 (0.2%)	-34
Area of WSS above 15 Pa (mm ²)	0.4 (0.4%)	3.0 (17.2%)	+650
Space and t-ave WSS in aneurysm (Pa)	5.7	9.4	+65
Max pressure on aneurysm wall (mmHg)*	122.4	140.8	+15
Area of elevated pressure (mm ²)*	3.0 (17.1%)	1.5 (8.5%)	-50%

NB: WSS; wall shear stress, OSI; oscillatory shear index, Max; maximum, ave; average, t; time, BC; boundary condition, * indicates the values at peak systole

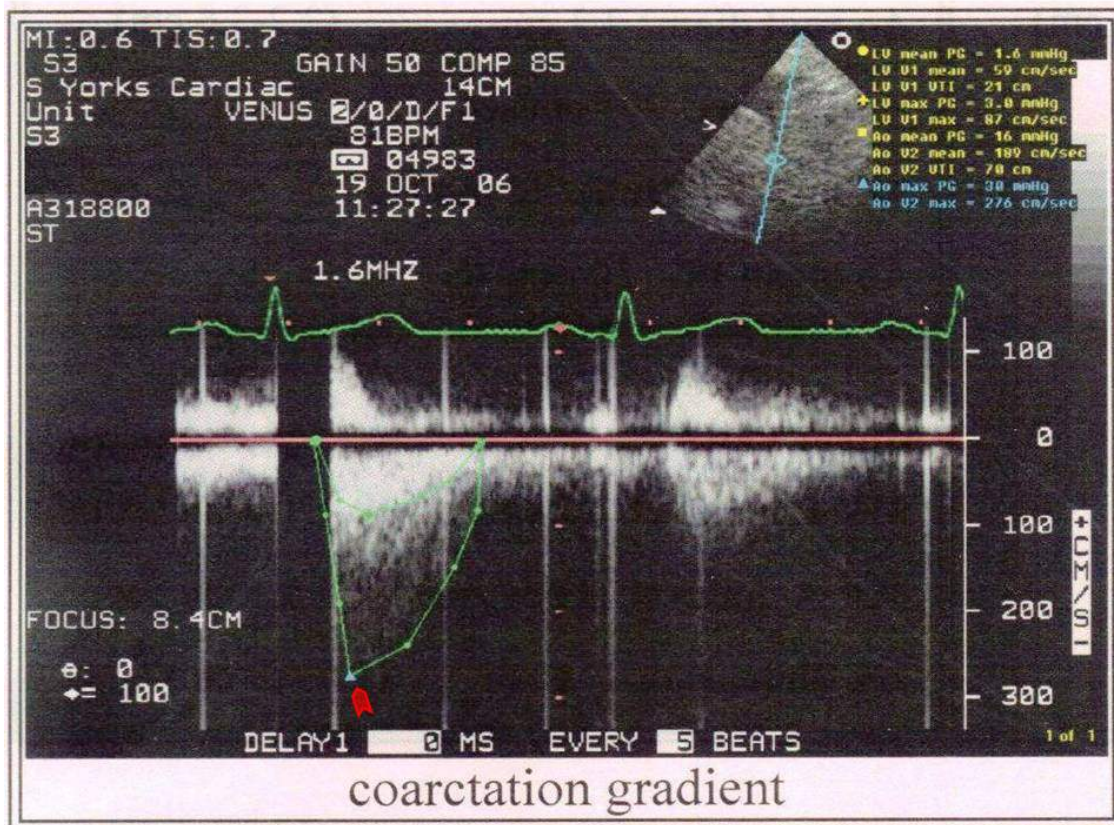


Figure-6.9: Transthoracic Doppler echocardiogram showing aortic coarctation with a diastolic tail. A coarctation gradient of 30-40mmHg was seen (arrowhead) while the average aortic pressure was 16mmHg. The peak velocity in aorta was 276cm/sec.

6.4.4 Discussion

The CoA is a connective tissue disorder accounting for 10% cases of congenital heart disease [Verheugt 2008]. The most common site of narrowing is distal to the left subclavian artery. Due to the mechanical outflow obstruction and extensive collateral formation a number of haemodynamic changes are seen in CoA. The most notable is a differential hypertension produced in the segment of aorta above the site of narrowing leading to increased aorto-cranial pressure gradients [Gupta1951, Abbott1928, Hom2008, Varaprasathan2002, Mohiaddin1993] and dilatation of cervicocephalic arteries [Rowe et al 1964, Abbot 1928]. The similar changes were seen in our patient (Figure-6.9). A pressure gradient of 30-40 mmHg was present at the site of coarctation. The peak velocity in aorta was also increased to 276 cm/sec as against the peak velocity of 80-90 cm/sec in the aorta of a normal person [Daley 1985]. As discussed in the previous sections, it is hypothesized here that the CBF in CoA patients should increase as a consequence of these changes.

It is surprising to see that such little attention is devoted on the effects of CoA on CBF. The first available study on the subject was conducted by Hafkenschiel et al [Hafkenschiel1949] in 1949. They measured CBF and cerebral oxygen consumption in two patients with CoA using nitrous oxide (NO) saturation method. They found that the CBF in patients with CoA was higher as compared to normal subjects.

A similar study was done by Rowe and colleagues [Rowe 1964] in 1964 that measured the CBF in 20 CoA patients using the same technique. The CBF was measured in these patients before and after the surgical correction of CoA and the results were compared with CBF values obtained in normal subjects in their previous study [Rowe 1959], as well as CBF values specific to hypertensive patients [Crompton 1955]. No significant differences were noted in the CBF pre and post surgical repair of coarctation and, between CoA patients and hypertensive patients. Interestingly, whereas authors conclude that there were no significant differences in the CBF in CoA patients and healthy volunteers, the values of average CBF measured by them (63 ± 13 ml/100 gm/ min) were approximately 21.2% higher compared to the CBF measured by same authors in 8 normal subjects (52 ± 12 ml/100 gm/ min) [Rowe 1959] using same methodology. Apart from that, the postoperative measurements in the study were taken at an average interval of 21 months (maximum 9.25 yrs.) from the time of surgery. Re-coarctation is a frequent complication of the coarctation surgery that can occur in 41-86% patients [Hesslein 1981]. The similar patterns were observed in our patient where 60-70% loss of luminal diameter occurred 14 years after repair. As Rowe and colleagues

did not assess the diameter of aorta at the time of CBF measurements, the possibility of re-coarctation in these patients cannot be ruled out which might account for the lack of difference in the CBF before and after surgical correction.

Moreover, being over 40-60 years old, the measurements in both the studies were performed using the oldest available technique based on NO diffusion and Fick's principle introduced by Kety and Schmidt in 1951 [Kety 1951]. The technique has several limitations. Apart from being cumbersome and difficult to perform, it only provides the measurements of global CBF rather than the regional values. The accuracy of measurements is dependent upon the reliability of the blood sample withdrawn from a single jugular vein, which can be influenced by the flow variations in dural sinuses and torcula [Joseph 2000]. With the advent of technology, the technique of CBF measurement has evolved tremendously. The use of pc-MR in this context is gaining a rapid popularity [Ueda 1999, Rordorf 1999, Buijs 1998, Enzmann 1993, Enzmann 1994, Yamashita 2007]. The CBF can be measured using this technique in a simple non-invasive manner without the need of any intravenous contrast administration and has been validated widely by means of *in vitro* and *in vivo* experiments [Caputo 1991, Kondo 1991, Evans 1993, Bakker 1995].

Apart from that, both the studies provide the estimation of global CBF in CoA patients. The recent evidence however indicates that it is the local variations in the haemodynamics that play an important role in the aetiopathogenesis of IAs [Gao 2008, Morimoto 2002, Handa 1983, Hashimoto 1987, Hashimoto 1980, Mantha 2006, Meng 2007, Wang 2009] highlighting the importance of assessing the local CBF. No previous study however has examined the local CBF in presence of CoA. According to the Hagan-Poiseuille's law I hypothesised that the local CBF should increase in patients with CoA. The results from current study demonstrate that my hypothesis is correct and the regional blood-flow in ICA and ACA of CoA patient was 27.1 to 54.9% higher (Table-6.9) when compared to healthy volunteers. Keeping in line with the increased flow-rates in the cerebral arteries in presence of CoA (Table-6.9) the space and time averaged velocity and max time average velocities inside the coincidental IA present in the same patient were also increased by 35-44% (Table-6.10) when the BCs specific to CoA were used.

I further hypothesize that this increased regional CBF can be an important contributory factor in the increased incidence of IAs in presence of CoA.

The possible mechanisms responsible for increased incidence of IAs in CoA patients are explored in the further sections of this manuscript.

Eppinger was the first person to draw attention towards the association between CoA and IAs in 1871 [Eppinger 1871]. Whereas the exact mechanisms responsible for this increased incidence remained obscure, arterial hypertension (HTN) has been suggested as a possible underlying cause by most of the authors (Table-6.11) [Stehbens 1989, 1962, Walton 1956, Patel 1971, Banna 1971, Orsi 1993, Ishii2001, Ahmetoğlu 2002]. Stehbens was the strongest proponent of this theory who particularly stressed on the importance of hypertension in this context while denying the role of all other factors including vessel wall abnormalities [Stebens 1989, 1962].

This assumption is probably based on two observations. First, HTN is often a constant feature in CoA patients. Second, HTN has been considered as a major risk factor for the development of IAs even without CoA [de la Monte 1985, Taylor 1995]. In spite of an increased prevalence of IAs in hypertensive patients many authors have questioned the role of HTN in this context. McCormick and Schmalstieg found no relationship between arterial HTN and IAs in 250 patients they studied [McCormick 1977]. In a similar study conducted in 212 cases Andrews and Spiegel [Andrews 1979] did not find significant elevation in the blood pressure in patients with IAs compared with the general population. However, studies supporting HTN as a risk factor for the development and rupture of IAs outnumber the studies refuting it. De la Monte et al [de la Monte 1985] found high degree of correlation ($p < 0.001$) between systemic hypertension and development of saccular IAs. In one of the largest studies conducted including 20,767 elderly patients Taylor et al [Taylor 1995] found HTN as an independent major risk factor for aneurysmal SAH.

It is argued here that whereas HTN can be an important contributory force in the aetiopathogenesis of IAs in these patients, it cannot be the sole perpetrator. Hudaoglu et al [Hudaoglu 2006] raised a question on HTN alone being a factor in the aetiopathogenesis of IAs in CoA patients. The fact is further supported by the observation that IAs may develop or rupture even in normotensive patients, years after the repair of CoA [Mercado2002, Forfang 1979, Laborde 1983, Ostergaard 1983]. Apart from that, HTN was not uniformly noted in the patients of CoA reported to have IAs [Connolly2003, Schievink1996]. The IAs were developed in our patient 17 years after the surgical correction of CoA. However, re-coarctation of the repaired segment occurred during this period ($>70\%$ reduction in aortic diameter), the patient remained completely

asymptomatic with a very well controlled blood pressure (Figure-6.5). My findings also indicate towards the presence of the some factors working independently of arterial HTN.

In their study conducted in 1960 Laitinen and Snellman [Laitinen1960] found that apart from CoA, aneurysms of Pericallosal artery region were also associated with other concomitant malformations such as craniosynostosis and kyphoscoliosis. They believed that coexistence of these malformations with IAs is secondary to a common developmental error-playing role in their aetiology. Embryologically- heart, aorta and cervicocephalic arteries all share a common origin from neural crest. After recognizing the association between a variety of congenital heart diseases and IAs, Schievink et al [Schievink1996] attributed the occurrence of IAs in CoA patients to the developmental errors of neural crest resulting in abnormal vessel wall collagen. The same theory was later supported many other authors (Table-6.11) [Mercado2002, Connolly2003, Cowan2004, Hudaoglu2006, Kan2007].

Haemodynamic stress due to increased blood flow has long been implicated in the pathogenesis of IAs. Development of IAs is reported in association with a wide range of conditions responsible for increased flow related WSS. Padget was first to draw attention towards the relationship between anatomical variations in CoW and increased incidence of IAs [Padget 1944]. The similar findings were confirmed by other workers [Riggs 1943, Stehbens 1963, Alpers 1963].

Kayambe et al [Kayambe 1984] observed that there was a definitive correlation between the site of vascular asymmetry and the location of IA formation. This increased incidence of IAs in presence of vascular asymmetry is thought to be caused by increased haemodynamic stress secondary to compensatory increase in blood flow [Kayambe 1984, Stehbens 1963, Stehbens 1972].

Iatrogenic carotid artery (ICA) ligation is a well-established technique to produce IAs in experimental animals [Jamous 2007, Handa 1983, Hashimoto 1987, Hashimoto 1978, Nagata 1980]. Increased haemodynamic shear stress has been considered a major factor in the production of these experimental IAs [Gao 2008, Jamous 2007, Handa 1983, Hashimoto1987, Hashimoto1987, Nagata 1980]. Apart from the carotid ligation, induced hypertension and administration of BAPN (beta aminopionitrile; a lathyrogen used to render arterial walls fragile), have also been common adjuncts of these experiments. One might argue here on the importance of haemodynamic shear stress on the development of

these IAs in these situations. In order to test this assumption Handa et al [Handa 1983] divided their experimental animals into three cohorts: no carotid ligation, unilateral carotid ligation and bilateral carotid ligation. Whereas, all rats were made hypertensive and fed on BAPN, no IA was induced where carotid artery was not ligated. Furthermore, the IAs were always formed corresponding to the sites where haemodynamic stress was expected to increase after carotid ligation.

Table-6.11: A comprehensive review of different mechanisms proposed for the increased incidence of IAs in CoA patients

Author/ Year	No. of Patients	IA location/ No.	HTN at the time IA diagnosed	Associated features	Proposed Mechanism(s)
Abbot (1928)	6	ACA, AComA, VA, PcomA, MCA	Yes	Reported one case of his own (MCA), rest 5 cases collected from literature	Congenital IA
Laitinen et al (1960)	1	Pericallosal/ Callosomarginal	Yes	Oxycephalic deformity of skull	Possible developmental errors
Patel et al (1971)	7	ICA, AComA (3), ACA (3), PcomA, BA	Yes	Only pediatric population (<19 yrs.) reviewed, 12% had CoA coexisting with IAs	HTN
Banna et al (1971)	1	PCA	NA	Source of SAH was dilated spinal collaterals	Medial hypoplasia of arteries of CoW + HTN
Stehbens (1989)	Review article				HTN
Orsi et al. (1993)	1	MCA, ICA	NA	-	HTN
Schievink et al (1996)	1	MCA	No	-	Development errors of Neural Crest leading to defective collagen and elastin formation
Ishii et al (2001)	1	AComA	Yes	Coarctation of abdominal aorta	HTN
Ahmetoğlu et al (2002)	1	B/L MCA	Yes	Coarctation of abdominal aorta	HTN ± Haemodynamic shear stress
Mercado et al. (2002)	3	ICA, PcomA (2), PeriA	Yes	Provided a comprehensive review of the distinct clinical behavior of IAs in presence of CoA	Development errors of Neural Crest
Connolley et al (2003)[10	ICA, MCA, PICA, PCA, PcomA, AChoA, BA tip	Yes (in 7 out of 10 patients)	Found 10% incidence of IAs in patients with CoA, no significant difference in BP of patients with and without IAs	Development errors of Neural Crest
Cowan et al (2004)	1	PcomA	No	Coexisting Alagille syndrome (arteriohepatic dysplasia), Progression of infundibulum to PcomA Aneurysm	Developmental defects
Harikrishnan (2005)	1	BA, VA	Yes	CoA of Descending aorta, coronary artery aneurysms	Atherosclerosis
Hudaoglu et al (2006)	1	PcomA	No	Raised strong suspicions about HTN alone being a factor for the increased incidence of IA in CoA	Development errors of Neural Crest
Kan et al (2007)	1	ICA	NA	Fusiform aneurysm associated with PHACES syndrome, positive family history of IAs	Development errors of Neural Crest
Singh et al (2009) (Present study)	1	ICA, MCA, PeriA	No	Measured the CBF in CoA patient and proposed WSS as an important factor in the formation of IAs in these patients	Haemodynamic WSS

NB: PHACES syndrome; posterior fossa malformations, facial haemangiomas, arterial anomalies, CoA, cardiac defects, eye abnormalities and sterna defects, NA; not available, B/L; bilateral, CoW; circle of Willis, BP; blood pressure, PeriA; pericallosal artery, AChoA; anterior choroidal artery, PCA; posterior cerebral artery, BA; basilar artery, VA; vertebral artery, PICA; posterior inferior cerebellar artery

Congenital absence of ICA [Chen 2008, Suyama 2009, Horie 2008], arteriovenous malformations (AVMs) [Meisel 2000, Redekop 1998, Thompson 1998], Takayasu's arteritis [Takayama 2008, Kanda 2004], Moyamoya disease [Kawaguchi 1996, Konishi 1985, Adams 1979] and presence of persistent fetal circulation [Zada 2008, Ali 2007, Li 2004] are other similar conditions where increased IAs are encountered due to flow related WSS. Development of IAs has also been observed following extra-intracranial bypass procedures [Kurokawa 2007, Nishimoto 2005, Fleischer 1979], again secondary to increased CBF. Resolution of these flow related IAs could occur once the cerebral haemodynamics is reestablished by addressing the underlying pathology [Takahashi 1997, Peltier 2008].

It is surprising to see that in spite of its very well established role in the aetiopathogenesis of IAs, nobody discussed the importance of haemodynamic WSS in this context. Ahmetoğlu et al (2002) indicated that arterial wall injury secondary to increased haemodynamic shear forces may be an important factor in the IA formation while discussing their case of abdominal aortic coarctation (AbCoA). However, the statement probably reflects their opinion towards the aetiopathogenesis of IAs in general population rather than in patients with CoA. Furthermore, the inference of was merely based on the literature based evidence rather than any experimental work. They finally concluded that hypertension was the main factor responsible for the rupture and growth of IAs in patients with AbCoA [Ahmetoğlu 2002].

I hypothesize that the higher WSS values secondary to increased flow-rates in cerebral circulation can be an important contributory factor in the pathogenesis of IAs in presence of CoA. WSS is a frictional force exerted tangentially on the arterial endothelium by flowing blood. It is proportional to the blood viscosity and velocity gradients. The average physiological range of arterial WSS has been suggested to lie between 1.5-2.0 Pa by Malek et al [Malek 1999]. It is widely accepted now that damage to the arterial and subsequently aneurysmal wall by haemodynamic forces plays a crucial role in the aetiopathogenesis of IAs [Burlison 1996, Gao 2008, Morimoto 2002, Handa 1983, Hashimoto1987, Hashimoto1987, Mantha 2006, Meng 2007, Wang 2009]. High supra-physiological and low infra-physiological values of WSS have been associated with initiation, growth and rupture of aneurysms [Malek 1999, Burlison 1996, Gao 2008, Morimoto 2002, Handa 1983, Hashimoto1987, Hashimoto 1987, Mantha 2006, Meng 2007, Wang 2009]. The values of space and time averaged WSS as well as the area affected by suprathreshold WSS (>15Pa) were increased in our patient by 65%

and 650%, respectively (Table-6.10). This exponential rise in the high supraphysiological WSS may play an important role in the aetiopathogenesis of IAs in patients with CoA.

Various authors have tried to explain the underlying mechanisms involved in the WSS induced vascular remodeling. The normal endothelial cell (EC) function and structure are regulated by WSS through a process called mechanotransduction [Davies 1993, Davies 1995]. The shear stress is sensed by a number of mechanoreceptors including basal adhesion points of ECs, cell junctions and nuclear membrane [Davies 1993, Davies 1995]. WSS also activates stretch-sensitive ion channels such as phospholipids and integrins in cellular membrane [Davies 1993, Davies 1995]. Increased production of matrix metalloproteinase (MMP-13) by ECs has been demonstrated after their prolonged exposure to high WSS, which, in turn, leads to degeneration of the internal elastic lamina [Sho et al [69]]. It has been demonstrated by a number of workers [Cooke 1990, Fukuda 2000, Pohl 1991] that WSS increases endothelial production of nitric oxide (NO) by inducing an enzyme responsible for its synthesis (iNOS; inducible nitric oxide synthase). Fukuda et al [Fukuda 2000] found a high concentration of iNOS at the site of IA formation, in both rat and human arteries and concluded that iNOS is a prerequisite for *de novo* development of IAs in cerebral vessels. In 1995, Wang et al [Wang 1995] showed that smooth muscle cells (SMCs) in arterial wall can also respond to WSS in intact arteries by virtue of interstitial flow generated by transmural flow gradients, further accentuating the vessel wall damage.

In addition to WSS, oscillatory shear index (OSI) has also been recognized as an important haemodynamic factor in the aneurysmal pathogenesis [Glor 2003, 2004, Goubergrits 2008, He 1996, Mantha 2006]. It is measure of the oscillatory nature of shear forces [Glor 2003, 2004, Goubergrits 2008, He 1996, Mantha 2006]. This index, which has a range of between 0 and 0.5, represents the fraction of the cardiac cycle over which the instantaneous shear force vector forms an angle greater than 90 degrees to the time-average direction of the same force. Consistently high values of OSI have been associated with EC dysfunction [He et al 1996]. Changes in cell structure secondary to cyclic mechanical stress have been demonstrated by Wang et al [Wang et al 1995] resulting in disruption of the actin cytoskeleton of ECs. Glor and colleagues propose 0.2 as a threshold value for OSI above which endothelial damage is initiated [Glor et al 2003, 2004]. Whereas, no change was observed in the maximum OSI in presence of CoA (Table-6.10), the values obtained from both analyses (0.3) remained above this critical threshold. This indicates towards the

possible role of high OSI in the EC damage in patients with IAs irrespective of presence or absence of CoA.

Apart from being a known risk factor for the formation of IAs, CoA has also been associated with increased incidence of IA rupture [Mercado 2002, Connolly 2003, Hudaoglu 2006, Weir 1996]. No satisfactory explanation is provided for this increased association. This increased tendency for early aneurysmal rupture can possibly be explained by analyzing the haemodynamic factors computed for our patient (Table-6.10). Whereas the values for maximum pressure on IA wall have increased by 15% in the patient with CoA, the area affected by high pressure is actually decreased by 50%. It means that CoA increases pressure applied per unit area. In other words, the pressure on the IA wall is more concentrated in nature in presence of CoA and may be an important underlying factor affecting the early aneurysmal rupture. Apart from that, high supra-physiological values of WSS have also been associated with endothelial cell dysfunction [Burlison et al. 1996, Handa et al 1996, Hashimoto et al 1978, Hashimoto et al 1980, Hashimoto et al 1987, Malek et al 1999, Mantha et al 2006, Meng et al 2007, Morimoto et al. 2002 Singh et al 2009, Wang et al 1995]. The exponential rise (by 650%) in the area affected by high supra-physiological WSS (>15Pa) may also play a role in early IA rupture in the patient with CoA.

6.4.5 Limitations of the study

Due to technical limitations, I could not perform extensive measurements in cerebral arteries other than ICA and ACA. It is however expected that the CBF will be increased in other arteries as well provided other parameters in the Hagan-Poiseuille's equation remain constant. The current study therefore reflects the need of further studies performed on bigger cohort of patients with CoA.

Moreover, as stated above the IAs are likely to share a multifactorial aetiology. Two other known risk factors in the formation of IAs are HTN and smoking. Whereas, our patient remained completely normotensive after the repair of her CoA (Figure-6.9) she had had high BP prior to surgery, managed by antihypertensives. Apart from that, she was also a chronic smoker smoking 10-15 cigarettes per day. The possibility of HTN and smoking playing some role in the formation of her IAs therefore cannot be ruled out.

6.4.6 Conclusions

My study demonstrates that the cerebral flow-rates in CoA patients are significantly higher when compared to average flow-rates in healthy

population. Furthermore, the values of space and time averaged WSS as well as the area affected by supraphysiological WSS ($>15\text{Pa}$) were increased in our patient by 65% and 650%, respectively. The values of maximum OSI however, remained unaffected by the presence of CoA. Increased haemodynamic WSS secondary to the increased flow-rates may play an important role in the pathogenesis of IAs in CoA patients. The increased per unit pressure on aneurysmal wall in CoA patients may be an important underlying factor affecting the early aneurysmal rupture.

IAs can develop in patients with CoA years after the surgical repair. I recommend that a high index of suspicion should be kept and all CoA patients should be carefully examined and followed-up by MRA for the possible presence of co-existing IAs. The lack of clear knowledge about the cerebral blood-flow in CoA patients and the existing controversies in the aetiopathogenesis of IAs in these patients emphasizes the importance of this study.

CHAPTER 7.0: CONCLUSIONS AND FUTURE WORK

Despite improvements in surgical and medical management, aneurysmal subarachnoid hemorrhage (SAH) remains a major cause of morbidity and mortality in neurosurgical patients. The current protocols used to treat the unruptured IAs are inadequate to provide clear guidelines, as they themselves remain descriptors for the poor prognosis for an intervention. In order to offer the best possible treatment to the patient with the least side effects, formulation of clear management protocols, directed by the natural history of unruptured IAs and, the risks associated with the active management, is required.

Whereas, the aetiopathogenesis of IA formation and rupture remains multifactorial, consistent with studies performed by other researchers, my work indicates haemodynamics playing an important role. An evaluation of patient-specific haemodynamic indices can provide a useful alternative to predict the behavior of an unruptured IA at an early stage.

In spite of their ability of guiding the correct management of IAs, limitations in current technology significantly restricts our ability to measure these haemodynamic indices in routine clinical practice. My studies demonstrate that Computational Fluid Dynamics (CFD) can provide a useful alternative to predict blood flows where detailed in vivo measurement of haemodynamic flow variables is not possible.

European Commission funded Project @neurIST was the first project of it's kind that brought together a number of multidisciplinary professionals from 32 European institutions and developed state of the art tools for personalised risk assessment and treatment IAs using CFD. These tools have been constantly improved and amended in the light of feedback gathered from their controlled exposures conducted world over, as described in the manuscript. However, need of a well-designed Randomized Controlled Trial in this context cannot be overemphasized, before these tools can be accepted by clinicians and patients.

In my study on the validation of different concepts used in CFD, I demonstrated that there is no added advantage of complex Womersley-flow-profile over the much simpler plug-flow profile.

One of my studies on initiation and rupture of IAs showed that the haemodynamic patterns of IAs during these two phases are significantly

different. Whereas, values of t -av-WSS_{min} and areas affected by supra-physiological WSS were higher in preaneurysmal lesion the corresponding values were lower in ruptured IA. The area affected by infra-physiological WSS (<0.4 Pa) was significantly higher in ruptured lesion as compared to preaneurysmal IA. Furthermore, heparin induces significant derangements in the haemodynamics of both, preaneurysmal as well as ruptured IA. In the light of current evidence, it is expected that whereas on the one hand such alterations in haemodynamics may facilitate the rupture of existing IAs, on the other hand they may suppress the formation of new IAs. Similar effects may be associated with other pharmacological agents, warranting further investigations.

Another study on Modeled vs. Patient-Specific Boundary Conditions demonstrated significant differences in the results obtained with these two methods. These are largely attributable to the underlying differences in the waveforms (similar peak but higher mean flow was observed in the measured values). It is most likely that in future patient-specific BCs will be provided as a part of the routine clinical procedure. The results of this study show that the 1D circulation model adopted by @neurIST performs better than other approaches found in the literature and offers a viable means to find correlation with rupture in large cohort size studies.

In the study on the effects of hypertension and smoking on the haemodynamic indices of an IA it was observed that when the high values of blood viscosity were used the values of WSS and OSI have increased significantly.

In the interesting study performed on Coarctation of Aorta (CoA), it was demonstrated that the cerebral flow-rates in CoA patients were significantly higher when compared to average flow-rates in healthy population. Furthermore, the values of space and time averaged WSS as well as the area affected by supraphysiological WSS (>15 Pa) were increased in our patient by 65% and 650%, respectively. The values of maximum OSI however, remained unaffected by the presence of CoA. Increased haemodynamic WSS secondary to the increased flow-rates may play an important role in the pathogenesis of IAs in CoA patients. The increased per unit pressure on aneurysmal wall in CoA patients may be an important underlying factor affecting the early aneurysmal rupture.

Due to the relatively low incidence of CoA in general population (1 in 5000) it may be difficult for the neurosurgeons and interventional neuroradiologists to get an opportunity to observe a case of IA coexisting with CoA. Moreover, IAs can develop in patients with CoA years after the

surgical repair. I recommend that a high index of suspicion should be kept and all CoA patients should be carefully examined and followed-up by MRA for the possible presence of co-existing IAs. The lack of clear knowledge about the cerebral blood-flow in CoA patients and the existing controversies in the aetiopathogenesis of IAs in these patients emphasizes the importance of this study.

In terms of future applications of the CFD in clinical practice there are a number of practical challenges that we will have to address before this dream could be realized. One of the most important factors is the validation of these tools in the field. Whereas, the CFD has been extensively validated and is a very well established technique in other fields, its validations in the field of Intracranial Aneurysms still in a preliminary stage. As reflected by the feedback form the workshops I conducted, mistrust shown by the clinicians in the CFD results clearly indicates the need for validations.

Before any technology or technique can be freely applied in clinical practice, one of the important prerequisite is conducting multi-centric, trials. Once the tools have been validated robustly and we are past the stage of mistrust, the second stage therefore will be need of a well designed multi-centric double blinded, randomized controlled clinical trial on a big cohort of patients. This again can be quite challenging especially due to the ethical issues related to making decisions of non-intervention treatment that can lead to the rupture of an aneurysm that obviously carries very high risk of mortality and morbidity. This can also lead to huge selection bias due to inherent inclination of clinicians to assign patient to the treatment group as against conservative. Apart from that, due to very long natural history of the Unruptured IAs, relatively longer period of observation will be required before any sensible conclusions can be drawn. All these factors can make logistics of conducting the clinical trials a herculean task.

However, in spite of all these challenges and limitations, the expected significant improvements in the outcome of the IA treatment when guided by CFD predictions, make this painstaking task worth accomplishing.

CHAPTER 8.0 REFERENCES

Anonymous

@neurist "integrated biomedical informatics for the management of cerebral aneurysms" In: Annex 1 - v6.1. Sixth Framework Programme PIST (Ed) Barcelona, Spain (2007). Project Identifier: IST-2004-027703.

ISUIA (1998). Unruptured intracranial aneurysms--risk of rupture and risks of surgical intervention. International study of unruptured intracranial aneurysms investigators. *N Engl J Med* (1998) 339(24):1725-1733.

A

Abbott ME: **Coarctation of aorta of adult type: II. A statistical study and historical retrospect of 200-recorded cases, with autopsy, of stenosis or obliteration of the descending arch in subjects above the age of two years.** *Am Heart J* (1928) 3):392-421.

Abruzzo T, Tun T, Sambanis A: **Efficient transmicrocatheter delivery of functional fibroblasts with a bioengineered collagen gel-platinum microcoil complex: Toward the development of endovascular cell therapy for cerebral aneurysms.** *AJNR Am J Neuroradiol* (2007) Sep;28(8):1586-1593.

Acevedo-Bolton G, Jou LD, Dispensa BP, Lawton MT, Higashida RT, Martin AJ, Young WL, Saloner D: **Estimating the haemodynamic impact of interventional treatments of aneurysms: Numerical simulation with experimental validation: Technical case report.** *Neurosurgery* (2006) 59(2):E429-430; author reply E429-430.

Adams HP, Jr., Kassell NF, Wisoff HS, Drake CG: **Intracranial saccular aneurysm and moyamoya disease.** *Stroke* (1979) 10(2):174-179.

Adamson J, Humphries SE, Ostergaard JR, Voldby B, Richards P, Powell JT: **Are cerebral aneurysms atherosclerotic?** *Stroke* (1994) 25(5):963-966.

Aenis M, Stancampiano AP, Wakhloo AK, Lieber BB: **Modeling of flow in a straight stented and nonstented side wall aneurysm model.** *J Biomech Eng* (1997) 119(2):206-212.

Agarwal R: **Computational fluid dynamics of whole-body aircraft.** *Annu Rev Fluid Mech* (1999) **31**(125-169).

Ahmetoğlu A, Koşucu, P. Sari, A. Gümele, HR.: **Abdominal aortic coarctation associated with multiple intracranial aneurysms.** *European Journal of Radiology* (2003) **Extra (46)**(38-41).

Alpers BJ, Berry RG: **Circle of Willis in cerebral vascular disorders. The anatomical structure.** *Arch Neurol* (1963) **8**(398-402).

Ali S, Walker MT: **Bilateral persistent trigeminal arteries associated with bilateral carotid aneurysms.** *J Vasc Interv Radiol* (2007) **18**(5):692-694.

Alfano JM, Kolega J, Natarajan SK, Xiang J, Paluch RA, Levy EI, Siddiqui AH, Meng H: **Intracranial aneurysms occur more frequently at bifurcation sites that typically experience higher haemodynamic stresses.** *Neurosurgery* (2013) **Jun 10**. [Epub ahead of print]

Alnaes MS, Isaksen J, Mardal KA, Romner B, Morgan MK, Ingebrigtsen T: **Computation of haemodynamics in the circle of Willis.** *Stroke* (2007) **38**(9):2500-2505.

Anderson JDJ: *Computational fluid dynamics: The basics with application.* McGraw-Hill, New York, USA (1995).

Anderson CS, Feigin V, Bennett D, Lin RB, Hankey G, Jamrozik K: **Active and passive smoking and the risk of subarachnoid hemorrhage: An international population-based case-control study.** *Stroke* (2004) **35**(3):633-637.

Ando J, Komatsuda T, Kamiya A: **Cytoplasmic calcium response to fluid shear stress in cultured vascular endothelial cells.** *In Vitro Cell Dev Biol* (1988) **24**(9):871-877.

Andrews RJ, Spiegel PK: **Intracranial aneurysms. Age, sex, blood pressure, and multiplicity in an unselected series of patients.** *J Neurosurg* (1979) **51**(1):27-32.

Aoki T, Kataoka H, Morimoto M, Nozaki K, Hashimoto N: **Macrophage-derived matrix metalloproteinase-2 and -9 promote the progression of cerebral aneurysms in rats.** *Stroke* (2007) **38**(1):162-169.

Aoki T, Kataoka H, Moriwaki T, Nozaki K, Hashimoto N: **Role of timp-1 and timp-2 in the progression of cerebral aneurysms.** *Stroke* (2007) **38**(8):2337-2345.

Aoki T, Kataoka H, Ishibashi R, Nozaki K, Hashimoto N: **Nifedipine inhibits the progression of an experimentally induced cerebral aneurysm in rats with associated down-regulation of nf-kappa b transcriptional activity.** *Curr Neurovasc Res* (2008) **5**(1):37-45.

Aoki T, Kataoka H, Ishibashi R, Nozaki K, Hashimoto N: **Simvastatin suppresses the progression of experimentally induced cerebral aneurysms in rats.** *Stroke* (2008) **39**(4):1276-1285.

Aoki T, Kataoka H, Ishibashi R, Nakagami H, Nozaki K, Morishita R, Hashimoto N: **Pitavastatin suppresses formation and progression of cerebral aneurysms through inhibition of the nuclear factor kappa b pathway.** *Neurosurgery* (2009) **64**(2):357-365; discussion 365-356.

Atkinson JL, Sundt TM, Jr., Houser OW, Whisnant JP: **Angiographic frequency of anterior circulation intracranial aneurysms.** *J Neurosurg* (1989) **70**(4):551-555.

B

Baek H, Jayaraman MV, Richardson PD, Karniadakis GE: **Flow instability and wall shear stress variation in intracranial aneurysms.** *Journal of the Royal Society, Interface / the Royal Society* (2010) **7**(47):967-988.

Bakker CJ, Kouwenhoven M, Hartkamp MJ, Hoogeveen RM, Mali WP: **Accuracy and precision of time-averaged flow as measured by nontriggered 2d phase-contrast mr angiography, a phantom evaluation.** *Magn Reson Imaging* (1995) **13**(7):959-965.

Balossino R, Pennati G, Migliavacca F, Formaggia L, Veneziani A, Tuveri M, Dubini G: **Computational models to predict stenosis growth in carotid arteries: Which is the role of boundary conditions?** *Computer methods in biomechanics and biomedical engineering* (2009) **12**(1):113-123.

Banna MM, Rose PG, Pearce GW: **Coarctation of the aorta as a cause**

of spinal subarachnoid hemorrhage. Case report. *J Neurosurg* (1973) 39(6):761-763.

Bark DL, Jr., Ku DN: **Wall shear over high degree stenoses pertinent to atherothrombosis. *J Biomech* (2010) 16(43(15)):2970-2977.**

Baskurt OK, Meiselman HJ: **Blood rheology and haemodynamics. *Semin Thromb Hemost* (2003) 29(5):435-450.**

Beckman JS, Beckman TW, Chen J, Marshall PA, Freeman BA: **Apparent hydroxyl radical production by peroxynitrite: Implications for endothelial injury from nitric oxide and superoxide. *Proc Natl Acad Sci U S A* (1990) 87(4):1620-1624.**

Bernardini A, Larrabide I, Morales HG, Pennati G, Petrini L, Cito S, Frangi AF: **Influence of different computational approaches for stent deployment on cerebral aneurysm haemodynamics. *Interface focus* (2011) 1(3):338-348.**

Bhagyalakshmi A, Frangos JA: **Mechanism of shear-induced prostacyclin production in endothelial cells. *Biochem Biophys Res Commun* (1989) 158(1):31-37.**

Bonert M, Myers JG, Fremes S, Williams J, Ethier CR: **A numerical study of blood flow in coronary artery bypass graft side-to-side anastomoses. *Ann Biomed Eng* (2002) 30(5):599-611.**

Bonita R: **Cigarette smoking, hypertension and the risk of subarachnoid hemorrhage: A population-based case-control study. *Stroke* (1986) 17(5):831-835.**

Bordas R, Seshadhri S, Janiga G, Skalej M, Thevenin D: **Experimental validation of numerical simulations on a cerebral aneurysm phantom model. *Interventional Medicine & Applied Science* (2012) 4(4):13.**

Born GV, Palinski W: **Unusually high concentrations of sialic acids on the surface of vascular endothelia. *Br J Exp Pathol* (1985) 66(5):543-549.**

Boussel L, Rayz V, McCulloch C, Martin A, Acevedo-Bolton G, Lawton M, Higashida R, Smith WS, Young WL, Saloner D: **Aneurysm growth occurs at region of low wall shear stress: Patient-specific correlation of haemodynamics and growth in a longitudinal study. *Stroke* (2008)**

39(11):2997-3002.

Bove EL, Migliavacca F, de Leval MR, Balossino R, Pennati G, Lloyd TR, Khambadkone S, Hsia TY, Dubini G: **Use of mathematic modeling to compare and predict haemodynamic effects of the modified blalock-taussig and right ventricle-pulmonary artery shunts for hypoplastic left heart syndrome.** *J Thorac Cardiovasc Surg* (2008) **136**(2):312-320 e312.

Brooks B: **The treatment of traumatic arteriovenous fistula.** *South Med J* (1930) **23**(100 –106).

Broderick JP, Viscoli CM, Brott T, Kernan WN, Brass LM, Feldmann E, Morgenstern LB, Wilterdink JL, Horwitz RI: **Major risk factors for aneurysmal subarachnoid hemorrhage in the young are modifiable.** *Stroke* (2003) **34**(6):1375-1381.

Brugger W, Imhof P, Muller P, Moser P, Reubi F: **Effect of nitroglycerin on blood rheology in healthy subjects.** *Eur J Clin Pharmacol* (1985) **29**(3):331-336.

Buijs PC, Krabbe-Hartkamp MJ, Bakker CJ, de Lange EE, Ramos LM, Breteler MM, Mali WP: **Effect of age on cerebral blood flow: Measurement with ungated two-dimensional phase-contrast mr angiography in 250 adults.** *Radiology* (1998) **209**(3):667-674.

Burleson AC, Strother CM, Turitto VT: **Computer modeling of intracranial saccular and lateral aneurysms for the study of their haemodynamics.** *Neurosurgery* (1995) **37**(4):774-782; discussion 782-774.

Burleson AC, Turitto VT: **Identification of quantifiable haemodynamic factors in the assessment of cerebral aneurysm behavior. On behalf of the subcommittee on biorheology of the scientific and standardization committee of the isth.** *Thromb Haemost* (1996) **76**(1):118-123.

Bulas D, Egloff A: **Benefits and risks of mri in pregnancy.** *Seminars in perinatology* (2013) **37**(5):301-304.

Busse R, Mulsch A: **Calcium-dependent nitric oxide synthesis in endothelial cytosol is mediated by calmodulin.** *FEBS Lett* (1990) **265**(1-2):133-136.

Butty VD, Gudjonsson K, Buchel P, Makhijani VB, Ventikos Y, Poulikakos D: **Residence times and basins of attraction for a realistic right internal carotid artery with two aneurysms.** *Biorheology* (2002) **39**(3-4):387-393.

Byrne JV, Guglielmi, G.: *Endovascular treatment of intracranial aneurysms.* Springer, (1998).

C

Caputo GR, Kondo C, Masui T, Geraci SJ, Foster E, O'Sullivan MM, Higgins CB: **Right and left lung perfusion: In vitro and in vivo validation with oblique-angle, velocity-encoded cine mr imaging.** *Radiology* (1991) **180**(3):693-698.

Carmichael R: **The pathogenesis of noninflammatory cerebral aneurysms.** *J Pathol Bacteriol* (1950) **62**(1):1-19.

Castro MA, Putman CM, Cebal JR: **Computational fluid dynamics modeling of intracranial aneurysms: Effects of parent artery segmentation on intra-aneurysmal haemodynamics.** *AJNR Am J Neuroradiol* (2006) **27**(8):1703-1709.

Castro MA, Putman CM, Cebal JR: **Patient-specific computational fluid dynamics modeling of anterior communicating artery aneurysms: A study of the sensitivity of intra-aneurysmal flow patterns to flow conditions in the carotid arteries.** *AJNR Am J Neuroradiol* (2006b) **27**(10):2061-2068.

Castro MA, Putman CM, Cebal JR: **Patient-specific computational modeling of cerebral aneurysms with multiple avenues of flow from 3d rotational angiography images.** *Acad Radiol* (2006c) **13**(7):811-821.

Cebal JR, Castro MA, Appanaboyina S, Putman CM, Millan D, Frangi AF: **Efficient pipeline for image-based patient-specific analysis of cerebral aneurysm haemodynamics: Technique and sensitivity.** *IEEE Trans Med Imaging* (2005) **24**(4):457-467.

Cebal JR, Lohner R, Choyke PL, Yim PJ: **Merging of intersecting triangulations for finite element modeling.** *Journal of biomechanics* (2001) **34**(6):815-819.

Cebral JR, Castro MA, Burgess JE, Pergolizzi RS, Sheridan MJ, Putman CM: **Characterization of cerebral aneurysms for assessing risk of rupture by using patient-specific computational haemodynamics models.** *AJNR Am J Neuroradiol* (2005) **26**(10):2550-2559.

Cebral JR, Castro MA, Putman CM, Alperin N: **Flow-area relationship in internal carotid and vertebral arteries.** *Physiol Meas* (2008) **29**(5):585-594.

Cebral JR, Hendrickson S, Putman CM: **Haemodynamics in a lethal basilar artery aneurysm just before its rupture.** *AJNR Am J Neuroradiol* (2009) **30**(1):95-98.

Cebral JR, Raschi M: **Suggested connections between risk factors of intracranial aneurysms: A review.** *Ann Biomed Eng* (2013) **Jul;41**(7):1366-1383.

Cellina GU, Honour AJ, Littler WA: **Direct arterial pressure, heart rate, and electrocardiogram during cigarette smoking in unrestricted patients.** *Am Heart J* (1975) **89**(1):18-25.

Chan BT, Lim E, Chee KH, Abu-Osman NA: **Review on cfd simulation in heart with dilated cardiomyopathy and myocardial infarction.** *Comput Biol Med* (2013) **1**(1;43(4)):377-385.

Chason JL, Hindman WM: **Berry aneurysms of the circle of willis; results of a planned autopsy study.** *Neurology* (1958) **8**(1):41-44.

Chatziprodromou I, Butty, V.D., Makhijani, V. B. P, D.,, Ventikos Y: **Pulsatile blood flow in anatomically accurate vessels with multiple aneurysms: A medical intervention planning application of computational haemodynamics.** *Flow, Turbulence and Combustion* (2003) **71**(333–346).

Chen L, Liu JM, Zhou D: **Congenital absence of the right common carotid artery, internal carotid artery and external carotid artery associated with anterior communicating artery aneurysm: A rare case.** *Neurol Sci* (2008) **29**(6):485-487.

Cheng C, Helderma F, Tempel D, Segers D, Hierck B, Poelmann R, van Tol A, Duncker DJ, Robbers-Visser D, Ursem NT, van Haperen R *et al*: **Large variations in absolute wall shear stress levels within one species and between species.** *Atherosclerosis* (2007) **195**(2):225-235.

Coata G, Ventura F, Lombardini R, Ciuffetti G, Cosmi EV, Di Renzo GC: **Effect of low-dose oral triphasic contraceptives on blood viscosity, coagulation and lipid metabolism.** *Contraception* (1995) **52**(3):151-157.

Cohen MM: **Cerebrovascular accidents; a study of two hundred one cases.** *AMA Arch Pathol* (1955) **60**(3):296-307.

Connolly HM, Huston J, 3rd, Brown RD, Jr., Warnes CA, Ammash NM, Tajik AJ: **Intracranial aneurysms in patients with coarctation of the aorta: A prospective magnetic resonance angiographic study of 100 patients.** *Mayo Clin Proc* (2003) **78**(12):1491-1499.

Cooke JP, Stamler J, Andon N, Davies PF, McKinley G, Loscalzo J: **Flow stimulates endothelial cells to release a nitrovasodilator that is potentiated by reduced thiol.** *Am J Physiol* (1990) **259**(3 Pt 2):H804-812.

Cooper BB: *Lectures on the principles and practice of surgery.* Blanchard & Lee, Philadelphia (1852).

Corbett SC, Ajdari A, Coskun AU, Nayeb-Hashemi H: **Effect of pulsatile blood flow on thrombosis potential with a step wall transition.** *ASAIO J* (2010) **Jul-Aug**;56(4):290-295.

Cowan JA, Jr., Barkhoudarian G, Yang LJ, Thompson BG: **Progression of a posterior communicating artery infundibulum into an aneurysm in a patient with alagille syndrome. Case report.** *J Neurosurg* (2004) **101**(4):694-696.

Crawford T: **Some observations on the pathogenesis and natural history of intracranial aneurysms.** *J Neurol Neurosurg Psychiatry* (1959) **22**(259-266).

Crompton MR: **The pathogenesis of cerebral infarction following the rupture of cerebral berry aneurysms.** *Brain* (1964) **87**(491-510).

Crompton MR: **Mechanism of growth and rupture in cerebral berry aneurysms.** *Br Med J* (1966) **1**(5496):1138-1142.

Crumpton CW, Rowe GG, Capps RC, Whitmore JJ, Murphy QR: **The effect of hexamethonium upon cerebral blood flow and metabolism in**

patients with premalignant and malignant hypertension. *Circulation* (1955) 11(1):106-109.

Crutchfield WG: Instruments for use in the treatment of certain intracranial vascular lesions. *J Neurosurg* (1959) 16(4):471-474.

D

Daley PJ, Sagar KB, Wann LS: Doppler echocardiographic measurement of flow velocity in the ascending aorta during supine and upright exercise. *Br Heart J* (1985) 54(6):562-567.

Dandy WE: Intracranial aneurysm of the internal carotid artery: Cured by operation. *Ann Surg* (1938) 107(5):654-659.

Danesh J, Collins R, Peto R, Lowe GD: Haematocrit, viscosity, erythrocyte sedimentation rate: Meta-analyses of prospective studies of coronary heart disease. *Eur Heart J* (2000) 21(7):515-520.

Damadian R, Goldsmith M, Minkoff L: Nmr in cancer: Xvi. Fonar image of the live human body. *Physiol Chem Phys* (1977) 9(1):97-100, 108.

Davies PF: Flow-mediated endothelial mechanotransduction. *Physiol Rev* (1995) 75(3):519-560.

Davies PF, Tripathi SC: Mechanical stress mechanisms and the cell. An endothelial paradigm. *Circ Res* (1993) 72(2):239-245.

de la Monte SM, Moore GW, Monk MA, Hutchins GM: Risk factors for the development and rupture of intracranial berry aneurysms. *Am J Med* (1985) 78(6 Pt 1):957-964.

de Simone G, Devereux RB, Chien S, Alderman MH, Atlas SA, Laragh JH: Relation of blood viscosity to demographic and physiologic variables and to cardiovascular risk factors in apparently normal adults. *Circulation* (1990) 81(1):107-117.

Dempere-Marco L, Oubel E, Castro M, Putman C, Frangi A, Cebal J: Cfd analysis incorporating the influence of wall motion: Application to intracranial aneurysms. *Med Image Comput Comput Assist Interv Int Conf Med Image Comput Comput Assist Interv* (2006) 9(Pt 2):438-445.

Dion JE, Gates PC, Fox AJ, Barnett HJ, Blom RJ: **Clinical events following neuroangiography: A prospective study.** *Stroke* (1987) **18**(6):997-1004.

Dodge JT, Jr., Brown BG, Bolson EL, Dodge HT: **Lumen diameter of normal human coronary arteries. Influence of age, sex, anatomic variation, and left ventricular hypertrophy or dilation.** *Circulation* (1992) **86**(1):232-246.

Doenitz C, Schebesch KM, Zoepfel R, Brawanski A: **A mechanism for the rapid development of intracranial aneurysms: A case study.** *Neurosurgery* (2010) **Nov**;67(5):1213-1221.

Dott NM: **Intracranial aneurysms: Cerebral arterio-radiography: Surgical treatment.** *Edinburgh Med J* (1933) **40**(219-234).

Drake CG: **Earlier times in aneurysm surgery.** *Clin Neurosurg* (1985) **32**(41-50).

Drake CG: **Progress in cerebrovascular disease. Management of cerebral aneurysm.** *Stroke* (1981) **12**(3):273-283.

Drexler H, Hornig B: **Endothelial dysfunction in human disease.** *J Mol Cell Cardiol* (1999) **31**(1):51-60.

DuBoulay GH: **Some observation on the natural history of intracranial aneurysms.** *Brit J Radiol* (1965) **38**(721-757).

Duncan J, Fraser TR: **On the treatment of aneurism by electrolysis: With an account of an investigation into the action of galvanism on blood and on albuminous fluids.** *Medico-Chir Soc Edinb Med J* (1867) **13**(101-120).

E

Ecker A, Riemenschneider PA: **Arteriographic demonstration of spasm of the intracranial arteries, with special reference to saccular arterial aneurysms.** *J Neurosurg* (1951) **8**(6):660-667.

Engelson E: **Catheter for guide-wire tracking.** In: 4739768. USPTO (Ed) USA (1986).

Ene-Iordache B, Remuzzi A: **Disturbed flow in radial-cephalic arteriovenous fistulae for haemodialysis: Low and oscillating shear stress locates the sites of stenosis.** *Nephrol Dial Transplant* (2011) **Jul 18**.([Epub ahead of print].

Enzmann DR, Marks MP, Pelc NJ: **Comparison of cerebral artery blood flow measurements with gated cine and ungated phase-contrast techniques.** *J Magn Reson Imaging* (1993) **3(5):705-712.**

Enzmann DR, Ross MR, Marks MP, Pelc NJ: **Blood flow in major cerebral arteries measured by phase-contrast cine mr.** *AJNR Am J Neuroradiol* (1994) **15(1):123-129.**

Eppinger H: **Pathogenesis (histogenesis and aetiology) der aneurysmen einschliesslich des aneurysma equi verminosum.** *Arch Klin Chir* (1887) **35(Suppl 1):1-563.**

Erbengi A, Inci S: **Pheochromocytoma and multiple intracranial aneurysms: Is it a coincidence? Case report.** *J Neurosurg* (1997) **87(5):764-767.**

Evans AJ, Iwai F, Grist TA, Sostman HD, Hedlund LW, Spritzer CE, Negro-Vilar R, Beam CA, Pelc NJ: **Magnetic resonance imaging of blood flow with a phase subtraction technique. In vitro and in vivo validation.** *Invest Radiol* (1993) **28(2):109-115.**

F

Fedorov BM, Sebekina TV, Sinitsyna TM, Strel'tsova EN, Vakulenko VM, Nikolaeva TG: **[stress and blood circulation in man].** *Kosm Biol Aviakosm Med* (1990) **24(3):35-40.**

Feng R, Xenos M, Girdhar G, Kang W, Davenport JW, Deng Y, Bluestein D: **Viscous flow simulation in a stenosis model using discrete particle dynamics: A comparison between dpd and cfd.** *Biomech Model Mechanobiol* (2011 [Epub ahead of print]) **Mar 3(**

Ferrua MJ, Singh RP: **Modeling the fluid dynamics in a human stomach to gain insight of food digestion.** *J Food Sci* (2010) **Sep;75(7):R151-162.**

Fifi JT, Meyers PM, Lavine SD, Cox V, Silverberg L, Mangla S, Pile-Spellman J: **Complications of modern diagnostic cerebral angiography**

in an academic medical center. *J Vasc Interv Radiol* (2009) **20**(4):442-447.

Fleischer AS, Faria MA, Jr., Hoffmann JC, Jr.: **Pseudoaneurysm complicating superficial temporal artery--middle cerebral artery bypass.** *Surg Neurol* (1979) **12**(4):305-306.

Fogarty TJ, Cranley JJ, Krause RJ, Strasser ES, Hafner CD: **A method for extraction of arterial emboli and thrombi.** *Surg Gynecol Obstet* (1963) **116**(241-244).

Forbus WD: **On the origin of miliary aneurysms of the superficial cerebral arteries.** *Bull Johns Hopkins Hosp* (1930) **47**(239-284).

Ford MD, Nikolov HN, Milner JS, Lownie SP, Demont EM, Kalata W, Loth F, Holdsworth DW, Steinman DA: **Piv-measured versus cfd-predicted flow dynamics in anatomically realistic cerebral aneurysm models.** *J Biomech Eng* (2008) **130**(2):021015.

Ford MD, Stuhne GR, Nikolov HN, Habets DF, Lownie SP, Holdsworth DW, Steinman DA: **Virtual angiography for visualization and validation of computational models of aneurysm haemodynamics.** *IEEE Trans Med Imaging* (2005) **24**(12):1586-1592.

Forfang K, Rostad H, Sorland S, Levorstad K: **Late sudden death after surgical correction of coarctation of the aorta. Importance of aneurysm of the ascending aorta.** *Acta Med Scand* (1979) **206**(5):375-379.

Formaggia L, Nobile F, Quarteroni A, Veneziani A: **Multiscale modelling of the circulatory system: A preliminary analysis.** *Comput Vis Sci* (1999) **2**(75-83).

Forbus WD: **On the origin of miliary aneurysms of the superficial cerebral arteries.** *Bull Johns Hopkins Hosp* (1930) **47**(239-284).

Foutrakis GN, Yonas H, Sclabassi RJ: **Saccular aneurysm formation in curved and bifurcating arteries.** *AJNR Am J Neuroradiol* (1999) **20**(7):1309-1317.

Fox C, Davies MJ, Webb-Peploe MM: **Length of left main coronary artery.** *Br Heart J* (1973) **35**(8):796-798.

Frawley P, Geron M: **Combination of cfd and doe to analyze and improve the mass flow rate in urinary catheters.** *J Biomech Eng* (2009) **Aug**;131(8):084501.

Frei EH, Driller J, Neufeld HN, Barr I, Bleiden L, Askenazy HN: **The pod and its applications.** *Med Res Eng* (1966) **5**(4):11-18.

Fukuda S, Hashimoto N, Naritomi H, Nagata I, Nozaki K, Kondo S, Kurino M, Kikuchi H: **Prevention of rat cerebral aneurysm formation by inhibition of nitric oxide synthase.** *Circulation* (2000) **101**(21):2532-2538.

G

Gaetani P, Tartara F, Tancioni F, Klersy C, Forlino A, Baena RR: **Activity of alpha 1-antitrypsin and cigarette smoking in subarachnoid haemorrhage from ruptured aneurysm.** *J Neurol Sci* (1996) **141**(1-2):33-38.

Gabrielsen TO, Greitz T: **Normal size of the internal carotid, middle cerebral and anterior cerebral arteries.** *Acta Radiol Diagn (Stockh)* (1970) **10**(1):1-10.

Gao L, Hoi Y, Swartz DD, Kolega J, Siddiqui A, Meng H: **Nascent aneurysm formation at the basilar terminus induced by haemodynamics.** *Stroke* (2008) **39**(7):2085-2090.

Gardner WJ: **Cerebral angiomas and aneurysms.** *Surg Clin North Am* (1936) **16**(1019–1030).

Geng Y, Hansson GK, Holme E: **Interferon-gamma and tumor necrosis factor synergize to induce nitric oxide production and inhibit mitochondrial respiration in vascular smooth muscle cells.** *Circ Res* (1992) **71**(5):1268-1276.

Gianturco C, Anderson JH, Wallace S: **Mechanical devices for arterial occlusion.** *Am J Roentgenol Radium Ther Nucl Med* (1975) **124**(3):428-435.

Glor FP, Long Q, Hughes AD, Augst AD, Ariff B, Thom SA, Verdonck PR, Xu XY: **Reproducibility study of magnetic resonance image-based computational fluid dynamics prediction of carotid bifurcation flow.** *Ann Biomed Eng* (2003) **31**(2):142-151.

Glor FP, Ariff B, Hughes AD, Crowe LA, Verdonck PR, Barratt DC, Mc GTSA, Firmin DN, Xu XY: **The integration of medical imaging and computational fluid dynamics for measuring wall shear stress in carotid arteries.** *Conf Proc IEEE Eng Med Biol Soc* (2004) **2**(1415-1418).

Glynn LE: **Medial defects in the circle of willis and their relation to aneurysm formation.** *J Pathol Bacteriol* (1940) **51**(213-222).

Gonzalez CF, Cho YI, Ortega HV, Moret J: **Intracranial aneurysms: Flow analysis of their origin and progression.** *AJNR Am J Neuroradiol* (1992) **13**(1):181-188.

Gonzalez-Alonso J, Dalsgaard MK, Osada T, Volianitis S, Dawson EA, Yoshiga CC, Secher NH: **Brain and central haemodynamics and oxygenation during maximal exercise in humans.** *J Physiol* (2004) **557**(Pt 1):331-342.

Goubergrits L, Kertzsch U, Schoneberg B, Wellnhofer E, Petz C, Hege HC: **Cfd analysis in an anatomically realistic coronary artery model based on non-invasive 3d imaging: Comparison of magnetic resonance imaging with computed tomography.** *Int J Cardiovasc Imaging* (2008) **24**(4):411-421.

Greenfield AJ: **Transcatheter vessel occlusion: Selection of methods and materials.** *Cardiovasc Intervent Radiol* (1980) **3**(4):222-228.

Greenhalgh RM, Laing S, Taylor GW: **Risk factors in carotid artery stenosis and intracranial aneurysms.** *J Cardiovasc Surg (Torino)* (1980) **21**(5):559-567.

Greenwood J, Jr.: **Two point coagulation: A follow-up report of a new technic and instrument for electrocoagulation in neurosurgery.** *Arch Phys Ther* (1942) **23**(9):552-554.

Guglielmi G: **History of the genesis of detachable coils. A review.** *J Neurosurg* (2009) **111**(1):1-8.

H

Hafkenschiel JH, Jr., Crumpton CW, Moyer JH: **Blood flow and oxygen consumption of the brain in coarctation of the aorta.** *Proc Soc Exp Biol Med* (1949) **71**(1):165-167.

Hajjar I, Selim M, Novak P, Novak V: **The relationship between nighttime dipping in blood pressure and cerebral haemodynamics in nonstroke patients.** *J Clin Hypertens (Greenwich)* (2007) **9**(12):929-936.

Handa H, Hashimoto N, Nagata I, Hazama F: **Saccular cerebral aneurysms in rats: A newly developed animal model of the disease.** *Stroke* (1983) **14**(6):857-866.

Handler FP, Blumenthal HT: **Inflammatory factor in pathogenesis of cerebrovascular aneurysms.** *J Am Med Assoc* (1954) **155**(17):1479-1483.

Harikrishnan S, Stigimon J, Tharakan JM: **Intracranial aneurysms, coronary aneurysms and descending aortic coarctation--unreported association.** *Int J Cardiol* (2005) **99**(2):329-330.

Hashimoto N, Handa H, Hazama F: **Experimentally induced cerebral aneurysms in rats.** *Surg Neurol* (1978) **10**(1):3-8.

Hashimoto N, Handa H, Nagata I, Hazama F: **Experimentally induced cerebral aneurysms in rats: Part v. Relation of haemodynamics in the circle of willis to formation of aneurysms.** *Surg Neurol* (1980) **13**(1):41-45.

Hashimoto N, Kim C, Kikuchi H, Kojima M, Kang Y, Hazama F: **Experimental induction of cerebral aneurysms in monkeys.** *J Neurosurg* (1987) **67**(6):903-905.

Hassan T, Ahmed YM, Hassan AA: **The adverse effects of flow-diverter stent-like devices on the flow pattern of saccular intracranial aneurysm models: Computational fluid dynamics study.** *Acta Neurochir (Wien)* (2011) **Aug;153**(8):1633-1640.

Hassan T, Ezura M, Timofeev EV, Tominaga T, Saito T, Takahashi A, Takayama K, Yoshimoto T: **Computational simulation of therapeutic parent artery occlusion to treat giant vertebrobasilar aneurysm.** *AJNR Am J Neuroradiol* (2004) **25**(1):63-68.

He X, Ku DN: **Pulsatile flow in the human left coronary artery bifurcation: Average conditions.** *J Biomech Eng* (1996) **118**(1):74-82.

Hesslein PS, McNamara DG, Morriss MJ, Hallman GL, Cooley DA: **Comparison of resection versus patch aortoplasty for repair of coarctation in infants and children.** *Circulation* (1981) **64**(1):164-168.

Hernandez M, Frangi AF: **Non-parametric geodesic active regions: Method and evaluation for cerebral aneurysms segmentation in 3dra and cta.** *Med Image Anal* (2007) **11**(3):224-241.

Hilal SK, Michelsen WJ, Driller J, Leonard E: **Magnetically guided devices for vascular exploration and treatment.** *Radiology* (1974) **113**(3):529-540.

Hillen B, Hoogstraten HW, Post L: **A mathematical model of the flow in the circle of willis.** *J Biomech* (1986) **19**(3):187-194.

Hitosugi M, Niwa M, Takatsu A: **Changes in blood viscosity by heparin and argatroban.** *Thromb Res* (2001) **104**(5):371-374.

Hoi Y, Meng H, Woodward SH, Bendok BR, Hanel RA, Guterman LR, Hopkins LN: **Effects of arterial geometry on aneurysm growth: Three-dimensional computational fluid dynamics study.** *J Neurosurg* (2004) **101**(4):676-681.

Holdsworth DW, Norley CJ, Frayne R, Steinman DA, Rutt BK: **Characterization of common carotid artery blood-flow waveforms in normal human subjects.** *Physiol Meas* (1999) **20**(3):219-240.

Holenstein R, Niederer P, Anliker M: **A viscoelastic model for use in predicting arterial pulse waves.** *J Biomech Eng* (1980) **102**(4):318-325.

Hom JJ, Ordovas K, Reddy GP: **Velocity-encoded cine mr imaging in aortic coarctation: Functional assessment of haemodynamic events.** *Radiographics* (2008) **28**(2):407-416.

Hop JW, Rinkel GJ, Algra A, van Gijn J: **Case-fatality rates and functional outcome after subarachnoid hemorrhage: A systematic review.** *Stroke* (1997) **28**(3):660-664.

Horie N, Tsutsumi K, Kaminogo M, Morikawa M, Kitagawa N, Nagata I: **Agensis of the internal carotid artery with transcavernous anastomosis presenting with an anterior communicating artery aneurysm--a case report and review of the literature.** *Clin Neurol Neurosurg* (2008) **110**(6):622-626.

Hounsfield GN: **Computerized transverse axial scanning (tomography). 1. Description of system.** *The British journal of radiology* (1973) **46**(552):1016-1022.

Hudaoglu O, Kurul S, Cakmakci H, Men S, Yis U, Dirik E: **Aorta coarctation presenting with intracranial aneurysm rupture.** *J Paediatr Child Health* (2006) **42**(7-8):477-479.

Hutchinson J: **Aneurism of internal carotid within the skull diagnosed eleven years before patient's death: Spontaneous cure.** *Trans Clin Soc Lond* (1875) **8**(127-131).

I

Ide K, Secher NH: **Cerebral blood flow and metabolism during exercise.** *Prog Neurobiol* (2000) **61**(4):397-414.

Inagawa T, Takechi A, Yahara K, Saito J, Moritake K, Kobayashi S, Fujii Y, Sugimura C: **Primary intracerebral and aneurysmal subarachnoid hemorrhage in izumo city, japan. Part i: Incidence and seasonal and diurnal variations.** *J Neurosurg* (2000) **93**(6):958-966.

Inagawa T: **Trends in incidence and case fatality rates of aneurysmal subarachnoid hemorrhage in izumo city, japan, between 1980-1989 and 1990-1998.** *Stroke* (2001) **32**(7):1499-1507.

Inagawa T: **Seasonal variation in the incidence of aneurysmal subarachnoid hemorrhage in hospital- and community-based studies.** *J Neurosurg* (2002) **96**(3):497-509.

Inagawa T: **Risk factors for aneurysmal subarachnoid hemorrhage in patients in izumo city, japan.** *J Neurosurg* (2005) **102**(1):60-67.

Inci S, Spetzler RF: **Intracranial aneurysms and arterial hypertension: A review and hypothesis.** *Surg Neurol* (2000) **53**(6):530-540; discussion 540-532.

Ishii K, Isono M, Kasai N, Nakano T, Kubo T, Inoue R, Nomura Y: **Midaortic syndrome in childhood associated with a ruptured cerebral aneurysm: A case report.** *Surg Neurol* (2001) **55**(4):209-212.

Isoda H, Ohkura Y, Kosugi T, Hirano M, Takeda H, Hiramatsu H, Yamashita S, Takehara Y, Alley MT, Bammer R, Pelc NJ *et al*: **In vivo haemodynamic analysis of intracranial aneurysms obtained by magnetic resonance fluid dynamics (mrfd) based on time-resolved three-dimensional phase-contrast mri.** *Neuroradiology* (2009).

J

Jakubowski J, Kendall B: **Coincidental aneurysms with tumours of pituitary origin.** *J Neurol Neurosurg Psychiatry* (1978) **41**(11):972-979.

Jamous MA, Nagahiro S, Kitazato KT, Tamura T, Aziz HA, Shono M, Satoh K: **Endothelial injury and inflammatory response induced by haemodynamic changes preceding intracranial aneurysm formation: Experimental study in rats.** *J Neurosurg* (2007) **107**(2):405-411.

Jeays AD, Lawford PV, Gillott R, Spencer P, Barber DC, Bardhan KD, Hose DR: **Characterisation of the haemodynamics of the superior mesenteric artery.** *J Biomech* (2007) **40**(9):1916-1926.

Joseph M, Nates, J.L.: **Stable xenon computed tomography cerebral blood flow measurement in neurological disease: Review and protocols.** *The Internet Journal of Emergency and Intensive Care Medicine* (2000) **4**(2).

Jou LD, Lee DH, Morsi H, Mawad ME: **Wall shear stress on ruptured and unruptured intracranial aneurysms at the internal carotid artery.** *AJNR Am J Neuroradiol* (2008).

Jou LD, Quick CM, Young WL, Lawton MT, Higashida R, Martin A, Saloner D: **Computational approach to quantifying haemodynamic forces in giant cerebral aneurysms.** *AJNR Am J Neuroradiol* (2003) **24**(9):1804-1810.

Jou LD, Wong G, Dispensa B, Lawton MT, Higashida RT, Young WL, Saloner D: **Correlation between luminal geometry changes and haemodynamics in fusiform intracranial aneurysms.** *AJNR Am J Neuroradiol* (2005) **26**(9):2357-2363.

Juvela S: **Risk factors for multiple intracranial aneurysms.** *Stroke* (2000) **31**(2):392-397.

Juvela S, Poussa K, Porras M: **Factors affecting formation and growth of intracranial aneurysms: A long-term follow-up study.** *Stroke; a journal of cerebral circulation* (2001) **32**(2):485-491.

Juvela S, Hillbom M, Numminen H, Koskinen P: **Cigarette smoking and alcohol consumption as risk factors for aneurysmal subarachnoid hemorrhage.** *Stroke* (1993) **24**(5):639-646.

K

Kan P, Liu JK, Couldwell WT: **Giant fusiform aneurysm in an adolescent with phaces syndrome treated with a high-flow external carotid artery-m3 bypass. Case report and review of the literature.** *J Neurosurg* (2007) **106**(6 Suppl):495-500.

Kanda M, Shinoda S, Masuzawa T: **Ruptured vertebral artery-posterior inferior cerebellar artery aneurysm associated with pulseless disease--case report.** *Neurol Med Chir (Tokyo)* (2004) **44**(7):363-367.

Karmonik C, Benndorf G, Klucznik R, Haykal H, Strother CM: **Wall shear stress variations in basilar tip aneurysms investigated with computational fluid dynamics.** *Conf Proc IEEE Eng Med Biol Soc* (2006) **1**(3214-3217).

Kashiwazaki D, Kuroda S: **On behalf of the sapporo sah study group. Size ratio can highly predict rupture risk in intracranial small (<5 mm) aneurysms.** *Stroke* (2013) **Jun 6**([Epub ahead of print]).

Kassell NF, Torner JC, Haley EC, Jr., Jane JA, Adams HP, Kongable GL: **The international cooperative study on the timing of aneurysm surgery. Part 1: Overall management results.** *J Neurosurg* (1990) **73**(1):18-36.

Kaufmann TA, Linde T, Cuenca-Navalon E, Schmitz C, Hormes M, Schmitz-Rode T, Steinseifer U: **Transient, three-dimensional flow field simulation through a mechanical, trileaflet heart valve prosthesis.** *ASAIO J* (2011) **57**(4):278-282.

Kawaguchi S, Sakaki T, Morimoto T, Kakizaki T, Kamada K: **Characteristics of intracranial aneurysms associated with moyamoya disease. A review of 111 cases.** *Acta Neurochir (Wien)* (1996) **138**(11):1287-1294.

Kayembe KN, Sasahara M, Hazama F: **Cerebral aneurysms and variations in the circle of willis.** *Stroke* (1984) **15**(5):846-850.

Keen W, DaCosta J: *Surgery its principles and practice.* WB Saunders, Philadelphia. (1916).

Kety SS: **The theory and applications of the exchange of inert gas at the lungs and tissues.** *Pharmacol Rev* (1951) **3**(1):1-41.

Khanna RK, Malik GM, Qureshi N: **Predicting outcome following surgical treatment of unruptured intracranial aneurysms: A proposed grading system.** *J Neurosurg* (1996) **84**(1):49-54.

Kharboutly Z, Deplano V, Bertrand E, Legallais C: **Numerical and experimental study of blood flow through a patient-specific arteriovenous fistula used for hemodialysis.** *Med Eng Phys* (2010) **Mar**;32(2):111-118.

Kim C, Cervos-Navarro J, Kikuchi H, Hashimoto N, Hazama F: **Alterations in cerebral vessels in experimental animals and their possible relationship to the development of aneurysms.** *Surg Neurol* (1992) **38**(5):331-337.

Kim EJ, Halim AX, Dowd CF, Lawton MT, Singh V, Bennett J, Young WL: **The relationship of coexisting extracranial aneurysms to intracranial hemorrhage in patients harboring brain arteriovenous malformations.** *Neurosurgery* (2004) **54**(6):1349-1357; discussion 1357-1348.

Kim C, Kikuchi H, Hashimoto N, Hazama F, Kataoka H: **Establishment of the experimental conditions for inducing saccular cerebral aneurysms in primates with special reference to hypertension.** *Acta Neurochir (Wien)* (1989) **96**(3-4):132-136.

Kinugasa K, Mandai S, Terai Y, Kamata I, Sugiu K, Ohmoto T, Nishimoto A: **Direct thrombosis of aneurysms with cellulose acetate polymer. Part ii: Preliminary clinical experience.** *Journal of neurosurgery* (1992) **77**(4):501-507.

Knekt P, Reunanen A, Aho K, Heliovaara M, Rissanen A, Aromaa A, Impivaara O: **Risk factors for subarachnoid hemorrhage in a longitudinal population study.** *J Clin Epidemiol* (1991) **44**(9):933-939.

Koffijberg H, Buskens E, Algra A, Wermer MJ, Rinkel GJ: **Growth rates of intracranial aneurysms: Exploring constancy.** *J Neurosurg* (2008) **109**(2):176-185.

Komotar RJ, Mocco J, Solomon RA: **Guidelines for the surgical treatment of unruptured intracranial aneurysms: The first annual j. Lawrence pool memorial research symposium--controversies in the management of cerebral aneurysms.** *Neurosurgery* (2008) **62**(1):183-193; discussion 193-184.

Kondo C, Caputo GR, Semelka R, Foster E, Shimakawa A, Higgins CB: **Right and left ventricular stroke volume measurements with velocity-encoded cine mr imaging: In vitro and in vivo validation.** *AJR Am J Roentgenol* (1991) **157**(1):9-16.

Kondo S, Hashimoto N, Kikuchi H, Hazama F, Nagata I, Kataoka H: **Cerebral aneurysms arising at nonbranching sites. An experimental study.** *Stroke* (1997) **28**(2):398-403; discussion 403-394.

Konishi Y, Kadowaki C, Hara M, Takeuchi K: **Aneurysms associated with moyamoya disease.** *Neurosurgery* (1985) **16**(4):484-491.

Kono K, Fujimoto T, Shintani A, Terada T: **Haemodynamic characteristics at the rupture site of cerebral aneurysms: A case study.** *Neurosurgery* (2012) **71**(6):E1202-1208; discussion 1209.

Krabbe-Hartkamp MJ, van der Grond J, de Leeuw FE, de Groot JC, Algra A, Hillen B, Breteler MM, Mali WP: **Circle of willis: Morphologic variation on three-dimensional time-of-flight mr angiograms.** *Radiology* (1998) **207**(1):103-111.

Krampe C: **Zeiss operating microscopes for neurosurgery.** *Neurosurg Rev* (1984) **7**(2-3):89-97.

Krayenbuehl H, Yasargil MG: *Cerebral angiography.* Thieme Medical Publishers., Stuttgart (1982).

Kuivaniemi H, Prockop DJ, Wu Y, Madhatheri SL, Kleinert C, Earley JJ, Jokinen A, Stolle C, Majamaa K, Myllyla VV, et al.: **Exclusion of mutations in the gene for type iii collagen (col3a1) as a common cause of intracranial aneurysms or cervical artery dissections: Results from sequence analysis of the coding sequences of type iii collagen from 55 unrelated patients.** *Neurology* (1993) **43**(12):2652-2658.

Kulikov VP, Grechishnikov VN, Sidor MV: **[response of cerebral haemodynamics to combined stress impacts]**. *Patol Fiziol Eksp Ter* (2005) 1):7-9.

Kurokawa T, Harada K, Ishihara H, Fujisawa H, Kato S, Kajiwara K, Suzuki M: **De novo aneurysm formation on middle cerebral artery branches adjacent to the anastomotic site of superficial temporal artery-middle cerebral artery bypass surgery in two patients: Technical case report**. *Neurosurgery* (2007) 61(5 Suppl 2):E297-298; discussion E298.

Kurze T: **Microtechniques in neurological surgery**. *Clin Neurosurg* (1964) 11(128-137).

Kwak R, Mizoi K, Katakura R, Suzuki J: **The correlation between hypertension in past history and the incidence of cerebral aneurysms**. *Tohoku J Exp Med* (1979) 128(3):267-271.

Kwan ES, Heilman CB, Shucart WA, Klucznik RP: **Enlargement of basilar artery aneurysms following balloon occlusion--"water-hammer effect"**. **Report of two cases**. *J Neurosurg* (1991) 75(6):963-968.

L

Laborde F, Bical O, Lemoine G, Neveux JY: **[rupture of a dissecting aneurysm of the ascending aorta 10 years after therapy of coarctation. Apropos of a case of a 10-year-old girl]**. *Sem Hop* (1983) 59(42):2937-2938.

Lagana K, Dubini G, Migliavacca F, Pietrabissa R, Pennati G, Veneziani A, Quarteroni A: **Multiscale modelling as a tool to prescribe realistic boundary conditions for the study of surgical procedures**. *Biorheology* (2002) 39(3-4):359-364.

Laitinen L, Snellman A: **Aneurysms of the pericallosal artery: A study of 14 cases verified angiographically and treated mainly by direct surgical attack**. *J Neurosurg* (1960) 17(447-458).

Lall RR, Eddleman CS, Bendok BR, Batjer HH: **Unruptured intracranial aneurysms and the assessment of rupture risk based on anatomical and morphological factors: Sifting through the sands of data**. *Neurosurg Focus* (2009) 26(5):E2.

Langewouters GJ: **Visco-elasticity of the human aorta in vitro in relation to pressure and age [thesis].** . In: University of Amsterdam, The Netherlands, Amsterdam, The Netherlands (1982).

Lauterbur PC: **Image formation by induced local interactions. Examples employing nuclear magnetic resonance. 1973.** *Clinical orthopaedics and related research* (1989) 244):3-6.

Leppala JM, Virtamo J, Fogelholm R, Albanes D, Heinonen OP: **Different risk factors for different stroke subtypes: Association of blood pressure, cholesterol, and antioxidants.** *Stroke* (1999) **30**(12):2535-2540.

Letcher RL, Chien S, Pickering TG, Laragh JH: **Elevated blood viscosity in patients with borderline essential hypertension.** *Hypertension* (1983) **5**(5):757-762.

Levitt MR, McGah PM, Aliseda A, Mourad PD, Nerva JD, Vaidya SS, Morton RP, Ghodke BV, Kim LJ: **Cerebral aneurysms treated with flow-diverting stents: Computational models with intravascular blood flow measurements.** *AJNR American journal of neuroradiology* (2014) **35**(1):143-148.

Li MH, Li WB, Pan YP, Fang C, Wang W: **Persistent primitive trigeminal artery associated with aneurysm: Report of two cases and review of the literature.** *Acta Radiol* (2004) **45**(6):664-668.

Li C, Wang S, Chen J, Yu H, Zhang Y, Jiang F, Mu S, Li H, Yang X: **Influence of haemodynamics on recanalization of totally occluded intracranial aneurysms: A patient-specific computational fluid dynamic simulation study.** *Journal of neurosurgery* (2012) **117**(2):276-283.

Linde T, Sandhagen B, Hagg A, Morlin C, Danielson BG: **Decreased blood viscosity and serum levels of erythropoietin after anti-hypertensive treatment with amlodipine or metoprolol: Results of a cross-over study.** *J Hum Hypertens* (1996) **10**(3):199-205.

Linge SO, Haughton V, Løvgren AE, Mardal KA, Helgeland A, Langtangen HP: **Effect of tonsillar herniation on cyclic csf flow studied with computational flow analysis.** *AJNR Am J Neuroradiol* (2011) **Sep**;32(8):1474-1481.

Lippi D: **An aneurysm in the papyrus of ebers (108, 3-9).** *Med Secoli* (1990) **2**(1-4).

Longstreth WT, Jr., Nelson LM, Koepsell TD, van Belle G: **Cigarette smoking, alcohol use, and subarachnoid hemorrhage.** *Stroke* (1992) **23**(9):1242-1249.

Lorensen WE, Cline, H.E.: **Marching cubes: A high resolution 3d surface construction algorithm.** *Computer Graphics* (1987) **21**(163-169).

Lougheed WM, Sweet WH, White JC, Brewster WR: **The use of hypothermia in surgical treatment of cerebral vascular lesions; a preliminary report.** *J Neurosurg* (1955) **12**(3):240-255.

Low M, Perktold K, Raunig R: **Haemodynamics in rigid and distensible saccular aneurysms: A numerical study of pulsatile flow characteristics.** *Biorheology* (1993) **30**(3-4):287-298.

Lu G, Huang L, Zhang XL, Wang SZ, Hong Y, Hu Z, Geng DY: **Influence of haemodynamic factors on rupture of intracranial aneurysms: Patient-specific 3d mirror aneurysms model computational fluid dynamics simulation.** *AJNR Am J Neuroradiol* (2011) **Aug;32**(7):1255-1261.

Luessenhop AJ, Spence WT: **Artificial embolization of cerebral arteries. Report of use in a case of arteriovenous malformation.** *J Am Med Assoc* (1960) **172**(1153-1155).

Luo XY, Hinton JS, Liew TT, Tan KK: **Les modelling of flow in a simple airway model.** *Med Eng Phys* (2004) **Jun;26**(5):403-413.

Luscher TF, Tanner FC: **Endothelial regulation of vascular tone and growth.** *Am J Hypertens* (1993) **6**(7 Pt 2):283S-293S.

M

Malek AM, Alper SL, Izumo S: **Haemodynamic shear stress and its role in atherosclerosis.** *JAMA* (1999) **282**(21):2035-2042.

Malvè M, Pérez-del-Palomar A, Chandra S, López-Villalobos JL, Mena A, Finol EA, Ginel A, Doblaré M: **Fsi analysis of a healthy and a**

stenotic human trachea under impedance-based boundary conditions. *J Biomech Eng* (2011) **Feb**;133(2):021001.

Mansfield P, Morris PG, Ordidge R, Coupland RE, Bishop HM, Blamey RW: **Carcinoma of the breast imaged by nuclear magnetic resonance (nmr).** *The British journal of radiology* (1979) **52**(615):242-243.

Mantha A, Karmonik C, Benndorf G, Strother C, Metcalfe R: **Haemodynamics in a cerebral artery before and after the formation of an aneurysm.** *AJNR Am J Neuroradiol* (2006) **27**(5):1113-1118.

Mark M, Walter R, Meredith DO, Reinhart WH: **Commercial taxane formulations induce stomatocytosis and increase blood viscosity.** *Br J Pharmacol* (2001) **134**(6):1207-1214.

Marzo A, Singh P, Larrabide I, Radaelli A, Coley S, Gwilliam M, Wilkinson ID, Lawford P, Reymond P, Patel U, Frangi A *et al*: **Computational haemodynamics in cerebral aneurysms: The effects of modeled versus measured boundary conditions.** *Ann Biomed Eng* (2011) **39**(2):884-896.

Marzo A, Singh P, Reymond P, Stergiopoulos N, Patel U, Hose R: **Influence of inlet boundary conditions on the local haemodynamics of intracranial aneurysms.** *Comput Methods Biomech Biomed Engin* (2009) **12**(4):431-444.

Matas R: *Surgery of the vascular system. Surgery, its principles and practice.* W.B. Saunders Company, Philadelphia, Pennsylvania (1914).

Matsuda M, Watanabe K, Saito A, Matsumura K, Ichikawa M: **Circumstances, activities, and events precipitating aneurysmal subarachnoid hemorrhage.** *J Stroke Cerebrovasc Dis* (2007) **16**(1):25-29.

Mattson DL, Maeda CY, Bachman TD, Cowley AW, Jr.: **Inducible nitric oxide synthase and blood pressure.** *Hypertension* (1998) **31**(1):15-20.

Mayberg MR, Batjer HH, Dacey R, Diringer M, Haley EC, Heros RC, Sternau LL, Torner J, Adams HP, Jr., Feinberg W, et al.: **Guidelines for the management of aneurysmal subarachnoid hemorrhage. A statement for healthcare professionals from a special writing group of the stroke council, american heart association.** *Stroke* (1994) **25**(11):2315-2328.

McCormick WF, Schmalstieg EJ: **The relationship of arterial hypertension to intracranial aneurysms.** *Arch Neurol* (1977) **34**(5):285-287.

Meisel HJ, Mansmann U, Alvarez H, Rodesch G, Brock M, Lasjaunias P: **Cerebral arteriovenous malformations and associated aneurysms: Analysis of 305 cases from a series of 662 patients.** *Neurosurgery* (2000) **46**(4):793-800; discussion 800-792.

Meng H, Tutino VM, Xiang J, Siddiqui A: **High wss or low wss? Complex interactions of haemodynamics with intracranial aneurysm initiation, growth, and rupture: Toward a unifying hypothesis.** *AJNR Am J Neuroradiol* (2013).

Meng H, Wang Z, Hoi Y, Gao L, Metaxa E, Swartz DD, Kolega J: **Complex haemodynamics at the apex of an arterial bifurcation induces vascular remodeling resembling cerebral aneurysm initiation.** *Stroke* (2007) **38**(6):1924-1931.

Mellado X, Larrabide, I. Hernandez, M. Frangi, A.F.: **Flux driven medial curve extraction.** *The Insight Journal* (2007) **1926**(

Mercado R, Lopez S, Cantu C, Sanchez A, Revuelta R, Gomez-Llata S, Bouffard JA, Pineda C: **Intracranial aneurysms associated with unsuspected aortic coarctation.** *J Neurosurg* (2002) **97**(5):1221-1225.

Mhurchu CN, Anderson C, Jamrozik K, Hankey G, Dunbabin D: **Hormonal factors and risk of aneurysmal subarachnoid hemorrhage: An international population-based, case-control study.** *Stroke* (2001) **32**(3):606-612.

Milner P, Kirkpatrick KA, Ralevic V, Toothill V, Pearson J, Burnstock G: **Endothelial cells cultured from human umbilical vein release atp, substance p and acetylcholine in response to increased flow.** *Proc Biol Sci* (1990) **241**(1302):245-248.

Mitsos AP, Kakalis NM, Ventikos YP, Byrne JV: **Haemodynamic simulation of aneurysm coiling in an anatomically accurate computational fluid dynamics model: Technical note.** *Neuroradiology* (2008) **50**(4):341-347.

Mohiaddin RH, Kilner PJ, Rees S, Longmore DB: **Magnetic resonance volume flow and jet velocity mapping in aortic coarctation.** *J Am Coll Cardiol* (1993) **22**(5):1515-1521.

Moniz E: **L'encephalographic arterielle dans la localisation des tumeurs cerebrales.** . *Rev Neurol (Paris)* (1927) **2**(72-90).

Morales HG, Kim M, Vivas EE, Villa-Uriol MC, Larrabide I, Sola T, Guimaraens L, Frangi AF: **How do coil configuration and packing density influence intra-aneurysmal haemodynamics?** *AJNR Am J Neuroradiol* (2011) **Nov-Dec;32**(10):1935-1941.

Morgagni JB: **De sebiuset causis morborumper anatomenin sagatis venetis et topog remondiana,** book 1, letter 4. (1761) **2**(VXCVI):298.

Morimoto M, Miyamoto S, Mizoguchi A, Kume N, Kita T, Hashimoto N: **Mouse model of cerebral aneurysm: Experimental induction by renal hypertension and local haemodynamic changes.** *Stroke* (2002) **33**(7):1911-1915.

Moyle KR, Antiga L, Steinman DA: **Inlet conditions for image-based cfd models of the carotid bifurcation: Is it reasonable to assume fully developed flow?** *J Biomech Eng* (2006) **128**(3):371-379.

Myers JG, Moore JA, Ojha M, Johnston KW, Ethier CR: **Factors influencing blood flow patterns in the human right coronary artery.** *Ann Biomed Eng* (2001) **29**(2):109-120.

N

Nagata I, Handa H, Hashimoto N, Hazama F: **Experimentally induced cerebral aneurysms in rats: Part vi. Hypertension.** *Surg Neurol* (1980) **14**(6):477-479.

Nishimoto T, Yuki K, Sasaki T, Murakami T, Kodama Y, Kurisu K: **A ruptured middle cerebral artery aneurysm originating from the site of anastomosis 20 years after extracranial-intracranial bypass for moyamoya disease: Case report.** *Surg Neurol* (2005) **64**(3):261-265; discussion 265.

Noordergraaf A: **Physical basis of ballistocardiography.** 's-Gravenhage: *Excelsior* (1956) 146.

Norlen G: **Some aspects of the surgical treatment of intracranial aneurysms.** *Clinical neurosurgery* (1963) **9**(214-222).

Numminen H, Kotila M, Waltimo O, Aho K, Kaste M: **Declining incidence and mortality rates of stroke in finland from 1972 to 1991. Results of three population-based stroke registers.** *Stroke* (1996) **27**(9):1487-1491.

O

Ohba M, Aoyama, M.: **Defibrinogenating effect of batroxobin (df-521) on plasma fibrinogen concentration of experimental animals: A comparative study on seven different species.** *Jpn J Med Pharmacol* (1985) **14**(1061-1071).

Oka S: *Cardiovascular hemorheology.* Cambridge, UK (1981).

Olesen SP, Clapham DE, Davies PF: **Haemodynamic shear stress activates a k⁺ current in vascular endothelial cells.** *Nature* (1988) **331**(6152):168-170.

Omodaka S, Sugiyama S, Inoue T, Funamoto K, Fujimura M, Shimizu H, Hayase T, Takahashi A, Tominaga T: **Local haemodynamics at the rupture point of cerebral aneurysms determined by computational fluid dynamics analysis.** *Cerebrovasc Dis* (2012) **34**(2):121-129.

Orsi P, Rosa G, Liberatori G, Lunardi PP, Ferrante L: **Repair of two unruptured intracranial aneurysms in the presence of coarctation of the aorta-anesthetic implications and management.** *J Neurosurg Anesthesiol* (1993) **5**(1):48-51.

Ortega HV: **Computer simulation helps predict cerebral aneurysms.** *Journal of medical engineering & technology* (1998) **22**(4):179-181.

Oshima M, Sakai H, Torii R: **Modelling of inflow boundary conditions for image-based simulation of cerebrovascular flow.** *Int J Numer Methods Fluids* (2005) **47**(603–617).

Ostergaard JR, Hog E: **Incidence of multiple intracranial aneurysms. Influence of arterial hypertension and gender.** *J Neurosurg* (1985) **63**(1):49-55.

P

Padgett DH: **The circle of willis: Its embryology and anatomy.** In: *Intracranial arterial aneurysms.* Dandy WE (Ed) Comstock Publishing Co., New York (1944):67-90.

Patel AN, Richardson AE: **Ruptured intracranial aneurysms in the first two decades of life. A study of 58 patients.** *J Neurosurg* (1971) **35**(5):571-576.

Peltier J, Vinchon M, Soto-Ares G, Dhellemmes P: **Disappearance of a middle cerebral artery aneurysm associated with moyamoya syndrome after revascularization in a child: Case report.** *Childs Nerv Syst* (2008) **24**(12):1483-1487.

Penn RD, Basati S, Sweetman B, Guo X, Linninger A: **Ventricle wall movements and cerebrospinal fluid flow in hydrocephalus.** *J Neurosurg* (2011) **Jul;115**(1):159-164.

Peters DG, Kassam A, St Jean PL, Yonas H, Ferrell RE: **Functional polymorphism in the matrix metalloproteinase-9 promoter as a potential risk factor for intracranial aneurysm.** *Stroke* (1999) **30**(12):2612-2616.

Pezzini A, Caso V, Zanferrari C, Del Zotto E, Paciaroni M, Bertolino C, Grassi M, Agnelli G, Padovani A: **Arterial hypertension as risk factor for spontaneous cervical artery dissection. A case-control study.** *J Neurol Neurosurg Psychiatry* (2006) **77**(1):95-97.

Phillips B: *A series of experiments performed for the purpose of showing that arteries may be obliterated without ligature, compression or the knife.* Pamphlet published in London, Longman & Co, London, Churchill, London (1832 (reference unverified)).

Pohl U, Herlan K, Huang A, Bassenge E: **Edrf-mediated shear-induced dilation opposes myogenic vasoconstriction in small rabbit arteries.** *Am J Physiol* (1991) **261**(6 Pt 2):H2016-2023.

Prasad A, To LK, Gorrepati ML, Zarins CK, Figueroa CA: **Computational analysis of stresses acting on intermodular junctions in thoracic aortic endografts.** *J Endovasc Ther* (2011) **Aug 18**(4):559-568.

Price JF, Mowbray PI, Lee AJ, Rumley A, Lowe GD, Fowkes FG: **Relationship between smoking and cardiovascular risk factors in the**

development of peripheral arterial disease and coronary artery disease: Edinburgh artery study. *Eur Heart J* (1999) **20**(5):344-353.

Q

Quarteroni A, Formaggia L: **Mathematical modelling and numerical simulation of the cardiovascular system.** *Handbook of Numerical Analysis* (2004) **12**(3-127).

Quarteroni A, Ragni S, Veneziani A: **Coupling between lumped and distributed models for blood flow problems.** *Comput Vis Sci* (2001) **4**(111–124).

Quigley MR, Heiferman K, Kwaan HC, Vidovich D, Nora P, Cerullo LJ: **Laser-sealed arteriotomy: A reliable aneurysm model.** *J Neurosurg* (1987) **67**(2):284-287.

Qureshi AI, Suarez JJ, Parekh PD, Sung G, Geocadin R, Bhardwaj A, Tamargo RJ, Ulatowski JA: **Risk factors for multiple intracranial aneurysms.** *Neurosurgery* (1998) **43**(1):22-26; discussion 26-27.

Quincke H: **Die lumbarpunktion des hydrocephalus.** *Klin Wochenscher* (1891) **28**(929-965).

R

Raaymakers TW, Rinkel GJ, Limburg M, Algra A: **Mortality and morbidity of surgery for unruptured intracranial aneurysms: A meta-analysis.** *Stroke* (1998) **29**(8):1531-1538.

Radaelli AG, Augsburger L, Cebal JR, Ohta M, Rufenacht DA, Balossino R, Benndorf G, Hose DR, Marzo A, Metcalfe R, Mortier P *et al*: **Reproducibility of haemodynamical simulations in a subject-specific stented aneurysm model--a report on the virtual intracranial stenting challenge 2007.** *J Biomech* (2008) **41**(10):2069-2081.

Rajasekaran H: **@neurist - towards a system architecture for advanced disease management through integration of heterogeneous data, computing, and complex processing services.** *Proceedings of the 2008 21st IEEE International Symposium on Computer-Based Medical Systems* (2008) **00**(

Ransohoff J: **A case of aortic aneurism treated by the insertion of wire.** *JAMA* (1886) **7**(481–485

Rayz VL, Boussel L, Acevedo-Bolton G, Martin AJ, Young WL, Lawton MT, Higashida R, Saloner D: **Numerical simulations of flow in cerebral aneurysms: Comparison of cfd results and in vivo mri measurements.** *J Biomech Eng* (2008) **130**(5):051011.

Rayz VL, Boussel L, Lawton MT, Acevedo-Bolton G, Ge L, Young WL, Higashida RT, Saloner D: **Numerical modeling of the flow in intracranial aneurysms: Prediction of regions prone to thrombus formation.** *Ann Biomed Eng* (2008) **36**(11):1793-1804.

Redekop G, TerBrugge K, Montanera W, Willinsky R: **Arterial aneurysms associated with cerebral arteriovenous malformations: Classification, incidence, and risk of hemorrhage.** *J Neurosurg* (1998) **89**(4):539-546.

Reifenstein GH, Levine, S.A. Gross, R.E.: **Coarctation of the aorta. A review of 104 autopsied cases of the "adult type", 2 years of age or older.** *Am Heart J* (1947) **33**:146-168.

Rengachary SS, Wilkins RH: *Principles of neurosurgery.* McGraw Hill, USA (1996).

Resnick N, Collins T, Atkinson W, Bonthron DT, Dewey CF, Jr., Gimbrone MA, Jr.: **Platelet-derived growth factor b chain promoter contains a cis-acting fluid shear-stress-responsive element.** *Proc Natl Acad Sci U S A* (1993) **90**(16):7908.

Reynold P, Merenda F, Perren F, Rufenacht D, Stergiopoulos N: **Validation of a one-dimensional model of the systemic arterial tree.** *Am J Physiol Heart Circ Physiol* (2009).

Rhoton AL, Jr.: **Anatomy of saccular aneurysms.** *Surg Neurol* (1980) **14**(1):59-66.

Riggs HE, Rupp C.: **Miliary aneurysms: Relations of anomalies of circle of willis to formation of aneurysms.** *Arch Neurol Psychiat* (1943) **49**:615-616.

Rinkel GJ, Djibuti M, Algra A, van Gijn J: **Prevalence and risk of rupture of intracranial aneurysms: A systematic review.** *Stroke* (1998) **29**(1):251-256.

Rinne J, Hernesniemi J, Puranen M, Saari T: **Multiple intracranial aneurysms in a defined population: Prospective angiographic and clinical study.** *Neurosurgery* (1994) **35**(5):803-808.

Rordorf G, Koroshetz WJ, Copen WA, Gonzalez G, Yamada K, Schaefer PW, Schwamm LH, Ogilvy CS, Sorensen AG: **Diffusion- and perfusion-weighted imaging in vasospasm after subarachnoid hemorrhage.** *Stroke* (1999) **30**(3):599-605.

Ronkainen A, Miettinen H, Karkola K, Papinaho S, Vanninen R, Puranen M, Hernesniemi J: **Risk of harboring an unruptured intracranial aneurysm.** *Stroke* (1998) **29**(2):359-362.

Rosenson RS, Tangney CC: **Antiatherothrombotic properties of statins: Implications for cardiovascular event reduction.** *JAMA* (1998) **279**(20):1643-1650.

Rossitti S: **Shear stress in cerebral arteries carrying saccular aneurysms. A preliminary study.** *Acta Radiol* (1998) **39**(6):711-717.

Rowe GG, Castillo CA, Afonso S, Young WP, Crumpton CW: **Cerebral blood flow in coarctation of the aorta.** *J Clin Invest* (1964) **43**(1922-1927).

S

Sacco RL, Wolf PA, Bharucha NE, Meeks SL, Kannel WB, Charette LJ, McNamara PM, Palmer EP, D'Agostino R: **Subarachnoid and intracerebral hemorrhage: Natural history, prognosis, and precursive factors in the framingham study.** *Neurology* (1984) **34**(7):847-854.

Sadasivan C, Fiorella DJ, Woo HH, Lieber BB: **Physical factors effecting cerebral aneurysm pathophysiology.** *Ann Biomed Eng* (2013) **Jul;41**(7):1347-1365.

Sadatomo T, Yuki K, Migita K, Taniguchi E, Kodama Y, Kurisu K: **Morphological differences between ruptured and unruptured cases in middle cerebral artery aneurysms.** *Neurosurgery* (2008) **62**(3):602-609; discussion 602-609.

Sah AL, Perett, G.E., Locksley, H.B. et al.: *Intracranial aneurysms sand sah: A co-operative study.* . JB Lippincott, Philadelphia (1969).

Sakai N, Nakayama K, Tanabe Y, Izumiya Y, Nishizawa S, Uemuara K: **Absence of plasma protease-antiprotease imbalance in the formation of saccular cerebral aneurysms.** *Neurosurgery* (1999) **45**(1):34-38; discussion 38-39.

Sakaki T, Tominaga M, Miyamoto K, Tsunoda S, Hiasa Y: **Clinical studies of de novo aneurysms.** *Neurosurgery* (1993) **32**(4):512-516; discussion 516-517.

San Millan Ruiz D, Yilmaz H, Dehdashti AR, Alimenti A, de Tribolet N, Rufenacht DA: **The perianeurysmal environment: Influence on saccular aneurysm shape and rupture.** *AJNR Am J Neuroradiol* (2006) **27**(3):504-512.

Sarner M, Crawford MD: **Ruptured intracranial aneurysm. Clinical series.** *Lancet* (1965) **2**(7425):1251-1254.

Sauerbeck LR, Hornung R, Moomaw CJ, Woo D, Curry R, Brown RD, Jr., Broderick J: **The effects of study participation in the familial intracranial aneurysm study on cigarette smoking.** *J Stroke Cerebrovasc Dis* (2008) **17**(6):370-372.

Schievink WI, Schaid DJ, Michels VV, Piepgras DG: **Familial aneurysmal subarachnoid hemorrhage: A community-based study.** *J Neurosurg* (1995) **83**(3):426-429.

Schmetterer L, Kemmler D, Breiteneder H, Alschinger C, Koppensteiner R, Lexer F, Fercher AF, Eichler HG, Wolzt M: **A randomized, placebo-controlled, double-blind crossover study of the effect of pentoxifylline on ocular fundus pulsations.** *Am J Ophthalmol* (1996) **121**(2):169-176.

Sekhar LN, Heros RC: **Origin, growth, and rupture of saccular aneurysms: A review.** *Neurosurgery* (1981) **8**(2):248-260.

Serbinnenko FA: **Balloon catheterization and occlusion of major cerebral vessels.** *J Neurosurg* (1974) **41**(2):125-145.

Sforza DM, Putman CM, Scrivano E, Lylyk P, Cebra JR: **Blood-flow characteristics in a terminal basilar tip aneurysm prior to its fatal rupture.** *AJNR Am J Neuroradiol* (2010) **Jun**;31(6):1127-1131.

Shearer WT, Rutman JY, Weinberg WA, Goldring D: **Coarctation of the aorta and cerebrovascular accident: A proposal for early corrective surgery.** *J Pediatr* (1970) **77**(6):1004-1009.

Shimogonya Y, Ishikawa T, Imai Y, Matsuki N, Yamaguchi T: **Can temporal fluctuation in spatial wall shear stress gradient initiate a cerebral aneurysm? A proposed novel haemodynamic index, the gradient oscillatory number (gon).** *J Biomech* (2009) **42**(4):550-554.

Sho E, Sho M, Singh TM, Nanjo H, Komatsu M, Xu C, Masuda H, Zarins CK: **Arterial enlargement in response to high flow requires early expression of matrix metalloproteinases to degrade extracellular matrix.** *Exp Mol Pathol* (2002) **73**(2):142-153.

Shojima M, Oshima M, Takagi K, Torii R, Hayakawa M, Katada K, Morita A, Kirino T: **Magnitude and role of wall shear stress on cerebral aneurysm: Computational fluid dynamic study of 20 middle cerebral artery aneurysms.** *Stroke* (2004) **35**(11):2500-2505.

Shojima M, Oshima M, Takagi K, Torii R, Nagata K, Shirouzu I, Morita A, Kirino T: **Role of the bloodstream impacting force and the local pressure elevation in the rupture of cerebral aneurysms.** *Stroke* (2005) **36**(9):1933-1938.

Singh PK, Marzo A, Coley SC, Berti G, Bijlenga P, Lawford PV, Villa-Uriol MC, Rufenacht DA, McCormack KM, Frangi A, Patel UJ *et al*: **The role of computational fluid dynamics in the management of unruptured intracranial aneurysms: A clinicians' view.** *Comput Intell Neurosci* (2009) 760364.

Siouffi M, Deplano V, Pélissier R: **Experimental analysis of unsteady flows through a stenosis.** *J Biomech* (1998) **31**(1):11-19.

Solenski NJ, Haley EC, Jr., Kassell NF, Kongable G, Germanson T, Truskowski L, Torner JC: **Medical complications of aneurysmal subarachnoid hemorrhage: A report of the multicenter, cooperative aneurysm study. Participants of the multicenter cooperative aneurysm study.** *Crit Care Med* (1995) **23**(6):1007-1017.

Solomon RA, Fink ME, Pile-Spellman J: **Surgical management of unruptured intracranial aneurysms.** *J Neurosurg* (1994) **80**(3):440-446.

St Jean P, Hart, B. Webster, M. Steed, D. Adamson, J. Powell, J. Ferrell, R.: **Alpha-1-antitrypsin deficiency in aneurysmal disease.** *Hum Hered* (1996) **46**(92-97).

Stehbens WE: **Medial defects of the cerebral arteries of man.** *J Pathol Bacteriol* (1959) **78**(179-185).

Stehbens WE: **Cerebral aneurysms and congenital abnormalities.** *Australas Ann Med* (1962) **11**(102-112).

Stehbens WE: **Histopathology of cerebral aneurysms.** *Arch Neurol* (1963) **8**(272-285).

Stehbens WE: **Aneurysms and anatomical variation of cerebral arteries.** *Arch Pathol* (1963b) **75**(45-64).

Stehbens WE: *Pathology of the cerebral blood vessels.* Mosby, St. Louis (1972).

Stehbens WE: **Aetiology of intracranial berry aneurysms.** *J Neurosurg* (1989) **70**(6):823-831.

Steiger HJ, Aaslid R, Keller S, Reulen HJ: **Growth of aneurysms can be understood as passive yield to blood pressure. An experimental study.** *Acta Neurochir (Wien)* (1989) **100**(1-2):74-78.

Steinman DA, Milner JS, Norley CJ, Lownie SP, Holdsworth DW: **Image-based computational simulation of flow dynamics in a giant intracranial aneurysm.** *AJNR Am J Neuroradiol* (2003) **24**(4):559-566.

Steinman DA: **Image-based computational fluid dynamics: A new paradigm for monitoring haemodynamics and atherosclerosis.** *Current drug targets Cardiovascular & haematological disorders* (2004) **4**(2):183-197.

Stergiopoulos N, Young DF, Rogge TR: **Computer simulation of arterial flow with applications to arterial and aortic stenoses.** *J Biomech* (1992) **25**(12):1477-1488.

Strother CM, Graves VB, Rappe A: **Aneurysm haemodynamics: An experimental study.** *AJNR Am J Neuroradiol* (1992) **13**(4):1089-1095.

Stuntz JT, Ojemann GA, Alvord EC, Jr.: **Radiographic and histologic demonstration of an aneurysm developing on the infundibulum of the posterior communicating artery. Case report.** *J Neurosurg* (1970) **33**(5):591-595.

Sun Q, Groth A, Aach T: **Comprehensive validation of computational fluid dynamics simulations of in-vivo blood flow in patient-specific cerebral aneurysms.** *Med Phys* (2012) **Feb**;39(2):742-754.

Sun Q, Groth A, Bertram M, Waechter I, Bruijns T, Hermans R, Aach T: **Phantom-based experimental validation of computational fluid dynamics simulations on cerebral aneurysms.** *Med Phys* (2010) **Sep**;37(9):5054-5065.

Suyama K, Mizota S, Minagawa T, Hayashi K, Miyazaki H, Nagata I: **A ruptured anterior communicating artery aneurysm associated with internal carotid artery agenesis and a middle cerebral artery anomaly.** *J Clin Neurosci* (2009) **16**(4):585-586.

Suzuki J, Hori S, Sakurai Y: **Intracranial aneurysms in the neurosurgical clinics in japan.** *J Neurosurg* (1971) **35**(1):34-39.

T

Takahashi M, Fujimoto T, Suzuki R, Asai J, Miyo T, Hokaku H: **[a case of spontaneous middle cerebral artery occlusion associated with a cerebral aneurysm angiographically disappearing after sta-mca anastomosis].** *No Shinkei Geka* (1997) **25**(8):727-732.

Takayama K, Nakagawa H, Iwasaki S, Taoka T, Myouchin K, Wada T, Sakamoto M, Fukusumi A, Kurokawa S, Kichikawa K: **Multiple cerebral aneurysms associated with takayasu arteritis successfully treated with coil embolization.** *Radiat Med* (2008) **26**(1):33-38.

Tang BT, Pickard SS, Chan FP, Tsao PS, Taylor CA, Feinstein JA: **Wall shear stress is decreased in the pulmonary arteries of patients with pulmonary arterial hypertension: An image-based, computational fluid dynamics study.** *Pulm Circ* (2012) **2**(4):470-476.

Tappura M: **Prognosis of subarachnoid haemorrhage. A study of 120 patients with unoperated intracranial aneurysms and 267 patients without vascular lesions demonstrable in bilateral carotid angiograms.** *Acta Med Scand Suppl* (1962) **392**(1):75.

Tateshima S, Murayama Y, Villablanca JP, Morino T, Nomura K, Tanishita K, Vinuela F: **In vitro measurement of fluid-induced wall shear stress in unruptured cerebral aneurysms harboring blebs.** *Stroke* (2003) **34**(1):187-192.

Tateshima S, Tanishita K, Omura H, Villablanca JP, Vinuela F: **Intra-aneurysmal haemodynamics during the growth of an unruptured aneurysm: In vitro study using longitudinal ct angiogram database.** *AJNR Am J Neuroradiol* (2007) **28**(4):622-627.

Taylor CL, Yuan Z, Selman WR, Ratcheson RA, Rimm AA: **Cerebral arterial aneurysm formation and rupture in 20,767 elderly patients: Hypertension and other risk factors.** *J Neurosurg* (1995) **83**(5):812-819.

Taylor CL, Yuan Z, Selman WR, Ratcheson RA, Rimm AA: **Cerebral arterial aneurysm formation and rupture in 20,767 elderly patients: Hypertension and other risk factors.** *J Neurosurg* (1995) **83**(5):812-819.

Thiex R, Norbash AM, Frerichs KU: **The safety of dedicated-team catheter-based diagnostic cerebral angiography in the era of advanced noninvasive imaging.** *AJNR Am J Neuroradiol* (2010) **31**(2):230-234.

Thompson RC, Steinberg GK, Levy RP, Marks MP: **The management of patients with arteriovenous malformations and associated intracranial aneurysms.** *Neurosurgery* (1998) **43**(2):202-211; discussion 211-202.

Tian G, Longest PW, Su G, Hindle M: **Characterization of respiratory drug delivery with enhanced condensational growth using an individual path model of the entire tracheobronchial airways.** *Ann Biomed Eng* (2011) **Mar**;39(3):1136-1153.

Toftdahl DB, Torp-Pedersen C, Engel UH, Strandgaard S, Jespersen B: **Hypertension and left ventricular hypertrophy in patients with spontaneous subarachnoid hemorrhage.** *Neurosurgery* (1995) **37**(2):235-239; discussion 239-240.

Tromp G, Gatalica Z, Skunca M, Berguer R, Siegel T, Kline RA, Kuivaniemi H: **Elevated expression of matrix metalloproteinase-13 in abdominal aortic aneurysms.** *Ann Vasc Surg* (2004) **18**(4):414-420.

Teunissen LL, Rinkel GJ, Algra A, van Gijn J: **Risk factors for subarachnoid hemorrhage: A systematic review.** *Stroke* (1996) **27**(3):544-549.

Turjman F, Massoud TF, Ji C, Guglielmi G, Vinuela F, Robert J: **Combined stent implantation and endosaccular coil placement for treatment of experimental wide-necked aneurysms: A feasibility study in swine.** *AJNR American journal of neuroradiology* (1994) **15**(6):1087-1090.

Turowski B, Hanggi D, Siebler M: **Intracranial bilateral vertebral artery dissection during anticoagulation after cerebral venous and sinus thrombosis (csvt).** *Acta Neurochir (Wien)* (2007) **149**(8):793-797; discussion 797.

U

Ujiie H, Tachibana H, Hiramatsu O, Hazel AL, Matsumoto T, Ogasawara Y, Nakajima H, Hori T, Takakura K, Kajiya F: **Effects of size and shape (aspect ratio) on the haemodynamics of saccular aneurysms: A possible index for surgical treatment of intracranial aneurysms.** *Neurosurgery* (1999) **45**(1):119-129; discussion 129-130.

Uihlein A: **Profound hypothermia and circulatory arrest in operations for intracranial aneurysms.** *Ann Chir Thorac Cardiovasc* (1962) **1**(811-812).

V

Varaprasathan GA, Araoz PA, Higgins CB, Reddy GP: **Quantification of flow dynamics in congenital heart disease: Applications of velocity-encoded cine mr imaging.** *Radiographics* (2002) **22**(4):895-905; discussion 905-896.

Vardoulis O, Coppens E, Martin B, Reymond P, Tozzi P, Stergiopoulos N: **Impact of aortic grafts on arterial pressure: A computational fluid dynamics study.** *Eur J Vasc Endovasc Surg* (2011) **Aug 31**.([Epub ahead of print]).

Verheugt CL, Uiterwaal CS, Grobbee DE, Mulder BJ: **Long-term prognosis of congenital heart defects: A systematic review.** *Int J Cardiol* (2008) **131**(1):25-32.

Vignon-Clementel IE, Figueroa C.A., Jansen K.E., Taylor C.A.: **Outflow boundary conditions for three-dimensional finite element modeling of blood flow and pressure in arteries.** *Comput Methods Appl Mech Eng* (2006) **195**(3776–3796)

Villa-Uriol MC, Berti G, Hose DR, Marzo A, Chiarini A, Penrose J, Pozo J, Schmidt JG, Singh P, Lycett R, Larrabide I *et al*: **@neurist complex information processing toolchain for the integrated management of cerebral aneurysms.** *Interface Focus* (2011) **Jun 6**(3):308-319.

Venugopal P, Valentino D, Schmitt H, Villablanca JP, Vinuela F, Duckwiler G: **Sensitivity of patient-specific numerical simulation of cerebral aneurysm haemodynamics to inflow boundary conditions.** *J Neurosurg* (2007) **106**(6):1051-1060.

Viceconti M, Astolfi, L., Leardini, A., Imboden, S., Petrone, M., Quadrani, P., Taddei, F., Testi, D., Zannoni, C.: **The multimod application framework.**:Abs 15-20. 2004.

Vignon-Clementel IE, Figueroa C.A., Jansen K.E., Taylor C.A.: **Outflow boundary conditions for three-dimensional finite element modeling of blood flow and pressure in arteries.** *Comput Methods Appl Mech Eng* (2006) **195**(3776–3796)

W

Waga S, Morikawa A: **Aneurysm developing on the infundibular widening of the posterior communicating artery.** *Surg Neurol* (1979) **11**(2):125-127.

Wagner CT, Durante W, Christodoulides N, Hellums JD, Schafer AI: **Haemodynamic forces induce the expression of heme oxygenase in cultured vascular smooth muscle cells.** *J Clin Invest* (1997) **100**(3):589-596.

Walker AE, Allegre GW: **The pathology and pathogenesis of cerebral aneurysms.** *J Neuropathol Exp Neurol* (1954) **13**(1):248-259.

Wang DM, Tarbell JM: **Modeling interstitial flow in an artery wall allows estimation of wall shear stress on smooth muscle cells.** *J Biomech Eng* (1995) **117**(3):358-363.

Wang Z, Kolega J, Hoi Y, Gao L, Swartz DD, Levy EI, Mocco J, Meng H: **Molecular alterations associated with aneurysmal remodeling are localized in the high haemodynamic stress region of a created carotid bifurcation.** *Neurosurgery* (2009) **65**(1):169-177; discussion 177-168.

Weichert F, Walczak L, Fisseler D, Opfermann T, Razzaq M, Münster R, Turek S, Grunwald I, Roth C, Veith C, Wagner M: **Simulation of intra-aneurysmal blood flow by different numerical methods.** *Comput Math Methods Med* (2013) **Epub 2013 Apr 15**(527654).

Weir B, Macdonald, R.L.: **Intracranial aneurysms and subarachnoid hemorrhage: An overview.** In: *Neurosurgery*. 2. Wilkins RH, Rengachary, S.S. (Ed) McGraw-Hill, New York (1996):2191–2213.

Wermer MJ, van der Schaaf IC, Velthuis BK, Algra A, Buskens E, Rinkel GJ, Group AS: **Follow-up screening after subarachnoid haemorrhage: Frequency and determinants of new aneurysms and enlargement of existing aneurysms.** *Brain* (2005) **128**(Pt 10):2421-2429.

Werner SC, Blackmore, A.H., King, B.C.: **Aneurysm of internal carotid artery within skull, wiring and electrothermic coagulation.** *JAMA* (1941) **116**(578-582).

Westerhof N, Bosman F, De Vries CJ, Noordergraaf A: **Analog studies of the human systemic arterial tree.** *J Biomech* (1969) **2**(2):121-143.

Wiebers DO, Whisnant JP, Huston J, 3rd, Meissner I, Brown RD, Jr., Piepgras DG, Forbes GS, Thielen K, Nichols D, O'Fallon WM, Peacock J *et al*: **Unruptured intracranial aneurysms: Natural history, clinical outcome, and risks of surgical and endovascular treatment.** *Lancet* (2003) **362**(9378):103-110.

Willis T: *Cerebri anatome cui accessit nervorum descriptio et usus.* (1664).

Wirth FP, Laws ER, Jr., Piepgras D, Scott RM: **Surgical treatment of incidental intracranial aneurysms.** *Neurosurgery* (1983) **12**(5):507-511.

Womersley JR: **Method for the calculation of velocity, rate of flow and viscous drag in arteries when the pressure gradient is known.** *J Physiol* (1955) **127**(3):553-563.

Wong GK, Poon WS: **Current status of computational fluid dynamics for cerebral aneurysms: The clinician's perspective.** *J Clin Neurosci* (2011) **Oct;18**(10):1285-1288.

X

Xu J, Yu Y, Wu X, Wu Y, Jiang C, Wang S, Huang Q, Liu J: **Morphological and haemodynamic analysis of mirror posterior communicating artery aneurysms.** *PLoS One* (2013) **8**(1):e55413.

Y

Yasui N, Magarisawa S, Suzuki A, Nishimura H, Okudera T, Abe T: **Subarachnoid hemorrhage caused by previously diagnosed, previously unruptured intracranial aneurysms: A retrospective analysis of 25 cases.** *Neurosurgery* (1996) **39**(6):1096-1100; discussion 1100-1091.

Yamashita K, Kashiwagi S, Kato S, Takasago T, Ito H: **Cerebral aneurysms in the elderly in yamaguchi, japan. Analysis of the yamaguchi data bank of cerebral aneurysm from 1985 to 1995.** *Stroke* (1997) **28**(10):1926-1931.

Yong-Zhong G, van Alphen HA: **Pathogenesis and histopathology of saccular aneurysms: Review of the literature.** *Neurol Res* (1990) **12**(4):249-255.

Z

Zada G, Breault J, Liu CY, Khalessi AA, Larsen DW, Teitelbaum GP, Giannotta SL: **Internal carotid artery aneurysms occurring at the origin of fetal variant posterior cerebral arteries: Surgical and endovascular experience.** *Neurosurgery* (2008) **63**(1 Suppl 1):ONS55-61; discussion ONS61-52.

Zeng Z, Kallmes DF, Durka MJ, Ding Y, Lewis D, Kadirvel R, Robertson AM: **Sensitivity of cfd based haemodynamic results in rabbit aneurysm models to idealizations in surrounding vasculature.** *J Biomech Eng* (2010) **Sep;132**(9):091009.

The Effects of Aortic Coarctation on Cerebral Hemodynamics and its Importance in the Etiopathogenesis of Intracranial Aneurysms

Abstract

Objectives: Hemodynamic changes in the cerebral circulation in presence of coarctation of aorta (CoA) and their significance in the increased intracranial aneurysms (IAs) formation in these patients remain unclear. In the present study, we measured the flow-rate waveforms in the cerebral arteries of a patient with CoA, followed by an analysis of different hemodynamic indices in a coexisting IA.

Pankaj K Singh, MRCS
 Alberto Marzo, PhD
 Cristina Staicu, PhD
 Matt G William, PhD
 Iain Wilkinson, PhD
 Patricia V Lawford, PhD
 Daniel A Rufenacht, MD
 Philippe Bijlenga, MD
 Alejandro F Frangi, PhD
 Rodney Hose, PhD
 Umang J Patel, FRCS
 Stuart C Coley, MD

Address Correspondence to:
 Pankaj K Singh, MRCS
 Clinical Research Fellow,
 Departments of Neurosurgery/Medical Physics,
 Royal Hallamshire Hospital, Sheffield, UK
 Email: neurosurgery2007@gmail.com
 Ph: +44 114 2712180
 Fax: +44 114 2713314

Materials and Methods: Phase-contrast Magnetic Resonance (pc-MR) volumetric flow-rate (VFR) measurements were performed in cerebral arteries of a 51 years old woman with coexisting CoA, and five healthy volunteers. Numerical predictions of a number of relevant hemodynamic indices were performed in an IA located in sub-clinoid part of left internal carotid artery (ICA) of the patient. Computations were performed using Ansys®-CFX™ solver using the VFR values measured in the patient as boundary conditions (BCs). A second analysis was performed using the average VFR values measured in healthy volunteers. The VFR waveforms measured in the patient and healthy volunteers were compared followed by a comparison of the hemodynamic indices obtained using both approaches. The results are discussed in the background of relevant literature.

Results: Mean flow-rates were increased by 27.1% to 54.9% (2.66-5.44 ml/sec) in the cerebral circulation of patients with CoA as compared to healthy volunteers (1.2-3.95 ml/sec). Velocities were increased inside the IA by 35-45%. An exponential rise of 650% was observed in the area affected by high wall shear stress (WSS >15Pa) when flow-rates specific to CoA were used as compared to population average flow-rates. Absolute values of space and time averaged WSS were increased by 65%. Whereas values of maximum pressure on the IA wall were increased by 15% the area of elevated pressure was actually decreased by 50%, reflecting a more focalized jet impingement within the IA of the CoA patient.

Conclusions: IAs can develop in patients with CoA several years after the surgical repair. Cerebral flow-rates in CoA patients are significantly higher as compared to average flow-rates in healthy population. The increased supra-physiological WSS (>15Pa), OSI (>0.2) and focalized pressure may play an important role in the etiopathogenesis of IAs in patients with CoA.

Keywords: Coarctation of aorta, intracranial aneurysms, cerebral circulation, flow-rates, hemodynamics, wall shear stress, computational fluid dynamics

Journal of Vascular and Interventional Neurology 2010;3(1) 17-30

Introduction:

Estimated annual incidence of IAs in most Western countries is estimated to be at 1 to 2%.^{7,49} Subarachnoid hemorrhage (SAH) can be a consequence with a high overall mortality rates approximating 45% (range 32-67%).⁴⁶ About 30% of survivors have moderate to severe disabilities and 66% of those who have 'successful' clip placement, never return to same quality of life as before SAH.^{23,46} The current evidence convincingly supports a multi-factorial basis for the initiation and rupture of IAs.^{88,92,108}

Amongst other etiologies proposed, CoA has been highlighted as a major risk factor in the etiopathogenesis of IAs.^{1,3,15,24,27,48,50,53,62,70,75,78,87} A wide range for the incidence of IAs in patients with CoA has been reported starting from 2.5%¹ to as high as 50%,⁸⁹ all above the estimated

incidence of IAs in general population. Connolly and colleagues in their recent study confirmed that the frequency of IAs among patients with CoA is approximately 5 times higher than that of the general population.¹⁵ The incidence of IA rupture in CoA patients (4.8%)^{70,83} is also higher than the estimated rate of rupture in the general population which is less than 1%.¹⁰⁶ In spite of CoA being a well-established risk factor for IA formation,^{1,3,15,24,27,48,50,53,62,70,75,78,87} the exact underlying mechanisms for this association remain poorly understood. Hypertension^{3,9,24,50,75,78,92,95} and developmental errors of neural crest resulting in abnormal vessel wall collagen^{15,17,48,53,62,70,87} are two main factors thought to facilitate the formation of IAs in presence of CoA. It is surprising to note that in spite of well established role of wall shear stress (WSS) in the genesis of IAs,^{11,32,38,40-42,65,69,72,91,104} none of the workers explored this important link in this context.

Owing to their direct origin from the pre-coarctation segment of aorta, cerebro-cephalic arteries are most likely to be affected by the hemodynamic changes occurring in this part of aorta. Secondary to the increased resistance to outflow, increased aorto-cranial pressure gradients have been demonstrated by a number of authors correlating to the severity of stenosis.^{1,36,45,71,102} Dilatation of cervico-cephalic arteries in CoA secondary to this increased pressure gradient is has also been reported.^{1,85}

An increase in the radius (r) of cerebral arteries and increased aorto-cranial pressure gradient (ΔP) in CoA are expected to result in an exponential rise in flow-rates (Q) as per the Hagan-Poiseuille law (Equation-1), given the viscosity (μ) and length (L) remain constant.

$$Q = \frac{\Delta P}{8\mu L} \pi r^4 \dots\dots\dots (\text{Eq-1})$$

Furthermore, bradycardia coupled with increased stroke volume

and cardiac output is a known feature of CoA.³⁶ These increments will further increase the cerebral blood-flow (CBF).

An increased flow-rate (Q), in turn is one of the major factors responsible for increased wall shear stress (WSS) in the intracranial arteries (Equation-2).

$$\tau = 4\mu \frac{Q}{\pi r^3} \dots\dots\dots (\text{Eq-2})$$

Where τ is WSS

Literature seems to be particularly deficient and controversial on the effects of CoA on cerebral arterial flow-rates. After a thorough search (PubMed®, Embase® and Google-Scholar™ searched from the year 1900 up to 2009) we could retrieve only two relevant studies. In 1949 Hafkenschiel et al³⁷ demonstrated a significant increase in cerebral arterial flow-rates in patients with CoA. Rowe and colleagues⁸⁵ found no significant differences in the flow-rates before and after the repair of CoA in their study done in 1964. No apparent efforts were done since then to measure the cerebral arterial flow-rates in patients with CoA. Paucity of information about the flow patterns inside the cerebral circulation in presence of CoA provided us a rationale to measure the cerebral arterial flow-rates in the present patient. Furthermore, given the widely accepted importance of hemodynamics in the etiopathogenesis of IAs^{11,32,38,40-42,65,69,72,91,104} it is logical to analyze the hemodynamic factors in the coexisting IA of our patient. A better understanding of the etiopathogenesis of the IA formation and rupture may help clinicians in preventing and treating the disease effectively.

In the current study, we preformed pc-MR measurements in the cerebral arteries of a CoA patient with coexisting IA and five healthy volunteers followed by an analysis of the different hemodynamic factors inside IA. The possible role of

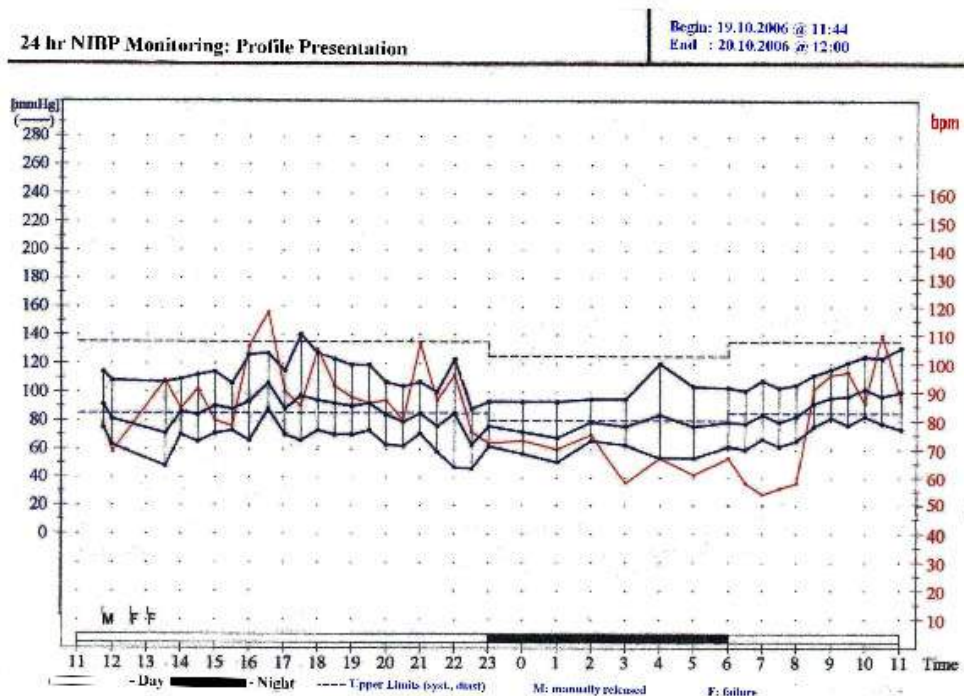


Figure 1: 24 hours ambulatory Non-invasive BP (NIBP) monitoring showing satisfactory BP control for both systolic and diastolic values.

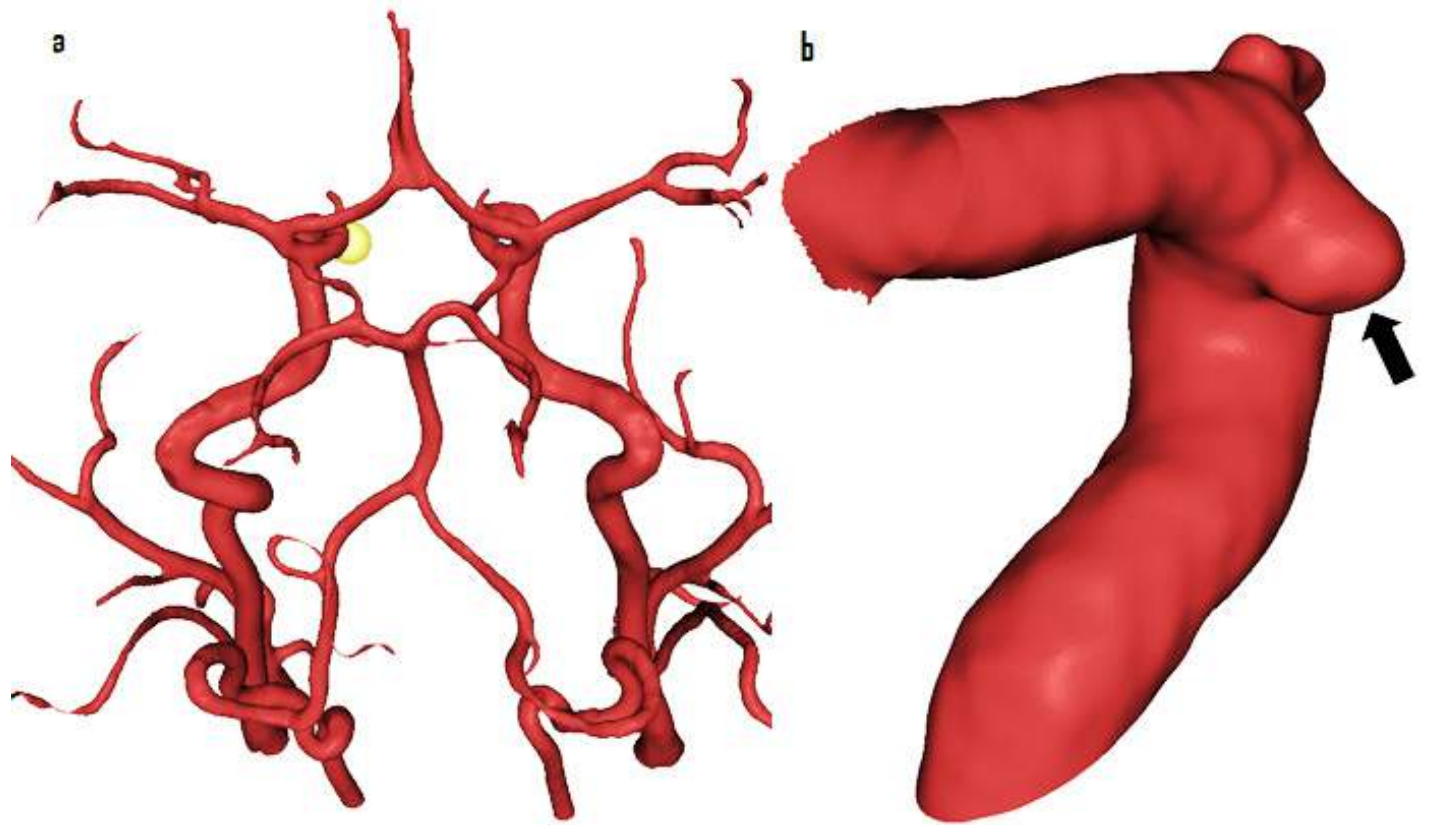


Figure 2: Intracranial aneurysm included in the study shown in (a) circle of Willis (yellow sphere- arrowhead) and (b) in subclinoid part of ICA (arrow)

hemodynamics is discussed in this context in a background of relevant literature.

Materials and methods

The study was conducted jointly in the departments of Neurosurgery and Neuroradiology, Royal Hallamshire Hospital, and the Academic Unit of Medical Physics, and Radiology, School of Medicine and Biomedical Sciences, University of Sheffield, Sheffield, UK. After obtaining appropriate consent and ethical approval the patient was recruited to the @neurIST project (www.aneurist.org).

Clinical details: This 51 years old woman, presented for the first time to cardiovascular surgeons in 1989 at the age of 31 years through obstetric unit. She had hypertension during both her pregnancies but was otherwise asymptomatic. She was a cigarette smoker, smoking 10-15 cigarettes per day. On clinical examination, she appeared fit and well with a blood pressure (BP) of 160/90 mm Hg. No femoral pulses were palpable and there was an ejection systolic murmur in the aortic area coupled with a continuous machinery murmur at left scapula. She was taking oral antihypertensives (Atenolol and Nifedipine) to control her hypertension. Subsequent investigations including DVI (digital vascular scan) done at that time revealed a severe (>80% reduction in diameter) post-ductal aortic coarctation distal to origin of left subclavian artery. X-ray chest showed typical inferior notching of 3rd and 8th ribs, bilaterally. No other congenital anomalies were detected apart from a pseudo-bicuspid aortic valve, without any

evidence of regurgitation or stenosis. One year later, the patient was treated with Dacron onlay patch graft (DOPG) repair for her coarctation with an uneventful postoperative recovery.

A follow-up MRI of heart done in July 2004 after 15 years of primary procedure demonstrated evidence of re-occurrence of coarctation with significant (60-70%) loss of luminal diameter. The stenosis occurred just distal to the origin of left subclavian artery coinciding with the site of repair. Presence of significant collaterals was also noted along with marginal concentric hypertrophy of left ventricle but adequate ejection fraction. A BRUCE treadmill stress test done to evaluate cardiac fitness demonstrated an appropriate exercise tolerance without any chest pain or ECG changes. A 24-hour BP monitoring further confirmed a satisfactory BP control (Fig-1). A completely asymptomatic status with no signs of cardiac failure was the reason to manage her conservatively.

The patient was referred to Neurosurgery in May 2007 with complaints of tingling and numbness affecting right side of her face. On further interrogation, she gave history of a similar episode three years back resulting in spontaneous resolution, but no other neurological symptoms. On clinical examination, she had no neurological deficits. An MRI demonstrated presence of two incidental IAs. First aneurysm was located in the pericallosal artery and was 4.2 mm in maximum diameter. A second small broad necked 1 mm aneurysm was also present at the origin of left anterior temporal artery arising from the proximal left middle cerebral artery (MCA). The findings were further confirmed by a

3D rotational angiogram (3DRA), which apart from two previous IAs, also revealed an approximately 1.8 mm aneurysm in the subclinoid segment of left internal carotid artery (ICA), pointing medially (Fig-2). The case was discussed in a multidisciplinary meeting with Neuroradiologists and it was found that due to its small neck the pericallosal IA was suitable for coil embolization.

3DRA acquisition: All medical images were obtained using rotational acquisition in a Philips® Integris™ Allura machine (Philips® Medical Systems, Best, The Netherlands), producing 100 images in 6 seconds, with 5 ms exposure per image. Voxel size in the reconstructed 3D images was 121 microns with reconstruction matrix of 512 x 512 x 512.

Endovascular Interventions: The pericallosal artery aneurysm was embolized under general anaesthesia in May 2008 with GDC® (Guglielmi Detachable Coils). A 6-french guided catheter was gently placed within the distal right internal carotid artery (ICA). The aneurysm was catheterized with an Excelsior® SL-10 microcatheter using a Transend® 14 guidewire (Boston Scientific, USA). The IA was packed satisfactorily using four Micrus® Cerecyte® endovascular bare platinum coils. She made an uneventful recovery from the procedure. Owing to their small size and anticipated difficulties for endovascular coiling (broad neck) remaining two aneurysms were decided to be observed by follow-up MRAs.

Flow Measurements & pc-MR protocol: MR imaging was performed

at high field strength (Achieva™ 3.0T, Philips® Medical Systems, Best, The Netherlands) using a standard 8-channel, radiofrequency receive-only head coil. The same radiographer imaged the patient and all volunteers to maximize reproducibility of overall acquisition technique. Macroscopic vascular flow and IA location were visualized using a qualitative Time-Of-Flight (TOF) MR angiography sequence (TR=25 ms; TE=3.5 ms; $\alpha=20^\circ$; visualization voxel size = $0.39 \times 0.39 \times 1.00 \text{ mm}^3$). Maximum intensity projections from this 3D dataset were used to define the placement of each quantitative phase contrast measurement plane perpendicular to the vessel under investigation. A 2D acquisition sequence (TR=8 ms; TE=4.4 ms; $\alpha=10^\circ$; field of view= $220 \times 179 \text{ mm}^2$; in-plane acquisition matrix= 128×112 ; slice thickness=5 mm) was used to acquire 40 velocity-encoded 'time points' over the cardiac cycle at each vascular location. Vector ECG triggering was used to standardize each quantitative acquisition.

The measurements were performed at three locations, both in healthy volunteers and in patient viz. left proximal ICA, left distal ICA, and left ACA A-1 segment. An appropriate maximum velocity-encoding (VENC) value was chosen (100 cm/sec) for ICA to ensure that appropriate dynamic ranges were sampled in all cases and no phase-aliasing occurred. As proximal vessels geometry has an important influence on intra-aneurysmal hemodynamics,¹³ measurements were taken at a distance of approximately 10 vessel diameters from the aneurysm location so that BCs to the numerical models could be applied at a sufficient distance from the location of the aneurysm. Measurement

Figure 3: A comparison of VFR waveforms from CoA patient (marked-red) measured in proximal ICA and average VFR waveforms from healthy volunteers (marked-blue) in the same location. The flow-rates in presence of CoA are 1.5 times higher (5.44 ml/sec) as compared with the normal healthy individuals (3.62 ml/sec). Solid horizontal lines represent average values of VFR for CoA (red) and typical (blue).

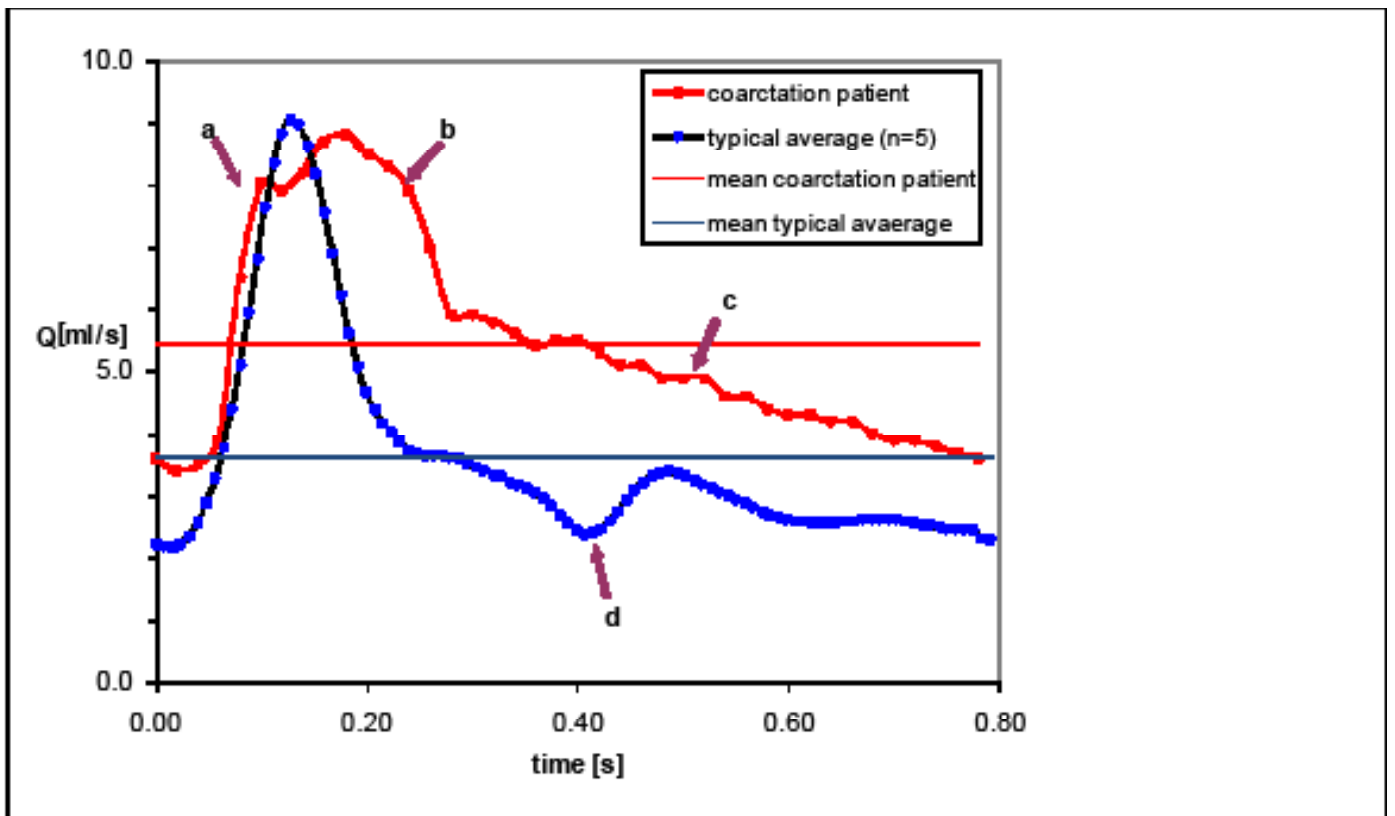


Table-1: Radiological characteristics of the IA included in the study, the pc-MR measurements in CoA patient and healthy volunteers along with the locations, types and methods of BC application

IA Location, Size* and Neck Size*		Q-flow measurements using pc-MR and BC application					
Lt ICA Subclinoid, 1.8mm, 3.1mm	Location of Q-Flow measurements	Q-av-Typical Healthy Volunteers (ml/s)	Q-av-CoA patient (ml/s)	Change (%)	BC location	BC type	BC Method†
	1. Lt ICA Proximal	3.95	5.44	+27.4	1. Lt ICA Proximal	Inlet/velocity	pc-MR
	2. Lt ICA Distal	3.7	5.07	+27.1	2. Lt ICA Distal	Outlet/velocity	pc-MR
	4. Lt ACA	1.2	2.66	+54.9	3. Lt OphthA	Outlet/pressure	Typical/population average

NB: Q-av; average blood flow, BC; boundary condition, Lt; left, Rt; right, ICA; internal carotid artery, MCA; middle cerebral artery, OphthA; ophthalmic artery, *size is reported as max diameter. †BC method refers to the analyses based on patient-specific BC from CoA patient.

location in distal vessels was approximately 3 diameters from the IA.

Measurements are reported in Fig-3 and Table-1. The manufacturer’s proprietary post-data-acquisition processing software (Q-Flow™, Philips® Medical Systems, Best, The Netherlands) was used to estimate VFR waveforms at each spatial location.

Transthoracic Doppler echocardiography: Flow and pressure measurements were performed using transthoracic Doppler echocardiography (Philips® Sonos™ 5500). The results are reported in Fig-5.

Numerical 3D models and computational fluid dynamics (CFD) analysis: The @neurIST computational tool-chain was used to reconstruct vessel and aneurysmal geometries, as described by Marzo et al.⁶⁶ The 3D transient Navier–Stokes equations were solved by using the finite-control-volume software ANSYS®-CFX™. Blood was assumed to be incompressible, with density $\rho=1060 \text{ kg/m}^3$ and Newtonian, with viscosity $\mu=0.0035 \text{ Pa}\cdot\text{s}$. The relevant hemodynamic indices were computed (Table-2) in the IA located in subclinoid part of left ICA (Fig-2) of the patient using the VFR values measured in the patient as BCs. A second analysis was performed with BCs derived from the average VFR values measured in healthy volunteers. Location, type and method of BC applied in the study are indicated in Table-1. All analyses were run in parallel on two Itanium2® 900 MHz 64-bit processors. The average time required to solve one cardiac cycle was approximately 8.6 Hr. Analyses were run for three cardiac cycles, to minimize the effects of the initial transient effects, and only results from the last cardiac cycle were post-processed.

Results

Flow measurements in intracranial arteries of healthy volunteers and patient with CoA

On comparing the patient-specific waveforms (Fig-3) from CoA patient (red) with that of typical normal individual (blue) it becomes apparent that the VFR waveform in the proximal ICA of CoA patient is higher than the one for the healthy volunteers. This is also reflected by the average values reported in Table-1 where the flow-rates for the CoA patient are 1.5 times higher (5.44 ml/sec) as compared to the normal healthy individuals (3.62 ml/sec).

The flow waveforms further illustrate that the cerebral arterial flow in CoA rises and falls slowly than that of a typical individual but the overall volume over one cardiac cycle is increased from 3.48 ml to 4.54 ml. A new broad hump (arrow-b) is seen just after the original peak (arrow-a). The systolic upstroke is delayed and slow; the peak is broader (between arrows a & b), slightly lower and dumped. The flow during diastole is almost a smooth decline curve (arrow-c) and the notch indicating the beginning of diastole is absent (arrow-d).

Contour plots for hemodynamic indices and their absolute values

Figure 4: Time-averaged WSS (top) and OSI (Oscillatory shear index) (bottom) contour plots in the left subclinoid intracranial aneurysm of the CoA patient. Whereas, areas affected by high WSS are increased in CoA patient (top, right) as compared with healthy volunteers (top, left) OSI patterns are minimally changed.

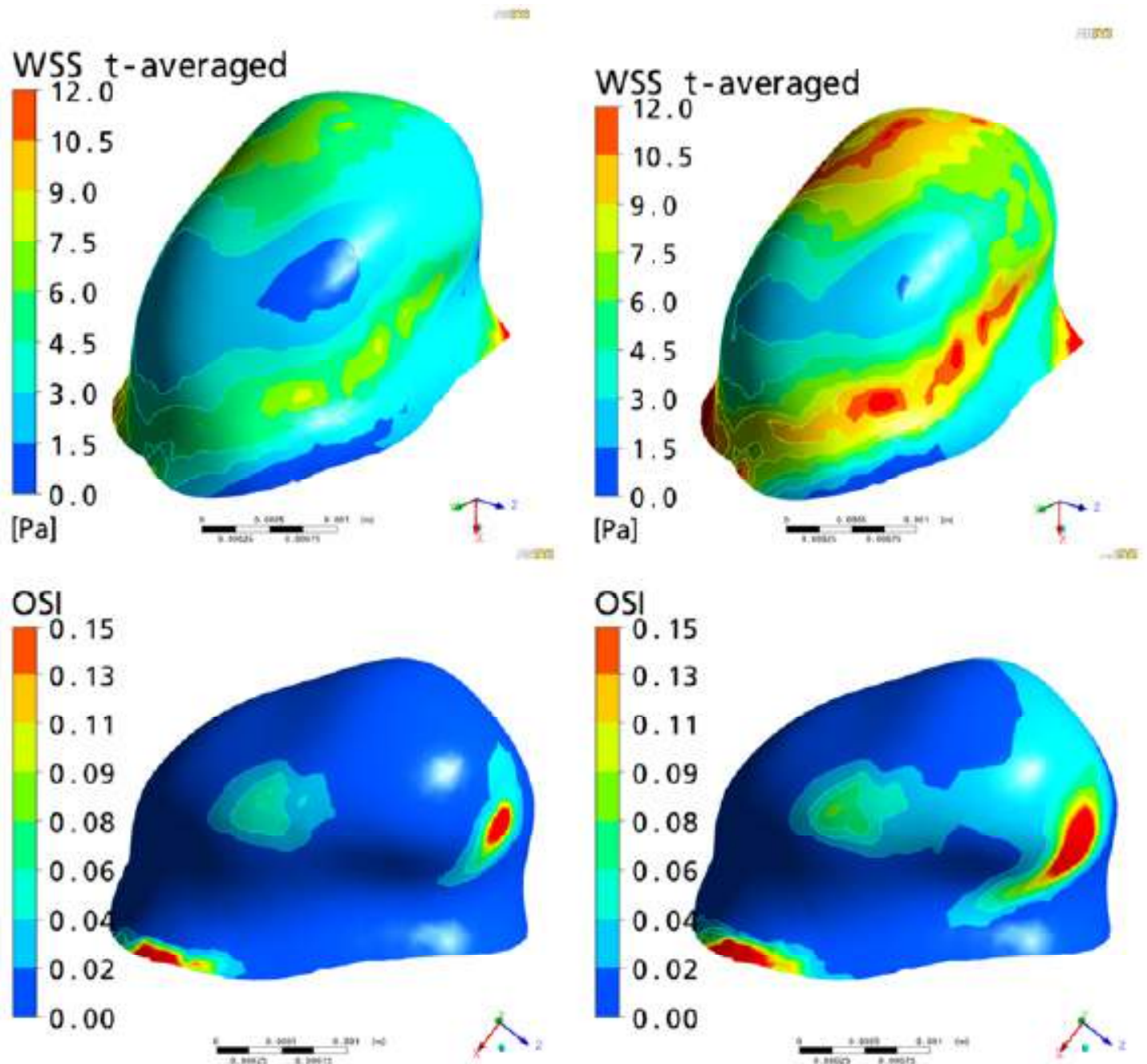
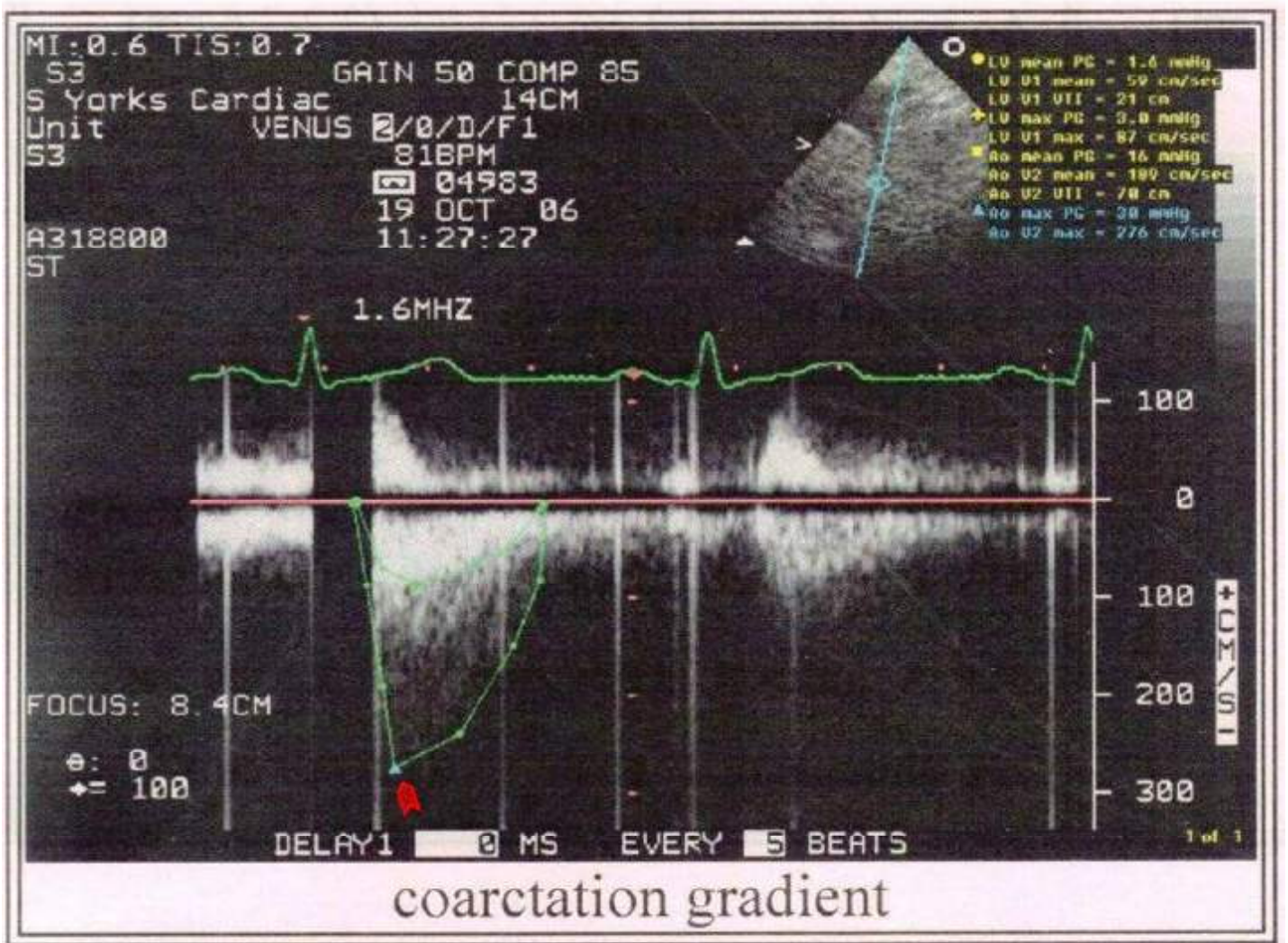


Table 2: Absolute values of WSS, OSI, velocity and pressure for IA, obtained using BCs derived from healthy volunteers and measurements taken in CoA patient by pc-MR

Hemodynamic Indices	BCs derived from healthy volunteers (without CoA)	BCs derived from patient (with CoA)	% difference
Max t-ave velocity (m/s)	0.5	0.72	+44
Space and t-ave velocity (m/s)	0.072	0.097	+35
Max OSI	0.3	0.3	0
Area of WSS below 0.4 Pa (mm ²)	0.05 (0.3%)	0.03 (0.2%)	-34
Area of WSS above 15 Pa (mm ²)	0.4 (0.4%)	3.0 (17.2%)	+650
Space and t-ave WSS in aneurysm (Pa)	5.7	9.4	+65
Max pressure on aneurysm wall (mmHg)*	122.4	140.8	+15
Area of elevated pressure (mm ²)*	3.0 (17.1%)	1.5 (8.5%)	-50%

NB: WSS; wall shear stress, OSI; oscillatory shear index, Max; maximum, ave; average, t; time, BC; boundary condition, * indicates the values at peak systole

Figure 5: Transthoracic Doppler echocardiogram showing aortic coarctation with a diastolic tail. A coarctation gradient of 30-40mmHg was seen (arrowhead) while the average aortic pressure gradient was 16 mmHg. The peak velocity in aorta was 276cm/sec.



Discussion

The CoA is a connective tissue disorder accounting for 10% of the cases of congenital heart disease.¹⁰³ The most common site of narrowing is distal to the left subclavian artery. Due to the mechanical outflow obstruction and extensive collateral formation a number of hemodynamic changes are seen in CoA. The most notable is a differential hypertension produced in the segment of aorta above the site of narrowing leading to increased aorto-cranial pressure gradients^{1,36,45,71,102} and dilatation of cervico-cephalic arteries.^{1,85} Similar changes were seen in our patient (Fig-5). A pressure gradient of 30-40 mmHg was present at the site of coarctation as compared to the mean aortic pressure gradient of 16 mmHg. The peak velocity in aorta was also increased to 276 cm/sec when compared to the peak velocity of 80-90 cm/sec in the aorta of a normal person.¹⁹ As discussed in the previous sections, it is hypothesized here that the regional cerebral blood flow (rCBF) in CoA patients should increase as a consequence of these changes.

It is surprising to see that such little attention is devoted on the effects of CoA on rCBF. The first available study on the subject was conducted by Hafkenschiel et al³⁷ in 1949. They measured rCBF and cerebral oxygen consumption in two patients with CoA using nitrous oxide (N₂O) saturation method and found that the rCBF in patients with CoA was higher as compared with normal subjects.

A similar study was done by Rowe and colleagues⁸⁵ in 1964 who measured the rCBF in 20 CoA patients using the same technique. The rCBF was measured in these patients before and after the surgical correction of CoA and the results were compared with rCBF values obtained in normal subjects in their previous study,⁸⁶ and rCBF values specific to hypertensive patients.¹⁸ No significant differences were noted in the rCBF pre and post surgical repair of coarctation and, between CoA patients and hypertensive patients. Interestingly, the comparison of rCBF in CoA patients and healthy volunteers suggested that the values of average rCBF measured by them (63±13 ml/100 gm/ min) were approximately 21% higher compared to the rCBF measured in 8 normal subjects (52±12 ml/100 gm/ min)⁸⁶ but not statistically significant. The postoperative measurements in this study were taken at an average interval of 21 months (maximum 9.25 yrs) from the time of surgery which may have obscured some of the differences. Re-occurrence of coarctation is a frequent complication following surgery that can occur in 41-86% patients.⁴⁴ The similar patterns were observed in our patient where 60-70% loss of luminal diameter occurred 14 years after repair. As the diameter of aorta was not assessed by Rowe and colleagues⁸⁵ at the time of rCBF measurements, the possibility of recoarctation in these patients cannot be ruled out which might account for the lack of difference in the rCBF before and after surgical correction.

The measurements of rCBF in both studies were performed using the oldest available technique based on N₂O diffusion and Fick's principle introduced by Kety and Schmidt in 1951.⁷⁷ The technique provides the measurements of global CBF rather than the regional values. The accuracy of measurements is

dependent upon the reliability of the blood sample withdrawn from a single jugular vein which can be influenced by the flow variations in dural sinuses and torcula.⁵² With the advent of new technology, the technique of rCBF measurement has evolved tremendously. The use of pc-MR in this context is gaining a rapid popularity.^{10,25,26,84,101,107} The rCBF can be measured using this technique in a simple non-invasive manner without the need of any intravenous contrast administration and has been validated widely by means of in vitro and in vivo experiments.^{8,12,28,58}

Recent evidence however indicates that the local variations in the hemodynamics that play an important role in the etiopathogenesis of IAs^{32,38,40-42,65,69,72,104} highlighting the importance of assessing the local flow patterns. No previous study however has examined the local hemodynamics in presence of CoA. According to the Hagan-Poiseuille law, we hypothesized that the local VFR should increase in patients with CoA. The pc-MR measurements performed prior to repair of the CoA in our study confirmed this hypothesis by demonstrating an increase of local regional CBF by 27.1 to 54.9% (Table-1) in ICA and ACA respectively, when compared to healthy volunteers. As a result space and time averaged velocity and max time average velocities inside the coincidental IA present were also increased by 35-44% (Table-2) when the BCs specific to CoA were used.

We further hypothesize that the increased VFR can be an important contributory factor in the increased incidence of IAs in presence of CoA. The possible mechanisms responsible for increased incidence of IAs in CoA patients are explored in the further sections of this manuscript. Eppinger was the first person to draw attention towards the association between CoA and IAs in 1871.²⁷ Whereas the exact mechanisms responsible for this increased incidence remained obscure, arterial hypertension has been suggested as a possible underlying cause by most of the authors (Table-3).^{3,9,24,50,75,78,92,95} Stehbens was the strongest proponent of this theory who particularly stressed on the importance of hypertension in this context while denying the role of all other factors including vessel wall abnormalities.^{92,95} This assumption is probably based on two observations. First, hypertension is often a constant feature in CoA patients. Second, hypertension has been considered as a major risk factor for the development of IAs even without CoA.^{22,99} In spite of an increased prevalence of IAs in hypertensive patients the role of hypertension in this context has been questioned by many authors. McCormick and Schmalstieg found no relationship between arterial hypertension and IAs in 250 patients they studied.⁶⁷ In a similar study conducted in 212 cases, Andrews and Spiegel⁶ did not find significant elevation in the blood pressure in patients with IAs compared with the general population. However, studies supporting hypertension as a risk factor for the development and rupture of IAs outnumber the studies refuting it. De la Monte et al²² found high degree of correlation ($p < 0.001$) between systemic hypertension and development of saccular IAs. In one of the largest studies conducted including 20,767 elderly patients Taylor et al⁹⁹ found hypertension as an independent major risk factor for aneurysmal SAH.

Although, hypertension can be an important contributory

Table-3: A comprehensive review of different mechanisms proposed for the increased incidence of IAs in CoA patients

Author/ Year	No. of Patients	IA location/No.	HTN at the time IA diagnosed	Associated features	Proposed Mechanism(s)
Abbot (1928) [1]	6	ACA, AcomA, VA, PcomA, MCA	Yes	Reported one case of his own (MCA), rest 5 cases collected from literature	Congenital IA
Laitinen et al (1960) [62]	1	Pericallosal/ Callosomarginal	Yes	Oxycephalic deformity of skull	Possible developmental errors
Patel et al (1971) [78]	7	ICA, AcomA(3), ACA(3), PcomA, BA	Yes	Only pediatric population (<19 yrs) reviewed, 12% had CoA coexisting with IAs	HTN
Banna et al (1971) [9]	1	PCA	NA	Source of SAH was dilated spinal collaterals	Medial hypoplasia of arteries of CoW + HTN
Stehbens (1989) [92]				Review article	HTN
Orsi et al. (1993) [75]	1	MCA, ICA	NA		HTN
Schievink et al (1996)[87]	1	MCA	No		Development errors of Neural Crest leading to defective collagen and elastin formation
Ishii et al (2001) [50]	1	AcomA	Yes	Coarctation of abdominal aorta	HTN
Ahmetoglu et al (2002) [3]	1	B/L MCA	Yes	Coarctation of abdominal aorta	HTN ± hemodynamic shear stress
Mercado et al. (2002)[70]	3	ICA, PcomA(2), PeriA	Yes	Provided a comprehensive review of the distinct clinical behavior of IAs in presence of CoA	Development errors of Neural Crest
Connolley et al (2003)[15]	10	ICA, MCA, PICA, PCA, PcomA, AChoA, BA tip	Yes (in 7 out of 10 patients)	Found 10% incidence of IAs in patients with CoA, no significant difference in BP of patients with and without IAs	Development errors of Neural Crest
Cowan et al (2004)[17]	1	PcomA	No	Coexisting Alagille syndrome (arteriohepatic dysplasia), progression of infundibulum to PcomA Aneurysm	Developmental defects
Harikrishnan (2005) [39]	1	BA, VA	Yes	CoA of Descending aorta, coronary artery aneurysms	Atherosclerosis
Hudaoglu et al (2006)[48]	1	PcomA	No	Raised strong suspicions about HTN alone being a factor for the increased incidence of IA in CoA	Development errors of Neural Crest
Kan et al (2007) [53]	1	ICA	NA	Fusiform aneurysm associated with PHACES syndrome, positive family history of IAs	Development errors of Neural Crest
Singh et al (2009) (Present study)	1	ICA, MCA, PeriA	No	Measured the CBF in CoA patient and proposed WSS as an important factor in the formation of IAs in these patients	Hemodynamic WSS

NB: PHACES syndrome; posterior fossa malformations, facial hemangiomas, arterial anomalies, CoA, cardiac defects, eye abnormalities and sterna defects, NA; not available, B/L; bilateral, CoW; circle of Willis, BP; blood pressure, PeriA; pericallosal artery, AChoA; anterior choroidal artery, PCA; posterior cerebral artery, BA; basilar artery, VA; vertebral artery, PICA; posterior inferior cerebellar artery, HTN; Hypertension, MCA, ICA & ACA; middle, internal & anterior cerebral arteries.

force in the etiopathogenesis of IAs in these patients, it cannot be the sole contributor. Hudaoglu et al⁴⁸ raised a question on hypertension alone being a factor in the etiopathogenesis of IAs in CoA patients. The fact is further supported by the observation that IAs may develop or rupture even in normotensive patients, years after the repair of CoA.^{30,61,70,76} Additionally, hypertension was not uniformly noted in the patients of CoA reported to have IAs.^{15,87} The IAs were developed in our patient 17 years after the surgical correction of CoA. However, recoarctation of the repaired segment occurred during this period (>70% reduction in aortic diameter), the patient remained completely asymptomatic with a very well controlled blood pressure (Fig-1). Our findings also indicate towards the role of other factors working independent of arterial hypertension.

Laitinen and Snellman⁶² in 1960 found that apart from CoA, aneurysms of Pericallosal artery region were also associated with other concomitant malformations such as craniosynostosis and kyphoscoliosis. They believed that coexistence of these malformations with IAs is secondary to a common developmental error playing a role in their etiology. Embryologically; heart, aorta and cervico-cephalic arteries all share a common origin from neural crest. After recognizing the association between a variety of congenital heart diseases and IAs, Schievink et al⁸⁷ attributed the occurrence of IAs in CoA patients to the developmental errors of neural crest resulting in abnormal vessel wall collagen. The same theory was later supported many other authors (Table-3).^{15,17,48,53,70}

Hemodynamic stress due to increased blood flow has long been implicated in the pathogenesis of IAs. Development of IAs is reported in association with a wide range of conditions responsible for increased flow related WSS. Padgett was first to draw attention towards the relationship between anatomical variations in circle of Willis and increased incidence of IAs.⁷⁷ The similar findings were confirmed by other workers.^{4,82,94} Kayambe et al⁵⁶ observed that there was a definitive correlation between the site of vascular asymmetry and the location of IA formation. This increased incidence of IAs in presence of vascular asymmetry is thought to be caused by increased hemodynamic stress secondary to compensatory increase in blood flow.^{56,93,94}

Iatrogenic carotid artery ligation is a well established technique to produce IAs in experimental animals.^{38,40-42,51,73} Increased hemodynamic shear stress has been considered a major factor in the production of these experimental IAs.^{32,38,40-42,51,73} Apart from the carotid ligation, induced hypertension and administration of BAPN (beta aminopionitrile; a lathyrogen used to render arterial walls fragile), can potentiate the occurrence of IAs in these models. Handa et al³⁸ divided their experimental animals into three cohorts: no carotid ligation, unilateral carotid ligation and bilateral carotid ligation. Whereas, all rats were made hypertensive and fed on BAPN, no IA was induced where carotid artery was not ligated. Furthermore, the IAs was always formed corresponding to the sites where hemodynamic stress was expected to increase after carotid ligation.

Congenital absence of ICA,^{14,47,96} arteriovenous malformations

(AVMs),^{68,81,100} Takayasu's arteritis,^{54,98} Moyamoya disease,^{2,55,59} and presence of persistent fetal circulation^{5,63,109} are other similar conditions where increased IAs are encountered due to increased-flow-related WSS. Development of IAs has also been observed following extra-intracranial bypass procedures,^{29,60,74} again secondary to increased rCBF. Resolution of these flow related IAs can occur once the cerebral hemodynamics is reestablished by addressing the underlying pathology.^{79,97}

The importance of hemodynamic WSS in the context of CoA is somewhat poorly explored. Ahmetoglu et al (2002)³ indicated that arterial wall injury secondary to increased hemodynamic shear forces may be an important factor in the IA formation while discussing their case of abdominal aortic coarctation (AbCoA). However, the statement probably reflects their opinion towards the etiopathogenesis of IAs in general population rather than in patients with CoA. Furthermore, the inference was merely based on the literature based evidence rather than any experimental work. They finally concluded that hypertension was the main factor responsible for the rupture and growth of IAs in patients with AbCoA.³

We hypothesize that the higher WSS values secondary to increased flow-rates in cerebral circulation can be an important contributory factor in the pathogenesis of IAs in presence of CoA. WSS is a frictional force exerted tangentially on the arterial endothelium by flowing blood. It is proportional to the blood viscosity and velocity gradients. The average physiological range of arterial WSS has been suggested to lie between 1.5-2.0 Pa by Malek et al.⁶⁴ It is widely accepted now that damage to the arterial and subsequently aneurysmal wall by hemodynamic forces plays a crucial role in the etiopathogenesis of IAs.^{11,32,38,40-42,65,69,72,91,104} High supra-physiological and low infra-physiological values of WSS have been associated with initiation, growth and rupture of aneurysms.^{11,32,38,40-42,65,69,72,91,104} The values of space and time averaged WSS as well as the area affected by supra-physiological WSS (>15Pa) were increased in our patient by 65% and 650%, respectively (Table-2). This exponential rise in the high supra-physiological WSS may play an important role in the etiopathogenesis of IAs in patients with CoA.

Various authors tried to explain the underlying mechanisms involved in the WSS induced vascular remodeling. The normal endothelial cell (EC) function and structure are regulated by WSS through a process called mechanotransduction.^{21,20} The shear stress is sensed by a number of mechanoreceptors including basal adhesion points of ECs, cell junctions, and nuclear membrane.^{21,20} WSS also activates stretch-sensitive ion channels such as phospholipids and integrins in cellular membrane.^{21,20} Increased production of matrix metalloproteinase (MMP-13) by ECs has been demonstrated after their prolonged exposure to high WSS which, in turn, leads to degeneration of the internal elastic lamina.⁹⁰ It has been demonstrated by a number of workers^{16,31,80} that WSS increases endothelial production of nitric oxide (NO) by inducing an enzyme responsible for its synthesis (iNOS; inducible nitric oxide synthase). Fukuda et al³¹ found a high concentration of iNOS at the site of IA formation, in both rat and human arteries and concluded that iNOS is a prerequisite for

de novo development of IAs in cerebral vessels. In 1995, Wang et al¹⁰⁴ showed that smooth muscle cells (SMCs) in arterial wall can also respond to WSS in intact arteries by virtue of interstitial flow generated by transmural flow gradients, further accentuating the vessel wall damage.

In addition to WSS, oscillatory shear index (OSI) has also been recognized as an important hemodynamic factor in the aneurysmal pathogenesis.^{33-35,43,65} It is a measure of the oscillatory nature of shear forces.^{33-35,43,65} This index, which has a range of between 0 and 0.5, represents the fraction of the cardiac cycle over which the instantaneous shear force vector forms an angle greater than 90 degrees to the time-average direction of the same force. Consistently high values of OSI have been associated with EC dysfunction.⁴³ Changes in cell structure secondary to cyclic mechanical stress have been demonstrated by Wang et al.¹⁰⁴ resulting in disruption of the actin cytoskeleton of ECs. Glor and colleagues propose 0.2 as a threshold value for OSI above which endothelial damage is initiated.^{33,34} Whereas, no change was observed in the maximum OSI in presence of CoA (Table-2), the values obtained from both analyses (0.3) remained above this critical threshold. This indicates towards the possible role of high OSI in the EC damage in patients with IAs irrespective of presence or absence of CoA.

Apart from being a known risk factor for the formation of IAs, CoA has also been associated with increased incidence of IA rupture (4.8%).^{15,48,70,106} No satisfactory explanation is provided for the association between the two entities. This increased tendency for early aneurysmal rupture can possibly be explained by analyzing the hemodynamic factors computed for our patient (Table-2). Whereas the values for maximum pressure on IA wall have increased by 15% in patient with CoA, the area affected by high pressure is actually decreased by 50%. In other words, in the context of our CoA patient, the pressure on the IA wall is more focal in nature in presence of CoA and may be an important underlying factor predisposing to early aneurysmal rupture. High supra-physiological values of WSS have also been associated with endothelial cell dysfunction.^{11,32,38,40-42,64,65,69,72,91,104} The exponential rise (by 650%) in the area affected by high supra-physiological WSS (>15Pa) may also play a role in early IA rupture in patient with CoA.

Limitations of the study

Due to technical limitations, we could not perform extensive measurements in cerebral arteries other than ICA and ACA. It is however expected that the VFR will increase in other arteries as well provided other parameters in the Hagan-Poiseuille (Eq-1) equation remain constant. The current study therefore reflects the need of further studies performed in larger cohort of patients with CoA.

Conclusions

Our study demonstrates that the cerebral arterial flow-rates in CoA patients are significantly higher when compared with average arterial flow-rates in healthy population. Furthermore,

the values of space and time averaged WSS and the area affected by suprathreshold WSS (>15Pa) were increased in our patient by 65% and 650%, respectively. The values of maximum OSI however, remained unaffected by the presence of CoA. Increased hemodynamic WSS secondary to the increased rCBF may play an important role in the pathogenesis of IAs in CoA patients. The more focalized pressure impingement on the aneurysmal wall in CoA patients may be an important underlying factor affecting the early aneurysmal rupture.

The lack of clear knowledge about the rCBF in CoA patients and the existing controversies in the etiopathogenesis of IAs in these patients emphasizes the importance of the findings of the current study.

Acknowledgements

The authors would like to extend their acknowledgments to Mr. David Capener and the MRI department to for their help in obtaining the pc-MR measurements. Furthermore, we are thankful to all developers of the @neurIST computational tool-chain and European Commission for funding this study.

Ethical Approvals

The project has appropriate ethical approvals for the required research. The ethical matters are managed by Project Ethical Committee, Oxford, UK (Oxfordshire Research Ethics Committee-A Study Number: 07/Q1604/53). A copy of the ethical approval can be provided as and when required.

References:

1. Abbott ME. A statistical study and historical retrospect of 200 recorded cases, with autopsy, of stenosis or obliteration of the descending arch in subjects above the age of two years. *Am Heart J*:1928;392-421.
2. Adams HP, Jr., Kassell NF, Wisoff HS, Drake CG. Intracranial saccular aneurysm and moyamoya disease. *Stroke* 10:1979;174-179.
3. Ahmetoğlu A, Koşucu P, Sari A, Gümele HR. Abdominal aortic coarctation associated with multiple intracranial aneurysms. *European Journal of Radiology Extra* (46):2003;38-41.
4. Alpers BJ, Berry RG. Circle of Willis in cerebral vascular disorders. The anatomical structure. *Arch Neurol* 8:1963;398-402.
5. Ali S, Walker MT. Bilateral persistent trigeminal arteries associated with bilateral carotid aneurysms. *J Vasc Interv Radiol*. 2007;18:692-694.
6. Andrews RJ, Spiegel PK. Intracranial aneurysms. Age, sex, blood pressure, and multiplicity in an unselected series of patients. *J Neurosurg*. 1979;51:27-32.
7. Atkinson JL, Sundt TMJ, Houser OW, Whisnant JP. Angiographic frequency of anterior circulation intracranial aneurysms. *J Neurosurg*. 1989;70:551-555.
8. Bakker CJ, Kouwenhoven M, Hartkamp MJ, Hoogeveen RM, Mali WP. Accuracy and precision of time-averaged flow as measured by nontriggered 2D phase-contrast MR angiography, a phantom evaluation. *Magn Reson Imaging*. 1995;13:959-965.
9. Banna MM, Rose PG, Pearce GW. Coarctation of the aorta as a cause of spinal subarachnoid hemorrhage. Case report. *J Neurosurg*. 1973;39:761-

- 763.
10. Buijs PC, Krabbe-Hartkamp MJ, Bakker CJ, et. al. Effect of age on cerebral blood flow: measurement with ungated two-dimensional phase-contrast MR angiography in 250 adults. *Radiology*. 1998;209:667-674.
 11. Burleson AC, Strother CM, Turitto VT. Computer modeling of intracranial saccular and lateral aneurysms for the study of their hemodynamics. *Neurosurgery*. 1995;37:774-82; discussion 782-7782; discussion 782-4.
 12. Caputo GR, Kondo C, Masui T, et. al. Right and left lung perfusion: in vitro and in vivo validation with oblique-angle, velocity-encoded cine MR imaging. *Radiology*. 1991;180:693-698.
 13. Castro MA, Putman CM, Cebral JR. Computational fluid dynamics modeling of intracranial aneurysms: effects of parent artery segmentation on intra-aneurysmal hemodynamics. *AJNR Am J Neuroradiol*. 2006;27:1703-1709.
 14. Chen L, Liu J-M, Zhou D. Congenital absence of the right common carotid artery, internal carotid artery and external carotid artery associated with anterior communicating artery aneurysm: a rare case. *Neurol Sci*. 2008;29:485-487.
 15. Connolly HM, Huston J 3rd, Brown RDJ, et. al. Intracranial aneurysms in patients with coarctation of the aorta: a prospective magnetic resonance angiographic study of 100 patients. *Mayo Clin Proc*. 2003;78:1491-1499.
 16. Cooke JP, Stamler J, Andon N, et. al. Flow stimulates endothelial cells to release a nitrovasodilator that is potentiated by reduced thiol. *Am J Physiol*. 1990;259:H804-12.
 17. Cowan JAJ, Barkhoudarian G, Yang LJS, Thompson BG. Progression of a posterior communicating artery infundibulum into an aneurysm in a patient with Alagille syndrome. Case report. *J Neurosurg*. 2004;101:694-696.
 18. Crumpton CW, Rowe GG, Capps RC, Whitmore JJ, Murphy QR. The effect of hexamethonium upon cerebral blood flow and metabolism in patients with premalignant and malignant hypertension. *Circulation*. 1955;11:106-109.
 19. Daley PJ, Sagar KB, Wann LS. Doppler echocardiographic measurement of flow velocity in the ascending aorta during supine and upright exercise. *Br Heart J*. 1985;54:562-567.
 20. Davies PF. Flow-mediated endothelial mechanotransduction. *Physiol Rev*. 1995;75:519-560.
 21. Davies PF, Tripathi SC. Mechanical stress mechanisms and the cell. An endothelial paradigm. *Circ Res*. 1993;72:239-245.
 22. de la Monte SM, Moore GW, Monk MA, Hutchins GM. Risk factors for the development and rupture of intracranial berry aneurysms. *Am J Med*. 1985;78:957-964.
 23. Drake CG. Progress in cerebrovascular disease. Management of cerebral aneurysm. *Stroke*. 1981;12:273-283.
 24. Du Boulay GH. Some observations on the natural history of intracranial aneurysms. *Br J Radiol*. 1965;38:721-757.
 25. Enzmann DR, Marks MP, Pelc NJ. Comparison of cerebral artery blood flow measurements with gated cine and ungated phase-contrast techniques. *J Magn Reson Imaging*. 1993;3:705-712.
 26. Enzmann DR, Ross MR, Marks MP, Pelc NJ. Blood flow in major cerebral arteries measured by phase-contrast cine MR. *AJNR Am J Neuroradiol*. 1994;15:123-129.
 27. Eppinger H. Stenosis aortae congenita seu isthmus persistans. *Vjschr Prakt aheilk*. 1871;112:31-67.
 28. Evans AJ, Iwai F, Grist TA, et. al. Magnetic resonance imaging of blood flow with a phase subtraction technique. In vitro and in vivo validation. *Invest Radiol*. 1993;28:109-115.
 29. Fleischer AS, Faria MAJ, Hoffmann JC. Pseudoaneurysm complicating superficial temporal artery--middle cerebral artery bypass. *Surg Neurol*. 1979;12:305-306.
 30. Forfang K, Rostad H, Sorland S, Levorstad K. Late sudden death after surgical correction of coarctation of the aorta. Importance of aneurysm of the ascending aorta. *Acta Med Scand*. 1979;206:375-379.
 31. Fukuda S, Hashimoto N, Naritomi H, et. al. Prevention of rat cerebral aneurysm formation by inhibition of nitric oxide synthase. *Circulation*. 2000;101:2532-2538.
 32. Gao L, Hoi Y, Swartz DD, et. al. Nascent aneurysm formation at the basilar terminus induced by hemodynamics. *Stroke*. 2008;39:2085-2090.
 33. Glor FP, Ariff B, Hughes AD, et. al. The integration of medical imaging and computational fluid dynamics for measuring wall shear stress in carotid arteries. *Conf Proc IEEE Eng Med Biol Soc*. 2004;2:1415-1418.
 34. Glor FP, Long Q, Hughes AD, et. al. Reproducibility study of magnetic resonance image-based computational fluid dynamics prediction of carotid bifurcation flow. *Ann Biomed Eng*. 2003;31:142-151.
 35. Goubergrits L, Kertzschner U, Schoneberg B, et. al. CFD analysis in an anatomically realistic coronary artery model based on non-invasive 3D imaging: comparison of magnetic resonance imaging with computed tomography. *Int J Cardiovasc Imaging*. 2008;24:411-421.
 36. Gupta TC, Wiggers CJ. Basic hemodynamic changes produced by aortic coarctation of different degrees. *Circulation*. 1951;3:17-31.
 37. Hafkenschiel JHJ, Crumpton CW, Moyer JH. Blood flow and oxygen consumption of the brain in coarctation of the aorta. *Proc Soc Exp Biol Med*. 1949;71:165-167.
 38. Handa H, Hashimoto N, Nagata I, Hazama F. Saccular cerebral aneurysms in rats: a newly developed animal model of the disease. *Stroke*. 1983;14:857-866.
 39. Harikrishnan S, Stigimon J, Tharakan JM. Intracranial aneurysms, coronary aneurysms and descending aortic coarctation--unreported association. *Int J Cardiol*. 2005;99:329-330.
 40. Hashimoto N, Handa H, Hazama F. Experimentally induced cerebral aneurysms in rats. *Surg Neurol*. 1978;10:3-8.
 41. Hashimoto N, Handa H, Nagata I, Hazama F. Experimentally induced cerebral aneurysms in rats: Part V. Relation of hemodynamics in the circle of Willis to formation of aneurysms. *Surg Neurol*. 1980;13:41-45.
 42. Hashimoto N, Kim C, Kikuchi H, et. al. Experimental induction of cerebral aneurysms in monkeys. *J Neurosurg*. 1987;67:903-905.
 43. He X, Ku DN. Pulsatile flow in the human left coronary artery bifurcation: average conditions. *J Biomech Eng*. 1996;118:74-82.
 44. Hesslein PS, McNamara DG, Morriss MJ, Hallman GL, Cooley DA. Comparison of resection versus patch aortoplasty for repair of coarctation in infants and children. *Circulation*. 1981;64:164-168.
 45. Hom JJ, Ordovas K, Reddy GP. Velocity-encoded cine MR imaging in aortic coarctation: functional assessment of hemodynamic events. *Radiographics*. 2008;28:407-416.
 46. Hop JW, Rinkel GJ, Algra A, van Gijn J. Case-fatality rates and functional outcome after subarachnoid hemorrhage: a systematic review. *Stroke*. 1997;28:660-664.
 47. Horie N, Tsutsumi K, Kaminogo M, et. al. Agenesis of the internal carotid artery with transcavernous anastomosis presenting with an anterior communicating artery aneurysm--a case report and review of the literature. *Clin Neurol Neurosurg*. 2008;110:622-626.
 48. Hudaoglu O, Kurul S, Cakmakci H, et. al. Aorta coarctation presenting with intracranial aneurysm rupture. *J Paediatr Child Health*. 2006;42:477-479.

49. Inagawa T. Trends in incidence and case fatality rates of aneurysmal subarachnoid hemorrhage in Izumo City, Japan, between 1980-1989 and 1990-1998. *Stroke*. 2001;32:1499-1507.
50. Ishii K, Isono M, Kasai N, et. al. Midaortic syndrome in childhood associated with a ruptured cerebral aneurysm: a case report. *Surg Neurol*. 2001;55:209-212.
51. Jamous MA, Nagahiro S, Kitazato KT, et. al. Endothelial injury and inflammatory response induced by hemodynamic changes preceding intracranial aneurysm formation: experimental study in rats. *J Neurosurg*. 2007;107:405-411.
52. Joseph M, Nates, JL. Stable Xenon Computed Tomography Cerebral Blood Flow Measurement In Neurological Disease: Review And Protocols. *The Internet Journal of Emergency and Intensive Care Medicine*. 2000;4(2).
53. Kan P, Liu JK, Couldwell WT. Giant fusiform aneurysm in an adolescent with PHACES syndrome treated with a high-flow external carotid artery-M3 bypass. Case report and review of the literature. *J Neurosurg*. 2007;106:495-500.
54. Kanda M, Shinoda S, Masuzawa T. Ruptured vertebral artery-posterior inferior cerebellar artery aneurysm associated with pulseless disease-- case report. *Neurol Med Chir (Tokyo)*. 2004;44:363-367.
55. Kawaguchi S, Sakaki T, Morimoto T, Kakizaki T, Kamada K. Characteristics of intracranial aneurysms associated with moyamoya disease. A review of III cases. *Acta Neurochir (Wien)*. 1996;138:1287-1294.
56. Kayembe KN, Sasahara M, Hazama F. Cerebral aneurysms and variations in the circle of Willis. *Stroke*. 1984;15:846-850.
57. Kety SS. The theory and applications of the exchange of inert gas at the lungs and tissues. *Pharmacol Rev*. 1951;3:1-41.
58. Kondo C, Caputo GR, Semelka R, et. al. Right and left ventricular stroke volume measurements with velocity-encoded cine MR imaging: in vitro and in vivo validation. *AJR Am J Roentgenol*. 1991;157:9-16.
59. Konishi Y, Kadowaki C, Hara M, Takeuchi K. Aneurysms associated with moyamoya disease. *Neurosurgery*. 1985;16:484-491.
60. Kurokawa T, Harada K, Ishihara H, et. al. De novo aneurysm formation on middle cerebral artery branches adjacent to the anastomotic site of superficial temporal artery-middle cerebral artery bypass surgery in two patients: technical case report. *Neurosurgery*. 2007;61:E297-8; discussion E298.
61. Laborde F, Bical O, Lemoine G, Neveux JY. [Rupture of a dissecting aneurysm of the ascending aorta 10 years after therapy of coarctation. Apropos of a case of a 10-year-old girl]. *Sem Hop*. 1983;59:2937-2938.
62. Laitinen L, Snellman A. Aneurysms of the pericallosal artery: a study of 14 cases verified angiographically and treated mainly by direct surgical attack. *J Neurosurg*. 1960;17:447-458.
63. Li MH, Li WB, Pan YP, Fang C, Wang W. Persistent primitive trigeminal artery associated with aneurysm: report of two cases and review of the literature. *Acta Radiol*. 2004;45:664-668.
64. Malek AM, Alper SL, Izumo S. Hemodynamic shear stress and its role in atherosclerosis. *JAMA*. 1999;282:2035-2042.
65. Mantha A, Karmonik C, Benndorf G, Strother C, Metcalfe R. Hemodynamics in a cerebral artery before and after the formation of an aneurysm. *AJNR Am J Neuroradiol*. 2006;27:1113-1118.
66. Marzo A, Singh P, Reymond P, et. al. Influence of inlet boundary conditions on the local haemodynamics of intracranial aneurysms. *Comput Methods Biomech Biomed Engin*. 2009;12:431-444.
67. McCormick WF, Schmalstieg EJ. The relationship of arterial hypertension to intracranial aneurysms. *Arch Neurol*. 1977;34:285-287.
68. Meisel HJ, Mansmann U, Alvarez H, et. al. Cerebral arteriovenous malformations and associated aneurysms: analysis of 305 cases from a series of 662 patients. *Neurosurgery*. 2000;46:793-800; discussion 800-800; discussion 800-2.
69. Meng H, Wang Z, Hoi Y, et. al. Complex hemodynamics at the apex of an arterial bifurcation induces vascular remodeling resembling cerebral aneurysm initiation. *Stroke*. 2007;38:1924-1931.
70. Mercado R, Lopez S, Cantu C, et. al. Intracranial aneurysms associated with unsuspected aortic coarctation. *J Neurosurg*. 2002;97:1221-1225.
71. Mohiaddin RH, Kilner PJ, Rees S, Longmore DB. Magnetic resonance volume flow and jet velocity mapping in aortic coarctation. *J Am Coll Cardiol*. 1993;22:1515-1521.
72. Morimoto M, Miyamoto S, Mizoguchi A, et. al. Mouse model of cerebral aneurysm: experimental induction by renal hypertension and local hemodynamic changes. *Stroke*. 2002;33:1911-1915.
73. Nagata I, Handa H, Hashimoto N, Hazama F. Experimentally induced cerebral aneurysms in rats: Part VI. Hypertension. *Surg Neurol*. 1980;14:477-479.
74. Nishimoto T, Yuki K, Sasaki T, et. al. A ruptured middle cerebral artery aneurysm originating from the site of anastomosis 20 years after extracranial-intracranial bypass for moyamoya disease: case report. *Surg Neurol*. 2005;64:261-5; discussion 265.
75. Orsi P, Rosa G, Liberatori G, Lunardi PP, Ferrante L. Repair of two unruptured intracranial aneurysms in the presence of coarctation of the aorta-anesthetic implications and management. *J Neurosurg Anesthesiol*. 1993;5:48-51.
76. Ostergaard JR, Hog E. Incidence of multiple intracranial aneurysms. Influence of arterial hypertension and gender. *J Neurosurg*. 1985;63:49-55.
77. Padget DH. The circle of Willis: its embryology and anatomy. In: Dandy WE, ed. *Intracranial Arterial Aneurysms*. New York, NY: Comstock Publishing Co; 1944:67-90.
78. Patel AN, Richardson AE. Ruptured intracranial aneurysms in the first two decades of life. A study of 58 patients. *J Neurosurg*. 1971;35:571-576.
79. Peltier J, Vinchon M, Soto-Ares G, Dhellemmes P. Disappearance of a middle cerebral artery aneurysm associated with Moyamoya syndrome after revascularization in a child: case report. *Childs Nerv Syst*. 2008;24:1483-1487.
80. Pohl U, Herlan K, Huang A, Bassenge E. EDRF-mediated shear-induced dilation opposes myogenic vasoconstriction in small rabbit arteries. *Am J Physiol*. 1991;261:H2016-23.
81. Redekop G, TerBrugge K, Montanera W, Willinsky R. Arterial aneurysms associated with cerebral arteriovenous malformations: classification, incidence, and risk of hemorrhage. *J Neurosurg*. 1998;89:539-546.
82. Riggs HE, Rupp C. Miliary aneurysms: Relations of anomalies of circle of Willis to formation of aneurysms. *Arch Neurol Psychiat* 49:1943;615-616.
83. Reifenshtein GH, Levine SA, Gross RE. Coarctation of the aorta. A review of 104 autopsied cases of the "adult type", 2 years of age or older. *Am Heart J* 1947; 33(2): 146-169.
84. Rordorf G, Koroshetz WJ, Copen WA, et. al. Diffusion- and perfusion-weighted imaging in vasospasm after subarachnoid hemorrhage. *Stroke*. 1999;30:599-605.
85. Rowe GG, Castillo CA, Afonso S, Young WP, Crumpton CW. Cerebral blood flow in coarctation of the aorta. *J Clin Invest*. 1964;43:1922-1927.
86. Rowe GG, Maxwell GM, Castillo CA, Freeman DJ, Crumpton CW. A study in man of cerebral blood flow and cerebral glucose, lactate and

- pyruvate metabolism before and after eating. *J Clin Invest.* 1959;38:2154-2158.
87. Schievink WI, Mokri B, Piepgras DG, Gittenberger-de Groot AC. Intracranial aneurysms and cervicocephalic arterial dissections associated with congenital heart disease. *Neurosurgery.* 1996;39:685-9; discussion 689-69; discussion 689-90.
 88. Sekhar LN, Heros RC. Origin, growth, and rupture of saccular aneurysms: a review. *Neurosurgery.* 1981;8:248-260.
 89. Shearer WT, Rutman JY, Weinberg WA, Goldring D. Coarctation of the aorta and cerebrovascular accident: a proposal for early corrective surgery. *J Pediatr.* 1970;77:1004-1009.
 90. Sho E, Sho M, Singh TM, et. al. Arterial enlargement in response to high flow requires early expression of matrix metalloproteinases to degrade extracellular matrix. *Exp Mol Pathol.* 2002;73:142-153.
 91. Singh PK, Marzo A, Coley SC, et. al. The role of computational fluid dynamics in the management of unruptured intracranial aneurysms: a clinicians' view. *Comput Intell Neurosci.* 2009;760364.
 92. Stehbens WE. Etiology of intracranial berry aneurysms. *J Neurosurg.* 1989;70:823-831.
 93. Stehbens WE. *Pathology of the Cerebral Blood Vessels.* St Louis, Mo: CV Mosby; 1972.
 94. Stehbens WE. Aneurysms and anatomical variation of cerebral arteries. *Arch Pathol.* 1963;75:45-64.
 95. Stehbens WE. Cerebral aneurysms and congenital abnormalities. *Australas Ann Med.* 1962;11:102-112.
 96. Suyama K, Mizota S, Minagawa T, et. al. A ruptured anterior communicating artery aneurysm associated with internal carotid artery agenesis and a middle cerebral artery anomaly. *J Clin Neurosci.* 2009;16:585-586.
 97. Takahashi M, Fujimoto T, Suzuki R, et. al. [A case of spontaneous middle cerebral artery occlusion associated with a cerebral aneurysm angiographically disappearing after STA-MCA anastomosis]. *No Shinkei Geka.* 1997;25:727-732.
 98. Takayama K, Nakagawa H, Iwasaki S, et. al. Multiple cerebral aneurysms associated with Takayasu arteritis successfully treated with coil embolization. *Radiat Med.* 2008;26:33-38.
 99. Taylor CL, Yuan Z, Selman WR, Ratcheson RA, Rimm AA. Cerebral arterial aneurysm formation and rupture in 20,767 elderly patients: hypertension and other risk factors. *J Neurosurg.* 1995;83:812-819.
 100. Thompson RC, Steinberg GK, Levy RP, Marks MP. The management of patients with arteriovenous malformations and associated intracranial aneurysms. *Neurosurgery.* 1998;43:202-11; discussion 211-2011; discussion 211-2.
 101. Ueda T, Yuh WT, Taoka T. Clinical application of perfusion and diffusion MR imaging in acute ischemic stroke. *J Magn Reson Imaging.* 1999;10:305-309.
 102. Varaprasathan GA, Araoz PA, Higgins CB, Reddy GP. Quantification of flow dynamics in congenital heart disease: applications of velocity-encoded cine MR imaging. *Radiographics.* 2002;22:895-905; discussion 905-905; discussion 905-6.
 103. Verheugt CL, Uiterwaal CSPM, Grobbee DE, Mulder BJM. Long-term prognosis of congenital heart defects: a systematic review. *Int J Cardiol.* 2008;131:25-32.
 104. Wang DM, Tarbell JM. Modeling interstitial flow in an artery wall allows estimation of wall shear stress on smooth muscle cells. *J Biomech Eng.* 1995;117:358-363.
 105. Wang Z, Kolega J, Hoi Y, et. al. Molecular alterations associated with aneurysmal remodeling are localized in the high hemodynamic stress region of a created carotid bifurcation. *Neurosurgery.* 2009;65:169-77; discussion 177-1677; discussion 177-8.
 106. Weir B, Macdonald, RL: Intracranial aneurysms and subarachnoid hemorrhage: an overview, in Wilkins RH, Rengachary SS (ed): *Neurosurgery*, ed 2. New York: McGraw-Hill;1996:2191–2213.
 107. Yamashita S, Isoda H, Hirano M, et. al. Visualization of hemodynamics in intracranial arteries using time-resolved three-dimensional phase-contrast MRI. *J Magn Reson Imaging.* 2007;25:473-478.
 108. Yong-Zhong G, van Alphen HA. Pathogenesis and histopathology of saccular aneurysms: review of the literature. *Neurol Res.* 1990;12:249-255.
 109. Zada G, Breault J, Liu CY, et. al. Internal carotid artery aneurysms occurring at the origin of fetal variant posterior cerebral arteries: surgical and endovascular experience. *Neurosurgery.* 2008;63:ONS55-61; discussion ONS61-61; discussion ONS61-2.

Research Article

The Role of Computational Fluid Dynamics in the Management of Unruptured Intracranial Aneurysms: A Clinicians' View

Pankaj K. Singh,¹ Alberto Marzo,² Stuart C. Coley,³ Guntram Berti,⁴ Philippe Bijlenga,⁵ Patricia V. Lawford,² Mari-Cruz Villa-Uriol,⁶ Daniel A. Rufenacht,⁷ Keith M. McCormack,² Alejandro Frangi,⁶ Umang J. Patel,⁸ and D. Rodney Hose²

¹Departments of Medical Physics and Neurosurgery, Royal Hallamshire Hospital, Sheffield, UK

²Academic Unit of Medical Physics, School of Medicine and Biomedical Sciences, University of Sheffield, Sheffield, UK

³Department of Neuroradiology, Royal Hallamshire Hospital, Sheffield, UK

⁴NEC Laboratories Europe, NEC Europe Ltd., 53757 St. Augustin, Germany

⁵Clinic of Neurosurgery, Department of Clinical Neurosciences, Geneva University Hospital, 1211 Geneva, Switzerland

⁶Biomedicine Communication Technologies Department, Center for Computational Imaging & Simulation Technologies, Pompeu Fabra University, Barcelona, Spain

⁷Department of Neuroradiology, Institute of Radiology, University Hospital Basel, Petersgraben, Basel, Switzerland

⁸Department of Neurosurgery, Royal Hallamshire Hospital, Sheffield, UK

Correspondence should be addressed to Pankaj K. Singh, neurosurgery2007@gmail.com

Received 11 February 2009; Revised 24 April 2009; Accepted 9 June 2009

Recommended by Francois Vialatte

Objective. The importance of hemodynamics in the etiopathogenesis of intracranial aneurysms (IAs) is widely accepted. Computational fluid dynamics (CFD) is being used increasingly for hemodynamic predictions. However, along with the continuing development and validation of these tools, it is imperative to collect the opinion of the clinicians. **Methods.** A workshop on CFD was conducted during the European Society of Minimally Invasive Neurological Therapy (ESMINT) Teaching Course, Lisbon, Portugal. 36 delegates, mostly clinicians, performed supervised CFD analysis for an IA, using the @neuFuse software developed within the European project @neurIST. Feedback on the workshop was collected and analyzed. The performance was assessed on a scale of 1 to 4 and, compared with experts' performance. **Results.** Current dilemmas in the management of unruptured IAs remained the most important motivating factor to attend the workshop and majority of participants showed interest in participating in a multicentric trial. The participants achieved an average score of 2.52 (range 0–4) which was 63% (range 0–100%) of an expert user. **Conclusions.** Although participants showed a manifest interest in CFD, there was a clear lack of awareness concerning the role of hemodynamics in the etiopathogenesis of IAs and the use of CFD in this context. More efforts therefore are required to enhance understanding of the clinicians in the subject.

Copyright © 2009 Pankaj K. Singh et al. This is an open access article distributed under the Creative Commons Attribution License, which permits unrestricted use, distribution, and reproduction in any medium, provided the original work is properly cited.

1. Introduction

The management of unruptured cerebral aneurysms remains one of the most controversial topics in neurosurgery. These uncertainties are multifactorial owing mainly to an incomplete understanding of the natural history of these lesions and risks associated with active management [1–4]. Recent evidence, however, suggests a good correlation between different hemodynamic factors and etiopathogenesis of IAs [5–8]. This, together with the fact that current technologies

do not allow detailed in vivo measurements of blood flow [9, 10] in cerebral arteries has given computational fluid dynamics (CFD) new strength and a chance to affirm itself as a technology that can help in the management of unruptured IAs. Many studies have been published where patient-specific medical images and CFD are used to predict relevant hemodynamic variables that correlate well with initiation, growth and rupture of an IA [9–15]. Until recently, these analyses were performed primarily by engineers, physicists or mathematicians in collaboration with select clinicians.

However, in order to make an impact on clinical practice and to enhance trust among clinicians, a controlled and extensive exposure of the software and its concepts to the broader clinical community is crucial along with its continuing validations.

The current study is the first effort of its kind where the concept and application of CFD software was exposed to the clinical community, followed by analysis of their views, understanding and performance.

2. Material and Methods

The first gathering of the European Society of Minimally Invasive Neurological Therapy (ESMINT) Teaching Course on IAs provided an ideal opportunity to expose the computational tools being developed within the European project @neurIST [16], to the attention of its audience. The workshop was held near the birthplace of angiography at the “Edifício Egas Moniz” of the Hospital Santa Maria in Lisbon, Portugal between 7th and 12th September 2008.

2.1. Participants’ Demography and Overview. The workshop was attended mainly by neurosurgeons and neuroradiologists. Out of all participants 86% had a clinical, 8% an engineering, and 6% a scientific background. Participants broadly fell into four age groups: 20–30 years old (3 participants, 8%), 31–40 (22, 61%), 41–50 (9, 25%), 50+ (2, 6%). Participants were prevalently male with a ratio $M : F = 8 : 1$. These data are summarized in Figure 1.

Participants were subdivided into groups of about 8 individuals per session to maximize teacher-to-attendee ratio. Two tutors were available during each session, one with a clinical background (neurosurgeon) and one with an engineering background (biomedical engineer). Teaching was delivered via a lecture of 75 minutes, which included a discussion of the clinical background and relevance of hemodynamic factors in etiopathogenesis of IAs, a brief introduction on the use of CFD in hemodynamic predictions, and explanation of key fluid dynamics concepts in this context, for example, wall shear stress (WSS), boundary conditions, and so forth. This was followed by a supervised hands-on experience with the software.

The exercise was presented to the audience via a clinical vignette of a typical difficult scenario encountered in the clinic, represented in Figure 2. The vignette illustrates a typical case of an incidentally-discovered IA in an anxious young patient. Due to its size (5 mm maximum diameter) and absence of any other major known risk factors the aneurysm should be managed conservatively as per ISUIA (International Studies for Unruptured Intracranial Aneurysms) guidelines [1, 4]. However due to patient’s concerns and insistence for active intervention the management plan becomes controversial.

The participants were then asked to use the software @neuFuse to extract additional and nonobservable hemodynamic data from the 3-dimensional rotational angiographic (3DRA) image of this case. Attendees performed the tasks independently with the help of a ready-reckoner containing

TABLE 1: Aneurysm radiological characteristics.

Localization	Carotid artery/ophthalmic segment/medial wall
Side	Left
Dome status	Unruptured
Depth	4.2 mm
Max diameter	5 mm
Max neck width	3.7 mm
Type	Side-wall, saccular
Aspect	Smooth

the complete guided procedure with illustrations to facilitate the exercise. One-to-one support and supervision was provided during each session, as required.

2.2. Image Acquisition and Processing. The medical image used in the workshop was obtained using rotational acquisition in a Philips Integris Allura machine (Philips Medical Systems, Best, The Netherlands), producing 100 images in 6 seconds, with 5 ms exposure per image. Voxel size in the reconstructed 3D images was 234 microns with reconstruction matrix $256 \times 256 \times 256$. Images were anonymized, respecting the @neurIST ethical approval for use of patient data. The characteristics of the aneurysm considered in this study are reported in Table 1.

The current version of the @neuFuse software (prototype 4), based on the Multimod Application Framework [17] and developed within the @neurIST project, was used to reconstruct the vessel surfaces, create the model and set up the hemodynamic analysis. The solvers used within @neuFuse to solve the fundamental equations describing the blood flow behavior within the region of interest were ANSYS-ICEM and ANSYS-CFX (Ansys, Inc., Canonsburg, PA, USA).

For the purpose of the workshop a simple stationary analysis (nonpulsatile but constant flow rate and pressure at the openings of the region of interest) was performed by the participants using Intel core duo 2.4 GHz machines, with 2 GB RAM and 512 MB of dedicated graphic memory.

2.3. CFD Analysis. Figure 3 shows the overall workflow of the operations performed from uploading the raw medical image to the software through the visualization of relevant hemodynamic data in @neuFuse.

Any CFD analysis requires knowledge of the volumetric region traversed by the fluid (i.e., aneurysm including connected surrounding vasculature) plus information about velocity and pressure of the fluid at the boundaries of the chosen region of interest (boundary conditions). Participants were asked to reconstruct the region of interest starting from the medical image, and specify the boundary conditions using the software @neuFuse. The first step was to launch @neuFuse and import the medical image (Figure 3(a)). The geometry of the vessel, including the IA, was then extracted from the imported image (Figure 3(b)). As only a subregion of the extracted vasculature around the

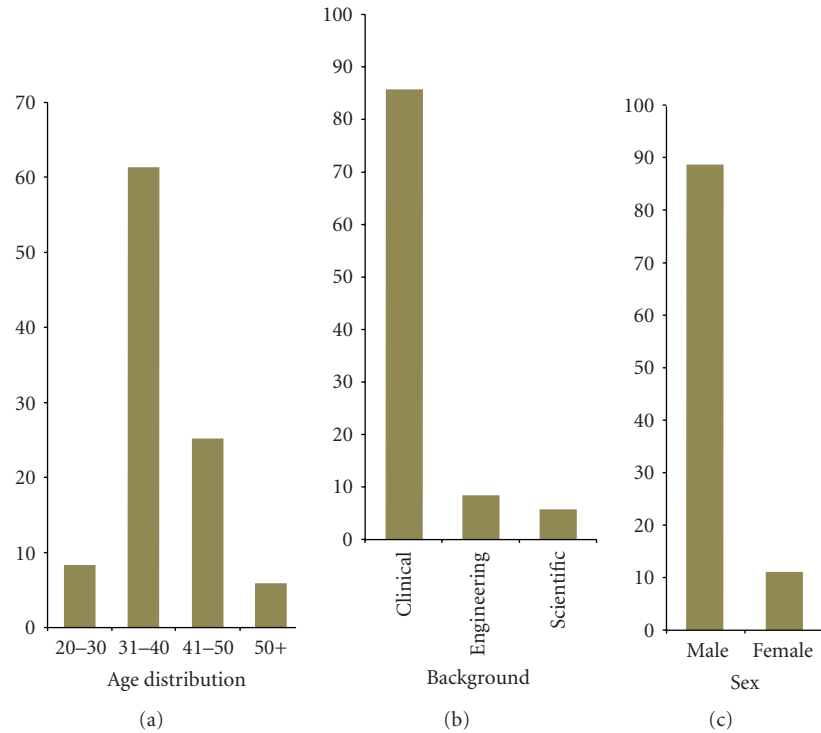


FIGURE 1: Participants' demographic constitution.

Clinical vignette:

A 23-year lady attends neurovascular clinic with her partner. Her mother died one month back due to subarachnoid hemorrhage from a cerebral aneurysm. She smokes around 10 cigarettes a day but is otherwise fit and asymptomatic. After a long discussion it was decided to screen her for the possibility of an intracranial aneurysm. The MRA revealed the presence of an aneurysm of 5 millimetre maximum diameter in the region of left terminal ICA. She expresses great concerns about the diagnosis and is keen on exploring the active treatment options rather than being observed by routine follow-up.

FIGURE 2: Clinical vignette: typical challenging case scenario.

aneurysm has influence on the hemodynamic computation, all vessels entering or leaving the IA were identified and cropped at desired locations to define the region of interest (ROI). The ascending carotid artery, which was an inlet (blood enters the domain through it), was cropped at ten vessel diameters proximal to the IA as shown in Figure 3(c). The distal carotid artery in the region of cavernous sinus and the ophthalmic artery were identified as the two outlets of ROI (blood exits the domain through these two vessels). These are shown in Figure 3(c). For the sake of simplicity and time constrains the mesh used in the analysis was coarse and was constructed using simple tetrahedral elements. As is often the case in real-life clinical situations, information

on pressure or velocity of the blood at these locations for the patient under examination was not available. Boundary conditions were therefore provided by using a 1D mathematical model of the systemic tree, which has been developed within @neurIST [18]. A representation of the @neurIST 1D circulation model is depicted in Figure 3(d). This model provides values of pressure and flow of blood at several locations along the systemic arterial tree, including locations in the circle of Willis for a typical individual. Plug-flow BCs were applied at inlet and pressure BC at outlet, using average values from the waveforms provided by the 1D circulation model. Typical values of blood viscosity ($\mu = 0.004 \text{ Pa}\cdot\text{s}$) and density ($\rho = 1066 \text{ kg/m}^3$) were applied to define the blood properties. Although the blood is a nonNewtonian fluid for the sake of simplicity and time-constraints, and also in view of recent findings from Cebra et al. [13], we decided to assume constant blood viscosity.

While arterial walls move under the effect of the propagating pressure waves, it has been shown that the effects of this movement on hemodynamic predictions are negligible [19, 20]. Fixed walls were thus considered in this analysis. The computation was automatically performed by the software and participants were asked to display different predicted hemodynamic variables like flow streamlines (Figure 3(e)), pressure distribution within the aneurysm or arterial wall, and WSS (Figure 3(f)). Participants were then asked to compare the WSS values computed within the aneurysm with the critical values found in the experimental studies of Malek et al. [21] below which the endothelium is affected by cell loss, desquamation and deranged activity of wall-growth regulators.

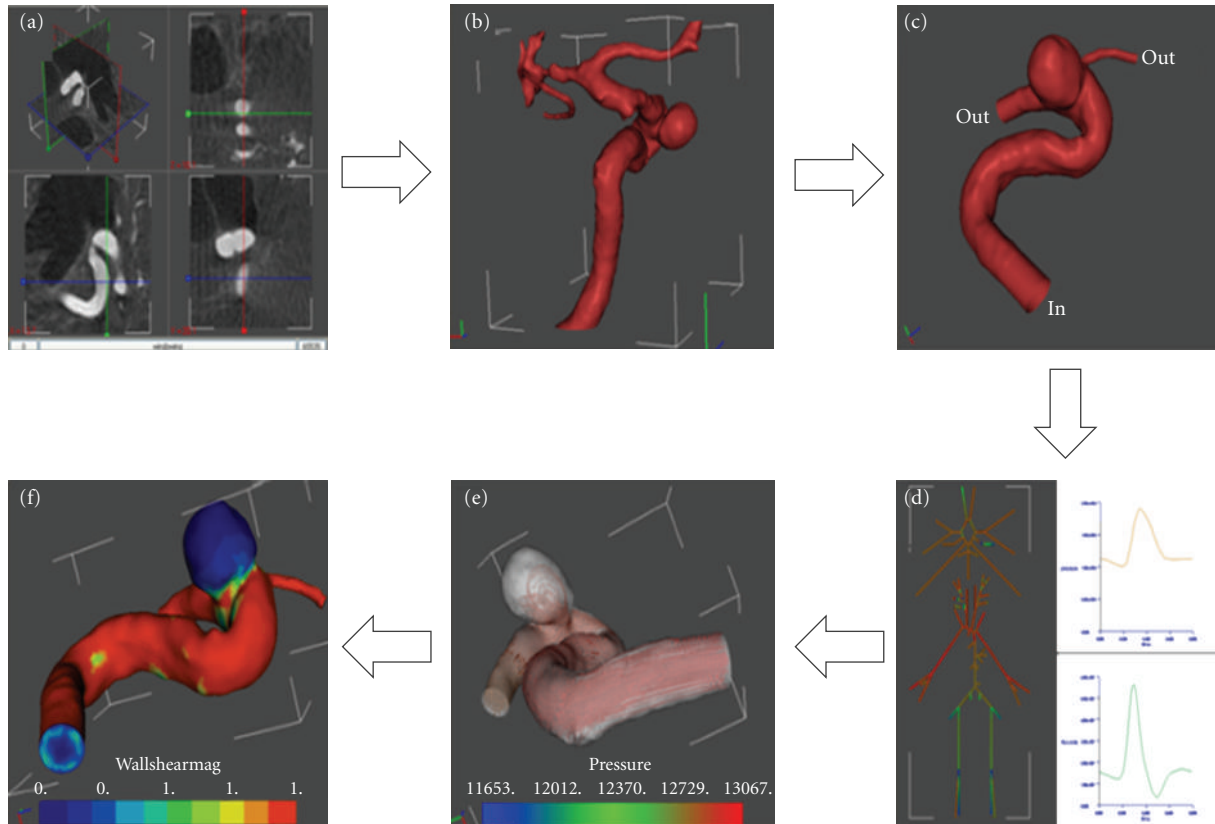


FIGURE 3: Operation workflow from medical image to hemodynamic results. (a) Orthoslice visualization of the 3DRA medical image in @neuFuse. (b) Visualization of the extracted vessel surface. (c) Visualization of reduced region of interest with location of inlet and outlet openings. (d) 1D circulation model. (e) Visualization of predicted streamlines. (f) Visualization of predicted wall shear stress.

2.4. Evaluation. Finally, the feedback was collected via a questionnaire consisting of 48 questions. These were broadly divided into 6 categories (Table 2): general feedback, course design and conduct, experience with the software, hemodynamics understanding, impact of CFD in neurosurgery, and bringing this software into routine use. Each section of the questionnaire was carefully designed to collect information on different aspects of the participant experience as described in Table 2. The questionnaire with the complete list of questions is reported in The questionnaire with the complete list of questions is reported in supplementary appendix questionnaire in Supplementary Material available online at doi:10.1155/2009/760364.

Performance of participants was measured by analyzing the file containing an audit trail of the operations performed during the analysis. The performance criteria were based on the analysis settings that have major influence on the outcome of the numerical predictions, namely, the quality of the reconstructed geometry, its extension, the locations in the 1D circulation model from which boundary conditions were extracted, and the correctness of the applied boundary condition type (i.e., whether it was correctly set to inlet or outlet). Each correct operation was assigned one point, leading to a maximum score of four. Expert performance was considered as gold standard (4 out of 4) and participants performance rate was compared against this.

3. Results

For each section of the questionnaire only data gathered for the most representative questions were reported in this manuscript. Results were represented using tables with percentage distribution for a ready appreciation of feedback across the participants. These are reported section by section below.

Section 1: General Feedback. As shown in Table 3, the overall feedback about the workshop was positive. The 86% of participants would recommend the software to a colleague, 75% found the workshop useful and 78% rated their overall experience between good and very good. Negative feedback was confined averagely within less than 5%. Most participants recognized the need to improve management of IAs and for 47% this was the main reason for attending the workshop.

Section 2: Course Design and Conduct. 80% of candidates found that the workshop to be of the right duration, 14% found that it to be too short while for 6% it was too long (Table 4). Participants-to-instructor ratio was right for 91% while 6% thought that there were too many participants. Most of the participants did not have any difficulty in understanding the instructions. On a scale of 1 to 5, where

TABLE 2: Questionnaire sections and objectives.

Section	Category	Objectives
1	General feedback	To gather impressions on the overall experience
2	Course design and conduct	To gather suggestions on possible improvements and identify any shortcomings in the design of the workshop
3	Experience with the software	To identify weak points as perceived by clinicians in the graphical user interface of the current version of the software
4	Haemodynamics understanding	To assess their current knowledge and understanding in the role of haemodynamics in the aetiopathogenesis of intracranial aneurysms
5	Impact of CFD in neurosurgery	To assess their faith in the principles of CFD and its use in the clinical environment, along with the need of validation through a multicentre trial
6	Bringing this software into routine use	To explore the participants view on cost related issues and gather information on future marketing potentials of this kind of software

1 is not clear and 5 is very clear, 86% rated it 4-5, while 14% were not sure. 94% of the participants thought that the course content was scientifically appropriate.

Section 3: Experience with the Software. 34% of the candidates found the current version of the software user friendly, 11% think that it needs some improvement, while 6% found that it was not user-friendly (Table 5). The remaining 46% were unsure. 48% of the participants think that clinicians with limited IT skills will find using the software challenging, 11% disagree with this assumption and 33% were not sure. 86% of all attendees were able to complete all the steps of the hemodynamic analysis within the time allocated (approximately 50 minutes). 11% missed one or more steps. Application of boundary conditions and clipping the region of interest were among the most difficult steps reported by majority of participants. These were equally distributed among participants with scientific and clinical background.

Section 4: Haemodynamics Understanding. Whereas for 78% of the participants it was easy to understand the technical concepts used throughout the course (Table 6), 19% faced

TABLE 3: General feedback.

Question/Answer options	Number of participants (%)	
<i>Would you recommend the software to a colleague?</i>		
Yes	31	(86)
No	3	(8)
n.a.	2	(6)
<i>Why did you decide to participate to this workshop?</i>		
Working in the field	16	(45)
Interested in CFD	2	(6)
Improve management of aneurysms	17	(47)
Other	1	(2)
<i>How useful did you find this workshop?</i>		
Not useful	1	(3)
Not sure	8	(22)
Useful	16	(45)
Very useful	11	(30)
<i>Rate your overall experience</i>		
Poor	1	(3)
Average	7	(19)
Good	15	(42)
Very good	13	(36)

TABLE 4: Course design and conduct.

Question/Answers	Number of participants (%)	
<i>Was the duration of the workshop...</i>		
Right	29	(80)
Short	5	(14)
Long	2	(6)
<i>Was the participant-to-instructor ratio...</i>		
Right	33	(91)
Too-many	2	(6)
n.a.	1	(3)
<i>Were the instructions given in a clear way?</i>		
Not sure	5	(14)
Clear	18	(50)
Very clear	13	(36)
<i>Was the content of the course scientifically appropriate?</i>		
Yes	34	(94)
No	2	(6)

some difficulties in understanding the terminology, mostly related to concepts such as boundary conditions and WSS.

TABLE 5: Experience with the software.

Question/Answers	Number of participants (%)	
<i>Do you find the software user friendly?</i>		
No	2	(6)
Needs improvement	4	(11)
Not sure	17	(46)
User friendly	11	(31)
Very user friendly	1	(3)
n.a.	1	(3)
<i>Will clinicians without tech/IT experience have trouble?</i>		
Yes	17	(48)
Not sure	12	(33)
No	4	(11)
n.a.	3	(8)
<i>Were you able to complete all the steps of the hemodynamic analysis?</i>		
Yes	30	(86)
No	4	(11)
n.a.	1	(3)

36% of the participants showed trust in the results predicted by the software and think that they are realistic. However, 58% were unsure. 48% believe that there is good scientific evidence to justify the role of hemodynamics in the etiopathogenesis of IAs, 3% did not agree with this. 43% of the candidates were not sure. Whereas 50% of the participants were aware of the use of CFD as a tool in the prediction of rupture in IAs, 42% were hearing the concept for the first time.

Interestingly, 84% of all participants were willing to read further peer-reviewed articles published on CFD and role of hemodynamics in IAs.

Section 5: Impact of CFD in Neurosurgery. Responding to the question “who should perform the CFD analysis for your patient”, 19% answered a consultant, 6% thought that it should be done by a registrar or a junior member of the team (Table 7). 25% believed that analysis should be performed by a dedicated clinical scientist/engineer, while 25% think that it can be done by anyone provided that they have adequate training.

84% of the participants were of the view that the software can be used as a diagnostic tool on outpatient basis, 8% did not agree with them. 84% of the participants were aware of similar software, whereas for 8% of them it was the first exposure to this kind of software. When asked about automated versus user controlled software, interestingly 35% expressed a wish to retain user control. 26% preferred a fully-automated tool, while 26% were unsure.

Although the majority of participants (88%) were convinced that there is a future for CFD as a risk prediction tool, and that there is a significant, or emerging clinical need for

TABLE 6: Haemodynamics understanding.

Question/Answers	Number of participants (%)	
<i>Did you have difficulty with the technical concepts (boundary conditions, wall shear stress, etc.)?</i>		
Yes	7	(19)
No	28	(78)
n.a.	1	(3)
<i>Are the results from this software realistic?</i>		
Yes	13	(36)
Not sure	21	(58)
No	0	(0)
n.a.	2	(6)
<i>Is current evidence sufficient to justify a role for haemodynamics in the pathogenesis of aneurysms?</i>		
No	1	(3)
Not sure	15	(43)
Yes	17	(48)
n.a.	2	6
<i>Were you previously aware of the use of CFD to predict the risk of rupture in intracranial aneurysms?</i>		
No	15	(42)
Yes	18	(50)
n.a.	3	(8)
<i>If you see a publication on computational predictions for IA in a peer-reviewed journal, will you read it?</i>		
No	3	(8)
Yes	30	(84)
n.a.	3	(8)

these kinds of innovative tools (84%), most of them (75%) thought that the current version of the software was not yet ready and would require refinement before it could be introduced into clinical practice.

64% of the candidates believed that an early prediction of the risk of rupture computed with the help of this software could influence their decision making in the management of an IA. Out of the 64% over half (39%) think that small asymptomatic unruptured cases specially falling in the border-line category based on current evidence, are the best cases where such software can provide definitive help. Interestingly, 19% thought that it could be useful in all cases. 69% of the participants were convinced of the need for a multicentric trial for the evaluation of the software and expressed their willingness to participate in it.

TABLE 7: Impact of CFD in neurosurgery.

Question/Answers	Number of participants (%)	
<i>Ideally, who should perform this type of computational analysis for patients?</i>		
Consultant	7	(19)
Dedicated clinical scientist	9	(25)
Registrar	2	(6)
Anyone with training	14	(38)
Office member	1	(3)
All	1	(3)
n.a.	2	(6)
<i>When ready could this software be used diagnostically in an outpatient clinic?</i>		
Yes	30	(84)
No	3	(8)
n.a.	3	(8)
<i>Are you aware of any similar software?</i>		
Yes	30	(84)
No	3	(8)
n.a.	3	(8)
<i>Should this type of analysis be fully automated, or is it better that the user has control?</i>		
Automated	10	(26)
User control	14	(35)
Not sure	10	(26)
n.a.	5	(13)
<i>Is there a future for computational tools for risk prediction of intracranial aneurysm rupture?</i>		
Yes	29	(80)
No	2	(6)
Not sure	2	(6)
n.a.	3	(8)
<i>How great a clinical need is there for this software?</i>		
Significant	17	(48)
Emerging	13	(36)
Low	3	(8)
n.a.	3	(8)
<i>Do you think that this type of analytical software is ready for introduction into the clinical environment?</i>		
Ready	4	(11)
Needs work	26	(75)
n.a.	5	(14)

TABLE 7: Continued.

Question/Answers	Number of participants (%)	
<i>In which cases might this software influence your decision-making about patient management?</i>		
All	7	(19)
Small unruptured asymptomatic	14	(39)
Other	2	(6)
Not sure	1	(3)
None	3	(8)
n.a.	9	(25)
<i>Would you be interested in participating in a multicentre trial on the evaluation of this software?</i>		
Yes	25	(69)
No	5	(14)
n.a.	6	(17)

TABLE 8: Bringing this software into routine use.

Question/Answers	Number of participants (%)	
<i>Would you expect this software to be provided as part of a scanner, or as a stand-alone product?</i>		
Scanner	11	(30)
Standalone	10	(27)
Both	12	(32)
n.a.	4	(11)
<i>Would the price of this software be an important factor in your deciding to obtain/use it?</i>		
Important	26	(72)
Low priority	6	(17)
n.a.	4	(11)
<i>Would you expect to pay for this software, or would you prefer a freeware/shareware arrangement?</i>		
Pay	4	(11)
Shareware	14	(37)
Freeware	17	(44)
n.a.	3	(8)

Section 6: Bringing This Software into Routine Use. Once the software is in routine use, 30% of the participants believed that it should be an integral part of the scanner (Table 8). 27% thought that it should be supplied as a standalone product, while 32% say it could be provided in either way.

Cost will be an important deciding factor for 72% and 81% prefer it to be a freeware or shareware. However, cost is a low priority for 17% and 11% will not mind paying for it.

TABLE 9: Attendees' performance.

	Score	%
<i>Average</i>	2.52	(63)
<i>Performance with age</i>		
20–30 years	2.58	(65)
31–40 years	2.50	(63)
41–50 years	2.36	(59)
50+ years	2.22	(56)
<i>Performance with background</i>		
Clinicians	2.5	(63)
Scientists	2.7	(68)

Performance. Attendees totaled an average score of 63% of experts' performance (Table 9). When age is taken into consideration youngest delegates in the group 20–30 years scored highest (65%) with score figures reducing progressively with age. Age group 50+ obtained the lowest scores (56%). Performance was slightly higher in scientific community (2.7), as compared to the clinicians (2.5).

4. Discussion

4.1. The Current Challenges Posed by Unruptured IAs. The easy availability and widespread use of relatively noninvasive and sophisticated neurodiagnostic modalities such as high resolution CT, MRI and MRA, have brought to clinical attention a large and ever increasing, group of patients harboring unruptured and asymptomatic IAs. These unruptured lesions are also diagnosed coincidentally at the time of catheter angiography carried out for a ruptured aneurysm in patients having multiple aneurysms. The increasing awareness of relatively bleak prognosis related to aneurysmal rupture in general public and clinicians, forces neurosurgeons to come up with a definitive answer for these unruptured lesions.

With the advancements in microsurgical techniques and improved neuroanesthetic and interventional neuroradiological approaches, the morbidity and mortality figures associated with active management of the *ruptured* IAs have improved significantly when compared to their conservative management. In other words, the indications for the active interventions in *ruptured* IAs are now well established. The situation unfortunately is not as straightforward in cases of *unruptured* IAs and, the management of these lesions remains one of the most controversial topics in Neurosurgery [1–4]. Most large series including the ISUIA studies, agree on the low risk of rupture for unruptured IAs. The cumulative rupture rates in the ISUIA studies were between 0.05 and <1 percent per annum [1, 4]. The fact that the prevalence of unruptured IAs in general population outnumbers the incidence of subarachnoid hemorrhage suggests that not all unruptured IAs share a common natural history. The annual prevalence of unruptured IAs in a population is around 5% while the incidence of subarachnoid hemorrhage in the corresponding population is observed up to a maximum of

10 cases per 100 000 persons per year [1]. It is clear from these figures that 80% to 85% of all IAs will never rupture.

The current uncertainties in the management of unruptured IAs are well acknowledged by the clinical community, and were among the most important motivating factors for the majority of the participants (47%, Table 3) to attend this workshop.

In order to offer the best possible treatment to the patient with the least side effects, formulation of a clear management protocol, directed by the natural history of unruptured IAs and the risks associated with the active management, is required. Whereas the endovascular coiling is increasingly being accepted as a preferred treatment modality for ruptured IAs, surgery is advocated as a first line treatment for unruptured lesions [2, 4]. Although there are no strict guidelines, most of the studies [22–24] including ISUIA trials [1, 4], almost unanimously recommend certain factors as indications of surgery in unruptured IAs, namely, large aneurysmal size, symptomatic lesions, evidence of growth, multiple lesions, posterior circulation location, and past history of SAH. All these criteria have been established to have good correlation with increased risk of rupture and hence, surgery is advocated in these situations to avoid the poor outcome. It is interesting to note that whereas on the one hand the above mentioned criteria are used to decide the need and suitability for surgery in an unruptured IA, all of these factors also remain the underlying descriptors for poor surgical outcome [25–27].

In the light of current evidence, it is clear that the group which will stand the best chance of an excellent outcome after surgery is the one with solitary, very small (<5 mm), truly asymptomatic IAs located in the anterior circulation, without any evidence of growth. Quite the contrary, current protocols dictate clinicians not to operate upon this group [1, 4, 25]; and in fact contraindicate any active management option in such patients [1, 4, 25]. Moreover, the small aneurysms of <5 mm size which are traditionally thought to be “safe”, are not “rupture-proof”. In a study Yasui et al. [28] found that in a group of 25 ruptured aneurysms, 16 (64%) were <5 mm in size. Similarly, Juvela et al. [29] who followed 142 patients with 181 aneurysms for a mean period of 13.9 years with an aneurysmal size of <4 mm, demonstrated a 19% rupture rate, that is, 27 out of 142 patients had a rupture.

In order to improve the surgical outcome if we choose to operate on these smaller and “safe” lesions, we have to operate on every single patient. The ideal situation, however, would be if we could identify the aneurysms at greater risk of rupture while they are still small in size and operate upon them, leaving others to be monitored expectantly.

4.2. The Emerging Need for New Alternatives. It is evident that, due to the limitations associated with conventional risk factors used to assess the risk of growth and rupture, it is currently impossible to identify those patients who are at an increased risk in this subset having a real need of an early surgery from those who can be monitored safely without any active intervention. The situation consequently leaves us

with no options other than searching some new descriptors which can predict the risk of rupture independently in small IAs before they join the cohort destined for a poor surgical outcome. This fact is in part reflected by the large number of participants' views (84%, Table 7), who believe that there is a significant or emerging need of new alternatives.

There is a rapidly growing body of literature affirming the importance of hemodynamics in the etiopathogenesis of IAs [5–8]. The hemodynamic variables often considered in these studies are WSS, oscillatory shear index (OSI), blood pressure and other quantities used to characterize blood flow. Proportional to blood viscosity and its velocity, WSS is the tangential frictional force exerted by the flowing blood on the walls of each vessel. High supra-physiological and low infra-physiological values of WSS have been associated with initiation, growth and rupture of aneurysms [7, 9, 11, 21, 30–33]. A measure of the oscillatory nature of these viscous forces is given by the OSI, often associated with endothelial cells degeneration [6, 15, 34]. Table 10 gives a comprehensive list of hemodynamic variables from literature and their association with IA evolution.

An evaluation of these variables can provide a useful alternative to predict the behavior of an unruptured IA at an early stage before it changes in size, shape or becomes symptomatic. Unfortunately, the detailed in vivo measurements of all relevant flow variables in the regions affected by the disease are currently impossible [9, 10].

4.3. Computational Fluid Dynamics: A Brief Overview. Motivated by the important role played by hemodynamics and the difficulty of conducting detailed in vivo observations of relevant hemodynamic variables, engineers and computer scientists have started using CFD to predict blood flows in IAs [9–15].

CFD is the science of predicting fluid flow, heat and mass transfer, chemical reactions, and related phenomena by solving numerically the set of mathematical equations that govern a particular physical system (conservation of mass, momentum, energy, species, etc.). Since its early development in the 1960s and 1970s in the field of aerospace, where it was used mainly to improve the design and efficiency of aircrafts [40], CFD has been successfully used in many other applications. In the past decades engineers used CFD in the automotive, nautical, and civil engineering industries for conceptual studies of new designs, troubleshooting redesign, or improving the physical understanding of a novel fluid mechanical phenomenon. Supported by experimental studies and a profound theoretical knowledge of the application at hand, CFD can be applied anywhere the flow of a fluid is important. Validation, through comparisons with experimental data, has always been a key aspect in successful applications of CFD. In the context of its use in IAs, although early validation work shows promising results [19, 41–43], a more systematic validation remains a prerequisite before CFD can be adopted as a routine tool in clinical practice. As it is evident from Table 7, 58% of the participants agreed that the results obtained using the software may influence their decision making in the small unruptured IA presented in the

clinical vignette or all cases, provided they are backed by a larger clinical trial. Whereas the software at the moment can successfully predict the relevant haemodynamic indices in the context of IAs, it is expected that after the larger clinical trials, significant statistical correlations can be established forming the basis of novel clinical protocols. Whereas the majority of participants (78%, Table 6) did not find any difficulty in understanding the technical concepts used in CFD, only 36% (Table 6) of them believed that the results produced by its application were realistic. The mistrust in the results emphasises the importance of validation. This is further supported by the fact that most of the participants (84%, Table 7) readily wanted to participate in a multicentric clinical trial.

Although participants showed a manifest interest in computational predictions (Table 6), there is a clear lack of awareness concerning the role of hemodynamics in the etiopathogenesis of IAs and the use of CFD in this context (42%, Table 6). More efforts therefore are required by the scientific community to enhance understanding of the role of hemodynamics and awareness of the use of CFD in this field.

4.4. The Concept of Controlled Exposure. The use of CFD in this context represents a significant change in the clinical workflow and a successful transfer of knowledge will only happen via carefully planned, controlled exposure. Clinical sites must be supported locally, underpinning the training for clinicians with the involvement of clinical scientists. The effectiveness of interdisciplinary transfer of knowledge is largely dependent on the course design and the methodology used. As reflected by the results (Table 9), a hands-on workshop using multimedia PowerPoint presentation, one-to-one supervision, and low participants-to-instructor ratio with a carefully designed course based on sound scientific principles, can lead to good results. The correct duration of such a course is also an important factor (Table 4). A close collaboration between engineers and the clinical community is also a prerequisite for successful transfer of knowledge. Supervision during this workshop was hence, jointly provided by a biomedical engineer and a clinician. Given a short training period of only 75 minute, the first ever exposure of the software and its concepts to most of the participants (Table 6), together with the fact that the software is still in its prototype stage, the overall response and average performance of 63% was remarkable. It is anticipated that performance can be enhanced to the level of the expert-user by means of a more user-friendly version of the software and more intensive training. The results also show a decline in performance with age. It may be associated with the IT skills necessary to use this type of software efficiently. This fact should be kept in mind when interpreting the results and formulating future training and translational requirements.

4.5. Software Design Improvement. Many valuable suggestions were collected from participants on the possible improvements in the software design and its functionalities. Among the important suggestions included automating the

TABLE 10: Literature-based evidence on the importance of hemodynamics in the etiopathogenesis of ICAs. NB: WSS; wall shear stress, MMP-13; matrixmetalloproteinases-13, iNOS; inducible-nitric oxide synthase, NO; nitric oxide, OSI; oscillatory shear index.

Hemodynamic factors	Intracranial aneurysm			Proposed mechanism(s)	References
	Initiation	Growth	Rupture		
<i>Dynamic</i>					
Wall shear stress (WSS)	High	Low	Low	Increased WSS increases the production of MMP-13 which in turn leads to vessel wall damage. Decreased WSS increases iNOS synthesis—NO induced damage to vessel wall. Low WSS increases endothelial proliferation and apoptosis	Boussel et al. [11], Fukuda et al. [30], Gao et al. [7], Jou et al. [31], Malek et al. [21], Meng et al. [32], Shojima et al. [9], Ujiie et al. [33]
Oscillatory shear index (OSI)	High/Low	High	High	Degenerative changes in endothelium	Glor et al. [35], Goubergrits et al. [34], Mantha et al. [15]
Jet of blood stream	Impingement	Impingement	Impingement	Localized endothelial cell injury	Foutrakis et al. [36], Cebal et al. [14], Cebal et al. [37]
Flow pattern	—	—	Complex	Statistical association	Cebal et al. [14, 37]
<i>Hydrostatic</i>					
Pressure	High	High	High	Passive yield/water hammer effect	Inci and Spetzler [38], Morimoto et al. [8] Steiger et al. [39]

steps for which user intervention is not strictly necessary, improving user friendliness through a more intuitive graphical user interface (GUI) where the user is guided through the number of operations required, or use of the icons in place of the more cumbersome operation from the menu bar and, finally graphical representation of the 1D circulation model for easier application of boundary conditions. After discussing the feasibility with developers, most of these suggestions were implemented in the latest version of the software @neuFuse.

4.6. The Expected Place of CFD in Neurosurgery. It is interesting to note that the majority of the participants (63%, Table 7) want these analyses to be performed either by an expert clinical scientist/engineer or by a person with the same level of expertise, rather than a clinician. The fact may reflect clinicians' reluctance to conduct the analyses themselves due to their understandable concern over time-constraints and may indicate the requirement of a dedicated team with sufficient infrastructure for the purpose. In spite of this, most of the clinicians (84%, Table 7) see the software as a handy tool which can be used on an outpatient basis (e.g., ophthalmoscope, otoscope, etc.) rather than a specialist department-based facility (e.g., 3DRA, MRA, etc.). On comparing the software in terms of the different properties of a diagnostic modality which makes it an ideal outpatient tool versus those requiring a dedicated setup, we find that this software has some important features of an ideal outpatient tool. It is noninvasive and is not directly performed on the patient (patients do not have to come prepared, e.g., empty stomach). As it is totally noninvasive, there is no risk of cross-infection or contamination. Due to no associated side effects, no admission or postoperative care is necessary. Although only time will decide, in authors' view only a dedicated department with sufficient IT facilities

and dedicated biomedical engineers can take the burden of the extensive computational time required by more realistic transient analyses and, effort to visualize and extract the hemodynamic characteristics required for clinical decision making.

Whereas the current study indicates a positive response among the clinical community for CFD and its use in IAs, it will be necessary to expose the software to a larger number of clinicians before definitive conclusions can be drawn.

5. Conclusions

Although participants showed a manifest interest in computational predictions, there is a clear lack of awareness concerning the role of hemodynamics in the etiopathogenesis of IAs and the use of CFD in this context. More efforts therefore are required by the scientific community to enhance awareness and understanding of the clinicians in the subject. There is a clear willingness to use such software as an outpatient tool. The mistrust in the results indicates the need for validations, and most of the participants supported with the need of a multicentric trial, when software is ready. Keeping in mind the very first exposure to CFD for most of the participants and the inherent difficulties associated with a developing-software, the average performance of 2.5 (63% of an expert) was remarkable. Adequate training, controlled exposure, and further development of these tools are necessary before these can be efficiently used by a common clinician.

Acknowledgments

The authors would like to thank the European Commission, VI Framework Program, Priority 2, Information Society

Technologies, a European Public Funded Organization, for funding @neurIST Project (2) (www.aneurist.org) and allowing this study (Research Grant no. IST-FP6-027703). The funding was provided in the form of financial support to first two authors along with the arrangement of necessary resources to conduct the workshop. The project has appropriate ethical approvals for the required research. The ethical matters are managed by Project Ethical Committee, Oxford, UK. A copy of the ethical approval can be provided as and when required. Special thanks go to Alessandro Chiarini, from BioComputing Competence Centre SCS s.r.l. (Bologna, Italy), Nacho Larrabide, from Universitat Pompeu Fabra (Barcelona, Spain), and the other developers from University of Bedfordshire, UK, for their dedicated efforts and support to make this software presentable and functional. Ian Jones from ANSYS Europe Inc. needs special mention for providing the ANSYS software to perform the analyses. The 1D circulation model used in the analyses is the result of the work done by Philippe Reymond and Nikos Stergiopoulos from the Laboratory of Hemodynamics and Cardiovascular Technology, Ecole Polytechnique, Fédérale de Lausanne EPFL, Switzerland. They also extend their special thanks to ESMINT (www.mitcourse.org) for providing the opportunity to conduct the workshop and, to all the participants of the workshop for their contribution.

References

- [1] “Unruptured intracranial aneurysms—risk of rupture and risks of surgical intervention. International Study of Unruptured Intracranial Aneurysms Investigators,” *The New England Journal of Medicine*, vol. 339, pp. 1725–1733, 1998.
- [2] S. Juvela, “Treatment options of unruptured intracranial aneurysms,” *Stroke*, vol. 35, no. 2, pp. 372–374, 2004.
- [3] T. W. M. Raaymakers, G. J. E. Rinkel, M. Limburg, and A. Algra, “Mortality and morbidity of surgery for unruptured intracranial aneurysms: a meta-analysis,” *Stroke*, vol. 29, no. 8, pp. 1531–1538, 1998.
- [4] D. O. Wiebers, J. P. Whisnant, J. Huston III, et al., “Unruptured intracranial aneurysms: natural history, clinical outcome, and risks of surgical and endovascular treatment,” *The Lancet*, vol. 362, no. 9378, pp. 103–110, 2003.
- [5] A. C. Burlison and V. T. Turitto, “Identification of quantifiable hemodynamic factors in the assessment of cerebral aneurysm behavior: on behalf of the Subcommittee on Biorheology of the Scientific and Standardization Committee of the ISTH,” *Thrombosis and Haemostasis*, vol. 76, no. 1, pp. 118–123, 1996.
- [6] J. V. Byrne and G. Guglielmi, *Endovascular Treatment of Intracranial Aneurysms*, Springer, New York, NY, USA, 1998.
- [7] L. Gao, Y. Hoi, D. D. Swartz, J. Kolega, A. Siddiqui, and H. Meng, “Nascent aneurysm formation at the basilar terminus induced by hemodynamics,” *Stroke*, vol. 39, no. 7, pp. 2085–2090, 2008.
- [8] M. Morimoto, S. Miyamoto, A. Mizoguchi, N. Kume, T. Kita, and N. Hashimoto, “Mouse model of cerebral aneurysm: experimental induction by renal hypertension and local hemodynamic changes,” *Stroke*, vol. 33, no. 7, pp. 1911–1915, 2002.
- [9] M. Shojima, M. Oshima, K. Takagi, et al., “Magnitude and role of wall shear stress on cerebral aneurysm: computational fluid dynamic study of 20 middle cerebral artery aneurysms,” *Stroke*, vol. 35, no. 11, pp. 2500–2505, 2004.
- [10] D. A. Steinman, J. S. Milner, C. J. Norley, S. P. Lownie, and D. W. Holdsworth, “Image-based computational simulation of flow dynamics in a giant intracranial aneurysm,” *American Journal of Neuroradiology*, vol. 24, no. 4, pp. 559–566, 2003.
- [11] L. Bousset, V. Rayz, C. McCulloch, et al., “Aneurysm growth occurs at region of low wall shear stress: patient-specific correlation of hemodynamics and growth in a longitudinal study,” *Stroke*, vol. 39, no. 11, pp. 2997–3002, 2008.
- [12] M. A. Castro, C. M. Putman, and J. R. Cebral, “Computational fluid dynamics modeling of intracranial aneurysms: effects of parent artery segmentation on intra-aneurysmal hemodynamics,” *American Journal of Neuroradiology*, vol. 27, no. 8, pp. 1703–1709, 2006.
- [13] J. R. Cebral, M. A. Castro, S. Appanaboyina, C. M. Putman, D. Millan, and A. Frangi, “Efficient pipeline for image-based patient-specific analysis of cerebral aneurysm hemodynamics: technique and sensitivity,” *IEEE Transactions on Medical Imaging*, vol. 24, no. 4, pp. 457–467, 2005.
- [14] J. R. Cebral, M. A. Castro, J. E. Burgess, R. S. Pergolizzi, M. J. Sheridan, and C. M. Putman, “Characterization of cerebral aneurysms for assessing risk of rupture by using patient-specific computational hemodynamics models,” *American Journal of Neuroradiology*, vol. 26, no. 10, pp. 2550–2559, 2005.
- [15] A. Mantha, C. Karmonik, G. Benndorf, C. Strother, and R. Metcalfe, “Hemodynamics in a cerebral artery before and after the formation of an aneurysm,” *American Journal of Neuroradiology*, vol. 27, no. 5, pp. 1113–1118, 2006.
- [16] Description of Work. @neurIST, “Integrated Biomedical Informatics for the management of cerebral aneurysms,” Sixth Framework Programme, Priority 2. Information Society Technologies. Project Identifier: IST-2004-027703.
- [17] M. Viceconti, L. Astolfi, A. Lardini, et al., “The multimod application framework,” in *Proceedings of the 8th International Conference on Information Visualisation (IV '04)*, pp. 15–20, 2004.
- [18] P. Reymond, F. Merenda, F. Perren, D. Rüfenacht, and N. Stergiopoulos, “Validation of 1D model of the systemic arterial tree including the cerebral circulation,” in *Proceedings of the Summer Bioengineering Conference (SBC '08)*, Proceedings of ASME, Marco Island, Fla, USA, 2008.
- [19] M. D. Ford, H. N. Nikolov, J. S. Milner, et al., “PIV-measured versus CFD-predicted flow dynamics in anatomically realistic cerebral aneurysm models,” *Journal of Biomechanical Engineering*, vol. 130, no. 2, Article ID 021015, 2008.
- [20] A. D. Jeays, P. V. Lawford, R. Gillott, et al., “Characterisation of the haemodynamics of the superior mesenteric artery,” *Journal of Biomechanics*, vol. 40, no. 9, pp. 1916–1926, 2007.
- [21] A. M. Malek, S. L. Alper, and S. Izumo, “Hemodynamic shear stress and its role in atherosclerosis,” *The Journal of the American Medical Association*, vol. 282, no. 21, pp. 2035–2042, 1999.
- [22] S. Juvela, M. Porras, and K. Poussa, “Natural history of unruptured intracranial aneurysms: probability and risk factors for aneurysm rupture,” *Neurosurgical Focus*, vol. 8, no. 5, preview 1, 2000.
- [23] R. J. Komotar, J. Mocco, and R. A. Solomon, “Guidelines for the surgical treatment of unruptured intracranial aneurysms: the first annual J. Lawrence pool memorial research symposium—controversies in the management of cerebral aneurysms,” *Neurosurgery*, vol. 62, no. 1, pp. 183–193, 2008.

- [24] M. R. Mayberg, H. H. Batjer, R. Dacey, et al., "Guidelines for the management of aneurysmal subarachnoid hemorrhage: a statement for healthcare professionals from a special writing group of the Stroke Council, American Heart Association," *Stroke*, vol. 25, no. 11, pp. 2315–2328, 1994.
- [25] R. K. Khanna, G. M. Malik, and N. Qureshi, "Predicting outcome following surgical treatment of unruptured intracranial aneurysms: a proposed grading system," *Journal of Neurosurgery*, vol. 84, no. 1, pp. 49–54, 1996.
- [26] R. A. Solomon, M. E. Fink, and J. Pile-Spellman, "Surgical management of unruptured intracranial aneurysms," *Journal of Neurosurgery*, vol. 80, no. 3, pp. 440–446, 1994.
- [27] F. P. Wirth, E. R. Laws Jr., D. Piepgras, and R. M. Scott, "Surgical treatment of incidental intracranial aneurysms," *Neurosurgery*, vol. 12, no. 5, pp. 507–511, 1983.
- [28] N. Yasui, S. Magarisawa, A. Suzuki, H. Nishimura, T. Okudera, and T. Abe, "Subarachnoid hemorrhage caused by previously diagnosed, previously unruptured intracranial aneurysms: a retrospective analysis of 25 cases," *Neurosurgery*, vol. 39, no. 6, pp. 1096–1101, 1996.
- [29] S. Juvela, M. Porras, and O. Heiskanen, "Natural history of unruptured intracranial aneurysms: a long-term follow-up study," *Journal of Neurosurgery*, vol. 79, no. 2, pp. 174–182, 1993.
- [30] S. Fukuda, N. Hashimoto, H. Naritomi, et al., "Prevention of rat cerebral aneurysm formation by inhibition of nitric oxide synthase," *Circulation*, vol. 101, no. 21, pp. 2532–2538, 2000.
- [31] L.-D. Jou, D. H. Lee, H. Morsi, and M. E. Mawad, "Wall shear stress on ruptured and unruptured intracranial aneurysms at the internal carotid artery," *American Journal of Neuroradiology*, vol. 29, no. 9, pp. 1761–1767, 2008.
- [32] H. Meng, Z. Wang, Y. Hoi, et al., "Complex hemodynamics at the apex of an arterial bifurcation induces vascular remodeling resembling cerebral aneurysm initiation," *Stroke*, vol. 38, no. 6, pp. 1924–1931, 2007.
- [33] H. Ujiie, H. Tachibana, O. Hiramatsu, et al., "Effects of size and shape (aspect ratio) on the hemodynamics of saccular aneurysms: a possible index for surgical treatment of intracranial aneurysms," *Neurosurgery*, vol. 45, no. 1, pp. 119–130, 1999.
- [34] L. Goubergrits, U. Kertzscher, B. Schoneberg, E. Wellnhofer, C. Petz, and H.-C. Hege, "CFD analysis in an anatomically realistic coronary artery model based on non-invasive 3D imaging: comparison of magnetic resonance imaging with computed tomography," *International Journal of Cardiovascular Imaging*, vol. 24, no. 4, pp. 411–421, 2008.
- [35] F. P. Glor, B. Ariff, A. D. Hughes, et al., "The integration of medical imaging and computational fluid dynamics for measuring wall shear stress in carotid arteries," in *Proceedings of the Annual International Conference of the IEEE Engineering in Medicine and Biology Society*, vol. 2, pp. 1415–1418, 2004.
- [36] G. N. Foutrakis, H. Yonas, and R. J. Scwabassi, "Saccular aneurysm formation in curved and bifurcating arteries," *American Journal of Neuroradiology*, vol. 20, no. 7, pp. 1309–1317, 1999.
- [37] J. R. Cebral, S. Hendrickson, and C. M. Putman, "Hemodynamics in a lethal basilar artery aneurysm just before its rupture," *American Journal of Neuroradiology*, vol. 30, no. 1, pp. 95–98, 2009.
- [38] S. Inci and R. F. Spetzler, "Intracranial aneurysms and arterial hypertension: a review and hypothesis," *Surgical Neurology*, vol. 53, no. 6, pp. 530–542, 2000.
- [39] H. J. Steiger, R. Aaslid, S. Keller, and H.-J. Reulen, "Growth of aneurysms can be understood as passive yield to blood pressure. An experimental study," *Acta Neurochirurgica*, vol. 100, no. 1-2, pp. 74–78, 1989.
- [40] J. D. J. Anderson, *Computational Fluid Dynamics: The Basics with Application*, McGraw-Hill, New York, NY, USA, 1st edition, 1995.
- [41] M. D. Ford, G. R. Stuhne, H. N. Nikolov, et al., "Virtual angiography for visualization and validation of computational models of aneurysm hemodynamics," *IEEE Transactions on Medical Imaging*, vol. 24, no. 12, pp. 1586–1592, 2005.
- [42] C. Karmonik, R. Klucznik, and C. Benndorf, "Blood flow in cerebral aneurysms: comparison of phase contrast magnetic resonance and computational fluid dynamics—preliminary experience," *RoFo Fortschritte auf dem Gebiet der Röntgenstrahlen und der Bildgebenden Verfahren*, vol. 180, no. 3, pp. 209–215, 2008.
- [43] A. G. Radaelli, L. Augsburg, J. R. Cebral, et al., "Reproducibility of haemodynamical simulations in a subject-specific stented aneurysm model—a report on the Virtual Intracranial Stenting Challenge 2007," *Journal of Biomechanics*, vol. 41, no. 10, pp. 2069–2081, 2008.

	Volume 112, issue 4, May 2010	ISSN 0303-8467 112(4) 265-364
Clinical Neurology and Neurosurgery		
Review		
Falls and gait disorders in geriatric neurology – H. Azev, M. Azev, H. Sauer, O.W. Witte, G. Hagemann (Jena, Germany)		265
Original articles		
Effect of anticoagulant and antiplatelet therapy in patients with spontaneous intra-cerebral hemorrhage: Does medication use predict worse outcome? – L.G. Steud, A. Jain (Rochester, NY, USA), M.F. Bellotti, A.O. Odofuge, R.K. Dhillon, V. Manivannan, R.M. Gilmore, A.A. Rabinstein, R. Chandru, L.A. Serrano, N. Nirmegonda, R. Polamuri, W.W. Decker (Rochester, MN, USA)		275
Degenerative parkinsonism in patients with psychogenic parkinsonism: A dopamine transporter imaging study – A.C. Pellico, C. Godino-Junior, T.S. Moriyma, M.C. Shih, M.Q. Rooster, V. Borges, S.M.A. Silva, P. de Carvalho Aguiar, L.A.Z. Andrade, R.A. Bressan, H.B. Fennz (Sao Paulo, Brazil)		282
Brain MRI findings in long-standing and disabling multiple sclerosis in 84 patients – D. Remard, G. Castelnuovo, P.-J. Boussquet (Nîmes, France), N. de Champfeur (Montpellier, France), J. de Seze (Strasbourg, France), F. Vermeersch (Lille, France), P. Labauge (Nîmes, France)		286
Adverse effects of carbamazepine, phenytoin, valproate and lamotrigine monotherapy in epileptic adult Chinese patients – K. Zeng, X. Wang, Z. Xi, Y. Yin (Chongqing, PR China)		291
Three-year survival after first-ever ischemic stroke is predicted by initial stroke severity: A hospital-based study – K.-C. Chung (Kaohsiung, Taiwan, Taiwan), H.-C. Lee (Taipei, Taiwan), M.-C. Cheng, Y.-C. Huang (Kaohsiung, Taiwan)		296
Factors influencing the symmetry of Parkinson's disease symptoms – J.C. Gómez-Esteban, B. Tijero, R. Cienfuegos, K. Berganzo, J. Somme, E. Lezcano, J.J. Zurrero (Vizcaya, Spain)		302
Effects of smoking and hypertension on wall shear stress and oscillatory shear index at the site of intracranial aneurysm formation – P.K. Singh, A. Muzum, B. Howard (Sheffield, UK), D.A. Bajbouj (Basel, Switzerland), P. Bijlenga (Geneva, Switzerland), A.R. Prings (Barcelona, Spain), P.S. Lanford, S.C. Coley, D.R. Hise, U.J. Patel (Sheffield, UK)		306
Prospective collection and analysis of error data in a neurosurgical clinic – J. Boström, A. Ylancub, J. Schimm (Germany)		314
The influence of cytochrome oxidase CYP2A6, CYP2B6, and CYP2C9 polymorphisms on the plasma concentrations of valproic acid in epileptic patients – L. Sun, J.-Y. Yu, Y.-P. Sun, J.-R. Ou, J.-H. Song, Y. Yu (Qingdao, China)		320
Increased expression of Akt2 and activity of PI3K and cell proliferation with the ascending of tumor grade of human gliomas – G. Wang, C. Kong, P. Pu (Tianjin, People's Republic of China)		324
Acute ischemic stroke treatment and the occurrence of seizures – J. De Ruck, G. Van Meule (Ghent, Belgium)		328
Workload of the emergency room neurologists and the neurological inpatient department in a Greek tertiary care hospital – J. Radoj, E.V. Demizakis, E. Kyriakopoulos (Thessaloniki, Greece), D. Nikolaidou (Patras, Greece), I. Grouva, V. Papadopoulos, I. Tripathis (Thessaloniki, Greece)		332
Case reports		
Bilateral diffuse intracerebral hemorrhagic infarction after cranioplasty with autologous bone graft – K.S. Fom, E.W. Kim, S.D. Kang (Seoul, Republic of Korea)		336
Spinal intradural haemorrhage in a patient with Wegener's Granulomatosis – M.R. Guffoy (Cambridge, UK), S. Khan (Norwich, UK), A. Henny, I. Jalloh, S. Thivedi, P.J. Kiripatrick (Cambridge, UK)		341
Meige's syndrome: A cranial dystonia treated with bilateral palatal deep brain stimulation – E. Merikaki, Z. Kyfiopoulou, M. Georgopoulos, A. Pitschak, C. Constantinou (Patras, Greece)		344
(contents continued on OBC)		

This article appeared in a journal published by Elsevier. The attached copy is furnished to the author for internal non-commercial research and education use, including for instruction at the authors institution and sharing with colleagues.

Other uses, including reproduction and distribution, or selling or licensing copies, or posting to personal, institutional or third party websites are prohibited.

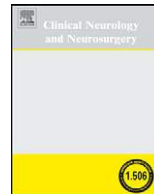
In most cases authors are permitted to post their version of the article (e.g. in Word or Tex form) to their personal website or institutional repository. Authors requiring further information regarding Elsevier's archiving and manuscript policies are encouraged to visit:

<http://www.elsevier.com/copyright>



Contents lists available at ScienceDirect

Clinical Neurology and Neurosurgery

journal homepage: www.elsevier.com/locate/clineuro

Effects of smoking and hypertension on wall shear stress and oscillatory shear index at the site of intracranial aneurysm formation

Pankaj K. Singh^{a,b,*}, Alberto Marzo^c, Bethany Howard^d, Daniel A. Rufenacht^e, Philippe Bijlenga^f, Alejandro F. Frangi^{g,h,i}, Patricia V. Lawford^c, Stuart C. Coley^j, D. Rodney Hose^c, Umang J. Patel^b

^a Department of Medical Physics, Royal Hallamshire Hospital, Sheffield, UK

^b Department of Neurosurgery, Royal Hallamshire Hospital, Sheffield, UK

^c Academic Unit of Medical Physics, School of Medicine and Biomedical Sciences, University of Sheffield, Sheffield, UK

^d Academic Unit of Medical Physics, School of Biomedical Sciences, University of Sheffield, Sheffield, UK

^e Department of Neuroradiology, Institute of Radiology, University Hospital Basel, Petersgraben, Basel, Switzerland

^f Clinic of Neurosurgery, Department of Clinical Neurosciences, Geneva University Hospital, Switzerland

^g Center for Computational Imaging & Simulation Technologies in Biomedicine, Universitat Pompeu Fabra (UPF), Barcelona, Spain

^h Center for Networked Biomedical Research on Bioengineering, Biomaterials and Nanomedicine (CIBER-BBN), Spain

ⁱ Institutió Catalana de Recerca i Estudis Avançats (ICREA), Barcelona, Spain

^j Department of Neuroradiology, Royal Hallamshire Hospital, Sheffield, UK

ARTICLE INFO

Article history:

Received 5 August 2009

Received in revised form 6 November 2009

Accepted 28 December 2009

Available online 21 January 2010

Keywords:

Blood viscosity

Computational fluid dynamics (CFD)

Hemodynamics

Hypertension

Initiation

Intracranial aneurysm

Smoking

Wall shear stress (WSS)

Oscillatory shear index (OSI)

ABSTRACT

Objective: The mechanisms by which smoking and hypertension lead to increased incidence of intracranial aneurysm (IA) formation remain poorly understood. The current study investigates the effects of these risk factors on wall shear stress (WSS) and oscillatory shear index (OSI) at the site of IA initiation.

Methods: Two ($n = 2$) IAs from two patients with history of smoking and hypertension were artificially removed with the help of software @neuFuse (Supercomputing Solutions®, Bologna, Italy) and the vessel geometry reconstructed to mimic the condition prior to IA formation. Two computational fluid dynamics (CFD) analyses were performed on each data-set by using in turn the normal physiological values of blood viscosity (BV), and high BV values specific to smoking and hypertension, obtained from literature.

Results: At normal BV, high WSS (>15 Pa) was observed at the site of IA initiation in both patients. When BV values specific to smoking and hypertension were used, both the areas affected by high WSS (>15 Pa) and the maximum WSS were increased whilst the magnitude and distribution of OSI showed no significant change.

Conclusions: Long-term exposure to high WSS may result in an increased risk of IA development. An incremental increase in areas of high WSS observed secondary to smoking and hypertension may indicate a further increase in the risk of IA initiation. Interestingly, the relationship between BV and the area of increased WSS was not linear, reflecting the need for patient-specific CFD analysis.

Crown Copyright © 2010 Published by Elsevier B.V. All rights reserved.

1. Introduction

Aneurysmal subarachnoid hemorrhage (SAH) remains a major cause of morbidity and mortality in neurosurgical patients [34,51]. Smoking and hypertension are well-established risk factors in IA formation [6,16,35,38,40]. However, their roles in the mechanisms that regulate aneurysm formation are poorly understood and are essentially limited to their statistical associations.

Recent evidence indicates WSS and OSI as important underlying hemodynamic factors in IA formation [9,11,24,49]. One of the important parameters influencing WSS is blood viscosity, which in turn is influenced by smoking and hypertension [17,41]. The current study employs CFD to predict the effect of smoking and hypertension on the WSS patterns at the site of IA initiation with aim to explore the possible underlying mechanisms leading to their formation.

2. Materials and methods

2.1.1. Study design and patients' recruitment

The study was conducted jointly in the Departments of Neurosurgery and Neuroradiology, Royal Hallamshire Hospital, and

* Corresponding author at: Department of Neurosurgery, Royal Hallamshire Hospital, Glossop Road, Sheffield S10 2JF, UK. Tel.: +44 114 2712180; fax: +44 114 2713314.

E-mail address: neurosurgery2007@gmail.com (P.K. Singh).

Table 1
Patients' demography, clinical presentations of IAs included in the study, their management and the known risk factors.

Pt	Age/sex	Clinical presentation	Ruptured/unruptured	Management	Location of IA	Smoking	Hypertension	Other risk factors
1	45/M	Asymptomatic	Unruptured	Observed	Lt terminal ICA	>60 cigarettes/day/25 years	Poorly controlled	None
2	45/F	Asymptomatic	Unruptured	GDC embolization	Rt terminal ICA	>40 cigarettes/day/22 years	Controlled on medication	None

NB: Pt, patient; GDC, Guglielmi detachable coils; Lt, left; Rt, right; ICA, internal carotid artery.

the Department of Cardiovascular Science, University of Sheffield, Sheffield, UK. A total of two ($n=2$) patients diagnosed with IAs between January 2004 and March 2009, were identified retrospectively and recruited with appropriate consent and ethical approval. In order to avoid age and sex bias both patients were selected from the same age group (45 years) with one male and one female. Their relevant demographic and clinical data are reported in Table 1.

2.1.2. 3DRA acquisitions

Medical images were obtained using rotational acquisition in a Philips® Integris™ Allura machine (Philips® Medical Systems, Best, The Netherlands), producing 100 images in 6 s, with 5 ms exposure per image. Voxel size in the reconstructed 3D images was 121 μm with reconstruction matrix 512 × 512 × 512.

2.1.3. Numerical 3D model

@neuFuse, the computational tool-chain developed within the EU project @neurIST was used to reconstruct vessel and aneurysmal geometries. Vessel triangular surfaces were reconstructed using a threshold iso-surface extraction tool, based on the marching cubes algorithm developed by Lorensen and Cline [42]. The removal of IAs was performed with the help of software @neuFuse. In order to mark the location of the IA in the parent artery after its removal, the image with IA in situ was superimposed over the image where the IA was removed. This step was done during the post-processing of data with the help of software ANSYS®-CFX Postprocess™. A virtual marker (a sphere) was placed at the location of IA in the parent vessel from where the IA was removed. Now the first image (image with IA intact) was taken out and the location of IA (as localized by the virtual marker) was displayed by the arrows. Understanding the importance of the issue authors have used exactly the same views for comparing the hemodynamic indices with and without intracranial aneurysms, so that the readers can make out the location of IAs easily in the view where there no IAs are present.

Volumetric meshes were generated using ANSYS® ICEM™ CFD 11.0 (Ansys®, Inc., Canonsburg, PA, USA) based on the octree approach. The mesh was refined at the wall (using prismatic elements) for more accurate computation of WSS and OSI. For computational efficiency a progressively coarser mesh was used towards the vessel axis. Tetrahedral elements were used for the discretization of the domain core, with three layers of prismatic elements adjacent to the wall, thus ensuring accurate computation of WSS and OSI. Element size and number were set according to

the outcome of a mesh dependency study performed on similar aneurysmal geometries [58]. In this study results were found to be grid independent for meshes greater than 1700 el/mm³. In order to maintain consistency across the meshes used for all geometries, similar element density and the same wall element size and maximum core element size were used in the discretization of the domains.

The 3D transient Navier–Stokes equations were solved using the finite-control-volume software, ANSYS®-CFX™. In view of the recent findings of [44] we used the ‘plug-flow’ or ‘flat’ velocity profile at inlet instead of Womersley flow profile. The default second-order high-resolution advection differencing scheme was used. Blood was assumed to be incompressible, with density $\rho=1060\text{ kg/m}^3$ and Newtonian, with viscosity $\mu_{\text{typical}}=3.5\text{ mPa}\cdot\text{s}$. The effects of hypertension and smoking were modelled by increasing BV values by 8.1% ($\mu_{\text{atypical}}=3.78\text{ mPa}\cdot\text{s}$) according to the findings of de Simone et al. [17] and Price et al. [55]. Boundary conditions (BCs) for the 3D models were provided in the form of typical volumetric flow rate waveforms at inlet and pressure waveforms at outlet. These were computed using the 1D circulation model developed by Raymond et al. [60]. The authors validated their model and found that the predictions of this 1D model have good agreement with the measurements performed in the real patient/healthy volunteers.

3. Results

Values of WSS and OSI were time-averaged for one cardiac cycle and a qualitative and quantitative comparison made for the two BVs. WSS contours reported in Figs. 1 and 2, and the data reported in Table 2, show that, in the case of both patients, the aneurysm formed at a location where WSS was higher than the mean value in the parent vessel. At physiological BV, the maximum WSS at the site of IA initiation for patient-1 (21.3 Pa) was approximately 5 times higher than the mean value in the parent vessel (4.5 Pa). Similarly, for patient-2, the maximum WSS at the initiation site (56.5 Pa) was approximately 5 times higher than in the parent vessel (12.1 Pa). OSI also followed the same trend with relatively higher values at the sites of aneurysmal development for both patients, compared to that in the respective parent vessel (Figs. 1 and 2 and Table 2). However, it must be noted that areas of relatively high WSS and OSI were not exclusively limited to the sites of IA formation.

The threshold value of 15 Pa for WSS used in the study was chosen as an arbitrary limit to highlight the areas of relatively

Table 2
Quantitative comparison of values of WSS and OSI obtained using two BVs; μ_{typical} and μ_{atypical} .

	Patient-1			Patient-2		
	μ_{typical}	μ_{atypical}	%Change	μ_{typical}	μ_{atypical}	%Change
Area of WSS >15 Pa at aneurysm location (mm ²)	1.24	1.42	+14.5	0.67	0.68	+1.5
Area of WSS >15 Pa in parent vessel (mm ²)	7.01	8.24	+17.5	148.8	160.0	+7.5
Maximum WSS at aneurysm location (Pa)	21.3	22.2	+4.2	56.54	58.73	+3.9
Average WSS in parent vessel (Pa)	4.5	4.7	+4.4	12.12	12.68	+4.6
Area of OSI >0.01 at location (mm ²)	0.83	0.79	−5.3	0.21	0.22	+5.1
Maximum OSI at location (mm ²)	0.018	0.019	+2.1	0.21	0.20	−2.8

NB: μ_{typical} , typical blood viscosity; μ_{atypical} , blood viscosity in smokers and hypertensive patients.

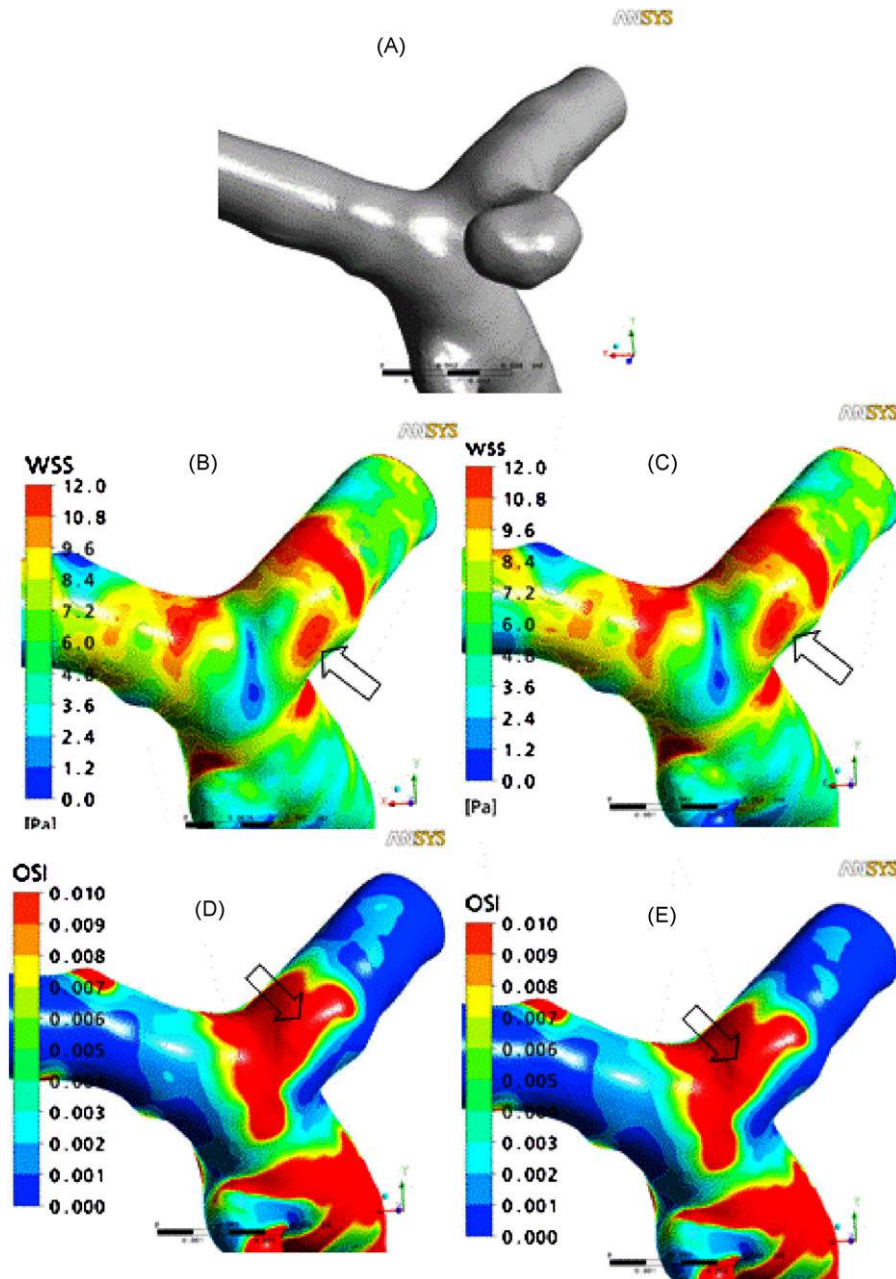


Fig. 1. Reconstructed geometry of the IA and surrounding vasculature for patient-1 (A). Contours of WSS (B and C) and OSI (D and E) for $\mu_{typical}$ (B and D) and $\mu_{atypical}$ (C and E) are displayed. Arrows indicate the site of IA along the parent vessel before removal.

Table 3

The literature-based evidence on the importance of WSS and OSI in the etiopathogenesis of IAs.

Hemodynamic factors	Intracranial aneurysm			Proposed mechanism(s)	References
	Initiation	Growth	Rupture		
Wall shear stress (WSS)	High	Low	Low	Increased WSS increases the production of MMP-13 which in turn leads to vessel wall damage Decreased WSS increases iNOS synthesis NO induced damage to vessel wall Low WSS increases endothelial proliferation and apoptosis	Boussel et al. [8], Fukuda et al. [22], Gao et al. [24], Jou et al. [37], Malek et al. [46], Meng et al. [47], Ujiie et al. [79]
Oscillatory shear index (OSI)	High	High	High	Degenerative changes in endothelium	Glor et al. [25,26], Goubergrits et al. [28], Mantha et al. [45]

NB: MMP-13, matrix metalloproteinases-13; NO, nitric oxide; iNOS, inducible-NO synthase.

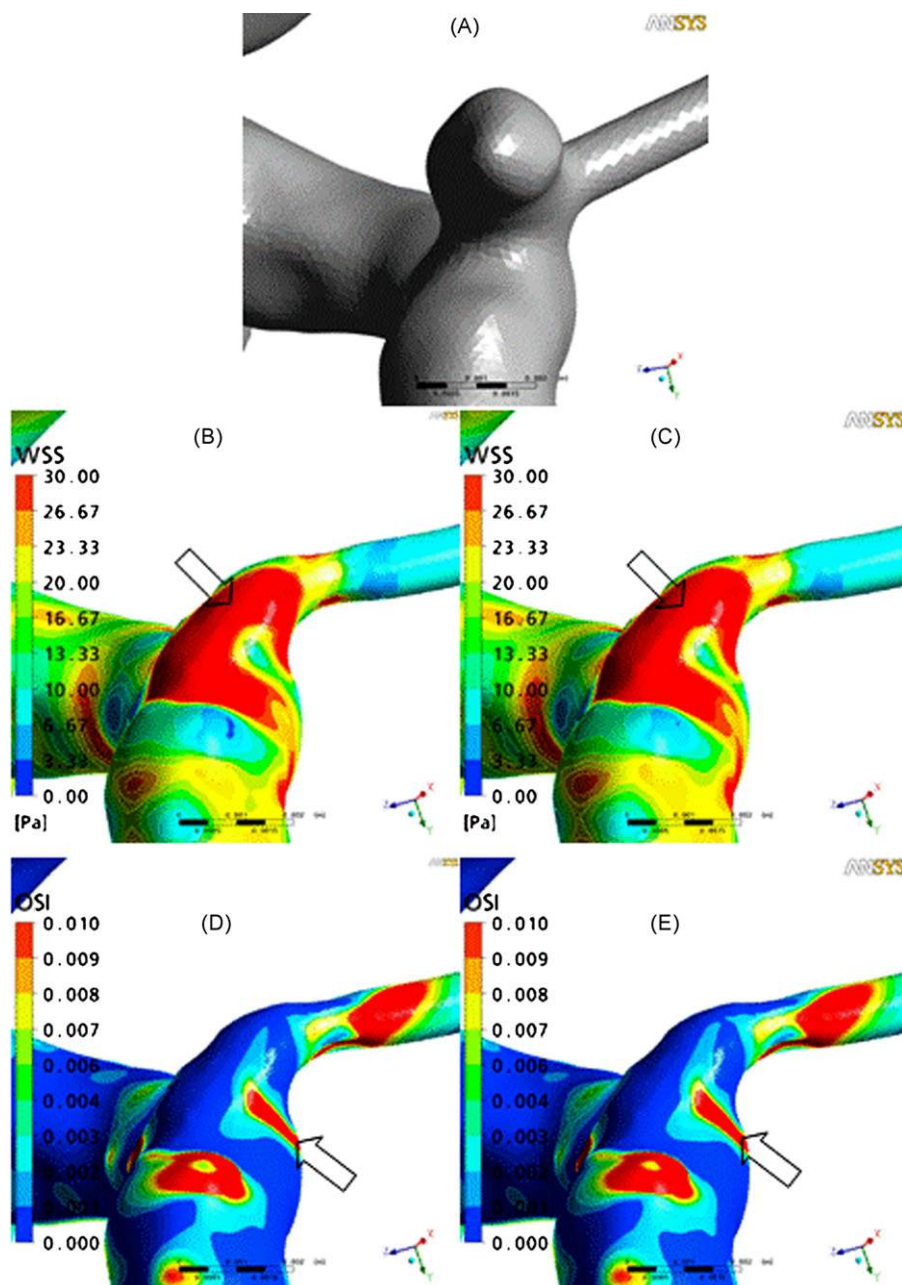


Fig. 2. Reconstructed geometry of the IA and surrounding vasculature for patient-2 (A). Contours of WSS (B and C) and OSI (D and E) for $\mu_{typical}$ (B and D) and $\mu_{atypical}$ (C and E) are displayed. Arrows indicate the site of IA along the parent vessel before removal.

higher WSS where the IAs were initiated and to appreciate/quantify the effects of changes in BV in smokers and hypertensives on WSS. Whereas it was possible to identify a threshold for infra-physiological WSS (<0.4 Pa) [46], no such values could be found in the literature for supra-physiological WSS. An increase in BV, to represent the effects of smoking and hypertension, is reflected in the values of WSS and OSI, reported in Table 2. For patient-1 the area of high WSS (>15 Pa) increased by 17.5%, whereas for patient-2 the increment was 7.5%. The maximum values of WSS at initiation sites followed a similar trend, but the increment was around 4% for both patients. Interestingly, the increase in the value of WSS does not correlate linearly with the increment in BV. Furthermore, from the data in Table 2, it can be seen that changes in BV do not have a significant or consistent effect on the value of OSI at the site of aneurysmal development.

4. Discussion

The exact etiopathogenesis of IA formation is poorly understood [69]. Whilst there is some indication of a congenital link [19], IAs are believed primarily to be acquired lesions [14,73]. Recent evidence suggests a strong correlation between different hemodynamic factors and the etiopathogenesis of IAs [9,11,24,49]. In particular, a number of studies suggest a link between aneurysmal initiation, growth and rupture and the magnitude and distribution of WSS and OSI (Table 3).

4.1. Wall shear stress (WSS)

WSS is a tangential frictional force exerted by flowing blood on the arterial endothelium, and is proportional to the blood viscosity and the velocity gradients. Mean arterial WSS has been suggested

by Malek et al. to lie within the range of 1.5–2.0 Pa [46]. There is an increasing body of literature suggesting that high WSS plays a role in the initiation of IAs [9,11,24,27,49,63]. This is further supported by the observation that IAs most frequently occur at bifurcations and arterial bends. These are regions which are exposed to constantly high WSS [21,62].

A number of different mechanisms have been proposed to explain how WSS influences the natural history of an IA. It has been established that the normal behaviour of arterial endothelial cells (ECs) is regulated by hemodynamic shear stress. Sho et al. [71] observed that increased WSS stimulates ECs to produce matrix metalloproteinase (MMP-13) which, in turn, leads to degeneration of the internal elastic lamina. In 1993 Luscher and Tanner [43] found that the release of EC-derived growth and relaxation factor (EDRF—later recognised as nitric oxide) is shear stress dependent and is responsible for vascular remodelling. It has been demonstrated by a number of workers [13,22,54] that WSS increases the production of NO by the ECs by inducing an enzyme responsible for its synthesis (iNOS, inducible nitric oxide synthase). Fukuda et al. [22] found a high localization of iNOS at the site of IA formation, in both rat and human arteries. They also demonstrated that iNOS inhibitors such as Aminoguanidine and Batroxobin (DF-521) attenuate the early degenerative changes associated with IA formation. The preventive effects of these drugs are thought to be mediated by lowering BV and hence WSS [22]. They concluded that iNOS is a prerequisite for *de novo* development of IAs in cerebral vessels. In 1995, Wang and Tarbell [81] showed that smooth muscle cells (SMCs) in arterial wall can also respond to WSS in intact arteries by

virtue of interstitial flow generated by transmural flow gradients, further accentuating the vessel wall damage.

A number of authors have attempted to explain the mechanisms linking WSS with EDRF/NO production. Experimental studies conducted by Busse and Mulsch [10] revealed that WSS activates calcium ion-dependent endothelial iNOS leading to its increased production. Furthermore, WSS augments the release of adenosine tri-phosphate (ATP) and substance-P from EC [48]. Increased concentrations of these two mediators are believed to enhance NO production in a paracrine manner [54]. More directly, increased WSS leads to hyperpolarization of the ECs by mobilizing the calcium ions from intracellular stores in cultured ECs [3] probably via activation of phospholipase-C [4] and/or K⁺ channels [52]. Several authors have attempted to explain the mechanism of WSS transduction by the endothelium [7,54,58]. Born and Palinski [7] identified 3D mechanoreceptors anchored to the endothelial membrane. They hypothesized that WSS acts on these mechanoreceptors, mechanically enhancing the interaction between regulatory proteins and their targets [7]. Resnick and colleagues [59] located a WSS-responsive element for iNOS on endothelial genes in 1993.

Table 4 gives an overview of the important mechanisms proposed on the role of WSS in vascular remodelling.

The findings of the current study support the correlation between high WSS and initiation of IA. Maximum values of WSS at the site of aneurysm formation were approximately 5 times higher than the mean values observed in the parent vessels, in both patients (Table 2).

Table 4
WSS-induced vascular remodelling: an overview of some important mechanisms proposed.

Author/journal/year	Proposed mechanism(s)/observations	Implications
Rossitti (Acta Radiol, 1998) [62], Foutrakis et al. (Neurol Res, 1997) [21]	IAs mostly occur at arterial bends and bifurcations exposed constantly to high WSS	High WSS can be a possible culprit in the development of IAs
Sho et al. (Exp Mol Pathol, 2002) [71]	Increased WSS stimulates endothelial cells to produce matrix metalloproteinases (MMP-13)	Degeneration of the arterial internal elastic lamina by MMP-13
Luscher and Tanner (Am J Hypertens, 1993) [43]	Release of endothelium derived EDRF is shear stress dependent	Vascular remodelling by WSS
Cooke et al. (Am J Physiol, 1990) [13], Pohl et al. (Am J Physiol, 1991) [54], Fukuda et al. (Circulation, 2000) [22]	WSS induces iNOS, an enzyme responsible for NO synthesis	Increased production of NO in the endothelium, EC injury
Fukuda et al. (Circulation, 2000) [22]	Found high concentrations of iNOS at the site of IA formation, both in rat and human arteries	Levels of iNOS correlate with IA initiation
Fukuda et al. (Circulation, 2000) [22]	iNOS inhibitors; Aminoguanidine and Batroxobin (DF-521) attenuate the early degenerative changes associated with IA formation	Aminoguanidine and Batroxobin (DF-521) have preventive effects on IA formation by lowering WSS
Wang and Tarbell (J Biomech Eng, 1995) [81]	SMCs in arterial walls also respond to shear stress	WSS induced vessel wall damage can extend to SMCs
Busse and Mulsch (FEBS Lett, 1990) [10]	WSS activate the calcium ion-dependent endothelial iNOS	WSS increases the synthesis of iNOS
Milner et al. (Proc Biol Sci, 1990) [48], Pohl et al. (Am J Physiol, 1991) [54]	WSS also augments the release of adenosine tri-phosphate (ATP) and substance-P from ECs	These two mediators increase EDRF production in a paracrine manner
Ando et al. (In Vitro Cell Dev Biol, 1988) [3]	High WSS leads to the hyperpolarization of the ECs by mobilizing the calcium ions from intracellular stores	EC damage
Bhagyalakshmi and Frangos (Biochem Biophys Res Commun, 1989) [4]	Hyperpolarization of ECs and mobilization of intracellular calcium is via activation of phospholipase-C	EC damage
Olesen et al. (Nature, 1988) [52]	Hyperpolarization of the ECs and mobilization of intracellular calcium is via activation of K ⁺ channels	EC damage
Born and Palinski (Br J Exp Pathol, 1985) [7]	Identified presence of 3D mechanoreceptors anchored to the EC membrane, WSS acts on these mechanoreceptors, mechanically enhancing the interaction between regulatory proteins and their targets	Link is established on how WSS transduces signals to ECs
Resnick et al. (Proc Natl Acad Sci USA, 1993) [59]	Located a WSS-responsive element for iNOS on EC genes	Role of WSS in EC damage
Fukuda et al. (Circulation, 2000) [22]	Both, the magnitude of WSS as well as the duration of exposure for the endothelium remain important determinants for the induction of iNOS	Duration and magnitude of WSS play important role in IA formation
Wagner et al. (J Clin Invest, 1997) [80]	Demonstrated that no iNOS was induced when the SMCs were exposed lower WSS (1.1–2.5 Pa) for shorter durations (<24 h)	Chronic and significant exposure of WSS are required for the initiation of IAs

NB: MMP-13, matrix metalloproteinases-13; NO, nitric oxide; iNOS, inducible-NO synthase; EC, endothelial cells.

4.2. Oscillatory shear index (OSI)

The OSI is a measure of the oscillatory nature of shear forces [25,26,28,44]. This index, which has a range of between 0 and 0.5, represents the fraction of the cardiac cycle over which the instantaneous shear force vector forms an angle greater than 90° to the time-average direction of the same force. Consistently high values of OSI have been associated with EC dysfunction [33] and changes in cell structure secondary to cyclic mechanical stress have been demonstrated by Wang and Tarbell [81] reporting disruption of the actin cytoskeleton of ECs.

Glor et al. propose that an OSI of 0.2 represents a threshold value above which endothelial damage is initiated [25,26]. Damage to ECs produced by high OSI may contribute in IA formation. Areas of relatively high OSI predicted at the site of aneurysm formation for patient-2 in our CFD simulations support such theories; the maximum values observed approached the threshold value of OSI (0.2) identified in the literature. In contrast, for patient-1, the OSI at the site of IA initiation fell well below the threshold. This may indicate a less significant role for OSI in IA formation, at least in the case of this particular patient.

Whilst, for both patients, areas of high WSS and OSI were located primarily at the bifurcations where the two IAs were observed, areas of high value for these indices were also predicted at other sites in the parent vessels. This raises a further question; why are these other critical areas unaffected? One explanation is that, in addition to the key hemodynamic triggers, IA initiation is governed by many other factors including amongst others; smoking, hypertension, genetics, polycystic kidney disease, Ehlers–Danlos syndrome, Marfan's syndrome, etc. In addition, the possibility of *de novo* IA formation in these patients in other locations in the future cannot be excluded without a long-term follow-up.

4.3. Role of smoking and hypertension in the IA formation

Smoking and hypertension are two well-established risk factors for IA formation. A number of clinical studies have highlighted the strong association between smoking [2,6,57,63,67] and hypertension [35,65,72,76,77] and *de novo* IA formation. Indeed, both risk factors also correlate with the presence of multiple IAs [18,38,53,57,61]. Experimental studies, where IA has been induced by hypertension, confirm these findings [30–32,39,40,50,56,75]. Furthermore, autopsy studies conducted to assess the relationship between the IA formation and hypertension demonstrate even stronger correlations [12,15,16,66,78].

Whilst being well-established risk factors for IA formation, the exact mechanisms by which smoking and hypertension lead to increased IA formation remain controversial [35]. A number of explanations have been offered including; endothelial cell injury, occlusion of *vasa vasorum* and disturbances in the synthesis of elastin and collagen [35]. It has been proposed that protease/protease-inhibitor factor imbalance is a factor in smokers and a quantitative deficiency of alpha-1-antitrypsin has been reported both in patients with SAH and in smokers [23,68,74]. Alpha-1-antitrypsin is an inhibitor of elastase, a proteolytic enzyme which enhances collagen catabolism. This link is not supported universally; Sakai et al. [64] attribute the increased plasma protease levels found in patients with IAs to leucocytosis after SAH thus disputing the significance of plasma protease/protease-inhibitor imbalance as a marker for IA formation. Another hypothesis suggests that IA formation is a part of a vascular degenerative process similar to atherosclerosis and that smoking leads to IA initiation by facilitating this process [1,29].

One widely recognised effect of smoking and hypertension is an increase in BV [17,55]. We propose that the missing link between these risk factors and increased IA formation is via high WSS sec-

ondary to an increase in BV. This hypothesis is supported by our findings which show an increase in the area of vessel wall subject to high WSS and elevated maximum values of WSS coincident with the IA initiation site for the two patients studied. For patient-1 both qualitative (Fig. 1) and quantitative (Table 2) comparisons show that increased BV results in a substantial increase in the maximum WSS of 4.2%. The area of wall affected by very high WSS (>15 Pa), up by 14.5% and 17.5% for the site of the IA and parent vessel respectively. Similar trends were observed for patient-2 but the relative differences were lower (Fig. 2 and Table 2).

There is strong evidence to indicate that induction of iNOS in ECs is dependent on both the magnitude and duration of exposure to WSS [22]. In an experimental study, Wagner et al. [80], found that iNOS was not induced when the vessel walls were exposed to low WSS (1.1–2.5 Pa) for short durations (<24 h). The study suggests that the chances of IA development are increased if an artery is exposed to high WSS on chronic basis. Both patients included in our study were exposed to these two risk factors chronically for an extended period (20–25 years). Long-term exposure to high WSS, and the increase in the area of vessel wall affected, may have led to EC damage in these patients and contributed to an increased risk of IA development.

Changes in OSI at the sites of IAs were less marked than changes in WSS, and had no consistent trend. Whilst OSI is not directly dependent on BV, changes in hemodynamics resulting from altered rheology may be reflected in the OSI. However the results indicate its less significant dependency from the hemodynamic changes secondary to altered BV.

It is important to note that our findings differ in some respects from those reported for previous studies, based on similar methodology [44,70]. These sought to develop novel indices in an attempt to link initiation with a hemodynamic trigger whilst indicating that WSS was relatively low at the site of IA initiation. Shimogonya et al. [70] reported a significant correlation between IA formation and a self-proposed hemodynamic index which they termed the 'gradient oscillatory number' (GON) and Mantha et al. [45] showed a correlation between IA initiation and their newly proposed hemodynamic index; aneurysm formation indicator (AFI). In considering these results in the light of the current work, it is important to note that Shimogonya et al. used a simplified geometry which may have influenced their results. Furthermore, as there are bodies of literature associating low [8,11,37,46] and high [9,11,22,24,27,49,62] WSS with endothelial dysfunction and the etiopathogenesis of IA, it could be argued that both supra-physiological and infra-physiological WSS lead to perturbation of normal EC behaviour. Our findings agree with the majority of studies [9,11,22,24,27,49,62] which support the role of high WSS in IA formation.

It is evident that the IA formation is likely to have a multifactorial etiology with hemodynamic factors acting as an important cog in this process. Many factors are likely to act in parallel rendering the vessel wall more susceptible to the effects of increased pressure and WSS.

4.4. Limitations of the study

Before drawing any conclusions it is important to emphasise that our study, in common with other CFD analyses, carries inherent limitations associated with the assumptions necessary to create the models. First, whilst very high quality images (3DRA) were used to reconstruct the vessel geometries, these represent the volume of the vessel occupied by contrast agent. If vessel filling with contrast is incomplete this may generate errors in surface prediction. Unfortunately, due to the limitations of current technology this remains an unresolved problem. Second, the BCs used in the analyses were obtained from a generic 1D circulation model and were not patient-specific [60]. Here it is important to note that recent validation of

this model against flow waveforms measured for young volunteers justify its use [60]. Third, despite being non-Newtonian, blood was considered as a Newtonian fluid for the purposes of these analyses. This assumption was based on the observations that, blood behaves as a Newtonian fluid at the high shear-rates which apply at most sites in the cerebral circulation ($>100 \text{ s}^{-1}$) [5], in particular in areas coinciding with sites of IA formation. Fourth, the arterial wall was considered rigid, neglecting wall motion, as this has been shown to have a negligible effect on CFD predictions [20,36]. Finally, the study was performed on a small cohort of two IAs. The work must be considered as a preliminary study; analyses will be required for a significantly larger number of IAs before firm conclusions can be drawn.

5. Conclusions

The current study suggests that long-term exposure to high WSS may affect the behaviour of ECs leading, in turn, to an increased risk of IA development. IA formation is likely to have a multi-factorial etiology with hemodynamics acting as an important component in the process. Increase in BV and hence WSS may be one of the important underlying mechanisms responsible for the increased incidence of IA formation in smokers and hypertensive patients. Trends in OSI patterns were less significant, with no consistent trend, and a less significant interdependency with BV. Interestingly, the relationship between BV and the area of increased WSS was not linear, reflecting the need for patient-specific CFD analysis.

Conflict of interest

Authors have nothing to declare under conflict of interests.

Ethical approvals

The project has appropriate ethical approvals for the required research. The ethical matters are managed by Project Ethical Committee, Oxford, UK (Oxfordshire Research Ethics Committee-A Study Number: 07/Q1604/53). A copy of the ethical approval can be provided as and when required.

Acknowledgements

The study was funded by European Commission, VI Framework Programme, Priority 2, Information Society Technologies, a European Public Funded Organization, under the banner of @neurIST Project (Research Grant No. IST-FP6-027703). The funding was provided in the form of financial support to first two authors along with the arrangement of necessary resources to conduct the workshop.

References

- Adamson J, Humphries SE, Ostergaard JR, Voldby B, Richards P, Powell JT. Are cerebral aneurysms atherosclerotic? *Stroke* 1994;25:963–6.
- Anderson CS, Feigin V, Bennett D, Lin RB, Hankey G, Jamrozik K. Active and passive smoking and the risk of subarachnoid hemorrhage: an international population-based case-control study. *Stroke* 2004;35:633–7.
- Ando J, Komatsuda T, Kamiya A. Cytoplasmic calcium response to fluid shear stress in cultured vascular endothelial cells. *In Vitro Cell Dev Biol* 1988;24:871–7.
- Bhagyalakshmi A, Frangos JA. Mechanism of shear-induced prostacyclin production in endothelial cells. *Biochem Biophys Res Commun* 1989;158:31–7.
- Bonert M, Myers JC, Fremes S, Williams J, Ethier CR. A numerical study of blood flow in coronary artery bypass graft side-to-side anastomoses. *Ann Biomed Eng* 2002;30:599–611.
- Bonita R. Cigarette smoking, hypertension and the risk of subarachnoid hemorrhage: a population-based case-control study. *Stroke* 1986;17:831–5.
- Born GV, Palinski W. Unusually high concentrations of sialic acids on the surface of vascular endothelia. *Br J Exp Pathol* 1985;66:543–9.
- Boussel L, Rayz V, McCulloch C, Martin A, Acevedo-Bolton G, Lawton M, et al. Aneurysm growth occurs at region of low wall shear stress. Patient-specific correlation of hemodynamics and growth in a longitudinal study. *Stroke* 2008.
- Burleson AC, Turitto VT. Identification of quantifiable hemodynamic factors in the assessment of cerebral aneurysm behavior. On behalf of the Subcommittee on Biorheology of the Scientific and Standardization Committee of the Isth. *Thromb Haemostasis* 1996;76:118–23.
- Busse R, Mulsch A. Calcium-dependent nitric oxide synthesis in endothelial cytosol is mediated by calmodulin. *FEBS Lett* 1990;265:133–6.
- Byrne JV, Guglielmi G. Endovascular treatment of intracranial aneurysms. Springer; 1998.
- Chason JL, Hindman WM. Berry aneurysms of the circle of Willis; results of a planned autopsy study. *Neurology* 1958;8:41–4.
- Cooke JP, Stamler J, Andon N, Davies PF, McKinley G, Loscalzo J. Flow stimulates endothelial cells to release a nitrovasodilator that is potentiated by reduced thiol. *Am J Physiol* 1990;259:H804–12.
- Crawford T. Some observations on the pathogenesis and natural history of intracranial aneurysms. *J Neurol Neurosurg Psychiatry* 1959;22:259–66.
- Crompton MR. The pathogenesis of cerebral infarction following the rupture of cerebral berry aneurysms. *Brain* 1964;87:491–510.
- de la Monte SM, Moore GW, Monk MA, Hutchins GM. Risk factors for the development and rupture of intracranial berry aneurysms. *Am J Med* 1985;78:957–64.
- de Simone G, Devereux RB, Chinali M, Best LG, Lee ET, Welty TK. Association of blood pressure with blood viscosity in American Indians: the Strong Heart Study. *Hypertension* 2005;45:625–30.
- Erbengi A, Inci S. Pheochromocytoma and multiple intracranial aneurysms: is it a coincidence? Case report. *J Neurosurg* 1997;87:764–7.
- Forbus WD. On the origin of miliary aneurysms of the superficial cerebral arteries. *Bull Johns Hopkins Hosp* 1930;47:239–84.
- Ford MD, Nikolov HN, Milner JS, Lownie SP, Demont EM, Kalata W, et al. PIV-measured versus CFD-predicted flow dynamics in anatomically realistic cerebral aneurysm models. *J Biomech Eng* 2008;130:021015.
- Fouttrakis GN, Yonas H, Scabassi RJ. Finite element methods in the simulation and analysis of intracranial blood flow. *Neurol Res* 1997;19:174–86.
- Fukuda S, Hashimoto N, Naritomi H, Nagata I, Nozaki K, Kondo S, et al. Prevention of rat cerebral aneurysm formation by inhibition of nitric oxide synthase. *Circulation* 2000;101:2532–8.
- Gaetani P, Tartara F, Tancioni F, Klersy C, Forlino A, Baena RR. Activity of alpha 1-antitrypsin and cigarette smoking in subarachnoid haemorrhage from ruptured aneurysm. *J Neurol Sci* 1996;141:33–8.
- Gao L, Hoi Y, Swartz DD, Kolega J, Siddiqui A, Meng H. Nascent aneurysm formation at the basilar terminus induced by hemodynamics. *Stroke* 2008;39:2085–90.
- Glor FP, Ariff B, Hughes AD, Crowe LA, Verdonck PR, Barratt DC, et al. Image-based carotid flow reconstruction: a comparison between MRI and ultrasound. *Physiol Meas* 2004;25:1495–509.
- Glor FP, Long Q, Hughes AD, Augst AD, Ariff B, Thom SA, et al. Reproducibility study of magnetic resonance image-based computational fluid dynamics prediction of carotid bifurcation flow. *Ann Biomed Eng* 2003;31:142–51.
- Gonzalez CF, Cho YI, Ortega HV, Moret J. Intracranial aneurysms: flow analysis of their origin and progression. *AJNR Am J Neuroradiol* 1992;13:181–8.
- Goubergrits L, Kertzschner U, Schoneberg B, Wellnhofer E, Petz C, Hege HC. CFD analysis in an anatomically realistic coronary artery model based on non-invasive 3D imaging: comparison of magnetic resonance imaging with computed tomography. *Int J Cardiovasc Imaging* 2008;24:411–21.
- Greenhalgh RM, Laing S, Taylor GW. Risk factors in carotid artery stenosis and intracranial aneurysms. *J Cardiovasc Surg (Torino)* 1980;21:559–67.
- Handa H, Hashimoto N, Nagata I, Hazama F. Saccular cerebral aneurysms in rats: a newly developed animal model of the disease. *Stroke* 1983;14:857–66.
- Hashimoto N, Kim C, Kikuchi H, Kojima M, Kang Y, Hazama F. Experimental induction of cerebral aneurysms in monkeys. *J Neurosurg* 1987;67:903–5.
- Hashimoto N, Handa H, Nagata I, Hazama F. Experimentally induced cerebral aneurysms in rats. Part V. Relation of hemodynamics in the circle of Willis to formation of aneurysms. *Surg Neurol* 1980;13:41–5.
- He X, Ku DN. Pulsatile flow in the human left coronary artery bifurcation: average conditions. *J Biomech Eng* 1996;118:74–82.
- Inagawa T. Trends in incidence and case fatality rates of aneurysmal subarachnoid hemorrhage in Izumo City, Japan, between 1980–1989 and 1990–1998. *Stroke* 2001;32:1499–507.
- Inci S, Spetzler RF. Intracranial aneurysms and arterial hypertension: a review and hypothesis. *Surg Neurol* 2000;53:530–40, discussion 540–532.
- Jeays AD, Lawford PV, Gillott R, Spencer P, Barber DC, Bardhan KD, et al. Characterisation of the haemodynamics of the superior mesenteric artery. *J Biomech* 2007;40:1916–26.
- Jou LD, Wong G, Dispensa B, Lawton MT, Higashida RT, Young WL, et al. Correlation between lumenal geometry changes and hemodynamics in fusiform intracranial aneurysms. *AJNR Am J Neuroradiol* 2005;26:2357–63.
- Juvela S. Risk factors for multiple intracranial aneurysms. *Stroke* 2000;31:392–7.
- Kim C, Cervos-Navarro J, Kikuchi H, Hashimoto N, Hazama F. Alterations in cerebral vessels in experimental animals and their possible relationship to the development of aneurysms. *Surg Neurol* 1992;38:331–7.
- Kondo S, Hashimoto N, Kikuchi H, Hazama F, Nagata I, Kataoka H. Cerebral aneurysms arising at nonbranching sites. An experimental study. *Stroke* 1997;28:398–403, discussion 403–394.
- Letcher RL, Chien S, Pickering TG, Laragh JH. Elevated blood viscosity in patients with borderline essential hypertension. *Hypertension* 1983;5:757–62.

- [42] Lorensen WE, Cline HE. Marching cubes: a high resolution 3D surface construction algorithm. *Comput Graph* 1987;21:163–9.
- [43] Luscher TF, Tanner FC. Endothelial regulation of vascular tone and growth. *Am J Hypertens* 1993;6:283S–93S.
- [44] Marzo A, Singh P, Reymond P, Stergiopoulos N, Patel U, Hose R. Influence of inlet boundary conditions on the local haemodynamics of intracranial aneurysms. *Comput Methods Biomech Biomed Eng* 2009;1025–5842.
- [45] Mantha A, Karmonik C, Benndorf G, Strother C, Metcalfe R. Hemodynamics in a cerebral artery before and after the formation of an aneurysm. *AJNR Am J Neuroradiol* 2006;27:1113–8.
- [46] Malek AM, Alper SL, Izumo S. Hemodynamic shear stress and its role in atherosclerosis. *JAMA* 1999;282:2035–42.
- [47] Meng H, Wang Z, Hoi Y, Gao L, Metaxa E, Swartz DD, et al. Complex hemodynamics at the apex of an arterial bifurcation induces vascular remodeling resembling cerebral aneurysm initiation. *Stroke* 2007;38:1924–31.
- [48] Milner P, Kirkpatrick KA, Ralevic V, Toothill V, Pearson J, Burnstock G. Endothelial cells cultured from human umbilical vein release ATP, substance P and acetylcholine in response to increased flow. *Proc Biol Sci* 1990;241:245–8.
- [49] Morimoto M, Miyamoto S, Mizoguchi A, Kume N, Kita T, Hashimoto N. Mouse model of cerebral aneurysm: experimental induction by renal hypertension and local hemodynamic changes. *Stroke* 2002;33:1911–5.
- [50] Nagata I, Handa H, Hashimoto N, Hazama F. Experimentally induced cerebral aneurysms in rats. Part VI. Hypertension. *Surg Neurol* 1980;14:477–9.
- [51] Numminen H, Kotila M, Waltimo O, Aho K, Kaste M. Declining incidence and mortality rates of stroke in Finland from 1972 to 1991. Results of three population-based stroke registers. *Stroke* 1996;27:1487–91.
- [52] Olesen SP, Clapham DE, Davies PF. Haemodynamic shear stress activates a K⁺ current in vascular endothelial cells. *Nature* 1988;331:168–70.
- [53] Ostergaard JR, Hog E. Incidence of multiple intracranial aneurysms. Influence of arterial hypertension and gender. *J Neurosurg* 1985;63:49–55.
- [54] Pohl U, Herlan K, Huang A, Bassenge E. EDRF-mediated shear-induced dilation opposes myogenic vasoconstriction in small rabbit arteries. *Am J Physiol* 1991;261:H2016–2023.
- [55] Price JF, Mowbray PI, Lee AJ, Rumley A, Lowe GD, Fowkes FG. Relationship between smoking and cardiovascular risk factors in the development of peripheral arterial disease and coronary artery disease: Edinburgh Artery Study. *Eur Heart J* 1999;20:344–53.
- [56] Quigley MR, Heiferman K, Kwaan HC, Vidovich D, Nora P, Cerullo LJ. Laser-sealed arteriotomy: a reliable aneurysm model. *J Neurosurg* 1987;67:284–7.
- [57] Qureshi AI, Suarez JL, Parekh PD, Sung G, Geocadin R, Bhardwaj A, et al. Risk factors for multiple intracranial aneurysms. *Neurosurgery* 1998;43:22–6, discussion 26–27.
- [58] Radaelli AG, Augsburger L, Cebal JR, Ohta M, Rufenacht DA, Balossino R, et al. Reproducibility of haemodynamical simulations in a subject-specific stented aneurysm model—a report on the Virtual Intracranial Stenting Challenge 2007. *J Biomech* 2008;41:2069–81.
- [59] Resnick N, Collins T, Atkinson W, Bonthron DT, Dewey Jr CF, Gimbrone Jr MA. Platelet-derived growth factor B chain promoter contains a cis-acting fluid shear-stress-responsive element. *Proc Natl Acad Sci USA* 1993;90:7908.
- [60] Reymond P, Merenda F, Perren F, Rufenacht D, Stergiopoulos N. Validation of a one-dimensional model of the systemic arterial tree. *Am J Physiol Heart Circ Physiol* 2009.
- [61] Rinne J, Hernesniemi J, Puranen M, Saari T. Multiple intracranial aneurysms in a defined population: prospective angiographic and clinical study. *Neurosurgery* 1994;35:803–8.
- [62] Rossitti S. Shear stress in cerebral arteries carrying saccular aneurysms. A preliminary study. *Acta Radiol* 1998;39:711–7.
- [63] Sacco RL, Wolf PA, Bharucha NE, Meeks SL, Kannel WB, Charette LJ, et al. Subarachnoid and intracerebral hemorrhage: natural history, prognosis, and precursive factors in the Framingham Study. *Neurology* 1984;34:847–54.
- [64] Sakai N, Nakayama K, Tanabe Y, Izumiya Y, Nishizawa S, Uemuura K. Absence of plasma protease-antiprotease imbalance in the formation of saccular cerebral aneurysms. *Neurosurgery* 1999;45:34–8, discussion 38–39.
- [65] Sakaki T, Tomimaga M, Miyamoto K, Tsunoda S, Hiasa Y. Clinical studies of de novo aneurysms. *Neurosurgery* 1993;32:512–6, discussion 516–517.
- [66] Sarner M, Crawford MD. Ruptured intracranial aneurysms. Clinical series. *Lancet* 1965;2:1251–4.
- [67] Sauerbeck LR, Hornung R, Moomaw CJ, Woo D, Curry R, Brown Jr RD, et al. The effects of study participation in the Familial Intracranial Aneurysm Study on cigarette smoking. *J Stroke Cerebrovasc Dis* 2008;17:370–2.
- [68] Schievink WI, Prakash UB, Piepgras DG, Mokri B. Alpha 1-antitrypsin deficiency in intracranial aneurysms and cervical artery dissection. *Lancet* 1994;343:452–3.
- [69] Sekhar LN, Heros RC. Origin, growth, and rupture of saccular aneurysms: a review. *Neurosurgery* 1981;8:248–60.
- [70] Shimogonya Y, Ishikawa T, Imai Y, Matsuki N, Yamaguchi T. Can temporal fluctuation in spatial wall shear stress gradient initiate a cerebral aneurysm? A proposed novel hemodynamic index, the gradient oscillatory number (GON). *J Biomech* 2009;42:550–4.
- [71] Sho E, Sho M, Singh TM, Nanjo H, Komatsu M, Xu C, et al. Arterial enlargement in response to high flow requires early expression of matrix metalloproteinases to degrade extracellular matrix. *Exp Mol Pathol* 2002;73:142–53.
- [72] Solenski NJ, Haley Jr EC, Kassell NF, Kongable G, Germanson T, Truskowski L, et al. Medical complications of aneurysmal subarachnoid hemorrhage: a report of the multicenter, cooperative aneurysm study. Participants of the Multicenter Cooperative Aneurysm Study. *Crit Care Med* 1995;23:1007–17.
- [73] Stehbens WE. Ultrastructure of aneurysms. *Arch Neurol* 1975;32:798–807.
- [74] St Jean P, Hart B, Webster M, Steed D, Adamson J, Powell J, et al. Alpha-1-antitrypsin deficiency in aneurysmal disease. *Hum Hered* 1996;46:92–7.
- [75] Strother CM, Graves VB, Rappe A. Aneurysm hemodynamics: an experimental study. *AJNR Am J Neuroradiol* 1992;13:1089–95.
- [76] Taylor CL, Yuan Z, Selman WR, Ratcheson RA, Rimm AA. Cerebral arterial aneurysm formation and rupture in 20,767 elderly patients: hypertension and other risk factors. *J Neurosurg* 1995;83:812–9.
- [77] Teunissen LL, Rinkel GJ, Algra A, van Gijn J. Risk factors for subarachnoid hemorrhage: a systematic review. *Stroke* 1996;27:544–9.
- [78] Toftdahl DB, Torp-Pedersen C, Engel UH, Strandgaard S, Jespersen B. Hypertension and left ventricular hypertrophy in patients with spontaneous subarachnoid hemorrhage. *Neurosurgery* 1995;37:235–9, discussion 239–240.
- [79] Ujiie H, Tachibana H, Hiramatsu O, Hazel AL, Matsumoto T, Ogasawara Y, et al. Effects of size and shape (aspect ratio) on the hemodynamics of saccular aneurysms: a possible index for surgical treatment of intracranial aneurysms. *Neurosurgery* 1999;45:119–29, discussion 129–130.
- [80] Wagner CT, Durante W, Christodoulides N, Hellums JD, Schafer AI. Hemodynamic forces induce the expression of heme oxygenase in cultured vascular smooth muscle cells. *J Clin Invest* 1997;100:589–96.
- [81] Wang DM, Tarbell JM. Modeling interstitial flow in an artery wall allows estimation of wall shear stress on smooth muscle cells. *J Biomech Eng* 1995;117:358–63.



Available online at
ScienceDirect
www.sciencedirect.com

Elsevier Masson France
EM|consulte
www.em-consulte.com



CORRESPONDENCE

Effects of heparin on the hemodynamic characteristics of intracranial aneurysms

A 58-year-old woman presented with a history of sudden onset of severe headache and loss of consciousness. She had a past medical history of deep vein thrombosis and was taking long-term warfarin for that. Her Glasgow Coma Scale score at the time of admission was 13. An urgent CT scan of the head revealed the presence of subarachnoid hemorrhage. The patient was recruited to the @neurIST project (www.aneurist.org) after obtaining the proper consent.

Four-vessel cerebral angiography demonstrated the presence of two intracranial aneurysms (Fig. 1). The first aneurysm (Aneu-1) was a tiny 'bleb'-type aneurysm located on the ophthalmic segment of the right internal carotid artery. It was considered a pre-aneurysm lesion. The second aneurysm (Aneu-2), which ruptured, was located at the origin of the right posterior communicating artery (PCoMMA) and was coiled with GDC® (Guglielmi Detachable Coils). Throughout her hospital stay, the patient received low-molecular weight (LMW) heparin (enoxaparin, Clexane®). However, as the tiny 'bleb' aneurysm was unsuitable for coiling, it was followed by magnetic resonance angiography (MRA).

Three-dimensional computer models of the intracranial aneurysms were created from 3D angiograms (Fig. 1). Boundary conditions were applied proximally at a distance of at least 10 vessel diameters and distally at 2–3 vessel diameters. Hemodynamic factors were computed with the help of @neuFuse software, using physiological values ($\mu_{\text{untreated}} = 0.0045 \text{ Pa s}$) of blood viscosity (BV). The analyses were then repeated, using the values of BVs specific to heparin ($\mu_{\text{heparin}} = 0.0025 \text{ Pa s}$), as reported in the literature. The latter simulates the effect of heparin at an average therapeutic concentration of 0.0075 mg/mL. The 3D unsteady Navier–Stokes equations were solved with the use of finite control volume ANSYS®-CFX™ software. Qualitative (Fig. 2) and quantitative (Table 1) comparisons were made between the hemodynamic parameters computed in both settings.

Findings showed that heparin administration decreased the maximum values of time-averaged wall shear stress (t-av-WSS) in both aneurysms, with a dramatic increase in the area affected by infraphysiological wall shear stress ($<0.4 \text{ Pa}$) in both lesions. The values for the oscillatory shear index (OSI) and pressure were decreased in the pre-aneurysm lesion, whereas an increase was observed in the ruptured lesion (Table 1).

Ruptured aneurysms remain a major cause of morbidity and mortality [1], and recent evidence indicates that hemodynamics are an important underlying factor in their etiopathogenesis [2]. As confirmed by others [3], the hemodynamics of the intracranial vasculature is dependent upon the rheological properties of blood, including BV. It is then logical to speculate that the factors affecting BV can also influence the hemodynamic environment of intracranial aneurysms, thereby affecting their initiation, growth and rupture.

In the present study, we investigated the effects of heparin on the hemodynamic characteristics of aneurysms. High wall shear stress (WSS) values have been associated with heparin initiation by increasing the production of MMP-13, while low values are thought to be responsible for aneurysm growth and rupture [4] by increasing inducible nitric-oxide (iNOS) synthesis, resulting in vessel wall damage. Heparin (and its derivative enoxaparin) is a widely used injectable anticoagulant for preventing venous thrombosis and pulmonary embolism. It inhibits the factors involved in blood-clotting (factor Xa), causing instantaneous inactivation of thrombin, thereby reducing BV [5] and, in turn,

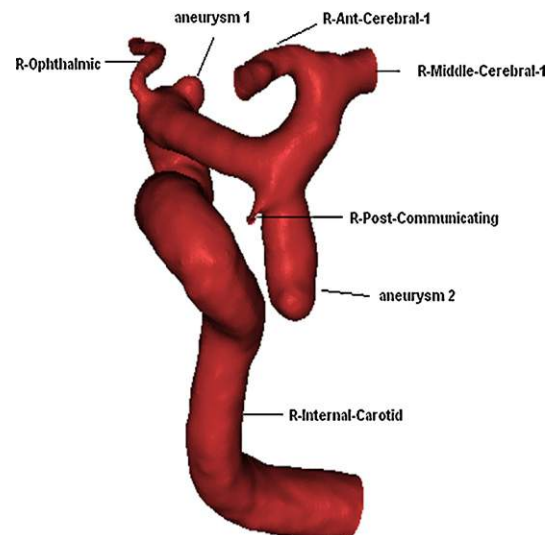


Figure 1 Reconstructed geometry showing the intracranial aneurysms and connecting vessels reconstructed with software from @neuFUSE. Labels indicate the openings where boundary conditions were applied.

Table 1 Quantitative comparison of the effects of heparin on hemodynamic indices.

	Aneu-1			Aneu-2		
	$\mu_{\text{untreated}}$	μ_{heparin}	Change (%)	$\mu_{\text{untreated}}$	μ_{heparin}	Change (%)
t-av-WSS _{min} (Pa)	1.066	1.086	+1.8	0.055	0.048	−12.7
t-av-WSS _{max} (Pa)	35.9	28.08	−21.8	67.75	45.11	−33.4
Area of infraphysiological WSS (< 0.4 Pa)	0.009%	0.07%	+677.8	0.8%	1.2%	+50.0
Area of suprphysiological WSS (> 1.5 Pa)	99.9%	99.6%	−0.3	91.2%	88.7%	−2.7
OSI _{max}	0.21	0.17	−19.0	0.43	0.46	+7.0
Area of elevated OSI (> 0.2)	0.1%	00%	−100.0	2.6%	4.1%	+57.7
Area of elevated pressure (%)	2.1%	2.5%	−19.0	3.5%	4.0%	+14.3

Area values were computed as a percentage of the overall aneurysm surface; Aneu-1: pre-aneurysm lesion; Aneu-2: ruptured aneurysm; $\mu_{\text{untreated}}$: untreated viscosity values used = 0.0045 Pa s; μ_{heparin} : heparinized viscosity values used = 0.0025 Pa s; WSS: wall shear stress; OSI: oscillatory shear index; t-av-WSS_{min}: minimum time-averaged wall shear stress; t-av-WSS_{max}: maximum time-averaged wall shear stress.

altering the hemodynamics of the blood circulation. Hitosugi and co-workers demonstrated a decrease in BV by 55.6% with the use of heparin at a therapeutic concentration of 0.75 IU/L.

However, heparin may also induce significant derangements of the hemodynamics of intracranial aneurysms and may even facilitate the rupture of existing aneurysms, albeit while perhaps inhibiting the formation of new aneurysms. In addition, similar effects might be achieved with other pharmacological agents, thus warranting further investigations. However, so far, it is difficult to draw any definitive conclusions based on only two aneurysms in one patient.

Conflict of interest statement

The authors have not declared any conflict of interest.

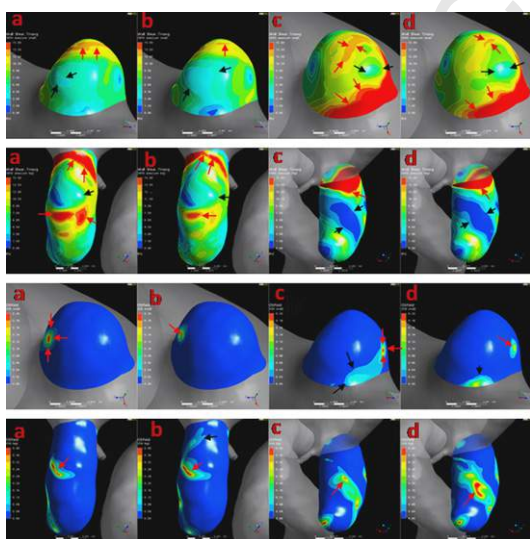


Figure 2 Qualitative differences in the patterns of time-averaged wall shear stress (t-av-WSS) and the oscillatory shear index (OSI) in pre- (a, c) and post-heparinized (b, d) blood. The upper two rows are contour plots for t-av-WSS, and the lower two rows are contour plots for OSI. (a, b) Anterior views; (c, d) posterior views; (rows 1, 3) Aneu-1; (rows 2, 4) Aneu-2.

References

- [1] Inagawa T. Trends in incidence and case fatality rates of aneurysmal subarachnoid hemorrhage in Izumo City, Japan, between 1980–1989 and 1990–1998. *Stroke* 2001;32:1499–507.
- [2] Shojima M, Oshima M, Takagi K, Torii R, Hayakawa M, Katada K, et al. Magnitude and role of wall shear stress on cerebral aneurysm: computational fluid dynamic study of 20 middle cerebral artery aneurysms. *Stroke* 2004;35:2500–5.
- [3] De Simone G, Devereux RB, Chien S, Alderman MH, Atlas SA, Laragh JH. Relation of blood viscosity to demographic and physiologic variables and to cardiovascular risk factors in apparently normal adults. *Circulation* 1990;81:107–17.
- [4] Cebal JR, Castro MA, Burgess JE, Pergolizzi RS, Sheridan MJ, Putman CM. Characterization of cerebral aneurysms for assessing risk of rupture by using patient-specific computational hemodynamics models. *AJNR Am J Neuroradiol* 2005;26:2550–9.
- [5] Hitosugi M, Niwa M, Takatsu A. Changes in blood viscosity by heparin and argatroban. *Thromb Res* 2001;104:371–4.

P.K. Singh^{a,b,*}

A. Marzo^c

H. Tahir^c

T.F. Weeratunge^c

K. Kumar^d

M. Boutarouch^e

R. Hose^c

U.J. Patel^a

S.C. Coley^f

^a Department of Neurosurgery, Royal Hallamshire Hospital, Sheffield, UK

^b Medical Physics, Royal Hallamshire Hospital, Sheffield, UK

^c Academic Unit of Medical Physics, School of Medicine and Biomedical Sciences, University of Sheffield, Sheffield, UK

^d Institute of Tropical Medicine, Berlin Germany

^e Department of Neurosurgery, Mohamed Vth University School of Medicine, Hospital des Spécialités ONO, Rabat 10100, Morocco

^f Department of Neuroradiology, Royal Hallamshire Hospital, Sheffield, UK

* Corresponding author.

E-mail address: neurosurgery2007@gmail.com (P.K. Singh)

Computational Hemodynamics in Cerebral Aneurysms: The Effects of Modeled Versus Measured Boundary Conditions

ALBERTO MARZO,¹ PANKAJ SINGH,² IGNACIO LARRABIDE,^{3,4,5} ALESSANDRO RADAELLI,⁶ STUART COLEY,⁷ MATT GWILLIAM,⁸ IAIN D. WILKINSON,⁹ PATRICIA LAWFORD,¹ PHILIPPE REYMOND,¹⁰ UMANG PATEL,¹¹ ALEJANDRO FRANGI,^{3,4,5} and D. ROD HOSE¹

¹Department of Cardiovascular Science, Academic Unit of Medical Physics, Faculty of Medicine and Biomedical Sciences, University of Sheffield, Beech Hill Road, S10 2RX Sheffield, UK; ²Departments of Medical Physics and Neurosurgery, Royal Hallamshire Hospital, Sheffield, UK; ³Centre for Computational Imaging and Simulation Technologies in Biomedicine, Universitat Pompeu Fabra (UPF), Barcelona, Spain; ⁴Centre for Networked Biomedical Research on Bioengineering, Biomaterials and Nanomedicine (CIBER-BBN), Barcelona, Spain; ⁵Institució Catalana de Recerca i Estudis Avançats (ICREA), Barcelona, Spain; ⁶Philips Healthcare, Best, The Netherlands; ⁷Department of Neuroradiology, Royal Hallamshire Hospital, Sheffield, UK; ⁸Medical Physics and Clinical Engineering, Sheffield Teaching Hospitals NHS, Sheffield, UK; ⁹Department of Human Metabolism, Academic Unit of Radiology, University of Sheffield, Sheffield, UK; ¹⁰Laboratory of Hemodynamics and Cardiovascular Technology (LHCT), École Polytechnique Fédérale de Lausanne, Lausanne, Switzerland; and Department of Neurosurgery, Royal Hallamshire Hospital, Sheffield, UK

(Received 8 June 2010; accepted 9 October 2010; published online 23 October 2010)

Associate Editor Peter E. McHugh oversaw the review of this article.

Abstract—Modeling of flow in intracranial aneurysms (IAs) requires flow information at the model boundaries. In absence of patient-specific measurements, typical or modeled boundary conditions (BCs) are often used. This study investigates the effects of modeled versus patient-specific BCs on modeled hemodynamics within IAs. Computational fluid dynamics (CFD) models of five IAs were reconstructed from three-dimensional rotational angiography (3DRA). BCs were applied using in turn patient-specific phase-contrast-MR (pc-MR) measurements, a 1D-circulation model, and a physiologically coherent method based on local WSS at inlets. The Navier–Stokes equations were solved using the Ansys®-CFX™ software. Wall shear stress (WSS), oscillatory shear index (OSI), and other hemodynamic indices were computed. Differences in the values obtained with the three methods were analyzed using boxplot diagrams. Qualitative similarities were observed in the flow fields obtained with the three approaches. The quantitative comparison showed smaller discrepancies between pc-MR and 1D-model data, than those observed between pc-MR and WSS-scaled data. Discrepancies were reduced when indices were normalized to mean hemodynamic aneurysmal data. The strong similarities observed for the three BCs models suggest that vessel and aneurysm geometry have the strongest influence on aneurysmal hemodynamics. In absence of patient-specific BCs, a distributed circulation model may represent the best option when CFD is used for large cohort studies.

Keywords—Computational fluid dynamics, Phase-contrast MRI, 1D circulation model.

INTRODUCTION

An aneurysm is a localized dilation in a blood vessel, which carries an inherent risk of rupture and consequent hemorrhage; for cerebral aneurysms rupture results in a subarachnoid hemorrhage (SAH). Despite improvements in surgical and medical management, SAH is still a major cause of morbidity and mortality.²⁰

Although the etiology of the disease remains unclear, there is a growing consensus that hemodynamics plays an important role in the growth, rupture, and initiation of intracranial aneurysms (IAs).^{6,38,40}

In this respect, a reliable prediction of stress or strain of the aneurysm wall would possibly offer a greater diagnostic capacity in the context of imminent rupture (it is likely that the event of rupture occurs when the tissue stress or strain exceeds some sustainable level). The stress and strain in the aneurysm can be calculated if the geometry, material characteristics, and boundary (support) conditions are known: unfortunately this will never be true for an individual and approximations would be required for all of them, thus compromising accuracy. The hemodynamic characterization returns parameters that might drive

Address correspondence to Alberto Marzo, Department of Cardiovascular Science, Academic Unit of Medical Physics, Faculty of Medicine and Biomedical Sciences, University of Sheffield, Beech Hill Road, S10 2RX Sheffield, UK. Electronic mail: a.marzo@shef.ac.uk, avmarzo@gmail.com

biological processes that are important in the evolution of an aneurysm toward a state in which it will rupture. This, despite a smaller diagnostic capacity might provide more accurate predictions, which might prove important with respect to correlation to rupture. Several hemodynamic indices and many biological patterns have been proposed that link hemodynamics to aneurysm formation, and evolution. These are well summarized by Singh *et al.*⁴² Two hemodynamic indices, wall shear stress (WSS) and oscillatory shear index (OSI), have received particular attention due to their influence on endothelial cell behavior.^{6,40}

Although studies from Rayz *et al.*,³⁶ Boussel *et al.*,¹ and Isoda *et al.*²² showed that *in vivo* measurement of these quantities is possible using magnetic resonance, inherent limitations in the current technology impede its use, especially for smaller aneurysms, in large cohort studies.

In this context, computational fluid dynamics (CFD) can provide detailed predictions of hemodynamics using input parameters derived from medical imaging, blood sampling, and other patient information. CFD has been used by many groups to investigate possible correlations between hemodynamics and risk of rupture or growth of IAs. For convenience, the spatial extent of the computational domain is often limited to a restricted area around the aneurysm and specification of boundary conditions (BCs) at the interfaces with the rest of the cardiovascular network remains a pre-requisite to find a numerical solution. This issue is approached in different ways by different authors.

Some studies use patient-specific BCs based on measurements obtained using phase-contrast-MR (pc-MR) or transcranial Doppler (TCD) ultrasound, to record blood velocity, and applanation tonometry, to infer pressure. More recently Ferns and colleagues¹³ have used a dual-sensor wire to measure *in vivo* pressure and blood flow velocity within intracranial vessels. These measurements are costly to perform, are currently rarely justifiable as part of the clinical routine and are inherently difficult to obtain for the small, intricate vessels of the cerebral vasculature hence, such studies often involve small cohorts and the results lack statistical significance.^{1,19,24}

Larger cohort studies, in contrast, rely on inflow BCs based on measurements taken from healthy individuals, that are, in some cases^{8,23,29,35,44} scaled in an attempt to achieve a more realistic mean WSS, and outflow BCs that arbitrarily assume the same pressure at all openings (zero pressure BCs). The assumptions associated with this approach may also lead to unrealistic results.

As detailed comparison with *in vivo* measurements is currently difficult, the validity of CFD tools in the

context of IA rupture-risk assessment relies upon the extent to which the correlations between hemodynamic predictions and rupture are statistically matched for a large cohort study. One of the important aims of @neurIST (www.aneurist.org), a multidisciplinary EU project of which this study forms a part, is to establish these correlations by processing a large number of cases. The lack of patient-specific data for use at computational boundaries remains an important limiting factor in the project. This issue has been addressed by deriving a complete set of BCs for 3D CFD analysis from a 1D model of the circulatory system.³⁷

This article analyses and compares the sensitivity of modeled hemodynamics within typical IAs to BCs derived using the 1D model, patient-specific pc-MR measurements, and other approaches described in the literature.

MATERIALS AND METHODS

Study Design, Demographics, and Clinical Details

The study was conducted as a co-operation between the Departments of Neurosurgery and Neuroradiology, Royal Hallamshire Hospital, and the Department of Cardiovascular Science, University of Sheffield, Sheffield, UK. A total of five patients diagnosed with IAs between Dec. 2006 and Jan. 2009, were identified retrospectively and followed prospectively upon appropriate ethical approval and patient consent. Table 1 shows the demographic constitution of the population along with the relevant aneurysm details. All IAs were side-wall saccular aneurysms with locations shown in Figs. 1 and 2.

X-ray Angiography Image Acquisition

The medical images used for surface reconstruction were obtained using 3D rotational acquisition (3DRA) in a Philips® Integris™ Allura machine (Philips® Medical Systems, Best, The Netherlands), producing

TABLE 1. Patient demographics and aneurysm radiological features.

Aneurysm	Sex	Age	Side	Location	Rupture	Size (diam/neck) (mm)
1	M	44	Left	ICA	No	5/4.3
2	M	52	Left	MCA	No	11.1/4.3
3	F	50	Left	ICA	No	3.4/3.1
4	F	41	Right	MCA	Yes	4.4/3
5	F	51	Left	ICA	No	2.9/3.1

ICA, internal carotid artery; MCA, middle cerebral artery bifurcation.

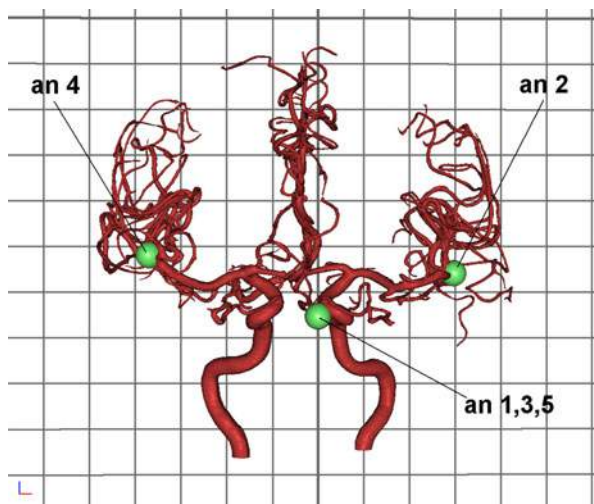


FIGURE 1. Locations of aneurysms 1–5 in typical cerebral vasculature (illustration generated using the @neurIST software).

100 images in 6 s, with 5 ms exposure per image. Voxel size in the reconstructed 3D images was 121 microns with reconstruction matrix of $512 \times 512 \times 512$.

pc-MR Protocol

All MR imaging was performed at high field strength (AchievaTM 3.0T, Philips[®] Medical Systems, Best, The Netherlands) using a standard eight-channel, radiofrequency receive-only head coil. The same radiographer imaged all patients to maximize the reproducibility of the overall acquisition technique.¹⁷ A pre-designed protocol guided the radiographer through the desired measurement locations for subsequent application of CFD BCs. As afferent vasculature has an important influence on intra-aneurysmal hemodynamics,^{2,30,32,33} proximal measurements were taken at a distance of approximately 10 parent vessel diameters from the aneurysm. Measurements in distal arteries were taken four diameters away from the IAs. To minimize patient discomfort, table-occupancy time was no greater than 1 h. Within this period it was difficult to ensure that all measurements were obtained for all patients. The tortuous nature of the vasculature also made slice selection perpendicular to the artery difficult to achieve. To maintain integrity in the final measurement data set, data was rejected if there was doubt about the placement of the measurement plane.

Locations of pc-MR measurements are reported Table 2. The manufacturer's proprietary post-data-acquisition software (Q-FlowTM, Philips[®] Medical Systems, Best, The Netherlands) was used to estimate volumetric flow rate (VFR) waveforms at each location.

1D Circulation Model

The model developed by Reymond *et al.*³⁷ was used to compute pressure and VFR waveforms at the desired interfaces with the 3D domains. The model solves the 1D form of the Navier–Stokes equation in a distributed model of the main human systemic arteries including the main arteries of the circle of Willis. It accounts for ventricular–vascular interaction and wall viscoelasticity, and it was recently validated through a comparison with *in vivo* flow measurements. Although the model could be personalized tuning input parameters such as heart rate, cardiac contractility, vessel elasticity, vessel geometry, and blood properties, in this study the model was used with the properties of a typical young individual as patient-specific data was not available for all patients. A typical analysis is solved in approximately 8 min.

3D Models

The @neurIST computational tool chain was used to reconstruct vessel and aneurysmal geometries, as described in Marzo *et al.*³⁰ The 3D transient Navier–Stokes equations were solved by using the finite-control-volume software, ANSYS[®]-CFXTM. Blood was assumed to be incompressible, with density $\rho = 1060 \text{ kg m}^{-3}$, and Newtonian, with viscosity $\mu = 0.0035 \text{ Pa s}$. BCs were applied using three different approaches, as reported in Table 2. *Method I* used pc-MR VFR measurements at the openings for which these could be measured, and 1D model pressure waveforms at every remaining interface. For aneurysm 1 and 5, measurements were available at all but one vessel opening. *Method II* used VFR and pressure waveforms from the 1D circulation model. *Method III* used the typical waveforms derived using the 1D model, where VFR curves were scaled to obtain a mean WSS of 1.5 Pa at inlets. For all velocity-based BCs a flat velocity profile was applied, in line with our recent finding.³⁰ Arterial walls were assumed to be rigid. The validity of this assumption has been tested in the context of IAs.¹¹ Tetrahedral elements were used to discretise the core of the computational domain, with three layers of prismatic elements at the wall to ensure accurate computation of the velocity gradients. Grid sizes with an average density of 2000 el/mm^3 were used following a mesh dependency study in which WSS, pressure and velocity values, were monitored at several points within the aneurysm and parent vessel.³⁵ Figure 2 shows the meshes and BC types used in the analyses. To be independent of the initial numerical conditions hemodynamic data were extracted from the last cardiac cycle of a three-cycle analysis. Analyses were run

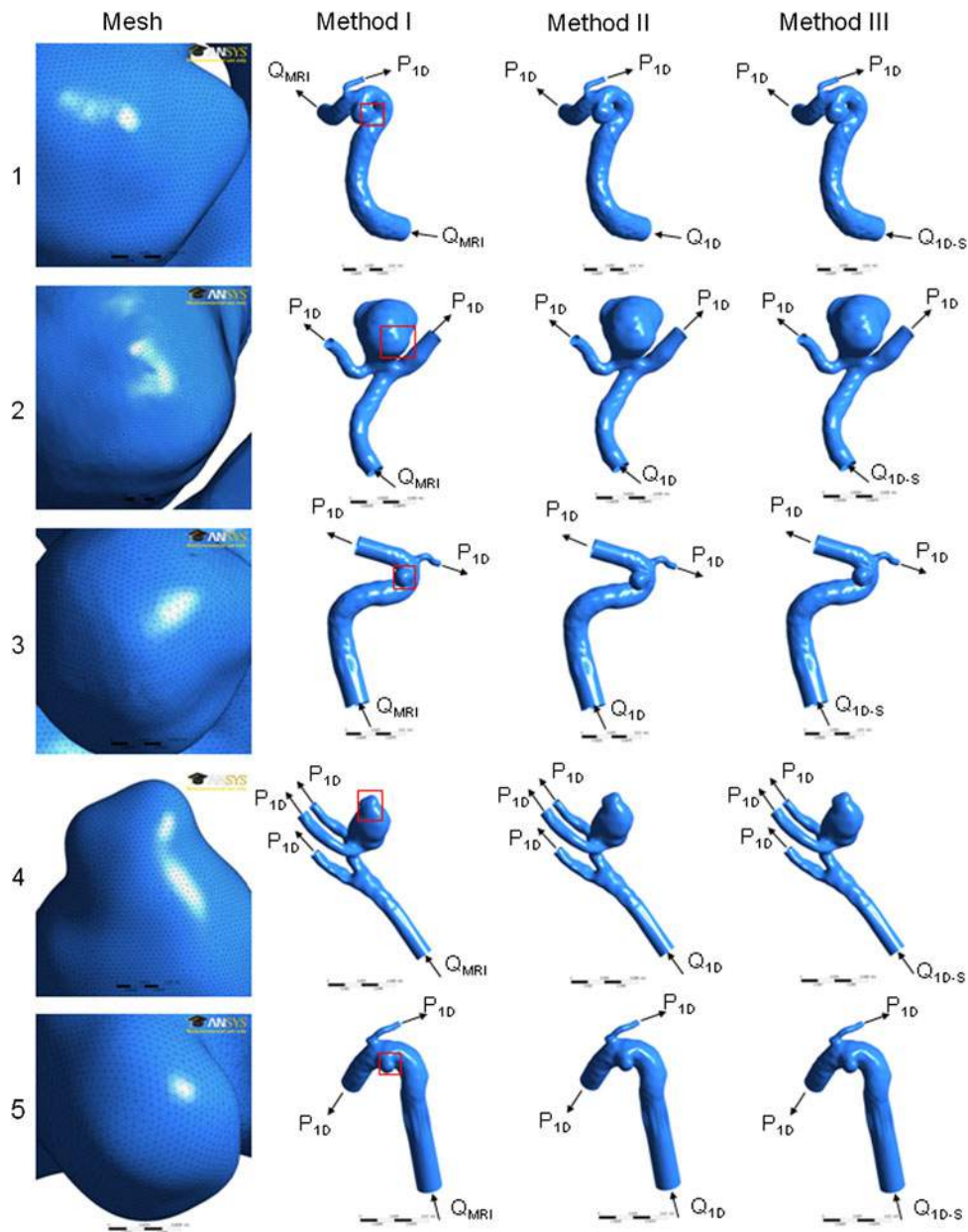


FIGURE 2. Mesh particulars and BC types used. Q_{MRI} is the velocity-based boundary condition from MRI patient-specific measurements, Q_{1D} is the velocity-based boundary condition from 1D model, Q_{1D-S} is the WSS-scaled velocity-based boundary condition from 1D model, and P_{1D} is the pressure boundary condition from 1D model.

in parallel using 30 cluster nodes (Xeon® 2.8 GHz, 2 GB RAM). The average time required to solve a complete three-cycle analysis was 5 h.

Statistical Analysis

Quantitative agreement between data obtained with the different BC methodologies was analyzed using boxplot diagrams.

RESULTS

Hemodynamic variables were compared qualitatively and quantitatively for the BC methods analyzed.

Qualitative Comparison

Figure 3 shows contour distributions of WSS time-averaged along the cardiac cycle (tavWSS) at the wall of the IAs. For all methods, in aneurysms 1, 2, areas of

TABLE 2. Boundary conditions location, type, and method.

Aneurysm	BC location	Type	Method I	Method II	Method III
1	ICA proximal	Inlet	pc-MR/velocity	1D/velocity	1D/velocity scaled
	ICA distal	Outlet	pc-MR/velocity	1D/pressure	1D/pressure
	OphthA	Outlet	1D/pressure	1D/pressure	1D/pressure
2	MCA M1	Inlet	pc-MR/velocity	1D/velocity	1D/velocity scaled
	MCA M2 supr	Outlet	1D/pressure	1D/pressure	1D/pressure
	MCA M2 infr	Outlet	1D/pressure	1D/pressure	1D/pressure
3	ICA proximal	Inlet	pc-MR/velocity	1D/velocity	1D/velocity scaled
	ICA distal	Outlet	1D/pressure	1D/pressure	1D/pressure
	OphthA	Outlet	1D/pressure	1D/pressure	1D/pressure
4	MCA M1	Inlet	pc-MR/velocity	1D/velocity	1D/velocity scaled
	TempA	Outlet	1D/pressure	1D/pressure	1D/pressure
	MCA M2 supr	Outlet	1D/pressure	1D/pressure	1D/pressure
	MCA M2 infr	Outlet	1D/pressure	1D/pressure	1D/pressure
5	ICA proximal	Inlet	pc-MR/velocity	1D/velocity	1D/velocity scaled
	ICA distal	Outlet	pc-MR/velocity	1D/pressure	1D/pressure
	OphthA	Outlet	1D/pressure	1D/pressure	1D/pressure

ICA, internal carotid artery; OphthA, ophthalmic artery; MCA M1, middle cerebral artery; MCA M2 supr/infr, superior/inferior division of the middle cerebral artery; TempA, temporal artery.

relatively high WSS were concentrated around the aneurysmal neck and apex, while in aneurysm 5, an area of relatively high WSS is also present in the body. In aneurysms 3 and 4 only the neck is affected by high WSS, with the remainder of the aneurysmal wall exposed to lower WSS. For all aneurysms, areas of relatively low WSS were found in their bodies.

From a visual comparison of the contour plots, the most pronounced differences between method I (pc-MR) and method II (1D model) are in the distribution of tavWSS for aneurysms 1, 3, and 5, whereas aneurysms 2 and 4 showed closer agreement. In terms of qualitative differences between patient-specific and 1D model waveforms tavWSS values were underestimated when 1D-model BCs were applied, for all IAs except IA2.

Qualitative comparison of method I (pc-MR) and method III (WSS scaled) revealed larger differences than those observed when comparing methods I and II, except for aneurysm 1 where contour values of tavWSS are closer to the predictions of method I. For all IAs, the values of tavWSS obtained with method III are lower than those observed for method I.

Figure 4 shows contours of normalized values of tavWSS (ntavWSS). Normalization was achieved by dividing the absolute values of tavWSS by the spatial average of tavWSS at the aneurysmal wall. Interestingly, for all methods, there is similarity in the overall distribution of areas of proportionally higher, or lower, WSS.

Figure 5 shows contour distributions of OSI on the aneurysmal surface. Although small differences can be observed, the OSI patterns are very similar.

As expected, areas of elevated OSI tend to be associated with low tavWSS . OSI values obtained with method II look closer to the pc-MR-based values, than those obtained using method III.

Quantitative Comparison

Figure 6 shows the boxplots diagrams of the percentage differences between method I and method II (top boxplot) and method I and method III (bottom boxplot) for selected indices computed within the aneurysmal sac, namely; maximum OSI (mOSI), normalized maximum value of time-average WSS (nmtavWSS), maximum time-average WSS (mtavWSS), maximum time-average velocity (mtavU) and spatial and time-average velocity (stavU). The percentage error was calculated from $(\text{index_value}_{\text{method I}} - \text{index_value}_{\text{method X}})100/\text{index_value}_{\text{method I}}$. As previously observed qualitatively, comparisons show that the smallest discrepancies are observed in the values of mOSI and nmtavWSS (median value 17.5–23.5% for mOSI and 11–20.5% for nmtavWSS). The hemodynamic index showing highest discrepancies is mtavWSS with median values of 46% for method I versus II and 69% for method I versus III.

When considering the cross-comparison of methods II (1D model) and III (WSS scaled) with method I (pc-MR) (which is assumed to be the gold standard), the largest discrepancies are observed for the comparison between methods I and III. If we consider only the median values of each index we observe that, for method I, all indices perform better than their counterpart in method III.

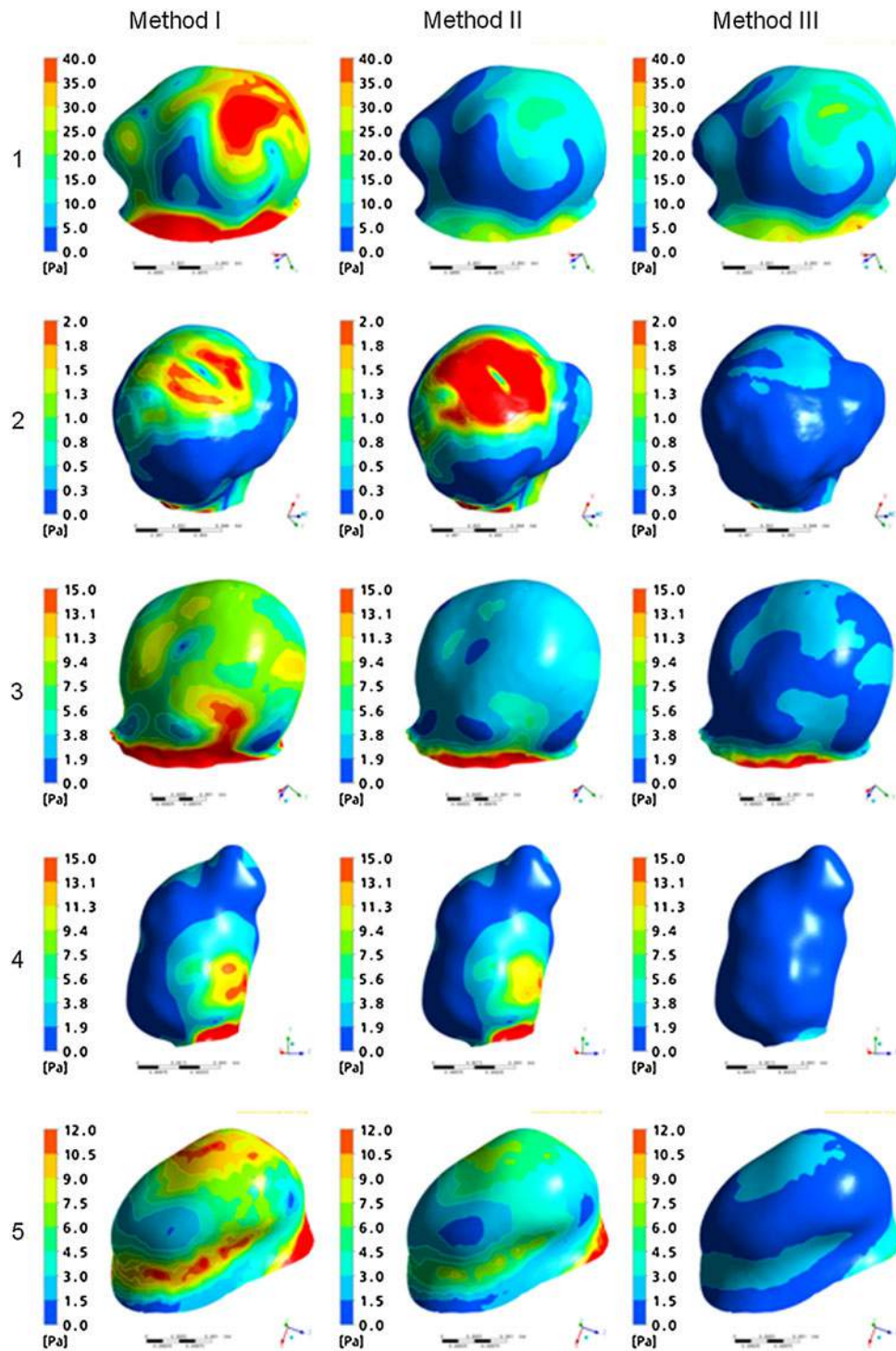


FIGURE 3. Contour plots of tavWSS for method I (pc-MR), method II (1D model), and method III (WSS scaled).

DISCUSSION

In creating a computational model to predict the hemodynamics in an IA, assumptions are often made that can adversely affect the numerical results. One of the most important areas where assumptions are

required is the application of BCs. Several authors have demonstrated the significant influence of BCs on computed hemodynamic indices.^{9,19,44}

Depending on the method of derivation, BCs can be broadly divided into two categories; those that are patient-specific and those that are non-patient-specific.

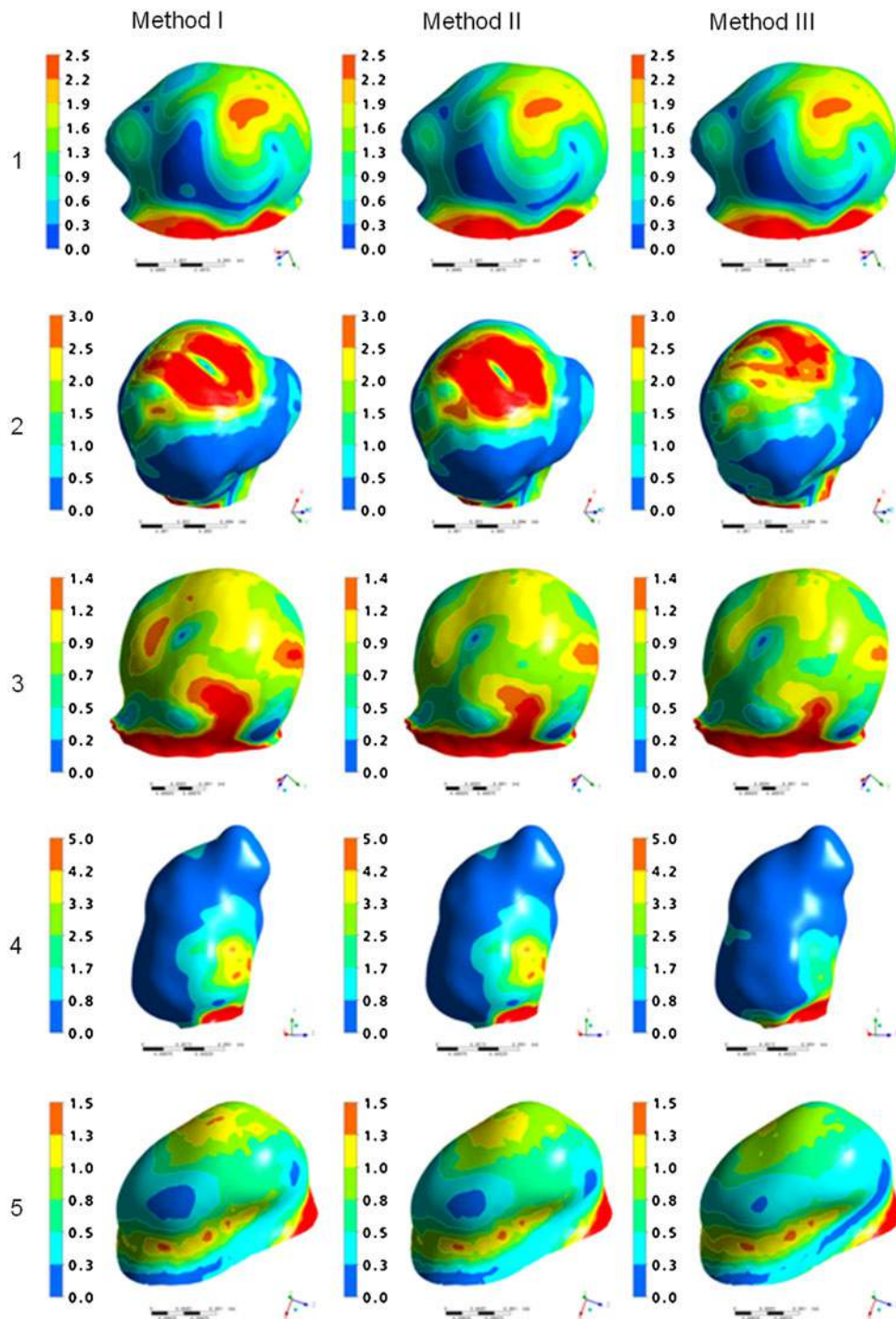


FIGURE 4. Contour plots of normalized values of tavWSS for method I (pc-MR), method II (1D model), and method III (WSS scaled).

Patient-Specific BC's

Patient-specific BCs are understandably considered the “gold standard.”^{9,19,44} Unfortunately, these are rarely available. Of 24 articles reviewed for this study (Table 3), only 6 (25%) used patient-specific BCs.^{1,19,24} pc-MR was the most common modality (5 out of 6)

used to obtain patient-specific measurements, with TCD used by one author.¹⁹ Most authors (5 out of 6), applied these measurements only at inlets. Only one group, Jou and colleagues,²⁵ used patient-specific pc-MR measurements at both inlets and outlet when analyzing a basilar artery fusiform aneurysm. Thus,

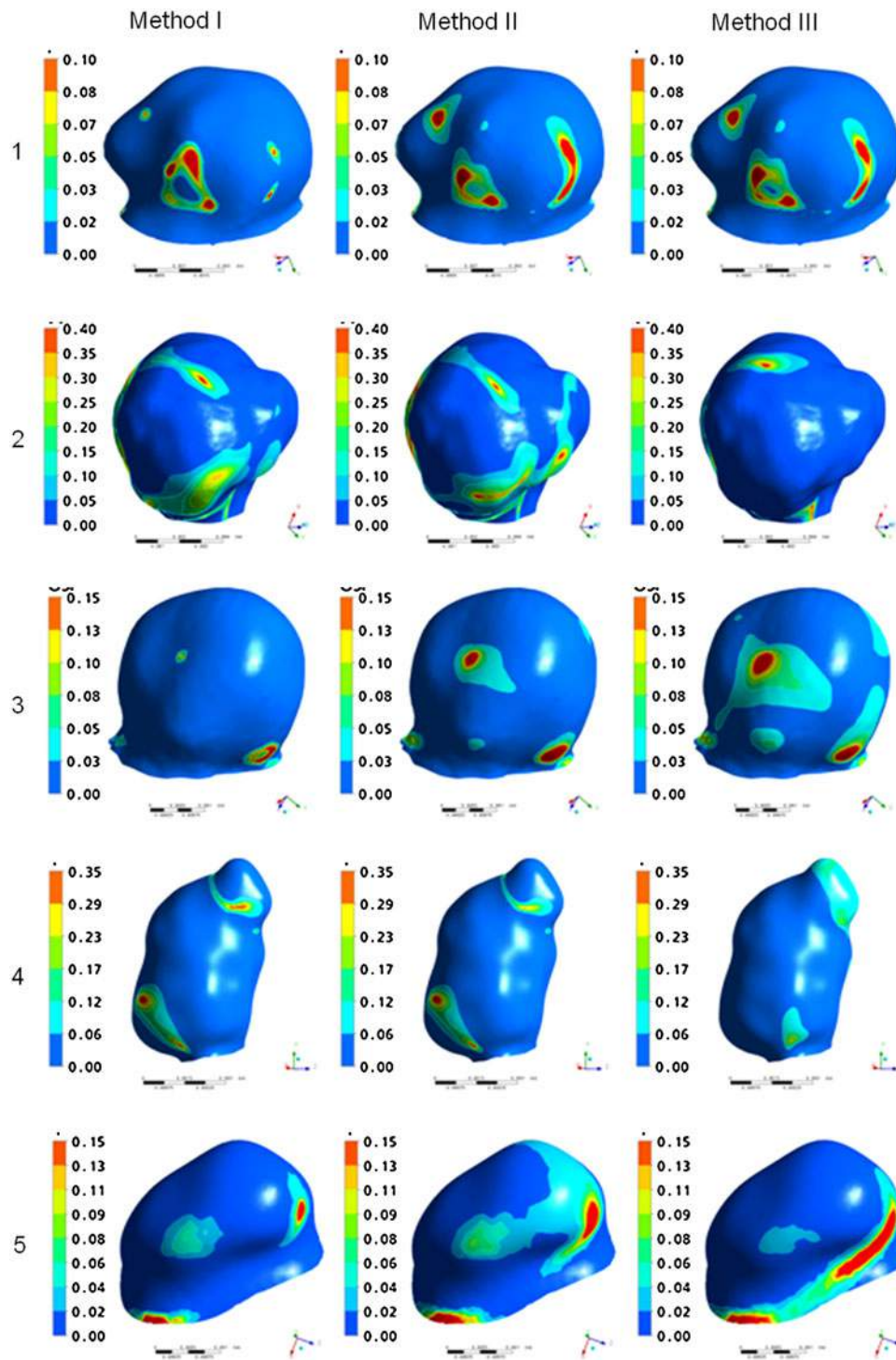


FIGURE 5. Contour plots of OSI for method I (pc-MR), method II (1D model), and method III (WSS scaled).

even when patient-specific measurements can be justified in a busy clinical setting, technical difficulties may compromise their application at all openings, further limiting their use in establishing statistical correlations with rupture. In fact, a major constraint when adopting patient-specific BCs is that due to current

restrictions in obtaining these measurements, they have not been applied in large cohort studies, thus compromising the possibility of using CFD to find significant statistical correlations between hemodynamics and aneurysmal evolution (initiation, growth, and rupture). In the current review, the mean cohort size

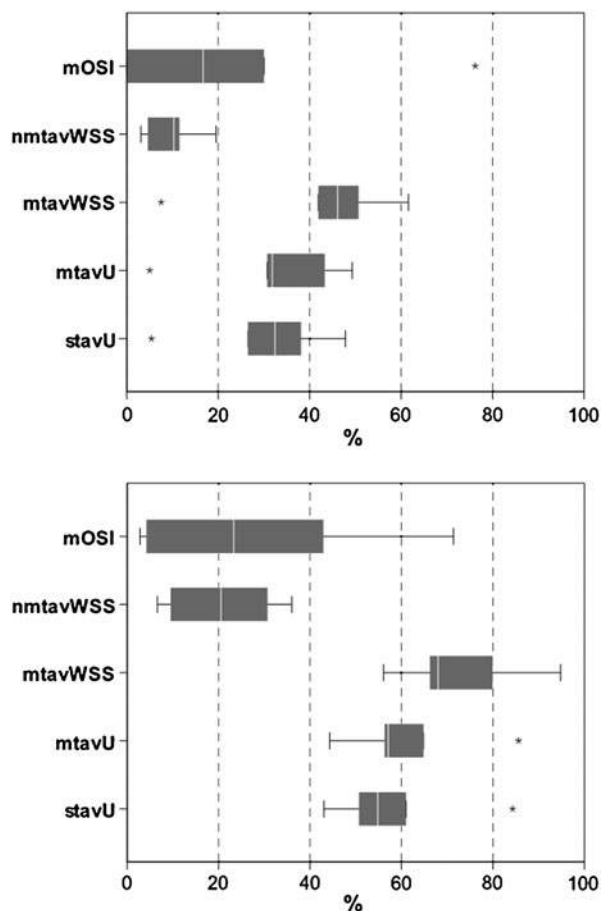


FIGURE 6. Boxplots showing the distribution percentage differences between method I and II (top) and method I and III (bottom). Asterisks denote outliers above or below 1.5 times the inter-quartile range.

for the patient-specific BC group was significantly smaller, i.e. 3 (range 1–7) compared to 9.5 (range 1–62) when non-patient-specific BCs were used. Another important aspect one has to consider: there may be significant diurnal variation in values for an individual associated with stress or anxiety,^{12,27} physical exertion,^{16,21} and other day-to-day activities.¹⁸ It can be argued that patient-specific BCs, invariably measured with a patient lying quietly in a scanner surrounded by an artificial environment or stressed by the overall clinical experience (e.g., white-coat hypertension), might not represent the normal day-to-day physiology for that individual, and thus might not represent exactly the type of BCs needed for statistical associations. Gonzalez-Alonso *et al.*¹⁶ recorded a population-average flow rate variation as high as 1 mL/s at the level of middle cerebral artery level between rest and exercise.

Another important aspect is the error associated with blood flow measurement. For quantitative MR angiography average measurement errors have

been reported to be as high as 7.6% for pulsatile flow.⁴⁵

Non-Patient-Specific BC

In absence of patient-specific BCs many investigators use typical or modeled BCs. Out of 24 papers, 18 (75%) used this approach. Waveforms are usually obtained from population-averaged measurements taken on healthy volunteers.^{14,43} While the use of such waveforms remains the most popular method of BC application (17 out of 18 non-patient-specific BCs in our review), the method carries important limitations. First, as these measurements are taken in a healthy population, they may not be representative of patient waveforms. This is illustrated in Fig. 7, where waveforms from a healthy volunteer show differences both in shape and values, when compared with those for patients 1, 3, and 5.

Second, these waveforms represent average values of pressure and velocity across the population, and lack adaptability in terms of location and vessel geometrical properties. In an attempt to address these issues and make these typical waveforms more patient-specific, Cebral and colleagues⁷ suggested “scaling” the inflow rates to the inflow boundary area to keep the WSS within a “physiological” range (around 1.5 Pa). The same approach has been adopted by other scientists.^{23,31,35} Although Cebral and co-workers found an important flow-area correlation based on experimental evidence at some specific vessel locations, their approach can be very sensitive to the boundary location along the vessel, due to diameter variations along the vessel, and to segmentation error and image modality. This approach may be appropriate for a typical healthy individual but, as reported by many authors in the field, it is predominantly atypical variations in hemodynamics (e.g., WSS) that are believed to influence the etiopathogenesis of IAs.^{38,40} Cheng *et al.*¹⁰ challenged this hypothesis in their recent review, which showed large variations of average WSS (range 0.2–1.6 Pa). Atypical values of WSS have been associated with other conditions such as maladaptive growth, congenital malformations, patent ductus arteriosus, and atherosclerosis.

Quarteroni and collaborators pioneered the concept of using lumped and 1D-circulation models in an attempt to provide realistic BCs to 3D models.^{15,28,34} More recently in 2009, we³⁰ introduced the use of a 1D-circulation model to derive BCs while studying hemodynamics within IAs. This model is used in the current study. The parameters of the 1D model used are relative to a healthy typical individual, an approach exposed to the limitations mentioned above for typical “healthy” waveforms. Indeed, this might

TABLE 3. A comprehensive review showing the methods adapted by different authors while applying BCs.

No.	Author/references	Cohort size (IAs)	IA location (s)	BC type/location	BC source (method)
1	Steinman <i>et al.</i> ⁴³	1	Terminal ICA	Inlet/ICA Outlets/MCA, ACA	Healthy subjects (pc-MR) Traction free
2	Chatziprodromou <i>et al.</i> ⁹	2	Supraclinoid ICA	Inlets/ICA Outlets/ICA	Idealized Traction free
3	Jou <i>et al.</i> ²⁴	1	BA (fusiform)	Inlets/VA Outlet/BA	Patient-specific (pc-MR) Patient-specific (pc-MR)
4	Hassan <i>et al.</i> ¹⁹	1	Vertebro-basilar	Inlet/VA Outlet/BA	Patient-specific (TCD) Traction free
5	Shojima <i>et al.</i> ⁴⁰	20	MCA	Inlets/MCA-M1 Outlets/MCA-M2	Healthy subjects (TCD) Traction free
6	Cebral <i>et al.</i> ⁶	62	ICA (22), MCA (14), Pcom (13), ACA (1), Post (9), (3 NA)	Inlets/ICA, MCA, ACA, BA Outlets/NA	Healthy subjects (pc-MR) NA
7	Jou <i>et al.</i> ²⁵	2	BA (fusiform)	Inlets/VA Outlets/PCA	Patient-specific (pc-MR) NA
8	Shojima <i>et al.</i> ⁴¹	29	ICA (14), MCA (14), ACA (1)	Inlets/ICA Outlets/ICA, MCA	Healthy subjects (TCD) Traction free
9	Cebral <i>et al.</i> ⁵	4	ICA (2), SCA (1), Pcom (1)	Inlets/NA Outlets/NA	Healthy subjects (pc-MR) Traction free
10	Karmonik <i>et al.</i> ²⁶	3	BA (top)	Inlets/BA, VA Outlet	Healthy subjects (pc-MR) NA
11	Castro <i>et al.</i> ²	4	Pcom (1), Acom (1), MCA (2)	Inlets/NA Outlets/NA	Healthy subjects (pc-MR) Traction free
12	Castro <i>et al.</i> ⁴	7	Acom (1), BA (1), ICA (2), MCA (1), SCA (1), PCA (1)	Inlets/NA Outlets/NA	Healthy subjects (pc-MR) Traction free
13	Castro <i>et al.</i> ³	2	Acom	Inlets/ICA Outlets/NA	Healthy subjects (pc-MR) Traction free
14	Mantha <i>et al.</i> ²⁹	3	ICA	Inlets/NA Outlets/NA	Healthy subjects (scaled) NA
15	Venugopal <i>et al.</i> ⁴⁴	1	Acom	Inlets/A1 Outlets/A2	Healthy subjects (scaled) Zero pressure
16	Boussel <i>et al.</i> ¹	7	BA (3), ICA (3), MCA (3)	Inlets/NA Outlets/NA	Patient-specific (pc-MR) NA
17	Mitsos <i>et al.</i> ³¹	1	Acom	Inlet/NA Outlet/NA	Healthy subjects (LDV) Traction free
18	Rayz <i>et al.</i> ³⁶	4	BA	Inlets/VA Outlets/PCA	Patient specific (pc-MR) Traction free
19	Radaelli <i>et al.</i> ³⁵	1	ICA	Inlet/ICA-proximal Outlet/ICA-distal	Healthy subjects (scaled) Traction free
20	Rayz <i>et al.</i> ³⁶	3	BA	Inlet/VA Outlet/PCA	Patient-specific (pc-MR) Likely traction free
21	Shimogonya <i>et al.</i> ³⁹	1	ICA	Inlet/ICA-proximal Outlet/ICA-distal	Healthy subjects waveforms Traction free
22	Jou <i>et al.</i> ²³	26	ICA-clinoidal	Inlets/ICA Outlet/NA	Healthy subjects (scaled) NA
23	Marzo <i>et al.</i> ³⁰	3	BA, ICA	Inlet/BA, ICA-proximal Outlet/BA, ICA-distal	Computed (1-D model) Traction free
24	Cebral <i>et al.</i> ⁸	1	BA (top)	Inlet/mid-BA Outlets/PCA	Healthy subjects (scaled) Traction free

BCs, boundary conditions; PC-MR, phase contrast magnetic resonance angiography; TCD, trans-cranial Doppler's ultrasound; LDV, laser Doppler velocimetry; ICA, internal carotid artery; ACA, anterior cerebral artery; Acom, anterior communicating artery; MCA, middle cerebral artery; Pcom, posterior communicating artery; SCA, superior cerebellar artery; BA, basilar artery; VA, vertebral artery; Post, posterior circulation.

explain, in part, the quantitative discrepancies observed. The use of a 1D model, however, has the advantage of allowing flexibility in the location of the model boundaries and, more importantly, has the potential for adaptation to patient-specific parameters,

when available, to obtain more representative values at the boundaries. The comparison in Fig. 6 (top) shows important differences between 1D model and pc-MR data ranging from a minimum median value of 11% (OSI) to a maximum of 46% (mtavWSS).

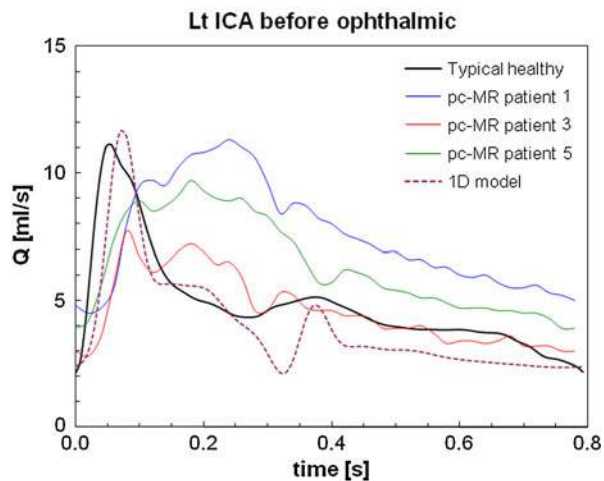


FIGURE 7. VFR waveforms for a typical healthy individual and aneurysm patients included in this study, measured using pc-MR at internal carotid level. Typical waveform was taken from Radaelli *et al.*³⁵

TABLE 4. Time-average volumetric flow rates and inlet radii for the five aneurysms.

	Q_{av-MR} (mL/s)	Q_{av-1D} (mL/s)	Q_{av-wss} (mL/s)	r_{pt} (mm)	r_{1D} (mm) ^a
Aneu-1	7.53	3.95	4.31	2.3	2.1–2.6
Aneu-2	1.46	1.90	0.74	1.3	1.4–1.5
Aneu-3	6.36	3.94	3.11	2.1	2.1–2.6
Aneu-4	2.00	1.91	0.42	1.1	1.4–1.5
Aneu-5	5.44	3.95	2.21	1.9	2.1–2.6

Aneu, aneurysm; Pt, patient; Q_{av-MR} , average flow measured using pc-MR; Q_{av-1D} , average flow predicted by 1D-model; Q_{av-WSS} , average flow predicted by 1D-model scaled to obtain $wss = 1.5$ Pa at boundary; r_{pt} , radius of the vessel as measured in the patient; r_{1D} , average radius of the vessel used in 1D-model.

^aMin and max radii in 1D model vessel where BCs was originated.

These discrepancies, however, are determined by differences in flow rates between the 1D model and patient-specific waveforms, which are of the same order of magnitude to physiological variations reported by Gonzalez-Alonso *et al.*¹⁶, see Table 4. While there are quantitative differences in hemodynamic indices obtained by the different methods, comparisons using normalized data showed that the distribution of WSS remains unchanged. This confirms once again the significance of geometry in determining the hemodynamic development within the aneurysm,^{5,30} but also some degree of linearity of the results with respect to the flow within the aneurysm. Table 5 shows information on geometry and flow immediately proximal to the aneurysm sac for all three methods considered. Re values show a certain degree of linearity with respect to the absolute values reported in Fig. 3.

Comparisons of OSI values showed good agreement between the three methods. This is to be expected

TABLE 5. Reynolds numbers of flow approaching aneurysm, aneurysm aspect ratios, and vessel radii.

Aneurysm	Re I	Re II	Re III	Surface ratio	r_{prox} (mm)
1	551	285	311	4.7	1.8
2	140	228	89	20.1	1.3
3	343	223	176	5.6	2.1
4	155	184	138	15.5	0.9
5	434	298	152	2.5	1.9

Re I–II–III, Reynolds numbers of flow approaching aneurysm for pc-MRI (I), 1D model (II), and WSS-scaled (III) boundary conditions methods measured at end diastole; Surface ratio, aneurysm surface area over neck surface area; r_{prox} , vessel radius proximal to aneurysm.

as OSI, in its definition, uses the normalization of local WSS.

Although blood is a non-Newtonian fluid, in this study we made the assumption of constant viscosity. This is a valid assumption in the context of a study whose aim is to evaluate the influence of BCs on intra-aneurysmal flow. In this respect, the use of a non-Newtonian model would have negligible influence on our findings as the same rheology model would be consistently used to study the influence of BCs. Also, Cebal *et al.*⁵ showed that the sensitivity of hemodynamic predictions to different rheology models is negligible in the context of aneurysmal hemodynamics.

The current study would benefit from a larger aneurysm cohort (although this would, of course, be subject to clinical limitations), and from a wider range of aneurysm locations (for example, aneurysm of the anterior communicating artery (AComMA) or basilar artery), which were not available in this study.

Summary

Whereas we can easily extract information about aneurysm and vessel geometry, measurements of blood flow to be used as BCs in numerical predictions are more difficult to determine. As hemodynamic factors are believed to be important in the aneurysm natural history, we investigated the variability of certain hemodynamic parameters with BCs. In this preliminary study differences were found between results obtained with patient-specific and modeled BCs. These are attributable to underlying differences in the Re of the flow approaching the aneurysms. In fact, discrepancies were significantly reduced when considering normalized indices, suggesting a certain degree of linearity in the results and the important role played by geometry in intraneurysmal hemodynamics. It is likely that in the future patient-specific BCs will be provided as a part of routine clinical procedure. Until then, affirmation of CFD will be based on finding statistical correlations using non-patient-specific BCs. The results

of this study show that modeled BCs allow realistic predictions of IA hemodynamics and offer a viable means for finding correlations with rupture in large cohort studies.

ACKNOWLEDGMENTS

The @neurIST project is funded by the European Commission, VI Framework Programme, Priority 2, Information Society Technologies (Oxfordshire Research Ethics Committee—A Study Number: 07/Q1604/53).

REFERENCES

- ¹Boussel, L., V. Rayz, *et al.* Aneurysm growth occurs at region of low wall shear stress: patient-specific correlation of hemodynamics and growth in a longitudinal study. *Stroke* 39(11):2997–3002, 2008.
- ²Castro, M. A., C. M. Putman, *et al.* Computational fluid dynamics modeling of intracranial aneurysms: effects of parent artery segmentation on intra-aneurysmal hemodynamics. *AJNR Am. J. Neuroradiol.* 27(8):1703–1709, 2006.
- ³Castro, M. A., C. M. Putman, *et al.* Patient-specific computational fluid dynamics modeling of anterior communicating artery aneurysms: a study of the sensitivity of intra-aneurysmal flow patterns to flow conditions in the carotid arteries. *AJNR Am. J. Neuroradiol.* 27(10):2061–2068, 2006.
- ⁴Castro, M. A., C. M. Putman, *et al.* Patient-specific computational modeling of cerebral aneurysms with multiple avenues of flow from 3D rotational angiography images. *Acad. Radiol.* 13(7):811–821, 2006.
- ⁵Cebral, J. R., M. A. Castro, *et al.* Efficient pipeline for image-based patient-specific analysis of cerebral aneurysm hemodynamics: technique and sensitivity. *IEEE Trans. Med. Imaging* 24(4):457–467, 2005.
- ⁶Cebral, J. R., M. A. Castro, *et al.* Characterization of cerebral aneurysms for assessing risk of rupture by using patient-specific computational hemodynamics models. *AJNR Am. J. Neuroradiol.* 26(10):2550–2559, 2005.
- ⁷Cebral, J. R., M. A. Castro, *et al.* Flow–area relationship in internal carotid and vertebral arteries. *Physiol. Meas.* 29(5):585–594, 2008.
- ⁸Cebral, J. R., S. Hendrickson, *et al.* Hemodynamics in a lethal basilar artery aneurysm just before its rupture. *AJNR Am. J. Neuroradiol.* 30(1):95–98, 2009.
- ⁹Chatziprodromou, I., V. D. Butty, *et al.* Pulsatile blood flow in anatomically accurate vessels with multiple aneurysms: a medical intervention planning application of computational haemodynamics. *Flow Turbul. Combust.* 71:333–346, 2003.
- ¹⁰Cheng, C., F. Helderman, *et al.* Large variations in absolute wall shear stress levels within one species and between species. *Atherosclerosis* 195(2):225–235, 2007.
- ¹¹Dempere-Marco, L., E. Oubel, *et al.* CFD analysis incorporating the influence of wall motion: application to intracranial aneurysms. *Med. Image Comput. Comput. Assist. Interv.* 9(Pt 2):438–445, 2006.
- ¹²Fedorov, B. M., T. V. Sebekina, *et al.* [Stress and blood circulation in man]. *Kosm. Biol. Aviakosm. Med.* 24(3):35–40, 1990.
- ¹³Ferns, S. P., J. J. Schneiders, *et al.* Intracranial blood-flow velocity and pressure measurements using an intra-arterial dual-sensor guidewire. *AJNR Am. J. Neuroradiol.* 31(2):324–326, 2010.
- ¹⁴Ford, M. D., H. N. Nikolov, *et al.* PIV-measured versus CFD-predicted flow dynamics in anatomically realistic cerebral aneurysm models. *J. Biomech. Eng.* 130(2):021015, 2008.
- ¹⁵Formaggia, L., J. F. Gerbeau, *et al.* On the coupling of 3d and 1d Navier–Stokes equations for flow problems in compliant vessels. *Comput. Methods Appl. Mech. Eng.* 191:561–582, 2001.
- ¹⁶Gonzalez-Alonso, J., M. K. Dalsgaard, *et al.* Brain and central haemodynamics and oxygenation during maximal exercise in humans. *J. Physiol* 557(Pt 1):331–342, 2004.
- ¹⁷Gwilliam, M. N., N. Hoggard, *et al.* MR derived volumetric flow rate waveforms at locations within the common carotid, internal carotid, and basilar arteries. *J. Cereb. Blood Flow Metab.* 29(12):1975–1982, 2009.
- ¹⁸Hajjar, I., M. Selim, *et al.* The relationship between nighttime dipping in blood pressure and cerebral hemodynamics in nonstroke patients. *J. Clin. Hypertens. (Greenwich)* 9(12):929–936, 2007.
- ¹⁹Hassan, T., M. Ezura, *et al.* Computational simulation of therapeutic parent artery occlusion to treat giant vertebrobasilar aneurysm. *AJNR Am. J. Neuroradiol.* 25(1):63–68, 2004.
- ²⁰Hop, J. W., G. J. Rinkel, *et al.* Case-fatality rates and functional outcome after subarachnoid hemorrhage: a systematic review. *Stroke* 28(3):660–664, 1997.
- ²¹Ide, K., and N. H. Secher. Cerebral blood flow and metabolism during exercise. *Prog. Neurobiol.* 61(4):397–414, 2000.
- ²²Isoda, H., Y. Ohkura, *et al.* In vivo hemodynamic analysis of intracranial aneurysms obtained by magnetic resonance fluid dynamics (MRFD) based on time-resolved three-dimensional phase-contrast MRI. *Neuroradiology* 52(10):921–928, 2010.
- ²³Jou, L. D., D. H. Lee, *et al.* Wall shear stress on ruptured and unruptured intracranial aneurysms at the internal carotid artery. *AJNR Am. J. Neuroradiol.* 29(9):1761–1767, 2008.
- ²⁴Jou, L. D., C. M. Quick, *et al.* Computational approach to quantifying hemodynamic forces in giant cerebral aneurysms. *AJNR Am. J. Neuroradiol.* 24(9):1804–1810, 2003.
- ²⁵Jou, L. D., G. Wong, *et al.* Correlation between luminal geometry changes and hemodynamics in fusiform intracranial aneurysms. *AJNR Am. J. Neuroradiol.* 26(9):2357–2363, 2005.
- ²⁶Karmonik, C., G. Benndorf, *et al.* Wall shear stress variations in basilar tip aneurysms investigated with computational fluid dynamics. *Conf. Proc. IEEE Eng. Med. Biol. Soc.* 1:3214–3217, 2006.
- ²⁷Kulikov, V. P., V. N. Grechishnikov, *et al.* [Response of cerebral hemodynamics to combined stress impacts]. *Patol. Fiziol. Eksp. Ter.* 1:7–9, 2005.
- ²⁸Lagana, K., G. Dubini, *et al.* Multiscale modelling as a tool to prescribe realistic boundary conditions for the study of surgical procedures. *Biorheology* 39(3–4):359–364, 2002.

- ²⁹Mantha, A., C. Karmonik, *et al.* Hemodynamics in a cerebral artery before and after the formation of an aneurysm. *AJNR Am. J. Neuroradiol.* 27(5):1113–1118, 2006.
- ³⁰Marzo, A., P. Singh, *et al.* Influence of inlet boundary conditions on the local haemodynamics of intracranial aneurysms. *Comput. Methods Biomech. Biomed. Eng.* 12(4): 431–444, 2009.
- ³¹Mitsos, A. P., N. M. Kakalis, *et al.* Haemodynamic simulation of aneurysm coiling in an anatomically accurate computational fluid dynamics model: technical note. *Neuroradiology* 50(4):341–347, 2008.
- ³²Moyle, K. R., L. Antiga, *et al.* Inlet conditions for image-based CFD models of the carotid bifurcation: is it reasonable to assume fully developed flow? *J. Biomech. Eng.* 128(3):371–379, 2006.
- ³³Oshima, M., H. Sakai, *et al.* Modelling of inflow boundary conditions for image-based simulation of cerebrovascular flow. *Int. J. Numer. Methods Fluids* 47:603–617, 2005.
- ³⁴Quarteroni, A., and L. Formaggia. Mathematical modeling and numerical simulation of the cardiovascular system. In: *Handbook of Numerical Analysis*, Vol. 12, edited by P. G. Ciarlet, and J. L. Lions. Amsterdam: Elsevier, 2004, pp. 3–127.
- ³⁵Radaelli, A. G., L. Augsburger, *et al.* Reproducibility of haemodynamical simulations in a subject-specific stented aneurysm model—a report on the Virtual Intracranial Stenting Challenge 2007. *J. Biomech.* 41(10):2069–2081, 2008.
- ³⁶Rayz, V. L., L. Bussel, *et al.* Numerical simulations of flow in cerebral aneurysms: comparison of CFD results and in vivo MRI measurements. *J. Biomech. Eng.* 130(5): 051011, 2008.
- ³⁷Reymond, P., F. Merenda, *et al.* Validation of a one-dimensional model of the systemic arterial tree. *Am. J. Physiol. Heart Circ. Physiol.* 297(1):H208–H222, 2009.
- ³⁸Sekhar, L. N., and R. C. Heros. Origin, growth, and rupture of saccular aneurysms: a review. *Neurosurgery* 8(2): 248–260, 1981.
- ³⁹Shimogonya, Y., T. Ishikawa, *et al.* Can temporal fluctuation in spatial wall shear stress gradient initiate a cerebral aneurysm? A proposed novel hemodynamic index, the gradient oscillatory number (GON). *J. Biomech.* 42(4): 550–554, 2009.
- ⁴⁰Shojima, M., M. Oshima, *et al.* Magnitude and role of wall shear stress on cerebral aneurysm: computational fluid dynamic study of 20 middle cerebral artery aneurysms. *Stroke* 35(11):2500–2505, 2004.
- ⁴¹Shojima, M., M. Oshima, *et al.* Role of the bloodstream impacting force and the local pressure elevation in the rupture of cerebral aneurysms. *Stroke* 36(9):1933–1938, 2005.
- ⁴²Singh, P. K., A. Marzo, *et al.* Effects of heparin on the hemodynamic characteristics of intracranial aneurysms. *J. Neuroradiol.* Apr 5.
- ⁴³Steinman, D. A., J. S. Milner, *et al.* Image-based computational simulation of flow dynamics in a giant intracranial aneurysm. *AJNR Am. J. Neuroradiol.* 24(4):559–566, 2003.
- ⁴⁴Venugopal, P., D. Valentino, *et al.* Sensitivity of patient-specific numerical simulation of cerebral aneurysm hemodynamics to inflow boundary conditions. *J. Neurosurg.* 106(6):1051–1060, 2007.
- ⁴⁵Zhao, M., S. Amin-Hanjani, *et al.* Regional cerebral blood flow using quantitative MR angiography. *AJNR Am. J. Neuroradiol.* 28(8):1470–1473, 2007.

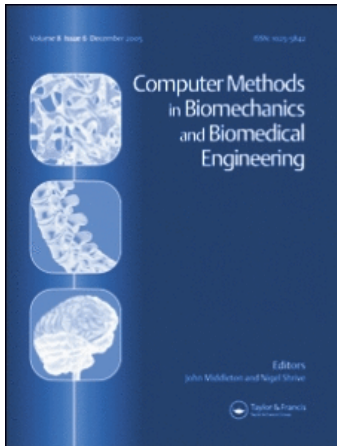
This article was downloaded by: [Warren, Gregg]

On: 2 February 2009

Access details: Access Details: [subscription number 781472160]

Publisher Taylor & Francis

Informa Ltd Registered in England and Wales Registered Number: 1072954 Registered office: Mortimer House, 37-41 Mortimer Street, London W1T 3JH, UK



Computer Methods in Biomechanics and Biomedical Engineering

Publication details, including instructions for authors and subscription information:

<http://www.informaworld.com/smpp/title-content=t713455284>

Influence of inlet boundary conditions on the local haemodynamics of intracranial aneurysms

Alberto Marzo ^a; Pankaj Singh ^{ab}; Philippe Reymond ^c; Nikos Stergiopoulos ^c; Umang Patel ^b; Rodney Hose ^a

^a Department of Medical Physics, School of Biomedical Sciences, University of Sheffield, Sheffield, UK ^b

Department of Neurosurgery, Royal Hallamshire Hospital, Sheffield, UK ^c Laboratory of Hemodynamics and Cardiovascular Technology, École Polytechnique Fédérale de Lausanne, Lausanne, Switzerland

First Published on: 26 January 2009

To cite this Article Marzo, Alberto, Singh, Pankaj, Reymond, Philippe, Stergiopoulos, Nikos, Patel, Umang and Hose, Rodney(2009)'Influence of inlet boundary conditions on the local haemodynamics of intracranial aneurysms',Computer Methods in Biomechanics and Biomedical Engineering,

To link to this Article: DOI: 10.1080/10255840802654335

URL: <http://dx.doi.org/10.1080/10255840802654335>

PLEASE SCROLL DOWN FOR ARTICLE

Full terms and conditions of use: <http://www.informaworld.com/terms-and-conditions-of-access.pdf>

This article may be used for research, teaching and private study purposes. Any substantial or systematic reproduction, re-distribution, re-selling, loan or sub-licensing, systematic supply or distribution in any form to anyone is expressly forbidden.

The publisher does not give any warranty express or implied or make any representation that the contents will be complete or accurate or up to date. The accuracy of any instructions, formulae and drug doses should be independently verified with primary sources. The publisher shall not be liable for any loss, actions, claims, proceedings, demand or costs or damages whatsoever or howsoever caused arising directly or indirectly in connection with or arising out of the use of this material.

Influence of inlet boundary conditions on the local haemodynamics of intracranial aneurysms

Alberto Marzo^{a*}, Pankaj Singh^{ab}, Philippe Reymond^c, Nikos Stergiopoulos^c, Umang Patel^b and Rodney Hose^a

^aDepartment of Medical Physics, School of Biomedical Sciences, University of Sheffield, Sheffield, UK; ^bDepartment of Neurosurgery, Royal Hallamshire Hospital, Sheffield, UK; ^cLaboratory of Hemodynamics and Cardiovascular Technology, École Polytechnique Fédérale de Lausanne, Lausanne, Switzerland

(Received 6 August 2008; final version received 25 November 2008)

Haemodynamics is believed to play an important role in the initiation, growth and rupture of intracranial aneurysms. In this context, computational haemodynamics has been extensively used in an effort to establish correlations between flow variables and clinical outcome. It is common practice in the application of Dirichlet boundary conditions at domain inlets to specify transient velocities as either a flat (plug) profile or a spatially developed profile based on Womersley's analytical solution. This paper provides comparative haemodynamics measures for three typical cerebral aneurysms.

Three dimensional rotational angiography images of aneurysms at three common locations, viz. basilar artery tip, internal carotid artery and middle cerebral artery were obtained. The computational tools being developed in the European project @neurIST were used to reconstruct the fluid domains and solve the unsteady Navier–Stokes equations, using in turn Womersley and plug-flow inlet velocity profiles. The effects of these assumptions were analysed and compared in terms of relevant haemodynamic variables within the aneurismal sac. For the aneurysm at the basilar tip geometries with different extensions of the afferent vasculature were considered to study the plausibility of a fully-developed axial flow at the inlet boundaries.

The study shows that assumptions made on the velocity profile while specifying inlet boundary conditions have little influence on the local haemodynamics in the aneurysm, provided that a sufficient extension of the afferent vasculature is considered and that geometry is the primary determinant of the flow field within the aneurismal sac. For real geometries the Womersley profile is at best an unnecessary over-complication, and may even be worse than the plug profile in some anatomical locations (e.g. basilar confluence).

Keywords: boundary conditions; haemodynamics; blood flow; Womersley; plug-flow; intracranial aneurysm

1. Introduction

An aneurysm is a localised dilation in a blood vessel, which carries an inherent risk of rupture and haemorrhage. Aneurysmal subarachnoid haemorrhage, despite improvement in surgical and medical management, remains a major cause of morbidity and mortality with high rates of case fatality (40–50%, Numminen et al. 1996; Inagawa 2001). Among different etiologies proposed so far (genetic, traumatic and inflammatory), haemodynamics is believed to play an important role in the initiation and the development of the disease (Sekhar and Heros 1981; Kayembe et al. 1984; Byrne and Guglielmi 1998; Shojima et al. 2004; Cebal et al. 2005b).

Detailed *in vivo* measurements of all relevant flow variables in the regions affected by the disease are currently impossible. Computational fluid dynamics (CFD) might represent a valuable tool to extract additional non-observable information from patient-specific data. Advances in image processing and vessel reconstruction techniques, together with the wider availability of significant computing power, have made possible the realisation of characterisation of the haemodynamics

of patient-specific geometries. Steinman (2004) has made the important observation that patient-specific CFD analyses are possible and that the onus is now on researchers to bring these technologies into a clinical setting. There are two steps in this process: the first is to establish a consistent analysis protocol and to undertake characterisation of large numbers of aneurysms to provide confidence in the association of haemodynamic measures with the event of rupture. The second is to deliver an effective and robust simulation workflow into the clinical environment.

Both of these steps are addressed in the @neurIST project (www.aneurist.org), which seeks to develop a robust, clinically-usable tool chain for the computation of relevant haemodynamic data associated with the initiation, growth and rupture of intracranial aneurysms. The specification of an analysis protocol that can be applied at all sites, both within and without the @neurIST project, that are interested in contribution to an extensive database of haemodynamic characterisations of patient-specific aneurysms is an important goal.

The computational technologies currently available limit the extension of the computational domain

*Corresponding author. Email: a.marzo@sheffield.ac.uk

to a restricted area around the aneurysm. The specification of boundary conditions at the interfaces with the rest of the cardiovascular network thus remains a pre-requisite for the solution of the governing equations.

Flow rate waveforms (describing area-integrated velocity at each instant in time) in the region of the aneurysm or in the afferent vessels might sometimes be available from Doppler ultrasound in the carotid, from transcranial Doppler ultrasound or from magnetic resonance imaging, but none of these is currently measured in routine clinical practice in the management of cerebral aneurysm. Invasive pressure measurements are even rarer. A viable alternative for description of flow and pressure waveforms might be 1D circulation models (Westerhof et al. 1969; Stergiopoulos et al. 1992; Vignon-Clementel 2006; Balossino et al. 2008; Bove et al. 2008). From whatever source flow or pressure measurements are available, it is unlikely or impossible that they include spatial resolution of the profiles. The solution of the 3D Navier–Stokes equations, on the other hand, requires these quantities to be specified as pointwise values at each node of the 3D boundary mesh. Assumptions made while completing such deficient data at boundaries is not trivial and can strongly perturb the numerical results.

Many authors rely on the theory of Womersley (1955) for the specification of the velocity profile of flowrate-based boundary conditions, assuming that flow is spatially developed to that associated with periodic flow in a circular pipe. This might be appropriate but it is known that geometry of the proximal vasculature remains the most important factor in describing the flow presented to the aneurysm (Cebal et al. 2005a; Oshima et al. 2005; Castro et al. 2006; Moyle et al. 2006). The over-complication of applying a Womersley velocity profiles might be unnecessary and in some circumstances unrealistic in the determination of the haemodynamics within the aneurysmal sac.

Myers et al. (2001) and Moyle et al. (2006) have assessed the effect of these assumptions on arterial haemodynamics and have shown that geometry takes over within a relatively short distance from the location of the inlet boundaries, thus nullifying the effects of careful specification of inlet velocity profiles.

However, there is relatively little data in the context of saccular cerebral aneurysms (Oshima et al. 2005), which often presents more complex haemodynamic patterns (Cebal et al. 2005a) when compared to the simpler geometries of the studies reported so far (Myers et al. 2001; Moyle et al. 2006).

The current study investigates the effects of inlet velocity profiles on the haemodynamics of intracranial aneurysms and demonstrates their secondary role when compared to anatomical geometry and extension of afferent vasculature in three typical anatomical locations.

2. Materials and methods

Three typical intracranial aneurysms found in the circle of Willis were considered in this study: an aneurysm at the tip of the basilar artery (herein called geom.1), an aneurysm of the right ophthalmic segment of the internal carotid artery (geom.2), and an aneurysm of the terminal bifurcation of the right middle cerebral artery (geom.3). Locations are illustrated in Figure 1. In order to study the flow development at the confluence of the vertebral arteries, an additional geometry for the basilar artery aneurysm was reconstructed (geom.1b), which contains the junction of the two vertebral arteries.

Some of the case studies had additional minor aneurysms. These are highlighted by black arrows in Figure 2, but were excluded from the study.

The aneurysm in each of geom.1 and 3 was saccular bilobular. The aneurysm in geom.2 was saccular with a single lobe. These geometries present a progressively higher level of tortuosity of the aneurysmal afferent loop from geom.1, where the basilar artery is only slightly curved, to geom.3, where the feeding vasculature presents several bends, changes in the lumen diameter and bifurcations, before reaching the aneurysm of interest. More details of the geometries of interest are reported in Table 1.

Rotational acquisitions were obtained using a Philips® Integris™ BV 5000 machine (Philips® Medical Systems, Eindhoven, The Netherlands), producing 100 images in 4 s, with 5 ms exposure per image. A built-in X-ray image

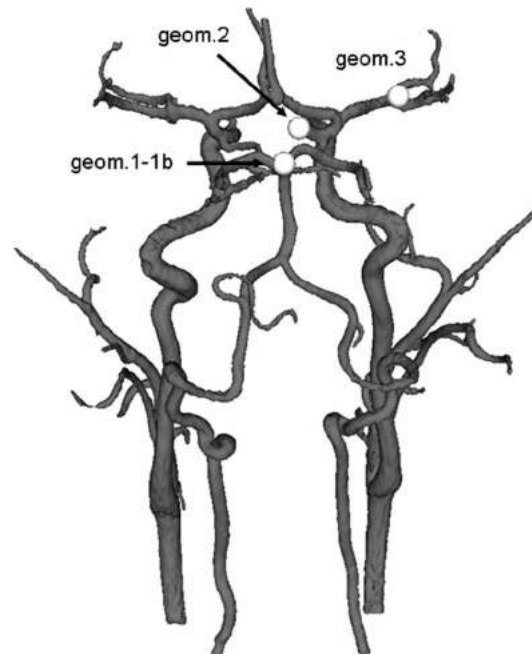


Figure 1. Representation in one of @neurIST application suites of a typical cerebral arterial tree, with locations of geom.1, 1b, 2 and 3 indicated by white spheres and black arrows.

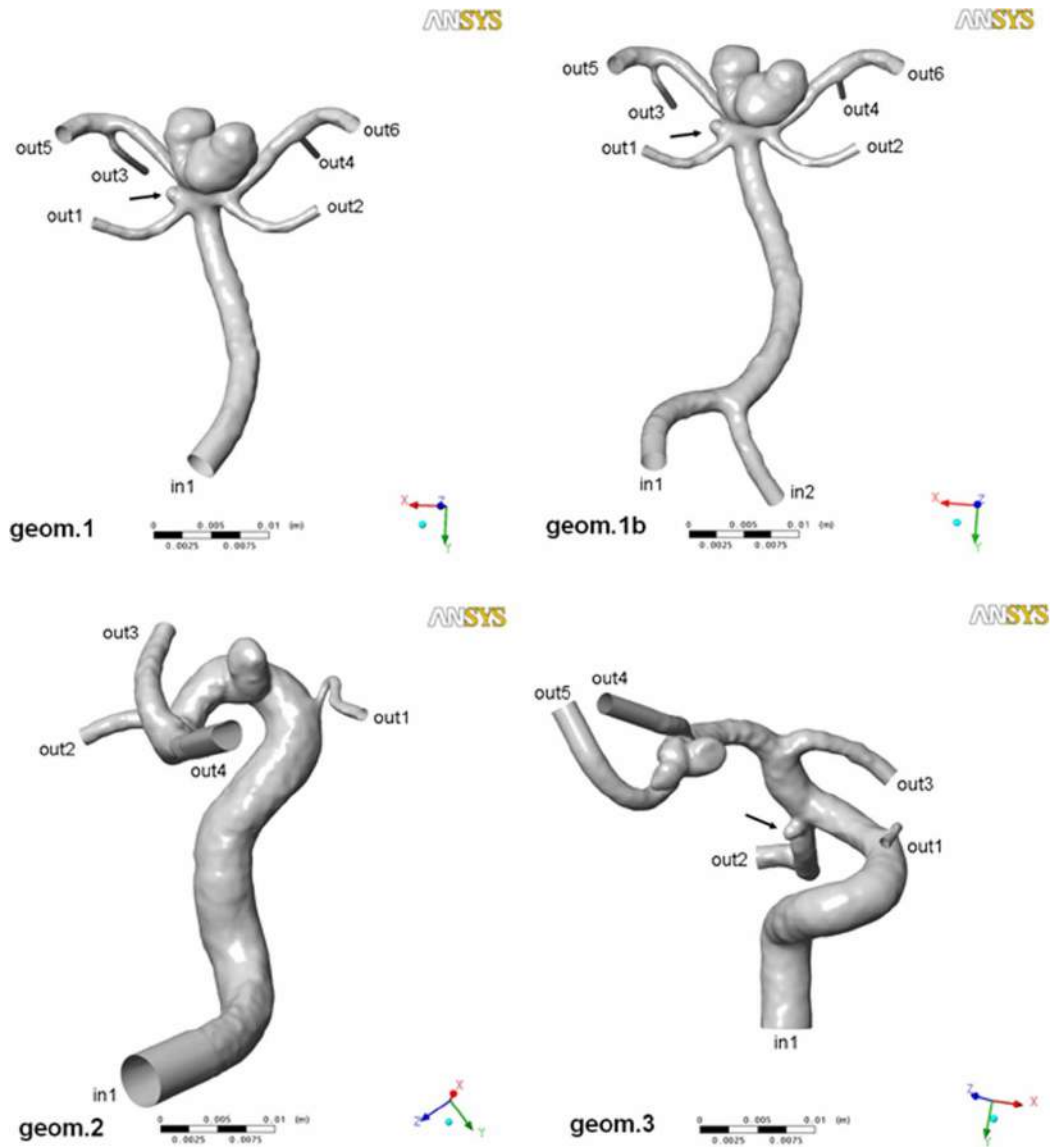


Figure 2. Reconstructed geometries: geom.1, basilar artery aneurysm; geom.1b, basilar artery aneurysm including vertebral arteries; geom.2, internal carotid artery aneurysm, geom.3, middle cerebral artery aneurysm. Black arrows show secondary smaller aneurysms, excluded from the study. Labels indicate the openings where boundary conditions were applied.

Table 1. Geometrical properties of geom.1–3.

	Aneurysm size (mm)			Length of afferent vessel (normalised with inlet diameter)	Complexity of afferent loop
	Depth	Max diameter	Neck (max width)		
Geom.1	5.5–6.5 ^a	4.6–5.8 ^a	5.5	10	Low
Geom.1b	5.5–6.5 ^a	4.6–5.8 ^a	5.5	12 ^b	Low
Geom.2	5.5	4.6	4.3	8.2	Medium
Geom.3	4.4–3.8 ^a	3.3–2.3 ^a	3.1	12	High

^a Values for the two lobes.

^b Values for both inlet afferent vessels of geom.1b, i.e. vertebral arteries.

intensifier was used, with a close-circuit-digital camera and software to correct for geometrical deformation. Voxel size in the reconstructed 3D images was $303\ \mu\text{m}$ with reconstruction matrix $512 \times 512 \times 512$. Images were anonymised, respecting the ethical approval for @neurIST's for use of patient data.

The @neurIST computational tool-chain was used to segment, extract and repair the vessel surfaces. In particular, vessel triangular surfaces were created using a threshold isosurface extraction tool, based on the marching cubes algorithm developed by Lorensen and Cline (1987). Artefacts and unnecessary vasculature were removed and surface repaired using tools based on the Visualisation Toolkit (www.vtk.org), first developed within the Multimod Application Framework (Viceconti et al. 2004) and further improved within the project @neurIST. All inlet openings were extruded and morphed into circular edges for the appropriate application of Womersley-based boundary conditions. Extrusion of some outlets was necessary to ensure that spatially constant pressure represented an appropriate boundary condition at the termination of the 3D domain. The results of the geometry reconstruction process are shown in Figure 2.

During vessel reconstruction, the neck of the aneurysms was manually identified and marked to define the aneurysmal sac that was used for the haemodynamic characterisation of each aneurysm.

Volumetric meshes were generated using ANSYS® ICEM CFD 11.0™ and based on the octree approach. Grids were made finer at the walls and progressively coarser towards the vessel axis. Tetrahedral elements were used for the discretisation of the domain core, with three layers of prismatic elements adjacent to the wall, thus ensuring accurate computation of wall shear stresses (WSS) and oscillatory shear indices (OSI). Element size and number were set accordingly to the outcome of a mesh dependency study performed on similar aneurysmal geometries (Radaelli et al. 2008, private communications). In this study, results were found to be grid independent for meshes greater than $1700\ \text{el}/\text{mm}^3$. In order to maintain consistency across the meshes used for all geometries, similar element density and the same wall element size and maximum core element size were used in the discretisation of the domains. Mesh details are reported in Table 2 below.

The 3D unsteady Navier–Stokes equations were solved by using the finite-control-volume software, ANSYS®-CFX™. The default second-order high-resolution advection differencing scheme was used. The solution algorithm is an implicit coupled solution scheme, based on an algebraic multigrid method for the coupled linear equations. Blood was assumed to be incompressible, with density $\rho = 1050\ \text{kg}/\text{m}^3$ and Newtonian, with viscosity $\mu = 0.0035\ \text{Pa}\cdot\text{s}$. All analyses were run in parallel, using the communication mode MPICH on two Itanium2 900 MHz 64-bit processors of a Tiger-2 Linux cluster node with 4 GB of registered DDR-SDRAM PC1600. The average time required to solve one cardiac cycle with the meshes considered was approximately 8.6 h.

2.1 Boundary conditions

Patient-specific flow measurements at boundaries were not available for the data sets under consideration, thus boundary conditions were derived from the flow-rate and pressure waveforms computed by using the 1D circulation model developed by Reymond et al. (2008), which is part of the @neurIST computational tool-chain. This is a distributed model of the entire systemic arterial tree, coupled to a heart model and including a detailed description of the cerebral arteries. The 1D form of the fluid equations are applied over each arterial segment and intimal WSS is modelled using the Womersley theory. Arterial wall was modelled with a non-linear viscoelastic constitutive law and arterial tree dimensions and properties were taken from literature and extended to include a description of the cerebral arterial tree obtained from real patient scans. In some more detail, the pressure dependency of compliance in thoracic and abdominal aortas, measured *ex vivo* and described by Langewouters (1982), was applied to the whole arterial tree. The elastic component of the compliance, which is function of the mean arterial lumen diameter, compliance, was described as a function of pulse wave velocity (Reymond et al. 2008). The viscoelastic behaviour of the arterial wall was described by the model developed by Holenstein et al. (1980). Geometrical properties of the arterial tree, including the circle of Willis, were taken from Noordergraaf (1956), Gabrielsen and Greitz (1970), Fox et al. (1973), Krayenbuehl and Yasargil (1982),

Table 2. Grid properties for geom.1–3.

	Volume (mm^3)	Elements	Nodes	Average density (el/mm^3)	Max el. size (mm)	Max wall el. size (mm)
Geom.1	433.9	1321449	411331	3046	0.4	0.12
Geom.1b	540.4	1678606	527615	3106	0.4	0.12
Geom.2	1375.5	3173174	912842	2307	0.4	0.12
Geom.3	848.2	2292777	694172	2703	0.4	0.12

Hillen et al. (1986), Dodge et al. (1992), Stergiopoulos et al. (1992), Krabbe-Hartkamp et al. (1998) and Holdsworth et al. (1999), and completed by interpolated real patient scans (3D rotational angiography and MRA).

Flow-rate waveforms were used for all primary inlets and pressure waveforms for all primary outlets. All pressure and flow rate waveforms used for the analyses are reported in Figure 3. Flow-rate waveforms were used to specify, in turn, plug-flow (i.e. flat velocity profile) and Womersley velocity profiles at the inlet boundaries. The waveforms were decomposed into Fourier series as indicated in Equation (1):

$$Q(t) = \sum_{n=0}^N Q_n e^{in\omega t}, \quad (1)$$

where N is the number of harmonics, and ω is the angular frequency derived from the period of the cardiac cycle $T = 0.8$ s. The Womersley velocity profile was expressed in terms of the Fourier representation of the flow rate waveforms as indicated in Equation (2):

$$\begin{aligned} v(r, t) = & \frac{2Q_0}{\pi R^2} \left[1 - \left(\frac{r}{R} \right)^2 \right] \\ & + \sum_{n=1}^N \frac{Q_n}{\pi R^2} \left[\frac{1 - \frac{J_0(\beta_n(r/R))}{J_0(\beta_n)}}{1 - \frac{2J_1(\beta_n)}{\beta_n J_0(\beta_n)}} \right] \cdot e^{in\omega t}, \end{aligned} \quad (2)$$

where R is the radius of the inlet boundary, Q_0 is the first harmonic coefficient responsible for the parabolic profile of a steady flow (i.e. Poiseuille flow), J_0 and J_1 are Bessel functions of order zero and one, respectively, and

$$\beta_n = i^{3/2} \cdot \alpha_n, \quad (3)$$

$$\alpha_n = R \cdot \sqrt{\frac{n \cdot \omega \cdot \rho}{\mu}}, \quad (4)$$

where α_n is the Womersley number of the n th harmonic. A Fortran subroutine was created and interfaced to the ANSYS[®]-CFX[™] solver for the computation of the velocity inlet profiles within each time loop.

Analyses were run for four cardiac cycles to nullify the transient artefacts generated by the initial conditions, and only data from the 4th cycle were used in the post-processing phase.

3. Results

Relevant haemodynamic variables were compared qualitatively and quantitatively for the two velocity profile assumptions both at two time-points along the cardiac cycle (corresponding to the lowest and highest Reynolds numbers achieved during diastole and systole, respectively), and as time-averaged quantities across the cardiac cycle.

The haemodynamic variables chosen for these comparisons have been associated with aneurysmal initiation, growth and rupture in the literature (Shojima et al. 2004; Cebal et al. 2005b).

3.1 Qualitative comparison using instantaneous velocity contours

Figure 4 shows the comparison between Womersley and plug-flow boundary conditions during diastole and systole, using velocity contours at specific cross sections. The cross-sections were selected as those, which subjectively, best illustrated the complexity of the flow within the three domains. Results for geom.1 show that for both flow regimes; the Womersley and plug-flow flow patterns are essentially the same with some minor discrepancy in the magnitude of the velocity field, as shown by the arrows in Figure. Results for geom.2 are consistent with geom.1 except that discrepancies in velocity magnitudes are more pronounced in the lower part of the cross section, representing the velocity patterns within the parent vessel. Finally, results for geom.3 show good agreement in the patterns as well as the magnitude of the velocity field. Contours in geom.2 and 3 show the presence of a jet of fluid entering the aneurysm and impinging onto the distal side of the aneurysmal wall. Moreover, results for all geometries show that flow is rather stable (according to the definition of Cebal et al. 2005b), exhibiting the same characteristics during diastole and systole.

3.2 Qualitative comparison using instantaneous WSS contours

Figure 5 shows the comparison between Womersley and plug-flow boundary conditions during diastole and systole, using contours of WSS on the wall of the aneurysmal sac. Results for geom.1 show that Womersley and plug-flow boundary conditions at inlet develop essentially the same WSS distribution in the aneurysm in both flow regimes. It was noticed that the bigger lobule of geom.1 is one, which is subjected to comparatively low WSS at both reported time-points in the cardiac cycle, whereas in the smaller lobule WSS values reach their highest values. Results for geom.2 and 3 show essentially the same WSS patterns for both inflow assumptions and for both flow regimes, with some minor variations for geom.2 during diastole near the aneurysmal neck, and for geom.3 during systole as shown by the arrows in Figure 5.

As for velocity distributions, WSS present similar patterns during diastole and systole, showing stability of the flow.

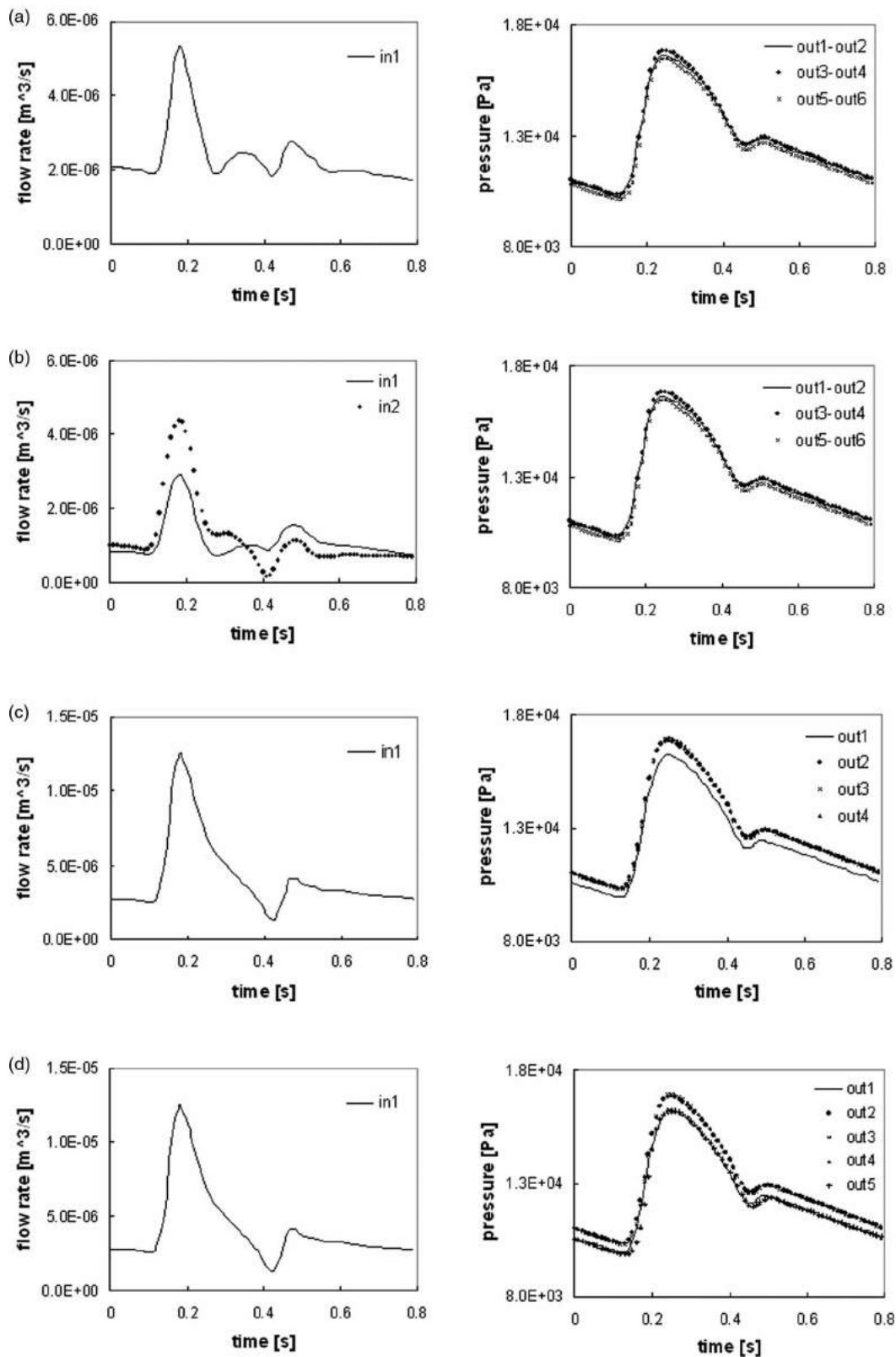


Figure 3. (a) Flow-rate (left) and pressure waveforms (right) applied in geom.1. (b) Flow-rate (left) and pressure waveforms (right) applied in geom.1b. (c) Flow-rate (left) and pressure waveforms (right) applied in geom.2 and (d) Flow-rate (left) and pressure waveforms (right) applied in geom.3.

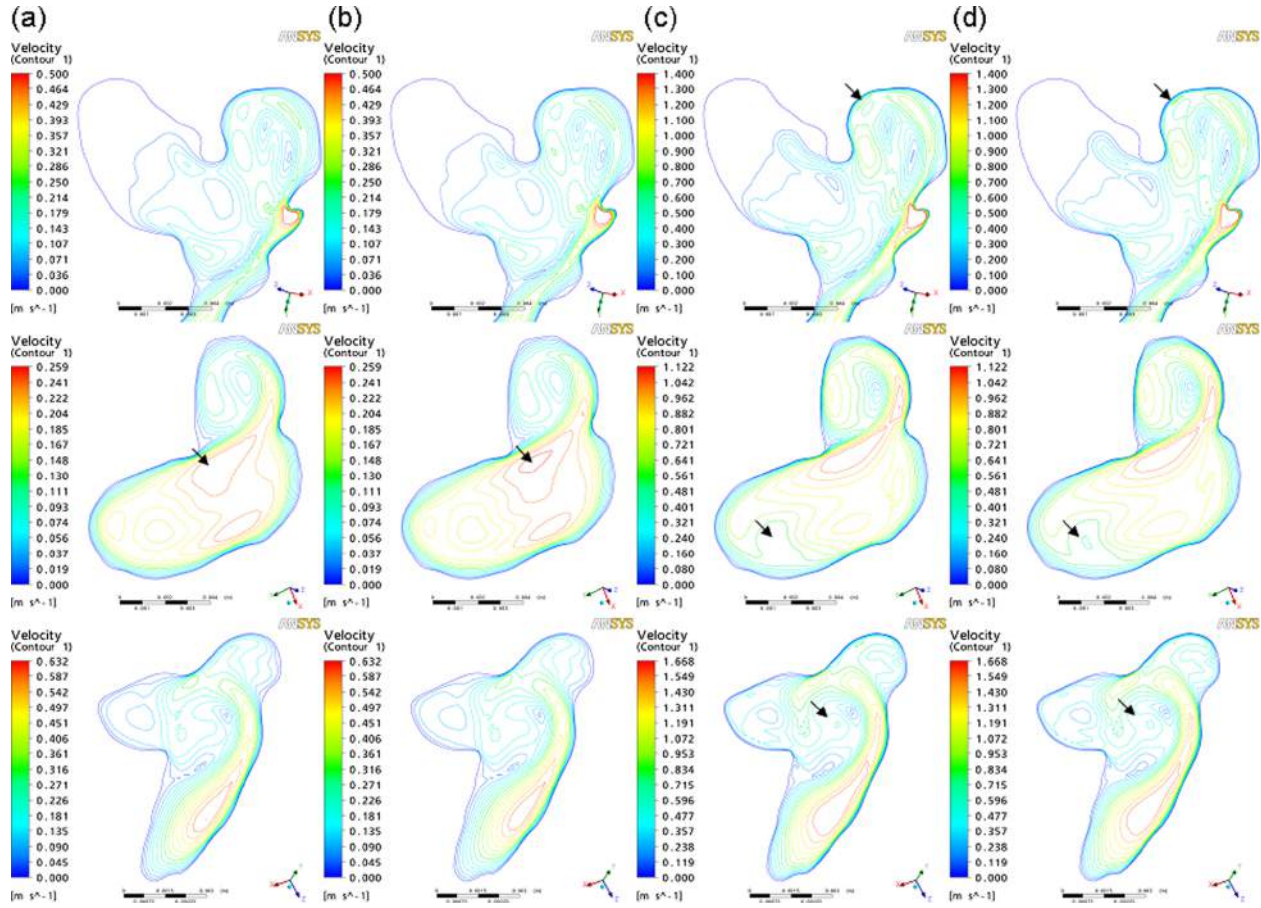


Figure 4. Velocity contours across the aneurysmal sac for (a) Womersley boundary conditions at lowest Re during diastole; (b) plug-flow boundary conditions at lowest Re during diastole; (c) Womersley boundary conditions at highest Re during systole and (d) plug-flow boundary conditions at highest Re during systole. From top to bottom: geom.1–3. Grey arrows indicate areas of discrepancies. Units for velocity are expressed in m/s.

3.3 Qualitative comparison using time-averaged WSS and OSI contours

Time-averaged haemodynamic quantities can be used to assess the agreement between results over the whole cardiac cycle, and not solely at specific snap-shots in time. Time-averaged WSS are reported, together with OSI for further comparison. OSI is defined in Equations (5) and (6), and was used to quantify the oscillatory shears experienced by the cells of the inner part of the arterial vessel and aneurysm (endothelial layer).

$$OSI = \frac{1}{2} \left(1 - \frac{\tau_{\text{mean}}}{\tau_{\text{abs}}} \right), \quad (5)$$

$$\tau_{\text{mean}} = \left| \frac{1}{T} \int_0^T t_s \cdot dt \right|, \quad (6)$$

where t_s represents the surface traction vector. Figures 6 and 7 show the time-averaged WSS and OSI contours, respectively, on the aneurysmal wall of all three

geometries and for both inlet boundary conditions. The results are consistent with those of the instantaneous measures, i.e. very little differences are observed between WSS and OSI patterns, and only minor differences in magnitudes, from Womersley and plug-flow boundary conditions. For these aneurysms, exhibiting stable flow patterns over the cardiac cycle, it is noted that the time-averaged WSS pattern is qualitatively very similar to that of its instantaneous counterparts.

3.4 Qualitative comparison on flow development

Figure 8(a),(b) shows the development of the flow for Womersley and plug-flow boundary conditions for geom.1. Although the two flows start from different assumptions at the inlet opening, both develop into a very similar velocity pattern before reaching the aneurysmal sac. Figure 8(c), illustrating the results for the extended domain of geom.1b, shows that the two converging vessels produce a ring-like velocity profile that is significantly different from both the Womersley and flat profiles, but

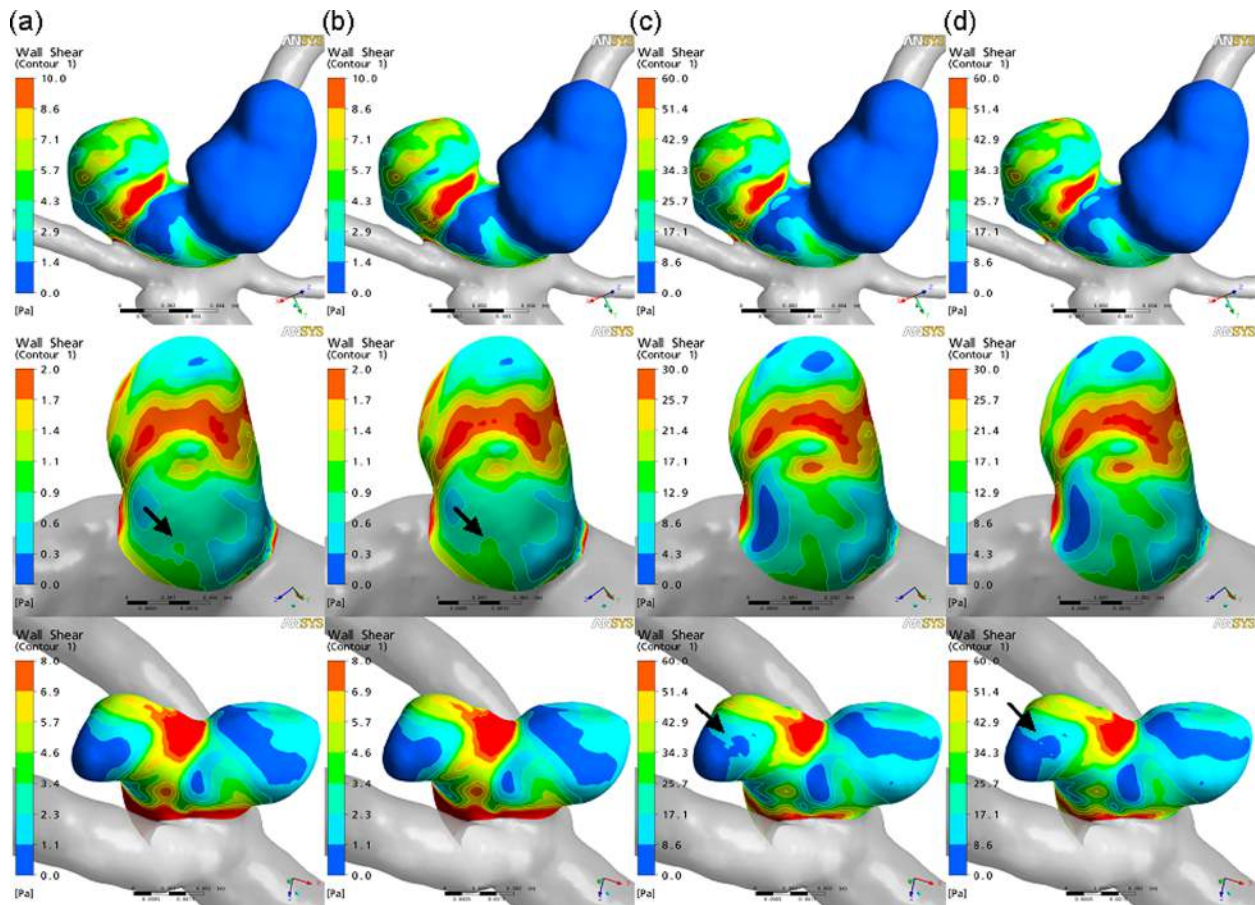


Figure 5. WSS contours for (a) Womersley boundary conditions at lowest Re during diastole; (b) plug-flow boundary conditions at lowest Re during diastole; (c) Womersley boundary conditions at highest Re during systole and (d) plug-flow boundary conditions at highest Re during systole. From top to bottom: geom.1–3. Units for WSS are expressed in Pa.

in fact closer to the latter. This indicates clearly that there are some geometries (of course those that are least like a straight tube) for which the Womersley profile is actually a worse choice than the flat profile. Nevertheless, once again the flow close to the aneurysm is relatively similar for all boundary conditions considered.

3.5 Quantitative comparison

For a more accurate and direct evaluation of the effects that different boundary conditions may have on local haemodynamics, several haemodynamic indices were extracted from the flow field of the three aneurysmal sacs, for both inflow boundary conditions. These are reported in Table 3 with the percentage discrepancy between Womersley and plug-flow results. In geom.1, the maximum discrepancy was observed in the spatial-average speed in the aneurysmal sac (4.3%) and in the area of elevated pressure in the aneurysmal wall (also 4.3%). Relatively high discrepancies were also observed in the values predicted for the maximum speed within the aneurysm at systole (2.3%) and the location of maximum

OSI (2.8%). In geom.2, the maximum discrepancy was observed in the predictions of area of elevated pressure (4.1%) and for geom.3 in the values of max OSI (3.7%) and its location (4.1%).

The root mean square of the errors of the different indices was also computed and is reported in the last row of Table 3.

Overall the maximum discrepancy between Womersley and plug-flow results was observed in geom.3, where the RMS is 2%. Lower RMS values were calculated for geom.1, $RMS = 1.9\%$ and geom.2, $RMS = 1.2\%$.

4. Discussion

The purpose of this paper is to compare the results from two common methods of application of proximal velocity boundary conditions for haemodynamic analysis of cerebral aneurysms. The context is that of specification of a robust protocol for routine haemodynamic analysis as part of a clinical workflow.

The isolation of the vessel of interest from the rest of the cardiovascular tree and its surroundings (e.g. tissues

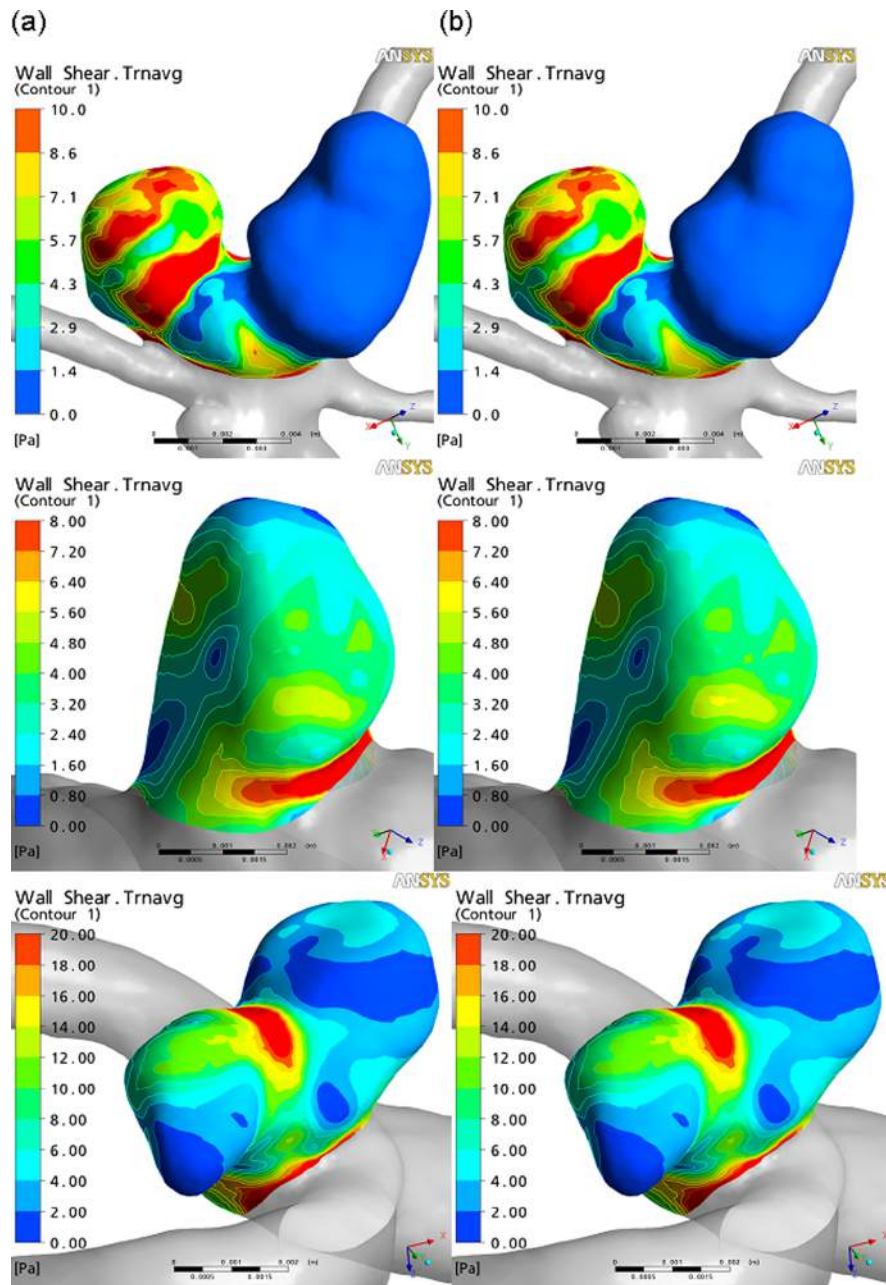


Figure 6. Time-averaged WSS contours for (a) Womersley boundary conditions; (b) plug-flow boundary conditions. From top to bottom: geom.1–3. Units for WSS are expressed in Pa.

and bones) implies that wall and flow conditions will have to be specified at the boundaries of the vessel. Patient-specific assessment of the properties of the vessel walls and its surroundings are difficult. There is some evidence that pulsatility of the vessel wall might have negligible effect on haemodynamics even when the wall motion is of the order of the radius of a vessel (Jeays et al. 2007) and even less so in the context of cerebral aneurysms in the confined compartment of the skull (Dempere-Marco et al. 2006). For the purposes of the current study (and probably

for a routine clinical analysis protocol) the walls of the vessel are considered fixed.

Patient-specific flow measurements are in principle attainable from MRI or Doppler ultrasound but the intricacy of the cerebral vasculature, the small size of its vessels, and the fact that these are not part of the clinical procedure make them rarely available. Even when they are, it is unusual to rely on the spatial distribution of velocity (due to resolution of MRI and difficulties of location of Doppler ultrasound measures). To overcome

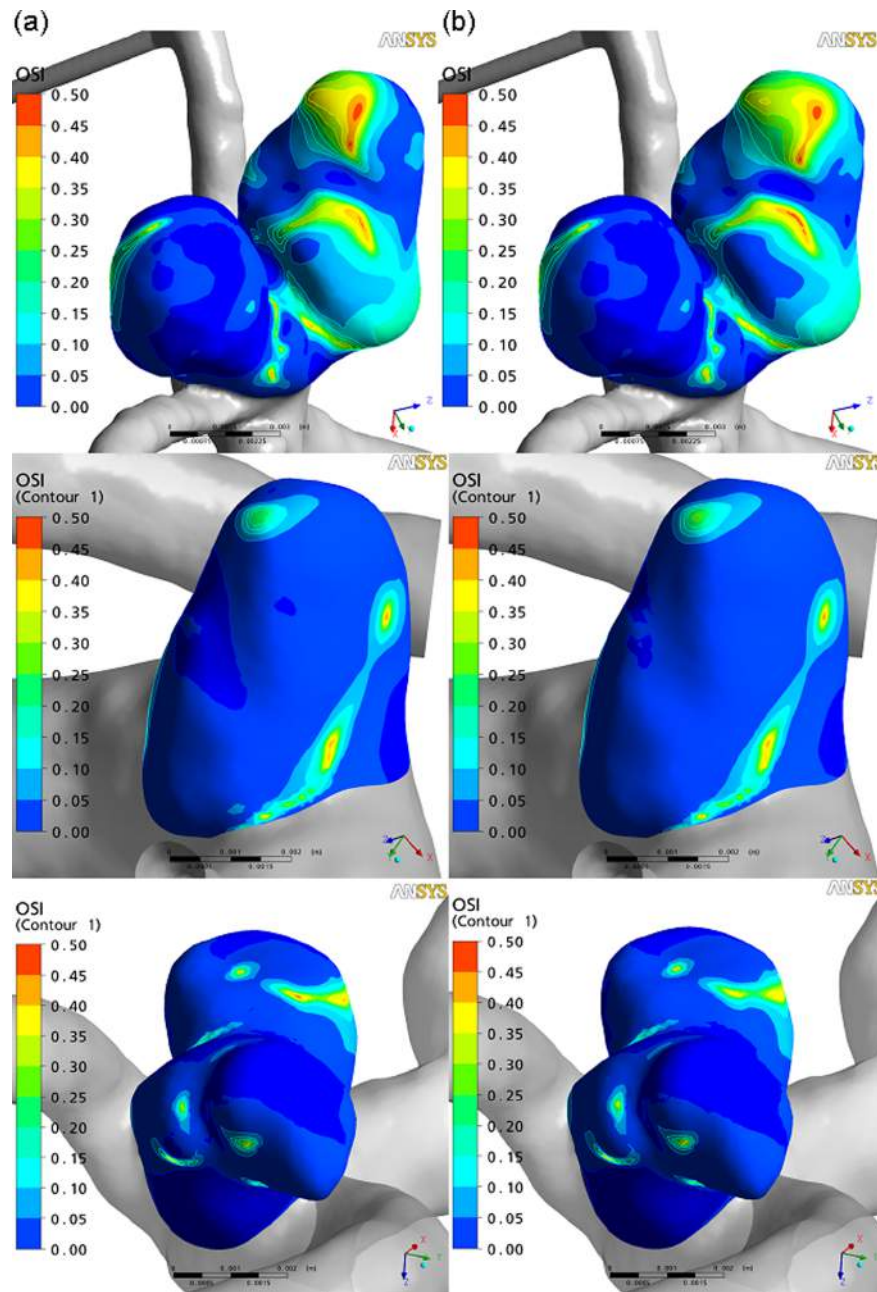


Figure 7. OSI contours for (a) Womersley boundary conditions; (b) plug-flow boundary conditions. From top to bottom: geom.1–3.

these difficulties several authors use lumped-parameters or 1D models for the description of the remaining vascular systems (Formaggia et al. 1999; Quarteroni et al. 2001). Flow boundary conditions, whether from patient-specific ultrasound or MRI measures, or computed using simple models of the cardiovascular system, are available as cross-sectional average values of velocity or pressure along the cardiac cycle. Thus assumptions on their 3D development across the same boundaries are to be made to match the level of details required by 3D modelling. While imposing inflow boundary conditions from the flow-rate

waveforms computed by a 1D distributed model, for instance, one assumption often imposed at the inlet boundary is that of axisymmetric flow with a velocity distribution determined by the Womersley theory.

The results of the comparative analyses with Womersley and flat velocity profiles indicate that there is no change in qualitative flow patterns, and detailed examination of the flow fields yields maximum differences of less than 5%, and RMS differences between 1 and 2%. It is suggested that these differences are unimportant in the context of interpretability against known thresholds, and particularly

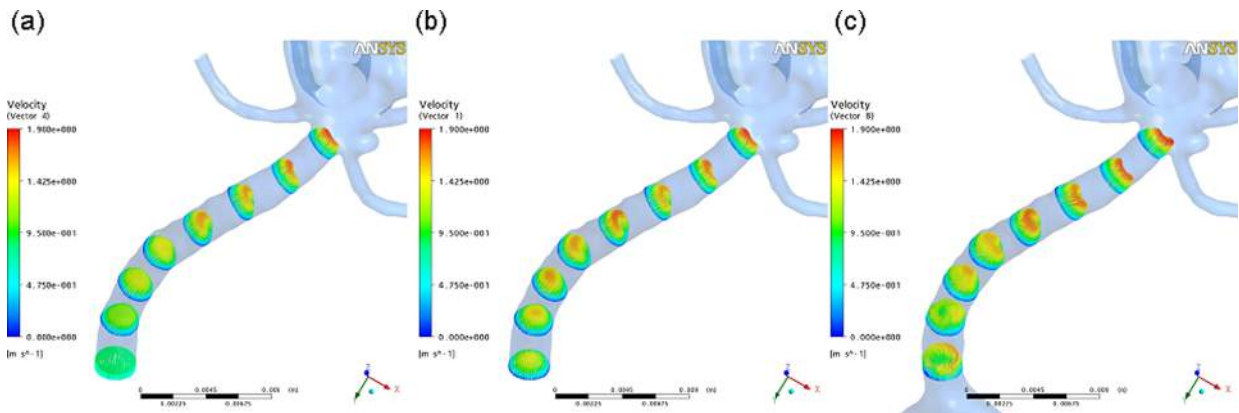


Figure 8. Velocity vectors on cross-sections along the afferent vessel at peak systole for geom.1 with plug-flow boundary conditions (a); geom.1 with Womersley boundary conditions (b) and geom.1b (c) with Womersley boundary conditions. The distance between the cross-sections is approximately $1.5D$, where D is the diameter of the inlet boundary in geom.1. Units for velocity are expressed in m/s.

in the context of other uncertainties in the analysis (patient blood pressure, beat-to-beat variations, alternative physiological states including exercise, patient haematocrit and viscosity models). Certainly, the errors are small compared with those that might arise from inaccurate segmentation of the patient specific geometry, when variabilities up to 48% have been reported (Moyle et al. 2006). Whilst the true significance and relevance of discrepancies between Womersley and plug-flow results can only be assessed once associations are found between haemodynamic indices and aneurysmal evolution, it is probably safe to assume that the uncertainties of any thresholds and the safety factors that will be built into any clinical interpretation and recommendations will always remain greater than that associated with analysis errors from the inlet velocity profile provided the inlet development domain is of adequate length.

The computational savings associated with a recommendation of the simplest inlet velocity boundary condition, that of a flat profile, are not significant. More important is that the simpler the analysis protocol adopted, the more likely it is that other centres will contribute to the growth of an established database of haemodynamic characterisations, ultimately reflecting on its power to provide meaningful, peer-reviewed and clinically implementable associations of the characteristic haemodynamic measures with observed clinical outcome. Until such associations are established, the impact of CFD on the management of cerebral aneurysms will be minimal.

A limitation of the current study is that results are reported for only three aneurysms, with one further variation. Nevertheless, these aneurysms have been selected as typical of those that arise most commonly in the cerebral vasculature and given the consistency of the results, and their resonance with expectations based on the physics of the problem, it is suggested that it provides strong evidence that haemodynamic characterisations are

indeed likely to be insensitive to details of the inlet velocity distribution.

Although specific analysis and comment on the haemodynamic results for any one aneurysm is not the focus of the current study, the analysis of geom.1 revealed some interesting haemodynamic characteristics that are worthy of mention. Primary haemodynamic activity is clearly confined to one of the lobules, whilst the other is subject to very low WSS. In fact, it is the smaller lobe that exhibits strong haemodynamic activity and the larger that is relatively stagnant. It is noted that the larger lobe has a more irregular shape. No follow-up data is available and so it is impossible to determine which, if either, lobe is growing or which might rupture. Nevertheless, it is noteworthy that the haemodynamic environment in the smaller of the lobes is more similar to that in the parent vasculature than that in the larger lobe, and that the mean shear stress in the larger lobe is below that threshold that has been associated with negative outcome and the onset of disease in other vascular applications (Malek et al. 1999).

5. Conclusions

Our final conclusions are as follows:

- (1) The haemodynamic characterisation of a cerebral aneurysm under given proximal flow conditions is relatively insensitive to the details of the velocity profile on inlet boundaries that are sufficiently far from the aneurysm.
- (2) Wider adoption of a given analysis protocol is more likely if it is simple to implement and the specification of a flat velocity profile at the inlet to a 3D domain provides an adequate and justifiable description for the purposes of haemodynamic characterisation.

Table 3. Haemodynamic indices extracted for geom.1–3 and percentage error between Womersley and plug-flow results.

	Geom.1			Geom.2			Geom.3		
	Wom	Plug	Err%	Wom	Plug	Err%	Wom	Plug	Err%
Max speed within aneurysm at systole (m/s)	1.774	1.733	-2.3	1.154	1.155	0.1	1.555	1.544	-0.7
Spatial mean speed in aneurysm at systole (m/s)	0.331	0.317	-4.3	0.557	0.557	0.0	0.619	0.619	0.0
Peak static wall pressure at systole (Pa)	16,131	15,950	-1.1	15,770	15,750	-0.1	14560	14,550	-0.1
Location X of max pressure (m)	3.51×10^{-2}	3.51×10^{-2}	0.0	4.20×10^{-2}	4.20×10^{-2}	0.0	1.73×10^{-2}	1.73×10^{-2}	0.0
Location Y of max pressure (m)	1.64×10^{-2}	1.64×10^{-2}	0.0	2.33×10^{-2}	2.33×10^{-2}	0.0	3.11×10^{-2}	3.11×10^{-2}	0.0
Location Z of max pressure (m)	-3.67×10^{-2}	-3.67×10^{-2}	0.0	-3.48×10^{-2}	-3.48×10^{-2}	0.0	-3.65×10^{-2}	-3.65×10^{-2}	0.0
Spatial mean static pressure in aneurysm at systole (Pa)	15,260	15,130	-0.9	15,140	15,120	-0.1	13,770	13,770	0.0
Area of elevated pressure ^a (m ²)	0.123×10^{-6}	0.118×10^{-5}	-4.3	4.18×10^{-6}	4.01×10^{-6}	-4.1	7.06×10^{-6}	7.13×10^{-6}	1.1
Max time-averaged WSS (Pa)	25.79	25.52	-1.1	16.44	16.87	2.6	49.07	50.52	2.95
Location X of max time-averaged WSS (m)	3.604×10^{-2}	3.604×10^{-2}	0.0	4.18×10^{-2}	4.18×10^{-2}	0.0	1.79×10^{-2}	1.79×10^{-2}	0.0
Location Y of max time-averaged WSS (m)	0.196×10^{-3}	0.196×10^{-3}	0.0	0.232×10^{-3}	0.232×10^{-3}	0.0	0.291×10^{-3}	0.291×10^{-3}	0.0
Location Z of max time-averaged WSS (m)	-3.48×10^{-2}	-3.48×10^{-2}	0.0	-3.49×10^{-2}	-3.49×10^{-2}	0.0	-3.36×10^{-2}	-3.36×10^{-2}	0.0
Area of elevated time-averaged WSS ^b (m ²)	1.83×10^{-6}	1.82×10^{-6}	-0.9	6.39×10^{-7}	6.39×10^{-7}	0.0	2.60×10^{-7}	2.56×10^{-7}	-1.4
Max OSI in aneurysmal wall	0.491	0.487	-0.8	0.471	0.472	0.2	0.494	0.475	-3.7
Location X of max OSI (m)	3.21×10^{-2}	3.12×10^{-2}	-2.8	4.13×10^{-2}	4.13×10^{-2}	0.0	1.95×10^{-2}	1.97×10^{-2}	1.2
Location Y of max OSI (m)	1.80×10^{-2}	1.79×10^{-2}	-0.9	2.34×10^{-2}	2.34×10^{-2}	0.0	3.12×10^{-2}	2.99×10^{-2}	-4.1
Location Z of max OSI (m)	-3.20×10^{-2}	-3.12×10^{-2}	-2.7	-3.75×10^{-2}	-3.75×10^{-2}	0.0	-3.67×10^{-2}	-3.68×10^{-2}	0.3
Area of elevated OSI (m ²)	6.44×10^{-5}	6.37×10^{-5}	-1.0	3.39×10^{-7}	3.35×10^{-7}	-1.2	7.30×10^{-7}	7.70×10^{-7}	5.4
RMS error (%)			1.9			1.2			1.98

^aElevation defined as 50% of peak pressure minus average pressure in the aneurysm at systole.^bElevation defined as 50% of maximum time-averaged WSS.

Acknowledgements

The authors would like to thank the European Commission, VI Framework Programme, Priority 2, Information Society Technologies, for funding @neurIST and allowing this study.

References

- Balossino R, Pennati G, Migliavacca F, Formaggia L, Veneziani A, Tuveri M, Dubini G. 2008. Computational models to predict stenosis growth in carotid arteries: which is the role of boundary conditions? *Comput Methods Biomech Biomed Engin.* Sep 1:1. [Epub ahead of Print].
- Bove EL, Migliavacca F, De Leval MR, Balossino R, Pennati G, Lloyd TR, Khambadkone S, Hsia TY, Dubini G. 2008. Use of mathematic modeling to compare and predict hemodynamic effects of the modified Blalock–Tausig and right ventricle–pulmonary artery shunts for hypoplastic left heart syndrome. *J Thorac Cardiovasc Surg.* 136(2):312–320.
- Byrne JV, Guglielmi G. 1998. Endovascular treatment of intracranial aneurysms. 1st ed. Chapter 1. Introduction to intracranial aneurysms: haemodynamic causes. Berlin: Springer-Verlag. p. 5–6.
- Castro MA, Putman CM, Cezbral JR. 2006. Computational fluid dynamics modeling of intracranial aneurysms: effects of parent artery segmentation on intra-aneurysmal hemodynamics. *AJNR Am J Neuroradiol.* 27:1703–1709.
- Cezbral JR, Castro MA, Appanaboyina S, Putman CM, Millan D, Frangi AF. 2005a. Efficient pipeline for image-based patient-specific analysis of cerebral aneurysm hemodynamics: technique and sensitivity. *IEEE Trans Med Imaging* 24:457–467.
- Cezbral JR, Castro MA, Burgess JE, Pergolizzi RS, Sheridan MJ, Putman CM. 2005b. Characterization of cerebral aneurysms for assessing risk of rupture by using patient-specific computational hemodynamics models. *AJNR Am J Neuro-radiol.* 26:2550–2559.
- Dempere-Marco L, Oubel E, Castro M, Putman C, Frangi A, Cezbral J. 2006. CFD analysis incorporating the influence of wall motion: application to intracranial aneurysms. *Med Image Comput Assist Interv Int Conf Med Image Comput Assist Interv.* 9:438–445.
- Dodge JT Jr, Brown BG, Bolson EL, Dodge HT. 1992. Lumen diameter of normal human coronary arteries. Influence of age, sex, anatomic variation, and left ventricular hypertrophy or dilation. *Circulation* 86(1):232–246.
- Formaggia L, Nobile F, Quarteroni A, Veneziani A. 1999. Multiscale modelling of the circulatory system: a preliminary analysis. *Comput Vis Sci.* 2:75–83.
- Fox C, Davies MJ, Webb-Peploe MM. 1973. Length of left main coronary artery. *Br Heart J.* 35(8):796–798.
- Gabrielsen TO, Greitz T. 1970. Normal size of the internal carotid, middle cerebral and anterior cerebral arteries. *Acta Radiol Diagn (Stockh)* 10(1):1–10.
- Hillen B, Hoogstraten HW, Post L. 1986. A mathematical model of the flow in the circle of Willis. *J Biomech.* 19(3):187–194.
- Holdsworth DW, Norley CJ, Frayne R, Steinman DA, Rutt BK. 1999. Characterization of common carotid artery blood-flow waveforms in normal human subjects. *Physiol Meas.* 20(3): 219–240.
- Holenstein R, Niederer P, Anliker M. 1980. A viscoelastic model for use in predicting arterial pulse waves. *J Biomech Eng.* 102(4):318–325.
- Inagawa T. 2001. Trends in incidence and case fatality rates of aneurysmal subarachnoid hemorrhage in Izumo city, Japan, between 1980–1989 and 1990–1998. *Stroke.* 32: 1499–1507.
- Jeays AD, Lawford PV, Gillott R, Spencer P, Barber DC, Bardhan KD, Hose DR. 2007. Characterisation of the haemodynamics of the superior mesenteric artery. *J Biomech.* 40:1916–1926.
- Kayembe KN, Sasahara M, Hazama F. 1984. Cerebral aneurysms and variations in the circle of Willis. *Stroke.* 15:846–850.
- Krabbe-Hartkamp MJ, Van der Grond J, De Leeuw FE, De Groot JC, Algra A, Hillen B, Breteler MM, Mali WP. 1998. Circle of Willis: morphologic variation on three-dimensional time-of-flight MR angiograms. *Radiology* 207(1):103–111.
- Krayenbuehl H, Yasargil MG. 1982. Cerebral angiography. Stuttgart: Thieme Medical Publishers.
- Langewouters GJ. 1982. Visco-elasticity of the human aorta *in vitro* in relation to pressure and age [thesis]. [Amsterdam (The Netherlands)]: University of Amsterdam.
- Lorenzen WE, Cline H. 1987. Marching cubes: a high resolution 3D surface construction algorithm. *Comput Graph.* 21(4): 163–169.
- Malek AM, Alper SL, Izumo S. 1999. Hemodynamic shear stress and its role in atherosclerosis. *JAMA* 282:2035–2042.
- Moyle KR, Antiga L, Steinman DA. 2006. Inlet conditions for image-based CFD models of the carotid bifurcation: is it reasonable to assume fully developed flow? *J Biomech Eng.* 128:371–379.
- Myers JG, Moore JA, Ojha M, Johnston KW, Ethier CR. 2001. Factors influencing blood flow patterns in the human right coronary artery. *Ann Biomed Eng.* 29:109–120.
- Noordergraaf A. 1956. Physical basis of ballistocardiography. 's-Gravenhage: Excelsior. p. 146.
- Numminen H, Kotila M, Waltimo O, Aho K, Kaste M. 1996. Declining incidence and mortality rates of stroke in Finland from 1972 to 1991. Results of three population-based stroke registers. *Stroke* 27:1487–1491.
- Oshima M, Sakai H, Torii R. 2005. Modelling of inflow boundary conditions for image-based simulation of cerebrovascular flow. *Int J Numer Methods Fluids* 47:603–617.
- Quarteroni A, Ragni S, Veneziani A. 2001. Coupling between lumped and distributed models for blood flow problems. *Comput Vis Sci.* 4:111–124.
- Radaelli AG, Augsburg L, Cezbral JR, Ohta M, Rufenacht DA, Balossino R, Benndorf G, Hose DR, Marzo A, Metcalfe R, et al. 2008. Reproducibility of haemodynamical simulations in a subject-specific stented aneurysm model – a report on the Virtual Intracranial Stenting Challenge 2007. *J Biomech.* 41:2069–2081.
- Reymond P, Merenda F, Perren F, Rufenacht D, Stergiopoulos N. 2008. Validation of 1D model of the systemic arterial tree including the cerebral circulation. In: Paper presented at: Summer Bioengineering Conference (SBC2008). Proceedings of ASME 2008 Conference; Florida, USA.
- Sekhar LN, Heros RC. 1981. Origin, growth, and rupture of saccular aneurysms: a review. *Neurosurgery* 8:248–260.
- Shojima M, Oshima M, Takagi K, Torii R, Hayakawa M, Katada K, Morita A, Kirino T. 2004. Magnitude and role of wall shear stress on cerebral aneurysm: computational fluid dynamic study of 20 middle cerebral artery aneurysms. *Stroke* 35:2500–2505.
- Steinman DA. 2004. Image-based computational fluid dynamics: a new paradigm for monitoring hemodynamics and atherosclerosis. *Curr Drug Targets Cardiovasc Haematol Disord.* 4:183–197.

- Stergiopoulos N, Young DF, Rogge TR. 1992. Computer simulation of arterial flow with applications to arterial and aortic stenoses. *J Biomech.* 25(12):1477–1488.
- Viceconti M, Astolfi L, Leardini A, Imboden S, Petrone M, Quadrani P, Taddei F, Testi D, Zannoni C. 2004. The multimod application framework. In: *Proceedings of the Information Visualisation, Eight International Conference*; 15–20.
- Vignon-Clementel IE, Figueroa CA, Jansen KE, Taylor CA. 2006. Outflow boundary conditions for three-dimensional finite element modeling of blood flow and pressure in arteries. *Comput Methods Appl Mech Eng.* 195: 3776–3796.
- Westerhof N, Bosman F, De Vries CJ, Noordergraaf A. 1969. Analog studies of the human systemic arterial tree. *J Biomech.* 2(2):121–143.
- Womersley JR. 1955. Method for the calculation of velocity, rate of flow and viscous drag in arteries when the pressure gradient is known. *J Physiol.* 127:553–563.

@neurIST complex information processing toolchain for the integrated management of cerebral aneurysms

M. C. Villa-Uriol^{1,2,*}, G. Berti⁴, D. R. Hose⁵, A. Marzo⁵,
A. Chiarini⁶, J. Penrose⁷, J. Pozo^{1,2}, J. G. Schmidt⁸, P. Singh⁵,
R. Lycett⁵, I. Larrabide^{2,1} and A. F. Frangi^{1,2,3}

¹*Centre for Computational Imaging and Simulation Technologies in Biomedicine (CISTIB), Information and Communication Technologies Department, Universitat Pompeu Fabra,*

²*Networking Research Center on Bioengineering, Biomaterials and Nanomedicine (CIBER-BBN), and*

³*Institució Catalana de Recerca i Estudis Avançats (ICREA), c/ Tanger 122–140, E08018 Barcelona, Spain*

⁴*Consulting in mathematical methods, Bonn, Germany*

⁵*Medical Physics Group, Faculty of Medicine, University of Sheffield, Sheffield, UK*

⁶*BioComputing Competence Centre SCS s.r.l., Casalecchio di Reno, Italy*

⁷*ANSYS UK, Ltd, Abingdon, UK*

⁸*University of Applied Science Koblenz, Germany*

Cerebral aneurysms are a multi-factorial disease with severe consequences. A core part of the European project @neurIST was the physical characterization of aneurysms to find candidate risk factors associated with aneurysm rupture. The project investigated measures based on morphological, haemodynamic and aneurysm wall structure analyses for more than 300 cases of ruptured and unruptured aneurysms, extracting descriptors suitable for statistical studies. This paper deals with the unique challenges associated with this task, and the implemented solutions. The consistency of results required by the subsequent statistical analyses, given the heterogeneous image data sources and multiple human operators, was met by a highly automated toolchain combined with training. A testimonial of the successful automation is the positive evaluation of the toolchain by over 260 clinicians during various hands-on workshops. The specification of the analyses required thorough investigations of modelling and processing choices, discussed in a detailed analysis protocol. Finally, an abstract data model governing the management of the simulation-related data provides a framework for data provenance and supports future use of data and toolchain. This is achieved by enabling the easy modification of the modelling approaches and solution details through abstract problem descriptions, removing the need of repetition of manual processing work.

Keywords: cerebral aneurysms; computational imaging and modelling; computational physiology; virtual physiological human

1. INTRODUCTION

Cerebral aneurysms are local pathological dilatations of arteries in the brain causing significant morbidity and mortality rates [1]. A large proportion (1–5%) of the population has unruptured aneurysms. Once an aneurysm ruptures, subarachnoid haemorrhage (SAH) usually occurs, and the impact is devastating. After SAH, patients have a 45 per cent 30 day mortality rate, and an estimated 30 per cent of survivors present moderate-

to-severe disability. As a consequence, SAH induces a serious burden for patients, their relatives and society.

A considerable debate regarding the optimal treatment of patients harbouring unruptured intracranial aneurysms has developed in recent years, stemming largely from the influence of several factors. Among them stand out the impact of recent technological improvements on diagnostic and interventional imaging, the appearance of a new generation of therapeutic devices, and the increase in the number of large-scale, randomized, multi-institutional studies centred in the outcome evaluation of existing treatments [2] as well as the evolution of unruptured aneurysms [3]. The combination of these factors and the sometimes contradictory

*Author for correspondence (cruz.villa@upf.edu).

One contribution of 17 to a Theme Issue 'The virtual physiological human'.

conclusions introduced by these studies have led to considerable uncertainty about the optimal treatment for patients harbouring unruptured intracranial aneurysms.

These efforts from the clinical community have caused an increasing interest in modelling the complex multi-factorial mechanisms thought to be involved in aneurysm genesis, growth and rupture, which include genetic, physical and environmental factors. This global approach to the disease links with the wide international interest in the construction of an integrated *in silico* human. The 'IUPS Physiome' [4,5] provides the framework for a hierarchy of models spanning the length scales from the molecule to the individual. Other activities exploring the development of multi-scale and multi-disciplinary physiological models up to specific organ level have resulted in the development of the virtual physiological human (VPH) [6–8], in the context of which we could frame this work.

1.1. The @neurIST project

This work was developed as part of the European project 'Integrated Biomedical Informatics for the Management of Cerebral Aneurysms' (@neurIST; <http://www.aneurist.org>) [9,10]. @neurIST was a 4 year project started in 2006 with a 17 million euro budget, gathering 28 public and private institutions of 12 European countries, including industrial, medical and academic institutions. Several organizations from the USA, New Zealand and Japan participated as external collaborators. The mission statement of the project was the following:

@neurIST will transform the management of cerebral aneurysms by providing new insights, personalized risk assessment, and methods for the design of improved medical devices and treatment protocols.

To fulfil this mission, four software suites (@neuRisk, @neuLink, @neuFuse and @neuEndo) and two infrastructure components (@neuCompute and @neuInfo) were developed to collaborate with each other [11–13]. @neuRisk provides personalized risk assessment and treatment guidelines to practitioners based on the analyses performed by the other three suites. @neuLink enables not only the study of the existing links between genetics and disease, but also provides links to the biomechanical indices extracted from @neuFuse. @neuFuse addresses the patient data fusion from different modalities and the extraction of such biomechanical indices. @neuEndo works closely to the other three suites facilitating the optimization and customization of medical devices used for patient treatment. The two infrastructure components allowing the interoperability and collaboration of the suites are @neuCompute, by providing high-performance-distributed computing capabilities, and @neuInfo, by enabling a homogeneous data access and storage to the heterogeneous data types handled in the suites. A more detailed description of the @neurIST system architecture is provided in Benkner *et al.* [14], where the authors introduce the developed service-oriented IT infrastructure supporting the seamless access to

distributed medical data and computational resources in an easy and secure manner.

From the previous, one can understand the role that @neurIST has in tackling a disease in a global manner, a concept which directly links to the VPH. The developed multi-scale paradigm could be extended to other diseases.

1.2. Finding biomechanical risk factors: approach and challenges

This paper describes the @neurIST complex information processing toolchain approach to provide physical models of cerebral aneurysms and derive representative descriptors that could be associated with their rupture.

To create a comprehensive basis for investigating potential physical risk factors, the project aimed to compute for a large number of cases many different characterizations based on the analysis of shape, blood flow (haemodynamics) and wall mechanics. To enable statistical analyses, the typically continuous output of these analyses had to be reduced to a finite number of descriptors suitable for finding statistical associations that would help understanding the natural history and the risks of available treatments.

To this end, @neurIST collected extremely heterogeneous data that included patient's clinical history, images and blood samples, for more than a total of 1400 patients with ruptured and unruptured aneurysms. Our goal was then to compute the whole set of physical characterizations mentioned before for the nearly 500 patients having associated medical images.

To reach these goals, we had to face three major challenges. **First**, to determine the details of the most representative biomechanical analyses to be performed and select the most meaningful physical descriptors that could be derived (§2). **Second**, to enable performing multi-case, multi-operator and multi-site analyses guaranteeing consistency and repeatability among users and processing sites, and to reduce the manual work needed (§3). And **third**, to preserve the provenance of the derived descriptors, to link back to the clinical data, and to permit revisions of the modelling decisions, allowing for future variations and extensions of the analysis (§4).

Section 5 gives an account on our practical experience with using the toolchain. Among others, the work needed to synchronize between different processing teams and feedback collected from exposure to clinicians, i.e. non-experts with respect to the tools. Finally, we discuss how relevant these results are for clinical practice and VPH research in general.

2. CHALLENGE 1: BIOMECHANICAL MODELLING AND DESCRIPTORS

The first challenge faced while designing the @neurIST toolchain was to identify the set of most representative biomechanical descriptors suitable for performing risk assessment and association studies, and to identify the most appropriate computational model of the underlying physical problem. Along the lines set by

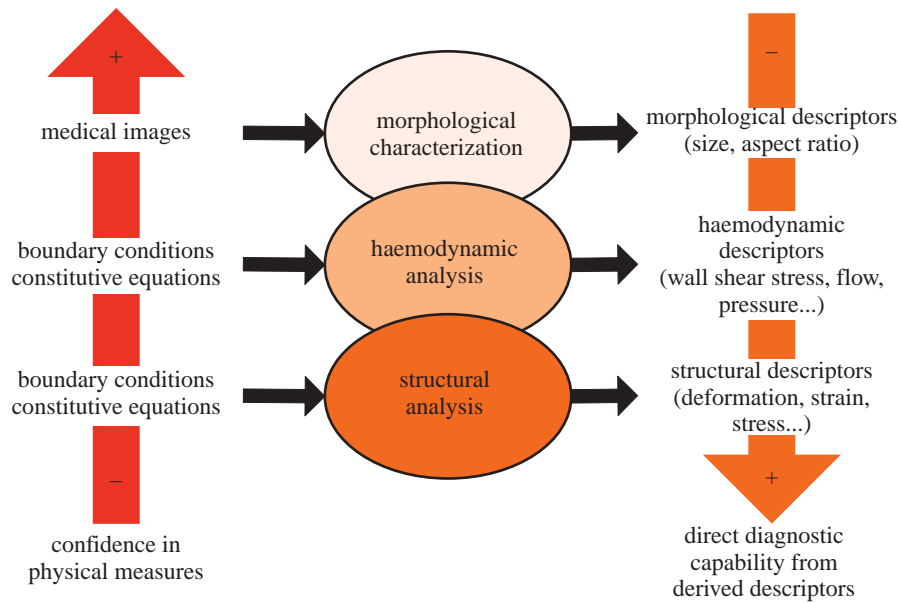


Figure 1. The theoretical diagnostic power (right) versus the practical reliability of physical measures (left) of the different analysis modes are inversely related [29].

Ma *et al.* [15] and Ma [16], three general analyses were chosen to be performed: morphological, haemodynamic and structural. These analyses have been linked in the literature to aneurysm genesis, growth and rupture [17–19]. Evidence indicating differences in morphology [20–23] and flow [18,24] between ruptured and unruptured aneurysms have been shown for reduced patient cohorts. Structural wall mechanics [25–28] has been used to justify the growth and remodelling happening at the aneurysm level.

The balance between merits and demerits of each analysis is sketched in figure 1. The theoretical level of confidence in the physical measures on which each of the analyses are based and the direct diagnostic capability derived from them varies inversely depending on the analysis. As an example, morphological characterizations have the least requirements in terms of the physical measures, only depending on the anatomical information extracted from the medical image. This is opposed to the difficulties in obtaining the physical measures needed to perform haemodynamic and structural analyses in this order of complexity. In the case of haemodynamics, the exact boundary conditions (inlet, outlet and wall movement) are usually unknown. For structural analysis, the situation is worse, as lack of information on the aneurysm wall (thickness, individual material properties) limits the analysis to provide qualitative results only. In contrast, the *theoretical* diagnostic capability would certainly be highest for a quantitatively correct wall mechanics analysis, as stresses exceeding the strength of the wall could be more directly associated with the mechanical processes inducing growth and remodelling phenomena and, therefore, linked to the event of rupture. Nevertheless, *practically*, morphological characterizations might currently have the highest predictive capabilities with respect to the other analyses.

Once these analyses were chosen, based on prior evidences found in the literature, and especially in the case

of the haemodynamic and structural analyses, the immediate need was to decide what to simulate and how to perform such simulations. Unfortunately, there is not a clear answer to this problem. Each of the modelling choices presented trade-offs [30] and needed to be judged in the light of the available input data and intended purpose of the output.

To address these issues, an analysis protocol was developed in two stages. During the first stage, an initial version of the protocol was created and where the fundamental alternatives were identified, the core processing steps and data entities were specified and the topics that needed further exploration were highlighted. As an example of the last, the need for performing sensitivity studies was discussed. An external scientific advisory board of experts reviewed the protocol and raised several questions, including the need of performing linear versus nonlinear wall mechanics studies, using moving versus fixed wall boundary conditions for haemodynamics, employing coupled or isolated models (fluid structure interaction being an option) and using a personalized versus generic systemic model.

As a result, a second version of the protocol was written [29] providing a high-level tool-independent description of the processing chain, clearly describing each major operation with the specification of inputs and outputs. In addition, it included references to several of the studies carried out by the project to evaluate aspects such as the sensitivity of flow simulations to the imaging modality [31] and inlet boundary conditions setting [32], and the relationship between patient-specific and generic boundary conditions [33].

3. CHALLENGE 2: IMPLEMENTATION OF THE TOOLCHAIN

The second challenge was to enable multi-case, multi-user and multi-site analyses, which guaranteed

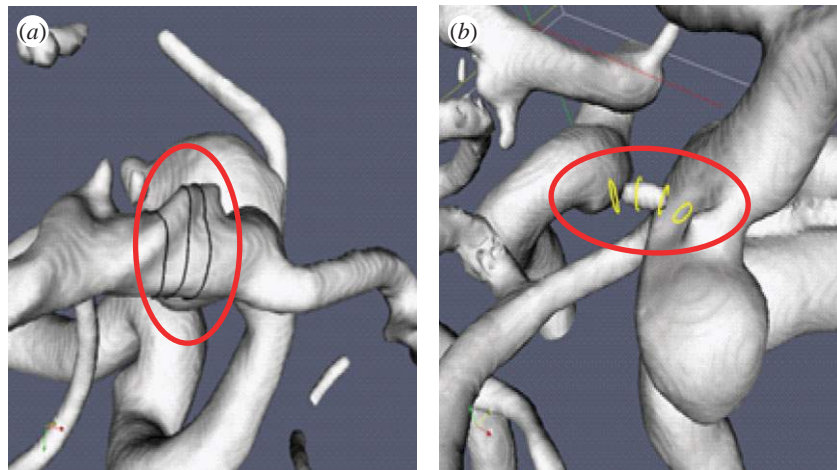


Figure 2. Examples of typical topological problems introduced during the segmentation because of low image quality: (a) touching vessels and (b) missing vessels.

consistency and repeatability among operators and geographically disperse processing sites, while minimizing the amount of required user manual intervention. However, some steps had to remain under user control and considerable efforts had to be devoted to synchronize the different operators in the various processing teams. In the current section, the actual implementation of the toolchain is discussed, highlighting the efforts made to automate or semi-automate it. The toolchain encompassed the whole process from reading a medical image to the extraction of the morphological, structural and haemodynamic descriptors selected in the analysis protocol. These were combined with information available from the patient record and stored within a structured data repository, as described in §4.

3.1. Vascular geometry creation

All three analyses specified in the analysis protocol get as an input a surface mesh. Therefore, the first stage in the toolchain proceeds to create a vascular geometry from a three-dimensional rotational angiographic image (3DRA). This imaging modality is currently considered the gold standard [34,35] for aneurysm detection owing to its superior spatial and contrast resolution. A three-dimensional triangulated surface mesh is obtained using an automatic segmentation method based on geodesic active regions (GAR) in combination with an image standardization technique [36,37], recently presented and validated by Bogunovic *et al.* [38]. The method eliminates most of the dependency on the operator, and on the specific imaging protocols and equipment used. The only possible choice for the operator is the selection of the region of interest to be segmented as opposed to other methods such as the manual iso-intensity surface extraction (ISE), where in addition the selection of a threshold is left to the operator. While the impact of the selection of the region of interest for both methods has shown to be negligible, GAR outperformed ISE qualitatively and quantitatively for 3DRA and time of flight magnetic resonance angiographic images obtained from clinical routine when compared with manual measurements performed

by clinicians. The dependency on the equipment used to image the patient is removed, thanks to the use of a training set and standardized images. The impact of the selection of images to build a training set has also shown to be minimal when compared with the inter-observer variability among clinicians when performing manual measurements. In terms of execution time, it was able to segment a region of interest with a size of 256^3 voxels in 17 ± 4 min (average \pm standard deviation) on a standard personal computer with an Intel quad-core 2.4 GHz processor and 4GB of memory.

Once the segmented surface mesh is available, it is manually manipulated to remove some of the artefacts not belonging to the cerebral vasculature or not relevant for the subsequent analyses (figure 2). A skeletonization algorithm [39] is used to extract the skeleton (medial axis) of this geometry. The skeleton acts as a reference to perform the perpendicular cuts where the flow boundary conditions need to be set, and as the linking point to the three-dimensional model of the human systemic circulation [40]. This first step in the toolchain is critical because the resulting vascular geometry is used as the basis for all further analyses. The impact of the chosen imaging modality and the quality of the image might have a strong influence in quantitative parameters extracted from flow simulations [31]. Therefore, the role of the operator in accepting or rejecting the images based on their quality before they are processed is fundamental for the accuracy of subsequent analyses. In our experience in @neurIST, the approximate discard rate of 3DRA images for all clinical centres involved in the data collection was between 30 and 40 per cent.

3.2. Morphological characterization chain

A collection of morphological descriptors of various complexity was selected among the wide variety available in the literature [21,22]. Basic size indices such as aspect ratio [20], non-sphericity index [22], aneurysm volume and surface area are calculated for the aneurysm sac. Aspect ratio relates the aneurysm depth and neck width, while non-sphericity index relates the aneurysm volume and surface area. To isolate the aneurysm sac,

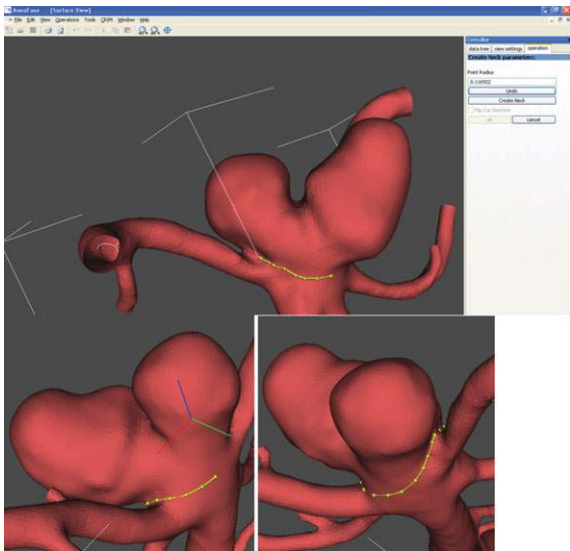


Figure 3. Example of the manual delineation of the aneurysm neck implemented in the @neurIST toolchain.

the aneurysm neck is manually delineated as shown in figure 3. A set of more sophisticated descriptors called three-dimensional Zernike moment invariants [23,41] are also used to characterize the aneurysm shape and a portion of the surrounding feeding vessels using a fixed cutting protocol at every inlet and outlet. Three-dimensional Zernike moments provide a complete three-dimensional morphological characterization of objects, and their invariants remove scale and orientation dependency. These have shown for a small heterogeneous population promising rupture prediction rates [42]. Finally, inlet and outlet vessel diameters are also calculated at the cut planes used to isolate the geometry for which the Zernike moment invariants are computed. All of these descriptors are automatically computed in real time from the isolated geometries of the sac and aneurysm plus a portion of the surrounding feeding vessels.

3.3. Haemodynamics analysis chain

Two complementary haemodynamic analyses are carried out as part of this chain: a global one and a local one, with an optional uni-directional coupling between them. The global one is based on a one-dimensional model of the human systemic circulation [40], including the main arteries of a complete circle of Willis, and predicts flow rate and pressure waveforms at predefined points (figure 4). The local analysis uses the full three-dimensional geometry near the region of interest, obtained by clipping the three-dimensional geometry at appropriate places [29,32].

As no patient-specific measurements of flow properties at the openings defined by the clipping are generally available, the results of the one-dimensional global analysis can be used to obtain boundary conditions for the local three-dimensional analysis. Using the skeletonized representation of the three-dimensional vasculature in the region of interest calculated during the vascular geometry extraction stage, the operator manually defines perpendicular clipping planes and links the appropriate nodes of the

one-dimensional circulation model to the corresponding points of the three-dimensional inlet and outlet boundaries, thus defining the boundary conditions for the three-dimensional model (figure 4).

The set of qualitative and quantitative descriptors (candidate risk factors) defined by the analysis protocol were extracted from the flow solution automatically, except a few qualitative ones such as flow stability and intra-aneurysmal flow type (figure 5) requiring expert judgement. Quantitative volumetric measures were performed within the aneurysm and at the neck. These included the maximum and mean velocities defined at peak systole and averaged over the cardiac cycle. Similarly, other measures were computed on the model surface, including areas of elevated pressure, impingement jet location, maximum static pressure on the wall at peak systole and the wall shear stress and derivatives such as the oscillatory shear index. Some of these measures are highly dependent on the location of the aneurysm neck, which unfortunately had to be manually defined as already mentioned in the morphological analysis. There have been several efforts in the literature aimed to solve this problem in an automated way, but to date none has been able to extract the aneurysm neck reliably in the general case [43–46].

The analysis protocol chose to model the transient blood flow by the Navier–Stokes equations under the assumption of rigid walls and a simple Newtonian rheology model with blood density of 1060 kg m^{-3} and viscosity of 0.0035 Pa s .

The production runs were performed using a commercial three-dimensional flow solver ANSYS CFX (Ansys Inc., Canonsburg, PA, USA), which is a finite-volume computational fluid dynamics (CFD) code solving for the Navier–Stokes flow equations across an unstructured three-dimensional discretization (known as mesh) of the vasculature volume. Such mesh was generated by the ANSYS ICEM 3D (Ansys Inc.) mesh generator that labelled the aneurysmal interior in a completely automatic manner.

3.4. Structural analysis chain

Of all types of analyses in figure 1, an ‘accurate’ structural analysis would have the largest predictive capabilities. Nevertheless, in practice it also is the analysis requiring the most assumptions and simplifications. Still it can be hoped to gain information about risk factors [28]. In @neurIST, and owing to the lack of patient-specific data, the assumptions being made included averaged material properties and aneurysmal wall thickness and spatially and temporally constant pressure, for simplicity assumed at diastole. However, the membrane code FEANOR [47], developed specifically for @neurIST, computes the zero-load state of the aneurysm under the above assumptions, which is a first step towards more realistic wall mechanics simulation.

The thickness of the aneurysm wall was set to a constant value of $86 \mu\text{m}$, the thickness of the vessel wall to $500 \mu\text{m}$, and was linearly interpolated in a transition region (figure 6a). Owing to this thin wall, computing the zero-load state is a numerically delicate process

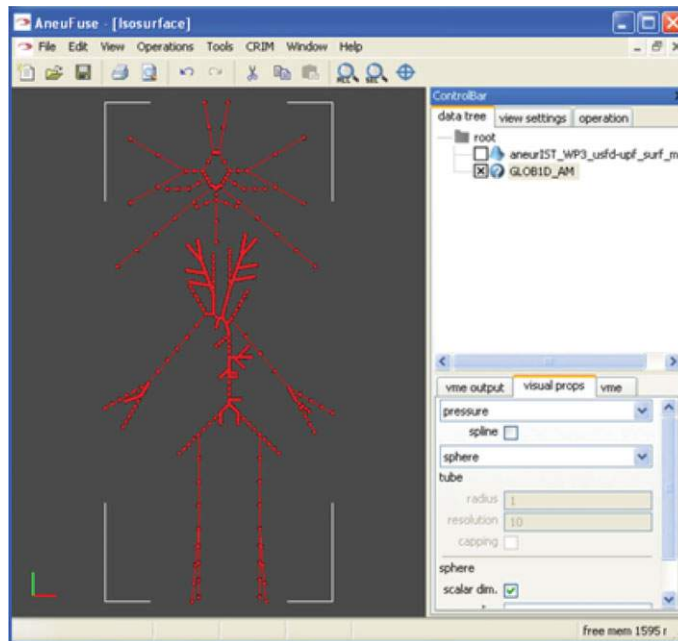


Figure 4. A view of the @neurIST one-dimensional model.

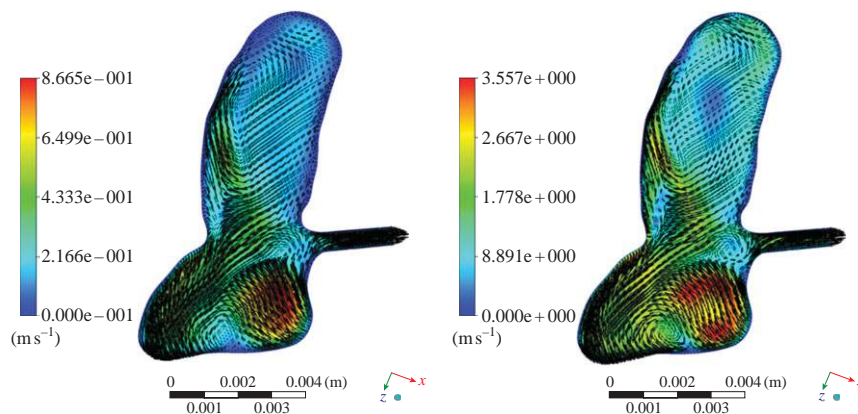


Figure 5. Example of unstable flow from (a) end diastole and (b) peak systole.

(figure 6) and great effort was required to make this numerically stable and hence automatic.

Two different protocols are supported. The first one uses a nonlinear material model and computation of a zero-load state, and the second uses a linear material model assuming zero stresses at diastole. Given the essential uncertainties in quantitatively estimating the model parameters, the characteristic measures include only relative measures like ratio of areas exceeding certain thresholds of maximum stress and strain, as these are expected to be less sensitive to variations of the unknown patient-specific values of aneurysm wall thickness and material properties.

4. CHALLENGE 3: A MODEL FOR @NEURIST SIMULATION DATA

4.1. Motivation and overview

The third challenge was to preserve the provenance of the derived descriptors, to be able to link back to the

clinical data and to permit future revisions of the modelling decisions, allowing for future variations and extensions of the analysis. This concern was partially originated by the huge amount of manual work going into the toolchain and into the data processing, despite the level of automation and semi-automation achieved during the implementation of the toolchain. Moreover, feeding the results into the sophisticated data mining machinery of @neuLink [11] meant that various subsets and combinations of the result data were possibly needed, in order to select statistically meaningful groups of cases and to provide the greatest flexibility in the search for patterns.

The answer was to design a systematic model of the different data entities involved to facilitate meeting these requirements. Relationships, mutual dependencies and history (provenance) needed to be clearly captured. In contrast to the general approaches for provenance recording described in Simmhan *et al.* [48], our approach is geared towards the specific needs of the @neurIST project. According to the taxonomy of

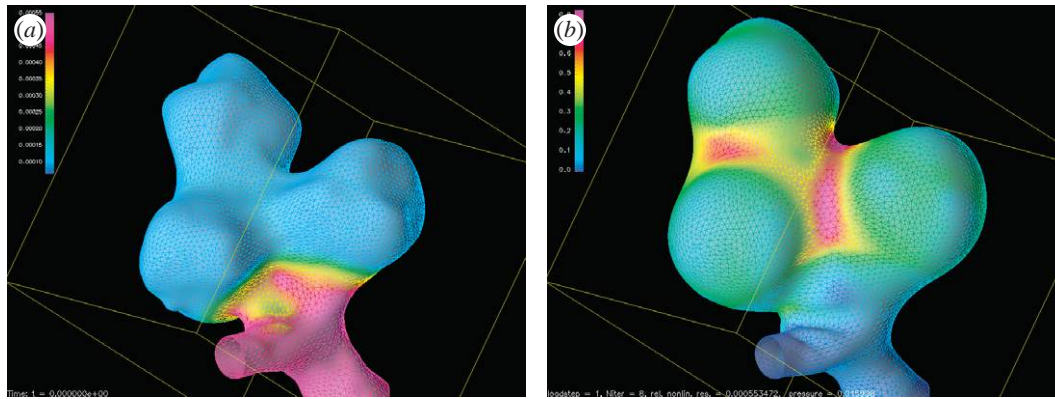


Figure 6. Computing the zero-load state leads to considerable wrinkling and is numerically delicate. (a) Computed zero-load configuration (with assumed thickness) and (b) stresses at 120 mmHg computed by using the nonlinear material model.

Simmhan *et al.* [48], we use a coarse-grained and somewhat abstracted replication recipe (see also below §4c on abstract problem descriptions (APDs)). At the same time, to maximize opportunities for future use, the entities in this model had to be represented in a sufficiently general way in order to distinguish from details specific to concrete tools and applications. That is, to abstract from information which will become obsolete sooner or later. This application-neutrality was already required within the @neurIST complex information toolchain, as it was designed to support different solvers for the same computational problem (e.g. ANSYS CFX and a Lattice–Boltzmann code for haemodynamics).

Our solution thus consisted of the following ingredients:

- A relational data model (using structured query language (SQL) as data definition language) linking the important classes of simulation (or ‘derived’) data to the clinical data, hence ‘derived data model’ (DDM).
- A set of tools automatically translating the abstract, application-neutral description of the DDM into complete input specifications for concrete simulation applications.
- A strategy for storing and retrieving bulk data, like raw simulation results, images, etc. While most of the bulk data is application-specific and can be reproduced using the high-level data and the two tools just mentioned, it may be worthwhile to keep it for a certain period of time, e.g. for visualization and review purposes.

4.2. A relational data model for derived data

The DDM forms the core of these developments. A high-level overview in the form of an entity-relationship (ER) diagram is shown in figure 7. The DDM covered the following major entities.

- *Aneurysm*. The anatomical structure in the focus of interest.
- *Image* (split in *imagingStudy* and *imagingSeries*). A medical image of the region of interest.
- *Processed geometry*. A valid geometric representation of one or more aneurysms with anatomically correct topology.

- *Analysis*. A high-level description of a computational model, e.g. blood flow through the vasculature surrounding an aneurysm.
- *Run*. An actual computation of an analysis with a simulation programme.
- *Index*. A discrete¹ characterization of an aneurysm, e.g. aspect ratio, collection of three-dimensional Zernike moment invariants or maximal wall shear stress inside the aneurysm.
- *Experiment*. A group of similar analyses suitable for finding statistical correlations.

Some of these entities (namely aneurysm and image) contained references to their counterparts in clinical databases that may be enhanced with additional information, such as image quality. The clinical databases containing the anonymized patient’s clinical record use their own data model developed in the project, the @neurIST clinical reference information model (CRIM). The DDM was kept deliberately separate from the CRIM to minimize dependencies.

The central use case of the DDM in our context of finding risk indicators is the ability to retrieve answers to questions (known as queries) like ‘for a set of aneurysms, retrieve rupture status and values of biomechanical characterizations A, B, and C’. This query could easily be refined by restriction to aneurysms in certain locations, or by excluding cases with certain irregularities (like bad image quality), and so on.

An important means to form meaningful groups of comparable analyses is the experiment entity. For instance, we used two different experiments for the wall mechanics analyses, one using a linear material model, and one using a non-linear model with computation of a zero-load state. Another example of use of experiments is for different conventions for geometry clipping in shape analysis. Clearly, it does not make sense to mix analyses pertaining to different experiments in a statistical evaluation.

4.3. Handling bulk data

The storage of the actual bulk data (meshes, pictures and full simulation results) can be handled in a quite flexible way, as the data model provides a placeholder

¹I.e. a small, finite set of values, as opposed to a continuum like a pressure field, which is not usable in a statistical clustering analysis.

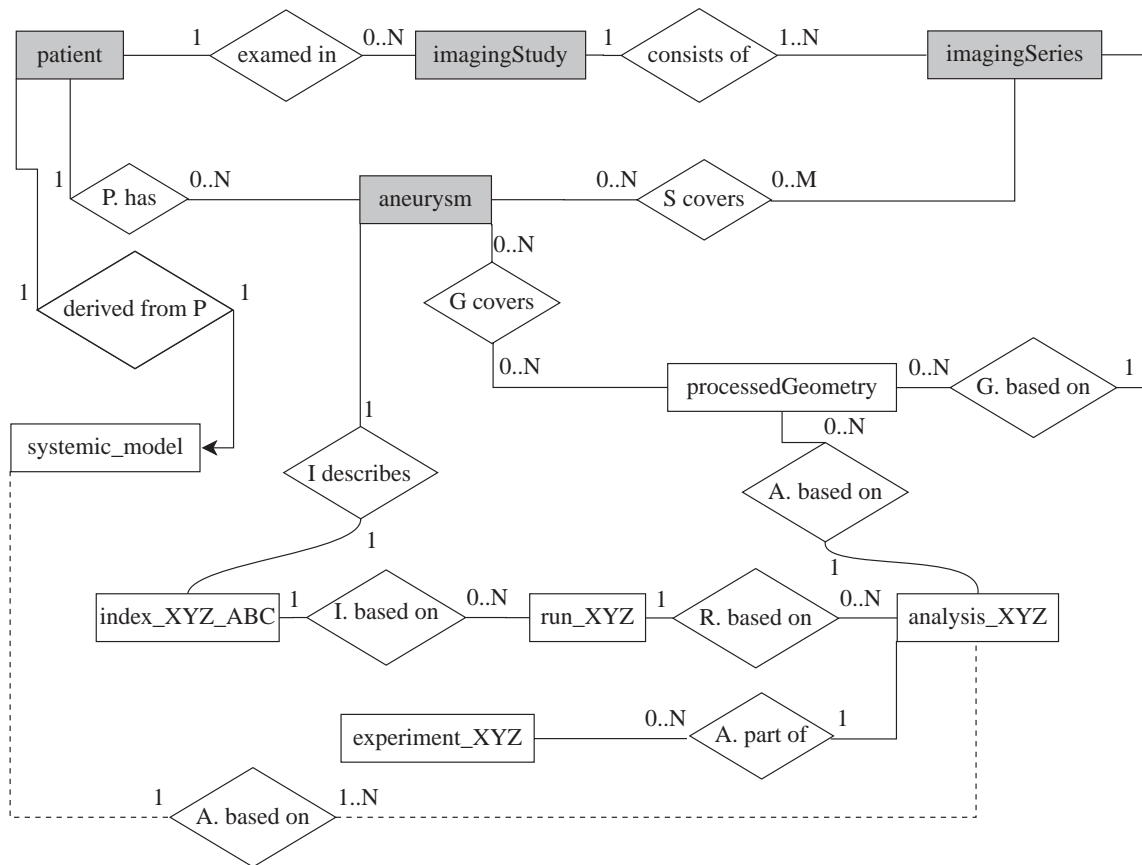


Figure 7. An entity-relationship diagram of the @neurIST derived data model [29]. Grey entities link to their counterparts in the clinical reference information model (CRIM) developed in the project, white ones to derived (i.e. computed) data. The diamond-shaped boxes describe the relationship of two entities, and the numbers give their multiplicities. For example, a processed geometry is based on exactly one imaging series, and each imaging series is the basis for 0 up to N processed geometries. The suffix XYZ is a placeholder for the different types of analysis.

for each such data entities, with the necessary meta-data as to where and how it is stored. Smaller data like surface meshes can even be stored directly in a data base management system (DBMS) as binary large object (BLOB). Data stored outside the DBMS can be referenced by URLs, or most generally, by endpoint references (EPR), containing the details for addressing a service delivering the data.

An important criterion to support decisions about whether to store a particular piece of data, such as raw simulation results or processed geometries, is the cost associated to (re-)generate them. This can be computational costly as well as, and more importantly, the amount of manual work needed to create them. For the case of the @neurIST toolchain, this differentiates processed geometries, possibly requiring a lot of manual work, see §3a, from simulation results, which can be generated automatically from their APDs, a concept we will discuss in more detail next.

4.4. An important concept: abstract problem descriptions

An APD is a high-level definition of a computational biomechanical problem, like a blood flow analysis through an aneurysm and surrounding vasculature. Despite their high-level nature, they contain or reference all information needed to generate input for any

concrete simulation application *run* computing the analysis. There could be different runs using different applications for the same analysis, which should yield the ‘same’ results (up to some limit of accuracy). Sets of different runs could be used for verification of the solver-independence of results.

The conversion of an APD into a concrete simulation input and the subsequent run is, in principle, a completely automatic task, as the APD contained all relevant information; all necessary pieces of data needing human intervention are generated and stored before creating the APD. In practice, the feasibility of automation is certainly dependent on the application; in the case of @neurIST, we fully automated this step for the supported simulation packages. An exception to this rule are some qualitative characterizations that inevitably required human intervention.

The precise but application-neutral representation of biomechanical problems in the APDs enables their long-term storage, making them insensitive to the rise and fall of simulation applications, or just incompatibilities between versions. For instance, we integrated two fundamentally different types of CFD solvers. First, ANSYS CFX based on a finite volume scheme on unstructured meshes, and, second, a Lattice-Boltzmann solver, based on regular structured grids (the latter was not used for production runs). Basically, this meant implementing specific preprocessors

translating the APD into either ANSYS CFX or Lattice–Boltzmann input. The abstractness of the representation also facilitates automatic transformation of analyses to yield variants implementing different experiments. For instance, it would be easy to implement features like changing the generation of boundary conditions or using a different material model. Such automatic transformations pave the way to practical future uses of the results, like doing parametric studies or setting up completely new modelling approaches.

5. PRACTICAL EXPERIENCE

Even if the degree of automation accomplished in the implementation of the complex information toolchain is beyond the state of the art, it was not sufficient to achieve consistent results across the different processing teams. To achieve this, training was fundamental, and verification of the level of understanding of the case processing rules was mandatory. To evaluate the overall impact of the operator decisions on the final-derived descriptors, six patient images were chosen as demonstrators and were fully processed by eight representatives of the processing teams. The objective was to synchronize the results of the operators for the shape, structural and haemodynamic analyses.

Several rounds of this synchronization were needed before a common agreement was reached and a set of accurate guidelines could be distilled. This process was simpler in the case of the morphological analysis and only two rounds were needed. As an example of the importance of this process, see in figure 8 the surprising variability in the results for some operators after the first synchronization iteration. In the case of the haemodynamic analysis, the synchronization took longer because of the elevated complexity of this chain as well as the impact that operator decisions could have on the final simulation results. Still, agreement was reached in the end and the @neurIST case processing was started.

In total, 15 operators from four case processing centres were involved and fully processed images from five hospitals producing descriptors for more than 300 aneurysms. The essential data items created during this process were stored using the mechanism described in §4 and are thus available for future work. Statistical associations are currently being analysed between these descriptors and the aneurysm rupture status information, among others.

In addition, we also wanted to evaluate the suitability of our toolchain for clinical practice. In this spirit, and to gain useful feedback, the toolchain has been officially exposed to more than 260 neurointerventionists, neurosurgeons and neurologists for their evaluation through hands-on workshops at different public events, where the participants worked under guidance through a simple case, from medical image to a three-dimensional blood flow simulation. They achieved results comparable to those obtained by experts users, with similar performance.

The main venues have been the 1st and 2nd European Society for Minimally Invasive Neurovascular

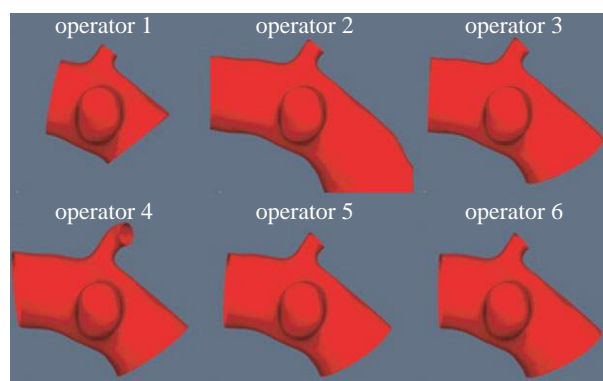


Figure 8. Results for the first synchronization round showing the differences among six of the eight operators during the manual isolation of the region of interest. Operators 1, 2 and 4 showed significant discrepancies with the correct geometries isolated by operators 3, 5 and 6.

Treatment (ESMINT) Teaching Courses, respectively, held in Lisbon, Portugal (7–12 September 2008) and Barcelona, Spain (13–18 December 2009), the 4th International Conference on Computational Bioengineering, Bertinoro, Italy (16–18 September 2009), the XIV World Congress of Neurological Surgery, Boston, USA (30 August–4 September 2009) and the Simposio Internacional de Neuroradiología Intervencional, Santiago de Chile, Chile (26–27 November 2009).

The collected feedback was used to further improve the subsequent releases of the toolchain. Some of the conclusions reached during the 1st ESMINT Teaching Course were reported and described in Singh *et al.* [49]. In general, clinicians recognized shortcomings in current management of cerebral aneurysms and the need for better understanding of the disease and the identification of novel and more efficient risk descriptors. Although most clinicians believe that physical characterization (mainly haemodynamics at that workshop) may offer better diagnostic value, there is a clear lack of awareness concerning the role of haemodynamics in the aetiopathogenesis of cerebral aneurysms and the use of CFD in this context.

6. DISCUSSION

A number of unique challenges were associated with the large-scale multi-case, multi-operator and multi-site biomechanical processing undertaken by @neurIST. The solutions we have developed to meet these challenges are, we believe, of interest not only for the field of aneurysm research, but also beyond that for the larger VPH community studying other diseases.²

The toolchain itself was developed and automated to a degree which proved sufficient to process more than 300 aneurysms minimizing and quantifying the impact of human operators, either by ensuring synchronization among operators through training or by performing

²Parts of the toolchain are available through the @neurIST web site <http://www.aneurist.org/>, as well as the data model SQL definition and the final analysis protocol document. Currently, there are efforts in the direction of making derived data available through the European Society of Minimally Invasive Neurological Therapy (ESMINT) society <http://www.esmint.eu/>.

several sensitivity studies. Also, more than 260 clinicians ran full blood flow simulations starting from medical images, using our toolchain during internationally renowned hands-on events. Their feedback convinced us that these kinds of tools will find their way into clinical practice. All together, the amount of practical usage, testing and continual improvement based on user feedback of this toolchain certainly surpasses that of most similar research-oriented efforts. There is, however, still room for improvements.

Our analysis protocol [29], with its detailed specifications and ample discussion of limitations versus modelling alternatives, is an ideal starting point for continuing and extending our efforts. It can also serve as a blueprint for transferring the approach to other diseases, which should be straightforward for vascular diseases.

The analysis of the biomechanical characterizations with respect to their diagnostic value is still ongoing. Some preliminary works [42,50–53] have already used the toolchain on a reduced number of cases. However, it can be expected that the larger the number of cases, the statistically more reliable conclusions will be achieved compared with similar prior works [53], but always under the strong and arguable assumption that aneurysms do not change over time.

Using the toolchain to simulate flow in the presence of virtual endovascular devices such as stents [54] currently allows evaluating the performance of endovascular devices from a haemodynamic point of view [55,56], benefiting from the ability of setting boundary conditions based on a one-dimensional model of the systemic circulation [32,33,40]. The inclusion in the project of genetics data has rendered already relevant results [57] to the scientific community in identifying three new risk loci, which still need to be linked to biomechanical factors through @neuLink [12].

The results of our processing are organized using the DDM and are available for future extensions of the our work, both by adding new cases or by varying the modelling approach. In this case, it might be interesting to enable the toolchain to investigate effects of certain drugs on blood viscosity and hence on the computed flow characterizations. The prospect of being able to run large-scale computational experiments with these many cases without having to invest a lot of human effort into manual case-by-case model adaptation is exciting.

We believe that our approach has the potential to serve as a model for organizing large-scale multi-case simulation in the VPH context in general, as it supports looking both into the past, by providing provenance information, and into the future, by providing a means to modify toolchain details (like replacing specific solvers) and to transform problem descriptions to support alternative modelling choices. Currently, the model only supports the coupling between the systemic and the local three-dimensional haemodynamics analyses; a particularly promising path for future evolution is to add explicit support for coupling between different analyses on different scales.

This work was supported by the @neurIST Integrated Project (co-financed by the European Commission through the

contract no. IST-027703). The authors would also like to thank for their contribution to the processing of cases as well as to the implementation of the toolchain the following researchers: C. Valencia, H. Tahir, H. Morales, A. J. Geers, M. Aguilar, M. Kim, C. Bludszuweit, D. Capdeferro, P. Watton, M. Giacomoni, H. Bogunovic, A. Radaelli and K. McCormack.

REFERENCES

- 1 Brisman, J., Song, J. & Newell, D. 2006 Medical progress: cerebral aneurysms. *New Engl. J. Med.* **355**, 928–939. (doi:10.1056/NEJMra052760)
- 2 Molyneux, A. J. & the International Subarachnoid Aneurysm Trial (ISAT) Collaborative Group. 2002 International subarachnoid aneurysm trial (ISAT) of neurological clipping versus endovascular coiling in 2143 patients with ruptured intracranial aneurysms: a randomised trial. *Lancet* **360**, 1267–1274. (doi:10.1016/S0140-6736(02)11314-6)
- 3 Wiebers, D. & the International Study of the Unruptured Intracranial Aneurysms Investigators. 2003 Unruptured intracranial aneurysms: natural history, clinical outcome, and risks of surgical and endovascular treatment. *Lancet* **362**, 103–110. (doi:10.1016/S0140-6736(03)13860-3)
- 4 Hunter, P., Robbins, P. & Noble, D. 2002 The IUPS human physiome project. *Eur. J. Physiol.* **445**, 1–9. (doi:10.1007/s00424-002-0890-1)
- 5 Hunter, P. & Borg, T. 2003 Integration from proteins to organs: the physiome project. *Nature* **4**, 237–243. (doi:10.1038/nrm1017)
- 6 STEP Consortium. 2007 Seeding the EuroPhysiome: a roadmap to the virtual physiological human. See <http://www.europhysiome.org/roadmap>.
- 7 Fenner, J. et al. 2008 The EuroPhysiome, STEP and a roadmap for the virtual physiological human. *Proc. R. Soc. A* **366**, 2979–2999. (doi:10.1098/rsta.2008.0089)
- 8 Viceconti, M., Clapworthy, G. & Van Sint Jan, S. 2008 The virtual physiological human—a European initiative for *in silico* human modelling. *J. Physiol. Sci.* **58**, 441–447. (doi:10.2170/physiolsci.RP009908)
- 9 Iavindrasana, J. et al. 2008 The @neurIST project. *Stud. Health Technol. Inform.* **138**, 161–164.
- 10 Dunlop, R. et al. 2008 @neurIST—chronic disease management through integration of heterogeneous data and computer-interpretable guideline services. *Stud. Health Technol. Inform.* **138**, 173–177.
- 11 Arbona, A., Benkner, S., Engelbrecht, G., Fingberg, J., Hofmann, M., Kumpf, K., Lonsdale, G. & Woehrer, A. 2007 A service-oriented grid infrastructure for biomedical data and compute services. *IEEE Trans. Nanobiosci.* **6**, 136–141. (doi:10.1109/TNB.2007.897438)
- 12 Friedrich, C. M., Dach, H., Gattermayer, T., Engelbrecht, G., Benkner, S. & Hofmann-Apitius, M. 2008 @neuLink: a service-oriented application for biomedical knowledge discovery. *Stud. Health Technol. Inform.* **138**, 165–172.
- 13 Hofmann-Apitius, M. et al. 2008 Knowledge environments representing molecular entities for the virtual physiological human. *Phil. Trans. R. Soc. A* **366**, 3091–3110. (doi:10.1098/rsta.2008.0099)
- 14 Benkner, S. et al. 2010 @neurist—infrastructure for advanced disease management through integration of heterogeneous data, computing, and complex processing services. *IEEE Trans. Info. Technol. BioMed.* **14**, 1365–1377. (doi:10.1109/TITB.2010.2049268)
- 15 Ma, B., Harbaugh, R., Lu, J. & Raghavan, M. 2004 Modeling the geometry, hemodynamics and tissue mechanics of cerebral aneurysms. In *Proc. of IMECE: ASME Int.*

- Mechanical Engineering Congress and Exposition, Advances in Bioengineering*, pp. 397–398. Washington, DC: ASME. (doi:10.1115/IMECE2004-60024)
- 16 Ma, B. 2004 Modeling the geometry, hemodynamics, and tissue mechanics of cerebral aneurysms. Ph.D. thesis, University of Iowa, USA.
 - 17 Humphrey, J. & Taylor, C. 2008 Intracranial and abdominal aortic aneurysms: similarities, differences, and need for a new class of computational models. *Annu. Rev. Biomed. Eng.* **10**, 221–246. (doi:10.1146/annurev.bioeng.10.061807.160439)
 - 18 Cebal, J. R., Castro, M. A., Appanaboyina, S., Putman, C. M., Millan, D. & Frangi, A. F. 2005 Efficient pipeline for image-based patient-specific analysis of cerebral aneurysm hemodynamics: technique and sensitivity. *IEEE Trans. Med. Imag.* **24**, 457–467. (doi:10.1109/TMI.2005.844159)
 - 19 Villa-Uriol, M. C. et al. 2010 Toward integrated management of cerebral aneurysms. *Phil. Trans. R. Soc. A* **368**, 2961–2982. (doi:10.1098/rsta.2010.0095)
 - 20 Ujiie, H. et al. 1999 Effects of size and shape (aspect ratio) on the hemodynamics of saccular aneurysms: a possible index for surgical treatment of intracranial aneurysms. *Neurosurgery* **45**, 119–130. (doi:10.1097/00006123-199907000-00028)
 - 21 Ma, B., Harbaugh, R. E. & Raghavan, M. L. 2004 Three-dimensional geometrical characterization of cerebral aneurysms. *Ann. Biomed. Eng.* **32**, 264–273. (doi:10.1023/B:ABME.0000012746.31343.92)
 - 22 Raghavan, M. L., Ma, B. & Harbaugh, R. E. 2005 Quantified aneurysm shape and rupture risk. *J. Neurosurg.* **102**, 355–362. (doi:10.3171/jns.2005.102.2.0355)
 - 23 Millan, R., Dempere-Marco, L., Pozo, J. M., Cebal, J. R. & Frangi, A. F. 2007 Morphological characterization of intracranial aneurysms using 3-D moment invariants. *IEEE Trans. Med. Imag.* **26**, 1270–1282. (doi:10.1109/TMI.2007.901008)
 - 24 Steinman, D., Milner, J., Norley, C., Lownie, S. & Holdsworth, D. 2003 Image-based computational simulation of flow dynamics in a giant intracranial aneurysm. *Am. J. Neuroradiol.* **24**, 559–566.
 - 25 Stehbens, W. 1963 Histopathology of cerebral aneurysms. *Arch. Neurol.* **8**, 272–285.
 - 26 Stehbens, W. 1981 Arterial structure at branches and bifurcations with reference to physiological and pathological processes, including aneurysm formation. In *Structure and function of the circulation*, vol. 2 (eds C. J. Schwarz, N. T. Werthessen & S. G. Wolf), pp. 667–693. New York, NY: Plenum Press.
 - 27 Seshaiyer, P., Hsu, F., Shah, A., Kyriacou, S. & Humphrey, J. 2001 Multiaxial mechanical behavior of human saccular aneurysms. *Comput. Methods Biomech. Biomed. Eng.* **4**, 281–289. (doi:10.1080/10255840108908009)
 - 28 Ma, B., Lu, J., Harbaugh, R. & Raghavan, M. 2007 Non-linear anisotropic stress analysis of anatomically realistic cerebral Aneurysms. *Trans. ASME J. Biomech. Eng.* **129**, 88–96. (doi:10.1115/1.2401187)
 - 29 Berti, G., Hose, R., Marzo, A., Villa-Uriol, M. C., Singh, P. & Lawford, P. 2010 Analysis protocols version 2. See http://www.aneurist.org/UserFiles/File/PUBLIC_DELIVERABLES/D23v2_v1.2_final.pdf.
 - 30 Taylor, C. & Humphrey, J. 2009 Open problems in computational vascular biomechanics: hemodynamics and arterial wall mechanics. *Comput. Methods Appl. Mech. Eng.* **198**, 3514–3523. (doi:10.1016/j.cma.2009.02.004)
 - 31 Geers, A. J., Larrabide, I., Radaelli, A. G., Bogunovic, H., Kim, M., van Andel, H. A. F. G., Majoie, C. B., VanBavel, E. & Frangi, A. F. 2011 Patient-specific computational hemodynamics of intracranial aneurysms from 3DRA and CTA: an *in vivo* reproducibility study. *Am. J. Neuroradiol.* (doi:10.3174/ajnr.A2306)
 - 32 Marzo, A., Singh, P., Reymond, P., Stergiopoulos, N., Patel, U. & Hose, D. R. 2009 Influence of inlet boundary conditions on the local haemodynamics of intracranial aneurysms. *Comput. Methods Biomech. Biomed. Eng.* **12**, 431–444. (doi:10.1080/10255840802654335)
 - 33 Marzo, A. et al. 2010 Computational haemodynamics in cerebral aneurysms: the effects of modelled versus measured boundary conditions. *Ann. Biomed. Eng.* **2**, 884–896 (doi:10.1007/s10439-010-0187-z)
 - 34 McKinney, A., Palmer, C., Truwit, C., Karagulle, A. & Teksam, M. 2008 Detection of aneurysms by 64-section multidetector CT angiography in patients acutely suspected of having an intracranial aneurysm and comparison with digital subtraction and 3D rotational angiography. *Am. J. Neuroradiol.* **29**, 594–602. (doi:10.3174/ajnr.A0848)
 - 35 van Rooij, W., Sprengers, M., de Gast, A., Peluso, J. & Sluzewski, M. 2008 3D rotational angiography: the new gold standard in the detection of additional intracranial aneurysms. *Am. J. Neuroradiol.* **29**, 976–979. (doi:10.3174/ajnr.A0964)
 - 36 Hernandez, M. & Frangi, A. F. 2007 Non-parametric geodesic active regions: method and evaluation for cerebral aneurysms segmentation in 3DRA and CTA. *Med. Image Anal.* **11**, 224–241. (doi:10.1016/j.media.2007.01.002)
 - 37 Bogunović, H., Radaelli, A., de Craene, M., Delgado, D. & Frangi, A. F. 2008 Image intensity standardization in 3D rotational angiography and its application to vascular segmentation. In *SPIE Medical Imaging 2008: Image Processing, San Diego, CA, USA*, vol. 6914 (eds J. Reinhardt & J. Pluim), p. 691419. Bellingham, WA: Society of Photo-Optical Instrumentation Engineers. (doi:10.1117/12.770564)
 - 38 Bogunovic, H. et al. 2011 Automated segmentation of cerebral vasculature with aneurysms in 3DRA and TOF-MRA using geodesic active regions: an evaluation study. *Med. Phys.* **38**, 210–222. (doi:10.1118/1.3515749)
 - 39 Mellado, X., Larrabide, I., Hernandez, M. & Frangi, A. F. 2007 Flux driven medial curve extraction. *Insight J.*
 - 40 Reymond, P., Merenda, F., Perren, F., Rüfenacht, D. & Stergiopoulos, N. 2009 Validation of a one-dimensional model of the systemic arterial tree. *Am. J. Physiol. Heart Circ. Physiol.* **297**, H208–H222. (doi:10.1152/ajpheart.00037.2009)
 - 41 Pozo, J. M., Villa-Uriol, M. & Frangi, A. F. 2011 Efficient 3D Geometric and Zernike moments computation from unstructured surface meshes. *IEEE Trans. Pattern Anal. Machine Intell.* **33**, 471–484. (doi:10.1109/TPAMI.2010.139)
 - 42 Valencia, C., Villa-Uriol, M. C., Pozo, J. M. & Frangi, A. F. 2010 Morphological descriptors as rupture indicators in middle cerebral artery aneurysms. In *Proc. IEEE EMBS. EMBC*, pp. 6046–6049. Buenos Aires, Argentina. Piscataway, NJ: IEEE Press. (doi:10.1109/IEMBS.2010.5627610)
 - 43 Lauric, A., Miller, E., Frisken, S. & Malek, A. M. 2010 Automated detection of intracranial aneurysms based on parent vessel 3D analysis. *Med. Image Anal.* **14**, 149–159. (doi:10.1016/j.media.2009.10.005)
 - 44 Ford, M., Hoi, Y., Piccinelli, M., Antiga, L. & Steinman, D. 2009 An objective approach to digital removal of saccular aneurysms: technique and applications. *Bri. J. Radiol.* **82**, S55–S61. (doi:10.1259/bjr/67593727)

- 45 Sgouritsa, E., Mohamed, A., Morsi, H., Shaltoni, H., Mawad, M. & Kakadiaris, I. 2010 Neck localization and geometry quantification of intracranial aneurysms. In *IEEE Int. Symp. Biomed. Imag.*, pp. 1057–1060. Piscataway, NJ: IEEE Press. Rotterdam, The Netherlands. (doi:10.1109/ISBI.2010.5490172)
- 46 Larrabide, I., Villa-Uriol, M. C., Cardenas, R., Pozo, J. M., Hose, D. & Frangi, A. F. 2010 Automated intracranial aneurysm isolation and quantification. In *Proc. IEEE EMBS. EMBC*, pp. 2841–2844. Argentina: Buenos Aires. Piscataway, NJ: IEEE Press. (doi:10.1109/IEMBS.2010.5626075)
- 47 Schmidt, J. G. 2010 The FEANOR source code. See <http://www.rheinahrcampus.de/~medsim>.
- 48 Simmhan, Y. L., Plale, B. & Gannon, D. 2005 A survey of data provenance in e-science. *SIGMOD Record* **34**, 31–36. (doi:10.1145/1084805.1084812)
- 49 Singh, P. et al. 2009 The role of computational fluid dynamics in the management of unruptured intracranial aneurysms: a clinicians' view. *Comput. Intell. Neurosci.* **2009**, 1–12. (doi:10.1155/2009/760364)
- 50 Radaelli, A. G., Sola Martínez, T., Vivas Díaz, E., Mellado, X., Castro, M. A., Putman, C. M., Guimaraens, L., Cebal, J. R. & Frangi, A. F. 2007 Combined clinical and computational information in complex cerebral aneurysms: application to mirror cerebral aneurysms. In *SPIE Medical Imaging: Physiology, Function, and Structure from Medical Images, San Diego, CA, USA* (eds A. Manduca & X. P. Hu). Lecture Notes on Computer Science 6511, p. 65111F. Bellingham, WA: Society of Photo-Optical Instrumentation Engineers. (doi:10.1117/12.708955)
- 51 Singh, P. et al. 2010 Effects of smoking and hypertension on wall shear stress and oscillatory shear index at the site of intracranial aneurysm formation. *Clin. Neurol. Neurosurg.* **112**, 306–313. (doi:10.1016/j.clineuro.2009.12.018)
- 52 Singh, P. et al. 2010 The effects of aortic coarctation on cerebral hemodynamics and its importance in the etio-pathogenesis of intracranial aneurysms. *J. Vasc. Interv. Neurol.* **3**, 17–30.
- 53 Cebal, J., Mut, F., Raschi, M., Scrivano, E., Ceratto, R., Lylyk, P. & Putman, C. 2010 Aneurysm rupture following treatment with flow-diverting stents: computational hemodynamics analysis of treatment. *Am. J. Neuroradiol.* **32**, 27–33. (doi:10.3174/ajnr.A2398)
- 54 Larrabide, I., Kim, M., Augsburger, L., Villa-Uriol, M., Rüfenacht, D. & Frangi, A. 2011 Fast virtual deployment of self-expandable stents: method and in vitro evaluation for intracranial aneurysmal stenting. *Med. Image Anal.* (doi:10.1016/j.media.2010.04.009)
- 55 Radaelli, A. et al. 2008 Reproducibility of haemodynamical simulations in a subject-specific stented aneurysm model: A report on the Virtual Intracranial Stenting Challenge 2007. *J. Biomech.* **41**, 2069–2081. (doi:10.1016/j.jbiomech.2008.04.035)
- 56 Kim, M., Larrabide, I., Villa-Uriol, M. C. & Frangi, A. F. 2009 Hemodynamic alterations of a patient-specific intracranial aneurysm induced by virtual deployment of stents in various axial orientation. In *IEEE Int. Symp. Biomed. Imag., Boston, MA, USA*, pp. 1215–1218. Piscataway, NJ: IEEE Press. (doi:10.1109/ISBI.2009.5193280)
- 57 Yasuno, K. et al. 2010 Genome-wide association study of intracranial aneurysm identifies three new risk loci. *Nat. Genet.* **42**, 420–425. (doi:10.1038/ng.563)

Risk of Rupture of Small Anterior Communicating Artery Aneurysms Is Similar to Posterior Circulation Aneurysms

Philippe Bijlenga

Stroke. published online July 30, 2013;
Stroke is published by the American Heart Association, 7272 Greenville Avenue, Dallas, TX 75231
Copyright © 2013 American Heart Association, Inc. All rights reserved.
Print ISSN: 0039-2499. Online ISSN: 1524-4628

The online version of this article, along with updated information and services, is located on the World Wide Web at:

<http://stroke.ahajournals.org/content/early/2013/07/30/STROKEAHA.113.001667>

Data Supplement (unedited) at:

<http://stroke.ahajournals.org/content/suppl/2013/07/30/STROKEAHA.113.001667.DC1.html>

Permissions: Requests for permissions to reproduce figures, tables, or portions of articles originally published in *Stroke* can be obtained via RightsLink, a service of the Copyright Clearance Center, not the Editorial Office. Once the online version of the published article for which permission is being requested is located, click Request Permissions in the middle column of the Web page under Services. Further information about this process is available in the [Permissions and Rights Question and Answer](#) document.

Reprints: Information about reprints can be found online at:
<http://www.lww.com/reprints>

Subscriptions: Information about subscribing to *Stroke* is online at:
<http://stroke.ahajournals.org/subscriptions/>

Risk of Rupture of Small Anterior Communicating Artery Aneurysms Is Similar to Posterior Circulation Aneurysms

Philippe Bijlenga; on behalf of the @neurIST investigators*

Background and Purpose—According to the International Study of Unruptured Intracranial Aneurysms (ISUIA), anterior circulation (AC) aneurysms of <7 mm in diameter have a minimal risk of rupture. It is general experience, however, that anterior communicating artery (AcoA) aneurysms are frequent and mostly rupture at <7 mm. The aim of the study was to assess whether AcoA aneurysms behave differently from other AC aneurysms.

Methods—Information about 932 patients newly diagnosed with intracranial aneurysms between November 1, 2006, and March 31, 2012, including aneurysm status at diagnosis, its location, size, and risk factors, was collected during the multicenter @neurIST project. For each location or location and size subgroup, the odds ratio (OR) of aneurysms being ruptured at diagnosis was calculated.

Results—The OR for aneurysms to be discovered ruptured was significantly higher for AcoA (OR, 3.5 [95% confidence interval, 2.6–4.5]) and posterior circulation (OR, 2.6 [95% confidence interval, 2.1–3.3]) than for AC excluding AcoA (OR, 0.5 [95% confidence interval, 0.4–0.6]). Although a threshold of 7 mm has been suggested by ISUIA as a threshold for aggressive treatment, AcoA aneurysms <7 mm were more frequently found ruptured (OR, 2.0 [95% confidence interval, 1.3–3.0]) than AC aneurysms of 7 to 12 mm diameter as defined in ISUIA.

Conclusions—We found that AC aneurysms are not a homogenous group. Aneurysms between 4 and 7 mm located in AcoA or distal anterior cerebral artery present similar rupture odds to posterior circulation aneurysms. Intervention should be recommended for this high-risk lesion group. (*Stroke*. 2013;44:00-00.)

Key Words: intracranial aneurysm ■ registries ■ risk factors ■ SAH ■ subarachnoid hemorrhage

The management of patients with unruptured cerebral aneurysms (UA) remains controversial because of their uncertain natural history. Although estimates of the prevalence of intracranial aneurysms range from 0.5% to 6% on radiological and autopsy studies, the incidence of aneurysmal subarachnoid hemorrhage (SAH) is 10/100,000 per year in the United States, leading to the conclusion that the majority of UAs do not rupture.^{1,2} The average risk of rupture of a UA is estimated to be between 1% and 2% per year.^{3,4} The International Study of Unruptured Intracranial Aneurysms (ISUIA) reported on a retrospective and prospective multicenter study in 1998 and 2003.^{5,6} In the latter, they observed that aneurysm location, size, and previous SAH were risk factors for rupture, with posterior circulation (PC) aneurysms collectively (including posterior communicating artery [PcoA] aneurysms) and aneurysms >7 mm located in the anterior circulation (AC) rupturing with at rates high enough to justify intervention. This observation seems to contradict the clinical perception that patients commonly present with ruptured small aneurysms. Moreover, aneurysm locations were segregated only as being either AC

or PC for risk assessment, raising concerns that the effects of pathophysiological mechanisms specific to individual arteries were combined reducing sensitivity to location as a risk factor. Work has since been published demonstrating the importance of aneurysm location, along with criteria such as patients' age, sex, ethnicity, and aneurysm morphology (size and shape) as risk factors for rupture. Recently, the Unruptured Cerebral Aneurysm Study of Japan (UCAS Japan) reported an annual rupture rate for UAs of 0.95%.⁷ It also found that aneurysms >7 mm in general, smaller aneurysms of the anterior communicating artery (AcoA) or internal carotid-PcoA, and aneurysms having a daughter sac were associated with increased rupture risk.

The aim of the present study was to assess whether AcoA aneurysms behave differently from other AC aneurysms. Furthermore, we provide a detailed comparison with previous studies of the risk factors for aneurysm rupture, and in doing so examine whether simply dividing UAs into anterior or PC locations along with aneurysm size, as proposed by ISUIA, remains adequate for rupture risk analysis.

Received April 15, 2013; accepted June 14, 2013.

From the Hôpitaux Universitaire de Genève et Faculté de médecine de Genève, Geneva, Switzerland.

*A list of @neurIST Investigators is given in the Appendix.

Preliminary findings from this study have been presented as a digital poster at the Annual Meeting of the Congress of Neurological Surgeons, San Francisco, CA, October 16–21, 2010 (<http://w3.cns.org/dp/2010CNS/38.pdf>) and as an oral presentation at the 62nd annual meeting of the German Society of Neurosurgery (DGNC), Hamburg, Germany, May 7–11, 2011.

The online-only Data Supplement is available at <http://stroke.ahajournals.org/lookup/suppl/doi:10.1161/STROKEAHA.113.001667/-/DC1>.

Correspondence to Philippe Bijlenga, Service de neurochirurgie, Département de neurosciences cliniques, Hôpitaux Universitaires de Genève, 4 rue Gabrielle-Perret-Gentil, 1211 Genève 14, Switzerland. E-mail philippe.bijlenga@hcuge.ch

© 2013 American Heart Association, Inc.

Stroke is available at <http://stroke.ahajournals.org>

DOI: 10.1161/STROKEAHA.113.001667

Methods

As part of the European Union's Sixth Framework Program Information Society Technologies priority, an information platform was designed, developed, and implemented by a group of clinical centers, universities, and companies from across Europe. Its purpose was to integrate complete biomedical information for the management of cerebral aneurysms. The system was used in the collection of the clinical data on aneurysm patients from multiple centers as described below.

Patients

Between November 1, 2006, and March 31, 2012, a total of 932 patients diagnosed with intracranial aneurysms were enrolled at 7 European clinical centers (Royal Hallamshire Hospital, Sheffield, United Kingdom; John Radcliffe Hospital, Oxford, United Kingdom; Erasmus Medical Center Rotterdam, The Netherlands; University Hospital of Geneva, Switzerland; University Hospital of Barcelona, Spain; General Hospital of Catalonia, Spain; University Hospital of Pécs, Hungary) using the platform. The data collection protocol was approved by individual local ethics committees, and written consent obtained from patients or where appropriate, next of kin, in all cases.

All clinical centers were made aware of the importance of consecutive recruitment from an identifiable catchment area but only 1 was able to verify and guarantee consecutive recruitment from a stable population. The University Hospital of Geneva embedded the data collection tool (@neuQuest) in the hospital's electronic information system and trained neurosurgical medical staff to use the platform as the basis of the electronic medical record. Regular checks were performed to ensure consistency between the administrative and medical databases. Thus, prospective and consecutive recruitment of all patients with a newly diagnosed intracranial aneurysm and known to be resident within this referral area was ensured, and the referral area did not vary during the course of data collection.

For analysis, the data were separated into 2 groups:

1. The Total @neurIST Cohort (TC), including all the cases of diagnosed intracranial aneurysm recruited prospectively or retrospectively by the 7 participating clinical centers. In the TC, 651 (70%) patients were recruited prospectively, and 281 (30%) patients were recruited retrospectively, for a total of 932 patients, of which 343 (36.8%) patients had no history of SAH and 589 (63.2%) patients had a SAH.
2. The Consecutive Cohort (CC), a subset of the TC, including cases prospectively and consecutively diagnosed with ≥ 1 saccular intracranial aneurysm, living within the hospital's recruitment area. Two patients were excluded from the analysis because they refused to give consent to participate (0.6%). The CC consisted of 404 patients: 194 (48%) patients without history of SAH and 210 (52%) patients recruited after SAH. Of the patients without SAH, 174 (89.7%) patients had incidentally discovered aneurysm(s) and 20 (10.3%) patients had symptomatic aneurysms causing cranial nerve palsy or focal strokes from upstream thrombosis.

Aneurysms and Clinical Information

For all recruited patients, data were collected relating to aneurysm location, characteristics, clinical history, and risk factors, some particulars of which are as follows.

Neurovascular Nomenclature

Adapted from the ISUIA study, aneurysm locations were defined as follows. The internal carotid artery (ICA), anterior cerebral artery (ACA), AcoA, middle cerebral artery (MCA), vertebral artery, basilar artery, and posterior cerebral artery were considered as parent vessels. In accordance with most neurovascular publications, we defined each parent artery segment as starting proximal to the origin of a branch and finishing proximal to the next branch artery. Each parent artery segment was then given the name of the branch that departs from

that segment. The following branches were taken into consideration: ophthalmic artery, PcoA anterior choroidal artery, pericallosal artery, posterior inferior cerebellar artery, and anterior inferior cerebellar artery, and superior cerebellar artery (Figure 1A).

For bifurcations, the segments were defined as per Rhoton,⁸ starting where the walls diverge and finishing at the cross-sections perpendicular to the flow within the daughter vessels where the projection of the parent vessel wall crosses the medial wall of the daughter vessel (see Figure 1B).

Risk Factors of Aneurysm Rupture and SAH

Risk factors considered in the study were those previously described for aneurysm rupture, including presence of an unruptured symptomatic aneurysms (relative risk [RR], 8.2 [95% confidence interval {CI}, 3.9–17.0]), aneurysms >10 mm (RR, 5.5 [95% CI, 3.3–9.5]), location in the PC (RR, 4.1 [95% CI, 1.5–11.0]), and female sex (RR, 2.1 [95% CI, 1.1–3.9]).^{9–15}

We also included those additional factors identified by a systematic Cochrane literature review of reviews¹⁶ as having significant RR associated with SAH in the general population, including positive family history (RR, 4.0 [95% CI, 2.7–6]), smoking (RR, 2.4 [95% CI, 1.8–3.4]), alcohol consumption of >150 g/wk (RR, 2.1 [95% CI, 1.5–2.8]), hypertension (RR, 2 [95% CI, 1.5–2.7]).

The @neurIST system was designed to serve the clinical management of patients with aneurysms. The data collected therefore included the above parameters as well as the patient's presenting history, symptoms, and signs, and details of any treatments and their follow-up. These records, coupled with angiographic imaging (eg, computed tomography angiogram, magnetic resonance angiogram, digital subtraction angiogram, digital rotational angiogram) and neurovascular morphological measurements and characterizations, were collated using elements (@neuQuest, @neuFuse, @neuInfo) of the purpose built information platform, developed during the course of the project. Prospective and retrospective clinical data were collected and the subject's residency could be determined from within the database.

Statistical Analysis

It has been postulated that the process leading to an aneurysmal SAH depends first on the formation of ≥ 1 aneurysm and, subsequently, the rupture of the aneurysm wall; our study is designed to estimate the latter risk.

The above data collection allowed us to count and compare the occurrence of newly diagnosed ruptured and unruptured aneurysms in each vessel segment. To evaluate the risk of rupture of an aneurysm located in a particular vessel segment, the odds of aneurysms being discovered ruptured versus being discovered unruptured was calculated for each vessel segment.

The role of size in AcoA aneurysm rupture was further compared with MCA aneurysms using groups composed of aneurysms with maximum dome sizes in the following ranges: 0 to 4, 4 to 7, 7 to 12, 12 to 25, and >25 mm. Again, the odds of aneurysms being discovered ruptured were calculated for comparison between AcoA and MCA locations.

To compare our observations with those reported in ISUIA, the TC data were analyzed for size and location effects, as per the categorizations used in the ISUIA report. This involved dividing the aneurysms by size into 2 groups: aneurysms of <7 mm in diameter and those between 7 and 12 mm, and then subdividing both groups by location. Observations on larger aneurysms groups are not reported because the rupture risk is known to be high and statistical robustness is low because of their relative rarity and limited population studied. In keeping with the ISUIA categorization, the PC group was composed of aneurysms located in the vertebrobasilar system, basilar tip, posterior cerebral artery, and PcoA segment of the ICA. The AC was formed by pooling all aneurysms located on the ICA (excluding PcoA), ACA (including AcoA), and MCA (ACA+ICA+MCA). To assess the place of AcoA aneurysms relative to this categorization system, subcomponents of the AC (namely the MCA-ICA, the ACA, and AcoA) were also considered separately. The 5-year cumulative

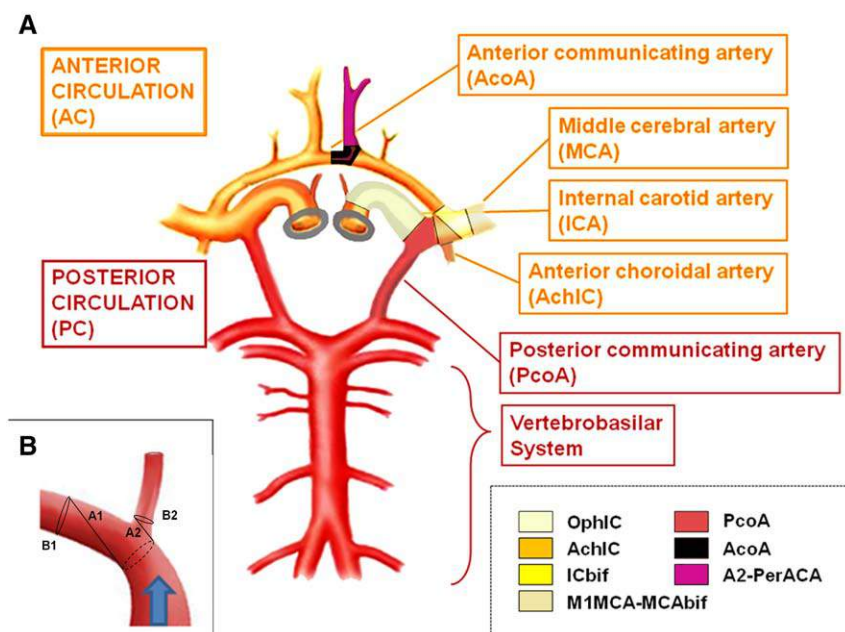


Figure 1. Left, Basis for attributing aneurysm locations according to the International Study of Unruptured Intracranial Aneurysms (ISUIA). Aneurysms of the internal carotid artery (ICA), middle cerebral artery (MCA), and anterior cerebral artery (ACA; excluding posterior communicating artery [PcoA]) belong to the anterior circulation (orange), whereas aneurysms of the vertebrobasilar system, PcoA, and PcoA segment of the ICA belong to the posterior circulation (red). Note that there is no subdivision in ISUIA between ACA and anterior communicating artery (AcoA). Right, Refined subdivision of neurovasculature as applied in this study: each parent vessel segment starts proximal to the origin of the branch and finishes proximal to the next branch and takes the name of the branch departing from the segment. Inset, As defined by Rhoton,⁸ a bifurcation begins where the walls diverge (dotted line) and ends on the cross-sections perpendicular to the flow (lines B1 and B2) located in the daughter vessels where the projection of the parent vessel wall (lines A1 and A2)

cross the medial wall of the daughter vessel. AC indicates anterior circulation; AchIC, anterior choroidal artery segment of the ICA; and PC, posterior circulation.

rupture risk of 2.6%, calculated by ISUIA for AC aneurysms between 7 and 12 mm, was taken as point of reference. The latter group was used as reference to calculated odds ratios (ORs).

To verify that the TC and CC were consistent, the risk factors and clinical characteristics of the cohorts were compared with each other and, to the extent possible, the same comparisons were made to the results in a 2002 report by Weir et al.¹⁴ Limited to UA patients with no previous history of SAH, similar comparisons were made between the @neurIST TC, Weir et al¹⁴ 2002, the ISUIA cohorts, and the 2012 UCAS report. For this, frequencies were calculated on a per patient basis and, for completeness, we also calculated per aneurysm statistics. The purpose of these comparisons was to identify differences between the cohorts that could affect the conclusions drawn from the observations either attributable to selection bias or to general changes in the population over time.

Case categorization and information extraction were performed using the @neuBrowser tool developed in the course of the @neurIST project. Statistics were produced using SPSS version 15.0 software (SPSS: IBM, NY) or MedCalc software (MedCalc software, Belgium), whichever was considered to be the most practical. Results for continuous variables are reported as mean±SD. The test of significance for mean differences was assessed using Student *t* test (significance level *P*<0.05). Odd ratios are reported with a 95% CI. Significance of differences in proportions was assessed by means of Fisher exact tests.

Results

Summaries of patient demographics, clinical histories, and risk factors obtained for the 2 @neurIST cohorts and their comparisons are given in the Table. In both the TC and CC, there was a ratio of ≈3 females for every male (Table). The average maximal unruptured aneurysm diameter was significantly higher in the TC than in the CC (6.35±4.8 versus 5.51±4.23 mm; *P*<0.05). However, there was a higher proportion of small (2–7 mm) aneurysms (63.9% versus 52.8%; *P*<0.05) and a significantly lower proportion of large (13–24 mm) aneurysms (6.3% versus 12.2%; *P*<0.05) reported in the CC (Table I in the online-only Data Supplement). The proportion

of symptomatic patients was significantly smaller in the CC (9% versus 16.9%; *P*<0.05). Both cohort populations were, however, comparable for all other variables studied (Table; Table I in the online-only Data Supplement).

Location and Size Dependence of Aneurysms and Rupture

AcoA was the vessel segment most commonly bearing a ruptured aneurysm (n=162), followed by the PcoA (n=121) and MCA bifurcation (n=72). The occurrence of SAH secondary to the rupture of aneurysms was more frequent in the AcoA and in the PcoA than in the MCA bifurcation (RR, 2.25 [95% CI, 1.7–3.0] and RR, 1.7 [95% CI, 1.2–2.25], respectively).

Figure 2 shows a forest plot reporting the ORs of aneurysms discovered ruptured or unruptured at each anatomic location (regardless of aneurysm size) in the TC. ORs to the right of the reference line (OR=1) reflect a higher than average proportion of aneurysms being ruptured at discovery. AcoA aneurysms had the highest OR (TC: 4.3 [95% CI, 2.8–6.5]; CC: 2.1 [95% CI, 1.4–3.2]) for rupture followed in order by basilar tip, A2 and pericallosal, and PcoA and posterior inferior cerebellar artery aneurysms. In contrast, aneurysms located in the ophthalmic segment of the ICA had the lowest OR for rupture. Observations were similar when analyzing the CC (Figure I in the online-only Data Supplement).

For different size subgroups, the odds of discovering ruptured AcoA aneurysms relative to that of similarly sized MCA aneurysms are compared in Figure 3. The OR for ruptured AcoA aneurysms was the highest in the size group 4 to 7 mm (OR, 8.3 [95% CI, 4.4–16]; *P*<0.001). At larger diameters, the differences decreased as the corresponding proportion of ruptured MCA aneurysms increased; at >12 mm diameter, no conclusions were drawn in light of the small sample size.

Table. Baseline Characteristics of Patients and Aneurysms for Cohorts

	Weir et al ¹⁴ (n=507)	Consecutive Cohort (n=404)	Total @neurIST Cohort (n=932)	PValue*	PValue†
Period of recruitment	1967–1987	2007–2012	2007–2012		
Baseline characteristics of patients					
Age, mean (SD)	47 (NA)	55.3 (14.11)	55.02 (13.24)	NA	NS
Sex ratio (% of female)	318/189 (62.7)	298/106 (74)	663/269 (71)	<0.005	NS
Ratio of multiple aneurysms (% of cases with multiple lesions)	111/396 (21.9)	134/270 (33)	278/654 (30)	<0.005	NS
Percentage of patients with SAH	86	53	63	<0.001	<0.001
Number of aneurysms		621	1347		
Max aneurysm diameter, mm; mean (SD)	9.7 (0.3 se)	6.2 (7.35)	6.76 (11.39)	<0.001	NS
Baseline characteristics of aneurysms					
Size of aneurysm, number of patients (%)					
0–1.9 mm		8 (2.0)	13 (1.4)		NS
2–6.9 mm	155 (38.5)	239 (59.2)	490 (52.6)	<0.001	<0.05
7–12 mm	144 (36.0)	117 (29.0)	316 (33.9)	NS	NS
13–24 mm	73 (18.0)	33 (8.2)	95 (10.2)	<0.001	NS
>24 mm	30 (7.5)	7 (1.7)	18 (1.9)	<0.001	NS
Location of aneurysm, number of patients (%)					
Cavernous part of carotid artery	18 (3.5)	26 (6)	50 (5)	NS	NS
Internal carotid artery	53 (10.4)	109 (27)	218 (23)	<0.001	NS
Anterior communicating or anterior cerebral artery	158 (31.2)	141 (35)	308 (33)	NS	NS
Middle cerebral artery	158 (31.2)	137 (34)	386 (31)	NS	NS
Posterior communicating artery	88 (17.4)	65 (16)	186 (20)	NS	NS
Vertebrobasilar system (other than basilar tip)	10 (2)	33 (8)	74 (8)	<0.001	NS
Tip of basilar artery	22 (4.3)	30 (7)	79 (8)	<0.005	NS

NA indicates not applicable; NS, not significant; SAH, subarachnoid hemorrhage; and se, standard error.

*P value comparing @neurIST Total Cohort (TC) with Weir et al.¹⁴

†P value between @neurIST cohorts.

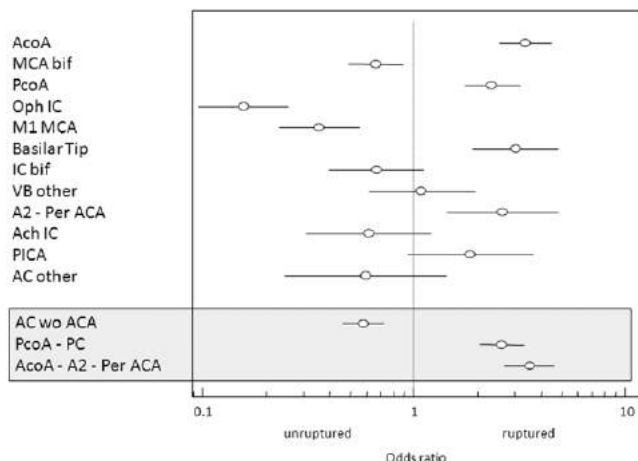
Reflecting the ISUIA classification of aneurysms by location (AC or PC) and size (<7 mm, 7–12 mm, or >12 mm in diameter), the incidences and ORs for ruptures of the subgroups are compared in Figure 4 (aneurysms >12 mm excluded). Also shown are the behaviors of separable AC components, broken down as AcoA, ACA (including A1, AcoA, A2, PerA, and Distal ACA aneurysms), or MCA+ICA aneurysms. The OR of ruptured AC aneurysms of <7 mm in size showed fewer ruptured aneurysms than the reference group, suggesting their rupture risk could be $\leq 2.6\%$ per 5 years. In contrast, aneurysms located in the PC showed a trend to higher ORs (1.29 [95% CI, 0.9–1.9]). These observations are in accordance with the ISUIA observations. We found however, that aneurysms of <7 mm in size in ACA locations in general, and AcoA aneurysms in particular, were more likely to be ruptured at presentation than other AC aneurysms, and that they showed ORs similar to PC lesions (ACA: 1.58 [95% CI, 1.10–2.30]; AcoA:

2.0 [95% CI, 1.31–3.03]). Interestingly, the OR for ruptured aneurysms <4 mm in the AcoA was smaller, although not significantly so, than the reference group (OR, 0.547 [95% CI, 0.279–1.073]). When separated from the AC aneurysms, a low OR for rupture of ICA+MCA became apparent even at diameters up to 12 mm (0.26 [95% CI, 0.18–0.37] for aneurysms <7 mm and 0.61 [95% CI, 0.39–0.95] for aneurysms between 7 and 12 mm; Figure 4).

Comparison With Previous Studies

Included in the Table, along with the details of the @neurIST cohorts, are summary data from Weir et al.¹⁴ 2002. A similar summary and analysis, limited to patients with UA at the time of recruitment, is given in Table I in the online-only Data Supplement. Because our interest here is in possible differences in bias between studies, or changes in the patient populations over time, below, we focus primarily on describing the

Total @neurIST cohort



N	OR	95% CI
243	3.5	2.6 to 4.5
217	0.6	0.5 to 0.9
202	2.4	1.8 to 3.2
151	0.2	0.1 to 0.3
121	0.3	0.2 to 0.6
79	3.2	1.9 to 4.9
64	0.6	0.4 to 1.1
46	1.2	0.6 to 1.9
47	2.5	1.4 to 4.8
40	0.6	0.3 to 1.2
31	1.7	0.9 to 3.7
22	0.6	0.2 to 1.4
615	0.5	0.4 to 0.6
358	2.6	2.1 to 3.3
290	3.6	2.7 to 4.6

Figure 2. Odds ratios of aneurysms discovered ruptured vs unruptured for each location compared with all other aneurysms included in the cohort. N is the number of aneurysms observed for each location or location cluster. AC indicates anterior circulation; AchIC, anterior choroidal artery segment of the ICA; AcoA, anterior communicating artery; CI, confidence interval; IC bif, ICA bifurcation; MCA, middle cerebral artery; Oph IC, ophthalmic segment of the ICA; OR, odds ratio; PcoA, posterior communicating artery; Per ACA, pericallosal segment of the ACA; PICA, posterior inferior cerebellar artery; and VB other, other location within the vertebrobasilar system.

points where significant differences were observed. Care has been taken to compare population of patients recruited according to the same criteria between studies. @neurIST cohorts are compared with Weir et al,¹⁴ whereas population of patients recruited with unruptured aneurysms and no history of SAH are compared with ISUIA and UCAS, and the subpopulation of patients recruited with unruptured aneurysms in Weir et al.¹⁴

Demographics, Signs, and Symptoms

The TC was populated with older patients, more females, more patients with multiple aneurysms, and fewer patients that had SAH than reported in Weir et al¹⁴ (Table).

The patients with unruptured aneurysms in the TC and ISUIA populations were similar in age (56±13.1 versus 55±13.1 years), whereas those in UCAS were older (65±10.4 years) and those in Weir et al¹⁴ were younger (46 years). Fewer of the @neurIST patients with unruptured aneurysms had multiple aneurysms or a family history of aneurysms than those in ISUIA. @neurIST patients had lower levels of alcohol and tobacco consumption and a trend toward fewer patients using

stimulants as compared with ISUIA (Table I in the online-only Data Supplement).

Relative to ISUIA, the comparable patient group in UCAS was older, and contained more males, whereas fewer patients were smokers, had multiple aneurysms, were symptomatic, or had a family history of SAH (Table IV in the online-only Data Supplement).

Ruptured Versus Unruptured

The population of patients with unruptured intracranial aneurysms (UA) corresponded to 37% of all cases recruited to the @neurIST (47% in the CC). This clearly contrasts with the observation made between 1967 and 1987 reported by Weir in 2002 wherein only 14% of patients were found to have UAs.

Location

@neurIST contained significantly more patients with internal carotid aneurysms than reported by Weir et al¹⁴ (CC: 27%, TC: 23%, Weir: 10.4%; *P*<0.001). Patients with PC aneurysms (vertebrobasilar and basilar tip) were also more frequent in @neurIST than in Weir et al (16% versus 6.3%; *P*<0.01; Table).

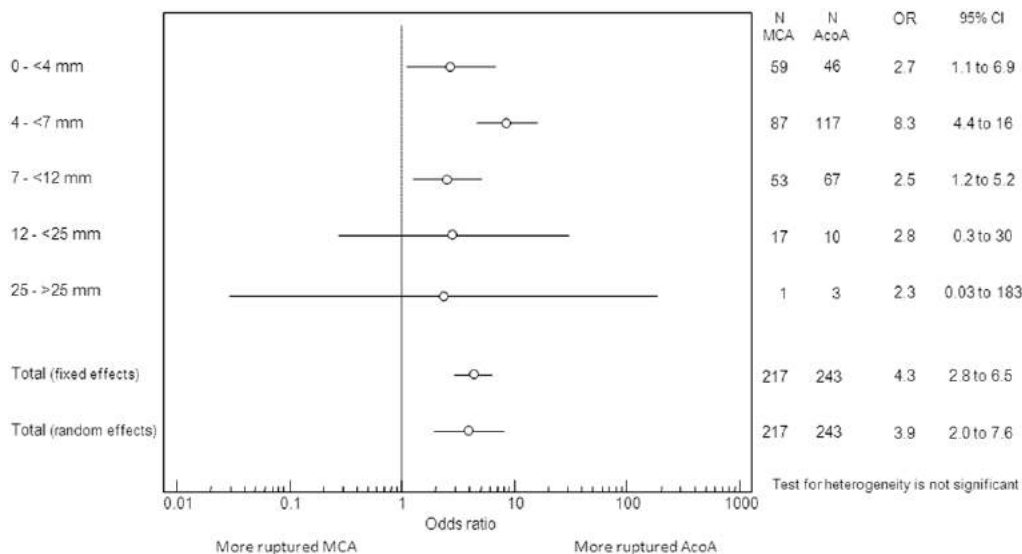


Figure 3. Odds ratios of anterior communicating artery (AcoA) aneurysms being discovered ruptured vs unruptured relative to those of the middle cerebral artery (MCA) stratified by size. CI indicates confidence interval; and OR, odds ratio.

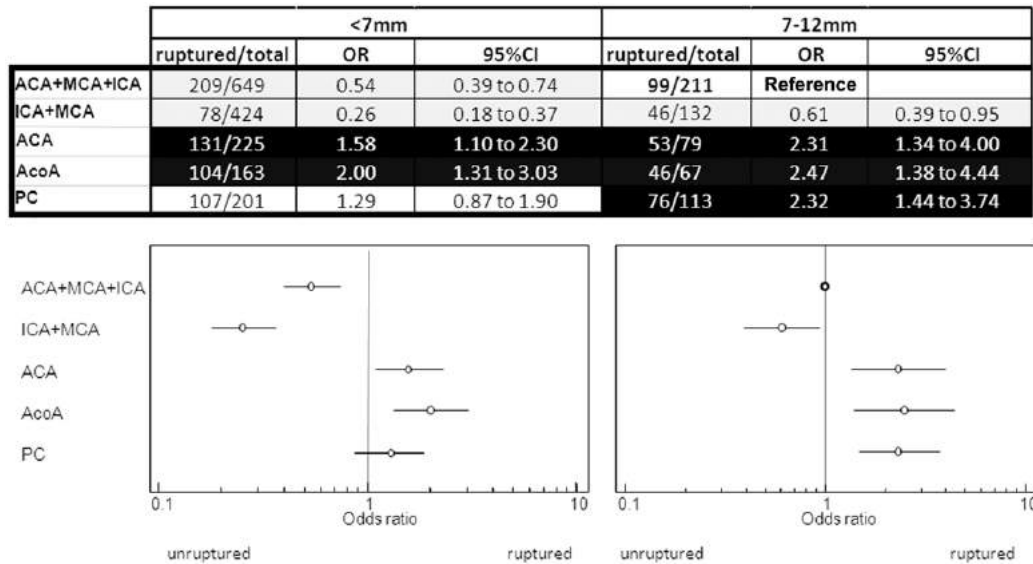


Figure 4. Odds of aneurysms discovered ruptured vs unruptured for groups clustered according to location and size compared with a reference group defined as aneurysms between 7 and 12 mm located in the anterior circulation aneurysm as defined by the International Study of Unruptured Intracranial Aneurysms, and for subsets of the anterior circulation. ACA indicates anterior cerebral artery; AcoA, anterior communicating artery; CI, confidence interval; ICA, internal carotid artery; MCA, middle cerebral artery; OR, odds ratio; and PC, posterior circulation.

Limited to patients with UAs, internal carotid aneurysms were significantly more represented in the @neurIST cohorts than in ISUIA and Weir et al¹⁴ (patient-based counting, respectively 35% versus 22.9% and 13.9%; $P<0.01$; Table I in the online-only Data Supplement). Comparing the distribution of aneurysms by location, aneurysms located in the ICA were significantly more frequent in @neurIST than in UCAS (aneurysm-based counting: 29% versus 19%; $P<0.001$); in contrast, aneurysms located in PcoA were significantly less frequent in @neurIST (11.9% versus 16.5%; $P<0.05$; Table III in the online-only Data Supplement). This latter observation may be attributable to differences in classifying aneurysms between the PcoA and the anterior choroidal artery segment of the ICA.

Unruptured AcoA aneurysms also formed a much greater fraction of the observed patients with aneurysms in the @neurIST cohort than those in Weir et al¹⁴ and ISUIA (24% versus 13.9% and 10.3%, respectively; $P<0.001$; Table I in the online-only Data Supplement). Comparing @neurIST and UCAS cohorts, a similar representation of unruptured AcoA aneurysm was observed (Table III in the online-only Data Supplement).

The pattern of aneurysm distribution varied slightly between @neurIST centers. Centers where neurosurgeons were less involved in the project reported fewer MCA and pericallosal segment of the ACA aneurysms ($P<0.001$) and proportionally more PcoA, basilar artery, and M1 aneurysms ($P<0.001$).

Size

The average aneurysm size was similar between UCAS and @neurIST CC (Table I in the online-only Data Supplement), with progressively larger average aneurysm sizes being seen in the @neurIST TC, ISUIA, and Weir et al¹⁴ studies.

However, concerning the distribution of aneurysm sizes, the @neurIST TC was close to that of Weir et al,¹⁴ whereas the distribution for the @neurIST CC was closer to that of ISUIA, with the former pairing having slightly fewer small and more midsized aneurysms relative to the latter pairing.

UCAS was populated with significantly more patients with aneurysms <7 mm than ISUIA, TC, and CC (78.4% versus 62%, 53.4%, 65.2% respectively; $P<0.01$; Table II in the online-only Data Supplement).

Discussion

This study was designed to evaluate AcoA aneurysm rupture risk relative to the anterior and PC location and size groupings used in ISUIA. Our motivation was the common perception that the behavior of AcoA aneurysms is not that suggested by the ISUIA results. Consistent with ISUIA, we found that aneurysms <7 mm in size and located in the AC (as defined in ISUIA) were less likely to be discovered ruptured than aneurysms in other locations or of larger size. More importantly, however, our results also provide statistical evidence that AcoA aneurysms rupture with smaller diameters than MCA aneurysms and, that generally, AcoA aneurysms rupture at least as frequently as those of the PC, in contrast to those in other AC locations. Furthermore, our data indicate that risk of rupture of aneurysms of <7 mm located in the internal carotid or MCA is low relative to the PC and AcoA, but not negligible. Thus, the AC as defined by ISUIA should not be considered homogeneous for aneurysm rupture, and we suggest that because of unknown factors (ie, embryogenesis or blood flow coherence), both AcoA and PcoA be considered with the PC for risk stratification.

The distinct rupture risk of AcoA aneurysms seen in the present study has important implications for our understanding of the ISUIA and UCAS studies. As mentioned by the authors of ISUIA, “the potential limitations of the study include the nonrandomised nature of the unoperated, surgical and endovascular cohorts, which led to asymmetries within groups;...” We think that the implications of this possible recruitment bias have not been fully appreciated by the medical community. The assignment of patients to one of the 2 ISUIA cohorts (treated

or not treated) was “based on whether surgical or endovascular treatment of ≥ 1 unruptured intracranial aneurysm was planned on clinical grounds at the time the patient was first seen at the ISUIA center.” Although the study coordinators took steps to minimize bias, there is no description or discussion of how consecutive the recruitment was. It may have been for various unstated reasons, for example, a reputation to rupture at small diameters or surgical accessibility, that more patients with unruptured AcoA aneurysms were treated and not observed in ISUIA. This may explain why patients with AcoA aneurysms represented only 13.5% of patients enrolled, as opposed to 24% in @neurIST, and why 10.3% were followed up without surgery. Other possible reasons for this difference include the following: (1) increased opportunities and improved quality of cerebral imaging, leading to more patients being diagnosed with incidental aneurysms, (2) a decrease in the incidence of rupture of existing aneurysms, resulting in an increase of the prevalence of unruptured lesions, (3) an aging population that may increase the prevalence of aneurysms, and (4) changes in an environmental risk factor such as increased prohibition of smoking in public areas. These factors apart, patients in ISUIA with ICA and AcoA aneurysms were significantly more frequently assigned to treatment than those with PcoA aneurysms. All together, our observations suggest that the AcoA location was under-represented in the ISUIA study, and that the particular behavior of lesions in that location could not be distinguished from lesions in other AC sites. This conclusion is supported by our finding that when all AC aneurysms are included in 1 single group, the increased rupture risk associated of AcoA aneurysms is masked (Figure 4).

Based on these considerations, we emphasize that the observation in ISUIA of a negligible rupture risk for AC aneurysms < 7 mm in size is only applicable in the situation where expert clinicians had considered observation as an acceptable alternative to treatment.

In order that our data be valid as a basis for the above comparison of our patient group with ISUIA, we sought to reduce case-selection bias as much as possible through a multicenter, population-based study (transversal study). Patients were recruited prospectively and consecutively in one of the clinical centers, and an audit was performed to verify that cases were not missed. All the other centers attempted to achieve these aims but were not able to provide checks that all cases were captured, and hence completeness in these sites is not guaranteed. To estimate and identify potential biases, a number of characteristics of patients and aneurysms reported when the lesion was initially discovered were examined between the @neurIST cohorts. We observed that the proportion of incidentally discovered aneurysms in @neurIST was significantly higher than in historical reports but also that this trend was more pronounced in the CC where all aneurysms identified within the clinical center were captured. However, the proportion of patients with known risk factors (familial history, symptomatic, multiple aneurysms) was lower. These observations suggest that selection biases are progressively attenuated because of the increased use and quality of head imaging. Despite differences in recruited populations, similar results were obtained in the 2 @neurIST cohorts and when analyzing separately cohorts recruited in each center.

All the studies of intracranial aneurysms, including the present, are affected by ≥ 2 limitations. First, the recruitment population can be naturally defined by the established, stable activity of the centers involved, but this is a difficult quantity to determine accurately. Furthermore, costs and ethical issues preclude screening for intracranial aneurysms in a randomly selected population. In consequence, we are not able to report absolute incidence, but rather must consider the odd ratios of aneurysm rupture associated with a condition in the fraction of the recruited population affected or not by the studied risk factor. Therefore, it can be assumed that the OR for rupture was overestimated because of undiagnosed unruptured aneurysms mentioned above. In counterpoint, the loss of information on patients with lethal hemorrhage and dying before being brought to medical attention and the impact on natural history in treated cases would lead to an underestimation of the OR. The validity of our observation may therefore be affected by the selection of a population where the distribution of unruptured aneurysms according to location and size does not match the distribution in the overall population.

When analyzing the odds of aneurysm rupture by location, the AcoA location was the most frequent site of aneurysm rupture followed by PcoA and MCA bifurcation in both the consecutive and TC. To determine whether the observed high frequency of ruptured aneurysms is associated with a higher prevalence of aneurysm or a higher risk of aneurysm rupture, the prevalence of aneurysm by location and size groups was estimated from the population of patients diagnosed with unruptured aneurysms. We could not identify factors that could explain why unruptured aneurysms in the AcoA should be underdiagnosed as compared with other locations. As for aneurysms located in the IC (close to bone structures), the incidence of unruptured aneurysms diagnosed increased between older and more recent studies.

Concerning risk associated with size, we made the assumption that if aneurysm rupture modifies the size or the morphology, it would happen regardless of location. Therefore, we decided to highlight the risk of rupture associated with aneurysm size by comparing AcoA with MCA, both locations sharing high anatomic similarities. Aneurysms between 4 and 7 mm in the AcoA were significantly more frequently observed ruptured than similar size aneurysms in the MCA location. This observation also held when the AcoA location was compared with other AC locations.

It has been debated whether the risk of rupture of an UA can or cannot be extrapolated from size or morphology observations of ruptured aneurysms as these features may be modified by the rupture itself.^{17,18} The Small Unruptured Intracranial Aneurysm Verification (SUAVe) study has demonstrated the different characteristics of aneurysms relative to their growth and rupture. Different types of aneurysm evolution have been described, from rapid aneurysm development and rupture at small sizes within days or months, to slower growing aneurysms with rupture occurring after years or remaining rupture free for decades. Based on a single evaluation at the time of diagnosis, our work is unsuited to answering questions of how aneurysms grow and what rupture rate to expect. Recently, the UCAS Japan reported results of a longitudinal follow-up study of patients enrolled from January 2001 through April

2004 and follow-up until April 2010. A total of 5720 patients with 6697 aneurysms were studied; of which, 3050 aneurysms were treated during follow-up, and 3647 aneurysms were left for observation. A total of 11 660 aneurysm-years were recorded with 111 aneurysm ruptures. The overall annual rupture rate in the untreated population of patients in Japan was estimated at 0.95% (95% CI, 0.79–1.15). The authors report that compared with MCA aneurysms, lesions located in the AcoA or in the PcoA are more likely to rupture with hazard ratio of 1.90 (95% CI, 1.12–3.21) and 2.02 (95% CI, 1.13–3.58), respectively. As stated by the UCAS authors, however, this type of study can never be entirely free of case-selection bias. A significant proportion of small aneurysms were treated, and the characteristics of these aneurysms were different from the studied group. Therefore, it is difficult to extrapolate the observed rupture rate to the general population of incidentally discovered aneurysms. It would be extremely interesting to compare the OR and the rate of rupture for aneurysms stratified in identical location and size groups for both @neurIST and UCAS. @neurIST continues to record rupture or treatment of unruptured aneurysms in the CC cohort to provide longitudinal data on top of the transversal information reported herein. We may then extrapolate rupture rates in the clinically pertinent population by comparing ORs with homogenous aneurysm groups with known rupture rates and be able to propose estimates.

Currently, most studies apply multiple univariate analyses in evaluating rupture risk but these may be inadequate because, as illustrated by our results, location, size, and many other factors may influence aneurysm behavior, such as sex, smoking, alcohol consumption, and hypertension. New tools are being developed to assess the risk of rupture using genetics, transcriptomics, morphodynamic evaluation, and simulations, and new treatments are being explored. This progress puts ever greater demands on the scale of aneurysm studies required for adequate and appropriate statistical analyses to be performed. The only way to achieve this is through wider multicentric collaboration and rigorous patient documentation practices. Further projects need to be launched to integrate all this information and help clinicians provide individualized recommendations to patients and the general population.

Conclusions

AcoA aneurysms with a size between 4 and 7 mm have a higher risk of rupture than was inferred from the ISUIA observations. We recommend that in the absence of complicating comorbidities, unruptured AcoA aneurysms >4 mm should be treated. Small aneurysms of <7 mm located in the internal carotid or middle cerebral arteries were seen to present lower risk of rupture. We recommend following these aneurysms with regular imaging.

Appendix

@neurIST Investigators

Project Board: Alejandro Frangi (Universitat Pompeu Fabra, Barcelona, Spain); Philippe Bijlenga (Hôpitaux Universitaires de Genève et Faculté de médecine de Genève, Geneva, Switzerland); Martin Hofmann-Apitius (Fraunhofer Institut Algorithmen und

Wissenschaftliches Rechnen, Sankt Augustin, Germany); Rod Hose (Royal Hallamshire Hospital and University of Sheffield, United Kingdom); Guy Lonsdale (NEC Laboratories Europe, IT Research Division, Sankt Augustin, Germany); Antonio Arbona (NEC Laboratories Europe, IT Research Division, Sankt Augustin, Germany); Peer Hasselmeyer (NEC Laboratories Europe, IT Research Division, Sankt Augustin, Germany); Daniel Rüfenacht (Hôpitaux Universitaires de Genève et Faculté de médecine de Genève, Geneva, Switzerland). Article writing team: Philippe Bijlenga (Hôpitaux Universitaires de Genève et Faculté de médecine de Genève, Geneva, Switzerland); Paul Summers (John Radcliffe Hospital, University of Oxford, Oxford, United Kingdom); Max Jägersberg (Hôpitaux Universitaires de Genève et Faculté de médecine de Genève, Geneva, Switzerland); Alister Rogers (Hôpitaux Universitaires de Genève et Faculté de médecine de Genève, Geneva, Switzerland); Karl Schaller (Hôpitaux Universitaires de Genève et Faculté de médecine de Genève, Geneva, Switzerland); James Byrne (John Radcliffe Hospital, University of Oxford, Oxford, United Kingdom). Ethical and legal review committee: Jessica Wright (Durham University Department of Law, United Kingdom); Jeremy Wilkins (Durham University Department of Law, United Kingdom); Derick Beyleveld (Durham University Department of Law, United Kingdom); Bernice Elger (Hôpitaux Universitaires de Genève et Faculté de médecine de Genève, Geneva, Switzerland). Information platform development and maintenance: Alan Waterworth (Royal Hallamshire Hospital and University of Sheffield, United Kingdom); Steven Wood (Royal Hallamshire Hospital and University of Sheffield, United Kingdom); Jimison Iavindrasana (Hôpitaux Universitaires de Genève et Faculté de médecine de Genève, Geneva, Switzerland); Rodolphe Meyer (Hôpitaux Universitaires de Genève et Faculté de médecine de Genève, Geneva, Switzerland); Christoph Friedrich (Fraunhofer Institut Algorithmen und Wissenschaftliches Rechnen, Sankt Augustin, Germany); Christian Ebeling (Fraunhofer Institut Algorithmen und Wissenschaftliches Rechnen, Sankt Augustin, Germany). Epidemiology and statistics: Christian Ebeling (Fraunhofer Institut Algorithmen und Wissenschaftliches Rechnen, Sankt Augustin, Germany); Philippe Bijlenga (Hôpitaux Universitaires de Genève et Faculté de médecine de Genève, Geneva, Switzerland); Roelof Risselada (Erasmus University Medical Center, Rotterdam, The Netherlands); Christoph Friedrich (Fraunhofer Institut Algorithmen und Wissenschaftliches Rechnen, Sankt Augustin, Germany); Miriam CJM Sturkenboom (Erasmus University Medical Center, Rotterdam, The Netherlands).

Participating Centers (In Order of Number of Recruited Patients)

Hôpitaux Universitaires de Genève et Faculté de médecine de Genève, Geneva, Switzerland (Philippe Bijlenga, Max Jägersberg, Alister Rogers, Bawarjan Schaflo, Patrick Teta, Karl Schaller, Vitor Mendes-Pereira, Ana Marcos Gonzalez, Ana Paula Narata, Karl O Lovblad, Daniel A. Rüfenacht); John Radcliffe Hospital, University of Oxford, Oxford, United Kingdom (Julia Yarnold, Paul Summers, Alison Clarke, Gulam Zilani, James Byrne); Hospital Clinic, Barcelona, Spain (Juan Macho, Jordi Blasco); University of Pécs Medical School, Pécs, Hungary (Peter Bukovics, Ferenc Kover, Istvan Hudak, Tamas Doczi); Erasmus University Medical Center, Rotterdam, The Netherlands (Roelof Risselada, Miriam CJM Sturkenboom); Royal Hallamshire Hospital, Sheffield, United Kingdom (Pankaj Singh, Alan Waterworth, Umang Patel, Stuart Coley, Patricia Lawford); Hospital General de Catalunya, San Cugat del Valles, Spain (Teresa Sola, Elio Vivas).

Acknowledgments

The authors are very grateful to all the trial participants and collaborators.

Sources of Funding

The study was supported by the 6th framework program of the European Commission @neurIST project (www.aneurist.org) FP6-IST-2004-027703.

Disclosures

Neither sponsor nor funder had any part in study design, data collection, analysis, or reporting, which were organized by the project board. The corresponding author had full access to all the data in the study and had final responsibility for the decision to submit for publication. The other authors have no conflict to report.

References

- Rinkel GJ, Djibuti M, Algra A, van Gijn J. Prevalence and risk of rupture of intracranial aneurysms: a systematic review. *Stroke*. 1998;29:251-256.
- Linn FH, Rinkel GJ, Algra A, van Gijn J. Incidence of subarachnoid hemorrhage: role of region, year, and rate of computed tomography: a meta-analysis. *Stroke*. 1996;27:625-629.
- Vlak MH, Algra A, Brandenburg R, Rinkel GJ. Prevalence of unruptured intracranial aneurysms, with emphasis on sex, age, comorbidity, country, and time period: a systematic review and meta-analysis. *Lancet Neurol*. 2011;10:626-636.
- Juvela S, Porras M, Heiskanen O. Natural history of unruptured intracranial aneurysms: a long-term follow-up study. *J Neurosurg*. 1993;79:174-182.
- Unruptured intracranial aneurysms—risk of rupture and risks of surgical intervention. International Study of Unruptured Intracranial Aneurysms Investigators. *N Engl J Med*. 1998;339:1725-33.
- Wiebers DO, Whisnant JP, Huston J III, Meissner I, Brown RD Jr, Piepgras DG, et al; International Study of Unruptured Intracranial Aneurysms Investigators. Unruptured intracranial aneurysms: natural history, clinical outcome, and risks of surgical and endovascular treatment. *Lancet*. 2003;362:103-110.
- UCAS Japan Investigators. The natural course of unruptured cerebral aneurysms in a Japanese cohort. *N Engl J Med*. 2012;366:2474-2482.
- Rhoton AL Jr. The supratentorial arteries. *Neurosurgery*. 2002;51:53-120.
- Ujji H, Sato K, Onda H, Oikawa A, Kagawa M, Takakura K, et al. Clinical analysis of incidentally discovered unruptured aneurysms. *Stroke*. 1993;24:1850-1856.
- Yasui N, Suzuki A, Nishimura H, Suzuki K, Abe T. Long-term follow-up study of unruptured intracranial aneurysms. *Neurosurgery*. 1997;40:1155-1159, discussion 1159.
- Morita A, Kimura T, Shojima M, Sameshima T, Nishihara T. Unruptured intracranial aneurysms: current perspectives on the origin and natural course, and quest for standards in the management strategy. *Neurol Med Chir (Tokyo)*. 2010;50:777-787.
- Sonobe M, Yamazaki T, Yonekura M, Kikuchi H. Small unruptured intracranial aneurysm verification study: SUAVe study, Japan. *Stroke*. 2010;41:1969-1977.
- Weir B. Unruptured intracranial aneurysms: a review. *J Neurosurg*. 2002;96:3-42.
- Weir B, Disney L, Karrison T. Sizes of ruptured and unruptured aneurysms in relation to their sites and the ages of patients. *J Neurosurg*. 2002;96:64-70.
- Wermer MJ, van der Schaaf IC, Algra A, Rinkel GJ. Risk of rupture of unruptured intracranial aneurysms in relation to patient and aneurysm characteristics: an updated meta-analysis. *Stroke*. 2007;38:1404-1410.
- Clarke M. Systematic review of reviews of risk factors for intracranial aneurysms. *Neuroradiology*. 2008;50:653-664.
- Kataoka K, Taneda M, Asai T, Yamada Y. Difference in nature of ruptured and unruptured cerebral aneurysms. *Lancet*. 2000;355:203.
- Wiebers DO, Whisnant JP, Sundt TM Jr, O'Fallon WM. The significance of unruptured intracranial saccular aneurysms. *J Neurosurg*. 1987;66:23-29.



Stroke

JOURNAL OF THE AMERICAN HEART ASSOCIATION

Supplementary Table I

Cohort	ISUIA	ref	Weir et al	p	UCAS	p	Consecutive C.			Total @neurist C.			
	no surgery (n=1692)		unruptured (n=170)		Not Surg (n=3647)		noSAH (N=191)	p	no SAH (N=343)	p	p*		
Period of recruitment	1991-1998		1967-1987		2001-2004		2007-2012			2007-2012			
Baseline characteristics of patients													
Age (mean [SD])	55.2 [13.1]		46[NA]	NA	65.0 [10.4]	<0.0001	57.35 [14.09]	0.03		56.67 [13.09]	NS	NS	
Gender ratio (% of female)	1261/431 (74.5%)		124/46 (72.9%)	NS	2480/1167 (68%)	<0.0001	148/43 (77%)	NS		262/81 (76%)	NS	NS	
ratio of multiple aneurysms (% cases with multiple lesions)	679/1013 (40.3%)		NA	NA	1003/2641 (27.5%)	<0.0001	59/132 (31%)	<0.05		96/247 (28%)	<0.001	NS	
symptomatic patients	186/1506 [11%]		9%	NA	171/5720 [3%]	<0.0001	18/173 [9.4%]	NS		58/285 [16.9%]	<0.01	<0.05	
number of aneurysms	2686		NA		6697		291			493			
Max aneurysm diameter (mm) (mean [SD])	7.4 [6.9]		7.76 [0.68*se"]	NS	5.3[3.3]	<0.0001	5.51 [4.23]	<0.001		6.35 [4.8]	<0.005	<0.05	
Baseline characteristics of aneurysms													
Size of aneurysm (number of patients [%])													
0-1.9mm							4 [2.1%]	NA		4 [1.2%]	NA	NS	
2-6.9mm	1049 [62%]		79 [55%]	NS			122 [63.9%]	NS		181 [52.8%]	<0.005	<0.05	
7-12mm	390 [23%]		40 [28%]	NS			50 [26.2%]	NS		108 [31.5%]	<0.005	NS	
13-24	198 [12%]		15 [11%]	NS			12 [6.3%]	<0.05		42 [12.2%]	NS	<0.05	
>24mm	55 [3%]		9 [6%]	NS			3 [1.6%]	NS		8 [2.3%]	NS	NS	
Location of aneurysm (number of patients [%] number of aneurysms [%])													
Cavernous part of carotid artery	210 [12.4%]		18 [10.6%]	NS			22 [12%]	25[3%]	NS	37 [11%]	42[3%]	NS	NS
Internal carotid artery	387 [22.9%]		22 [13.9%]	<0.01			68 [36%]	81[28%]	<0.0005	121 [35%]	144[29%]	<0.0001	NS
Anterior communicating or anterior cerebral artery	175 [10.3%]		22 [13.9%]	NS			58 [30%]	61[21%]	<0.0001	82 [24%]	87[18%]	<0.0001	NS
Middle cerebral artery	475 [28.1%]		61 [35.9%]	<0.05			65 [34%]	82[28%]	NS	114 [33%]	139[28%]	NS	NS
Posterior communicating artery	246 [14.5%]		37 [21.8%]	<0.05			18 [9%]	19[6%]	NS	39 [11%]	41[8%]	NS	NS
Vertebrobasilar system (other than basilar tip)	87 [5.1%]		5 [2.9%]	NS			15 [8%]	15[5%]	NS	21 [6%]	21[4%]	NS	NS
Tip of basilar artery	112 [6.6%]		5 [2.9%]	NS			8 [4%]	8[3%]	NS	19 [6%]	19[4%]	NS	NS

NS: non significant

NA: not available

p: p-value compared to ISUIA

p*: p-value comparing both @neurIST cohorts

Supplementary Table II

Cohort	UCAS				@neurIST							
	Total UCAS cohort (N = 6697)		Not Surgically Treated before Rupture (N = 3647)		Surgically Treated before Rupture (N = 3050)		Consecutive cohort No SAH (N=187)			Total cohort No SAH (N=339)		
							p	p*		p	p*	
maximal aneurysm size												
≥7 mm	1711 [25.5]		786 [21.6]		925 [30.3]		65 [34.8]	<0.01	<0.0001	158 [46.6]	<0.0001	<0.0001
3-4 mm	3132 [46.8]	4986 [74.5]	2000 [54.8]	2861 [78.4]	1132 [37.1]	2125 [69.7]	122 [65.2]	<0.01	<0.0001	181 [53.4]	<0.0001	<0.0001
5-6 mm	1854 [27.7]		861 [23.6]		993 [32.6]							

p = compared to Total UCAS cohort

p* = compared to Not Surgically Treated before Rupture group from UCAS

Supplementary Table III

	UCAS						@neurIST							
	Total	Not surgically treated before rupture		Surgically treated before rupture		Consecutive cohort no SAH				Total @neurIST C. no SAH				
		%		%			%	p	p*		%	p	p*	
Middle cerebral artery	2425	36.2	1210	33.2	1215	39.8	82	31	NS	NS	139	31	<0.05	NS
Anterior communicating artery	1037	15.5	530	14.5	507	16.6	47	18	NS	NS	63	14	NS	NS
Internal carotid artery	1245	18.6	696	19.1	549	18	77	29	<0.001	<0.001	131	29	<0.001	<0.001
Internal carotid–posterior communicating artery	1037	15.5	602	16.5	435	14.3	23	9	<0.005	<0.001	54	12	<0.05	<0.05
Basilar tip and basilar–superior cerebellar artery	445	6.6	327	9	118	3.9	13	5	NS	<0.05	25	6	NS	<0.05
Vertebral artery–posterior inferior cerebellar artery and vertebrabasilary junction	123	1.8	80	2.2	43	1.4	8	3	NS	NS	13	3	NS	NS
Other	385	5.7	202	5.5	183	6	16	6	NS	NS	27	6	NS	NS
Total	6697		3647		3050		266				452			

p = probability their is a difference compared to UCAS total

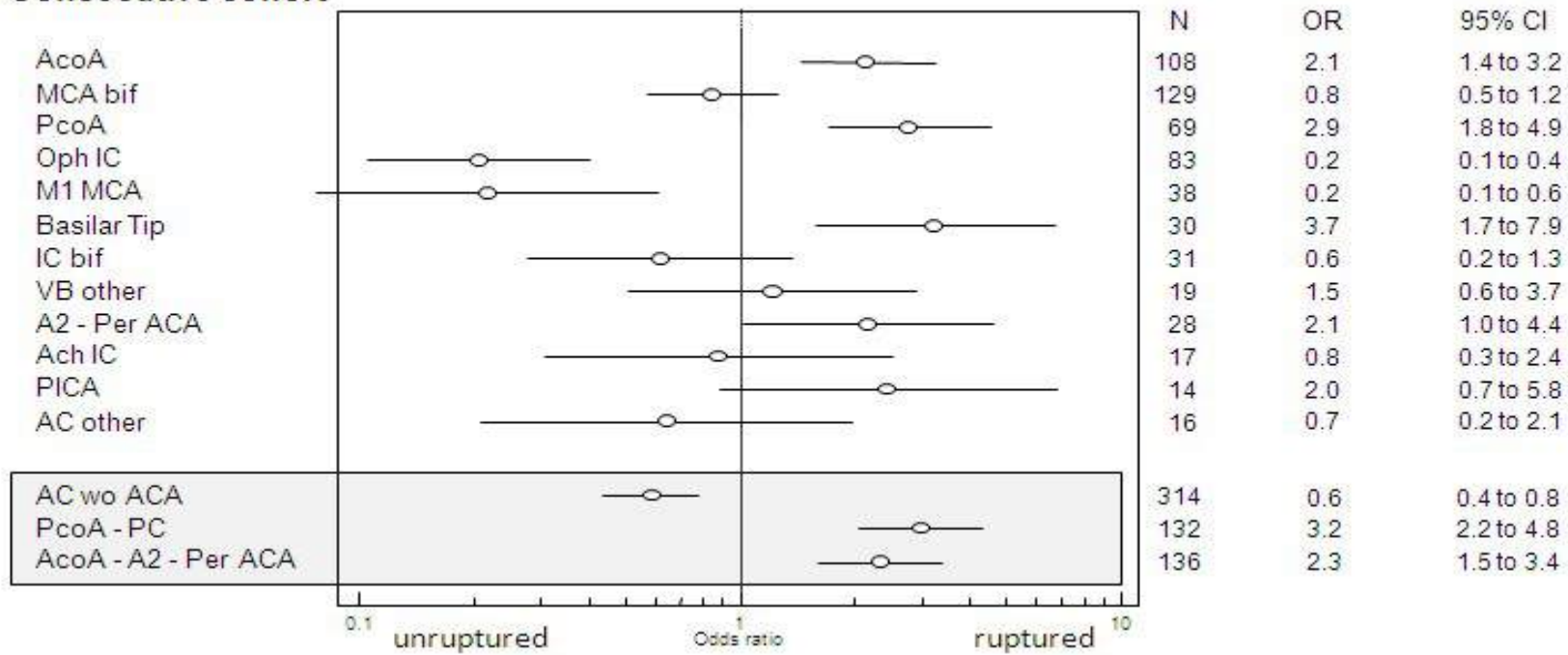
p* = probability their is a difference compared to UCAS Not surgical group

Supplementary Table IV

Cohort	ISUIA no surgery (n=1692)	ref	UCAS Not Surg (n=3647)	p	Consecutive C. noSAH (N=191)	p	Total @neurist C. no SAH (N=343)	p	p*	Consecutive cohort (N=404)	p	Total @neurist cohort (N=932)	p	p*
Medical History														
Hypertension	732 (43.6%)		1665 (45.6%)	NS	68 (35.6%)	<0.05	144(42.0%)	NS	NS	110 (27.2 %)	<0.001	320 (34.3 %)	<0.001	<0.01
Hypertension therapy	637 (37.8%)				60 (31.4%)	NS	126(36.7%)	NS	NS	88 (21.7 %)	<0.001	258 (27.7 %)	<0.001	<0.001
Valvular disease	37 (2.2%)				3/158 (1.9%)	NS	4/305(1.3 %)	NS	NS	3 (1 %)	NS	8 (1 %)	<0.05	NS
Family History														
Aneurysms	276 (18.4%)		416 (11.4%)	<0.0001	15 (7.9%)	<0.005	45 (13.1%)	NS	NS	22 (5.4%)	<0.001	88 (9.4 %)	<0.001	NS
Behavioural history														
Alcohol (>5 drinks per week)	502 (30.2%)				29 (15.2%)	<0.0001	54 (15.7%)	<0.0001	NS	58 (14.4 %)	<0.001	175 (18.7 %)	<0.001	NS
Current smoker	693 (41.1%)		551 (15%)	<0.0001	54 (28.3%)	<0.001	92 (26.8%)	<0.0001	NS	98 (24.2 %)	<0.001	258 (28 %)	<0.001	NS
Former smoker	602 (35.7%)				30 (15.7%)	<0.0001	78 (22.7%)	<0.0001	NS	57 (14.1 %)	<0.001	204 (22 %)	<0.001	<0.001
Use of stimulants	79 (4.7%)				5 (2.6%)	NS	10 (2.9%)	NS	NS	6 [1.5%]	<0.005	12 (1.3 %)	<0.0001	NS
Associated disorders														
Coarctation of aorta	9 (0.5%)				2 (0.9%)	NS	3 (0.9%)	NS	NS	3 (0.7%)	NS	4 (0.4%)	NS	NS
Polycystic kidney disease	25 (1.6%)		11 (0.3%)	<0.0001	7 (3.6%)	NS	10 (3%)	<0.05	NS	8 (1.8%)	NS	12(1.3%)	NS	NS
Arteriovenous malformation	34 (2.0%)				2 (0.9%)	NS	3 (0.9%)	NS	NS	3 (0.7%)	<0.06	7 (0.7%)	<0.01	NS
Ehlers-Danlos syndrome	0 (0%)				1 (0.5%)	NS	1(0.3%)	NS	NS	1 (0%)	NS	1(0.1%)	NS	NS
Neurofibromatosis	0 (0%)				0 (0%)	NS	0 (0%)	NS	NS	0 (0%)	NS	1 (0.1%)	NS	NS
Tuberous sclerosis	0 (0%)				0 (0%)	NS	0 (0%)	NS	NS	0 (0%)	NS	0 (0%)	NS	NS
Moyamoya disease	0 (0%)				0 (0%)	NS	1 (0.3%)	NS	NS	1 (0.2%)	NS	2 (0.2%)	NS	NS
Hypocoagulable state	6 (0.4%)				0 (0%)	NS	2 (0.6%)	NS	NS	0 (0%)	NS	3 (0.3%)	NS	NS
Fibromuscular disease	14 (0.9%)				0 (0%)	NS	0 (0%)	NS	NS	0 (0%)	NS	2 (0.2%)	NS	NS

Supplementary Figure I

Consecutive cohort



Supplemental Table and Figure Legends

Supplementary table I:

Base line characteristics of patients and aneurysms for cohorts of cases with unruptured aneurysms.

Supplementary table II:

Distribution of aneurysms by size in UCAS and @neurIST no SAH cohorts.

Supplementary table III:

Distribution of aneurysms by location in UCAS and @neurIST no SAH cohorts.

Supplementary table IV:

Medical, family and behavioural history and associated disorders characteristics for all cohorts.

Supplementary figure I:

Odds of aneurysms discovered rupture versus unruptured for each location compared to the odds of all other aneurysms included in the consecutive cohort (CC). N is the number of aneurysms observed for each location or location cluster.

Genome-wide association study of intracranial aneurysm identifies three new risk loci

Katsuhito Yasuno^{1–3*}, Kaya Bilguvar^{1–3}, Philippe Bijlenga⁴, Siew-Kee Low⁵, Boris Krischek⁶, Georg Auburger⁷, Matthias Simon⁸, Dietmar Krex⁹, Zulfikar Arlier^{1–3}, Nikhil Nayak^{1–3}, Ynte M Ruigrok¹⁰, Mika Niemela¹¹, Atsushi Tajima¹², Mikael von und zu Fraunberg¹³, Tamas Doczi¹⁴, Florentina Wirjatijasa⁷, Akira Hata¹⁵, Jordi Blasco¹⁶, Agi Oszvald¹⁷, Hidetoshi Kasuya¹⁸, Gulam Zilani¹⁹, Beate Schoch²⁰, Pankaj Singh^{21,22}, Carsten Stüer²³, Roelof Risselada²⁴, Jürgen Beck¹⁷, Teresa Sola²⁵, Filomena Ricciardi⁷, Arpo Aromaa²⁶, Thomas Illig²⁷, Stefan Schreiber²⁸, Cornelia M van Duijn^{29,30}, Leonard H van den Berg¹⁰, Claire Perret³¹, Carole Proust³¹, Constantin Roder⁶, Ali K Ozturk^{1–3}, Emília Gaál^{1–3,11}, Daniela Berg³², Christof Geisen³³, Christoph M Friedrich³⁴, Paul Summers¹⁹, Alejandro F Frangi³⁵, Matthew W State^{3,36,37}, H Erich Wichmann²⁷, Monique M B Breteler^{29,30}, Cisca Wijmenga³⁸, Shrikant Mane³⁹, Leena Peltonen⁴⁰, Vivas Elio²⁵, Miriam C J M Sturkenboom²⁶, Patricia Lawford⁴¹, James Byrne¹⁹, Juan Macho¹⁶, Erol I Sandalcioglu²⁰, Bernhard Meyer²³, Andreas Raabe¹⁷, Helmuth Steinmetz⁷, Daniel Rüfenacht⁴², Juha E Jääskeläinen¹³, Juha Hernesniemi¹¹, Gabriel J E Rinkel¹⁰, Hitoshi Zembutsu⁵, Ituro Inoue¹², Aarno Palotie⁴⁰, François Cambien³¹, Yusuke Nakamura⁵, Richard P Lifton^{3,43,44} & Murat Günel^{1–3} 

Saccular intracranial aneurysms are balloon-like dilations of the intracranial arterial wall; their hemorrhage commonly results in severe neurologic impairment and death. We report a second genome-wide association study with discovery and replication cohorts from Europe and Japan comprising 5,891 cases and 14,181 controls with ~832,000 genotyped and imputed SNPs across discovery cohorts. We identified three new loci showing strong evidence for association with intracranial aneurysms in the combined dataset, including intervals near *RBBP8* on 18q11.2 (odds ratio (OR) = 1.22, $P = 1.1 \times 10^{-12}$), *STARD13-KL* on 13q13.1 (OR = 1.20, $P = 2.5 \times 10^{-9}$) and a gene-rich region on 10q24.32 (OR = 1.29, $P = 1.2 \times 10^{-9}$). We also confirmed prior associations near *SOX17* (8q11.23–q12.1; OR = 1.28, $P = 1.3 \times 10^{-12}$) and *CDKN2A-B* (9p21.3; OR = 1.31, $P = 1.5 \times 10^{-22}$). It is noteworthy that several putative risk genes play a role in cell-cycle progression, potentially affecting the proliferation and senescence of progenitor-cell populations that are responsible for vascular formation and repair.

Intracranial aneurysms affect approximately 2% of the general population and arise from the action of multiple genetic and environmental risk factors¹. We previously reported the first genome-wide association study (GWAS) of intracranial aneurysms² that identified three risk loci on chromosomes 8q11.23–q12.1, 9p21.3 and 2q33.1 with $P < 5 \times 10^{-8}$.

This previous study had limited power to detect loci imparting genotypic relative risk (GRR) < 1.35 (Supplementary Table 1).

To increase the power to detect additional loci of similar or smaller effect, we ascertained and whole-genome sequenced two new European case cohorts ($n = 1,616$) and collected genotyping data from five additional European control cohorts (Supplementary Note, $n = 11,955$). We also increased the size of the original Japanese replication cohort and added a new Japanese replication cohort (2,282 affected individuals (cases) and 905 controls) (Table 1). The new combined cohort had nearly threefold more cases than the original cohort and increased our power to detect variants with modest effect sizes. For example, this study had 89% and 64% average power to detect common variants (minor allele frequencies (MAF) $\geq 10\%$) with GRR of 1.25 and 1.20, respectively (Supplementary Table 1).

All subjects were genotyped using the Illumina platform. The new as well as the previously analyzed genotyping data were subjected to well-established quality-control measures (Supplementary Table 2). We sought to eliminate potential confounding due to population stratification and gender^{1,3} by matching cases and controls of the same gender based on inferred genetic ancestry. As previous studies demonstrated that the Finnish population forms an ancestry cluster distinct from other European populations similar to those included in this study^{4,5}, we analyzed our Finnish cohort independently from the others. To maximize opportunities for genetic matching and analytic power, we analyzed all subjects in the remaining European cohorts together. The resulting matched case-control data consisted of 808

*A full list of author affiliations appears at the end of the paper.

Table 1 Overview of the study cohorts

	Cohort	Case (n)	Control (n)	Quality control-passed SNPs (n)	GIF
Discovery	Finland (FI)	808	4,393	1,303,876	1.070
	Combined European (CE)	1,972	8,122	905,906	1.090
	Total discovery	2,780	12,515	831,532	1.007
CE sub-cohorts	NL	708	3,954	905,906	1.110
	DE	789	2,228	905,906	1.060
	AN	475	1,940	905,906	1.060
	Total CE	1,972	8,122	905,906	1.090
Replication	Japan 1 (JP1)	829	761	12	
	Japan 2 (JP2)	2,282	905	13	
	Total replication	3,111	1,666	12	
	Total	5,891	14,181	12	

Combined European cohort consisted of all European subjects who were not ascertained in Finland. Sub-cohorts of the European cohort were defined on the basis of case series; NL, cases from The Netherlands with matched controls; DE, German cases with matched controls; AN, @neurIST cases with matched controls. NL, DE and AN were exclusive subsets of the European cohort (see also **Supplementary Table 3**). AN cases consisted of subjects from Germany, Great Britain, Hungary, The Netherlands, Switzerland and Spain. JP1 and JP2 were two independent Japanese case-control cohorts. Genomic inflation factors of the Finnish and European cohorts (as well as NL, DE and AN) were calculated for 1,303,876 and 905,906 SNPs, respectively. The genomic inflation factor of the discovery cohort (total discovery) was based on the meta-analysis result for 831,532 SNPs after correcting each cohort for genomic control. The discovery data (combined Finnish and European cohorts) was not corrected for genomic control. GIF, genomic inflation factor.

cases and 4,393 controls in the Finnish cohort and 1,972 cases and 8,122 controls in the rest of the combined European cohort (**Supplementary Table 3**). We used the genotype data that passed quality-control filters and phased chromosomes from the HapMap CEU sample to impute missing genotypes⁶. We based our further analyses on 831,534 SNPs that passed the quality-control filters both in the Finnish and European samples (**Table 1** and **Supplementary Table 2**).

We tested for association of each quality control-passed SNP with intracranial aneurysms using conditional logistic regression, assuming a log-additive effect of allele dosage. We corrected each cohort for residual overdispersion (**Table 1**) using genomic control⁷, and combined the results from the Finnish and European cohorts to obtain *P* values, ORs and CIs for the discovery cohort of 2,780 cases and 12,515 controls using a fixed-effects model.

To evaluate the strength of association, in addition to obtaining *P* values, we employed a Bayesian approach⁸. We used the Bayes factor that represents the fold-change of the odds of association before and after observing the data⁹ and the posterior probability of association (PPA), calculated through the Bayes factor, that provides a simple probabilistic measure of the evidence of association^{8,10}. For every SNP, we assumed a uniform prior probability of association of 1/10,000 and set the prior of the logarithm of the per-allele OR as a normal distribution with a 95% probability for the OR to be between 0.67 and 1.5, with larger weights for smaller effect sizes^{9,11}.

From the discovery results, we eliminated two imputed SNPs that showed PPAs of 0.97 and 0.94 because their association signals

Figure 1 Genome-wide association analysis results in the discovery cohort.

(a) The PPAs for 831,532 quality control-passed SNPs that were analyzed specifying a prior probability of association of 1/10,000 are plotted against genomic locations of SNPs. A gray horizontal line at PPA = 0.5 indicates the cutoff value for follow-up genotyping. (b) Quantile-quantile plots of *P* values ($-\log_{10}$ scale) are shown for all the SNPs analyzed (black; $n = 831,532$); SNPs after excluding those within previously identified regions (red; $n = 830,907$); and SNPs after excluding all within the final associated intervals (blue; $n = 830,158$). (c) A scatter plot of $-\log_{10} P$ versus \log_{10} Bayes factors is shown with color for each point indicating the range of PPA values. There are very close relationships among the *P* values for association, the Bayes factor and the PPA value. Note that, given a uniform prior probability of association, the PPA increases as the Bayes factor increases. A vertical line indicates the minimum PPA threshold at 0.5 (Bayes factor = 1.0×10^4) for follow-up.

were not supported by surrounding genotyped SNPs and because their genotypes were not confirmed by direct genotyping results (data not shown). This resulted in 831,532 SNPs that passed quality control (**Supplementary Table 2**).

We observed three regions that showed very high PPA (>0.995 ; **Fig. 1a**) and also a substantial excess of SNPs with $P < 1 \times 10^{-3}$ (1,295 SNPs versus 831 SNPs expected by chance) even after excluding those within previously identified associated regions² (**Fig. 1b**). Moreover, we observed a strong correlation between the *P* values and Bayes factors for the upper tail of the distribution (**Fig. 1c**).

We focused on five genomic regions (**Fig. 1a**) that contained at least one SNP with PPA >0.5 for which the hypothesis of association with intracranial aneurysm was more likely than the null hypothesis of no

association. The PPAs of the most highly associated SNPs in these intervals ranged from 0.6621 to >0.9999 and the *P* values ranged from 7.9×10^{-7} to 2.2×10^{-16} (**Supplementary Table 4**). The five chromosomal segments included three newly identified SNP clusters at 10q24.32, 13q13.1 and 18q11.2. The remaining two regions were previously identified loci at 8q11.23–q12.1 and 9p21.3 (**Fig. 2**; ref. 2). The third locus identified in our previous study, at 2q33, did not contain any SNPs with PPA >0.5 . Furthermore, consistent with our previous results², detailed analysis of the 8q11.23–q12.1 region detected two independent association signals within the <100 -kb interval that spans the *SOX17* locus (**Fig. 2** and **Supplementary Fig. 1**); these two signals are hereafter referred to as 5′-*SOX17* and 3′-*SOX17*. Thus, the five chromosomal segments comprised six independent association signals for follow-up.

We performed replication genotyping in two Japanese cohorts including 3,111 cases and 1,666 controls (JP1 and JP2, see **Table 1**). For each independent signal, we selected for replication the genotyped SNP with the highest PPA and added up to two additional SNPs per locus. For the 5′-*SOX17* region, we selected two SNPs analyzed previously, as they tag the best SNP in the current study (**Supplementary Fig. 1**).

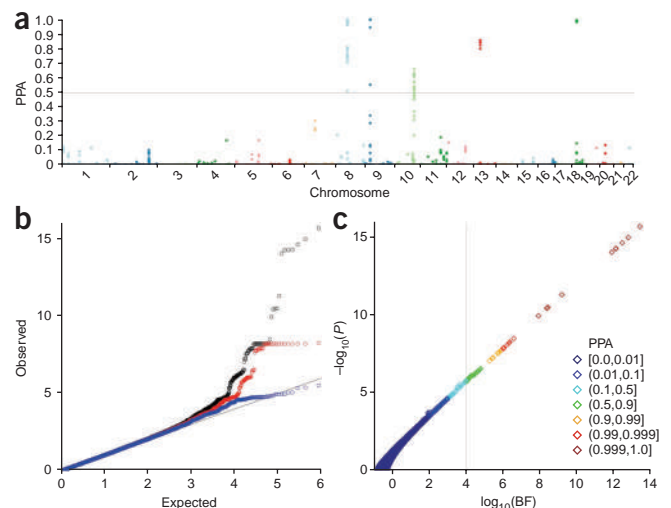
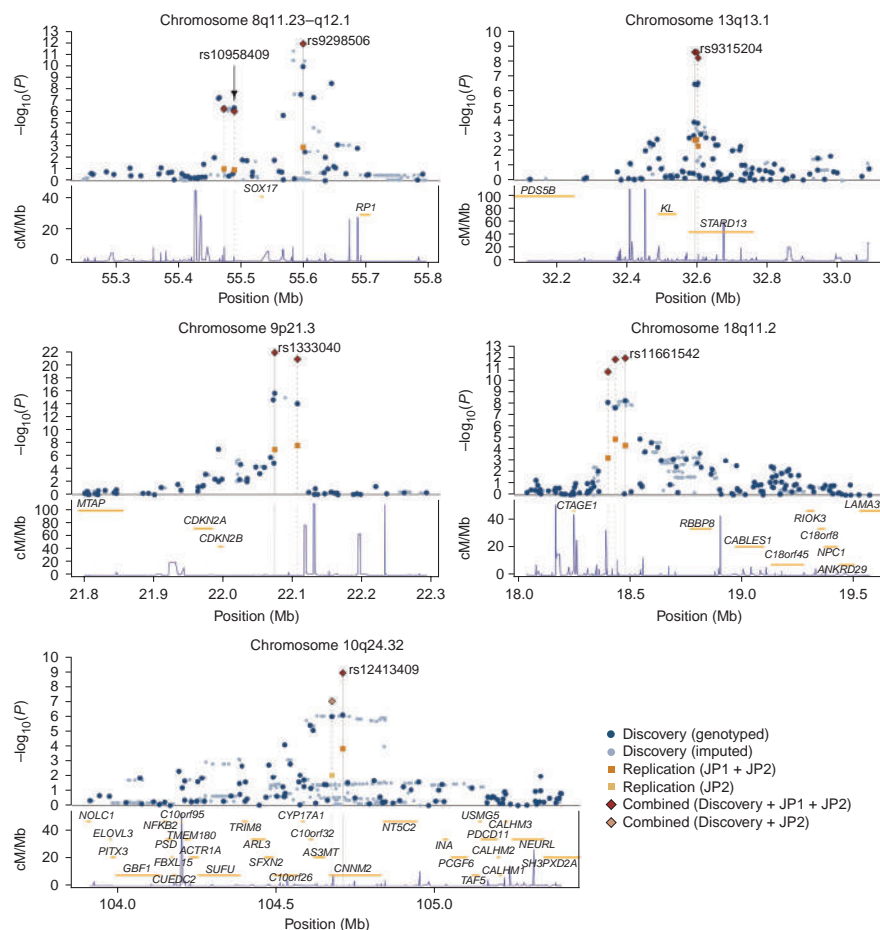


Figure 2 Regional plots for associated regions. For each chromosomal interval, $-\log_{10} P$ values for association are plotted against the genomic coordinates (NCBI build 36) above; the recombination rates obtained from the HapMap database and the RefSeq genes (hg18) within the regions are shown below. Above, rs identifiers of SNPs listed in **Table 2** are shown and their positions are indicated by gray vertical lines. Gray dashed lines indicate locations of other SNPs genotyped in the replication cohorts. Dark blue and light blue dots represent results of genotyped and imputed SNPs for the discovery cohort, respectively; orange and light orange squares represent association results for the replication cohort using JP1 combined with JP2 and also JP2-only, respectively; combined results for SNPs genotyped both in the discovery and the replication cohort using JP1 plus JP2 and JP2-only are shown by red and light red diamonds, respectively.



All but one of the SNPs (rs12411886 on 10q24.32 in JP1) were successfully genotyped and passed quality-control filters. We tested for association of each SNP with intracranial aneurysm using logistic regression stratified by gender, specifying the same model as for the discovery cohort (**Supplementary Table 5**). We combined results from JP1 and JP2 using a fixed-effects model (**Table 2** and **Supplementary Table 4**). We considered an association to be replicated if the Bayes factor increased the odds of association more than tenfold after observing the replication data.

Of the six candidate loci, all but the 5′-*SOX17* interval were replicated, with replication P values ranging from 0.0019 to 1.0×10^{-7} , and the odds of association with intracranial aneurysm increasing by 22.9-fold to 1.5×10^5 -fold, yielding robust evidence for replication for each interval (**Table 2**).

We combined the discovery and replication results using a fixed-effects model. All of the five loci that replicated in the Japanese cohort surpassed the conventional threshold for genome-wide significance ($P < 5 \times 10^{-8}$), with P values ranging from 2.5×10^{-9} to 1.5×10^{-22} , and all also had PPAs ≥ 0.998 (**Table 2**).

In order to determine each cohort's contribution to the observed association and to assess the consistency of the effect size across cohorts, we analyzed each ascertained cohort separately (**Table 1** and **Supplementary Table 5**) and then combined the results from the six cohorts using a random-effects model. The association results remained highly significant (**Fig. 3**). For the five loci that were replicated in the Japanese cohorts, we found no evidence of significant heterogeneity across cohorts ($P > 0.1$). Every cohort had the same risk allele and provided support for association with the exception of JP1 cohort for the 3-*SOX17* locus, consistent with our previous study² (**Fig. 3**).

The most significant association was detected in the previously reported² 9p21.3 region near *CDKN2A* and *CDKN2B* with $P = 1.5 \times 10^{-22}$ (OR = 1.32, PPA > 0.9999). All of the newly studied cohorts strongly supported this association with intracranial aneurysm (**Fig. 3**). These same alleles are also associated with coronary artery disease, but not with type 2 diabetes¹². Similarly, the previously reported 8q11.23-q12.1 region showed significant association. The 3′-*SOX17*

interval (rs9298506) showed robust association with $P = 1.3 \times 10^{-12}$ (OR = 1.28, PPA > 0.9999) and all new cohorts supported the association of this SNP with intracranial aneurysm (**Fig. 3**). For the 5′-*SOX17* region (rs10958409), the new cohorts introduced a substantial heterogeneity across cohorts, lowering the PPA to 0.016 (**Fig. 3**).

Among the newly identified loci, the strongest association was found at rs11661542 on 18q11.2 (OR = 1.22, $P = 1.1 \times 10^{-12}$, PPA > 0.9999). A cluster of SNPs that are associated with intracranial aneurysm spans the interval between 18.400 Mb and 18.509 Mb and are strongly correlated with rs11661542 (**Fig. 2**). A single gene, *RBBP8* (encoding the retinoblastoma binding protein 8), is located within an extended linkage disequilibrium interval (**Fig. 2**).

The second strongest new association was at rs12413409 on 10q24.32 (OR = 1.29, $P = 1.2 \times 10^{-9}$, PPA = 0.9990), which maps to intron 1 of *CNNM2* (encoding cyclin M2) (**Fig. 2**). A cluster of SNPs strongly correlated with rs12413409 and located within a ~247-kb interval in the same linkage disequilibrium block supported the association (**Fig. 2**).

The third new locus is defined by rs9315204 at 13q13.1 (OR = 1.20, $P = 2.5 \times 10^{-9}$, PPA = 0.9981) in intron 7 of *STARD13* (encoding the STAR-related lipid transfer (START) domain containing 13) (**Fig. 2**). Two SNPs, rs1980781 and rs3742321, that are strongly correlated with rs9315204 ($r^2 > 0.9$) also showed significant association with intracranial aneurysm (**Fig. 2** and **Supplementary Table 4**). These two SNPs are missense (lysine to arginine) and synonymous coding variants of *STARD13*, respectively. Another gene that has been implicated in aging phenotypes, *KL* (also known as *KLOTHO*), is located nearby¹³.

Table 2 Representative SNPs analyzed both in the discovery and replication cohorts

Locus	SNP	Position	Genes	Risk allele	Cohort	P value	log ₁₀ (Bayes)	PPA	Per-allele OR (95% CI)	Control RAF	Case RAF
8q11.23	rs10958409	55,489,644	SOX17	A	Discovery	4.2 × 10 ⁻⁷	4.64	0.8128	1.24 (1.14–1.35)	0.15, 0.19	0.18, 0.22
					Replication	0.12	-0.11		1.08 (0.98–1.20)	0.28	0.29
					Combined	9.0 × 10 ⁻⁷	4.30	0.6685	1.17 (1.10–1.25)		
8q12.1	rs9298506	55,600,077	SOX17	A	Discovery	1.2 × 10 ⁻¹⁰	7.94	0.9999	1.33 (1.22–1.45)	0.81, 0.76	0.85, 0.81
					Replication	0.0012	1.56		1.21 (1.08–1.36)	0.79	0.81
					Combined	1.3 × 10 ⁻¹²	9.85	1.0–1.4 × 10 ⁻⁶	1.28 (1.20–1.38)		
9p21.3	rs1333040	22,073,404	CDKN2A, CDKN2B	T	Discovery	2.5 × 10 ⁻¹⁶	13.41	1.0–3.9 × 10 ⁻¹⁰	1.32 (1.24–1.41)	0.56, 0.45	0.63, 0.53
					Replication	1.0 × 10 ⁻⁷	5.18		1.31 (1.19–1.45)	0.66	0.72
					Combined	1.5 × 10 ⁻²²	19.48	1.0–3.3 × 10 ⁻¹⁶	1.32 (1.25–1.39)		
10q24.32	rs12413409	104,709,086	CNNM2	G	Discovery	7.9 × 10 ⁻⁷	4.29	0.6621	1.38 (1.22–1.57)	0.91, 0.91	0.94, 0.93
					Replication	0.00014	2.34		1.23 (1.10–1.37)	0.74	0.77
					Combined	1.2 × 10 ⁻⁹	7.00	0.9990	1.29 (1.19–1.40)		
13q13.1	rs9315204	32,591,837	KL, STARD13	T	Discovery	3.3 × 10 ⁻⁷	4.73	0.8443	1.21 (1.13–1.31)	0.21, 0.33	0.24, 0.39
					Replication	0.0019	1.36		1.18 (1.06–1.31)	0.24	0.27
					Combined	2.5 × 10 ⁻⁹	6.72	0.9981	1.20 (1.13–1.28)		
18q11.2	rs11661542	18,477,693	RBBP8	C	Discovery	5.6 × 10 ⁻⁹	6.39	0.9959	1.21 (1.14–1.30)	0.49, 0.44	0.54, 0.47
					Replication	4.5 × 10 ⁻⁵	2.79		1.22 (1.11–1.34)	0.61	0.65
					Combined	1.1 × 10 ⁻¹²	9.92	1.0–1.2 × 10 ⁻⁶	1.22 (1.15–1.28)		

Genomic locations for SNPs are based on NCBI build 36, and risk alleles are aligned to the forward strand of the reference sequence. Control and case risk allele frequencies (RAFs) for the discovery cohort are shown in the form: RAF of European cohort, RAF of Finnish cohort. Log₁₀ (Bayes) indicates the logarithm of the Bayes factor in favor of association. PPA, posterior probability of association. Genes closest to the listed SNPs within the same LD regions are shown.

A search of the gene-expression database (eQTL browser, see URLs) for all the intracranial aneurysm-risk loci did not reveal any consistent pattern of association of intracranial aneurysm SNPs with variation in gene expression levels.

In this second GWAS of intracranial aneurysm, which included nearly three times as many cases as the initial study, we detected three new risk loci and obtained strong independent evidence for association of two previously identified loci. The evidence that these are

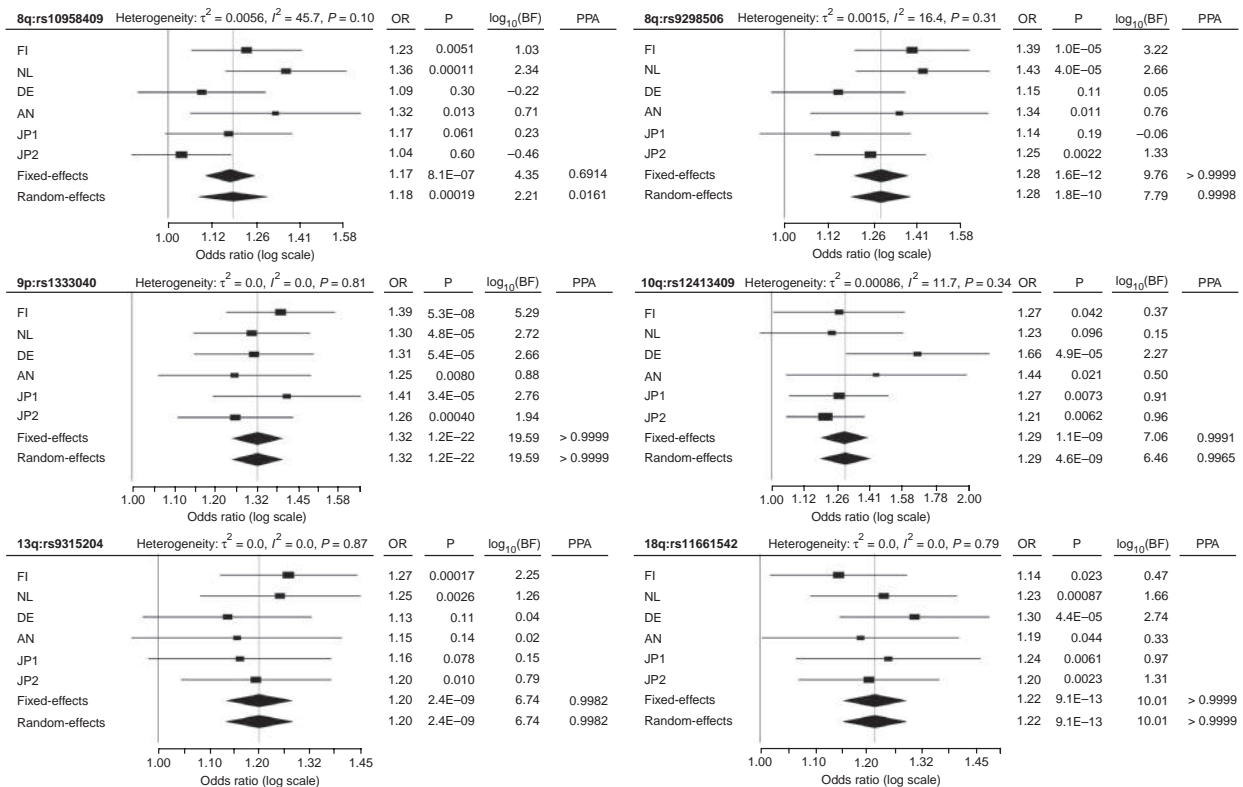


Figure 3 Consistency of association across cohorts. Forest plots are shown for meta-analysis of the SNPs listed in **Table 2**. Squares and horizontal segments represent estimated per-allele ORs and 95% CIs for individual cohorts. Diamonds represent the summary OR estimates and 95% CIs for the meta-analyses of six cohorts (using fixed- and random-effects models). Log₁₀ (Bayes factor) > 0 supports association with intracranial aneurysm, whereas log₁₀ (Bayes factor) < 0 supports no association with intracranial aneurysm. Analyzing the results here as six distinct cohorts rather than four cohorts (as in the primary analysis) resulted in only minor differences due to different weights given to sub-cohorts of the combined European cohort associated with genomic control correction.

bona fide risk loci for intracranial aneurysm is very strong from both Bayesian measures and conventional *P* values.

Given our power (~90%) to detect variants that confer risk of intracranial aneurysm with GRR = 1.25 and MAFs ≥ 10%, we expect that we have identified most of these variants, limited principally by potential gaps in SNP coverage. Indeed, across the rest of the genome, there was no locus with PPA >0.22 and MAF ≥10%, whereas there were 14 loci with PPAs between 0.1 and 0.22 and ORs between 1.16 and 1.25 (data not shown). We expect that a fraction of these loci are genuine intracranial aneurysm risk loci, as suggested by the excess of SNPs with $P < 1 \times 10^{-3}$ (Fig. 1b); exploring this possibility will require analysis of larger intracranial aneurysm cohorts and/or genotyping of alleles with lower MAF.

Based on the results of the first GWAS of intracranial aneurysm and the role of the implicated gene products, encoded by *SOX17* and in individuals with the genotype *P15*^{INK4b}, *P16*^{INK4a}, we previously hypothesized² that the genes associated with intracranial aneurysm might play a role in determining cell cycle progression, and may affect the proliferation¹⁴ and senescence of progenitor-cell populations and/or the balance between production of progenitor cells versus cells committed to differentiation. Genes located within the newly identified regions support this idea. The protein encoded by *RBBP8*, located within the 18q11.2 region, influences progression through the cell cycle by interacting with *BRCA1*¹⁵. Similarly, of the two genes located within the 13q13.1 interval, *STARD13* contains the Rho-GAP and C-terminal STAR-related lipid transfer (START) domains and its overexpression results in suppression of cell proliferation¹⁶. The other gene implicated here, *KL*, encodes a transmembrane protein that modulates FGF receptor specificity¹⁷; mice lacking *KL* show accelerated aging in diverse organ systems¹³.

On the assumption that there is a fourfold increase in the risk of intracranial aneurysm among siblings of cases^{18,19} and that the SNPs combine to increase log-odds of disease in an additive fashion, the five intracranial aneurysm risk loci explain 5.2% (within the Finnish cohort), 4.0% (in the European cohort) and 3.5% (in the combined JP1 and JP2 cohort) of the familial risk of intracranial aneurysm. Under this model, the odds of developing an intracranial aneurysm varies 4.99- to 7.63-fold across the top and bottom 1% of genetic risk profiles at these loci in the populations studied here and 3.61- to 4.64-fold across the 5% extremes (Supplementary Fig. 2). When combined with traditional risk factors such as gender, blood pressure and smoking, these findings form the basis of future work aimed at preclinical identification of individuals who are at high risk of intracranial aneurysm formation and rupture.

URLS. eQTL browser, <http://eqtl.uchicago.edu/>.

METHODS

Methods and any associated references are available in the online version of the paper at <http://www.nature.com/naturegenetics/>.

Note: Supplementary information is available on the Nature Genetics website.

ACKNOWLEDGMENTS

We are grateful to the participants who made this study possible. We thank A. Chamberlain, B. Mesek-Selchow and members of the Keck Foundation Biotechnology Resource Laboratory for their technical help. This study was supported by the Yale Center for Human Genetics and Genomics and the Yale Program on Neurogenetics, the US National Institute of Health (NIH) grants R01NS057756 (M.G.) and U24 NS051869 (S.M.) and the Howard Hughes Medical Institute (R.P.L.). The @neurIST project was funded by European Commission, VI Framework

Programme, Priority 2, Information Society Technologies, a European Public Funded Organization (Research Grant No. IST-FP6-027703). The Frankfurt case cohort collection was supported by BMBF (01GI9907), Utrecht Control cohort by the Prinses Beatrix Fonds and the Adessium foundation (L.H.v.d.B.). S.M. was supported in part by the Clinical and Translational Science Award ULI RR024139, National Center for Research Resources, NIH. We would also like to acknowledge the use of Yale University Biomedical High Performance Computing Center (NIH grant: RR19895).

AUTHOR CONTRIBUTIONS

Study Cohorts: ascertainment, characterization and DNA preparation: M.N., M.v.u.z.F., E.G., J.E.J., J.H. and A.P. (Finnish case-control); Y.M.R. and G.J.E.R. (NL cases); P.B., T.D., J. Blasco, G.Z., P.S., R.R., T.S., C.M.F., P.S., A.F.F., V.E., M.C.J.M.S., P.L., J. Byrne, J.M. and D.R. (@neurIST case series); B.K., G.A., M.S., D.K., F.W., A.O., B.S., C.S., J. Beck, F.R., C.R., D.B., C.G., E.J.S., B.M., A.R. and H.S. (DE case series); A.T., A.H., H.K. and I.I. (JP1); S.-K.L., H.Z. and Y.N. (JP2). **Control Cohorts:** A.A., L.P. and A.P. (Health2000); A.A., L.P. and A.P. (NFBC1966); C.M.v.D. and M.M.B.B. (Rotterdam Study); L.H.v.d.B. and C.W. (Utrecht); T.I. and H.E.W. (KORA-gen); S.S. (PopGen). **Genotyping:** K.B., Z.A., N.N., A.K.O., E.G., S.M., R.P.L. and M.G. (Yale); C. Perret, C. Proust and F.C. (Aneurist); S.-K.L., H.Z. and Y.N. (JP2). **Data management and informatics:** K.Y., K.B., Z.A., N.N. and M.G. (Yale); S.-K.L., H.Z. and Y.N. (JP2 cohort); **Statistical analysis:** K.Y. and M.G. **Writing team:** K.Y., K.B., M.W.S., R.P.L. and M.G. **Study design and analysis plan:** K.Y., R.P.L. and M.G.

COMPETING FINANCIAL INTERESTS

The authors declare competing financial interests: details accompany the full-text HTML version of the paper at <http://www.nature.com/naturegenetics/>.

Published online at <http://www.nature.com/naturegenetics/>.

Reprints and permissions information is available online at <http://npg.nature.com/reprintsandpermissions/>.

- Rinkel, G.J., Djibuti, M., Algra, A. & van Gijn, J. Prevalence and risk of rupture of intracranial aneurysms: a systematic review. *Stroke* **29**, 251–256 (1998).
- Bilguvar, K. *et al.* Susceptibility loci for intracranial aneurysm in European and Japanese populations. *Nat. Genet.* **40**, 1472–1477 (2008).
- Iwamoto, H. *et al.* Prevalence of intracranial saccular aneurysms in a Japanese community based on a consecutive autopsy series during a 30-year observation period. The Hisayama study. *Stroke* **30**, 1390–1395 (1999).
- Salmela, E. *et al.* Genome-wide analysis of single nucleotide polymorphisms uncovers population structure in Northern Europe. *PLoS One* **3**, e3519 (2008).
- Jakkula, E. *et al.* The genome-wide patterns of variation expose significant substructure in a founder population. *Am. J. Hum. Genet.* **83**, 787–794 (2008).
- Marchini, J., Howie, B., Myers, S., McVean, G. & Donnelly, P. A new multipoint method for genome-wide association studies by imputation of genotypes. *Nat. Genet.* **39**, 906–913 (2007).
- Devlin, B. & Roeder, K. Genomic control for association studies. *Biometrics* **55**, 997–1004 (1999).
- Wakefield, J. A Bayesian measure of the probability of false discovery in genetic epidemiology studies. *Am. J. Hum. Genet.* **81**, 208–227 (2007).
- Wellcome Trust Case Control Consortium. Genome-wide association study of 14,000 cases of seven common diseases and 3,000 shared controls. *Nature* **447**, 661–678 (2007).
- Stephens, M. & Balding, D.J. Bayesian statistical methods for genetic association studies. *Nat. Rev. Genet.* **10**, 681–690 (2009).
- Wacholder, S., Chanock, S., Garcia-Closas, M., El Ghormli, L. & Rothman, N. Assessing the probability that a positive report is false: an approach for molecular epidemiology studies. *J. Natl. Cancer Inst.* **96**, 434–442 (2004).
- Helgadottir, A. *et al.* The same sequence variant on 9p21 associates with myocardial infarction, abdominal aortic aneurysm and intracranial aneurysm. *Nat. Genet.* **40**, 217–224 (2008).
- Kuro-o, M. *et al.* Mutation of the mouse *klotho* gene leads to a syndrome resembling ageing. *Nature* **390**, 45–51 (1997).
- Visel, A. *et al.* Targeted deletion of the 9p21 non-coding coronary artery disease risk interval in mice. *Nature* **464**, 409–412 (2010).
- Yun, M.H. & Hiom, K. CtIP-BRCA1 modulates the choice of DNA double-strand-break repair pathway throughout the cell cycle. *Nature* **459**, 460–463 (2009).
- Leung, T.H. *et al.* Deleted in liver cancer 2 (DLC2) suppresses cell transformation by means of inhibition of RhoA activity. *Proc. Natl. Acad. Sci. USA* **102**, 15207–15212 (2005).
- Urakawa, I. *et al.* *Klotho* converts canonical FGF receptor into a specific receptor for FGF23. *Nature* **444**, 770–774 (2006).
- Schievink, W.I. Genetics of intracranial aneurysms. *Neurosurgery* **40**, 651–662 discussion 662–663 (1997).
- Cannon Albright, L.A. *et al.* A genealogical assessment of heritable predisposition to aneurysms. *J. Neurosurg.* **99**, 637–643 (2003).

¹Department of Neurosurgery and ²Department of Neurobiology, Yale University School of Medicine, New Haven, Connecticut, USA. ³Department of Genetics, Yale Program on Neurogenetics, Yale Center for Human Genetics and Genomics, Yale University School of Medicine, New Haven, Connecticut, USA. ⁴Department of Clinical Neurosciences, Service de Neurochirurgie, Geneva University Hospital, Geneva, Switzerland. ⁵Human Genome Center, Institute of Medical Science, University of Tokyo, Tokyo, Japan. ⁶Department of Neurosurgery, University of Tuebingen, Tuebingen, Germany. ⁷Department of Neurology, Goethe University, Frankfurt am Main, Germany. ⁸Department of Neurosurgery, University of Bonn, Bonn, Germany. ⁹Klinik und Poliklinik für Neurochirurgie Universitätsklinikum Carl Gustav Carus der Technischen Universität Dresden, Dresden, Germany. ¹⁰Department of Neurology, Rudolf Magnus Institute of Neuroscience, University Medical Center Utrecht, Utrecht, The Netherlands. ¹¹Department of Neurosurgery, Helsinki University Central Hospital, Helsinki, Finland. ¹²Division of Molecular Life Science, School of Medicine, Tokai University, Isehara, Kanagawa, Japan. ¹³Department of Neurosurgery, Kuopio University Hospital, Kuopio, Finland. ¹⁴Neurosurgery, University of Pécs Medical School, Pécs, Hungary. ¹⁵Department of Public Health, School of Medicine, Chiba University, Chiba, Japan. ¹⁶Department of Vascular Radiology, Hospital Clinic, Barcelona, Spain. ¹⁷Department of Neurosurgery, Goethe University, Frankfurt am Main, Germany. ¹⁸Department of Neurosurgery, Medical Center East, Tokyo Women's University, Tokyo, Japan. ¹⁹Nuffield Department of Surgery, John Radcliffe Hospital, University of Oxford, Oxford, UK. ²⁰Department of Neurosurgery, University Hospital, Essen, Germany. ²¹Department of Medical Physics and ²²Department of Neurosurgery, Royal Hallamshire Hospital, Sheffield, UK. ²³Department of Neurosurgery, Technical University of Munich, Munich, Germany. ²⁴Department of Medical Informatics, Erasmus University Medical Center, Rotterdam, The Netherlands. ²⁵Therapeutic Neuroangiography, Hospital General de Catalunya, San Cugat del Valles, Spain. ²⁶Department of Health and Functional Capacity, National Public Health Institute, Helsinki, Finland. ²⁷Institute of Epidemiology, German Research Center for Environmental Health, Helmholtz Zentrum München, Munich, Germany. ²⁸Institute for Clinical Molecular Biology, Christian-Albrechts-University, Kiel, Germany. ²⁹Genetic Epidemiology Unit, Department of Epidemiology and Biostatistics and ³⁰Department of Clinical Genetics, Erasmus Medical Center, Rotterdam, The Netherlands. ³¹UMR Institut National de la Santé et de la Recherche Médicale (INSERM) S937—University Pierre and Marie Curie, Paris, France. ³²Center of Neurology, Department of Neurodegeneration and Hertie Institute for Clinical Brain Research, University of Tuebingen, Tuebingen, Germany. ³³Institute of Transfusion Medicine and Immunohaematology, Department of Molecular Haemostasis, DRK Blood Donor Service Baden Wuerttemberg and Hessen, Frankfurt am Main, Germany. ³⁴Fraunhofer-Institut for Algorithms and Scientific Computing, Sankt Augustin, Germany. ³⁵Center for Computational Imaging and Simulation Technologies in Biomedicine, Universitat Pompeu Fabra, Barcelona, Spain. ³⁶Department of Psychiatry and ³⁷Child Study Center, Yale University School of Medicine, New Haven, Connecticut, USA. ³⁸Department of Genetics, University Medical Center Groningen and University of Groningen, Groningen, The Netherlands. ³⁹Keck Foundation Biotechnology Resource Laboratory, Yale University, New Haven, Connecticut, USA. ⁴⁰Wellcome Trust Sanger Institute, Wellcome Trust Genome Campus, Hinxton, Cambridge, UK. ⁴¹Academic Unit of Medical Physics, School of Medicine and Biomedical Sciences, University of Sheffield, Sheffield, UK. ⁴²Neuroradiology - SNI - Clinic Hirslanden, Zürich, Switzerland. ⁴³Howard Hughes Medical Institute and ⁴⁴Department of Internal Medicine, Yale University School of Medicine, New Haven, Connecticut, USA. Correspondence should be addressed to R.P.L. (richard.lifton@yale.edu) or M.G. (murat.gunel@yale.edu).

ONLINE METHODS

Genotyping. Whole-genome genotyping for the discovery cohort was performed on the Illumina platform according to the manufacturer's protocol (Illumina). Bead chips used for individual cohorts are presented in **Supplementary Table 2**. Replication genotyping in the JP1 cohort was performed using either Taqman (Applied Biosystems) or MassARRAY (Sequenom) assays. For the JP2 cohort, genotyping for cases was performed using the multiplex PCR-based Invader assay (Third Wave Technologies Inc.); genotyping for controls was performed on an Illumina platform as described previously²⁰.

Ethics. The study protocol was approved by the Yale Human Investigation Committee (HIC protocol #7680). Institutional review board approval for genetic studies, along with written consent from all study participants, was obtained at all participating institutions.

Data storage and analysis tools. We used PLINK²¹ v1.06 and R statistical environment v2.9.0 (in particular, the `snpMatrix` package²²) for storage of genotype data and data analysis.

Preprocessing. Prior to the analysis of genotyping data, we excluded SNPs that were located either on mitochondrial DNA or sex chromosomes, SNPs with A/T or C/G alleles, those for which all subjects were assigned as 'no call', and those that were assayed on Hap300v1 or 550v1 but were dropped from newer versions.

Sample quality control. We excluded subjects in the discovery cohort who did not conform to our study design on the basis of genotyping and information quality, cryptic relatedness and population outliers. We summarize the sample exclusion steps in **Supplementary Table 2**. This filtering process resulted in the inclusion of 835 cases and 6,529 controls in the Finnish cohort and 2,000 cases and 8,722 controls in the rest of the combined European cohort.

Imputation. We performed imputation analysis with the HapMap phase II CEU reference panel (release 24) using the IMPUTE v1 software⁶. The analysis was performed separately for the Finnish and European cohorts. We converted posterior probabilities of three possible genotypes to fractional allele dosage scores (between 0 and 2) and used these scores for association tests in order to take into account the imputation uncertainty²³. For the quality assessment of imputed SNPs, we also converted the posterior probabilities to the most likely genotypes with the threshold at 0.9.

Case-control matching. Population stratification and independent genotyping of cases and controls are major causes of confounding in GWAS²⁴. Because our study consisted of multiple independently ascertained cohorts that were genotyped separately, we performed a stringent analysis to control for these biases by inferring the genetic ancestries of subjects^{25,26}. We used the Laplacian eigenmaps²⁷ to infer population structure. Following the determination of the number of dimensions ($K + 1$) using the threshold given in Lee *et al.*²⁸, we used the K -dimensional nontrivial generalized eigenvectors²⁹ to calculate the Euclidean distance between any two subjects.

In the course of this analysis, we excluded 'isolated' subjects who were identified by using the nearest-neighbor distance distributions in any of the two-dimensional sections. After excluding these subjects, we observed 13 dimensions in the Finnish cohort and 5 dimensions in the European cohort. The larger dimensions observed in the Finnish population could be attributable to the presence of many isolated populations in Finland⁵.

Before matching, we stratified data into males and females because female gender is a known risk factor of intracranial aneurysm^{1,3}. We also set the maximum distance between cases and controls to match to be less than 0.028 in the Finnish cohort and 0.009 in the and European cohort. These values were determined by examining the distribution of the nearest-neighbor distances in K dimensions (data not shown). We matched cases and controls using the fullmatch function in the R-package `optmatch`^{30,31}.

SNP quality control. For both genotyped and imputed SNPs in the discovery cohort, we applied quality-control filters to individual cohorts and to cases

and controls separately on the basis of the missing rate, MAF and the P value of the exact test of Hardy-Weinberg equilibrium³². For imputed SNPs, we also assessed imputation quality using the average posterior probability, MAF and allelic R^2 metric³³. Finally, we assessed differential missingness between cases and controls (**Supplementary Table 2**).

Any genotyped SNP that passed the quality-control filters both in the European and Finnish cohorts was referred to as a 'genotyped SNP', and any one for which we used the quality control-passed imputation data either in one or both of the cohorts was classified as an 'imputed SNP'.

For genotyping data of the replication cohorts, we excluded SNPs if any of the following three conditions were met in either cases or controls: (i) missing rate >0.05 ; (ii) P value of the exact test of Hardy-Weinberg equilibrium <0.001 ; or (iii) MAF <0.01 .

Statistical analysis. Cohort-wise association analysis. We tested for association between each quality control-passed SNP and intracranial aneurysm using conditional and unconditional logistic regression for the discovery and replication cohorts, respectively³⁴. For the discovery cohort, we used the matched strata to correct for potential confounding due to population stratification and gender and for the replication cohorts we adjusted for gender. We assumed the log-additive effect of allele dosage on disease risk. We obtained P values from the score test (two-sided) and estimated the logarithm of per-allele ORs with standard errors (s.e.m.) by maximizing the conditional or unconditional likelihood. Both the test statistic and the s.e.m. of the log of the OR were corrected using genomic control⁷. We performed the association analysis for the Finnish and European cohorts, as well as sub-cohorts of the European group that consisted of NL cases, DE cases or @neurIST cases and their matched controls (**Table 1** and **Supplementary Table 3**). We used the following R functions to perform the association analysis: `clogit`, `glm` and `snp.rhs.tests`²².

Meta-analysis. We combined the cohort-wise per-allele ORs in the Finnish and European cohorts using a fixed-effects model of meta-analysis for 831,534 quality control-passed SNPs to obtain the discovery results. For SNPs analyzed both in the discovery and replication cohorts, we combined JP1 and JP2 to obtain replication results and all four cohorts to obtain combined results. Our primary analysis was based on the fixed-effects model²³. To assess the heterogeneity of the effect size between cohorts, we first divided the European cohort into three groups as described above, aiming to analyze the data without averaging effect sizes over the combined European cohorts, and then combined our six cohorts using the random-effects model. We employed the restricted maximum likelihood procedure to estimate the between-cohort heterogeneity variance (τ^2) using the R function `MiMa`³⁵ (see URLs). From this estimate, we calculated the Cochran's Q statistic and the I^2 statistic³⁶.

Bayesian evaluation of the strength of association. To evaluate the strength of association with intracranial aneurysm, we used a Bayesian approach^{9,37}. A limitation of the use of P values alone is that variability in factors such as effect size, MAF and sample size can result in identical statistics that might correspond to markedly different levels of evidence regarding the strength of association¹⁰. The Bayes factor provides an alternative that compares the probabilities of the data under the alternative hypothesis of association versus the null hypothesis of no association. For computational simplicity, we approximated the Bayes factor as described by Wakefield⁸. For all SNPs, we assumed a single prior for the log-OR: a normal distribution with mean of 0 and a standard deviation of $\log(1.5)/\Phi^{-1}(0.975)$, where Φ is the normal distribution function⁹.

The PPA¹⁰ provides a simple probabilistic measure of evidence by introducing the prior probability of association, π_1 . We assumed a uniform prior, $\pi_1 = 1/10,000$, for all the SNPs¹¹. For Bayes factor $>10^6$, changing π_1 to a more conservative value of $1/100,000$ would result in little change in the PPA.

To combine the results from multiple cohorts, we extended the formula³⁸ to be applicable to multiple (>2) cohorts.

Conditional analysis. For each region that contained a SNP with PPA >0.5 , we examined the number of independent association signals by testing for association of every genotyped SNP with intracranial aneurysm by adjusting for the effect of a specified SNP (**Supplementary Fig. 1**).

Two-locus interaction analysis. We tested for deviation from a linear model, which assumes that two SNPs combine to increase the log-odds of disease in an additive fashion, using conditional (in the Finnish and European cohorts)

or unconditional (in JP1 plus JP2, stratified by cohorts and gender) logistic regression. There was no significant deviation from the linear model (data not shown).

Cumulative effect. We evaluated potential clinical implications of the genetic profiles of the five intracranial aneurysm risk loci following the approach described by Clayton³⁹. We fitted a five-locus conditional (Finnish and European cohorts) or unconditional (Japanese cohorts) logistic regression model including the additive and dominance-deviation terms for each locus. Using the estimated effect sizes and each individual's genotype, we calculated the risk scores for every individual. The receiver-operating characteristic curve for each ethnic cohort (Finnish, European and Japanese) was depicted using the risk score.

We also calculated the ratio of the exponential of the mean of the risk scores for control subjects within the top versus bottom 5% or 1% of each cohort to obtain approximated odds ratios of disease between these classes.

The sibling recurrence risk was estimated by assuming the polygenic model that fits well to our data³⁹. Fraction of the sibling recurrence risk attributable to all of the five loci was calculated by taking the ratio of the logarithm of this value and epidemiologically estimated value of 4^{18,19}.

URLs. The R function MiMa, <http://www.wvbauer.com/>.

20. Kamatani, Y. *et al.* A genome-wide association study identifies variants in the HLA-DP locus associated with chronic hepatitis B in Asians. *Nat. Genet.* **41**, 591–595 (2009).
21. Purcell, S. *et al.* PLINK: a tool set for whole-genome association and population-based linkage analyses. *Am. J. Hum. Genet.* **81**, 559–575 (2007).
22. Clayton, D. & Leung, H.T. An R package for analysis of whole-genome association studies. *Hum. Hered.* **64**, 45–51 (2007).
23. de Bakker, P. *et al.* Practical aspects of imputation-driven meta-analysis of genome-wide association studies. *Hum. Mol. Genet.* **17**, R122–R128 (2008).
24. Clayton, D.G. *et al.* Population structure, differential bias and genomic control in a large-scale, case-control association study. *Nat. Genet.* **37**, 1243–1246 (2005).
25. Patterson, N., Price, A.L. & Reich, D. Population structure and eigenanalysis. *PLoS Genet.* **2**, e190 (2006).
26. Price, A.L. *et al.* Principal components analysis corrects for stratification in genome-wide association studies. *Nat. Genet.* **38**, 904–909 (2006).
27. Belkin, M. & Niyogi, P. Laplacian eigenmaps for dimensionality reduction and data representation. *Neural Comput.* **15**, 1373–1396 (2003).
28. Lee, A., Luca, D., Klei, L., Devlin, B. & Roeder, K. Discovering genetic ancestry using spectral graph theory. *Genet. Epidemiol.* **34**, 51–59 (2009).
29. von Luxburg, U. A tutorial on spectral clustering. *Stat. Comput.* **17**, 395–416 (2007).
30. Rosenbaum, P. A characterization of optimal designs for observational studies. *J. R. Statist. Soc. B* **53**, 597–610 (1991).
31. Hansen, B. & Klopfer, S. Optimal full matching and related designs via network flows. *J. Comput. Graph. Statist.* **15**, 609–627 (2006).
32. Wigginton, J., Cutler, D. & Abecasis, G. A note on exact tests of Hardy-Weinberg equilibrium. *Am. J. Hum. Genet.* **76**, 887–893 (2005).
33. Browning, B. & Browning, S. A unified approach to genotype imputation and haplotype-phase inference for large data sets of trios and unrelated individuals. *Am. J. Hum. Genet.* **84**, 210–223 (2009).
34. Breslow, N. & Day, N. Statistical methods in cancer research. Volume I—the analysis of case-control studies. *IARC Sci. Publ.* 5–338 (1980).
35. Viechtbauer, W. Bias and efficiency of meta-analytic variance estimators in the random-effects model. *J. Educ. Behav. Stat.* **30**, 261–293 (2005).
36. Higgins, J., Thompson, S., Deeks, J. & Altman, D. Measuring inconsistency in meta-analyses. *Br. Med. J.* **327**, 557–560 (2003).
37. Goodman, S. Toward evidence-based medical statistics. 2: The Bayes factor. *Ann. Intern. Med.* **130**, 1005–1013 (1999).
38. Wakefield, J. Reporting and interpretation in genome-wide association studies. *Int. J. Epidemiol.* **37**, 641–653 (2008).
39. Clayton, D. Prediction and interaction in complex disease genetics: experience in type 1 diabetes. *PLoS Genet.* **5**, e1000540 (2009).